Mapping the MicroRNA Landscape in Central Nervous System Malignancies: Functional Role and Clinical Relevance

Author: Denis Mustafov

Primary supervisor: Dr Maria Braoudaki,

Supervisory team: Professor Emmanouil Karteris, Dr Shoib Siddiqui, Dr Maria Dimitriadi

Submitted to the University of Hertfordshire in partial fulfilment of the requirement of the degree of Doctor of Philosophy

September 2024

Abstract

Glioblastoma (GB) is the most aggressive and lethal brain tumour found in adults and is characterised by poor prognosis and limited treatment options. Identifying putative biomarkers for early diagnosis and developing new therapeutic strategies are necessary to improve patient outcomes. Liquid biopsy-based microRNAs (miRNAs) have emerged as promising diagnostic biomarkers due to their stability in body fluids and their ability to reflect tumour-specific changes. This study aimed to identify miRNA diagnostic biomarkers for GB and evaluate alternative therapeutic approaches. The primary focus was to assess the dysregulation of miRNAs and their target genes, explore their potential as diagnostic tools, and evaluate new therapies, including in-house synthesised anticancer compounds.

Initially, we performed *in silico* analyses to identify the most dysregulated miRNAs in GB and their associated target genes. Selected miRNAs and their target genes were further validated using reverse transcription quantitative polymerase chain reaction (RT-qPCR) in GB cell lines. Western blotting, immunofluorescence (IF) and immunohistochemistry (IHC) were used to further confirm the expression profiles of selected proteins in GB cells and patient samples, respectively. To expand the clinical relevance of the study, the expression of selected miRNAs and their target genes was also assessed in highly malignant paediatric brain tumours, such as medulloblastomas (MBs). To evaluate liquid biopsy-based diagnostics, exosomes from GB patients were extracted and analysed using small RNA-sequencing (sRNA-seq) and proteomics to screen the miRNome and proteome in these patients. Transient transfections and functional assays were conducted to understand the mechanisms underlying selected miRNAs and their roles as alternative therapeutics for GB and MB tumours. Additionally, two newly synthesised anticancer compounds were evaluated as potential therapeutics against GB cell line models. *In vitro* functional assays, further bioinformatics analyses, and sRNA-seq were utilised to assess the cytotoxic effects and the impact of these compounds on the miRNome of GB cells. Data from these analyses were integrated to determine the therapeutic potential of both natural and synthetic compounds, particularly focusing on their ability to modulate miRNAs involved in GB progression.

Our *in silico* analyses revealed that miR-34a and miR-128a were downregulated in GB and targeted the potential oncogenes *CORO1C* and *SV2B*, demonstrating their tumour-suppressive properties. However, the affinity of miR-34a and miR-128a towards *CORO1C* and *SV2B* was relatively weak, leading to the selection of miR-206 and miR-383 for further analysis. MiR-206 and miR-383 demonstrated stronger targeting affinity for *CORO1C* and *SV2B*, respectively, as shown by our *in silico* analyses, making them more suitable candidates for potential miRNA-mimic therapies aimed at suppressing these oncogenes in GB. Notably, *CORO1C* was particularly elevated in paediatric patients with high synaptic plasticity, highlighting its diagnostic potential for aggressive brain tumours. Elevated *SV2B* expression was associated with shorter survival, emphasising its role in tumour prognosis. Western blotting and IF analyses confirmed these findings by showing the upregulation and cytoplasmic cellular appearance of CORO1C and SV2B in GB and MB cell lines, suggesting their potential roles in tumour progression. Immunohistochemistry results further supported our *in vitro* findings, showing elevated protein expression of CORO1C and SV2B in both GB and MB patient tissues. Additionally, sRNA-seq of paediatric MB patient samples showed the downregulation of miR-206 and miR-383, whilst transcriptomic analysis revealed upregulation of *CORO1C* and *SV2B*. However, exosomal GB sRNA-seq and proteomics analysis did not show these miRNAs or proteins as dysregulated, suggesting that CORO1C and SV2B may have specialised roles in intracellular processes rather than in exosome-mediated communication.

Functional assays demonstrated that miR-206 and miR-383 effectively targeted and downregulated *CORO1C* and *SV2B*, leading to reduced cell viability and impaired colony formation in GB and MB cells. In addition, two synthesised compounds, SHG-8 and SHG-44 were evaluated for their therapeutic potential in GB. Both compounds significantly inhibited cell viability, migration, and proliferation in GB cells. SHG-8 downregulated *CORO1C* and inhibited the Wnt signalling pathway, while SHG-44 modulated GB-associated oncomiRs and tumour suppressor miRNAs.

This study identified miR-206/*CORO1C* and miR-383/*SV2B* axes as highly promising therapeutic targets due to their observed tumour-suppressive effects *in vitro*. MiR-206 and miR-383 were shown to effectively downregulate their respective targets, *CORO1C* and *SV2B*, resulting in significant reduction in cell viability and tumour progression, emphasising their potential use in targeted miRNA-mimic therapies for brain malignancies. Furthermore, the synthesised compounds SHG-8 and SHG-44 exhibited strong inhibitory effects on GB cells, demonstrating their potential as alternative treatments by modulating key miRNAs and oncogenic pathways, including the suppression of *CORO1C* and the Wnt signalling pathway. These findings enhance our understanding of miRNA-based diagnostics and therapeutics in brain cancer, highlighting the miR-206/*CORO1C* and miR-383/*SV2B* axes as candidates in the development of personalised treatment strategies and improving patient outcomes in neuro-oncology.

Keywords: microRNAs, glioblastoma, medulloblastoma, diagnostic biomarkers, therapy

Dedication

I am dedicating this work to my parents, Gyuner Sakinov and Slavena Sakinova, for their constant support, love, and encouragement throughout this journey.

Acknowledgements

I am sincerely grateful to my primary supervisor, Dr Maria Braoudaki, whose exceptional guidance, expertise, and continuous support were invaluable throughout my PhD. Her encouragement and insightful feedback broadened my research scope and enriched the quality of my work. Beyond her role as a supervisor, her kind and understanding approach provided me with the confidence and motivation needed to complete this journey.

I would also like to express my appreciation to the rest of my supervisory team, Professor Emmanouil Karteris, Dr Maria Dimitriadi, and Dr Shoib Siddiqui, for their dedicated support and input throughout my PhD. Their diverse expertise, thoughtful advice, and collaborative spirit played an important role throughout my research, ensuring the successful completion of my thesis. I am truly fortunate to have had such a knowledgeable and supportive team guiding me along the way.

I also wish to acknowledge all my colleagues, especially Mohammed Ahmad, Altin Kocinaj, and Dr Ladislav Klena, for their friendship and encouragement. Their constant support, willingness to share their knowledge and the positive atmosphere they brought to our work environment made a great difference throughout my research journey. Their friendship and teamwork made even the most challenging days manageable and enjoyable.

My thanks extend to the technical team in the Nexus Building for their consistent support in the laboratories. Their expertise and assistance with the day-to-day technical aspects of my experiments were a great help and support throughout my research.

I would also like to express my gratitude to my collaborators, Dr Irshad Ahmad, Dr Shagufta, Dr Georgios Giamas, and Dr George Lambrou, for their contributions to my research. Their expertise and insightful discussions further enhanced the quality and depth of my work. Their collaborative spirit and commitment to advancing our research objectives were inspiring and greatly influenced the focus and development of my studies.

Lastly, I am grateful to my friends and family for their consistent encouragement and support. Their patience, understanding, and belief in my capabilities were constant sources of strength and motivation. Whether through their words of encouragement or simply by being there, their support has been an essential part of my success.

Table of contents

Abstract **2**

Dedication **4**

Acknowledgements **5**

List of figures **12**

List of tables **16**

Abbreviations **18**

Chapter 1. Introduction **21**

1.1. Primary brain tumours 21

1.2. Glioblastoma 24

1.2.1. Epidemiological characteristics 24

1.2.2. Clinical Presentation 25

1.2.3. Initial assessment 25

1.2.4. Differential diagnosis and Neuroimaging 26

1.2.5. Advanced neuroimaging 28

1.2.6. Histopathology 29

1.2.7. Molecular profiling, altered molecular pathways and molecular biomarkers 30

1.2.7.1. Molecular profiling 30

1.2.7.2. Altered molecular pathways 35

1.2.8. Molecular biomarkers 36

1.2.8.1. Isocitrate dehydrogenase 36

1.2.8.2. O6-methylguanine-DNA methyltransferase (MGMT) promoter methylation 37

1.2.8.3. Epidermal growth factor receptor 37

1.2.9. Tumour microenvironment in GB 38

1.2.9.1. Glioma stem cells 39

1.2.9.2. Astrocytes 40

1.2.9.3. Neurones 41

1.2.9.4. Oligodendrocytes 41

1.2.9.5. Immune cells 41

1.2.10. Therapeutic management 42

1.2.10.1. Surgery 42

1.2.10.2. Intra-operative neuroanatomical navigation systems 43

1.2.10.3. Ultrasound 43

1.2.10.4. Fluorescent dyes 44

1.2.10.6. Awake surgery 44

1.2.11. Radiotherapy 45

1.2.12. Chemotherapy 46

1.2.12.1. Temozolomide 46

1.2.12.2. Lomustine 47

1.2.12.3. Bevacizumab 48

1.2.13. Immunotherapy 48
1.2.13.1. Chimeric antigen receptor T cell therapy 49
1.2.13.2. Oncolytic Viruses 49
1.2.13.3. Immune checkpoint inhibitors 50
1.2.14. Combination Therapies 50
1.2.15. Prediction benefit 51
1.3. MicroRNAs 51
1.3.1. Introduction to miRNAs 51
1.3.2. MiRNA biogenesis 52
1.3.2.1. The canonical pathway 52
1.3.2.2. The non-canonical pathway 55
1.3.3. Dysregulation of miRNAs 57
1.3.3.1. Dysregulated miRNAs in GB 58
1.3.3.2. Overexpressed miRNAs in GB 59
1.3.3.3. Downregulated miRNAs in GB 61
1.3.4. MiRNAs as diagnostic biomarkers for GB 63
1.4. Liquid Biopsies 64
1.4.1. Liquid biopsies versus tissue biopsies 65
1.4.2. Types of liquid biopsies 67
1.4.3. Types of liquid biopsy biomarkers 68
1.4.3.1. Cell-free DNA 68
1.4.3.2. Circulating Tumour Cells 69
1.4.3.3. Extracellular vesicles 69
1.4.3.4. Proteins 70
1.4.3.5. Liquid biopsy-based miRNAs 70
1.5. miRNAs as therapeutics 71
1.5.1. Challenges associated with miRNA therapeutics 75
1.6. Aims and objectives 76
1.6.1. Liquid biopsy-based miRNA diagnostic biomarkers 76
1.6.2. GB alternative therapies 76
Chapter 2. Identification of new miRNA biomarkers through bioinformatics 77
2.1. Introduction 77
2.1.2. Aims and research questions 80
2.1.2.1. Aims 80
2.1.2.2. Research Questions 80
2.2. Materials and Methods 81
2.2.1. *In silico* miRNA analysis 81
2.2.2. *In silico* miRNA: mRNA interaction analysis 81
2.2.3. *In silico* target gene analysis 82
2.2.4. *In silico* target protein analysis 83

2.2.5. Statistics 83
2.3. Results 84
2.3.1. *In silico* miRNA analysis 84
2.3.2. *In silico* miRNA: mRNA interaction analysis 87
2.3.3. MiRNA-centric network analysis 90
2.3.4. Sfold miRNA: mRNA analysis 92
2.3.5. *CORO1C* gene expression analysis in normal tissues and brain 94
2.3.6. *CORO1C* gene expression analysis in different cancer types and GB 97
2.3.7. *CORO1C* mRNA expression analysis in GB cells 102
2.3.8. *CORO1C* survival analysis in GB cases 105
2.3.9. CORO1C pathway and protein analysis 105
2.3.10. *SV2B* gene expression analysis in normal tissues and brain 107
2.3.11. *SV2B* gene expression analysis in different cancer types and GB 110
2.3.12. *SV2B* mRNA expression analysis in GB cells 115
2.3.13. *SV2B* survival analysis in GB cases 118
2.3.14. SV2B pathway and protein analysis 118
2.4. Discussion 120

Chapter 3. *In vitro* validations 138

3.1. Introduction 138
3.1.1. Aims and research questions 143
3.1.1.1. Aims 143
3.1.1.2. Research Questions 143
3.2. Materials and Methods 144
3.2.1. Cell culture 144
3.2.2. Total RNA extraction 144
3.2.3. Organic miRNA extraction 145
3.2.4. cDNA synthesis 146
3.2.5. RT-qPCR 147
3.2.6. Protein quantification via western blotting 148
3.2.7. Immunofluorescence 149
3.2.8. Transient transfections 150
3.2.9. Cell viability assay 151
3.2.10. Colony forming assay 151
3.2.11. Statistics 151
3.3. Results 152
3.3.1. RT-qPCR validations of miRNA expression profiles in GB cells 152

3.3.2. RT-qPCR validations of gene expression profiles in GB cells 154
3.3.3. RT-qPCR validations of miRNA expression profiles in MB cells..... 155
3.3.4. RT-qPCR validations of gene expression profiles in MB cells 157
3.3.5. Protein quantification via western blotting..... 157
3.3.6. Immunofluorescence protein visualisation 159
3.3.7. Transient transfections of GB cells..... 162
3.3.8. Transient transfections of MB cells 170
3.4. Discussion..... 176

Chapter 4: Patient tissue and liquid biopsy-based biomarkers..... 186

4.1. Introduction..... 186
4.1.2. Aims and research questions..... 190
4.1.2.1. Aims..... 190
4.1.2.2. Research questions 190
4.2. Materials and Methods 191
4.2.1. Patient's samples..... 191
4.2.2. Immunohistochemistry 192
4.2.3. Small RNA-sequencing 193
4.2.4. Clustering and sequencing..... 194
4.2.5. Data analysis..... 194
4.2.6. Comparative analysis..... 194
4.2.7. Target gene functional annotation..... 194
4.2.8. Quantification of miRNA expression levels 195
4.2.9. Differential expression analysis..... 195
4.2.10. GO enrichment and KEGG pathway enrichment analysis 195
4.2.11. Transcriptomics..... 196
4.2.12. Extracellular vesicles extractions 196
4.2.13. Nanoparticle tracking analysis..... 196
4.2.14. Western blotting..... 197
4.2.15. Protein and miRNA extractions from exosomes 197
4.2.16. Proteomics of GB exosomes..... 198
4.2.17. Mass spectrometry analysis 199
4.2.18. Database search and bioinformatics analyses..... 199
4.2.19. Data availability..... 199
4.2.20. Statistics..... 200
4.3 Results..... 201
4.3.1. Immunohistochemistry for CORO1C..... 201

4.3.2. Immunohistochemistry for SV2B 204
4.3.3. sRNA-seq analysis of MB tissue profiles 208
4.3.4. Transcriptomics analysis of MB tissue profiles 213
4.3.5. Exosome extraction and validation 217
3.4.6. sRNA-seq of GB exosome profiles 220
3.4.7. Proteomics analysis of GB exosome profiles 225
4.4. Discussion 229

Chapter 5. New GB therapies 237

5.1. Introduction 237
5.1.2. Aims and research questions 240
5.1.2.1. Aims 240
5.1.2.2. Research questions 240
5.2. Materials and Methods 242
5.2.1. SHG-8 synthesis and characterisation 242
5.2.2. SHG-44 synthesis and characterisation 243
5.2.3. Cell culture 243
5.2.4. Cell viability assay 244
5.2.5. Colony formation assay 244
5.2.6. Scratch assay 245
5.2.7. Reactive oxygen species assay 246
5.2.8. 4′,6-diamidino-2-phenylindole, dihydrochloride staining 247
5.2.9. Acridine Orange/Ethidium bromide staining 247
5.2.10. RNA isolation, preparation of samples for sRNA-seq, and sRNA-seq 248
5.2.11. TaqMan Expression Assays 249
5.2.12. Molecular docking 250
5.2.13. *In silico* analysis of SHG-8 and SHG-44 and their metabolites 251
5.2.14. Data availability 251
5.2.15. Statistics 251
5.3. Results 252
5.3.1. Synthesis and characterisation of SHG-8 252
5.3.2. Synthesis and characterisation of SHG-44 256
5.3.3. SHG-8 and SHG-44 cell viability assays 260
5.3.4. Small RNA-sequencing of SHG-8 and SHG-44 treated U87MG cells 262
5.3.5. RT-qPCR validation 269
5.3.6. SHG-8 and SHG-44 impaired the colony formation within GB cells 271
5.3.7. SHG-8 and SHG-44 disrupted the migratory abilities in both GB cell lines 276

5.3.8. Reactive oxygen species determination post-exposure to SHG-8 and SHG-44 282
5.3.9. SHG-8 and SHG-44 mediated apoptosis in U87MG and U251MG glioma cells 286
5.3.10. Molecular docking 295
5.3.11. RT-qPCR gene analysis following molecular docking 299
5.3.12. *In silico* analysis of the pharmacokinetic and pharmacodynamic characteristics of SHG-8 and SHG-44 301
5.4. Discussion 305

Chapter 6. Final Discussion 319

References 327

Appendices 393

Appendix 1. Continuous professional development 393
1.1. Attended workshops and seminars 393
1.2. Attended conferences and webinars 393

Appendix 2. Publications and extended abstracts 394
2.1. Peer-reviewed journal publications 394
2.2. Journal papers in press 394
2.3. Journal papers in preparation 395
2.4. Extended abstracts (peer-reviewed) 395
2.5. Book chapters 395

Appendix 3. Poster and oral presentations 396
3.1. Poster presentations 396
3.2. Oral presentations 396

Appendix 4. Awards and grants 397

Appendix 5. Ethics approval notification 398

Appendix 6. Relevant publications to work done in Chapter 2, Journal: *Non-coding RNA* 400

Appendix 7. Relevant publications to work done in Chapters 2, 3 & 4, Journal: *Scientific reports* 418

Appendix 8. Relevant publications to work done in Chapter 5, Journal: *ACS omega* 431

List of figures

Chapter 1

Figure 1. Global incidence and distribution of brain tumours based on GLOBOCAN Data (2022) 23
Figure 2. Routine imaging assessment of suspected brain neoplasms 27
Figure 3. Histopathological analysis of GB 30
Figure 4. Key genetic alternations crucial for gliomagenesis 32
Figure 5.A flowchart summarising key genetic alterations in gliomagenesis as outlined by the WHO CNS5 classification, organised by glioma type 33
Figure 6. The complex tumour microenvironment in GB. 39
Figure 7. An overview of the canonical and non-canonical pathways of miRNA biogenesis. 56
Figure 8. Examples of some commonly overexpressed and under-expressed miRNAs in GB 59
Figure 9. Benefits of liquid biopsies in their use of cancer monitoring 65
Figure 10. The use of liquid biopsies in GB management 68
Figure 11. Therapeutic applications of miRNAs 72

Chapter 2

Figure 12. Flowchart summarising the in silico methodology for miRNA analysis in GB 85
Figure 13. KEGG pathway analysis depicted the most differentially expressed miRNA profiles in 529 GB cases (grade 4) 86
Figure 14. A Venn diagram incorporating miRSystem, TargetScan, miRWalk, and ENCORI databases 88
Figure 15. A Venn diagram incorporating miRSystem, TargetScan, miRWalk, and ENCORI databases 89
Figure 16. Interactome analysis of important miRNAs involved in the overall gene regulation for *CORO1C* co-expressed genes 91
Figure 17. Interactome analysis of important miRNAs involved in the overall gene regulation for *SV2B* co-expressed genes. 92
Figure 18. Sfold analysis of miRNA binding sites for *CORO1C.* 93
Figure 19. Sfold analysis of miRNA binding sites for *SV2B*. 94
Figure 20. Detection of *CORO1C* mRNA across different tissue types. 95
Figure 21. Detection of *CORO1C* mRNA across the normal brain. 95
Figure 22. Detection of *CORO1C* mRNA across normal brain cells. 96
Figure 23. Heatmaps of log2 expression values from six patients obtained through microarray experiments (Allen Brain Atlas). 97
Figure 24. Expression of *CORO1C* in various cancerous tissues. 98
Figure 25. *CORO1C* expression levels across different GB age groups. 99
Figure 26. *CORO1C* expression levels in male and female GB patients compared to normal controls. 100
Figure 27. *CORO1C* expression levels across different racial groups in GB patients. 101
Figure 28. *CORO1C* expression levels across different paediatric brain tumours. 102
Figure 29. Single-cell *CORO1C* analysis of GB cell clusters from paediatric and adult patients. 104
Figure 30. Survival analysis of *CORO1C* expression in glioblastoma cases. 105
Figure 31. CORO1C pathway analysis and its role in cellular processes associated with tumour progression and metastasis. 106

Figure 32. CORO1C protein interaction network. 106
Figure 33. Detection of *SV2B* mRNA across different tissue types. 108
Figure 34. Detection of *SV2B* mRNA across the normal brain. 108
Figure 35. Detection of *SV2B* mRNA across normal brain cells. 109
Figure 36. Heatmaps of log2 expression values from six patients obtained through microarray experiments (Allen Brain Atlas). 110
Figure 37. Expression of *SV2B* in various cancerous tissues. 111
Figure 38. *SV2B* expression across different age groups in GB patients. 112
Figure 39. *SV2B* expression in male and female GB patients compared to normal controls. 113
Figure 40. *SV2B* mRNA expression across different racial groups in GB patients compared to controls 114
Figure 41. *SV2B* expression across different types of paediatric brain malignancies. 115
Figure 42. Single-cell *SV2B* analysis of GB cell clusters from paediatric and adult patients. 117
Figure 43. Survival analysis of *SV2B* expression in glioblastoma cases 118
Figure 44. Integrated KEGG pathway analysis of SV2B. 119
Figure 45. SV2B protein interaction network. 119

Chapter 3

Figure 46. MiRNA RT-qPCR expression analyses in GB cells. 153
Figure 47. Gene RT-qPCR expression analyses in GB cells. 154
Figure 48. MiRNA RT-qPCR expression analyses in MB cells. 156
Figure 49. Gene RT-qPCR expression analyses in MB cells. 157
Figure 50. Western blotting protein quantification analyses. 158
Figure 51. IF analysis of CORO1C localisation and quantification in HA-bs, U251MG, U87MG, and DAOY cells. 160
Figure 52. IF analysis of SV2B localisation and quantification in HA-bs, U251MG, U87MG, and DAOY cells. 161
Figure 53. IF analysis of β-actin localisation and quantification in HA-bs, U251MG, U87MG, and DAOY cells. 162
Figure 54. RT-qPCR of miRNA expression in GB cells post-transfection. 164
Figure 55. RT-qPCR of gene expression in GB cells post-transfection. 165
Figure 56. MTT assays in GB cells post-transfection with miR-206 or miR-383 mimics. 166
Figure 57. Colony-forming assays in GB cells post-transfection with miR-206 or miR-383 mimics. 167
Figure 58. Western blotting of U251MG GB cells post-transfection with miR-206 or miR-383 mimics. 168
Figure 59. Western blotting of U87MG GB cells post-transfection with miR-206 ormiR-383 mimics. 169
Figure 60. RT-qPCR of miRNA expressions in MB cells post-transfection. 171
Figure 61. RT-qPCR of gene expressions in MB cells post-transfection. 172
Figure 62. MTT assays in MB cells post-transfection with miR-206 or miR-383 mimics. 173
Figure 63. Colony-forming assays in MB cells post-transfection with miR-206 or miR-383 mimics. 174
Figure 64. Western blotting of DAOY MB cells post-transfection with miR-206 or miR-383 mimics. 175

Chapter 4

Figure 65. Immunohistochemistry analyses of CORO1C. 202-204
Figure 66. Immunohistochemistry analyses of SV2B. 205-207
Figure 67. Comprehensive sRNA-seq analysis of MB tissue miRNA profiles. 209
Figure 68. KEGG pathway analysis.....210
Figure 69. Molecular function analysis.. 211
Figure 70. Biological process analysis.....212
Figure 71. Comprehensive transcriptomics analysis of MB tissue profiles.....213
Figure 72. Pathway enrichment analysis. 214
Figure 73. Molecular function analysis. 215
Figure 74. Biological process analysis.....216
Figure 75. Assessment of EV enrichment and purity.....219
Figure 76. Ponceau staining and western blotting. 220
Figure 77. Comprehensive sRNA-seq analysis of GB exosomal miRNA profiles.....221
Figure 78. KEGG pathway analysis.....222
Figure 79. Molecular function analysis.. 223
Figure 80. Biological process analysis.....224
Figure 81. Comprehensive proteomics analysis of GB exosome samples. 225
Figure 82. KEGG pathway analysis.....226
Figure 83. Reactome protein analysis......227
Figure 84. Gene ontology analysis.....228

Chapter 5

Figure 85. SHG-8 synthesis reaction. 253
Figure 86. FT-IR spectrum of SHG-8. 253
Figure 87. ^{1}H NMR spectrum of SHG-8 in $CDCl_3$.....254
Figure 88. ^{13}C NMR spectrum of SHG-8 in $CDCl_3$.....255
Figure 89. ESI-MS spectrum of SHG-8.....255
Figure 90. High-resolution mass spectrum of SHG-8. 256
Figure 91. SHG-44 synthesis reaction. 257
Figure 92. FT-IR spectrum of SHG-44. 257
Figure 93. ^{1}H NMR spectrum of SHG-44 in $CDCl_3$.....258
Figure 94. ^{13}C NMR spectrum of SHG-44 in $CDCl_3$.....259
Figure 95. High-resolution mass spectrum of SHG-44. 259
Figure 96. U251MG and U87MG glioma cell viability and proliferation in response to varying concentrations of SHG-8. 260
Figure 97. U251MG and U87MG glioma cell viability and proliferation in response to varying concentrations of SHG-44.. 261
Figure 98. U251MG and U87MG glioma cell viability and proliferation in response to cis-platin treatment. 261
Figure 99. sRNA-seq of U87MG cells (SHG-8). 263
Figure 100. KEGG pathway analysis (SHG-8).....264
Figure 101. Molecular function analysis (SHG-8). 264
Figure 102. Biological process analysis (SHG-8).....265
Figure 103. Cellular component enrichment analysis (SHG-8).....265
Figure 104. sRNA-seq of U87MG cells (SHG-44). 266
Figure 105. KEGG pathway analysis (SHG-44).....267
Figure 106. Molecular function analysis (SHG-44).. 267

Figure 107. Biological process analysis (SHG-44).....268
Figure 108. Cellular component enrichment analysis (SHG-44).....269
Figure 109. RT-qPCR validation.....270
Figure 110. Colony formation of U87MG post-SHG-8 treatment.....272
Figure 111. Colony formation of U251MG post-SHG-8 treatment.....273
Figure 112. Colony formation of U87MG post-SHG-44 treatment.....274
Figure 113. Colony formation of U251MG post-SHG-44 treatment.....275
Figure 114. Colony formation of U251MG and U87MG post-cis-platin treatment.....276
Figure 115. Cell migration of U87MG cells post-SHG-8 exposure. 278
Figure 116. Cell migration of U251MG cells post-SHG-8 exposure. 279
Figure 117. Cell migration of U87MG cells post-SHG-44 exposure. 280
Figure 118. Cell migration of U251MG cells post-SHG-44 exposure. 281
Figure 119. SHG-8 induced the release of ROS in U87MG treated cells. 283
Figure 120. SHG-8 induced the release of ROS in U251MG treated cells. 284
Figure 121. SHG-44 induced the release of ROS in U87MG treated cells. 285
Figure 122. SHG-44 induced the release of ROS in U251MG treated cells.. 286
Figure 123. DAPI staining of U87MG and U251MG cells treated with SHG-8.....288
Figure 124. DAPI staining of U87MG and U251MG cells treated with SHG-44.....289
Figure 125. Acridine orange/ethidium bromide staining of U87MG cells post-SHG-8 treatment. 291
Figure 126. Acridine orange/ethidium bromide staining of U251MG cells post-SHG-8 treatment. 292
Figure 127. Acridine orange/ethidium bromide staining of U87MG cells post-SHG-44 treatment.. 293
Figure 128. Acridine orange/ethidium bromide staining of U251MG cells post-SHG-44 treatment. 294
Figure 129. Molecular docking between SHG-8 and CORO1C.....296
Figure 130. Molecular docking between SHG-8 and SV2B.....297
Figure 131. Molecular docking between SHG-44 and CORO1C.....298
Figure 132. Molecular docking between SHG-44 and SV2B.....299
Figure 133. RT-qPCR analysis of gene expression following SHG-8 and SHG-44 treatments. 300
Figure 134. Metabolites of SHG-8 predicted by Biotransformer 3.1. 302
Figure 135. Metabolites of SHG-44 predicted by Biotransformer 3.1. 302

Chapter 6

Figure 136. MiRNA axes and therapeutics in high grade brain malignancies.....326

List of tables

Chapter 1

Table 1. Overview of tumour types, grades, and key molecular markers in brain tumours 34
Table 2. Summary of ongoing and completed liquid biopsy studies for GB (Eibl & Schneemann, 2023, modified). 66
Table 3. MiRNAs in clinical trials for cancer therapies (Kim & Croce, 2023, modified).....74

Chapter 2

Table 4. Identification of miRNAs and associated target genes.. 84
Table 5. Identification of gene targets of miR-34a-5p and miR-128a-3p. 87
Table 6. miRSystem analysis of miRNA: mRNA interactions. 87
Table 7. Common miRNAs (62) in "miRSystem ", "TargetScan", "miRWalk" and "ENCORI" found to target CORO1C. 90
Table 8. Common miRNAs (26) in "miRSystem", "TargetScan", "miRWalk" and "ENCORI" found to target SV2B. 90

Chapter 3

Table 9. Assay IDs for gene expression analysis. 147
Table 10. Assay IDs for miRNA expression analysis. 148
Table 11. Assay IDs for siRNA transient transfections assays....150

Chapter 4

Table 12. Comparison of protein concentration and NTA size in control and patient extracellular vesicle samples....218

Chapter 5

Table 13. Treatment concentrations of SHG-8 and SHG-44 in U87MG and U251MG cells (Cell viability assay). 244
Table 14. Treatment concentrations of SHG-8 and SHG-44 in U87MG and U251MG cells (Colony formation assay)....245
Table 15. Treatment concentrations of SHG-8 and SHG-44 in U87MG and U251MG cells (Scratch assay) 246
Table 16. Treatment concentrations of SHG-8 and SHG-44 in U87MG and U251MG cells (ROS assay). 247
Table 17. Treatment concentrations of SHG-8 and SHG-44 in U87MG and U251MG cells (DAPI assay). 247
Table 18. Treatment concentrations of SHG-8 and SHG-44 in U87MG and U251MG cells (acridine orange/ethidium bromide staining assay). 248
Table 19. Thermal cycler settings for cDNA synthesis. The table shows the cDNA synthesis settings used for mRNA and miRNA profiling. 250
Table 20. Settings for RT-qPCR. This table shows the RT-qPCR steps for mRNA and miRNA profiling....250
Table 21. Molecular docking sites and binding affinities between the large molecule receptor protein CORO1C and the small molecule ligand SHG-8. 296

Table 22. Molecular docking sites and binding affinities between the large molecule receptor protein SV2B and the small molecule ligand SHG-8. 297
Table 23. Molecular docking sites and binding affinities between the large molecule receptor protein CORO1C and the small molecule ligand SHG-44. 298
Table 24. Molecular docking sites and binding affinities between the large molecule receptor protein SV2B and the small molecule ligand SHG-44. 299
Table 25. Prediction of absorption, distribution, and toxicity properties of SHG-8 and its metabolites, alongside aspirin and ibuprofen analysis.....303
Table 26. Prediction of absorption, distribution, and toxicity properties of SHG-44 and its metabolites, alongside aspirin and ibuprofen analysis.....304

Abbreviations

ADC - Apparent Diffusion Coefficient
ADMET - Absorption, Distribution, Metabolism, Excretion, and Toxicity
Ago - Argonaute
ANOVA - Analysis of Variance
ATP - Adenosine Triphosphate
BAX - BCL2 Associated X, Apoptosis Regulator
BCA - Bicinchoninic Acid
BCL-xL - B-cell lymphoma-extra-large
BBB - Blood-Brain Barrier
BrdU - Bromodeoxyuridine
CAIX - Carbonic Anhydrase IX
CBTRUS - Central Brain Tumour Registry of the United States
CDS - Coding Sequence
CEST - Chemical Exchange Saturation Transfer
CL - Classical
CNS - Central Nervous System
CNNC - Cytosine-any nucleotide-nucleotide-cytosine
CPAN - Comprehensive Perl Archive Network
CORO1C - Coronin 1C
CSF - Cerebrospinal Fluid
CT - Computer Tomography
CTLA-4 - Cytotoxic T-lymphocyte-associated Protein 4
DAB - Diaminobenzidine
DAPI - 4',6-Diamidino-2-Phenylindole
DEG - Differentially Expressed Genes
DGCR8 - DiGeorge Syndrome Critical Region Gene 8
DIPG - Diffuse Infiltrative Pontine Glioma
DMSO - Dimethyl Sulfoxide
DNT - Dysembryoplastic Neuroepithelial Tumor
DNA - Deoxyribonucleic Acid
DTI - Diffusion Tensor Imaging
DWI - Diffusion-Weighted Imaging
ECM - Extracellular Matrix
EGFR - Epidermal Growth Factor Receptor
EMA - European Medicines Agency
EMT - Epithelial-Mesenchymal Transition
ENCORI - Encyclopedia of RNA Interactomes
ESI - Electrospray Ionization
EV - Extracellular Vesicles
FDA - Food and Drug Administration
FBS - Fetal Bovine Serum
FDG - Fluoro-2-deoxy-D-glucose
FGFR - Fibroblast Growth Factor Receptor
FLAIR - Fluid-Attenuated Inversion Recovery
FPKM - Fragments Per Kilobase of Exon Per Million
FTIR - Fourier Transform Infrared Spectroscopy
G-CIMP - Glioma Cytosine-Phosphate-Guanine Island Methylator Phenotype
GAMs - Glioma-Associated Microglia/Macrophages

GB - Glioblastoma
GHG - Glycine-Histidine-Glycine
GNG - Ganglioglioma
GO - Gene Ontology
GSCs - Glioma Stem Cells
GTEx - Genotype-Tissue Expression
GTR - Gross Total Resection
HDAC - Histone Deacetylase
HIF-1α - Hypoxia-Inducible Factor 1-Alpha
HMGA2 - High Mobility Group AT-Hook 2
HRMS - High-Resolution Mass Spectrometry
HRP - Horseradish Peroxidase
iMRI - Intraoperative MRI
iUS - Intraoperative Ultrasound
IC50 - Half Maximal Inhibitory Concentration
IDH - Isocitrate Dehydrogenase
IF - Immunofluorescence
IHC - Immunohistochemistry
IL-6 - Interleukin 6
KEGG - Kyoto Encyclopedia of Genes and Genomes
KM - Kaplan-Meier
LC-MS - Liquid Chromatography-Mass Spectrometry
MAPK - Mitogen-Activated Protein Kinase
MB - Medulloblastoma
MDM2 - Mouse Double Minute 2 Homolog
MEG - Magnetoencephalography
MGMT - O-6-methylguanine-DNA Methyltransferase
MHC - Major Histocompatibility Complex
miRNA - MicroRNA
MoCA - Montreal Cognitive Assessment
MRI - Magnetic Resonance Imaging
MRS - Magnetic Resonance Spectroscopy
mRNA - Messenger RNA
MTIs - MicroRNA:mRNA Target Interactions
MTT - Methyl Thiazolyl Tetrazolium
nTPM - Normalized Transcripts Per Million
NCBI - National Center for Biotechnology Information
NCS - Neural Stem Cells
ncRNA - Non-coding RNA
NF1 - Neurofibromin 1
NICE - National Institute for Health & Care Excellence
NMR - Nuclear Magnetic Resonance
NTA - Nanoparticle Tracking Analysis
NSC - Neural Stem Cell
OPCs - Oligodendrocyte Precursor Cells
OS - Overall Survival
PARP - Poly (ADP-Ribose) Polymerase
PBS - Phosphate-Buffered Saline
PCV – Procarbazine/Lomustine/Vincristine regimen for GB
PFA - Paraformaldehyde

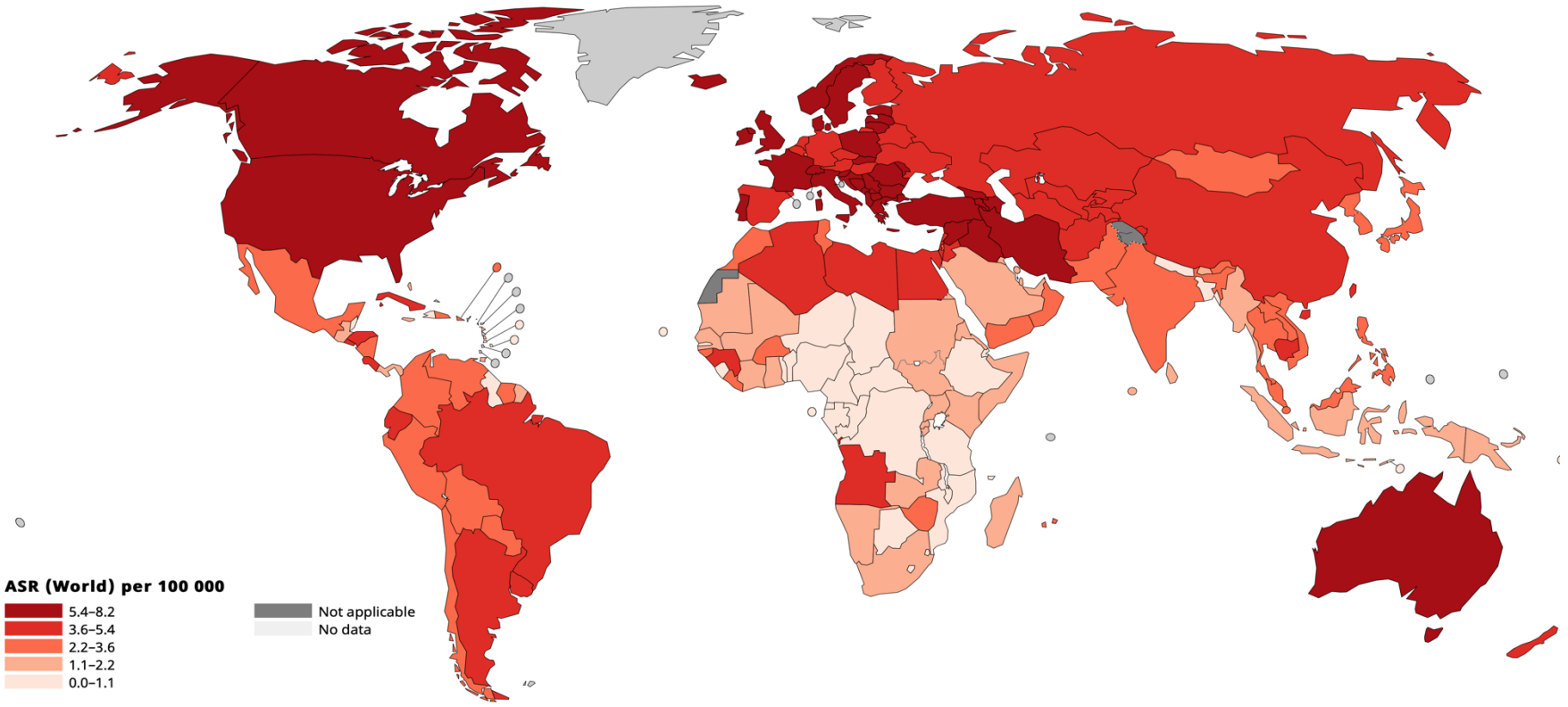
PFS - Progression-Free Survival
PET - Positron Emission Tomography
PI3K - Phosphoinositide-3-Kinase
PpIX - Protoporphyrin IX
PPI - Protein-Protein Interaction
PTEN - Phosphatase and Tensin Homolog
RISC - RNA-Induced Silencing Complex
RNA - Ribonucleic Acid
RNA-seq - RNA Sequencing
ROS - Reactive Oxygen Species
RT - Room Temperature
RT-qPCR - Reverse Transcription Quantitative Polymerase Chain Reaction
RTK - Receptor Tyrosine Kinase
sRNA-seq - Small RNA Sequencing
SCTR - Secretin Receptor
SDS - Sodium Dodecyl Sulfate
siRNA - Small Interfering RNA
SHG-8 - b3-(4-bromophenyl)-1-phenyl-3-(phenylamino)propan-1-one
SHG-44 - (E)-1-(4-chlorophenyl)-3-(p-tolyl)prop-2-en-1-one
SHH – Sonic Hedgehog
SRS - Stereotactic Radiosurgery
SV2B - Synaptic Vesicle Glycoprotein 2B
SYT1 - Synaptotagmin 1
t-SNE – t-distributed neighbour embedding
TBST - Tris-Buffered Saline with Tween 20
TCGA - The Cancer Genome Atlas
TEM - Transmission Electron Microscopy
TGF-β - Transforming Growth Factor Beta
TILs - Tumour-Infiltrating Lymphocytes
TLE - Tumour Microenvironment
TMZ - Temozolomide
TMS - Tetramethylsilane
TP53 - Tumour Protein p53
TPM - Transcripts Per Million
TRX - Thioredoxin
TSC - Tuberous Sclerosis Complex
U1 snRNA - U1 Small Nuclear RNA
UALCAN - University of Alabama at Birmingham Cancer Data Analysis Portal
UG - Uridine-Guanosine
UGU - Uridine-Guanosine-Uridine
UK - United Kingdom
US - United States
UV - Ultraviolet
VAR – Variant
VEGF - Vascular Endothelial Growth Factor
VWF - Von Willebrand Factor
WHO - World Health Organization
XPO5 - Exportin-5

Chapter 1. Introduction

1.1. Primary brain tumours

Brain tumours are an abnormal growth of cells that can occur within the brain or in nearby areas, such as the cranial nerves, the pituitary gland, the pineal gland, or the membranes (meninges) covering the brain (Mezzacappa & Thorell, 2022). Brain tumours are generally divided into two main categories: primary brain tumours, which originate in the brain, and secondary (or metastatic) brain tumours, which arise when cancer from another part of the body spreads to the brain (Tandel, *et al.,* 2019). According to GLOBOCAN, around 297,000 new cases of brain tumours are diagnosed globally each year, making up approximately 2% of all cancers (Figure 1). Despite their rarity, brain tumours contribute a reduced overall survival (OS) and 7% of all cancer-related deaths due to their aggressive nature and complex treatment **(**Rachet, Mitry, Quinn, Cooper & Coleman, 2008). Additionally, an estimate of 85,000 patients in the United States are diagnosed with primary brain tumours annually, nearly a third (29%) of which are malignant (Ostrom, Cioffi, Waite, Kruchko & Barnholtz-Sloan, 2021**).** The global incidence rate is about 3 to 4 cases per 100,000 people annually. Men are slightly more prone to brain tumours, particularly glioblastomas (GBs), compared to women (Carrano, Juarez, Incontri, Ibarra & Guerrero Cazares, 2021). These tumours occur across all age groups with paediatric tumours like medulloblastomas (MBs) being more common in children, while aggressive forms like GBs are more prevalent in adults (Greuter, Guzman & Soleman, 2021). High-income countries report higher incidence rates due to better diagnostic tools, while underreporting is common in low- and middle-income regions (Ilic & Ilic, 2023). As healthcare improves globally, incidence rates are expected to rise (Figure 1). Diffuse gliomas are the most common primary central nervous system (CNS) tumours in adults, but a wide array of less frequent CNS tumour types also exist. They arise sporadically and without known cause from supporting cells within the brain and the spinal cord (Mesfin & Al-Dhahir, 2023). The tumour's lineage is determined by the initial glial cell type involved, such as astrocytes or oligodendrocytes. The recent 2021 World Health Organisation (WHO) classification of CNS tumours has reflected the growing importance of distinct tumour molecular characteristics by placing a strong emphasis on molecular diagnostics for tumour classification (Louis, *et al.,* 2021). Based on the 2021 WHO classification, the three most common adult gliomas include: astrocytoma, isocitrate dehydrogenase (IDH)-mutant; oligodendroglioma, IDH-mutant; glioblastoma, IDH-wild-type. The location of primary brain tumours presents significant

challenges to current therapeutic interventions, limiting their effectiveness in patients (Tarev & Cekov, 2024). Most current drug and chemotherapeutic delivery strategies face difficulties in crossing the blood-brain barrier (BBB) due to the tight junctions formed by intracranial endothelial cells, which restrict passive diffusion to small gas and lipophilic molecules (Haumann, Videira, Kaspers, van Vuurden & Hulleman, 2020). This barrier poses significant constraints on chemotherapy treatments and the effective delivery of therapeutic drugs to brain tumours, thereby reducing treatment efficacy.



All rights reserved. The designations employed and the presentation of the material in this publication do not imply the expression of any opinion whatsoever on the part of the World Health Organization / International Agency for Research on Cancer concerning the legal status of any country, territory, city or area or of its authorities, or concerning the delimitation of its frontiers or boundaries. Dotted and dashed lines on maps represent approximate borderlines for which there may not yet be full agreement.

Cancer TODAY | IARC
https://gco.iarc.who.int/today
Data version: Globocan 2022 (version 1.1) - 08.02.2024
© All Rights Reserved 2024

International Agency for Research on Cancer
World Health Organization

Figure 1. Global incidence and distribution of brain tumours based on GLOBOCAN Data (2022). This figure illustrates the global incidence of brain tumours, highlighting the total estimated new cases (approximately 297,000) and the distribution across different regions. The incidence rate varies globally, with high-income regions such as North America and Europe showing higher rates (3–4 per 100,000 people) due to advanced diagnostic capabilities, while lower-income regions, including parts of Africa and Asia, report lower incidence, likely due to underdiagnosis and limited access to healthcare.

1.2. Glioblastoma

Glioblastoma is a particularly aggressive and rare form of adult primary brain malignancy. Originating from gliomas, this subtype accounts for 81% of malignant intracranial tumours in adults (Ostrom, *et al.,* 2014a). Despite substantial efforts, the five-year survival rate for GB patients remains low at only 6.8%, with a median survival period of approximately 8 months (Wen, *et al.,* 2020). Complete resection of brain tumours is often unachievable due to the intricate anatomical structure of the cranial and brainstem nerves. Even with surgical interventions aimed at improving prognosis, most GB tumours exhibit resistance to chemotherapeutic treatments, significantly reducing their efficacy (Hanif, Muzaffar, Perveen, Malhi & Simjee, 2017). Diagnosing adult gliomas involves a multi-step approach, starting with evaluating the symptoms and the medical history of the patient, followed by neurological exams and imaging, like magnetic resonance imaging (MRI) (Hoggarth, *et al.,* 2024). Biopsies or surgical resections may be needed to confirm the type and grade of the tumour (Sanai & Berger, 2018). Treatment options vary based on the tumour characteristics and patient health, but typically involve surgery to remove as much of the tumour as possible (Molinaro, *et al.,* 2020). Radiation and chemotherapy are often used to target remaining or inoperable tumours (Alexander & Cloughesy, 2017).

1.2.1. Epidemiological characteristics

Glioblastoma is the most frequent form of primary brain malignancy in adults, with a median age at diagnosis of 65 years (Gillespie, *et al.,* 2022). It is about 1.6 times more common in males than in females, although the reason for this discrepancy remains unclear (Grochans, *et al.,* 2022). In England, over three decades (1995-2017), approximately 32% of all diagnosed primary brain tumours are classified as GBs (Wanis, Møller, Ashkan & Davies, 2021). Glioblastoma accounts for nearly 3,350 newly diagnosed cases annually in the United Kingdom (UK), with OS rate between 6 to 17 months (Gillespie, *et al.,* 2022). While GB is primarily diagnosed in adults, it can also be identified in children. Paediatric GB (pGB) makes up only 2%–3% of all childhood brain tumours (Ostrom, *et al.,* 2014b). Data from the Central Brain Tumour Registry of the United States (CBTRUS) indicates a low incidence of around 0.85 cases per 100,000 children (Ostrom, *et al.,* 2015). In the UK, fewer than 30 children are diagnosed with high-grade glioma annually, representing approximately 8% of all childhood brain and spinal cord tumours (NHS England, 2024). The demographic characteristics of GB vary across regions, with higher incidence rates in Europe and North America compared to Asia and Africa (Ozair, *et al.,* 2023).

1.2.2. Clinical Presentation

The initial presentation of patients with GB is often non-specific. The experienced symptoms are common to other primary or secondary brain tumours and to other benign neurological neoplasms (Kanderi, Munakomi & Gupta, 2024). Approximately half of GB patients are diagnosed after an emergency hospital visit. Most of these patients had previously consulted their general practitioner (GP) regarding their experienced symptoms (Wasilewski, Serventi, Kamalyan, Wychowski & Mohile, 2017). A national UK campaign called HeadSmart has led to an improvement in recognising early brain tumour symptoms in children, reducing the time from symptom onset to diagnosis (HeadSmart Be Brain Tumour Aware, 2016). However, a similar strategy for adult patients has not yet developed due to the variability of symptoms experienced by adults (Penfold, Joannides, Bell & Walter, 2017). The symptoms are often mistaken for common issues related to aging, stress, or other routine health problems. Symptoms such as persistent headaches, memory problems, fatigue, and mood changes may develop gradually and be attributed to normal aging or conditions like anxiety or depression. Headache is the most common early symptom associated with brain tumours, but only 1-2 in 1000 patients who see their GP for headaches are later diagnosed with a brain tumour. Glioblastoma-related headaches are common upon waking, but they can vary based on the tumour's location, size, and growth rate (Kanderi, *et al.,* 2024). Their frequency and severity tend to increase over time. The presence of additional neurological symptoms, such as weakness or cognitive dysfunction, alongside headaches significantly increases the likelihood of an underlying brain tumour by 44 and 59-fold, respectively (Ozawa, *et al.,* 2019). Furthermore, about 20% of GB patients present with seizures, with an additional 20% developing seizures later from the onset of the malignancy (Englot, Chang & Vecht, 2016). The combinations of these symptoms, especially if progressive, significantly increase the likelihood of identifying brain neoplasm on an MRI scan.

1.2.3. Initial assessment

During the initial assessment of a patient who is suspected to present with a brain malignancy, it is crucial to establish the nature and progression of their presenting symptoms (Penfold, Joannides, Bell & Walter, 2017). For patients presenting with headaches, high-risk clinical features may raise suspicion of a brain tumour. These include factors, such as systemic malignancy, previous radiation exposure, or a family history of inheritable cancer syndromes

(Weller, *et al.,* 2021). Each of these factors independently could potentially increase the likelihood of a brain tumour diagnosis.

Additionally, focal neurological deficits associated with brain tumours often develop gradually from the onset of the neoplasm. If the patient has experienced seizures, descriptive information about the event of the seizure is collected (Chen, *et al.,* 2017). Temporal lobe seizures present as sudden changes in behaviour and may be preceded by abnormal smells, tastes, or gastric sensations (Ehara, Ohka, Motomura & Saito, 2024). Recently, clinicians have considered collecting informative collateral history from family members, friends, or colleagues that can be very beneficial, as patients are often unaware of indirect changes in their behaviour and personality over time. A recent qualitative study on brain tumour diagnosis experiences found that most patients and their families had noticed multiple mild symptoms or changes (e.g., phrases like "My head felt fuzzy") at least six months before the initial presentation (Walter, *et al.,* 2019). Thus, a thorough review of the patient's history must be conducted, and evaluation of all risk factors must be considered.

Further tests are considered as beneficial during the initial assessment of patients with suspected brain tumours. A thorough neurological examination, including assessments of the cranial nerves, motor, sensory, and cerebellar systems, is suggested (Robinson, Biggs & Walker, 2015). However, a Mini-Mental State Examination (MMSE) or Montreal Cognitive Assessment (MoCA) test is not recommended for patients with suspected GB, as this test lacks sensitivity for detecting subtle, domain-specific neurocognitive deficits (van Kessel, Baumfalk, van Zandvoort, Robe & Snijders, 2017).

1.2.4. Differential diagnosis and Neuroimaging

The differential diagnosis of brain malignancies depends on the duration, chronological sequence, and anatomical location of symptoms and signs experienced by the patient. Patients presenting with elevated intracranial pressure (ICP), such as headaches accompanied by papilledema, should immediately be referred to the emergency department for same-day assessment and initial investigation using contrast-enhanced computer tomography (CT) head scan (McKinnon, Nandhabalan, Murray & Plaha, 2021). For patients suspected of having a brain tumour but do not exhibit suggestive symptoms, such as raised ICP or seizure activity, an urgent MRI brain scan is requested. In resource-limited settings, a contrast-enhanced CT

head scan is a valuable alternative for initial investigation, although it is less sensitive (Zienius, *et al.,* 2019).

The standard MRI scan employed in the diagnosis of GB includes pre- and post-gadolinium contrast T1-weighted, T2-weighted, fluid-attenuated inversion recovery (FLAIR), and diffusion-weighted imaging (DWI) (Martucci, *et al.,* 2023). The classic appearance of GB on these scans includes a mass lesion with peripheral contrast-enhancement on T1-weighted imaging, indicating blood-brain barrier disruption, central hypointensity on T2-weighted images, indicating necrosis, and surrounding hyperintensity on T2-weighted and FLAIR images, representing vasogenic edema or infiltrating tumour (Martucci, *et al.,* 2023) (Figure 2).

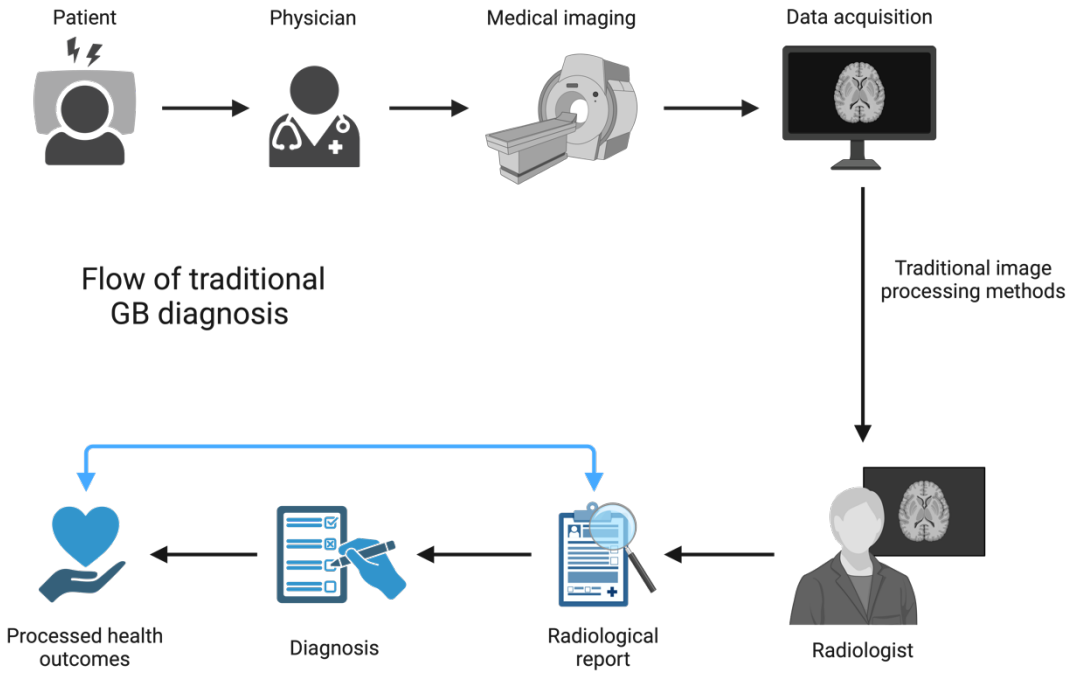


Figure 2. Routine imaging assessment of suspected brain neoplasms. The standard MRI for diagnosing GB includes pre- and post-gadolinium contrast T1-weighted, T2-weighted, FLAIR, and DWI sequences. Glioblastomas typically appear as mass lesions with peripheral contrast-enhancement on T1-weighted imaging, central hypointensity on T2-weighted images, and surrounding hyperintensity on T2-weighted and FLAIR images, indicating blood-brain barrier disruption, necrosis, and vasogenic edema or infiltrating tumour, respectively. Designed using BioRender: https://biorender.com.

Furthermore, advanced imaging techniques are beneficial for distinguishing GB from other types of brain neoplasms. Diffusion-weighted imaging aids in distinguishing GB from other contrast-enhancing brain lesions like cerebral abscesses or CNS lymphoma by measuring the apparent diffusion coefficient (ADC) to indirectly assess the tumour's cellularity by quantifying water diffusivity (Schob, *et al.,* 2016). Glioblastoma is typically characterised by a lower ADC value compared to lower-grade gliomas, whereas primary CNS lymphoma demonstrates even lower ADC values in comparison to GB (Ahn, Shin, Chang & Lee, 2014).

Urgent neuroimaging access varies across the UK. In England, the National Institute for Health & Care Excellence (NICE) recommends the referral of patients over 24 years old for an urgent MRI brain scan within two weeks if they present with progressive, sub-acute loss of central neurological function (NHS England, 2023). Conversely, NHS Scotland recommends an urgent referral to a specialist, such as a neuro-oncologist, who subsequently arranges the necessary neuroimaging (Scottish Referral Guidelines for Suspected Cancer, 2024). Patients presenting with a suspected primary headache disorder without high-risk factors for brain tumours may still be referred for a scan. Thus, at the time of referral, it is important to inform patients that their neuroimaging is for reassurance that there is no serious underlying cause (Martucci, *et al.,* 2023).

Patients with a suspected primary headache disorder pose a dilemma for GPs who should evaluate unnecessary investigations with the concern of missing a brain tumour diagnosis (Walter, *et al.,* 2019). Furthermore, there are potential risks associated with neuroimaging, such as radiation exposure and anaphylaxis from contrast agents. Research has also demonstrated that approximately 1 in every 37 MRI brain scans will yield an incidental abnormality, considered as false positive, which may require further specialist management or follow-up (Sunny, *et al.,* 2022). There is also a lack of scientific evidence to suggest that earlier neuroimaging of patients with GB who initially present with headaches would translate to a difference in their clinical outcomes.

1.2.5. Advanced neuroimaging

Dynamic susceptibility contrast MRI has been employed to quantify the cerebral blood volume (CBV) of brain tumours (Essig, *et al.,* 2013). This provides an indirect measure of total tumour vascularity. Alternatively, dynamic contrast-enhanced MRI assesses the permeability of the tumour surface area, providing information for vascular leakiness (Essig, *et al.,* 2013). Both

parameters are useful in distinguishing glioblastoma from lower-grade gliomas. Isocitrate dehydrogenase (IDH)-wild-type brain neoplasms have significantly higher relative CBV values when compared to IDH-mutant tumours (van Santwijk, Kouwenberg, Meijer, Smits & Henssen, 2022).

Chemical exchange saturation transfer (CEST) is an alternative MRI technique that measures the exchange rate of amide protons between proteins and bulk water, inversely correlated with tissue pH (Chan, *et al.,* 2021). Current research involving IDH-wild-type GB has demonstrated a diagnostic sensitivity and specificity of 90% (Peach, *et al.,* 2018). Furthermore, positron emission tomography (PET) utilises the use of radiolabelled molecules to explore the biological characteristics of brain neoplasms (Herholz, 2017). Glucose transporters are found upregulated in gliomas, showing high affinity for [18F]-2-fluoro-2-deoxy-D-glucose (FDG) tracers (Cui, Zorrilla-Veloz, Hu, Guan & Ma, 2021). However, FDG tracers are also characteristic for inflammatory conditions and are physiologically taken up by the cerebral parenchyma, resulting in low diagnostic specificity and a poor signal-to-noise ratio for defining gliomas (Herholz, 2017). To challenge these limitations, radiolabelled amino acid tracers are now under wide exploration (Prather, *et al.,* 2022). Clinically, these tracers are valuable for the precise outlining of tumour boundaries, especially in normal-appearing tissue, aiding in radiotherapy and surgical planning.

1.2.6. Histopathology

The conventional diagnosis of GB primarily relies on its histopathological characteristics (Figure 3). According to the WHO classification guidelines for CNS tumours, GBs are grade 4 diffuse gliomas (Louis, *et al.,* 2021). Histologically, diffuse gliomas can be astrocytic or oligodendroglial, with astrocytoma WHO grade 4 being the most common subtype, accounting for approximately 50% of all primary malignant brain tumours (Lan, Li & Zhang, 2024). GB is characterised by several classic morphologic features, including nuclear atypia, cellular pleomorphism, mitotic activity, microvascular proliferation, and necrosis (Lan, *et al.,* 2024). GB can be further classified into primary and secondary (Oronsky, Reid, Oronsky, Sandhu & Knox, 2021). Primary GBs arise *de novo*, typically in patients over 50 years of age, and lack a known clinical precursor. Secondary GBs develop from a pre-existing lower-grade glioma and usually affect younger patients. Although primary and secondary GBs are morphologically indistinguishable and respond similarly to conventional therapies, they exhibit different molecular profiles (Tan, *et al.,* 2020a). Despite their similar histological appearances, IDH-

wild-type GB has a more aggressive phenotype with a median survival of 15 months in comparison to 31 months for IDH-mutant grade 4 astrocytoma (Molinaro, Taylor, Wiencke & Wrensch, 2019).

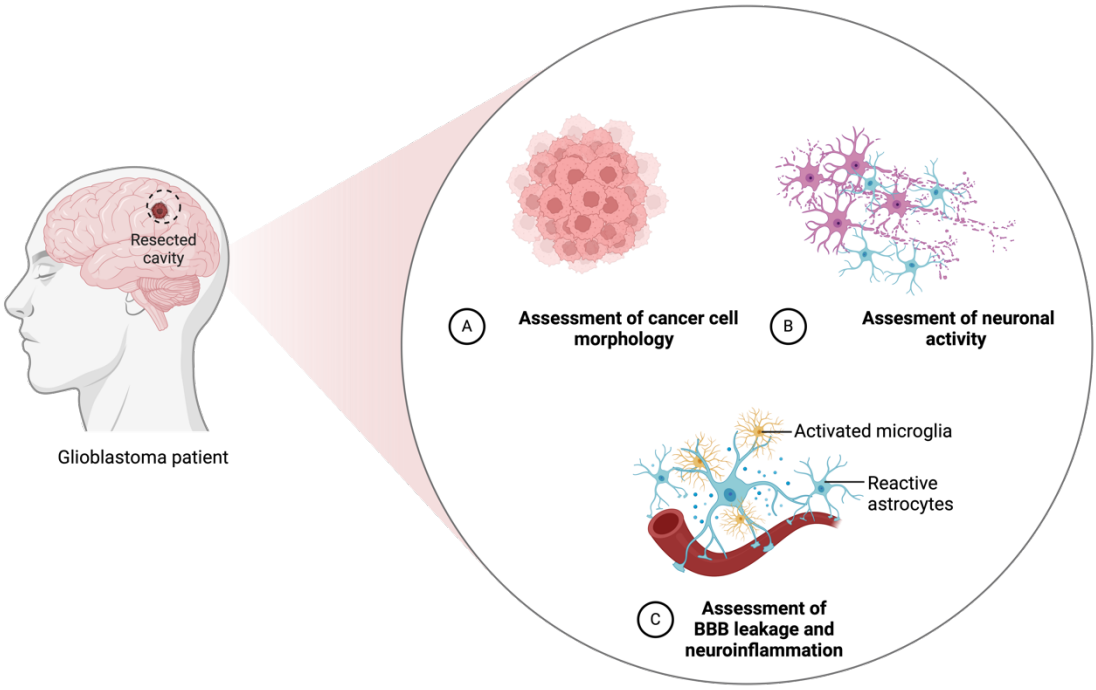


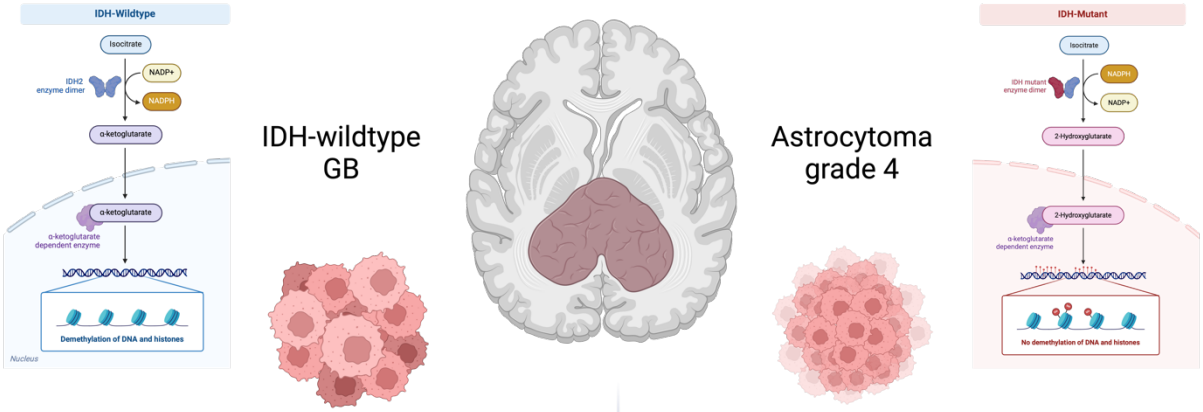
Figure 3. Histopathological analysis of GB. GB is characterised by several classic morphologic features, including nuclear atypia, cellular pleomorphism, mitotic activity, microvascular proliferation, and necrosis. Designed using BioRender: https://biorender.com.

1.2.7. Molecular profiling, altered molecular pathways and molecular biomarkers

1.2.7.1. Molecular profiling

Glioblastomas are characterised by their invasive nature and resistance to therapy. These tumours can originate anywhere in the CNS, but they are most commonly found in the frontal or temporal lobes (Hanif, *et al.,* 2017). Revisions in the 2021 WHO classification of CNS brain malignancies emphasised the utilisation of molecular prefiling alongside histopathological criteria for the classification of GB (Louis, *et al.,* 2021). For GBs, IDH mutation status is now a central criterion. Glioblastomas are now classified as IDH-wild-type, which constitute about 90% of all cases. However, tumours previously classified as GB IDH-mutant are now categorised as "astrocytoma, IDH-mutant, WHO grade 4", accounting for approximately 10% of all cases (Antonelli & Poliani, 2022) (Figure 4 and Figure 5).

The updated WHO CNS 5 incorporates additional molecular characteristics into the definition of gliomas, such as cyclin-dependent kinase inhibitor 2A/B (*CDKN2A/B*) homozygous deletion mutation, telomerase reverse transcriptase (*TERT*) promoter mutation, epidermal growth factor receptor (*EGFR*) gene amplification, and the combined gain of entire chromosome 7 and loss of entire chromosome 10 (+7/−10), which are diagnostic criteria for IDH-wild-type GB (Table 1) (Louis, *et al.,* 2021). Glioblastoma is characterised by key genetic alternations, such as the mutations in the *TERT* promoter, deletion of the phosphatase and tensin homolog (*PTEN*) tumour suppressor gene, high-level amplification of the proto-oncogene *EGFR*, alpha thalassemia/mental retardation syndrome X-linked (*ATRX*) mutation, and tumour protein p53 (*TP53*) mutation (Lan, *et al.*, 2024). Primary IDH-wild-type GB is commonly associated with *TERT* promoter mutation, *PTEN* deletion, and *EGFR* amplification (Lan, *et al.,* 2024). Conversely, thioredoxin (*TRX*) mutation and *TP53* mutation are more common in secondary IDH-mutant GB, now described as grade 4 astrocytoma (Louis, *et al.,* 2021). Multiple genetic alterations with relevance to GB also include mutations in neurofibromin 1 (*NF1*), platelet-derived growth factor receptor alpha (*PDGFRA*), phosphoinositide-3-kinase regulatory subunit 1 (*PIK3R1*), phosphoinositide-3-kinase catalytic subunit alpha (*PIK3CA*), retinoblastoma 1 (*RB1*), *CDKN2A/B,* mouse double minute 2/4 homolog (*MDM2* and *MDM4*), cyclin-dependent kinase 4 (*CDK4*), and H3 histone family member 3A (*H3F3A*). The genetic abnormalities reported in GB contribute mainly to three tumorigenic processes: initiating tumour growth, evading senescence, and enabling immortal growth (Testa, Castelli & Pelosi, 2018). These genetic defects are crucial for gliomagenesis through the modulation of several key signalling pathways.



Mutations	Frequency	Reference
TERT	80.7%	(Jonsson, *et al.*, 2019)
PTEN	37.8%	(Jonsson, *et al.*, 2019)
TP53	34.0%	(Jonsson, *et al.*, 2019)
EGFR	21.2%	(Jonsson, *et al.*, 2019)
NF1	18.6%	(Jonsson, *et al.*, 2019)
RB1	12.8%	(Jonsson, *et al.*, 2019)
ATRX	11.7%	(Jonsson, *et al.*, 2019)

Mutations	Frequency	Reference
IDH1	50.6%	(Ceccarelli, *et al.*, 2016)
TP53	39.7%	(Ceccarelli, *et al.*, 2016)
ATRX	25.6%	(Ceccarelli, *et al.*, 2016)
TTN	13.4%	(Ceccarelli, *et al.*, 2016)
PTEN	13.3%	(Ceccarelli, *et al.*, 2026)
EGFR	10.7%	(Ceccarelli, *et al.*, 2016)
CIC	9.7%	(Ceccarelli, *et al.*, 2016)

Figure 4. Key genetic alternations crucial for gliomagenesis. According to the WHO, CNS 5 *TERT, EGFR, PTEN,* and *TP53* mutation are some of the leading genetic alternations causative of GB. *IDH1, TRX, TP53*, and titin (*TTN*) mutations are more common in IDH-mutant GB, now described as grade 4 astrocytoma. Designed using BioRender: https://biorender.com

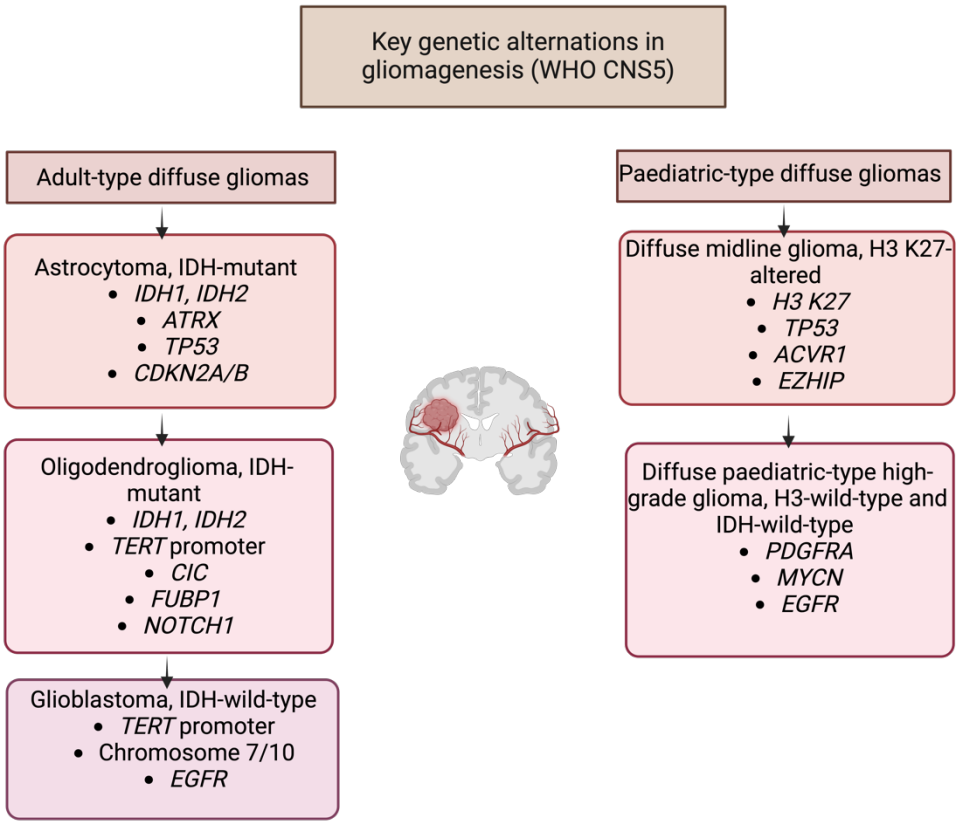


Figure 5.A flowchart summarising key genetic alterations in gliomagenesis as outlined by the WHO CNS5 classification, organised by glioma type. Adult-type diffuse gliomas (e.g., IDH-mutant astrocytoma, IDH-wild-type glioblastoma) and paediatric-type diffuse gliomas (e.g., H3 K27-altered diffuse midline glioma) show distinct genetic markers. Arrows indicate hierarchical relationships within each glioma type.

Table 1. Overview of tumour types, grades, and key molecular markers in brain tumours (Torp, Solheim & Skjulsvik, 2022, modified). Abbreviations: B-Raf proto-oncogene, serine/threonine kinase (*BRAF*), H3 histone family member (*H3*), mitogen-activated protein kinase (*MAPK*), O-6-methylguanine-DNA methyltransferase (*MGMT*), MYB proto-oncogene, transcription factor (*MYB*), MYB proto-oncogene like 1 (*MYBL1*), Yes-associated protein 1 (*YAP1*), and zinc finger translocation associated (*ZFTA*).

Molecular marker	Clinical significance and tumour grading
***ATRX* mutation**	Commonly found in astrocytoma, IDH-mutant but absent in oligodendrogliomas. Also associated with diffuse hemispheric glioma, H3 G34-mutant.
***BRAF* V600 mutation**	Frequently present in pleomorphic xanthoastrocytoma, ganglioglioma, and epithelioid GB.
***CDKN2A/B* homozygous deletion**	Found in astrocytoma, IDH-mutant; linked to poor prognosis.
***EGFR* gene amplification**	Common in GB, IDH-wild-type (WHO Grade 4). Also observed in astrocytomas, IDH-wild-type (WHO Grades 2 or 3), indicating progression to GB (WHO Grade 4).
***EGFR* mutations**	EGFRvIII is the most frequent variant in GB, IDH-wild-type (WHO Grade 4).
***H3* G34 mutation (histone *H3.3* G34)**	Present in hemispheric diffuse gliomas, IDH-wild-type, typically affecting children and young adults with poor prognosis.
***H3* K27M mutation (histone *H3* K27M)**	Defining feature of diffuse midline glioma, H3 K27M-altered. Can also appear in non-midline gliomas like pilocytic astrocytoma and ependymoma.
***IDH1/2* mutations**	Frequently mutated in diffuse gliomas (astrocytomas and oligodendrogliomas), associated with better prognosis compared to IDH-wild-type gliomas.
***KIAA1549-BRAF* gene fusion**	Often found in pilocytic astrocytoma and observed in diffuse leptomeningeal glioneuronal tumours, pilomyxoid astrocytoma, and ganglioglioma.
***MAPK* alterations**	Common in paediatric type diffuse low-grade gliomas.
***MGMT* promoter methylation**	Predicts good response to alkylating agents, such as temozolomide, in GB, IDH-wild-type.
***MYB* or *MYBL1* alterations**	Typically found in paediatric low-grade gliomas.
***TERT* promoter mutation**	Present in most oligodendrogliomas. Also found in diffuse astrocytomas, IDH-wild-type (WHO Grades 2 and 3), indicating progression to GB (WHO Grade 4).
***TP53* mutation**	Present in most astrocytomas, IDH-mutant, but rare in oligodendrogliomas.
***YAP1* fusions**	Found in some supratentorial ependymomas, especially in paediatric cases.
***ZFTA* fusions**	Present in certain supratentorial ependymomas.
Gain of Chromosome 7/Loss of Chromosome 10 (+7/−10)	Common alteration in GB, IDH-wild-type (WHO Grade 4).
Loss of Chromosome 1p/19q	Essential for the diagnosis of oligodendroglioma.

1.2.7.2. Altered molecular pathways

The receptor tyrosine kinase (RTK) pathway is the most frequently altered signalling cascade in GB, particularly in IDH-wild-type tumours. Receptor tyrosine kinases are cell-surface receptors that bind growth factors, including EGFR, PDGFR, transforming growth factor receptor (TGFR), fibroblast growth factor receptor (FGFR), MET proto-oncogene, receptor tyrosine kinase (MET), and vascular endothelial growth factor receptor (VEGFR), crucial for signalling transduction and intercellular communication (Tilak, Holborn, New, Lalonde & Jones, 2021). In GB, RTK signalling activation through the PI3K/AKT/mTOR pathway stimulates cell proliferation, migration, differentiation, and survival. EGFR and PTEN are primary targets within this pathway, with EGFR often playing an oncogenic role due to amplification or mutation, leading to its overexpression (Rascio, *et al.,* 2021). Conversely, *PTEN* acts as a tumour suppressor, and its mutation or deletion facilitates pathway activation, promoting cell migration, invasion, and survival. Another frequently altered RTK pathway in GB is the Ras pathway (Ras/BRAF/MEK), where active Ras (Ras-GTP) drives cell cycle progression, survival, and migration via downstream effectors (Lan, *et al.*, 2024).

The well-known tumour suppressor and transcription factor TP53 plays a crucial role in tumour prevention by regulating various cellular processes such as invasion, migration, proliferation, and evasion of apoptosis. Deregulation of the TP53/MDM2/CDKN2A pathway occurs in 84% of GB patients and 94% of GB cell lines (Zhang, *et al.,* 2018). *In vitro* cell lines often undergo selective pressures that favour the survival of aggressive, genetically unstable cells leading to a higher representation of deregulated TP53/MDM2/CDKN2A pathways, which confer advantages in growth and survival (He, *et al.,* 2023). Over time, cell lines become genetically homogeneous, with dominant clones expanding, unlike the heterogeneous nature of patient tumours (Marusyk & Polyak, 2010). Additionally, cell lines adapt to artificial conditions that can further promote specific genetic alterations, such as those affecting the TP53 pathway. TP53 inactivation is observed in approximately one-third of IDH-wild-type GB, resulting in the loss of its tumour suppressive functions and enhanced GB tumorigenesis (Suwala, *et al.,* 2021). Additionally, MDM2 facilitates *p53* degradation, further promoting tumorigenesis. *MDM2* amplification is mutually exclusively with TP53 mutation and is more prevalent in primary GBs lacking TP53 mutations (Kung & Weber, 2022). Meanwhile, *CDKN2A*, another critical regulator of the TP53 pathway, exhibits homozygous deletion in 22-35% of all GBs, 16-47% in IDH-mutant grade 4 astrocytoma and approximately 58% in IDH-wild-type GB, leading to TP53 pathway inactivation (Huang, 2022).

One of the most altered pathways in GB, crucially involved in regulating its tumorigenesis, is the retinoblastoma protein (RB) pathway. Phosphorylation of the RB protein by the CDK4/Cyclin D1 complex leads to inhibition of cell cycle progression from G1 to S phase by binding E2F transcription factors. CDKN2A connects the RB pathway to the TP53 pathway, activating RB and TP53 through its Ink4a and Arf proteins, respectively (Egger, Lane, Antonucci, Dedi & Krucher, 2016). In GB, the growth inhibition function of the RB pathway is often disrupted due to *CDKN2A/CDKN2B* and *RB1* inactivation, alongside *CDK4* and *CDK6* amplification (Lan, *et al.*, 2024). Decreased RB1 expression and functionality as a cell-cycle checkpoint thereby leads to dysregulated cell cycle and uncontrolled cell proliferation of GB cells.

1.2.8. Molecular biomarkers

1.2.8.1. Isocitrate dehydrogenase

Despite GB's genetic heterogeneity, several biomarkers have shown great potential in the clinical management of the malignancy: *IDH1, MGMT,* and *EGFR* (Table 1). In 2008, a comprehensive genetic analysis of GB patient samples revealed mutations in the *IDH1* gene in 18 out of 149 tumours (Parsons, *et al.,* 2008). The observed mutations were predominantly found in younger GB patients, originating from lower-grade gliomas, and correlated with improved survival rates (Parsons, *et al.,* 2008). The most common mutation identified was the single nucleotide change substitution from histidine to arginine (R132H), accounting for approximately 90% of all mutations (Von Deimling, Korshunov & Hartmann, 2011). This substitution affects the enzyme's isocitrate binding site, altering its metabolic function. Instead of converting isocitrate to α-ketoglutarate, it converts α-ketoglutarate to 2-hydroxyglutarate, thereby influencing both the metabolic and epigenetic profiles of tumour cells (Han, *et al.,* 2020) (Figure 4). Mutations in *IDH1/2* were seen to contribute to abnormal neomorphic activity, leading to DNA and histone methylation and resulting in the glioma cytosine-phosphate-guanine (CpG)-island methylator phenotype (G-CIMP) (Han, *et al.,* 2020). The IDH mutational status has become a pivotal molecular marker in the latest WHO classification of brain tumours and is crucial for patients' prognosis. The previously termed IDH-mutant GB, now referred to as astrocytoma, IDH-mutant, grade 4, exhibits a markedly better prognosis (Yan, *et al.,* 2009). Due to its prognostic benefits and uncomplicated testing, IDH status is now essential for all ongoing therapeutic trials. Moreover, clinical trials are underway to specifically target IDH-mutant gliomas, either by directly inhibiting the enzyme or utilising treatments

tailored to the epigenetic and DNA repair alterations associated with these mutations (Platten, *et al.,* 2021).

1.2.8.2. O6-methylguanine-DNA methyltransferase (MGMT) promoter methylation

The levels of O6-methylguanine-DNA methyltransferase (MGMT) promoter methylation differ among GB patients, where hypermethylation is associated with reduced chemoresistance and an increased survival rate by approximately 6.8 months (Gibson, *et al.,* 2024). MGMT is a repair protein that undergoes a unique self-modification process, transferring a methyl group from O6 of guanine to a cysteine residue at position 145 (Gerson, 2004). This irreversible modification results in alkylated MGMT, which is subsequently targeted for degradation. MGMT plays a critical role in GB by counteracting the effects of alkylating agents, such as temozolomide (TMZ)/lomustine, thereby resulting in resistance to these drugs by the tumour cells. Clinical evidence has shown that MGMT silencing through hypermethylation significantly improves the response to TMZ in GB patients (Hegi *et al.,* 2005). As a result, MGMT methylation status has become an important factor in guiding adjuvant therapy decisions for GB patients (Mansouri et al., 2019). Moreover, MGMT serves as a molecular biomarker playing a key role in assessing and developing new therapeutic strategies for GB treatment (Mansouri et al., 2019).

1.2.8.3. Epidermal growth factor receptor

The most frequently observed amplified and altered proto-oncogene in GB is *EGFR*, found in approximately 40% of all GB cases (Cancer Genome Atlas Research Network, 2008). The predominant mutation, EGFR variant III (*EGFRvIII*), represents a persistently active form of EGFR. The use of both mutations as prognostic biomarkers remains controversial, with no definitive evidence suggesting a significant impact on OS (Li, Liang, Song, Xiang & Liu, 2018). However, given the prevalence of EGFR alterations in GB, researchers have focused on EGFR-targeting drugs and immunotherapy trials. Nonetheless, current therapies have shown limited efficacy in GB treatment. As of now, no EGFR-targeted drugs are approved for clinical use in GB outside of clinical trials (Rodriguez, *et al.,* 2023).

1.2.9. Tumour microenvironment in GB

The understanding of GB tumour growth has expanded over the past few years and has shined light on the complex interactions within the tumour microenvironment (TME) (Figure 6). Recent evidence has highlighted the presence of transcriptionally distinct cells in different microenvironments within a single tumour (Crivii, *et al.,* 2022). Since different tumours originate from various cell types and grow in diverse environments, these interactions differ between tumour types and even subtypes. Additionally, as tumours grow and evolve, they modify their environment, which in turn influences tumour cell evolution. The heterogeneity of GB is observed in both inter-patient (between patients) and intra-patient (within individual tumours) (Ramón Y Cajal, *et al.,* 2020). For this reason, GB tumours are often classified into three main distinct subtypes based on their mRNA expression profile: classical (CL), mesenchymal (MES), and pro-neural (PN) (Steponaitis & Tamasauskas, 2021). However, the clinical application of these molecular profiles for GB diagnosis and classification is often limited due to the tumour's dynamic microenvironment and its ability to transition between different molecular subtypes, thus not accounting for the heterogeneous and dynamic expression of these subtypes within a single tumour.

Researchers have suggested that GB develops due to the gradual accumulation of somatic mutations in neural stem cells (NSCs) and glial precursor cells, providing these cells with selective growth advantages and leading to uncontrolled proliferation (Kim, Park & Lee, 2021). Furthermore, changes were observed in stromal and innate immune cell distributions within the tumour TME, suggesting that TME reorganisation may influence, or be influenced by, GB subtype switching (Steponaitis, Kucinskas, Golubickaite, Skauminas & Saudargiene, 2022). Therefore, treatments targeting specific GB subtypes are often inadequate, as the persistence of other subtypes within different microenvironments leads to tumour recurrence.

Understanding the complex interplay between GB behaviours and surrounding noncancerous brain cells is crucial for effectively targeting and preventing GB growth and invasion. Numerous noncancerous cells, such as astrocytes, oligodendrocytes, neurons, resident immune cells, tumour-infiltrating circulating immune cells, and vascular endothelial cells, comprise the dynamic TME in GB (Sharma, Aaroe, Liang & Puduvalli, 2023). Additionally, noncellular molecules such as extracellular matrix (ECM) components, paracrine signalling molecules, exosomes, and chemical factors like acidity and oxygen availability also influence the GB TME (Sharma, *et al.,* 2023). For instance, high expression and secretion of the ECM glycoprotein

tenascin-C (TNC) by glioma stem cells (GSCs) at the tumour's leading edge create a TME that facilitates tumour cell migration away from the tumour mass (Marino, *et al.,* 2023). Furthermore, invading GB cells have been observed to effetely utilise their surrounding TME and thus regulate shifts in their osmotic potential via Cl^- and K^+ channels, allowing invasion into smaller spaces (Griffin, Khan, Basu & Smith, 2020). This heterogeneous mix of cells and molecules leads to many direct cell-to-cell communications and the potential for various signalling pathway alternations. Therefore, to improve our understanding of the drivers of GB genesis, growth, and invasion, deeper insights into the mechanisms and effects of TME-tumour interactions are necessary.

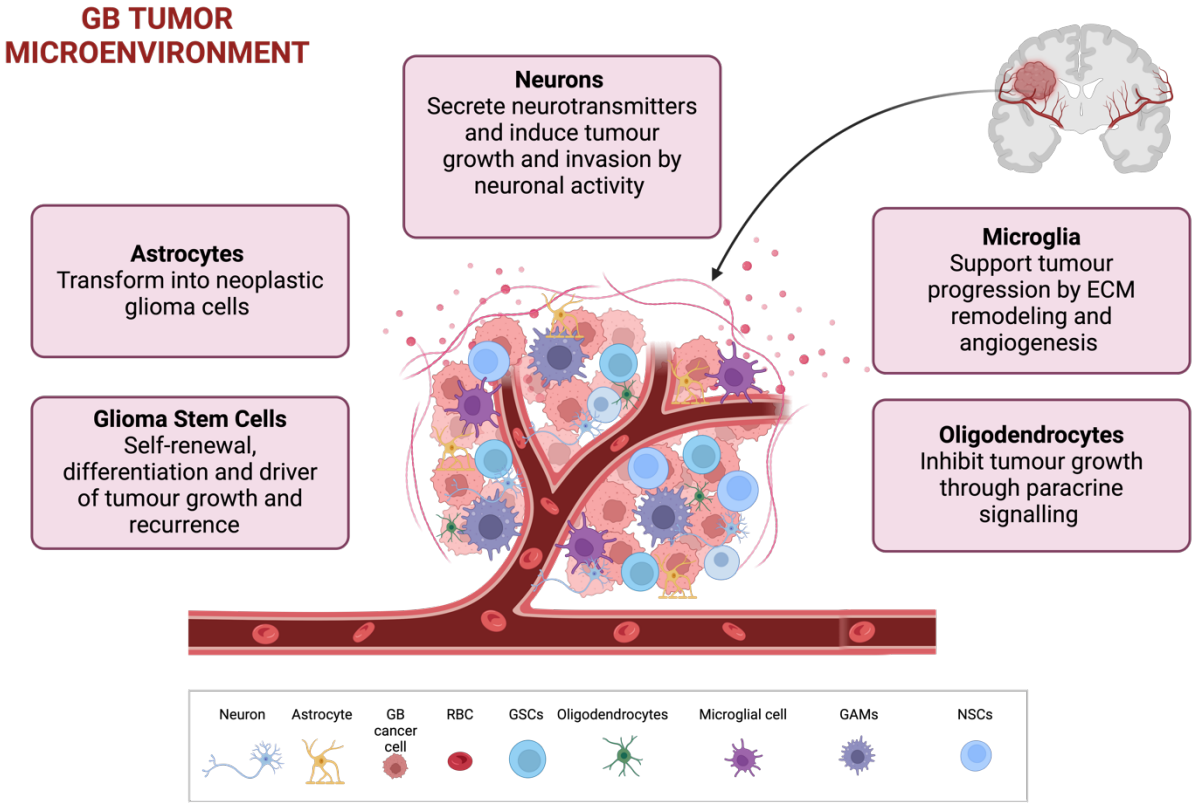


Figure 6. The complex tumour microenvironment in GB. The complexity of the tumour microenvironment in GB, highlighting the interactions between tumour cells, immune cells, neurones, astrocytes and oligodendrocytes. Designed using BioRender: https://biorender.com.

1.2.9.1. Glioma stem cells

The GSC subpopulation of cells comprise as few as 1% of all the tumour's cells within GB. They are widely recognised as key regulators of GB growth, maintenance, invasion, treatment evasion, and recurrence, contributing to the aggressive nature of GB (Tan, *et al.,* 2019). These cells maintain stem-like properties similar to NCSs, enabling them to self-renew and produce various cell lineages, which sustain the intratumoral heterogeneity in GB. It has been observed

that their heterogenetic variations across patient tumours are aided through amplifications of RTKs, allowing GB to interact with diverse cell types, facilitating adaptation and modification of the TME (Furnari, *et al.,* 2015). The GSCs also exhibit prominent resistance to chemotherapeutic agents and radiotherapy. This resistance is attributed to several mechanisms, including the upregulation of anti-apoptotic genes like B-cell lymphoma-extra-large (*BCL-xL*) and the activation of DNA damage repair proteins such as checkpoint kinase 1 (Chk1) (Auffinger, Spencer, Pytel, Ahmed & Lesniak, 2015). In the case of Chk1, phosphorylation occurs in response to DNA damage and activates its role in DNA damage repair, thus activating Chk1 and enabling it to help the cells manage and repair damaged DNA (Zhang & Hunter, 2014a). Therefore, there is a significant focus on specifically targeting these treatment-resistant, tumour-initiating GSCs. However, considering their existence within a complex microenvironment that supports their stemness, these therapies have not shown promising results.

1.2.9.2. Astrocytes

Comprising approximately 50% of all brain cells, astrocytes represent the most abundant cellular compartment in the brain. They play a crucial role in maintaining brain homeostasis (Akdemir, Huang & Deneen, 2020). It is believed that NSC-derived astrocytes are one of the main three cell types, alongside NSCs and oligodendrocyte precursor cells (OPCs), that can give rise to GB (Zong, Parada & Baker, 2015). These glial cells are heterogeneous and phenotypically different across different brain regions, performing different functions, including maintaining the BBB, regulating inhibitory and excitatory transmission, and supporting tissue repair mechanisms. Following brain injury, local astrocytes undergo astrogliosis, becoming reactive astrocytes that transcribe components necessary for growth, such as growth factors, signalling receptors, and cell adhesion proteins to repair the site of injury (Wei & Morrison, 2024). Subsequently, GB can recognise this response, transforming astrocytes into tumour-associated reactive astrocytes (TARAs). These TARAs then promote GB growth and invasion through various signalling mechanisms, including direct signalling, paracrine signalling, and structural enhancement via the secretion factors like transforming growth factor beta (TGF-β) and interleukin 6 (IL-6), which increase GB proliferation and invasion, respectively (Zhang, Wang, Liu, Wang & Jia, 2023).

1.2.9.3. Neurones

The unique ability of GB to remodel neuronal circuits, thereby enhancing neuronal activity and aiding tumour growth, has been exclusively observed (Krishna, *et al.,* 2023). Well-characterised pathways such as PI3K-mTOR activation in GB cells following neurotrophin-3 secretion from neurons have been associated with promoting GB growth (Yan, Zhang & Li, 2020). Given that GB is highly interconnected, with gap junctions between glioma cells throughout the tumour, electrical impulses can propagate widely leading to various outcomes, such as increased microtubule turnover and, thus, facilitated invasion (White, White, Wickremesekera, Peng & Gray, 2024). It has been demonstrated that the excitatory activity at electrical synapses connecting neurons (pre-synaptic) to tumour GB cells (post-synaptic) correlated with increased growth and invasion (Venkatesh, *et al.,* 2019). These bidirectional interactions between neurons and GB create a stimulated environment for tumour growth, with higher neuronal activity correlating with reduced survival rates.

1.2.9.4. Oligodendrocytes

Oligodendrocytes are a type of glial cells that play important roles in regulating neuronal activity and supporting axon myelination (Yalçın & Monje, 2021). They are frequently found at the invasion front and resection border of GB tumours, indicating their potential role in both invasion and recurrence. Evidence has demonstrated that oligodendrocytes enhance GB migration, though not proliferation, through the release of cytokines like angiopoietin-2 (Erices, *et al.,* 2023). Blocking this cytokine has been shown to reduce migration and extend patient survival. Furthermore, oligodendrocytes have been observed to promote angiogenesis in GB, thus enhancing tumorigenicity (Huang, *et al.,* 2014). The involvement of oligodendrocytes in tumour recurrence has also been suggested. It has been observed that oligodendrocytes contribute to the promotion of GSC niches (Hide, *et al.,* 2018). Consequently, this led to the induction of stemness and chemo- and radio-resistance in GB cells aided by GSC proliferation invasion at the borders of the tumour following resection.

1.2.9.5. Immune cells

Glioblastomas are mainly associated with the presence of immune cells, such as microglia and tumour-infiltrating macrophages. The immune cell population accounts for approximately 30-50% of all cells present within the GB microenvironment (Wu, *et al.,* 2024). Once associated with GB, these cells are referred to as glioma-associated microglia/macrophages (GAMs). The

positive correlation between the presence of GAMs and poor prognosis and reduced OS within GB patients has been previously observed (Lin, Wang & Xu, 2023). GAMs are involved in the production of anti-inflammatory cytokines, tumour-promoting factors, and angiogenesis-promoting factors (Sharma, *et al.,* 2023). Their presence in the TME is associated with increased glioma proliferation, migration, ECM degradation, angiogenesis, and T-cell apoptosis. The resistance of GSCs to immune responses has been extensively documented, with mechanisms including the expression of checkpoint inhibitors, downregulation of antigen presentation molecules, and induction of immunosuppressive GAMs (Wang, *et al.,* 2023a). Furthermore, myeloid-derived suppressor cells (MDSCs) can inhibit glucose uptake within T-cells, thus impairing their activation and leading to enhanced preferential glucose metabolism by GSCs, promoting tumour growth (Wu, Yi, Niu, Mei & Wu, 2022b). The role of GSCs in immune evasion in GB was further highlighted by an observed correlation between the percentage of c-Met and FasL (GSC markers) and the frequency of GAMs (Khan, *et al.,* 2022).

1.2.10. Therapeutic management

1.2.10.1. Surgery

Following neuroimaging, if a suspected brain tumour lesion is detected, the patient is referred to a specialist neuro-oncology multidisciplinary team (MDT) for diagnostic confirmation and further management. The primary treatment for a suspected GB is maximal surgical resection, aiding in controlling the tumour locally before adjuvant therapy (Weller, *et al.,* 2021). The primary aims of surgery are to remove as much of the neoplastic tissues as possible, to obtain tissue for histopathological diagnosis, to improve neurological function, to extend survival, and to enhance quality of life (Królikowska, *et al.,* 2022). Less invasive biopsy procedures are recommended for elderly patients with poor performance status or patients with tumours unsuitable for surgical resection. In cases where the biopsy risk is too high, or the patients' prognosis is very poor, the MDT recommends supportive care or a short course of palliative radiotherapy (Alieva, van Rheenen & Broekman, 2018).

A current systematic review and meta-analysis demonstrated that maximal tumour resection correlated with a better OS in GB patients (Wach, Vychopen, Kühnapfel, Seidel & Güresir, 2023). Nevertheless, the risks from intra-operative injury in critical brain regions that control movement, sensation, or speech are associated with reduced quality of life and OS (Ghatol & Widrich, 2024). To maximise resection extent while minimising post-operative disability, various surgical implications have been developed, including intra-operative neuroanatomical

navigation systems, ultrasound, fluorescent dyes for visualising tumour tissue, spectroscopy, and cortical mapping in awake patients.

1.2.10.2. Intra-operative neuroanatomical navigation systems

Structural and functional image guidance is now an essential part of GB surgery. However, due to individual neuroanatomy variability, traditional anatomical identification of functional areas is often insufficient. Neuronavigation, alongside diffusion tensor imaging (DTI) tractography, magnetoencephalography (MEG), and functional MRI (fMRI), aid in the creation of anatomical and functional brain maps, allowing for an individualised understanding of functional areas and their relationship to brain tumours (Kokkinos, Chatzisotiriou & Seimenis, 2023). Diffusion tensor imaging is increasingly used to identify critical white fibber tracts both preoperatively and intraoperatively, enhancing the safe and effective resection of tumours (Abdullah, Lubelski, Nucifora & Brem, 2013). The UK's multicentre randomised control trial, FUTURE-GB, is currently investigating the additional benefits of intraoperative DTI and ultrasound (Plaha, *et al.,* 2023). Compared to direct cortical and subcortical stimulation mapping, fMRI shows a sensitivity and specificity of 91% and 64% for identifying Broca's area, 93% and 18% for identifying Wernicke's area, and 100% and 98% for motor areas (Bizzi, *et al.,* 2008). With an individualised map, surgeons could plan their approach to a tumour preoperatively and ensure maximal tumour resection while preserving critical subcortical fibre tracts intraoperatively.

1.2.10.3. Ultrasound

The major challenges associated with intraoperative neuronavigation are related to brain shift caused by tumour resection, cerebrospinal fluid loss, and cerebral edema. These obstacles can be partially addressed via the utilisation of intraoperative MRI (iMRI) and intraoperative ultrasound (iUS) (Incekara, *et al.,* 2021). These techniques allow surgeons to reassess the surgical field after they believe gross total resection (GTR) has been achieved. If any residual tumour mass is identified via iMRI, surgery can continue. However, the high setup costs of iMRI limit its use in the UK, where it is available in only a few neurosurgical units and is not yet standard care (Trevisi, Barbone, Treglia, Mattoli & Mangiola, 2020). Meanwhile, the considerably cheaper iUS technique is easier to use intraoperatively, but it is more user-dependent and has a longer learning curve. Consequently, iUS is associated with a relatively low sensitivity (49.6%) (Kubben, *et al.,* 2011). Studies such as FUTURE-GB aim to accelerate this learning curve and adoption within the clinical setting (Plaha, *et al.,* 2022).

1.2.10.4. Fluorescent dyes

The heme precursor, 5-aminolevulinic acid (5-ALA), is a fluorescent agent that when administered exogenously, leads to increased accumulation of the fluorophore protoporphyrin IX (PpIX) within GB (Stummer, *et al.,* 2006). This intraoperative technique utilises an operative microscope under blue light which allows the visualisation of the tumour, particularly at resection margin regions. In a randomised trial, the use of 5-ALA significantly increased gross GTR rates from 36% to 65%, with a corresponding rise in 6-month progression-free survival (PFS) from 21.1% to 41% and OS from 11.8 months to 16.7 months (Stummer, *et al.,* 2006). The NICE has approved the routine use of 5-ALA for all patients undergoing surgical resection of GB in the UK (Fernandes, *et al.,* 2017). Nevertheless, increased GTR has been associated with a higher incidence of early post-operative neurological deficits at 48 hours (26.2% vs. 14.5%), but not at 3 months (19.6% vs. 18.6%) (Ontario Health (Quality), 2020). Furthermore, PpIX also acts as a photosensitiser, which is activated by bright light, and it produces reactive oxygen species, leading to local cytotoxicity to cancer cells (Schipmann, *et al.,* 2020). Thus, the use of PpIX for local photodynamic therapy (PDT) has been under exploration for GB patients, but further studies are necessitated to determine its efficacy.

1.2.10.5. Spectroscopy

Another biophotonic tool, called Raman spectroscopy, has demonstrated efficient in the distinguishment between various tissue types and GB. It has been seen that this spectroscopy method could effectively differentiate GB tissue from normal tissue (Livermore, *et al.,* 2020). Furthermore, it can also differentiate between IDH-wild-type GB from other mutated tumours (Livermore, *et al.,* 2019). Raman spectroscopy offers a real-time intraoperative diagnosis of brain tumours when combined with machine learning, showing a sensitivity of 93% and specificity of 91% (Jermyn, *et al.,* 2015). However, its effectiveness at tumour margins has not been fully tested. Furthermore, this rather diagnostic approach also requires the use of probe machine learning and validation for each probe in each location, which vary between different probes and conditions and thus may limit its widespread clinical use.

1.2.10.6. Awake surgery

GB surgery often involves a delicate balance between achieving maximal tumour resection and avoiding permanent neurological damage. The advantages of awake surgery allow for the intraoperative mapping of important brain areas to maximise resection while protecting

essential brain functions (Watts & Sanai, 2016). Awake surgery has primarily been used for low-grade gliomas due to the infiltrative nature of high-grade GBs, which are often located in delicate brain regions. Even though GBs are more aggressive and infiltrative, they usually present with a clearer margin between the tumour and normal brain tissue. In such cases, awake surgery can help to increase the extent of resection and reduce post-operative morbidity (Ius, *et al.,* 2023). A recent meta-analysis of 14 studies involving 278 GB patients who underwent awake surgery showed a GTR rate of 74.7%, with early post-operative deficits in 34.5% of cases, dropping to 1.9% after three months (Zhang, *et al.,* 2020a). However, further evidence is required to evaluate the effectiveness and clinical benefits of an awake surgery. The ongoing SAFE-Trial (NCT03861299) compares awake craniotomy to surgery under general anaesthesia, aiming to provide further insights (Gerritsen, *et al.,* 2020).

1.2.11. Radiotherapy

One of the most effective adjuvant treatments for GB is fractionated radiotherapy. Post the excision of the brain tumour or biopsy, follow-up treatment depends on the patient's age and performance status. In the UK, patients over the age of 70 years who are capable of independent self-care and have a Karnofsky performance status ≥ 70 receive a standard treatment of daily fractionated radiation therapy over six weeks alongside TMZ, an oral alkylating chemotherapy, for up to six months (Weller, *et al.,* 2021). Patients above the age of 70 years with a similar performance status could be recommended a course of hypofractionated radiotherapy with concurrent and adjuvant TMZ for up to 12 months (Weller, *et al.,* 2021). A recent meta-analysis suggested that hypofractionation is comparable to standard treatment, offering the advantage of a shorter duration, which is beneficial for elderly GB patients. The Radiation Therapy Oncology Group randomised trial (RTOG 93-05) investigated the addition of stereotactic radiosurgery (SRS) to standard radiotherapy (Souhami, *et al.,* 2004). The results revealed that there was no survival benefit (13.5 versus 13.6 months) compared with conventional therapy. Additionally, there was no improvement in quality of life or cognitive function of the patients.

The standard course of radiation therapy should begin within 3 to 6 weeks post-surgery and involve the administration of 60 Gy over 6 weeks in 30 fractions of 2 Gy (Stupp, *et al.,* 2009). This is usually delivered concurrently with TMZ. Temozolomide intake is continued 4 weeks after radiation completion, typically for 5 consecutive days every 28 days over 6 monthly cycles. In a clinical trial with 573 participants, this regimen significantly improved survival compared to radiation alone (14.6 months versus 12.1 months) (Stupp, *et al.,* 2005). A group

of 92 patients with epigenetic silencing of the DNA-repair protein MGMT showed improved median OS when TMZ was combined with radiation (21.7 months versus 15.3 months) (Hegi, *et al.,* 2005). However, radiation alone, compared to radiation plus TMZ, led to similar health-related quality of life in those patients. Short-course radiotherapy alone (40 Gy in 15 fractions) and combined radiotherapy with TMZ were compared in a group of 562 patients aged 65 years or older (Perry, *et al.,* 2017). The results demonstrated improved OS with combination therapy (9.3 months versus 7.6 months). However, some patients cannot tolerate combined radiotherapy with chemotherapy. These patients are recommended to either undergo radiotherapy alone (if MGMT is unmethylated) or chemotherapy alone (if MGMT is methylated) (Weller, *et al.,* 2021).

1.2.12. Chemotherapy

Chemotherapy is an essential treatment strategy for GB management with its primary aim being to either control or eliminate cancer cells via the use of cytotoxic agents (Taal, Bromberg & van den Bent, 2015). It is often combined with other treatments, such as surgery or radiotherapy to improve outcomes (Amjad, Chidharla & Kasi, 2023). For instance, in GB, the current standard of care is chemoradiotherapy with TMZ, which maximises tumour control, especially when surgical resection is incomplete (Wu, *et al.,* 2021). When combined with other treatments, chemotherapy can improve outcomes by sensitising tumours to radiation (chemoradiotherapy) or targeting specific pathways (Bayat Mokhtari, *et al.,* 2017). However, the efficacy varies depending on the molecular profile of the tumour, such as MGMT promoter methylation status, which can predict responsiveness to alkylating agents like TMZ (Ortiz, *et al.,* 2021). In recurrent gliomas, chemotherapy remains an important option, though often with limited effectiveness, underscoring the need for continued clinical trials to explore novel therapeutic combinations and drugs (Kamiya-Matsuoka & Gilbert, 2015). The timing and integration of chemotherapy into the broader treatment strategy are key in optimising patient outcomes, particularly in high-risk and recurrent glioma cases.

1.2.12.1. Temozolomide

The first-line chemotherapeutic drug used for primary GB is TMZ. The alkylating agent discovered in the 1970s causes DNA damage, leading to cell death. As already mentioned, Stupp and colleagues demonstrated that combinational TMZ and radiotherapy led to increased OS by over 2.5 months (14.6 months versus 12.1 months) and provided a 2-year survival advantage of 16.1% (26.5% versus 10.4%) (Stupp, *et al.,* 2005). This protocol, introduced as

the standard of care in 2005, remains the last significant change in the management of primary GB. Nevertheless, this therapeutic regimen was associated with a 7% incidence of grade 3/4 haematological adverse events (Ma, de Pennington, Hofer, Blesing & Stacey, 2013). The effectiveness of TMZ was observed to be enhanced in patients with *MGMT* gene silencing. The *MGMT* gene encodes a DNA repair enzyme known to counteract the effects of the alkylating agent TMZ. In IDH-wild-type GB, the response to TMZ chemotherapy can be predicted by the promoter methylation status (Kitange, *et al.,* 2009). Epigenetic silencing in *MGMT* promoter-methylated tumours led to an increased response to TMZ and improved survival, with only marginal effects in *MGMT* promoter-unmethylated tumours (Rivera, *et al.,* 2010). However, due to the lack of effective treatments and the fact that TMZ is still effective in patients with active *MGMT*, the chemotherapeutic is administered to all patients under 70 in the UK, regardless of *MGMT* status (Kanderi, *et al.*, 2024).

1.2.12.2. Lomustine

Due to the limited effective treatment options, there are no established guidelines for the management of recurrent GB. Lomustine is an alkylating agent considered as the primary chemotherapy for recurrent GB (Weller & Le Rhun, 2020). Lomustine is traditionally administered alongside procarbazine and vincristine as part of the PCV regimen for GB. Before the discovery of TMZ's greater efficacy, PCV was used as a first-line treatment for GB (Fernandes, *et al.,* 2017). Among these three agents, lomustine has been associated with the greatest anti-GB activity. In the UK, PCV has been replaced by TMZ for the adjuvant treatment of primary GB and is now primarily used for recurrent GB. However, there is accumulating evidence that has suggested beneficial use of TMZ for recurrent GB (Perry, *et al.,* 2010). A large phase II study indicated that continuous dose-intense TMZ is a viable option for patients who experienced tumour recurrence within their first six cycles of TMZ or those who had a disease-free interval followed by recurrence (Perry, *et al.,* 2010). There has been an attempt for a clinical trial exploring the combined use of TMZ and lomustine that has suggested an improved survival in patients with primary *MGMT* methylated GB (Herrlinger, *et al.,* 2019). However, factors such as slow recruitment resulting in insufficient statistical power led to the stop of this trial. A larger trial is being planned to further investigate this potential benefit.

1.2.12.3. Bevacizumab

One of the characteristic features of GB is its significant microvascular proliferation and disruption of the BBB. This feature is observed through the contrast enhancement on MRI and CT scans. Bevacizumab, a monoclonal antibody against vascular endothelial growth factor A (VEGF-A), has been seen as beneficial for the treatment of GB. The drug targets the overexpressed *VEGF* in GB (Gilbert, *et al.,* 2014). Several large clinical trials, including two major phase-III randomised controlled trials, demonstrated that bevacizumab treatment resulted in a notable radiological response and increased progression-free survival (PFS) (10.6–10.7 months versus 6.2–7.3 months) (Chinot, *et al.,* 2014). However, there was no improvement in OS (15.7–16.8 months versus 16.1–16.7 months) for patients with primary GB. As a result, bevacizumab is not licensed for GB treatment in the UK but is approved for recurrent GB in the USA, Switzerland, Japan, and Australia (Green, *et al.,* 2023).

1.2.13. Immunotherapy

Immunotherapy has emerged as a promising approach for treating various cancers by enhancing the body's immune system to target and eliminate tumour cells. Immune checkpoint inhibitors, such as pembrolizumab, nivolumab, and ipilimumab, have shown significant success in cancers like melanoma and non-small cell lung cancer (NSCLC) (Shiravand, *et al.,* 2022; Tang, *et al.,* 2022a). These drugs work by blocking immune checkpoints, such as programmed cell death protein 1 (PD-1), programmed death-ligand 1 (PD-L1), and cytotoxic T-lymphocyte-associated protein 4 (CTLA-4), which cancer cells use to evade immune surveillance (Wojtukiewicz, *et al.,* 2021). By inhibiting these checkpoints, T-cell activity against cancer cells is restored, allowing the immune system to generate a stronger anti-tumour response. However, the application of immunotherapy in GB has faced some challenges. Although early preclinical studies suggested potential benefits, clinical trials in GB have produced mixed results. For instance, the Checkmate 143 phase III trial found that nivolumab, a PD-1 inhibitor, did not improve survival outcomes in recurrent GB compared to bevacizumab (Weenink, French, Sillevis Smitt, Debets & Geurts, 2020). The challenges of using immunotherapy in GB primarily arise from the unique immunosuppressive microenvironment of the brain (Sharma, Aaroe, Liang & Puduvalli, 2023). Additionally, the BBB limits the ability of immune cells and drugs to access the tumour, while the lack of a conventional lymphatic system in the brain and the reduced levels of antigen-presenting cells (APCs) further obstruct immune activation (Razavi, *et al.,* 2016). These issues create significant obstacles to the success of immunotherapy in GB.

1.2.13.1. Chimeric antigen receptor T cell therapy

Chimeric antigen receptor (CAR) T cell therapy is an emerging approach for GB therapy. The CAR-T cells are engineered to express single-chain receptors with an antibody-like antigen-binding domain linked to an intracellular T-cell activating domain (Sadelain, Rivière & Riddell, 2017). They recognise antigens independently of the major histocompatibility complex (MHC) and directly activate T-cells rather than relying on antibody-dependent cell-mediated cytotoxicity (Sun, *et al.,* 2023). Various CAR-T cells have been evaluated, showing promising results in preclinical and clinical trials. These include the EGFRvIII (NCT01454596, NCT02664363, NCT02209376), interleukin receptor 13Rα2 (IL13Rα2) (NCT02208362), and ephrin type-A receptor 2 (NCT02575261) trails (Prapa, *et al.,* 2021; Knudson, *et al.,* 2022; Hsu, *et al.,* 2021). A CAR-T therapy against GSCs via targeting B7-H3 has shown anti-tumour efficiency against GSC-enriched neurospheres and differentiated GB cell lines (Li, *et al.,* 2024). While there have been some successes, such as with IL13Rα2 CAR-T cells showing tumour regression for over seven months with repeated cerebrospinal fluid (CSF) infusions, the efficacy of these treatments is often limited. This is because the targeted tumour-associated antigens are not present in all GB tumours and are only expressed in a portion of the tumour cells (Luksik, Yazigi, Shah & Jackson, 2023). Thus, further research into the mechanisms of GB and immune population interactions may enhance the effectiveness of CAR T-cell therapies, facilitating their translation into clinical practice.

1.2.13.2. Oncolytic Viruses

The use of native or genetically modified viruses has also been implicated in the fight against GB. The so-called oncolytic viruses have been used to selectively infect and replicate within tumour cells (Asija, *et al.,* 2023). Several oncolytic viruses have been trailed for GB treatment, including herpes simplex virus (HSV), adenovirus, poliovirus, parvovirus, reovirus, measles virus, and more recently, Zika virus (Hamad, Yusubalieva, Baklaushev, Chumakov & Lipatova, 2023). The first studied oncolytic virus approach for targeting GB was published in 1991. Modified HSV was incorporated in targeting rapidly dividing GB cells *in vitro* and showed tumour regression *in vivo* (Martuza, Malick, Markert, Ruffner & Coen, 1991). This has been followed by many phase-I trials in humans, which have proven safety. An example is M032, a modified HSV virus including the human interleukin 12 (*IL12*) gene, currently in a phase-I trial (NCT02062827) (Estevez-Ordonez, *et al.,* 2023). The success of these therapies requires a balance between effective viral replication and an active immune response against the infected

cells. Any imbalance can lead to uncontrolled viral infection or, more likely, eradication of the virus without therapeutic effect. Thus, further investigations and clinical trials are necessitated.

1.2.13.3. Immune checkpoint inhibitors

The anti-programmed cell death protein 1 (PD-1) and anti-cytotoxic T-lymphocyte-associated protein 4 (CTLA-4) are immune checkpoint inhibitors that have been utilised in the therapeutic management of different types of metastatic tumours, such as melanoma, NSCLC, and renal carcinoma (Buchbinder & Desai, 2016). As many as 88% of GB tumours are observed to express very high levels of PD-L1 (Hölzl, *et al.,* 2021). Additionally, the tumour-infiltrating lymphocytes (TILs) within GB are also PD-1 positive, suggesting that checkpoint inhibitors could be an effective treatment (Berghoff, *et al.,* 2015). The largest clinical trial studying immune checkpoint inhibitors to date, the CheckMate 143 trial, has indicated that although some patients showed partial responses and other patients had stable disease with checkpoint inhibitor therapy, there was no OS benefit in any cohort (Reardon, *et al.,* 2020). In the UK, the Ipi-Glio trial is currently investigating the use of ipilimumab (anti-CTLA-4) for patients diagnosed with primary GB (Brown, *et al.,* 2020).

1.2.14. Combination Therapies

Considering the limitations associated with individual therapies, researchers and clinicians are increasingly adopting combinatorial approaches. Such therapies, especially those involving checkpoint inhibitors, might be regarded as promising due to their current success in treating other cancers, such as melanoma. As described above, various combinations have been explored to enhance their efficacy in GB malmanagement. These strategies are still in the early stages, and the results from them must be carefully evaluated before their clinical application (Ghosh, Nandi & Bhattacharjee, 2018). Nevertheless, it is important to consider that combination therapies, while promising, are challenging to develop and analyse. Furthermore, possible antagonistic side effects might be experienced by patients who receive combinations of highly toxic drugs, such as the interaction between TMZ and immunotherapies (Wu & Lim, 2023). Temozolomide can induce lymphopenia, which compromises the immune system, potentially counteracting the benefits of immunotherapy. This interaction can lead to more side effects, reducing the effectiveness of immune-based treatments and making it harder for patients to tolerate long-term therapy (Sengupta, Marrinan, Frishman & Sampath, 2012). Even when tolerated, it can be difficult to determine the contribution of each therapy to the overall efficacy of the combination, anticipating the need for further studies.

1.2.15. Prediction benefit

The median survival for adult patients under the age of 70 years who do not undergo surgery is approximately 3-4.5 months. This median survival is improved to 8-10 months if the patient receives chemotherapy, with or without radiotherapy, following a tissue biopsy (Fernandes, *et al.,* 2017). The longest median survival of around 15-16 months is achieved with maximal treatment involving GTR followed by chemoradiotherapy (Mohammed, Dinesan & Ajayakumar, 2022). Given the incurable nature of GB, it is highly important to inform patients about the potential adverse effects associated with the current therapeutic strategies and how this could affect their quality of life. This is especially important for elderly patients and those with poor performance status who have a particularly poor prognosis. Elderly patients who receive only supportive care have a median survival of less than 4 months. Patients over the age of 65 years who undergo biopsy or resection, followed by hypofractionated radiotherapy and chemotherapy, have an improved median survival from 7 to 9 months (Mak, Agarwal, Qureshi & Truong, 2017). However, adding adjuvant chemotherapy has a negative effect on their quality of life despite the survival advantage.

1.3. MicroRNAs

1.3.1. Introduction to miRNAs

Found in all plants and animals, microRNAs (miRNAs) are a major class of conserved (~22 nucleotides) non-coding single-stranded RNA molecules that have emerged as post-transcriptional regulators of gene expression (Friedman, Farh, Burge & Bartel, 2009). The first miRNA, lin-4, was described by Ambros and Ruvkun in 1993. While studying the gene *lin-4* in *Caenorhabditis elegans*, Victor Ambros, Rosalind Lee, and Rhonda Feinbaum discovered that *lin-4* did not encode a protein but instead produced a small RNA molecule that was complementary to sequences in the 3' untranslated region (UTR) of another gene, *lin-14* (Lee, Feinbaum & Ambros, 1993). They identified that lin-4 post-transcriptionally downregulated the expression of *lin-14* in the nematode. Gary Ruvkun's lab also contributed to the discovery by identifying that *lin-14*'s regulation by lin-4 was due to a novel RNA-RNA interaction (Wightman, Ha & Ruvkun, 1993). MiRNAs exert their regulatory mechanisms by direct targeting the messenger RNAs (mRNAs) of key metabolic genes, leading to decreased protein production and subsequent modulation of metabolic activity (Ha & Kim, 2014). Additionally, miRNAs can indirectly regulate metabolism by affecting signalling pathways that govern these processes. At present, it is estimated that miRNAs regulate the expression of approximately 60% of all protein-coding genes (de Rooij, *et al.,* 2022). A

systematic review identified more than 300 miRNAs implicated in GB tumorigenesis, with 253 being overexpressed and 95 under-expressed (Buruiană, *et al.,* 2020). Due to their short size, miRNAs can bind imperfectly or complementarily to multiple mRNAs, allowing them to regulate several targets. It is estimated that approximately 10,000 mRNAs can be regulated by this mechanism, enabling a single miRNA to target multiple genes directly or indirectly (Giza, Vasilescu & Calin, 2014). Their impact extends to various aspects of metabolism, such as glucose and lipid homeostasis, insulin sensitivity, embryogenesis, and mitochondrial function. Dysregulation of miRNAs has been linked to the development of metabolic diseases such as obesity, diabetes, neurodegenerative and cardiovascular disorders, and cancer (Li, Lei & Sun, 2023; Zhou, *et al.,* 2018). Their multifunctional nature has suggested that miRNAs could serve as candidates for promising diagnostic and prognostic biomarkers, as well as potential therapeutic agents (Ho, Clark & Le, 2022). To fully harness this potential, a thorough understanding of miRNA biogenesis and their modulatory mechanisms is crucial. The biogenesis of miRNAs begins with post- or co-transcriptional processing by RNA polymerase II/III (Borchert, Lanier & Davidson, 2006). Most intragenic miRNAs are transcribed from the introns of protein-coding genes, while very few are synthesised from the exons. Intergenic miRNAs possess their own promoter regions and are transcribed independently of their host genes (Shang, Lee, Senavirathne & Lai, 2023). The biogenesis pathways of miRNAs can be categorised into two major routes: canonical and non-canonical.

1.3.2. MiRNA biogenesis

1.3.2.1. The canonical pathway

The canonical miRNA biogenesis pathway is a multistep process that converts primary miRNA transcripts (pri-miRNAs) into functional, mature single-stranded miRNAs. These miRNAs associate with Argonaute (Ago) proteins to form the RNA-induced silencing complex (RISC). The mature miRNA strand then binds to its target mRNA, guiding the Ago proteins to execute mRNA degradation or translational repression (Shang, *et al.,* 2023) (Figure 7).

The synthesis of miRNAs begins in the nucleus, where RNA polymerase II transcribes a DNA sequence encoding a miRNA gene, though some pri-miRNAs are produced by RNA polymerase III (Bofill-De Ros & Vang Ørom, 2024). This transcription results in the formation of a long, 5′ capped, and 3′ polyadenylated RNA molecule known as a pri-miRNA. Pri-miRNAs typically exhibit a characteristic hairpin structure with a double-stranded RNA stem, an upper stem of approximately 22 base pairs, a lower stem of about 13 base pairs, a single-

stranded RNA terminal loop of around 10 nucleotides, and two flanking single-stranded RNA sequences (ssRNAs) adjacent to the double-stranded stem at both the 5' and 3' ends of the pri-miRNA hairpin structure (Cai, Hagedorn & Cullen, 2004). The lower stem end, flanked by the two ssRNAs, forms a basal junction, while the upper stem end, preceding the terminal loop, forms an apical junction.

Within the nucleus, the pri-miRNA encounters the microprocessor complex, consisting of one Drosha and two DiGeorge syndrome critical region gene 8 (DGCR8) molecules. Drosha, an RNase III enzyme, recognises and cleaves the pri-miRNA 11 base pairs from the basal junction, releasing a shorter, hairpin-shaped RNA molecule called a precursor miRNA (pre-miRNA) (Nguyen, Nguyen, Nguyen & Nguyen, 2019). The DGCR8 dimer acts as an RNA-binding protein that stabilises Drosha on the pri-miRNA, facilitating precise cleavage. Several motifs and cofactors assist in the binding and recognition of Drosha and DGCR8 to the miRNA (Shang, *et al.,* 2023). These include the uridine-guanosine (UG) motif, uridine-guanosine-uridine (UGU) motif, cytosine-any nucleotide-nucleotide-cytosine (CNNC) motif, the hemin cofactor, and the glycine-histidine-glycine (GHG) motif.

The UG motif near the 5' ssRNA flank (basal junction) is crucial for Drosha binding to the pri-miRNA, directing cleavage at the basal junction. Conversely, the UGU motif in the terminal loop facilitates DGCR8 binding at the apical junction (Nguyen, Park, Dang, Choi & Kim, 2018). Additionally, the CNNC motif recruits SRSF3, which promotes Drosha binding at the basal junction. Hemin, a ferrous iron ($Fe2^{+}$) cofactor, strengthens the DGCR8-UGU motif interaction (Kim, Nguyen, Li & Nguyen, 2018). Finally, the mismatched GHG motif in the lower stem enhances Drosha cleavage efficiency (Nguyen, Nguyen & Nguyen, 2021). Following Drosha-DGCR8 processing, the pre-miRNA is exported from the nucleus to the cytoplasm, facilitated by the Exportin-5 (XPO5)/RanGTP complex. XPO5 interacts with the pre-miRNA in a sequence-independent manner in the presence of the GTP-binding nuclear protein Ran (RanGTP) (Wu, He, Pu & Peng, 2018b).

Once in the cytoplasm, the pre-miRNA encounters the Dicer complex. Dicer, another RNase III enzyme, recognises the pre-miRNA and cleaves it at a defined position, generating a short, double-stranded miRNA duplex containing the mature miRNA and its passenger strand (Shang, *et al.,* 2023). An optimal pre-miRNA structure, essential for Dicer's recognition affinity and cleavage efficiency, typically includes a single-stranded terminal loop, a double-

stranded RNA (dsRNA) stem, a 3′ overhang of two nucleotides, and a 5′ monophosphate (Nguyen, Trinh, Bao & Nguyen, 2022).

Three competing models describe Dicer's cleavage mechanism. In the 3′ counting rule, the PAZ domain recognises the 3′ overhang and measures approximately 22 nucleotides for cleavage. In the 5′ counting rule, the PAZ domain recognises the 5′ monophosphate end and measures approximately 22 nucleotides for cleavage (Park, *et al.,* 2011). The loop counting rule establishes precise cleavage when a 2-nucleotide gap exists between the 5′ ends of miRNA-3p and the bulge/apical junction; deviations from this 2-nucleotide gap leads to multiple miRNA isoforms (Lee, Kim & Kim, 2023b). Interestingly, recent studies have identified a motif called GYM (consisting of a paired G, a paired pyrimidine, and either a mismatched C or A nucleotide) next to the Dicer cleavage site. This motif promotes the specific cleavage of the pre-miRNA independently of the counting rule models (Le, Nguyen & Nguyen, 2024).

Once the miRNA duplex is formed, it is loaded into an Ago protein with the assistance of the Hsc70/Hsp90 chaperone machinery in an ATP-dependent manner (Lee, *et al.,* 2023a). This miRNA duplex can be incorporated into any of the four Ago proteins. Among the four human Ago paralogs, Ago2 is the most abundant and essential for slicing activity (Nakanishi, 2022). However, recent research has suggested that Ago3 may also possess slicing capabilities for specific miRNAs like miR-20a (Nakanishi, 2022). Upon association with the Ago complex, one strand of the miRNA duplex (the mature guide miRNA) is retained, while the other strand (the passenger strand) is discarded, forming a single-stranded RISC. Notably, both 5' (5p) and 3' (3p) derived miRNAs can be functional, denoted by -5p and -3p suffixes (Medley, Panzade & Zinovyeva, 2021).

The mature miRNA loaded onto the RISC complex guides it to its complementary mRNA targets within the cytoplasm. Target recognition primarily relies on base-pairing interactions between the miRNA seed region (nucleotides 2-7/8 of the mature miRNA) and the complementary sequence within the mRNA 3′ UTR (Hwang, Chang & Baek, 2023; Braoudaki & Lambrou, 2015). This interaction leads to various modes of gene silencing; however, in some cases, the binding of miRNA to its target site may activate translation rather than repressing it (Ørom, Nielsen & Lund, 2008). Although the most frequent target sequence is the 3' UTR, miRNAs can also bind to the 5′ UTR and the coding sequence (CDS) (Brümmer & Hausser, 2014). The efficiency of miRNA targeting is influenced by the complementarity at the binding

sites. 8mer sites (a perfect match at nucleotides 2-7 and 8 of the miRNA, with a complementary nucleotide and an mRNA adenine opposite site) are the most effective, followed by 7mer-m8 and 7mer-A1 sites (Agarwal, Bell, Nam & Bartel, 2015).

The RISC complex can inhibit ribosome assembly on the target mRNA by preventing the union of the 60S and/or 40S subunits. Additionally, the RISC complex can inhibit ribosome elongation, induce ribosome drop-off, or initiate proteolysis (Pratt & MacRae, 2009). The RISC complex can also interact with a deadenylase complex formed by CCR4-NOT1, leading to deadenylation of the poly(A) tail. This process is followed by the decapping of the 5′ terminals (Pavanello, Hall & Winkler, 2023). Finally, the translationally repressed mRNAs accumulate in P-bodies or GW bodies, where the final steps of mRNA degradation occur (Luo, Na & Slavoff, 2018).

1.3.2.2. The non-canonical pathway

In addition to the canonical pathway, several non-canonical pathways exist. They bypass some of the steps observed in the canonical pathway or employ different enzymes in the miRNA biogenesis (Figure 7).

Drosha/DGCR8-independent pathways involve several mechanisms. In certain cases, the splicing complex and debranching enzymes generate introns that mimic the structure of typical pre-miRNAs. These introns, termed mirtrons, bypass processing by the microprocessor complex and instead enter the cytoplasm through the Exportin-5 complex, continuing miRNA biogenesis via Dicer (Westholm & Lai, 2011). Furthermore, the tRNA-derived miRNAs pathway is observed in the biogenesis of miRNAs from murine herpesvirus (MHV68). During tRNA-derived miRNA biogenesis, a polymerase III transcribes a viral tRNA-like sequence into a pri-miRNA, which is processed by tRNase Z rather than the microprocessor complex (Zhao, *et al.,* 2023a). Additionally, pre-miRNAs capped with 7-methylguanosine (m7G) typically have their 5′ ends aligned with transcription start sites and their 3′ ends produced during transcription termination (Lee, Lee, Kim, Kim & Roh, 2023c). These capped pre-miRNAs are transported via the Exportin-1 (XPO1) pathway instead of the canonical XPO5 pathway. Following cleavage by Dicer, only the 3p-miRNA is effectively incorporated into the RISC complex, forming a functional miRNA.

The Dicer-independent pathway is exclusively followed by miR-451. In this pathway, the microprocessor complex generates pre-miR-451, which is then exported via the XPO5 complex

(Annese, Tamma, De Giorgis & Ribatti, 2020). Dicer cannot process this pre-miRNA into a miRNA duplex. Instead, Ago2 cleaves the pre-miRNA into a mature miRNA, followed by 3′ trimming by the ribonuclease enzyme PARN. Consequently, this pathway can only generate functional 3p-miRNA.

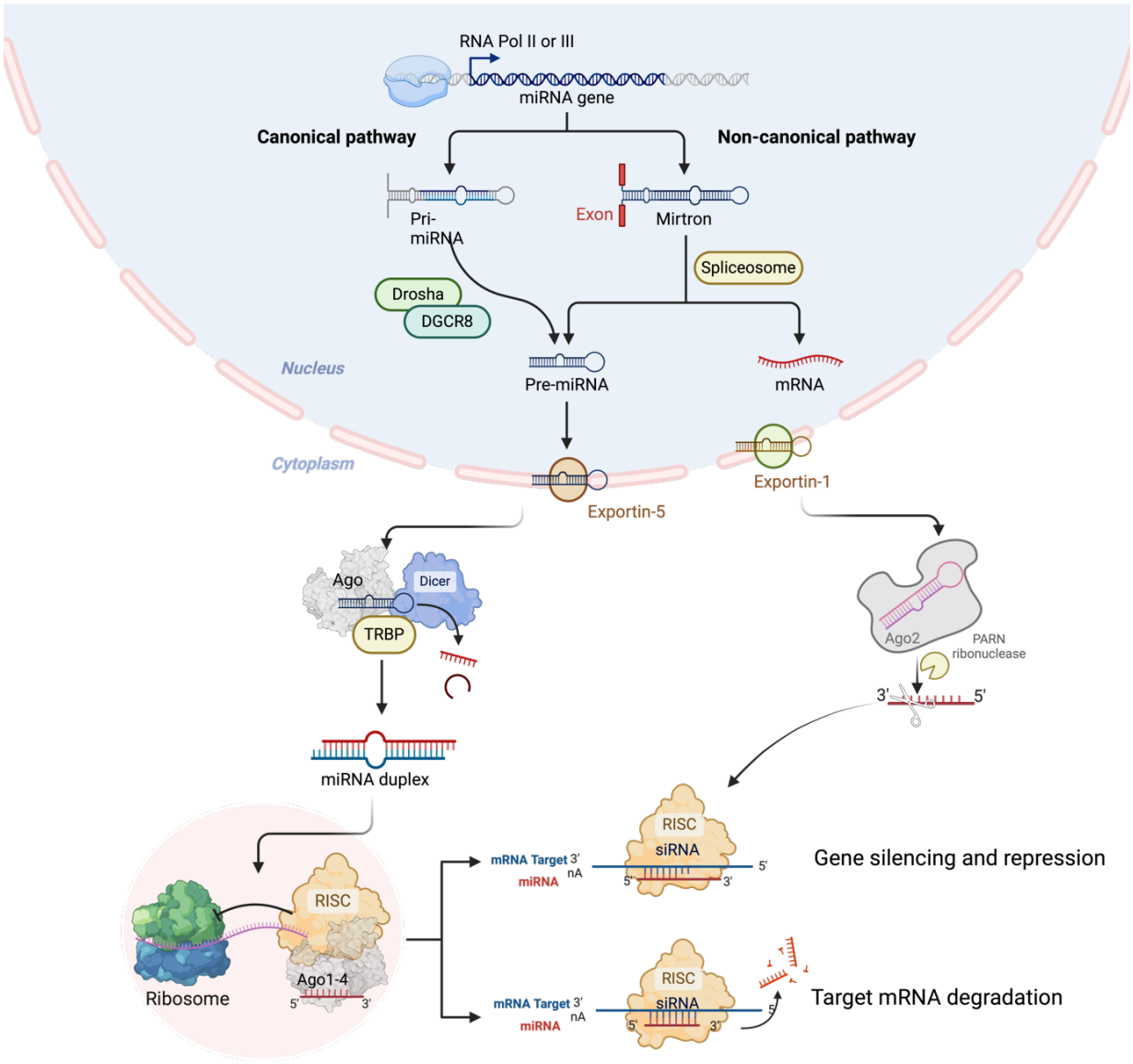


Figure 7. An overview of the canonical and non-canonical pathways of miRNA biogenesis. The canonical miRNA biosynthesis initiates with the transcription of miRNA genes by RNA polymerase II or III, producing primary miRNA transcripts (pri-miRNA) that can range from several hundred to thousands of nucleotides (nts) in length and may contain multiple hairpin structures. In the nucleus, the pri-miRNA is recognised and cleaved by the Drosha enzyme (an RNase III enzyme) and its co-factor, DiGeorge Syndrome Critical Region 8 (DGCR8), forming a microprocessor complex. This complex identifies the RNA stem loop and cleaves the pri-miRNA to generate precursor-miRNA (pre-miRNA) approximately 65-70 nts long, characterised by a two-nucleotide-long 3' overhang. This pre-miRNA is then recognised by exportin 5, a transmembrane protein that facilitates its export to the cytoplasm. In the

cytoplasm, the pre-miRNA undergoes further processing by Dicer, which, together with the TAR-RNA binding protein (TRBP) cofactor, forms the Dicer-TRBP complex. This complex removes the terminal loop of the pre-miRNA, producing mature double-stranded miRNA (dsRNA). The mature dsRNA, about 18-22 nts long, consists of a miRNA-guide strand and a miRNA-passenger strand (miRNA/miRNA* or miR-3p/miR-5p, respectively). The guide strand, typically the one with lower 5'-end stability, associates with an RNA-induced silencing complex (RISC) containing Argonaute (AGO 1-4) proteins. The miRNA-RISC complex then targets a complementary mRNA sequence, acting as a post-transcriptional regulator by inducing degradation or translational inhibition of the target mRNA at its 3' untranslated region (UTR). The non-canonical miRNA biosynthesis pathways include mechanisms such as mirtron processing, which bypasses the Drosha/DGCR8 microprocessor complex. Instead, spliceosomes or other debranching enzymes in the nucleus cleave introns to exclude the pre-miRNA hairpin, making it ready for export by exportin 5/1 and subsequent processing by Dicer. Another non-canonical pathway involves the generation of miR-3p strands without Dicer cleavage, where Ago2 and PARN ribonucleases remove the pre-miRNA hairpin structure to produce a miR-3p strand capable of targeting mRNA. Designed using BioRender: https://biorender.com.

1.3.3. Dysregulation of miRNAs

As previously demonstrated, many miRNAs are dysregulated in cancer, primarily due to alterations in transcription factors (TFs) and epigenetic mechanisms that control their transcription. Transcription factors play a role in regulating miRNA expression levels by directly influencing the transcription of miRNA genes (Chiarella, Aloisio, Scicchitano, Bond & Mesuraca, 2021). MiRNAs and TFs coordinate through two autoregulatory feedback loops: unilateral or reciprocal negative feedback loops and double-negative feedback loops (Chiarella, Aloisio, Scicchitano, Bond & Mesuraca, 2021). In the first loop, the miRNA downregulates the TF, while the TF activates the miRNA (Arora, Rana, Chhabra, Jaiswal & Rani, 2013). In the second, the miRNA represses the TF by binding to its mRNA, while the TF represses the miRNA at the transcriptional level (Krol, Loedige & Filipowicz, 2010). Transcription factors also modulate gene expression through cis-regulatory modules (CRMs) and feed-forward loops (FFLs) (Wu, Qin, Zhao & He, 2015). Feed-forward loops can be miRNA-mediated, where miRNAs repress both the TF and target genes, or TF-mediated, where TFs regulate miRNAs and target genes (Wu, *et al.,* 2015). These regulatory networks are essential for maintaining gene expression balance and play key roles in biological processes and cancer development, especially when dysregulated (Feng, Wu, Gao, Yu & Cui, 2017). However, miRNA expression can be affected by a variety of other factors beyond the influence of TFs. Several miRNAs show dysregulated expression patterns in GB, which are due to epigenetic modifications, errors in their multistep biogenesis process and environmental factors such as hypoxia (Ahmed, Castresana & Shahi, 2021). Epigenetic modifications, such as DNA methylation and histone modifications, can alter miRNA expression by modifying the accessibility of miRNA genes to

the transcriptional machinery (Arif, Elliott, Haupt & Griffiths, 2020). For example, the downregulation of miR-127 in cell lines is caused by methylation of CpG sites and histone deacetylation around its promoter region (Chuang & Jones, 2007). Additionally, mutations in miRNA genes or in regions that regulate their transcription can lead to either overexpression or downregulation of specific miRNAs. For instance, mutations in Drosha or Dicer cleavage sites can impair or alter the precision of cleavage affecting the balance of isomiRs or creating new ones (Tomasello, Distefano, Nigita & Croce, 2021). Furthermore, seed region mutations can prevent proper target recognition or lead to the recognition of new targets (Galka-Marciniak, *et al.,* 2019). Environmental factors, such as hypoxia, inflammation, or exposure to certain drugs or toxins, can also induce changes in miRNA expression (Miguel, *et al.,* 2018). Additionally, variations in the 3' UTR regions of target genes, can create or disrupt miRNA binding sites, altering miRNA-target interactions and the downstream regulatory effects (Yuan & Weidhaas, 2019). Together, these various mechanisms contribute to the dynamic regulation of miRNA expression and their functional outcomes in different biological processes and cancer states.

1.3.3.1. Dysregulated miRNAs in GB

Many miRNAs are involved in key pathways in GB biology, including tumour formation, immune evasion, rapid growth, vascularisation, cell diversity, stem-cell-like cell formation, and chemoresistance (Figure 8). MiRNAs exhibit pleiotropic effects: one miRNA can modulate multiple targets, and one target gene may be regulated by several miRNAs simultaneously (Yang, *et al.,* 2018). This property could be employed to identify key miRNAs in cancer with significant effects on the transcriptional regulatory network. There are two general classes of miRNAs in cancer: oncomiRs and tumour suppressors (Svoronos, Engelman & Slack, 2016). OncomiRs, often upregulated in GB, promote tumorigenesis, cell growth, survival, and immune evasion and should be downregulated as a therapeutic strategy. Tumour suppressor miRNAs, which inhibit tumour growth and are downregulated in GB, should be overexpressed for therapeutic benefits. High throughput sequencing techniques have been utilised in studying the expression patterns of miRNAs in GB. MiRNAs like miR-9, miR-10b, miR-15a, miR-16, miR-17, miR-19a, miR-20a, miR-21, miR-25, miR-28, miR-93, miR-130b, miR-140, and miR-210 have been identified as upregulated in both GB cell lines and clinical samples of grade II gliomas progressing to grade IV secondary GB (Valle-Garcia, *et al.,* 2024). Conversely, miR-7, miR-29b, miR-32, miR-34, miR-181 family members, miR-184, and miR-328 are among the downregulated miRNAs in GB progression (Valle-Garcia, *et al.,* 2024). These changes in

miRNA expression significantly impact GB hallmarks such as proliferation, angiogenesis, immune evasion, resistance to cell death, metastasis, and the development of chemoresistance, through their regulation of target genes.

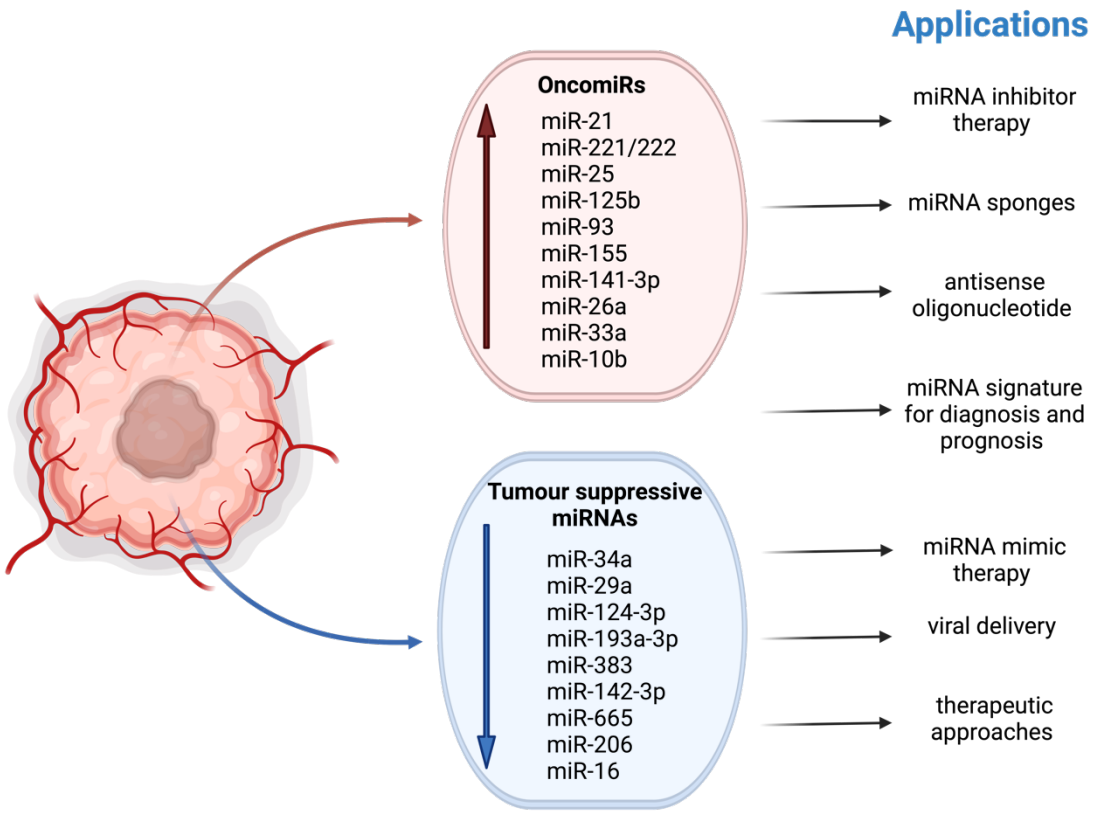


Figure 8. Examples of some commonly overexpressed and under-expressed miRNAs in GB. OncomiRs are upregulated miRNAs that can promote tumorigenesis, cell growth, survival, and immune evasion and should be downregulated as a therapeutic strategy. Conversely, tumour suppressor miRNAs can inhibit tumour growth and should be overexpressed for therapeutic benefits. Designed using BioRender: https://biorender.com.

1.3.3.2. Overexpressed miRNAs in GB

The identification of miRNA signatures in primary brain tumours has opened new avenues for GB diagnosis, prognosis, and patient monitoring. Among the well-studied miRNAs with diagnostic, prognostic, and potential therapeutic significance in high-grade GBs are miRNA-21, miRNA-10b, miR-221, and miR-222.

MiR-21, which is aberrantly expressed in many cancer types such as colorectal, lung, pancreas, leukaemia, and GB, is located within the vacuole membrane protein 1 (*VMP1*) locus on chromosome 17 (Cheng & Zhang, 2010). The mature miR-21 is transcribed from two primary miRNAs of approximately 3.5kb and 4.3kb in size. MiR-21 plays a crucial role in the tumorigenesis of GB, and its diagnostic and prognostic properties are well characterised. Post-

tumour resection, miR-21 levels significantly decrease, making it a useful biomarker for monitoring patients and detecting early relapse (Qu, Guan & Liu, 2015). High miR-21 levels in blood samples correlate with a poor prognosis for GB patients, as miR-21 downregulates insulin-like growth factor-binding protein 3 (IGFBP3) and other caspases, inhibiting programmed cell death (Yang, *et al.,* 2014a). The upregulated profile of miR-21 across various cancers highlights its potential role as an oncomiR. Extracellular miR-21 has been validated as a diagnostic biomarker for GB, with previous research showing high accuracy and specificity in predicting GB (Bautista-Sánchez, *et al.,* 2020). The distinctive properties of miR-21 in gliomas differentiate it from other brain tumours, a finding demonstrated by Ivo D'Urso and colleagues, who reported a 90% sensitivity and 100% specificity for miR-21 and miR-16 (Ivo D'Urso, *et al.,* 2015). MiR-21's diagnostic relevance in CSF is linked to its action on the TGF-β/Smad3 signalling pathway (Qu, *et al.,* 2016). However, CSF sample screening poses challenges and potential complications. Elevated miR-21 levels have also been detected in plasma samples from GB patients, indicating increased expression.

Another miRNA with high oncogenic potential in GB is miR-10b, which is virtually undetectable in normal brain tissue but abundantly expressed in low- and high-grade brain tumours (Liang, Han & Guo, 2020). Located within the *HOXD* genomic locus, miR-10b participates in pathways associated with the proliferation, invasion, and metastasis of malignant GB (Teplyuk, *et al.,* 2015). Although dysregulated in various tumours, including ovarian and gastric, miR-10b regulation appears cell- and context-specific (Fasoulakis, *et al.,* 2023; Liu, Shi, Liu, Li & Xu, 2021a). High miR-10b levels in the serum of GB patients' post-bevacizumab therapy indicated its potential as a prognostic marker (Sufianov, Begliarzade, Ilyasova, Liang & Beylerli, 2022). A negative correlation has been observed between high miR-10b/miR-21 levels and GB size. This was not observed in patients treated with TMZ. Thus, miR-10b, combined with miR-21, could be used to monitor bevacizumab-treated patients (Buruiană, *et al.,* 2020). MiR-10b is specifically detectable in the CSF of advanced and metastatic brain tumour patients, whereas miR-21 is expressed in various cancer types and normal brain tissue, lacking exclusive specificity for GB (Teplyuk, *et al.,* 2012). Remission in GB patients showed low or absent miR-10b and miR-21 levels, with increases during relapse, suggesting their combined use as monitoring and prognostic biomarkers for advanced GB.

The miR-221/222 cluster is associated with GB infiltration and poorer survival. The gene cluster encoding miR-221/222, located on chromosome X (Xp11.3), is highly conserved in

vertebrates, sharing an identical seed region (Di Martino, *et al.,* 2022). Previous research has demonstrated significantly high plasma levels of miR-221/222 in glioma patients, correlating with poorer survival rates in 95% of the patient cohort (Song, He, Zhang & Xu, 2020a). These miRNAs promote cell cycle progression and inhibit apoptosis, with miR-221/222 directly targeting the 3' UTR regions of *p27* and *p57*, reducing their expression and enhancing cell proliferation (Song, *et al.,* 2019). They also regulate glioma cell invasion via the tissue inhibitor of metalloproteinase 3 (*TIMP3*). Knockdown studies in xenograft models showed normal *TIMP3* levels restoration and reduced tumour growth (Zhang, *et al.,* 2012). The cluster could serve as a therapeutic agent by increasing radiosensitivity in GB cells through PTEN-independent Akt pathway activation. Post-radiotherapy, low *PTEN* levels suggested that miR-221/222 could inhibit GB growth post-radiation (Song, Zhang, He & Xu, 2020b). The prognostic and therapeutic significance of miR-221/222 in high-grade gliomas is strengthened by their interactions with tumorigenic genes such as *TIMP3, p27, p53,* and *PTEN*.

1.3.3.3. Downregulated miRNAs in GB

MiRNAs offering potential for diagnostic, prognostic, and therapeutic applications also include miR-128, miR-34, and miR-7. These miRNAs are downregulated in GB patients and function as tumour suppressors.

MiR-128, a brain-enriched intronic miRNA, is encoded by *miR-128-1* and *miR-128-2*, located on chromosomes 2q21.3 and 3p23.p, respectively (Lanza, Cuzzocrea, Oddo, Esposito & Casili, 2023). Normal expression of miR-128 is crucial for brain development (Franzoni, *et al.,* 2015). However, assays using quantitative real-time polymerase chain reaction (RT-qPCR), and western blot analyses showed that miR-128 was downregulated in aggressive brain tumours, such as GB and MB, compared to adjacent normal brain tissue (Novakova, Slaby, Vyzula & Michalek, 2009). When overexpressed, miR-128 inhibits proliferation, influences apoptosis and drug resistance, regulates epithelial to mesenchymal transition, and prevents tumour cell invasion and motility (Banelli, *et al.,* 2017). Previous research has demonstrated the high analytical specificity and sensitivity of miR-21 and miR-128 as diagnostic markers for GB (Bautista-Sánchez, *et al.,* 2020). The significant downregulation of miR-128 was observed in the peripheral blood of 20 GB patients, with an accuracy of 81% and sensitivity and specificity of 79% and 81%, respectively (Roth, *et al.,* 2011). However, the small sample size necessitates further validation in a larger cohort. Overexpression of miR-128a led to inhibit GB

development by promoting apoptosis in the U87MG GB cell line, although its exact molecular mechanism remains unclear (Nie, *et al.,* 2015). MiR-128a expression varies in different cancers, suggesting distinct roles in cancer development. For instance, miR-128a is overexpressed in acute lymphoblastic leukaemia (Mendiola-Soto, *et al.,* 2023). Previous study has demonstrated that miR-128a targets the polycomb complex protein BMI1 and E2F transcription factor 3 (E2F3), inhibiting GB cell proliferation by targeting *E2F3a* (Makowska, Smolarz & Romanowicz, 2023). Thus, miR-128a possesses diagnostic and therapeutic potential for GB management.

In addition, miR-34a has emerged as a potential therapeutic agent for GB patients. Located on chromosome 1p36, miR-34a is encoded by its own two highly conserved transcripts (Li, *et al.,* 2009). This miRNA acts as a tumour suppressor via the p53 pathway, with *p53* binding sites in its gene promoters (Navarro & Lieberman, 2015). Lower miR-34a levels have been identified in patients with mutated *p53* compared to wild-type *p53* GB samples (Gao, Zhao & Xiang, 2013). Gao and colleagues also reported significantly lower levels of miR-34a in high-grade gliomas compared to adjacent normal brain tissue, suggesting its potential as a diagnostic and predictive biomarker for GB. The downregulation of miR-34a in GB correlates with poorer prognosis and is associated with the expression of oncogenes such as *CDK6, Notch1*, and *Notch2*. The Notch signalling pathway relies on Jagged protein receptors, such as Jagged1, encoded by the jagged 1 (*JAG1*) gene, which has a prognostic value for GB (Hai, *et al.,* 2018). Overexpression of the oncogene *CDK6* is observed in brain tumours, particularly in advanced stages of GB (Li, *et al.,* 2017). MiR-34a, when overexpressed *in vitro,* can induce apoptosis and inhibit proliferation in GB cell lines, highlighting its therapeutic potential in targeting aberrant genes like *JAG1* and *CDK6* to restore normal cellular processes (Li, Ren & Tang, 2014).

MiR-7 is another miRNA downregulated in GB tissues. It is encoded by *miR-7a-1, miR-7a-2,* and *miR-7b* on different chromosomes, with identical mature sequences (Zhao, *et al.,* 2015). MiR-7 is highly expressed in normal brain tissue and plays significant roles in various physiological and pathological processes (Zhao, *et al.,* 2020). When overexpressed, miR-7-5p inhibited GB cell migration and invasion by targeting the special AT-rich sequence binding protein (SATB1) (Yin, Kong, Jiang, Xu & Zhao, 2019). Yin and colleagues demonstrated the suppressive effect of miR-7-5p on *SATB1* in U87MG and U373 GB cell lines, resulting in reduced cell migration and invasion. Immunohistochemical analysis of 122 glioma samples

indicated significant expression of phosphorylated SATB1 in high-grade gliomas, correlating with poorer OS (Yin, *et al.,* 2019). MiR-7-5p's suppressive effect on *SATB1* provides a potential therapeutic pathway. Delivery of miR-7-5p in DNA-cationic liposome complexes to GB cells significantly inhibited growth and metastasis *in vivo* (Wang, *et al.,* 2013). MiR-7 also antagonises the epidermal growth factor receptor (EGFR), inhibiting downstream effectors such as ERK, Akt, and Stat3, leading to enhanced apoptosis and reduced proliferation and migration in GB cells (Liu, *et al.,* 2014). Thus, the low levels of miR-7 in GB highlight its potential in targeted therapies for GB patients.

1.3.4. MiRNAs as diagnostic biomarkers for GB

MiRNAs possess the ideal biomarkers' properties for GB due to their stability in biological fluids, tissue-specific expression patterns, and ability to regulate multiple genes involved in tumour progression (Huang, Ali, Zhong & Shi, 2018). MiRNAs can reflect the molecular heterogeneity of GB, capturing the dynamic changes within the tumour microenvironment (Suzuki, Katsura, Matsuyama & Miyazono, 2015). Moreover, their differential expression profiles between normal and tumour tissues make them highly specific for identifying disease states, monitoring treatment responses, and predicting patient outcomes, enhancing their utility in personalised medicine (Nikolova, *et al.,* 2024). Previous studies have demonstrated that miRNA expression in GB tumour tissues significantly differs from that in normal control tissues (Kim, *et al.,* 2011; Parker, *et al.,* 2013). Extensive research has been conducted on various miRNAs that are dysregulated in GB. Patients exhibiting different miRNA expression patterns often have distinct prognoses and respond differently to treatments (Malzkorn, *et al.,* 2010). Consequently, miRNAs may serve as valuable tools for classifying, diagnosing, and predicting the clinical outcomes of brain tumour patients. Moreover, miRNAs are considered ideal biomarkers for GB due to their stability, tissue specificity, and involvement in regulating key pathways associated with tumour growth, progression, and resistance to therapy (Buruiană, *et al.,* 2020). They are highly conserved and can be easily detected in bodily fluids making them accessible through non-invasive methods (Condrat, *et al.,* 2020) This makes them particularly useful for monitoring tumour progression and response to treatment over time. However, as of now, no miRNAs have been officially approved as diagnostic biomarkers for GB by regulatory agencies such as the U.S. Food and Drug Administration (FDA) or European Medicines Agency (EMA). This is due to the need for them to be verified in a large pool of prospective studies to ensure their reliability, consistency, and clinical utility before being

considered for regulatory approval as diagnostic biomarkers for GB (He, Jiang, Liu, Zuo & Zeng, 2021).

1.4. Liquid Biopsies

For diagnosing many diseases and conditions, especially cancers, the initial step often involves obtaining a tissue biopsy. By examining the tissue biopsy, medical professionals can detect abnormal cells and determine disease severity, prognosis, and appoint an appropriate treatment strategy (Connolly, *et al.,* 2003). Despite the existence of various biopsy methods, most are considered painful and highly invasive, often requiring surgery. For instance, obtaining biopsies for GB involves a surgical procedure called a stereotactic biopsy, where a small tissue sample is resected from the brain using a precisely guided needle (Lim, Kim, Na & Cho, 2023). The employment of this invasive procedure is necessary due to the tumour's location within the brain, often requiring careful planning and execution to minimise risks and ensure accurate diagnosis of the patient (Wick& Platten, 2018). As an alternative to tissue biopsies, liquid biopsy assays could detect biomarkers in biological fluids. Liquid biopsies allow for the analyses of various fluids, including blood, saliva, urine, sweat, and CSF, for biomarkers associated with different diseases (Connal, *et al.,* 2023). By focusing on fluids rather than tissue samples, liquid biopsies offer a less invasive method for disease detection and monitoring, significantly improving patient comfort and clinical outcomes (Figure 9).

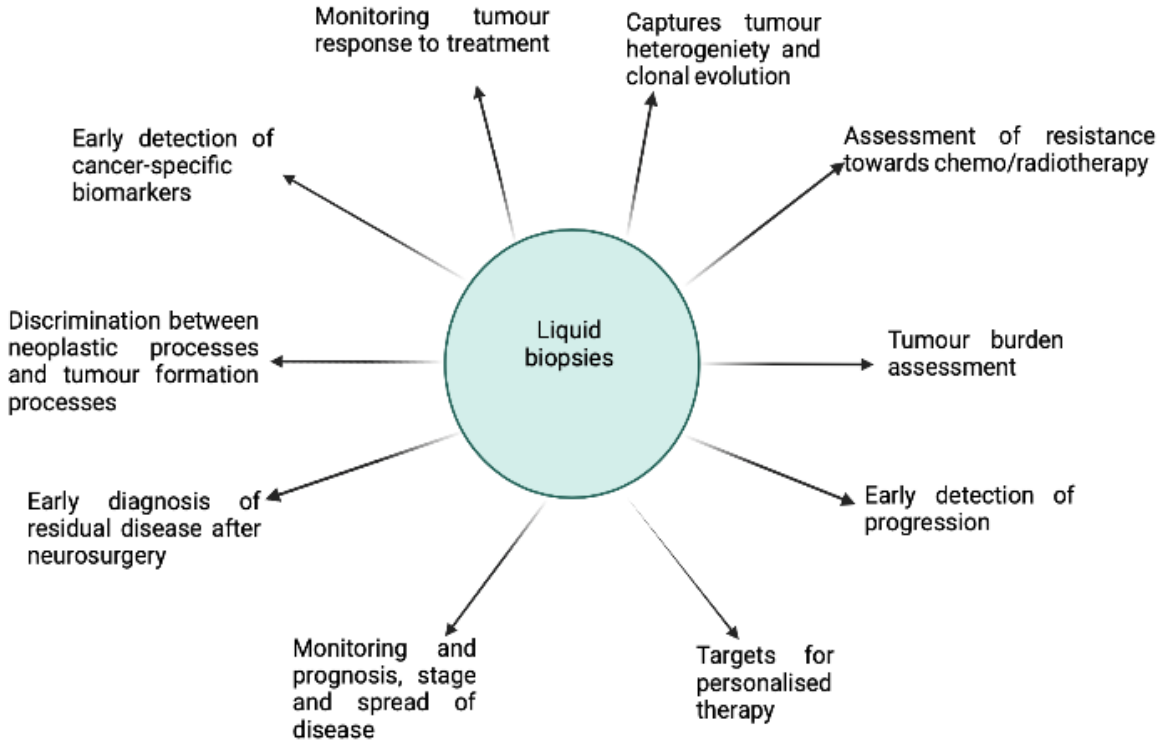


Figure 9. Benefits of liquid biopsies in their use of cancer monitoring. Molecular biomarkers found in liquid biopsies could aid in understanding various stages of cancer development, monitoring, progression, and response to treatment in individual patients. Designed using BioRender: https://biorender.com.

1.4.1. Liquid biopsies versus tissue biopsies

Cancer diagnosis involves sampling a section of tumour tissue for histological analysis, which is typically invasive and painful, often requiring anaesthesia and recovery time. In contrast, liquid biopsies, such as blood tests, are minimally invasive and useful for tumours in difficult-to-sample locations, such as GB (Lone, *et al.,* 2022). Due to the invasive nature of many cancers, tissue biopsies can only be performed a limited number of times, posing challenges for analysing metastatic cancer or relapse. Multiple surgeries are often not feasible due to cancer progression, patient condition, and tissue availability (Brennan, *et al.,* 2021). Liquid biopsies address this issue by enabling ongoing biomarker analysis throughout diagnosis and treatment without compromising patient safety (Ju, *et al.,* 2022). Furthermore, tumours can change over time, especially in response to treatment. These changes can be detected in real time through serial liquid biopsies. For example, a study on breast cancer patients showed that minimal residual disease (MRD) could be detected four years before clinically detectable metastatic condition appeared (Stergiopoulou, *et al.,* 2023). Liquid biopsies facilitate real-time prognosis prediction, drug resistance identification, and MRD assessment. Although not yet

widely available in clinics, initial studies have suggested that liquid biopsy results have a faster turnaround time compared to tissue biopsies. For instance, a study in NSCLC patients found that liquid biopsy next-generation sequencing (NGS) results were returned an average of 26.8 days faster than tissue biopsy results (Raez, *et al.,* 2023). Faster results can lead to reduced time-to-treatment and improved survival outcomes. Additionally, liquid biopsies can investigate the genetic makeup of tumour cells over time and across different locations (Gilson, Merlin & Harlé, 2022). By analysing tumours from metastatic sites, molecular alterations in clones from various spatially distinct tumour sites can be detected. Serial liquid biopsies also track tumour heterogeneity over time. An example is the TRACERx Lung study, where circulating tumour DNA (ctDNA) analysis in NSCLC patients was used to create phylogenetic profiles of cancer evolution (Abbosh, *et al.,* 2017). Table 2 summarises the ongoing and completed studies from various countries that have investigated the clinical use of liquid biopsy for GB, focusing on the detection of ctDNA, circulating tumour cells (CTCs), and other biomarkers, as well as their potential in improving diagnosis, monitoring, and treatment outcomes.

Table 2. Summary of ongoing and completed liquid biopsy studies for GB (Eibl & Schneemann, 2023, modified).

Study	Location	Participants	Study Focus	Trial ID
UCLA Interventional Study (2020-2024)	California, USA	Recurrent GB patients	Monitoring liquid biopsy gene expression signature from peripheral blood before/after treatment.	NCT04201873
Tessa Jowell BRAIN MATRIX Study (2020-2025)	UK	1,000 glioma patients (grades 2-4)	Matching tumour and blood, but not CSF, for targetable mutations.	NCT04274283
CircTeloDIAG Study (2021-2024)	Lyon, France	150 patients (gliomas grades 2-4)	Detecting *IDH, TERT,* and *ATRX* mutations in blood ctDNA (also CTCs) liquid biopsies for diagnosis and monitoring of relapse.	NCT04931732
PLANET Study (2021-2025)	France	500 advanced GB and chronic lymphocytic leukaemia patients	Sequential analysis of tumour and liquid biopsy ctDNA before/after chemotherapy.	NCT05099068

Paediatric CNS Tumours Study (Pagès, *et al.*, 2022)	France	258 paediatric high grade glioma tumours	Children with brain tumours have low levels of ctDNA in blood, CSF, and urine, making molecular profiling feasible only in a small subset of high-grade tumours.	-
Microbubble Resonator Study (2022-2023)	USA	57 GB patients	Monitoring cfDNA before/after BBB disruption using microbubble resonator.	NCT05383872
CTC Antigen Profile Study (2009-2013)	USA	130 GB patients	Investigating CTC antigen profiles with a cluster of differentiation signature.	NCT01135875

1.4.2. Types of liquid biopsies

Most liquid biopsy assays typically involve a standard blood test, requiring only a small volume of blood for analysis (Figure 10). Blood samples, when processed via ultracentrifugation, are separated into their components: serum (or plasma), white blood cells and platelets, and red blood cells. These components can then be further analysed to isolate and quantify the biomarkers of interest (Connal, *et al.,* 2023). Furthermore, saliva presents clear advantages for liquid biopsy tests as it can be collected from nearly all patients regardless of age, health complications, or disease progression (Patel, Patel, Patel & Tanavde, 2022). Additionally, no specialist equipment or training is necessary, reducing the cost and complexity of sampling. Saliva-based liquid biopsies have shown considerable promise in detecting head and neck cancer (HNC) (Patel, *et al.,* 2022). Like blood-based assays, saliva liquid biopsies can detect ctDNA, CTCs, extracellular vesicles (EVs), and metabolites that provide information for the diagnosis, prognosis, and treatment of patients (Wang, *et al.,* 2024). In 2021, Viome, a biotech company, received approval for an early detection diagnostic liquid biopsy assay for oral and throat cancer (Queensland University of Technology, 2021). Additionally, urine, like saliva, is another non-invasive and easily sampled fluid. It can be collected more frequently and in larger quantities than blood, allowing for sample concentration through centrifugation (Salfer, Li, Wong & Zhang, 2022). Although urine-based liquid biopsies have shown promising results in detecting various conditions, including cancer, the number of FDA and EMA liquid biopsy

trials using urine is relatively low, with only 20 trials compared to over 400 for blood plasma cfDNA in 2022 (Salfer, *et al.,* 2022). On the other hand, CSF sampling is more invasive than saliva and urine collection, usually requiring a lumbar puncture. However, given the lack of effective blood-based liquid biopsy assays for brain tumours and neurological malignancies, such as GB, CSF assays may offer a promising alternative (Friedman, Hertz, Karajannis & Miller, 2022). Cerebrospinal fluid provides several advantages over traditional blood testing. CtDNA is enriched in CSF compared to plasma, resulting in higher concentrations and improved detection rates for brain cancers. Consequently, ctDNA genetic aberrations can be detected more readily than in plasma without requiring high sequencing read depth (Hickman, Miller & Arcila, 2023). Overall, due to the ease of sampling and reduced invasiveness, liquid biopsy assays are considered the future of cancer screening, with some assays capable of detecting up to 50 different cancer types simultaneously (Connal, *et al.,* 2023).

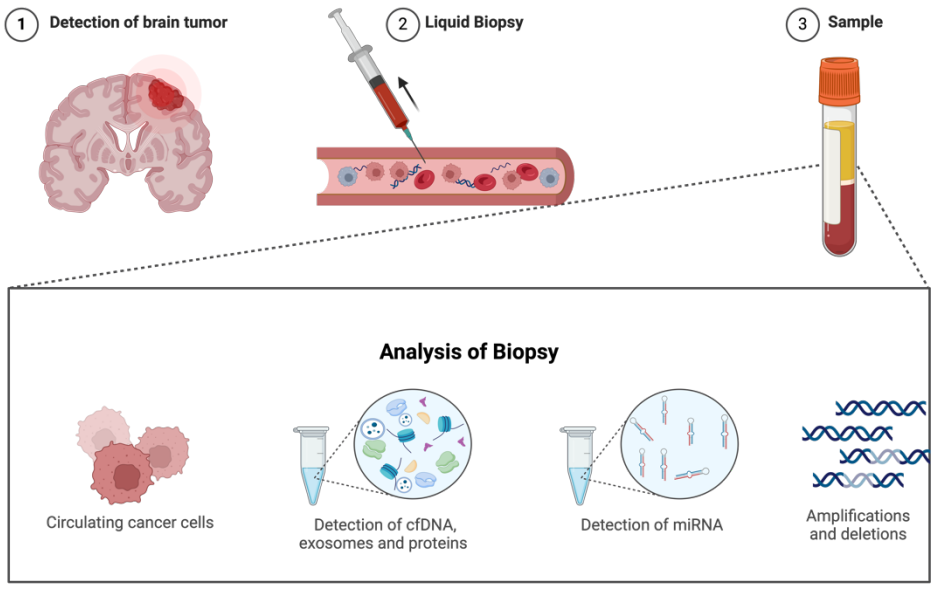


Figure 10. The use of liquid biopsies in GB management. Liquid biopsies provide a non-invasive method for GB management by analysing circulating tumour cells and DNA, proteins, exosomes, and miRNAs in body fluids such as blood and CSF. This technique enables real-time monitoring of tumour dynamics, detection of genetic mutations, and assessment of treatment response. Designed using BioRender: https://biorender.com.

1.4.3. Types of liquid biopsy biomarkers

1.4.3.1. Cell-free DNA

Cell-free DNA has become one of the most prominent biomarkers in liquid biopsies. CfDNA refers to any extracellular nucleic acid found in circulation, released from either tumour or non-

cancerous cells, and can be detected in various bodily fluids, including CSF, pleural fluid, urine, saliva, and blood plasma (Yan, *et al*., 2021) CtDNA, a subset of cfDNA, is particularly significant for cancer detection. The release of DNA from tumour cells was first documented in 1977 when researchers observed elevated free DNA levels in the blood serum of cancer patients (Leon, Shapiro, Sklaroff & Yaros, 1977). Subsequent analysis confirmed that this DNA originated from tumour cells and carried the genetic mutations characteristic of the tumour. These DNA alterations can now be identified and analysed using PCR and NGS technologies (Jee, *et al.,* 2022). Detection of ctDNA mutations is a major focus of many liquid biopsy studies. Besides point mutations, various properties of ctDNA, such as methylation patterns and fragmentation length, have clinical applications in oncology (Kirchweger, Wundsam & Rumpold, 2022). Analysis of ctDNA levels and mutations plays numerous clinical roles, including predicting survival, allowing for targeted therapy, and monitoring drug resistance (Cao, *et al.,* 2020).

1.4.3.2. Circulating Tumour Cells

Circulating tumour cells are another widely analysed biomarker in cancer-related liquid biopsies. Like ctDNA, CTCs originate from tumours and circulate in the blood, providing crucial information about cancer heterogeneity and evolution (Chudasama, *et al.,* 2019). While both ctDNA and CTCs come from tumours, the information obtained from their analysis can vary significantly. Importantly, analysing CTCs offers genetic, transcriptomic, and proteomic data at single-cell resolution. This detailed information serves as biomarkers for diagnosis, prognosis, and therapy monitoring in many solid cancers (Lin, *et al.,* 2021). Despite the benefits of CTC analysis, enriching and isolating this biomarker is technically challenging due to the low number of CTCs in patient blood samples, ranging from 1 to 100 cells per millilitre of peripheral blood (Ju, *et al.,* 2022). Additionally, CTCs are heterogeneous, expressing various surface protein markers, which complicates their isolation.

1.4.3.3. Extracellular vesicles

Extracellular vesicles are cell-derived granules secreted into the extracellular environment, playing a crucial role in cell-to-cell signalling processes (Robinson, *et al.,* 2024). Their main function is to deliver cellular cargo to recipient cells, which includes nucleic acids (such as mRNA and non-coding RNAs), proteins, lipids, and metabolites (Irmer, Chandrabalan, Maas, Bleckmann & Menck, 2023). A notable subset of EVs are exosomes, small vesicles that facilitate long-distance intercellular communication. As carriers of biomolecules, EVs

circulating in bodily fluids are prime targets for liquid biopsy analysis (Yu, *et al.,* 2022). There is growing interest in EV biomarkers for various diseases, including cancer, CNS-related pathologies, and infectious diseases (Monteiro-Reis, *et al.,* 2021). Extracellular vesicles also play a key role in intercellular communication within the TME by delivering various molecular cargos to nearby and distant cells, influencing processes such as angiogenesis, immune suppression, invasion, and drug resistance. They reflect the phenotype of the TME, making them potential biomarkers for diagnosis, prognosis, and treatment monitoring (Simon, Jackson & Giamas, 2020). Additionally, EVs can cross the blood-brain barrier, offering potential for drug delivery in GB therapy. EV-based liquid biopsies provide extensive information beyond genomic alterations, with miRNA biomarkers showing promise in predicting cancer progression (Irmer, *et al.,* 2023). Compared to CTCs, EVs are significantly more abundant (~10^9 particles per mL) and more stable due to their lipid bilayer, which allows them to survive in harsh conditions. This abundance and stability make EVs a valuable resource for disease biomarker analysis (Liu, *et al.,* 2021b).

1.4.3.4. Proteins

Proteins represent another promising target for liquid biopsy, serving as a readout of cellular activity. Similar to nucleic acids, protein biomarkers can be found in circulation or within circulating cells and EVs. Protein biomarkers have shown useful applications for the identification of various diseases (Ding, Wang, Ji & Chen, 2022). Hundreds of protein biomarkers have been approved by the FDA for clinical diagnostic use, such as prostate-specific antigen (PSA) for prostate cancer and carbohydrate antigen 125 (CA 125) for ovarian cancer (Ding, *et al.,* 2022). Furthermore, analysis of EV protein content has revealed new biomarkers associated with several neurodegenerative conditions, including Parkinson's disease, amyotrophic lateral sclerosis (ALS), and multiple sclerosis (MS) (Malhotra, Miras, Pappolla, Montalban & Comabella, 2023). Despite its potential, progress in the proteomics field has lagged compared to other liquid biopsy biomarkers. This delay may be attributed to the vast and dynamic nature of the proteome, which continuously changes in response to cellular demands (Armakolas, Kotsari & Koskinas, 2023).

1.4.3.5. Liquid biopsy-based miRNAs

MiRNAs have emerged as promising biomarkers for liquid biopsy due to their stability in bodily fluids, such as blood and CSF. Once isolated, the miRNAs are quantified and analysed using techniques like RT-qPCR, NGS, or microarray analysis. These methods allow for the

precise measurement of miRNA expression levels, which can then be correlated with GB-specific signatures (Garcia & Toms, 2020). MiRNAs offer several advantages as liquid biopsy biomarkers in GB. Firstly, their stability in circulation makes them suitable for non-invasive testing, which is crucial for a disease where traditional biopsy methods are highly invasive and risky (Condrat, *et al.,* 2020). MiRNAs can reflect the tumour's genetic and epigenetic alterations, providing a real-time snapshot of the disease state (Condrat, *et al.,* 2020). Specific miRNAs, such as miR-21, miR-221/222, and miR-10b, have been found to be dysregulated in GB and can serve as diagnostic and prognostic markers as outlined in section 1.3.3.2. Moreover, miRNAs can provide insights into treatment response and resistance. For example, changes in miRNA expression levels after therapy can indicate the effectiveness of the treatment and the likelihood of recurrence (Cervena, *et al.,* 2021). Additionally, targeting specific miRNAs therapeutically offers a new avenue for treatment, as modulating miRNA levels can influence tumour growth and progression (Valle-Garcia, *et al.,* 2024).

1.5. miRNAs as therapeutics

Mature miRNAs regulate gene expression in the cytoplasm and targeting steps in their biogenesis pathway could yield promising therapeutic agents in the treatment of GB. However, miRNA processing in GB remains underexplored, and no strategies currently exist to modify any step of their biogenesis pathway (Valle-Garcia, *et al.,* 2024). Current evidence suggests that miRNA dysregulation may be a causal factor rather than a consequence of cancer, as shown in both *in vitro* and *in vivo* models and large patient cohorts (Iorio, & Croce, 2012). Therapeutically, miRNAs can be modulated using mimics to restore the function of downregulated tumour-suppressive miRNAs or inhibitors to silence oncogenic miRNAs (Figure 11). This targeted approach offers an alternative mechanism to interfere with critical pathways involved in GB progression, potentially enhancing the efficacy of existing treatments and improving patient outcomes (Kim & Croce, 2023).

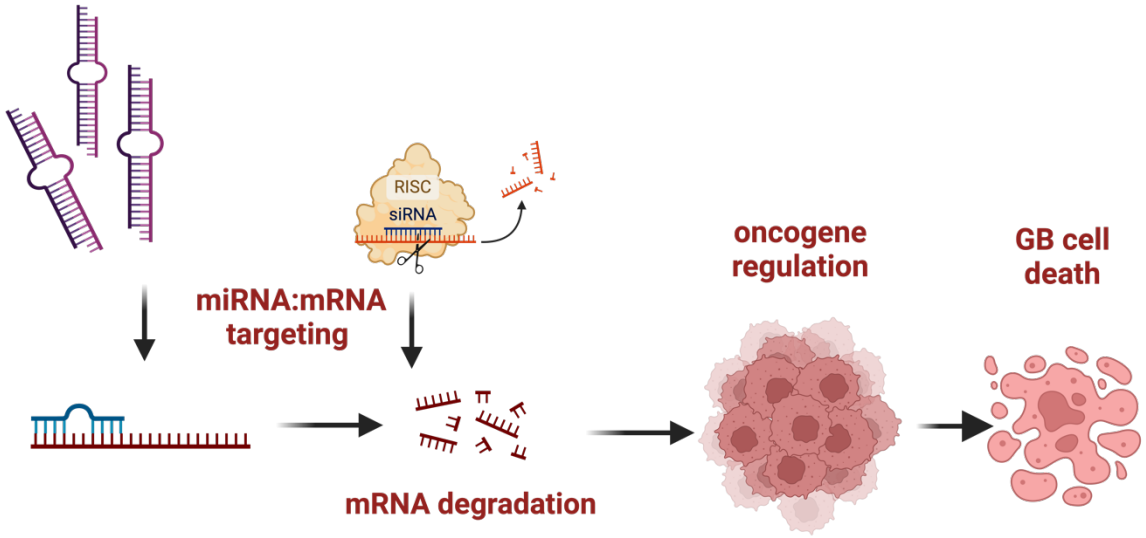


Figure 11. Therapeutic applications of miRNAs. MiRNAs bind to complementary sequences on target mRNAs, leading to mRNA degradation or inhibition of translation. This regulation can downregulate the expression of oncogenes. By inhibiting oncogene expression, miRNAs play a crucial role in controlling cell proliferation, differentiation, and apoptosis, thus acting as tumour suppressors and contributing to cancer prevention. Designed using BioRender: https://biorender.com.

A single miRNA can act as an oncomiR or tumour suppressor depending on the cellular context, making it essential to understand its role and effects in specific contexts for effective therapeutic targeting (Svoronos, *et al.,* 2016). To alter miRNA expression, synthetic mimics can enhance miRNA levels, delivered as double- or single-stranded RNA molecules or vectors containing natural or synthetic miRNA precursors (Lam, Chow, Zhang & Leung, 2015). To decrease miRNA expression, antagomiRs (antisense oligonucleotides) or miRNA sponges can be used. AntagomiRs are RNA molecules designed to complement miRNA sequences, sequestering miRNAs without degradation due to their enhanced stability (Stenvang, Petri, Lindow, Obad & Kauppinen, 2012). MiRNA sponges are circular RNAs with multiple miRNA binding sites, sequestering miRNAs and allowing original targets' expression (Sakshi, Jayasuriya, Ganesan, Xu & Ramkumar, 2021). Circular RNAs (circRNAs) contain multiple binding sites for specific miRNAs allowing them to sequester and inhibit these miRNAs, preventing them from binding to their target mRNAs (Sakshi, Jayasuriya, Ganesan, Xu & Ramkumar, 2021). This reduces the miRNA's ability to downregulate its target genes, thereby influencing gene expression. By modulating miRNA activity, circRNAs can indirectly control various cellular processes, such as proliferation, apoptosis, and differentiation (Ikeda, *et al.,*

2023). Sponges can target several miRNAs if different miRNA target sequences are included but are technically more challenging to produce and deliver than small single-stranded RNAs. Table 3 outlines the miRNAs that have been involved, are currently undergoing, or are in the preclinical stages of clinical trials for cancer therapy.

Table 3. MiRNAs in clinical trials for cancer therapies (Kim & Croce, 2023, modified).

miRNA	Drug Name	Drug Type	Phase	Status	Description
miR-16 NCT02369198 (van Zandwijk, *et al.*, 2017)	TargomiR	Double stranded synthetic mimic	Phase I	Completed	A Phase I study of TragomiRs as 2nd or 3rd line treatment for **malignant pleural mesothelioma and non-small cell lung cancer**
miR-155 NCT02580552 (Anastasiadou, *et al.*, 2021)	Cobomarsen	Locked nucleic acid inhibitor	Phase I	Phase I - Completed	A Phase I study of safety, tolerability and pharmacokinetics of Cobomarsen (MRG-106) in patients with **cutaneous T-cell lymphoma, mycosis fungoides, and chronic lymphocytic leukaemia**
miR-34a NCT01829971 (Hong, *et al.*, 2020)	MRX34	Double stranded mimic	Phase I	Phase I – Terminated	A Phase I study of miR-RX34 liposomal injection **primary liver cancer, lymphoma, melanoma, multiple myeloma, renal cell carcinoma, and non-small cell lung cancer**
miR-10b (Ghosh, *et al.*, 2023)	TTX-MC138	AntagomiR	Preclinical	-	A preclinical study of TTX-MC138 for **metastatic breast cancer, glioblastoma, pancreatic cancer, small cell lung carcinoma, osteosarcoma**
miR-10b (Kim & Croce, 2023)	RGLS5579	AntagomiR	Preclinical	-	A preclinical study of RGLS5579 for **GB**
miR-193a-3p NCT04675996 (Yang, *et al.*, 2023)	INT-1B3	Mimic	Phase I	Recruiting	A Phase I study of INT-1B3 in patients with **advanced solid tumours**
miR-221 NCT04811898 (Tassone, *et al.*, 2023)	LNA-i-miR-221	AntagomiR	Phase I		A Phase I study of dose escalation of LNA-i-miR-221 in **multiple myeloma and advanced solid tumours**

1.5.1. Challenges associated with miRNA therapeutics

MiRNA-based therapeutics face several challenges, particularly due to their broad gene regulation, which can lead to off-target effects and associated toxicities (Segal & Slack, 2020). Since each miRNA can influence multiple genes and pathways, unwanted effects may occur in non-target tissues, as seen in the clinical trial of MRX34, which was terminated due to severe immune-related adverse effects (Arif, Elliott, Haupt & Griffiths, 2020). Additionally, miRNAs can have different functions across various cells within the TME, complicating therapeutic outcomes (Raue, Frank, Syed & Brüne, 2021). Delivery challenges are also an obstacle for the utilisation of miRNA therapeutics, with miRNAs potentially affecting unintended tissues and leading to unwanted side effects (Segal, *et al.,* 2020). Furthermore, the inherent complexity of miRNA regulation, where one miRNA can control multiple genes, and one gene may be regulated by multiple miRNAs, adds another layer of difficulty in predicting and managing therapeutic outcomes (Xu, *et al.,* 2020a). Immunogenic responses to viral delivery systems and other delivery vehicles, such as nanoparticles or artificial miRNAs, remain a concern (Dasgupta & Chatterjee, 2021). Despite these difficulties, miRNAs hold promise as therapeutic agents, especially if these challenges can be addressed through better delivery and precise targeting methods.

1.6. Aims and objectives

The aim of this research project was to identify liquid biopsy-based miRNA diagnostic biomarkers and evaluate new therapies for GB, in collaboration with the University of Ras Al-Khaimah in the United Arab Emirates (UAE). The primary objectives included:

1.6.1. Liquid biopsy-based miRNA diagnostic biomarkers

1. *In silico* analysis to identify the most dysregulated miRNAs in GB and their target genes.
2. Validation of the expression profiles of selected miRNAs and target genes in GB cell lines via RT-qPCR.
3. Validation of targeted proteins via western blotting and immunohistochemistry.
4. Assessing the expression of selected miRNAs and their target genes in highly malignant paediatric brain tumours, such as MBs.
5. Screening the miRNome and transcriptome of MB tumour samples.
6. Extraction of exosomes from GB patients and screening of the miRNome and proteome of these patient samples via sRNA-seq and proteomics, respectively.
7. Functional and *in vitro* assays to identify the mechanisms underlying selected miRNAs and their target genes and how they could act as alternative therapeutics for GB and MB tumours.
8. Overall data analysis and interpretation for the identification of new liquid-based miRNA GB diagnostic biomarkers and potential therapeutic targets.

1.6.2. GB alternative therapies

1. Synthesis of anticancer compounds and bioinformatic analysis of their biological significance.
2. sRNA-seq to assess their effects on the miRNome of GB cells.
3. Functional assays to evaluate their cytotoxic effects on GB cells.
4. Overall data analysis and interpretation to determine the therapeutic potential of natural and synthetic compounds.

Chapter 2. Identification of new miRNA biomarkers through bioinformatics

2.1. Introduction

Glioblastoma accounts for approximately 50% of all gliomas and 15% of all intracranial tumours and is characterised by a highly heterogeneous molecular profile (Delgado-Martín & Medina, 2020). The application of molecular profiles in the clinical diagnosis of GB is often challenging due to the tumour's dynamic microenvironment and its ability to transition between various molecular subtypes (Ramón Y Cajal, *et al.,* 2020). Current diagnostic methods rely primarily on MRI, but the use of MRI alone for definitive diagnosis can sometimes lead to inaccuracies (Bernstock, *et al.,* 2022). As a result, tissue biopsy is almost always required in the diagnostic process. However, this approach has significant drawbacks, including its invasive nature, the inability to monitor malignancy serially, tissue heterogeneity, and the potential risk of neurological damage (Kanderi, Munakomi & Gupta, 2022). In light of these challenges, research efforts are increasingly focusing on miRNAs as potential diagnostic and therapeutic tools.

In GB, specific miRNA profiles correlate with different stages of the tumour and could potentially help in defining its diagnosis, prognosis and therapeutic management (Shea, *et al.,* 2016). Several miRNAs with high diagnostic value for GB have been identified and discussed in Chapter 1, indicating that diagnosis could potentially be made based on miRNA levels in blood or cerebrospinal fluid (Ivo D'Urso, *et al.,* 2015). Functional analyses have suggested that GB-specific miRNAs can act as both oncogenes and tumour suppressors contributing to chemotherapy and radiotherapy resistance, promoting angiogenesis and proliferation, and regulating the cell cycle and apoptosis (Makowska, Smolarz & Romanowicz, 2023). While these findings emphasise the importance of miRNA expression in GB pathogenesis and offer promising diagnostic and prognostic applications, a complete understanding of the mechanisms by which miRNAs regulate cellular processes is still lacking, delaying their potential use as therapeutic targets (Sempere, Azmi & Moore, 2021).

The detection of miRNA dysregulation in primary brain tumours has opened new avenues for assessing diagnosis, prognosis, and patient monitoring (Nikolova, *et al.,* 2024). TargetScan is a database that is often employed to predict miRNA target sites, which is important for identifying potential interactions between miRNAs and their target mRNAs (Riolo, Cantara,

Marzocchi & Ricci, 2020). By locating miRNA binding sites in the 3'UTRs of mRNAs, TargetScan helps to understand the regulatory impact of specific miRNAs on gene expression (Riolo, *et al.,* 2020). Following target prediction, miRSystem is usually employed in pathway analysis by integrating multiple target prediction algorithms to assess the functional impact of miRNAs on biological pathways (Lu, *et al.,* 2012). This is regarded as a valuable tool for exploring how miRNAs influence complex cellular networks and contribute to various diseases, including GB. To enhance these predicted interactions, miRWalk and The Encyclopedia of RNA Interactomes (ENCORI) are utilised to explore miRNA expression profiles across different tissues and conditions, such as cancer versus normal tissues (Kariuki, *et al.,* 2023). These tools strengthen the reliability of predictions and ensure that the observed interactions are biologically relevant, advancing miRNA research toward clinical applications. Additionally, the software for statistical folding of nucleic acids and studies of regulatory RNAs (Sfold) contributes to the structural understanding of miRNA function by predicting the folding patterns of miRNAs and their interactions with target mRNAs (Long, Chan & Ding, 2008). These bioinformatics approaches are essential for understanding the complex role of miRNAs in GB and their potential use as diagnostic and therapeutic biomarkers.

In GB research, studying miRNA targets and their regulatory roles requires the integration of multiple databases that provide diverse types of data. Although our understanding of miRNA regulation in GB is growing, there is still much to be elucidated, and the development of robust bioinformatics tools is essential for advancing research in this area. While no single tool exists for comprehensive miRNA analysis, a reliable pipeline for studying GB dysregulated miRNAs could be established by using existing resources (Chen, *et al.,* 2019). Data sets for miRNA analysis can be obtained from public databases, and relevant literature can be retrieved from sources like PubMed (Chou, *et al.,* 2018). Expression data, including miRNA sequencing and miRNA microarrays are available from platforms such as The Cancer Genome Atlas (TCGA) (Tomczak, Czerwińska & Wiznerowicz, 2015). The Cancer Genome Atlas has been instrumental in advancing cancer research by providing comprehensive genomic profiles of over 30 tumour types through large-scale sequencing and multi-dimensional analyses (Tomczak, *et al.,* 2015). Its publicly available datasets have contributed to improving diagnostic methods and treatment strategies, as well as to understanding tumorigenesis across various cancers, including GB (Han & Puri, 2018). In addition to TCGA, the Human Protein Atlas (HPA) utilises some of the TCGA data, specifically RNA-sequencing information to enhance the understanding of protein expression across various cancer tissues, including

gliomas (Thul & Lindskog, 2018). On the other hand, the Allen Brain Atlas provides detailed gene expression data specific to the brain, offering further insights into how miRNAs might regulate genes in the brain (Gilbert, 2018). Thus, this tool aids in understanding the expression patterns of target genes across the brain and helps in elucidating the influence of miRNAs in specific brain regions.

Furthermore, comprehensive cancer transcriptomics data offered by the University of ALabama at Birmingham CANcer data analysis Portal (UALCAN) allows the exploration of the differentially expressed target genes across different cancer stages and patient subgroups (Chandrashekar, *et al.,* 2022). Consequently, this allows the identification of miRNA targets that are associated with poor prognosis or treatment resistance in GB. The Single Cell Portal provides an additional layer of insight by allowing the exploration of single-cell RNA sequencing data. This enables the identification of specific cell populations in the tumour that may be more influenced by miRNA regulation (Wang, *et al.,* 2019d). Additionally, the Xena Functional Genomic Explorer utilises multiple cancer genomics datasets, including TCGA that enable the study of the correlation between miRNA expression and genomic alterations in GB (Goldman, *et al.,* 2020). To facilitate the exploration of target protein interactions within a larger network, STRING protein-protein interaction analysis is usually performed. This leads to deeper insights into how miRNAs may affect not just individual proteins but entire signalling pathways in GB progression (Szklarczyk, *et al.,* 2019). Together, these databases provide a powerful framework for studying the role of miRNA targets in GB.

Validating miRNA biomarkers could represent a significant advancement in the identification and treatment of brain cancer, offering the potential to predict tumour behaviour and response to targeted therapies (O'Brien, *et al.,* 2018). However, their clinical adoption remains limited due to uncertainties in experimental findings, often restricted by the small number of patient samples used in research (Lam, Chow, Zhang & Leung, 2015). Despite these obstacles, combining different computational methods provides a reliable framework and valuable guidance in cancer research, offering important insights for the identification of new biomarkers and therapeutic targets.

2.1.2. Aims and research questions

2.1.2.1. Aims

The aim of this chapter was to utilise various miRNA-based analysis tools to identify the most dysregulated miRNAs in GB and subsequently determine their target genes. By integrating multiple bioinformatics approaches, we attempted to identify the most dysregulated miRNAs involved in GB progression and the pathways they regulate, providing potential for their utilisation as diagnostics, prognostics, or therapeutics.

2.1.2.2. Research Questions

1. Which miRNAs are most significantly dysregulated in GB compared to normal brain tissue, and what potential roles do they play in tumour development and progression?
2. What are the specific target genes of the identified dysregulated miRNAs in GB, and how these miRNA-mRNA target interactions could contribute to GB tumorigenesis?
3. Can the identified miRNA-target pathways serve as potential diagnostic or prognostic biomarkers and/or therapeutic targets for improving GB treatment outcomes?

2.2. Materials and Methods

2.2.1. *In silico* miRNA analysis

A comprehensive bioinformatic analysis was conducted to identify miRNAs with potential clinical relevance in the diagnosis, prognosis, and treatment of GB. The National Center for Biotechnology Information (NCBI) database was utilised in the identification of dysregulated genes associated with GB (www.ncbi.nlm.nih.gov). The keyword "glioblastoma" was typed in the search bar of the NCBI website. Once the result was generated, the option "gene" was selected. To generate a data table with all identified genes, the following steps were performed in the outlined order: select *Homo sapiens* organism → select "Send to" in the right top corner above the gene's table → select "File" → select "Download 2,084 items" → select format "Tabular (text)" → choose sort by "Relevance" → select "Create file". The gene selection process employed the "Popular" filter category, which included current Entrez Gene records, gene records annotated on RefSeq chromosome or contig accessions, gene records linked to gene-specific reports in dbSNP (variant (VAR)), and genes with entries in the ClinVar database. When the text file was downloaded, the data were transferred in an Excel file by performing the following: open Excel → select "Data" from the main tab menu → select "Get data" → select "Get data from text" → no other functions selected → press "Finish". The miRSystem database (http://mirsystem.cgm.ntu.edu.tw/index.php) (Lu, *et al.,* 2012) was then used to generate a report of miRNAs targeting the dysregulated genes in GB identified from the NCBI report by following the steps: select "Target genes to miRNAs" → paste the genes' names from the Excel file in the "Enter gene symbol" box → select species "Human" → press "Submit" → select "miRNA summary report" and download the report. To enhance the reliability of the results, the default parameter in miRSystem was set to three algorithm hits. Subsequently, the Kyoto Encyclopedia of Genes and Genomes (KEGG; https://www.genome.jp/kegg/pathway.html) was employed to analyse differentially expressed miRNAs and genes associated with GB and their role in tumorigenesis. The study included a sample size of 529 GB cases (Kanehisa, Furumichi, Tanabe, Sato & Morishima, 2017).

2.2.2. *In silico* miRNA: mRNA interaction analysis

Post-identifying miRNAs with potential diagnostic, prognostic, or therapeutic relevance for GB management, a subsequent miRNA: mRNA interaction analysis was incorporated to

provide robust evidence for functional miRNA: mRNA target interactions (MTIs) and to minimise the likelihood of false positive results. A Venn diagram of miRNAs targeting for selected genes was created using Venny 2.1.0 (https://bioinfogp.cnb.csic.es/tools/venny/) (Oliveros, 2007-2015). Four different miRNA tools were incorporated to create the Venn diagram: miRSystem, miRWalk (http://mirwalk.umm.uni-heidelberg.de/), TargetScan (https://www.targetscan.org/vert_80/), and ENCORI (https://starbase.sysu.edu.cn/) (Lu, *et al.,* 2012; Sticht, De La Torre, Parveen & Gretz, 2018; Agarwal, Bell, Nam & Bartel, 2015; Kariuki, *et al.,* 2023). Following this, the miRNA-centric network visual analytics platform miRNet2.0 (https://www.mirnet.ca/) was used to construct a network of miRNA-target interactions between the genes commonly co-expressed with the selected genes (Fan, *et al.,* 2016). The organism *Homo sapiens* was selected, followed by the incorporation of a gene list with official gene symbols. All other parameters were set as default. Lastly, Sfold was then utilised to provide the probable binding sites of selected miRNAs to their gene targets (Ding, Chan & Lawrence, 2004). Sfold predicted the probable RNA secondary structures through structure ensemble sampling and centroid predictions, with an emphasis on assessing RNA target accessibility (https://sfold.wadsworth.org/cgi-bin/index.pl).

2.2.3. *In silico* target gene analysis

A comprehensive miRSystem analysis was employed to identify the gene targets of highly deregulated selected miRNAs identified through the miRNA *in silico* analysis. The HPA (https://www.proteinatlas.org/) was then incorporated to analyse the mRNA expression levels of identified target genes (Thul & Lindskog, 2018). HPA-RNA-sequencing data was utilised to demonstrate the normal tissue expression of selected genes across various tissue types. To investigate the tissue-specific gene expression of selected genes, the GTEx Bulk database (https://gtexportal.org/home/) was incorporated (GTEx Consortium, 2013). Expression values were presented in normalised transcripts per million (nTPM). Box plots were depicted showing the median along with the 25th and 75th percentiles. Any data points exceeding 1.5 times the interquartile range were considered as outliers. Visualisation of selected proteins' expression across six brain donors was conducted using the Allen Brain Atlas (https://portal.brain-map.org/) (Sunkin, *et al.,* 2013). The results are displayed as heatmaps of log2 expression. Additionally, the tool generated data on the mRNA expression of selected genes across 17 different types of cancer. This data was obtained from the TCGA database and measured in fragments per kilobase of exon per million (FPKM) (Tomczak, Czerwińska & Wiznerowicz, 2015). A bar chart displaying the normal neuronal cell cluster was also available on the HPA,

where the mRNA expression of selected genes was measured in nTPM within individual brain cell clusters. Furthermore, UALCAN (http://ualcan.path.uab.edu/) was used to evaluate the mRNA expression levels of selected genes across different GB age groups, races and various paediatric brain phenotypes (Chandrashekar, *et al.,* 2022). Additionally, the Single Cell Portal was employed to analyse the log2 expression of selected genes within 28 GB cases, which included 8 paediatric and 20 adult samples (https://singlecell.broadinstitute.org/single_cell) (Tarhan, *et al.,* 2023). The Xena Functional Genomics Explorer (https://xenabrowser.net/) was used to assess the impact of differential expression of selected genes on GB survival, selecting the TCGA Glioblastoma study (631 GB patient samples, grade 4) for analysis (Goldman, *et al.,* 2020). Recurrent GB tumour samples were excluded, resulting in 619 primary GB tumour samples (grade 4; 10–89 years of age; n = 230 females; n = 389 males).

2.2.4. *In silico* target protein analysis

To elucidate the role of selected proteins in specific biological pathways, KEGG Pathway and STRING analyses were performed. STRING analysis (https://string-db.org/cgi/input?sessionId=bLTkmworrpXG&input_page_show_search=on) was conducted to identify protein-protein interactions (PPI) using defined parameters for the queried protein (Szklarczyk, *et al.,* 2021). The resulting PPI network highlighted both functional and physical associations among an initial set of five protein targets. Further expansion of the PPI network for the queried protein identified an additional five interactive protein targets, all with a high confidence interval of more than 0.900.

2.2.5. Statistics

Significance of the TPM values utilised by UALCAN for the generation of boxplots was determined using a *t*-test PERL script with Comprehensive Perl Archive Network (CPAN) module “Statistics: Student’s t-test”. Values of $p<0.05$ were considered statistically significant. The Xena software was used to generate Kaplan-Meier (KM) survival plots, and the statistical test performed was the log-rank test (also known as the Mantel-Cox test) to compare survival curves between different groups (normal versus GB). Values of $p<0.05$ were considered statistically significant.

2.3. Results

2.3.1. *In silico* miRNA analysis

Throughout our bioinformatics analysis, summarised in Figure 12 and Table 4, we examined miRNAs and their gene targets using formatted miRNA summary reports from the NCBI and miRSystem databases. Based on the NCBI report, a total of 2085 genes were associated with GB. Subsequent miRSystem analysis identified that a total of 707 miRNAs were associated with one or more GB genes. The analysis of interactions between miRNAs and their target genes enabled us to identify three miRNAs with significant relevance to GB pathogenesis: miR-21-5p (also referred as miR-21), miR-34-5p (also referred as miR-34a), and miR-128a-3p (also referred as miR-128a). Among these, miR-34-5p exhibited the highest number of interactions with GB oncogenes. Subsequent KEGG pathway analysis illustrated the differential expression profiles of three of these miRNAs, showing that miR-34a and miR-128a were downregulated in GB, while miR-21a was upregulated (Figure 13).

Table 4. Identification of miRNAs and associated target genes. The three depicted miRNAs: miR-21-5p, miR-34-5p and miR-128-3p, aligned against the oncogenes *CDK6, NOTCH1, NOTCH2, JAG1, TIPM3, E2F3,* and *BMI1* found in GB.

	Gene name and Total no. of hits							
Name of miRNAs	***CDK6***	***NOTCH1***	***NOTCH2***	***JAG1***	***TIMP3***	***E2F3***	***BMI1***	**Total**
miR-21-5p	5	0	0	7	7	3	0	22
miR-34a-5p	7	7	8	8	0	8	0	38
miR-128a-3p	5	0	0	4	0	8	7	24

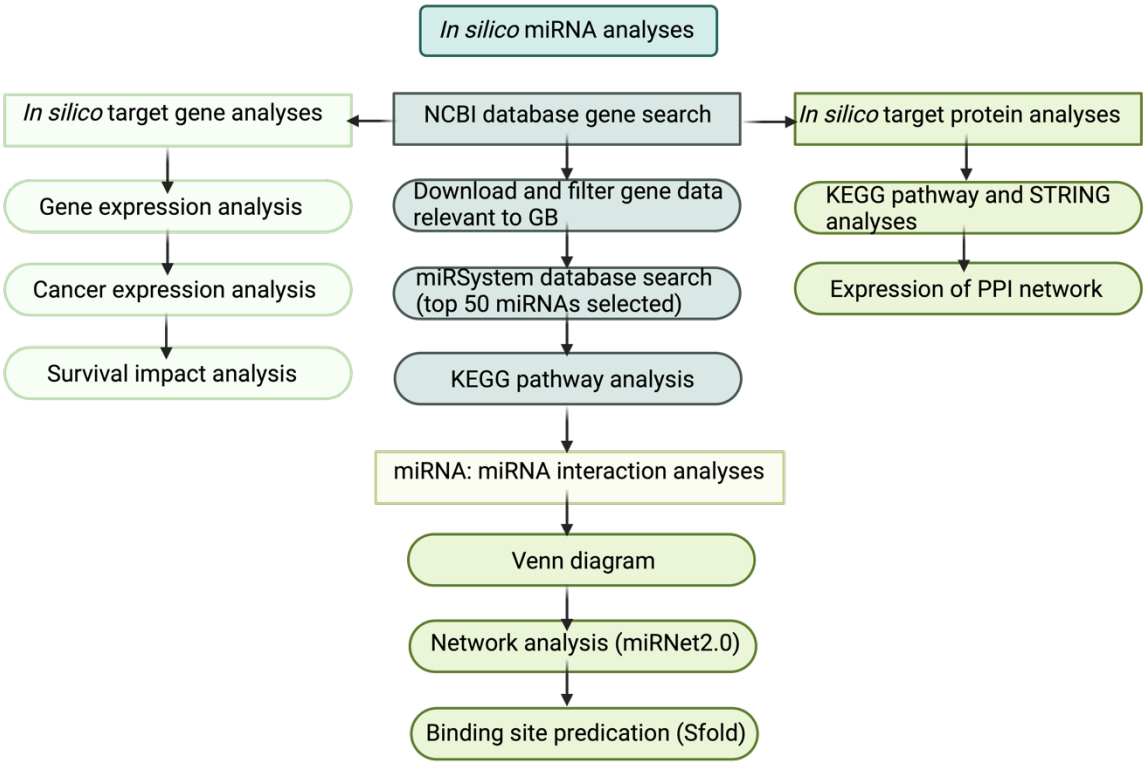


Figure 12. Flowchart summarising the *in silico* methodology for miRNA analysis in GB. Key stages include identifying GB-associated genes and top 50 miRNAs, analysing miRNA-mRNA interactions and target genes, and exploring protein-protein interactions. Each stage builds sequentially to support miRNA-target identification and pathway analysis in GB.

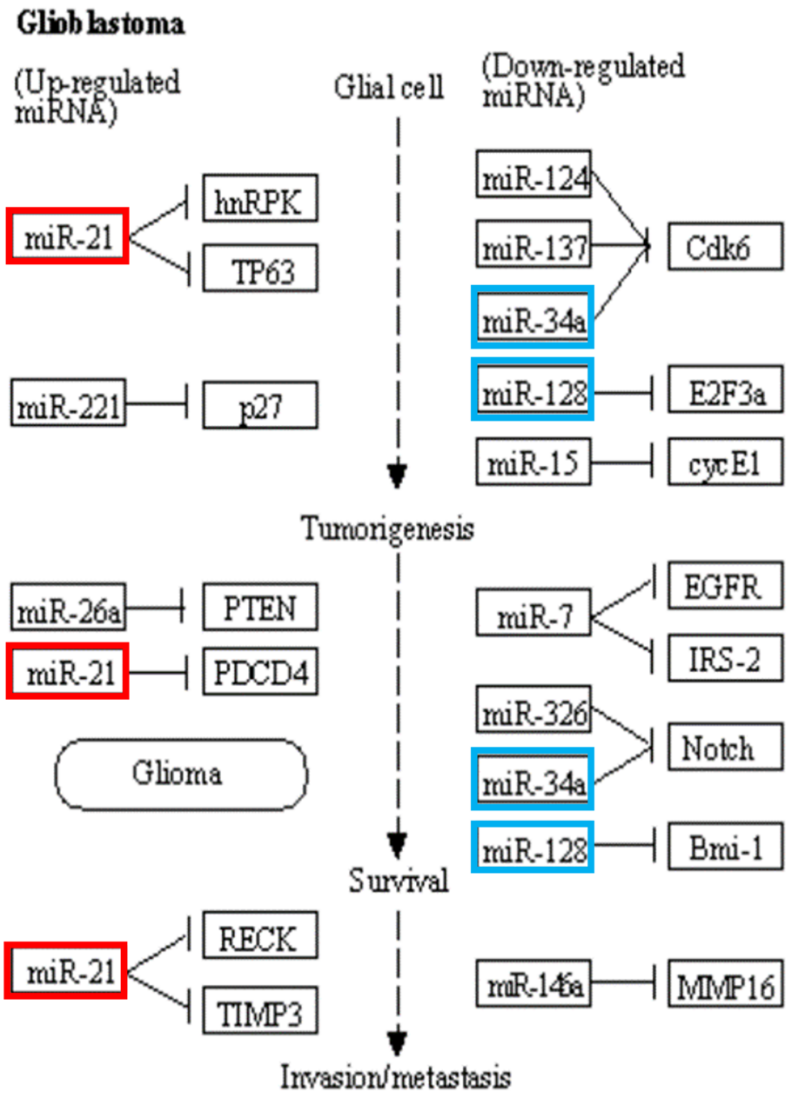


Figure 13. KEGG pathway analysis depicted the most differentially expressed miRNA profiles in 529 GB cases (grade 4). MiR-21 (red boxes) was seen to be upregulated, whereas miR-34a and miR-128 (blue boxes) were downregulated.

2.3.2. *In silico* miRNA: mRNA interaction analysis

Further *in silico* miRNA: mRNA interaction analysis depicted that miR-34-5p and miR-128-3p were targeting the Coronin 1C (*CORO1C*) and synaptic vesicle glycoprotein 2B (*SV2B*) genes. As miR-34a-5p and miR-128a-3p were already seen downregulated, their interactions with the *CORO1C* and *SV2B* genes were studied further (Table 5). As seen in Table 5 below, miR-34a-5p and miR-128a-3p had a greater affinity towards *CORO1C*, whilst *SV2B* was primarily targeted by miR-128a-3p.

Table 5. Identification of gene targets of miR-34a-5p and miR-128a-3p.

Gene name and Total no. of hits			
Name of miRNAs	***CORO1C***	***SV2B***	**Total**
miR-34a-5p	6	1	7
miR-128a-3p	5	3	8

A subsequent miRNA: mRNA interaction analysis was incorporated to provide robust evidence for functional miRNA: mRNA target interactions (MTIs) and to minimise the likelihood of false positive results. In this analysis, the direct targets for *CORO1C* and *SV2B* were identified as miR-206 and miR-383, respectively (Table 6). The miRNA: mRNA interaction analysis identified that miR-206 was directly targeting the *CORO1C* gene. This interaction was validated across six miRNA: mRNA interactome databases (Table 6). Furthermore, miR-383 was observed to directly target the *SV2B* gene, which was confirmed in five miRNA: mRNA databases (Table 6).

Table 6. miRSystem analysis of miRNA: mRNA interactions. The analysis depicted that miR-206 and miR-383 were targeting the *CORO1C* and *SV2B* genes, respectively. The interactions were validated across seven publicly available miRNA: mRNA interactome databases (Diana, Miranda, Mirbridge, Pictar, Pita, RNA22, TargetScan).

miRNA	Total hit	Validation	Diana	Miranda	Mirbridge	Pictar	Pita	RNA22	TargetScan
miR-206	6	*CORO1C*	✓		✓	✓	✓	✓	✓
miR-383-5p	5	*SV2B*	✓	✓	✓		✓	✓	

Subsequently, Venn diagrams for miRNAs targeting *CORO1C* and *SV2B* were generated via selected miRNA databases: miRSystem, TargetScan, miRWalk, and ENCORI. The *CORO1C* results, illustrated in Figure 14, revealed 62 (2.6%) common miRNA targeting this gene across all four miRNA analysis tools (Table 7). Among these common miRNAs, miR-34a-5p, miR-128-3p and miR-206 were identified as common miRNAs targeting *CORO1C*. The *SV2B* results indicated that 26 common miRNAs were targeting the gene (1%) (Table 8). These were identified across all four databases. Among these shared miRNAs, miR-34a-5p and miR-383-5p were identified as CORO1C-targeting miRNAs (Figure 15).

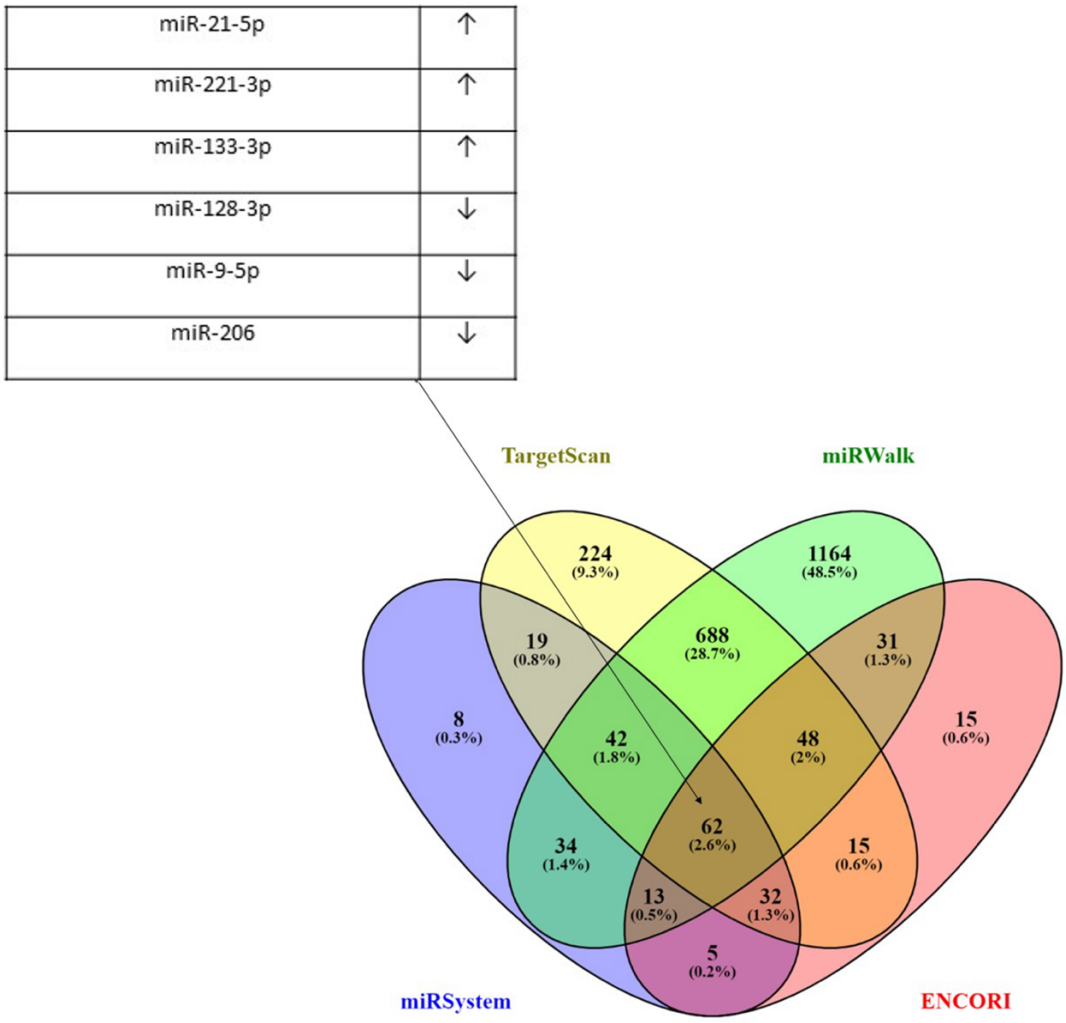


Figure 14. A Venn diagram incorporating miRSystem, TargetScan, miRWalk, and ENCORI databases. In total, 62 miRNAs were found to overlap between the four miRNA analysis tools (2.6%). Of these, miR-34a-5p, miR-128-3p and miR-206 were identified as targeting *CORO1C*.

miR-210-5p	↑
miR-136-5p	↑
miR-34a-5p	↓
miR-9-5p	↓
miR-383-5p	↓

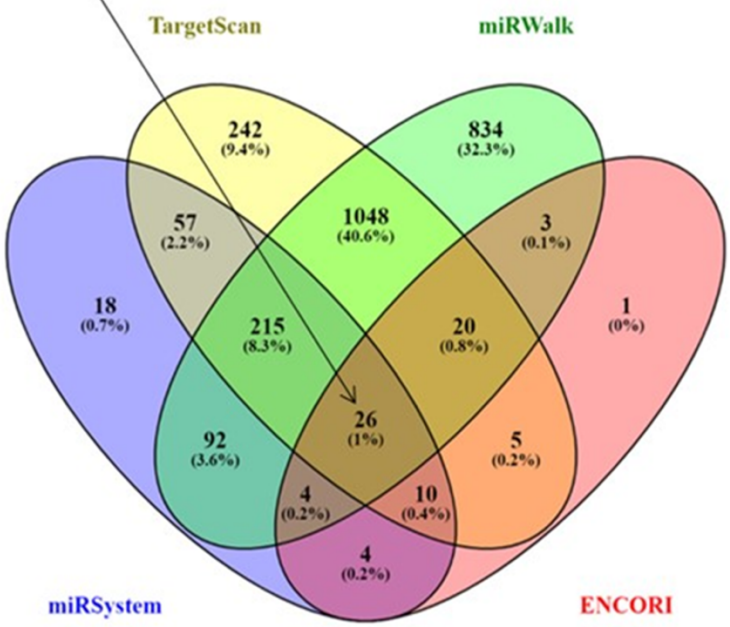


Figure 15. A Venn diagram incorporating miRSystem, TargetScan, miRWalk, and ENCORI databases. In total, 26 miRNAs were found to overlap between the four miRNA analysis tools (2.6%). Of these, miR-34a-5p and miR-383-5p were identified as targeting *SV2B*.

Table 7. Common miRNAs (62) in "miRSystem ", "TargetScan", "miRWalk" and "ENCORI" found to target *CORO1C*.

hsa-miR-125b-5p	hsa-miR-300	hsa-miR-524-5p
hsa-miR-128-3p	hsa-miR-31-5p	hsa-miR-543
hsa-miR-129-2-3p	hsa-miR-326	hsa-miR-552-3p
hsa-miR-129-5p	hsa-miR-330-5p	hsa-miR-579-3p
hsa-miR-133b	hsa-miR-338-3p	hsa-miR-588
hsa-miR-135b-5p	hsa-miR-34a-5p	hsa-miR-613
hsa-miR-136-5p	hsa-miR-34c-5p	hsa-miR-616-3p
hsa-miR-141-3p	hsa-miR-381-3p	hsa-miR-708-5p
hsa-miR-149-5p	hsa-miR-409-3p	hsa-miR-874-3p
hsa-miR-150-5p	hsa-miR-433-3p	hsa-miR-125a-5p
hsa-miR-181a-5p	hsa-miR-449a	hsa-miR-96-5p
hsa-miR-181b-5p	hsa-miR-449b-5p	hsa-miR-204-5p
hsa-miR-181d-5p	hsa-miR-494-3p	hsa-miR-206
hsa-miR-182-5p	hsa-miR-495-3p	hsa-miR-21-5p
hsa-miR-185-5p	hsa-miR-508-3p	hsa-miR-211-5p
hsa-miR-194-5p	hsa-miR-512-3p	hsa-miR-214-3p
hsa-miR-197-3p	hsa-miR-519c-5p	hsa-miR-221-3p
hsa-miR-200a-3p	hsa-miR-519e-5p	hsa-miR-222-3p
hsa-miR-200b-3p	hsa-miR-520d-5p	hsa-miR-26a-5p
hsa-miR-200c-3p	hsa-miR-520f-3p	hsa-miR-28-5p
hsa-miR-9-5p	hsa-miR-942-5p	

Table 8. Common miRNAs (26) in "miRSystem", "TargetScan", "miRWalk" and "ENCORI" found to target *SV2B*.

hsa-miR-143-3p	hsa-miR-324-5p	hsa-miR-96-5p
hsa-miR-150-5p	hsa-miR-330-3p	hsa-miR-1269a
hsa-miR-186-5p	hsa-miR-34a-5p	hsa-miR-216b-5p
hsa-miR-383-5p	hsa-miR-362-5p	hsa-miR-27a-3p
hsa-miR-495-3p	hsa-miR-449a	hsa-miR-27b-3p
hsa-miR-520d-5p	hsa-miR-506-3p	hsa-miR-205-5p
hsa-miR-524-5p	hsa-miR-513a-5p	hsa-miR-210-3p
hsa-miR-556-3p	hsa-miR-532-3p	hsa-miR-136-5p
hsa-miR-9-5p	hsa-miR-182-5p	

2.3.3. MiRNA-centric network analysis

Further analysis of the genes commonly co-expressed with *CORO1C*, along with their regulating miRNAs, revealed that miR-206, miR-128-3p, and miR-34a-5p play a role in regulating the *CORO1C* gene hub in brain tissue (Figure 16). Similarly, the analysis of *SV2B*

and its co-expressed genes identified miR-383-5p, miR-34a, and miR-128a as miRNAs involved in regulating both the *SV2B* gene and its associated gene hub (Figure 17).

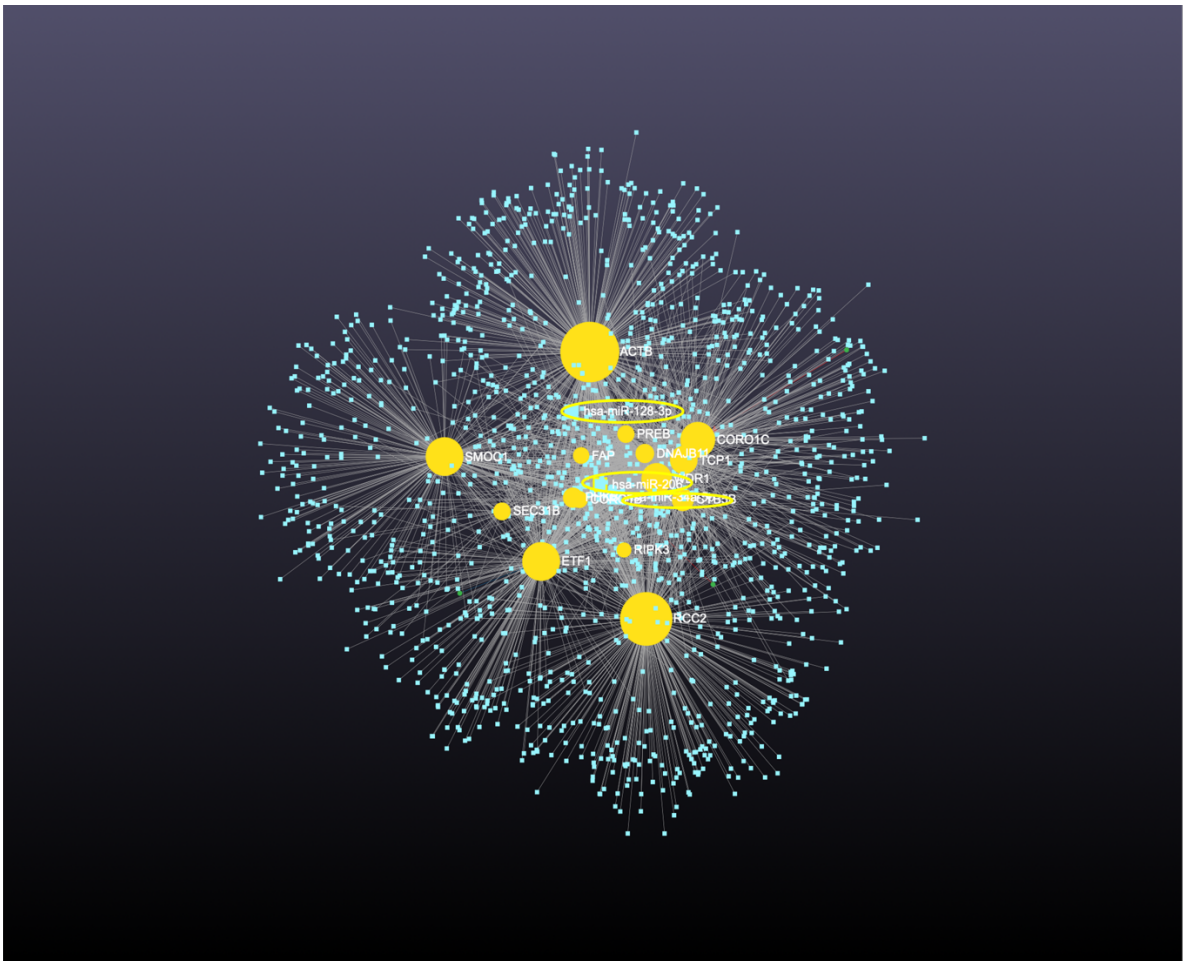


Figure 16. Interactome analysis of important miRNAs involved in the overall gene regulation for *CORO1C* co-expressed genes (coronin 1B (*CORO1B*), WD repeat domain 1 (*WDR1*), eukaryotic translation termination factor 1 (*ETF1*), cytochrome B5 type B (*CYB5B*), regulator of chromosome condensation 2 (*RCC2*), SEC31 homolog B, COPII coat complex component (*SEC31B*), T-complex 1 (*TCP1*), actin-beta (*ACTB*), phosphorylase kinase regulatory subunit beta (*PHKB*), fibroblast activation protein alpha (*FAP*), prolactin regulatory element binding (*PREB*), SPARC related modular calcium binding 1 (*SMOC1*), receptor interacting serine/threonine kinase 3 (*RIPK3*), and DnaJ heat shock protein samily (Hsp40) member B11 (*DNAJB11*)). MiR-34a-5p, miR-128-3p, and miR-206-5p were identified in regulating *CORO1C* and the gene hub (yellow circles – gene names; blue quadrats – miRNAs; yellow margin circles – highlighted miRNAs).

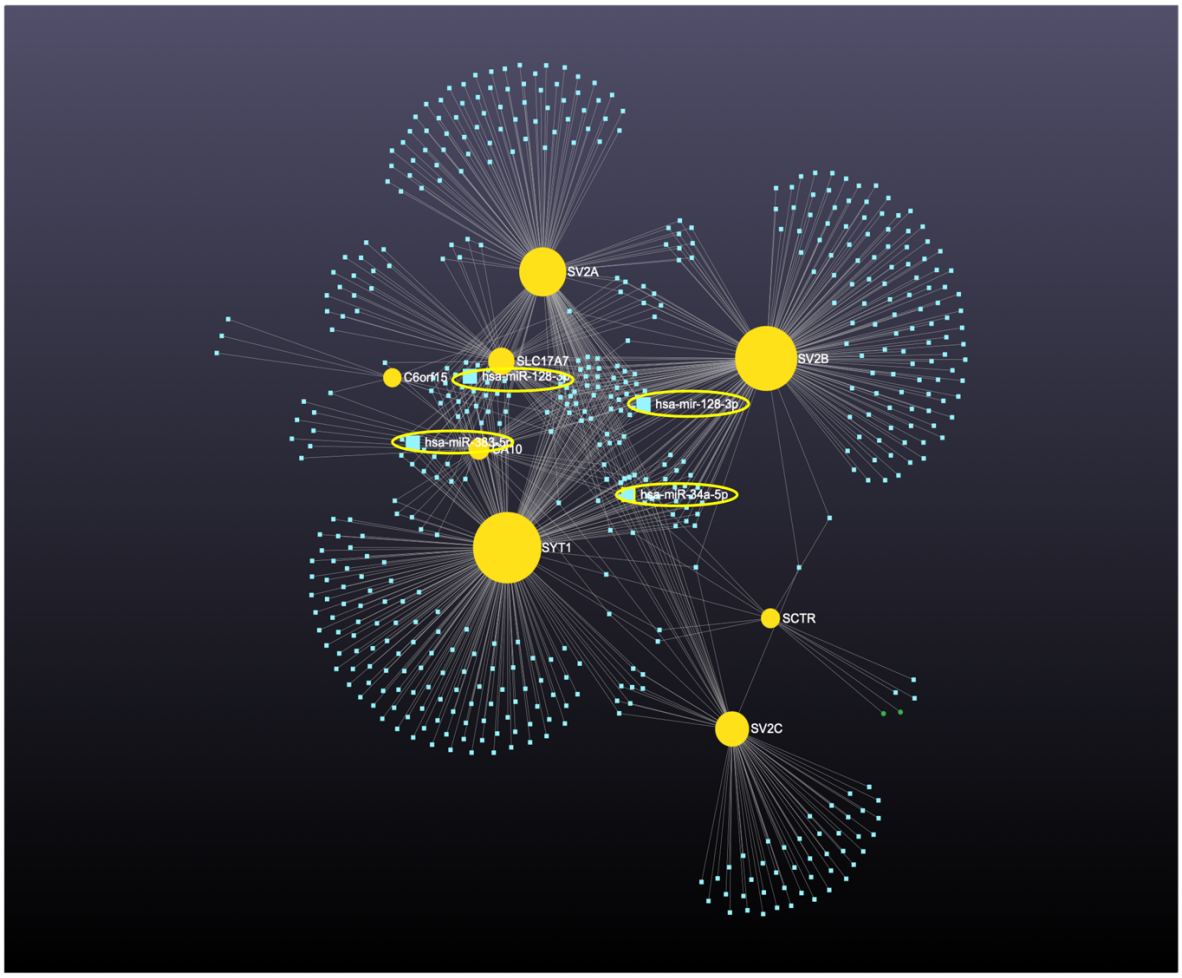


Figure 17. Interactome analysis of important miRNAs involved in the overall gene regulation for *SV2B* co-expressed genes (chromosome 6 open reading frame 15 (*C6orf15*), secretin receptor (*SCTR*), synaptotagmin 1 (*SYT1*), synaptic vesicle glycoprotein 2C (*SV2C*), carbonic anhydrase 10 (*CA10*), synaptic vesicle glycoprotein 2A (*SV2A*), and solute carrier family 17 member 7 (*SLC17A7*)). MiR-34a-5p, miR-128-3p, and miR-206-5p were identified in regulating *SV2B* and the gene hub (yellow circles – gene names; blue quadrats – miRNAs; yellow margin circles – highlighted miRNAs).

2.3.4. Sfold miRNA: mRNA analysis

We selected the downregulated miR-34a-5p, and miR-128a-3p, alongside miR-206-5p and miR-383-5p for subsequent Sfold base-pair matching analysis with *CORO1C* and *SV2B*. As shown in Figure 18a, miR-34a-5p had one binding site at the 3'UTR of *CORO1C* at position 1604-1624, with a predicted hybridisation free energy (ΔG hybrid) value of −30.300 kcal/mol. This binding type was described as an 8mer, suggesting full complementarity binding. Furthermore, miR-128a-3p was also seen to bind *CORO1C* at position 2021-2037. This was the only binding site for miR-128a-3p and the 3'UTR region of *CORO1C*, described as a 7mer-A1, suggesting partial complementarity. The ΔG hybrid value of -25.100 kcal/mol (Figure 18b). Further Sfold analysis showed that there were two binding sites between miR-206 and

the 3'UTR of *CORO1C*. The interaction between miR-206 and the 3′UTR of *CORO1C* at site position 1614-1639 was described as an 8mer with an ΔG hybrid of −23.4 kcal/mol (Figure 18c). The second binding site position between miR-206 and *CORO1C* (site position 1655-1675) has ΔG hybrid of −20.6 kcal/mol and was also an 8mer (Figure 18d). Analysis of the interactions between miR-34a and the 3′UTR of *SV2B* revealed a binding site at position 3909–3932, with a ΔG hybrid value of −27.500 kcal/mol. The binding type was 7mer-A1 (Figure 19a). Sfold also predicted three binding sites between SV2B and miR-128a-3p at site positions 9532–9552, 8986–8999, and 5671–5685. The hybrid binding interactions at these sites had ΔG hybrid values of −19.300 kcal/mol, −17.900 kcal/mol, and −17.600 kcal/mol, respectively. The seed type interactions were described as 7mer-A1 for the first two sites and 6mer for the latest also suggesting partial complementarity (Figures 19b, 19c, and 19d). The binding interaction between miR-383-5p and the 3′UTR of *SV2B* relieved a binding site at position 3239-3263. The predicted ΔG hybrid for this interaction was −20.3 kcal/mol, and the binding type was described as an 8mer (Figure 19e).

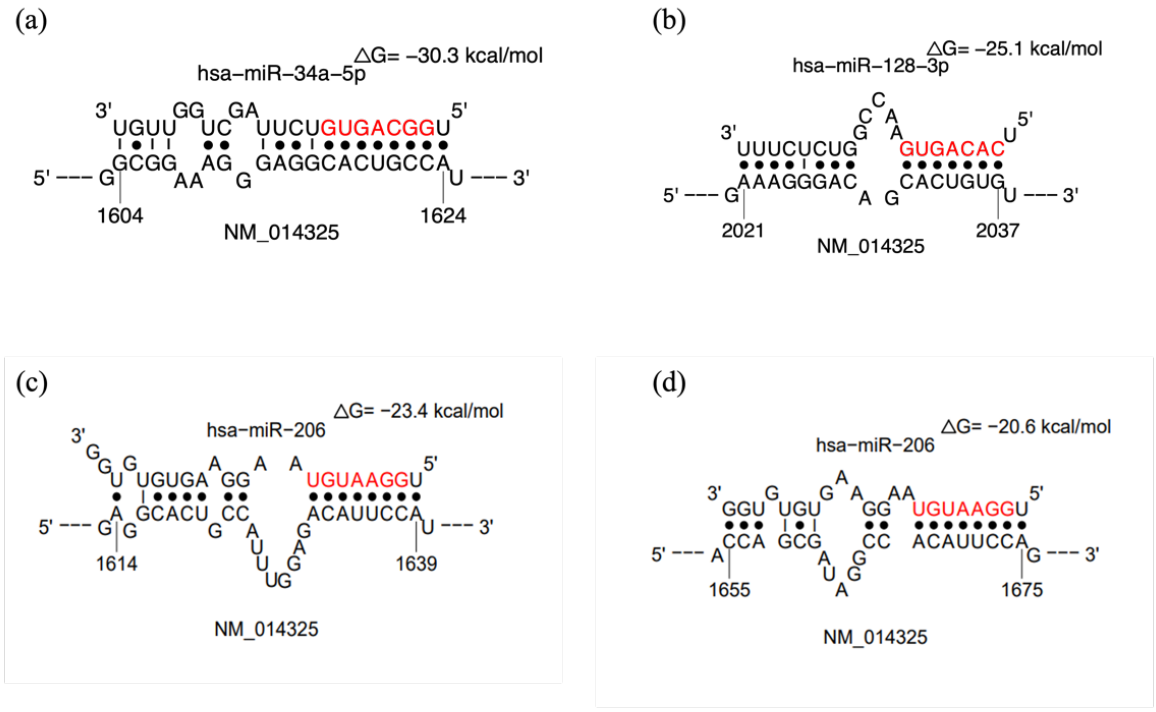


Figure 18. Sfold analysis of miRNA binding sites for *CORO1C*. (a) 3'UTR of *CORO1C* and miR-34a-5p binding at site position 1604-1624, ΔG hybrid =−30.300 kcal/mol. (b) 3'UTR of *CORO1C* and miR-128a-3p binding at site position 2021-2037, ΔG hybrid =-25.100 kcal/mol. (c) 3′UTR of *CORO1C* and miR-206 binding at site position 1614-1639, ΔG hybrid =−23.4 kcal/mol. (d) 3′UTR of *CORO1C* and miR-206 binding at site position 1655-1675, ΔG hybrid =−20.6 kcal/mol.

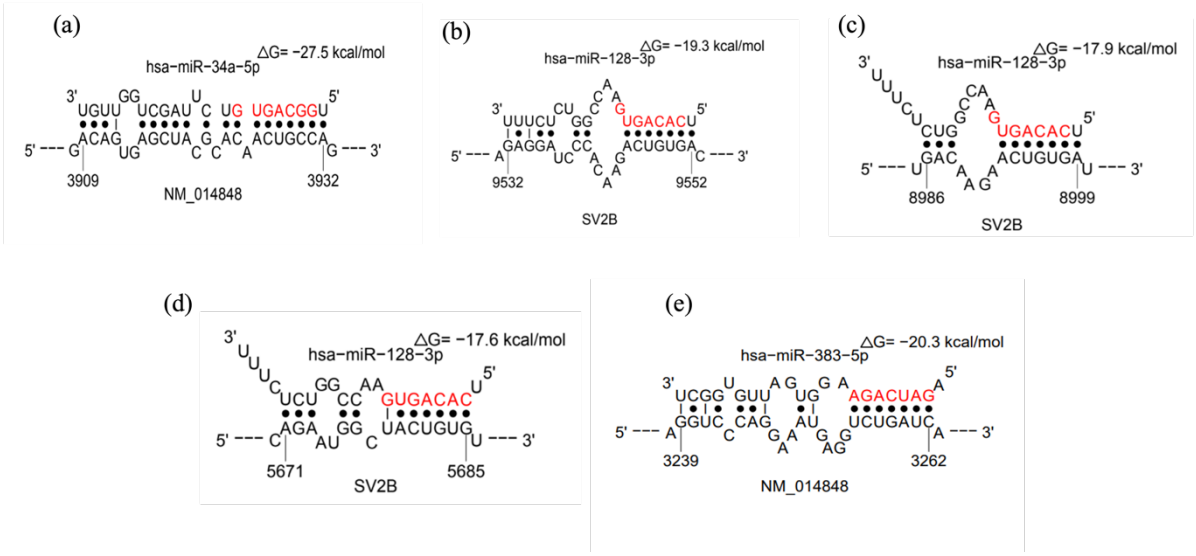


Figure 19. Sfold analysis of miRNA binding sites for *SV2B*. (a) 3′UTR of *SV2B* and miR-34a binding at site position 3909–3932, ΔG hybrid =−27.500 kcal/mol. (b) 3′UTR of *SV2B* and miR-128-3p binding at site position 9532–9552, ΔG hybrid =−19.300 kcal/mol. (c) 3′UTR of *SV2B* and miR-128-3p binding at site position 8986–8999, ΔG hybrid =−17.900 kcal/mol. (d) 3′UTR of *SV2B* and miR-128-3p binding at site position 5671–5685, ΔG hybrid =−17.600 kcal/mol. (e) 3′UTR of *SV2B* and miR-383-5p binding at site position 3239-3263, ΔG hybrid =−20.3 kcal/mol.

2.3.5. *CORO1C* gene expression analysis in normal tissues and brain

Figure 20 illustrates the mRNA expression profile of *CORO1C* in normal tissues. Specifically, the highest expression, measured in normalised transcripts per million (nTPM), was detected in smooth muscle tissue (275.4 nTPM), followed by the endometrium (227.9 nTPM), urinary bladder (180.1 nTPM), adipose tissue (167.4 nTPM), and lung (133.2 nTPM). When brain tissue and its associated regions were analysed separately, the average *CORO1C* expression across all regions was 68.25 nTPM (Figure 21). Notably, high expression of *CORO1C* mRNA was observed in the white matter (100.1 nTPM), medulla oblongata (82.0 nTPM), thalamus (77.3 nTMP), and hippocampal formation (75.3 nTPM). Single-cell analysis of the brain revealed that *CORO1C* was highly expressed within neuronal cells. Within the glial cluster, which includes astrocytes, oligodendrocytes, oligodendrocyte precursor cells, and microglial cells, *CORO1C* was highly expressed in all glial cell types except for astrocytes, cluster c-35 (Figure 22). The expression of *CORO1C* in various brain regions of six patients was assessed using heatmaps of log2 expression values obtained via microarrays. High expression of *CORO1C* was observed in the hippocampal formation. Figure 23 illustrates the MRI scans and heatmaps from six healthy individuals who died from causes other than brain tumours. The expression was predominantly present in the CA1 (log2 expression 7.2 ± 2.5 and 7.5 ± 2.5),

CA2 (log2 expression 7.7 ± 2.5), CA3 (log2 expression 7.0 ± 2.5), and CA4 (log2 expression 6.7 ± 2.5) regions of the hippocampus. Additionally, high expression levels of *CORO1C* were observed in the myelencephalon region (log2 expression 6.5 ± 2.5), as depicted in the heatmaps.

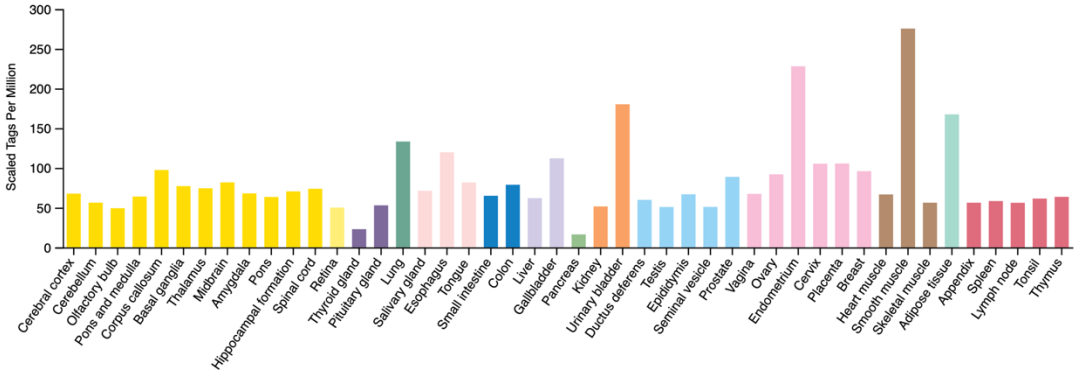


Figure 20. Detection of *CORO1C* mRNA across different tissue types. Elevated expression levels were observed in smooth muscle, endometrium, urinary bladder, adipose, and lung tissues.

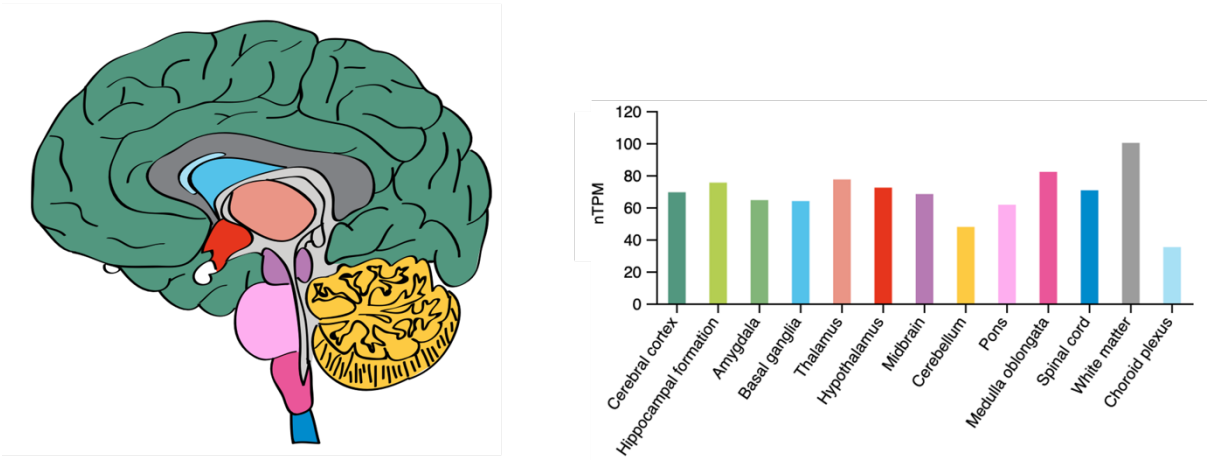


Figure 21. Detection of *CORO1C* mRNA across the normal brain. Analysis of *CORO1C* mRNA distribution within the brain revealed high expression in the white matter, medulla oblongata, and hippocampal formation.

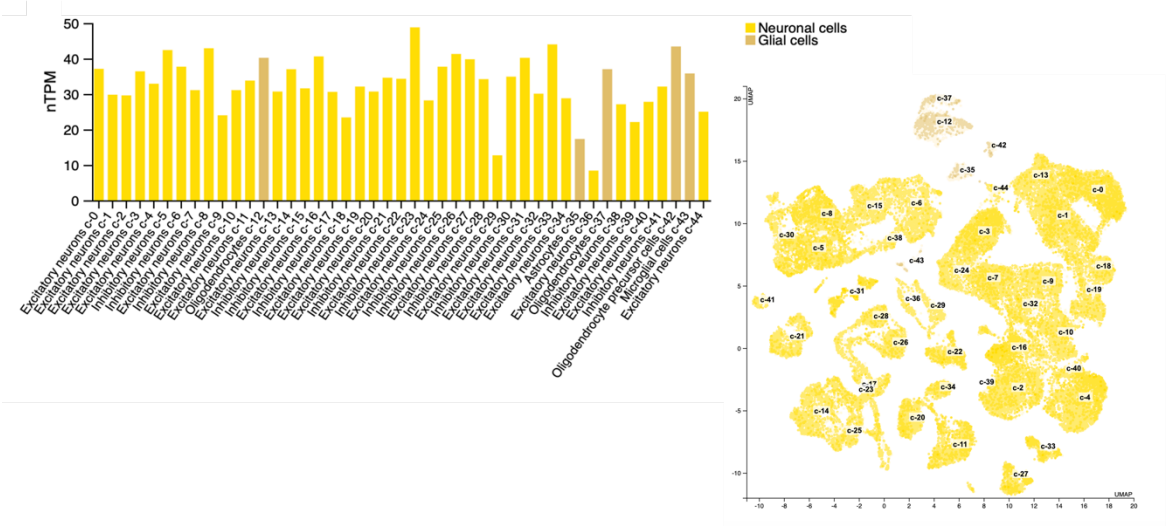


Figure 22. Detection of *CORO1C* mRNA across normal brain cells. Single-cell cluster analysis of normal brain tissue indicated significant expression of *CORO1C* in neuronal cells, oligodendrocytes, oligodendrocyte precursor cells, and microglial cells.

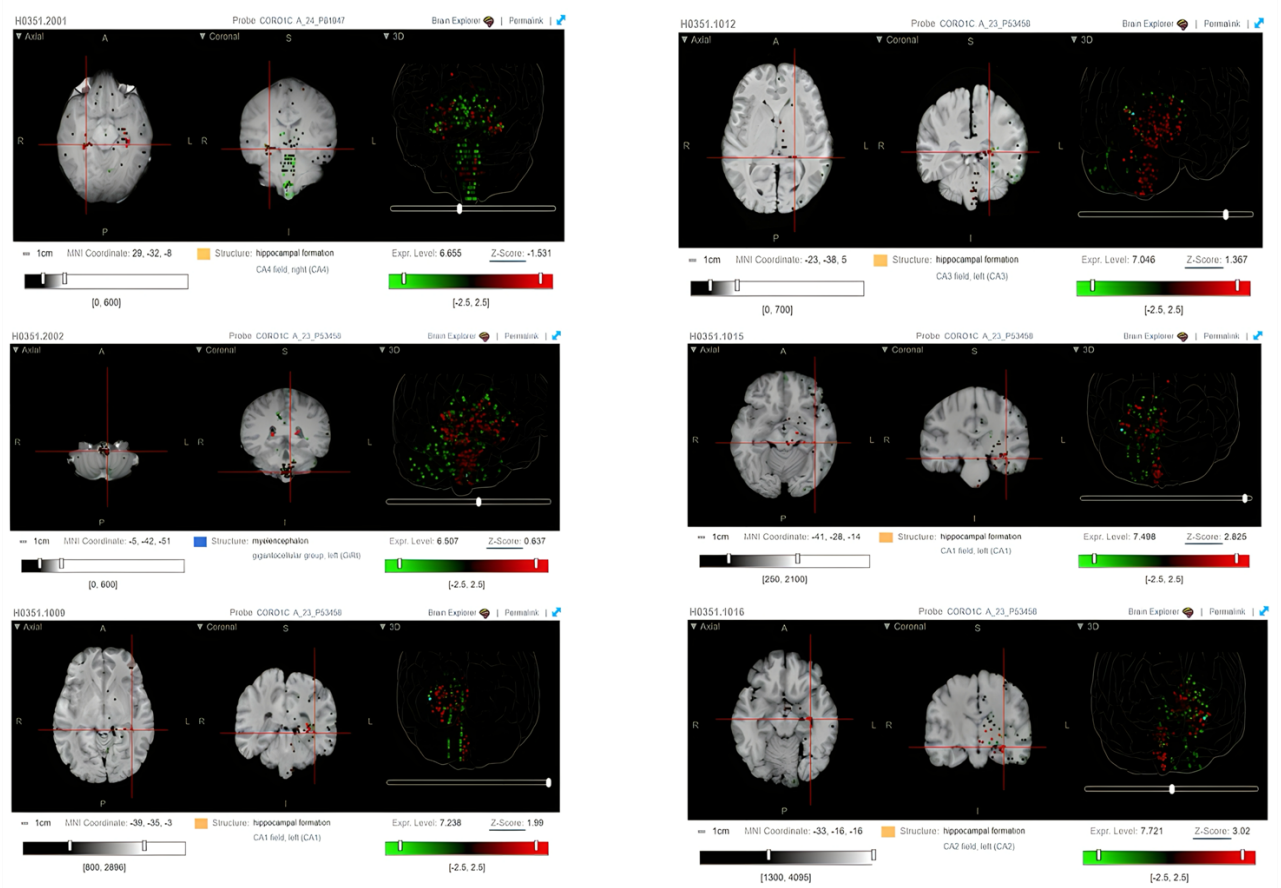


Figure 23. Heatmaps of log2 expression values from six patients obtained through microarray experiments (Allen Brain Atlas). The analysis indicated that *CORO1C* is highly expressed in the hippocampal formation and myelencephalon regions of the brain.

2.3.6. *CORO1C* gene expression analysis in different cancer types and GB

Figure 24 shows RNA-seq data from the TCGA database, highlighting the specificity of *CORO1C* expression across various cancer types. The RNA-seq data is presented as median FPKM values. Among the 17 different cancer types analysed, *CORO1C* expression was highest in head and neck cancers and gliomas, with median FPKM values of 33.4 and 33.2, respectively. Additionally, *CORO1C* expression was notably high in melanoma, with a median of 32.3 FPKM. The expression of *CORO1C* based on patients' ages is illustrated in Figure 25. Three GB age groups (21–80 years) showed significantly increased *CORO1C* total expression levels when compared to their normal counterparts. The most significant difference in median expression was observed between normal samples and the 21–40 years GB age group (111.92 nTPM), followed by the 41–60 years (109.19 nTPM) and 61–80 years age groups (91.63 nTPM). The age group of 81-100 years had the lowest median *CORO1C* expression in comparison to the other age groups (80.56 nTPM), but still significantly higher than their control normal counterparts. Furthermore, the analysis showed that the expression of *CORO1C*

was significantly higher in both males and females in comparison to their normal counterparts (Figure 26). Males expressed slightly higher levels of *CORO1C* than females (100.92 nTPM versus 93.43 nTPM), but this difference did not reach statistical significance. Figure 27 provides a deeper insight into *CORO1C* expression levels in different racial groups. Caucasian and African-Americans had significantly higher *CORO1C* expression in comparison to normal samples (98.18 nTPM and 81.51 nTPM, respectively). Asians had a high median *CORO1C* expression of 127.68 nTPM that did not reach statistical significance when compared to their normal counterparts. Figure 28 shows the expression of *CORO1C* in different types of paediatric brain malignancies. The highest median expression was detected in neurofibroma, chondroma, schwannoma, high-grade glioma (PHGG), and diffuse intrinsic pontine glioma (DIPG) (70 nTPM, 69.4 nTPM, 68.0 nTPM, 62.8 nTPM, and 60.7 nTPM, respectively). The median expression of *CORO1C* within medulloblastoma samples (MBL) was 42.23 nTPM. Overall, *CORO1C* expression levels in low-grade glioma (PLGG), DIPG, craniopharyngioma (CRANIO), supratentorial or spinal cord primitive neuroectodermal (PTEN), Ewings sarcoma (ES), dysembryoplastic neuroepithelial tumour (DNT), and choroid plexus papilloma (CPP) paediatric brain cancer subtypes were significantly lower compared to PHGG.

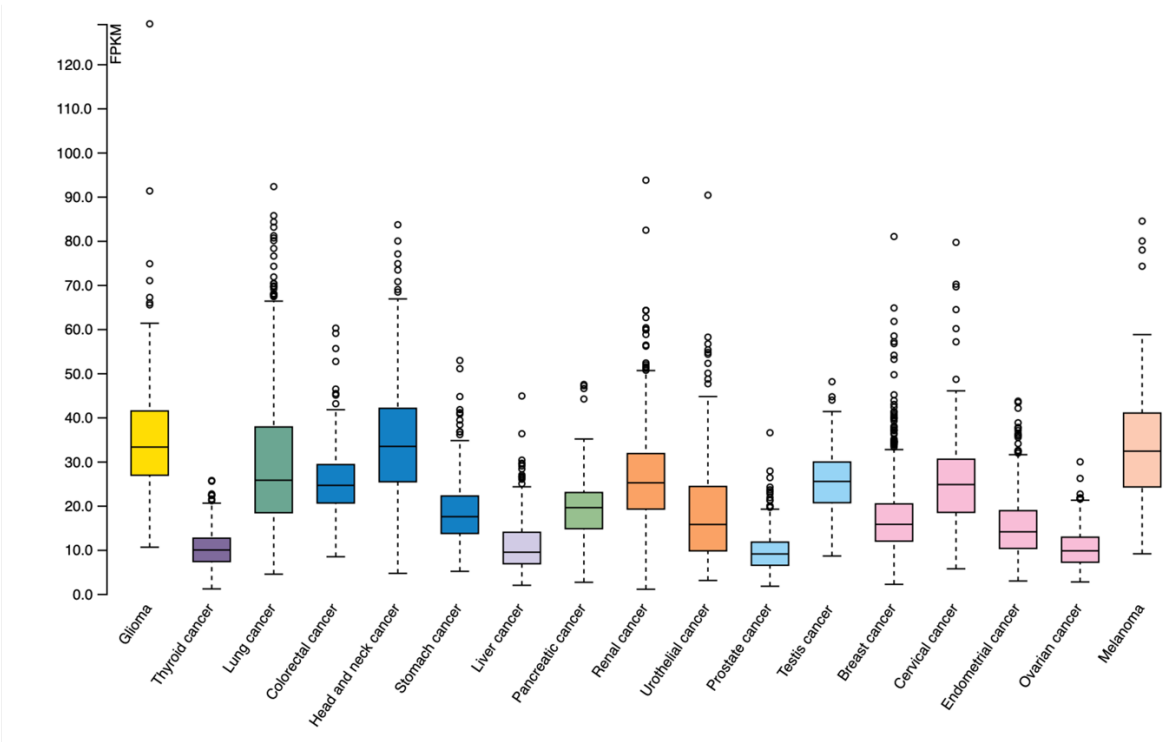


Figure 24. Expression of *CORO1C* in various cancerous tissues. Analysis of *CORO1C* expression across 17 different cancer types revealed high expression levels in head and neck cancer, gliomas, and melanomas.

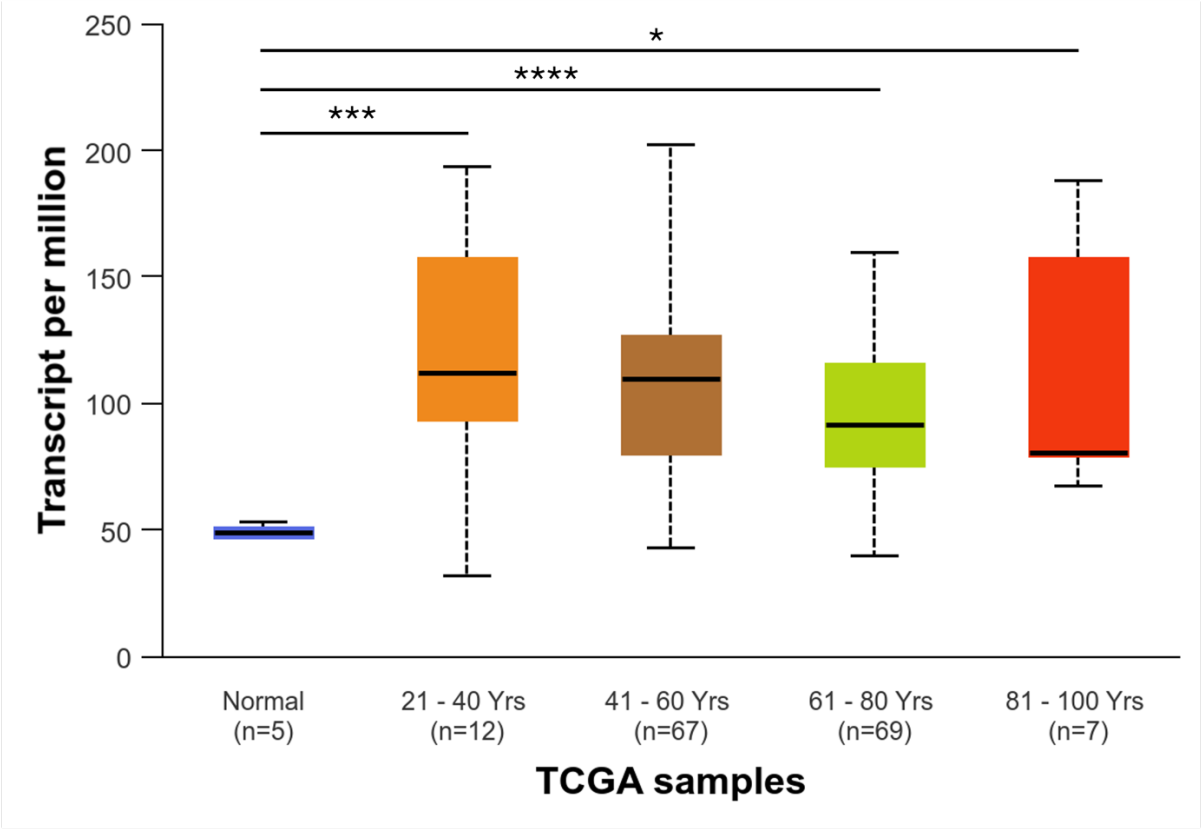


Figure 25. *CORO1C* expression levels across different GB age groups. There were significantly elevated *CORO1C* total expression levels in GB patients across three age groups (21–40, 41–60, and 61–80 years) compared to their normal counterparts ($p<0.003$, $p<0.0001$, and $p<0.0001$, respectively). The 81–100 years age group exhibited the lowest but still significant median *CORO1C* expression in comparison to normal controls ($p<0.014$).

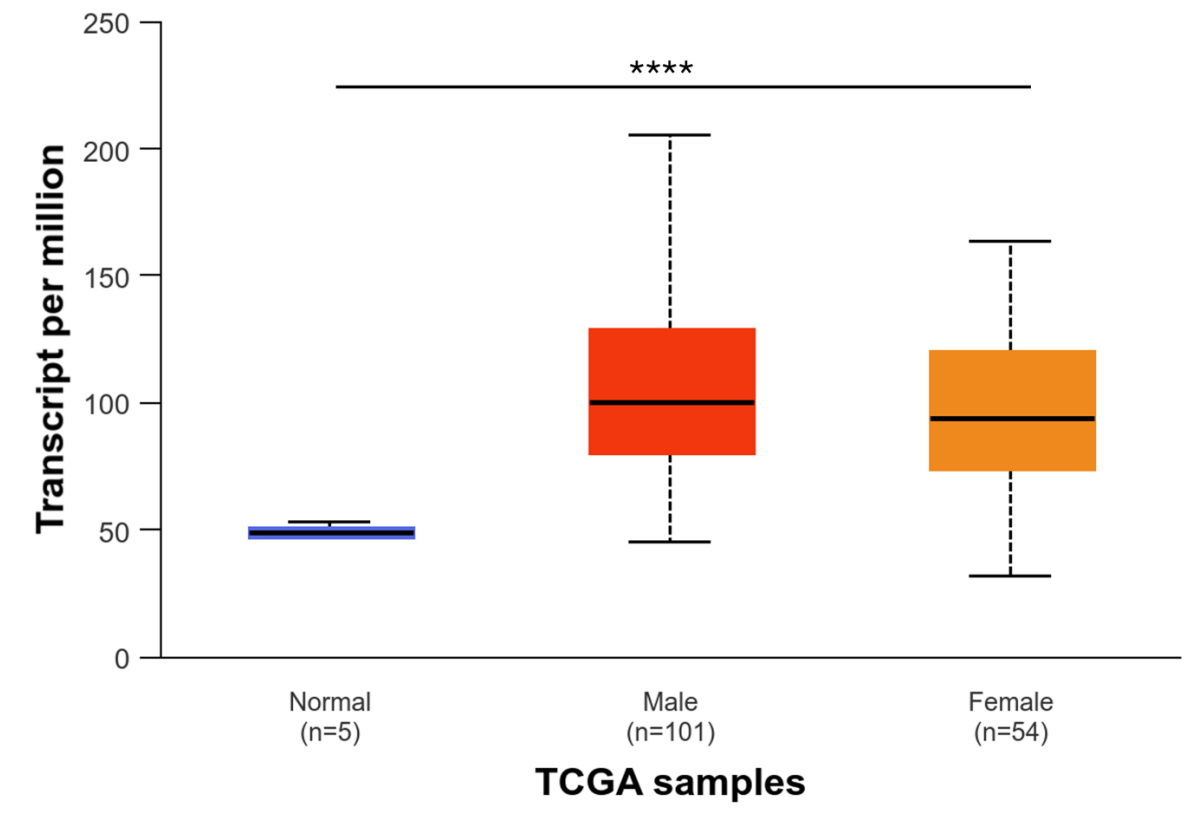


Figure 26. *CORO1C* expression levels in male and female GB patients compared to normal controls. The analysis revealed that both males and females exhibited significantly higher *CORO1C* expression levels in GB tissues compared to their normal counterparts ($p<0.0001$ and $p<0.0001$, respectively).

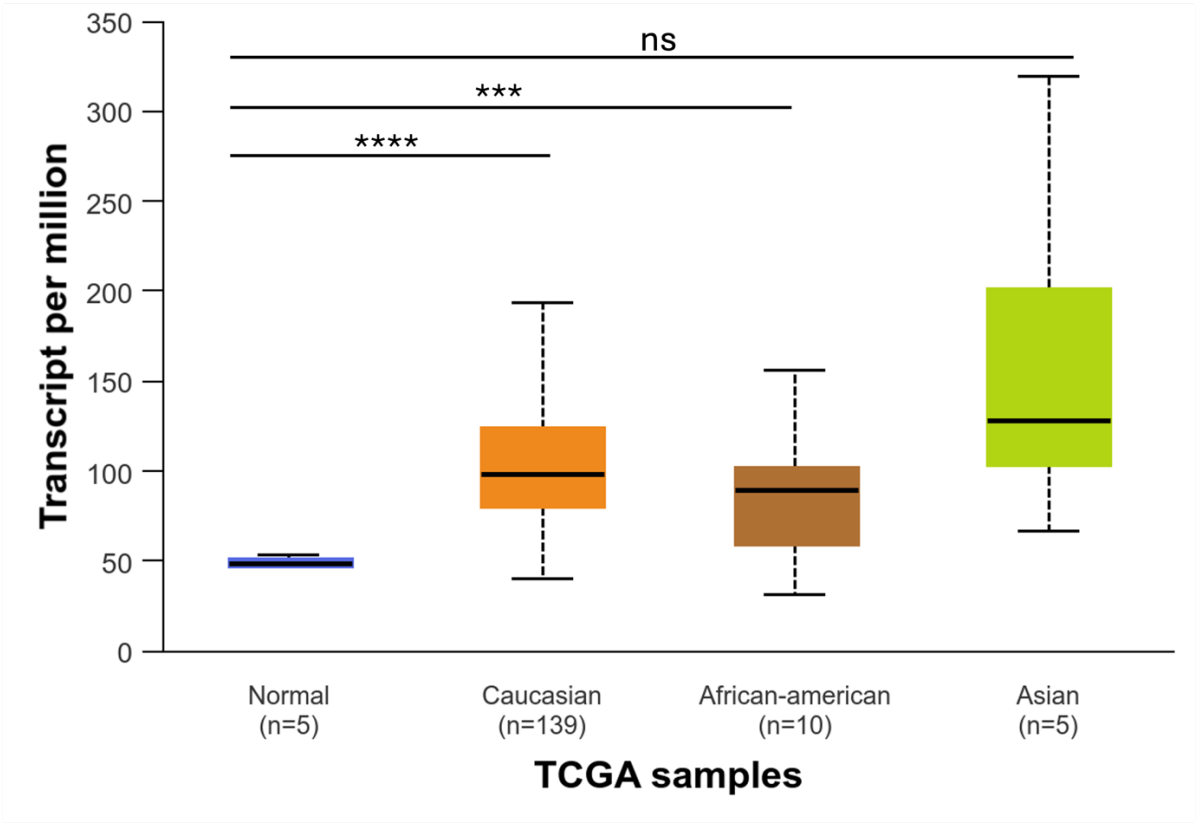


Figure 27. *CORO1C* expression levels across different racial groups in GB patients. The figure illustrated significantly higher *CORO1C* expression in Caucasian and African-American patients compared to their normal counterparts ($p<0.0001$ and $p<0.001$, respectively). Although Asian patients exhibited a high median *CORO1C* expression, this increase did not reach statistical significance when compared to normal samples.

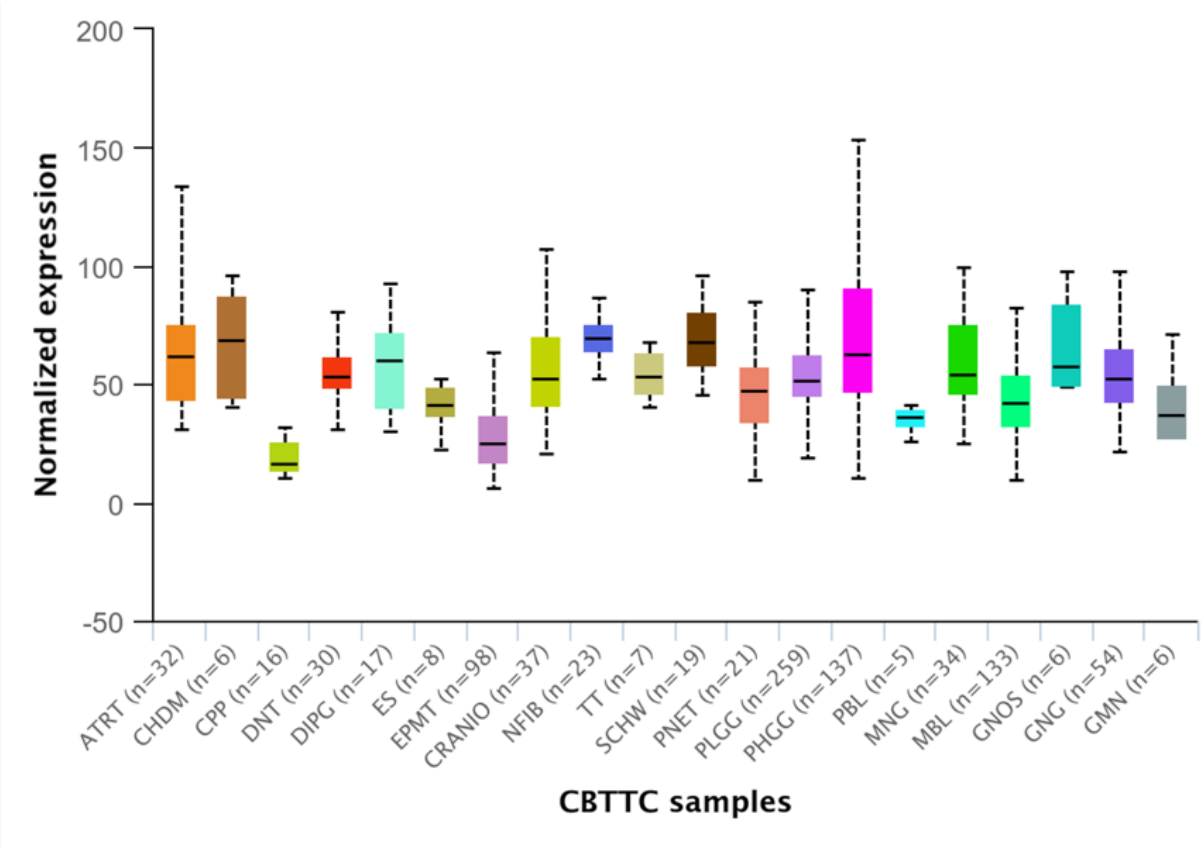


Figure 28. *CORO1C* expression levels across different paediatric brain tumours. Neurofibroma (NFIB), chondroma (CHDM), schwannoma (SCHW), PHGG, and DIPG exhibited the highest levels of *CORO1C* expression. Among these, neurofibromas showed significantly higher *CORO1C* expression compared to PHGG ($p<0.03$). In contrast, the PLGG, DIPG, CRANIO, PTEN, ES, DNT, and CPP subtypes displayed significantly lower *CORO1C* expression levels relative to PHGG (PLGG versus PHGG, $p<0.000002$; DIPG versus PHGG, $p<0.003$; CRANIO versus PHGG, $p<0.005$; PTEN versus PHGG, $p<0.002$; ES versus PHGG, $p<0.0000005$; DNT versus PHGG, $p<0.01$; CPP versus PHGG, $p<0.0001$). The CBTTC UALCAN analysis compares mean gene expression levels in paediatric brain tumour samples to those in normal tissues (not shown) or between different tumour subgroups.

2.3.7. *CORO1C* mRNA expression analysis in GB cells

Different types of cell clusters were obtained from 28 individuals spanning both adult and paediatric GB cohorts, including macrophages, T-cells, malignant cells, and oligodendrocytes. In Figure 29a, the t-distributed neighbour embedding (tSNE) heatmap shows *CORO1C* expression primarily within the left half of the malignant cell cluster, almost entirely across the macrophage cluster, and the centre of the oligodendrocyte cell cluster, with limited expression observed in the T-cell cluster (lower panel). The expression levels of the protein ranged between logTPM of 4 and logTPM of 8 in these areas. The expression of *CORO1C* was further evaluated via a two-dimensional representation of each cellular state, including astrocyte-like (AC-like), oligodendrocyte precursor cells (OPC-like), mesenchymal-like (MES-like), and

neural-progenitor-like cells (NPC-like). The heatmap of logTPM expression in Figure 29b revealed that *CORO1C* was expressed globally across all cellular states, with expression levels exceeding 4 logTPM. Notably, the expression of the mRNA within the NPC-like state was slightly higher compared to the other cellular states, exceeding 6 logTPM (lower panel). Figure 29c presents a comparison between eight paediatric cell populations and their 20 adult counterpart cell populations. *CORO1C* expression within the paediatric cluster was higher, ranging between logTPM of 6 and logTPM of 8, compared to cells from the adult cluster. The results indicated that paediatric cells occupied the left side of the malignant cell cluster, almost the entire macrophage cluster, and the centre of the oligodendrocyte cell cluster, corroborating the earlier observation of increased log2 expression of *CORO1C* in these regions (lower panel).

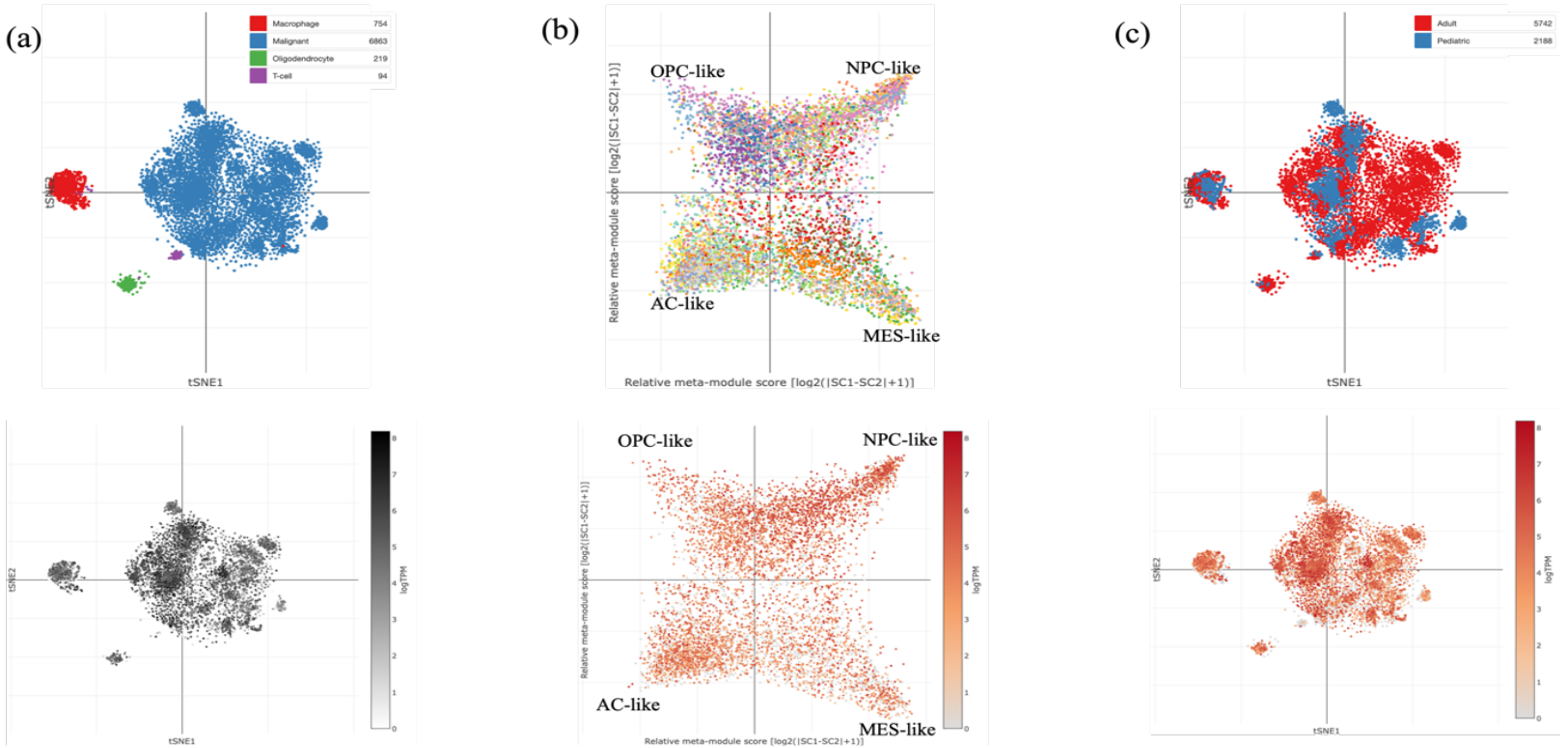


Figure 29. Single-cell *CORO1C* analysis of GB cell clusters from paediatric and adult patients. (a) The tSNE heatmap displayed *CORO1C* expression predominantly within the left half of the malignant cell cluster (blue), almost exclusively across the macrophage cluster (red), and the centre of the oligodendrocyte cell cluster (green). Minimal to no expression was observed within the T-cell cluster (purple). (b) Expression of *CORO1C* across different cellular states, including astrocyte-like (AC-like), oligodendrocyte precursor cells (OPC-like), mesenchymal-like (MES-like), and neural-progenitor-like cells (NPC-like), demonstrated global expression. The NPC-like state exhibited slightly higher protein expression levels (logTPM of 6). (c) *CORO1C* expression within the paediatric cluster (blue) was higher, ranging between logTPM of 6 and logTPM of 8, compared to cells from the adult cluster (red).

2.3.8. *CORO1C* survival analysis in GB cases

CORO1C survival analysis of primary GB samples revealed that patient groups with higher *CORO1C* expression levels had significantly longer OS and disease-specific survival compared to those with lower expression levels ($p<0.03$ and $p<0.02$, respectively) (Figures 30a and 30b). However, the differences in *CORO1C* expression profiles did not show statistically significant variations in the PFS analysis of GB (Figure 30c).

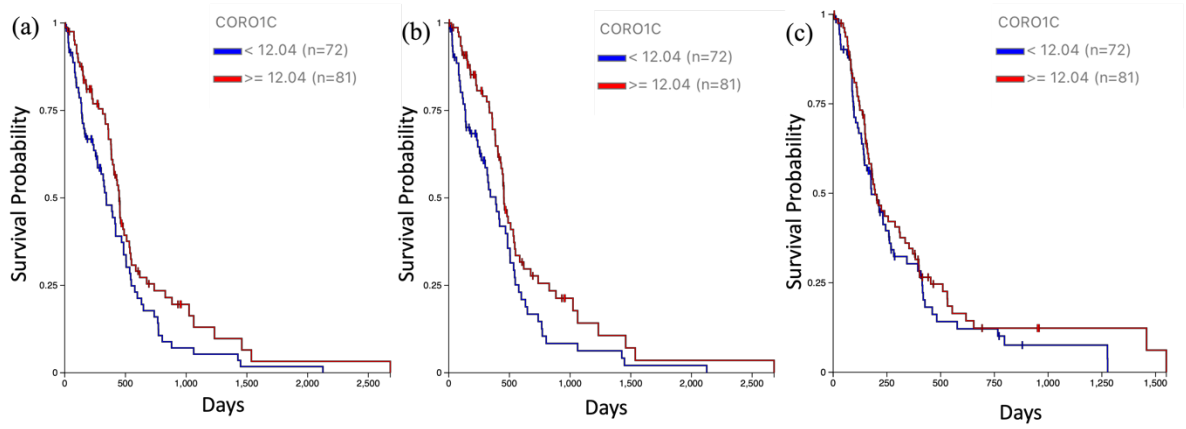


Figure 30. Survival analysis of *CORO1C* expression in glioblastoma cases. (a) Survival analysis showed that higher *CORO1C* levels were associated with significantly longer OS ($p<0.03$). (b) Disease-specific survival analysis indicated that elevated *CORO1C* expression correlated with longer disease-specific survival ($p<0.02$). (c) Progression-free survival analysis in GB did not reveal statistically significant differences ($p<0.27$).

2.3.9. CORO1C pathway and protein analysis

The CORO1C pathway was analysed to elucidate its role in various cellular processes associated with tumour progression and metastasis (Figure 31). The network diagram highlighted the central role of CORO1C in regulating multiple critical functions related to actin filament dynamics. CORO1C appeared to directly influence a variety of processes, including tumour cell invasion, metastasis, cell shape, and intracellular transport, as well as immune-related functions such as immune synapse formation and immune cell migration. Figure 31 also indicates that CORO1C interacts with important signalling molecules such as Rac1 and Cdc42. The analysis of CORO1C protein interactions revealed that it had the strongest interaction physical interaction with CORO1B (Figure 32a). Further investigation using the GeneMANIA database provided a comprehensive interaction network, highlighting physical interactions between CORO1C and several other proteins. The database identified physical

associations with CORO1B, WDR1, ETF1, CYB5B, RCC2, SEC31B, TCP1, ACTB, PHKB, FAP, PREB, SMOC1, RIPK3, and DNAJB11 (Figure 32b).

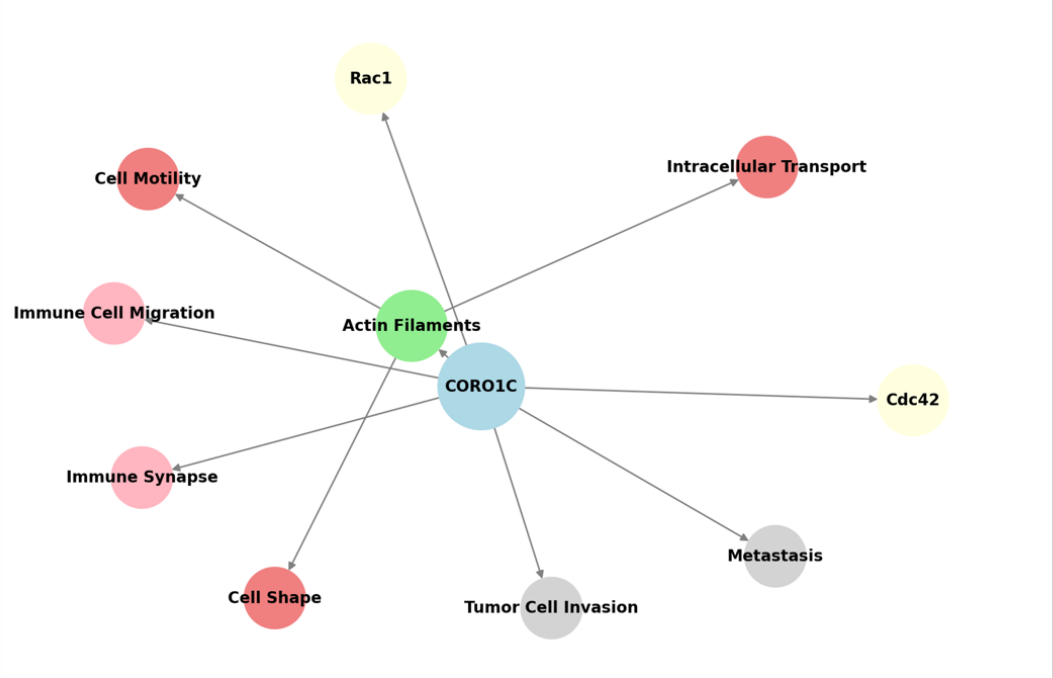


Figure 31. CORO1C pathway analysis and its role in cellular processes associated with tumour progression and metastasis. The diagram illustrated the central role of CORO1C in regulating critical functions related to actin filament dynamics and processes such as tumour cell invasion, metastasis, cell shape, and intracellular transport. The interactions between CORO1C and key signalling molecules, such as Rac1 and Cdc42, were also observed.

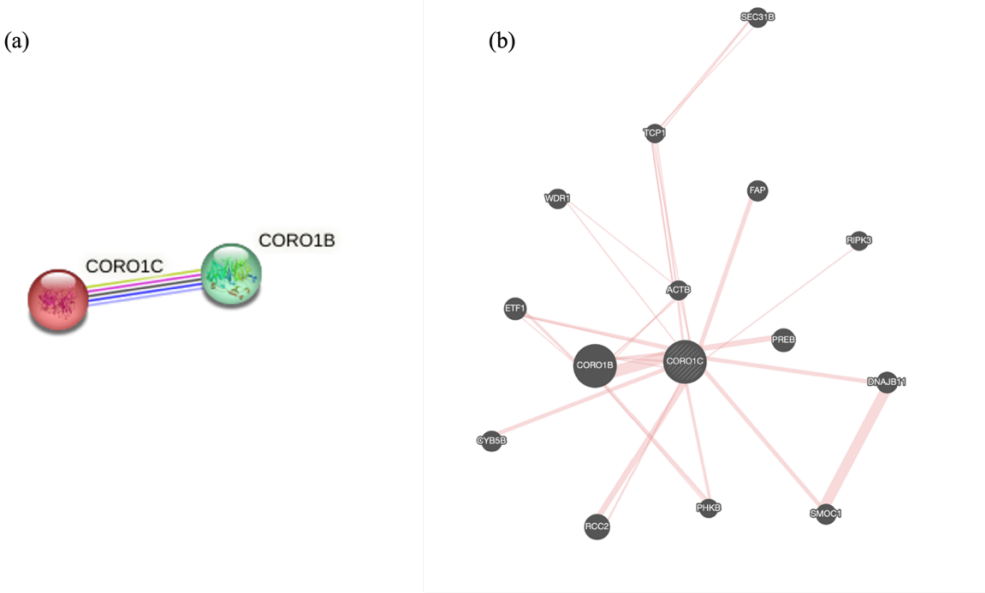


Figure 32. CORO1C protein interaction network. (a) The STRING analysis revealed that CORO1C has the strongest physical interaction with CORO1B. (b) A broader investigation using the GeneMANIA database identified additional physical interactions of CORO1C with multiple proteins, including CORO1B, WDR1, ETF1, CYB5B, RCC2, SEC31B, TCP1, ACTB, PHKB, FAP, PREB, SMOC1, RIPK3, and DNAJB11.

2.3.10. *SV2B* gene expression analysis in normal tissues and brain

Figure 33 shows the mRNA expression profile of *SV2B* in normal tissues. The highest expression measured nTPM, was detected in areas of the brain, such as the cerebral cortex (312.9 nTPM), followed by the cerebellum (305.5 nTPM), pons (253.5 nTPM), olfactory bulb (215.0 nTPM), and hippocampal formation (190.8 nTPM). When other tissues were analysed separately, the average *SV2B* expression was observed in the pancreas (18.9 nTPM), heart muscle (17.1 nTPM), adipose tissue (14.6 nTMP), and pituitary gland (11.9 nTPM). When analysed separately, the highest expression of SV2B in the brain revealed expression in the cerebral cortex and white matter (139.7 nTPM and 95.5 nTPM, respectively) (Figure 34). Single-cell analysis of the brain revealed that *SV2B* was highly expressed within excitatory neuronal cells. Within the glial cluster, which includes astrocytes, oligodendrocytes, oligodendrocyte precursor cells, and microglial cells, the expression of *SV2B* was particularly low (Figure 35). These included clusters c-12, c-35, c-37, and c-42. The expression of *SV2B* in various brain regions of six patients was assessed using heatmaps of log2 expression values obtained via microarrays. High expression of *SV2B* was observed in the hippocampal formation, cerebral cortex, and frontal and temporal lobes. Figure 36 illustrates the MRI scans and heatmaps from six healthy individuals who died from causes other than brain tumours. The expression was predominantly present in the hippocampal formation (log2 expression 12.5 ± 2.5), cerebral cortex (log2 expression 12.2 ± 2.5), frontal lobe (log2 expression 7.5 ± 2.5), and temporal lobe (log2 expression 12.5 ± 2.5). Additionally, high expression levels of *SV2B* were observed in the claustrum (log2 expression 12.9 ± 2.5) and parietal lobe (log2 expression 7.8 ± 2.5).

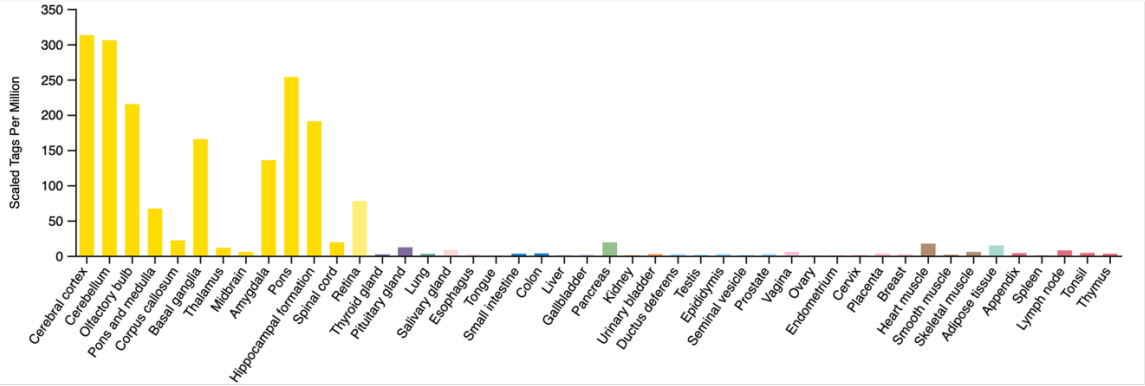


Figure 33. Detection of *SV2B* mRNA across different tissue types. Elevated expression levels were observed in the cerebral cortex, followed by the cerebellum, pons, olfactory bulb, and hippocampal formation.

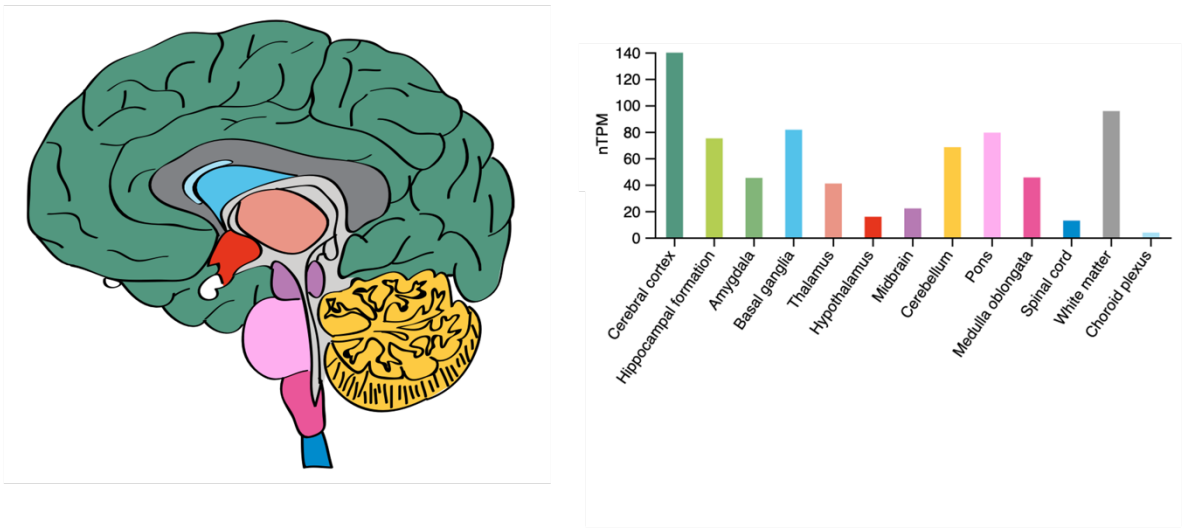


Figure 34. Detection of *SV2B* mRNA across the normal brain. Analysis of *SV2B* mRNA distribution within the brain revealed high expression in the cerebral cortex and white matter.

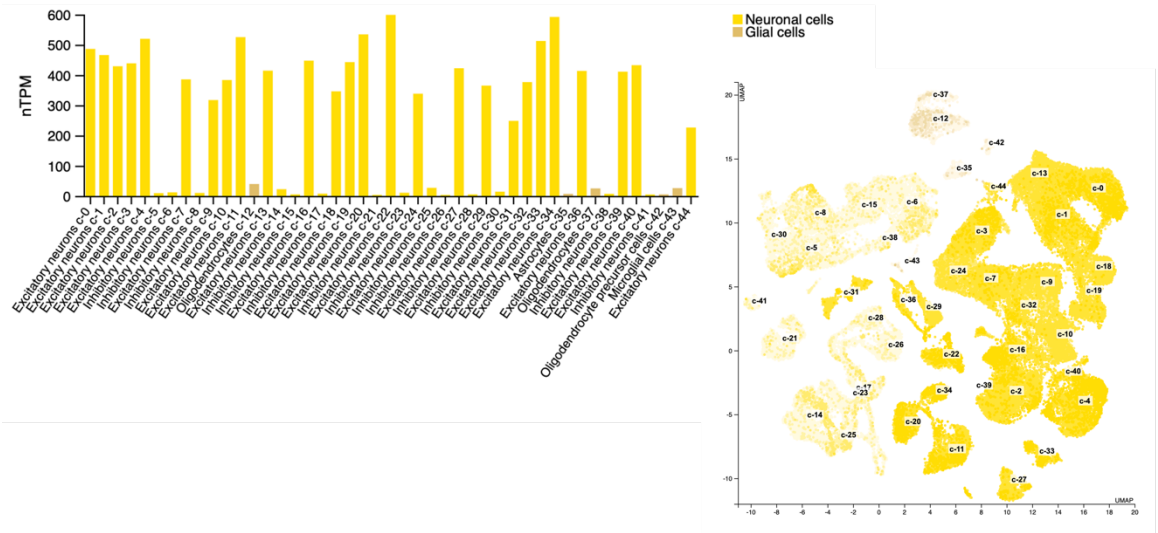


Figure 35. Detection of *SV2B* mRNA across normal brain cells. Single-cell cluster analysis of normal brain tissue indicated significant expression of *SV2B* in excitatory neuronal cells, whilst astrocytes, oligodendrocytes, oligodendrocyte precursor cells, and microglial cells showed very low *SV2B* mRNA levels.

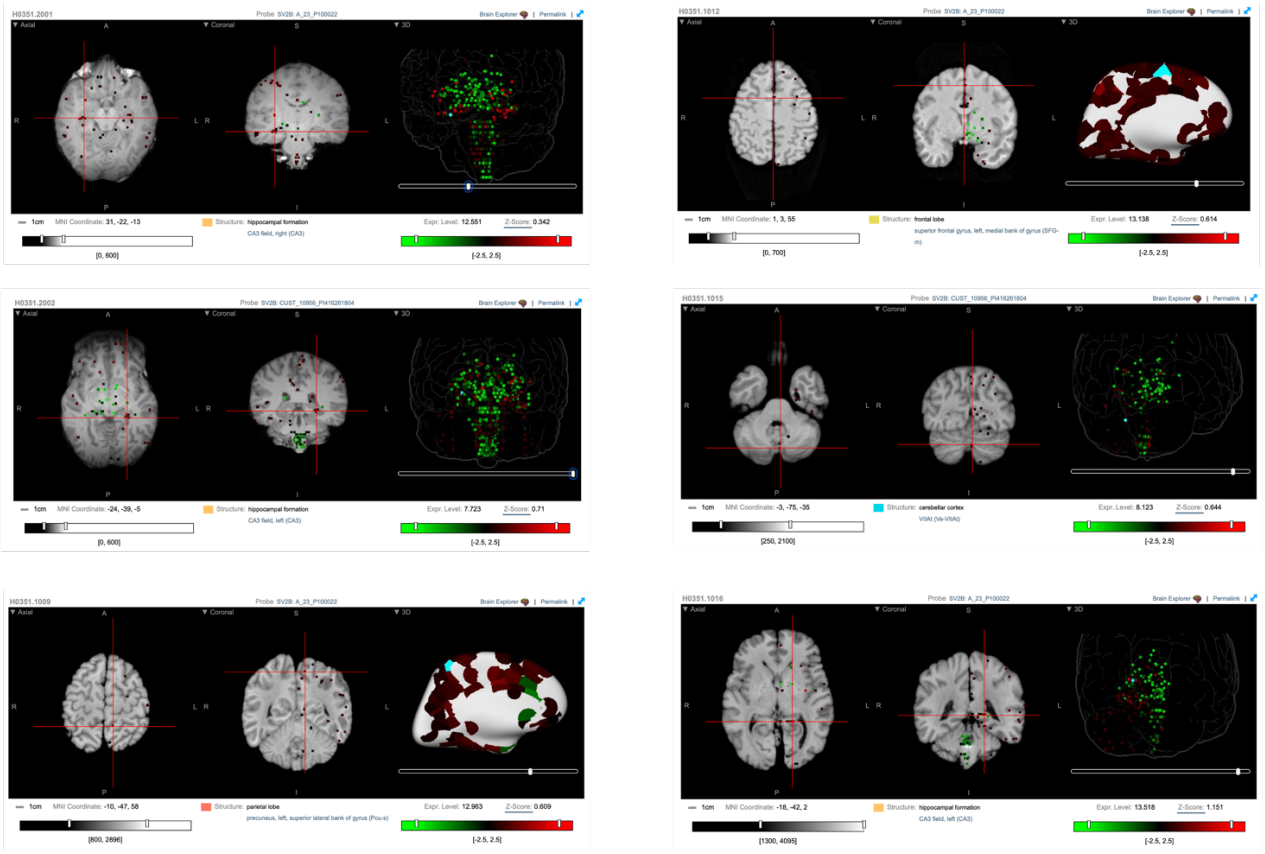


Figure 36. Heatmaps of log2 expression values from six patients obtained through microarray experiments (Allen Brain Atlas). The analysis indicated that *SV2B* is highly expressed in the hippocampal formation, cerebral cortex, frontal and temporal lobes.

2.3.11. *SV2B* gene expression analysis in different cancer types and GB

Figure 37 illustrates TCGA RNA-seq data, highlighting the expression of *SV2B* across various cancer types. Among the 17 cancer types analysed, *SV2B* expression was highest in pancreatic cancer and gliomas, with median FPKM values of 0.4 and 0.4, respectively. Figure 38 depicts *SV2B* expression based on patients' ages. Three GB age groups (21–80 years) exhibited significantly lower median *SV2B* expression levels compared to their normal counterparts. There was also a significant difference between the age groups 21-40 years (0.39 nTPM) and 41-60 years (0.49 nTPM), with the later expressing higher levels of the mRNA. Additionally, the analysis showed that *SV2B* has significantly lower median expression in both males and females compared to their normal counterparts (Figure 39). Even though the expression was lower than the control cohort, males expressed slightly higher levels of SV2B in comparison to females (0.83 nTPM versus 0.5 nTPM). Significantly low levels of *SV2B* mRNA were also detected in all GB races (Figure 40). *SV2B* median expression among different racial groups was significantly lower compared to the control group. However, there was no significant

differences in the expression of the mRNA between the racial groups part of the analysis (Caucasian 0.83 nTPM; African-America 2.10 nTPM; Asian 0.36 nTPM). Figure 41 shows SV2B expression in different types of paediatric brain malignancies. The highest median expression was detected in medulloblastomas (38.97 nTPM), followed by pineoblastoma (PBL), gangliogliomas (GNG) and DNT (37.23 nTPM, 10.29 nTPM and 8.93 nTPM). Medulloblastoma samples showed significantly higher expression of *SV2B* in comparison to all other paediatric brain tumours.

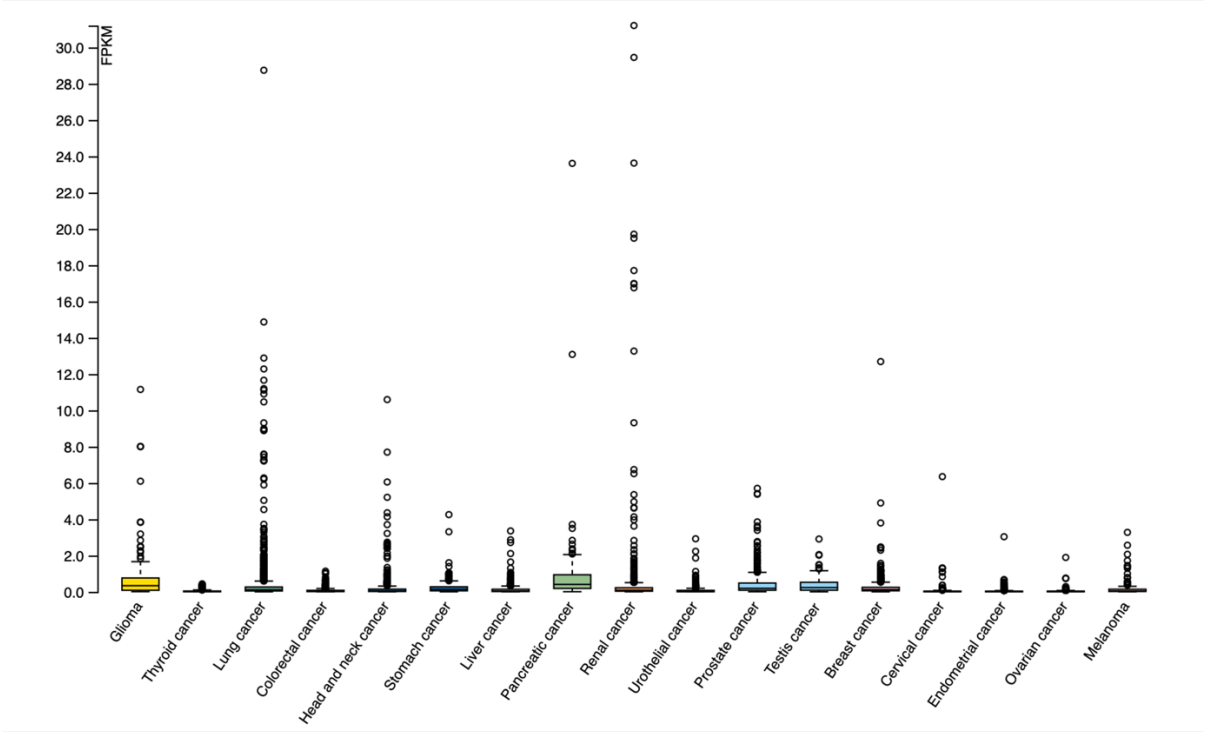


Figure 37. Expression of *SV2B* in various cancerous tissues. *SV2B* expression was most elevated in pancreatic cancer and gliomas.

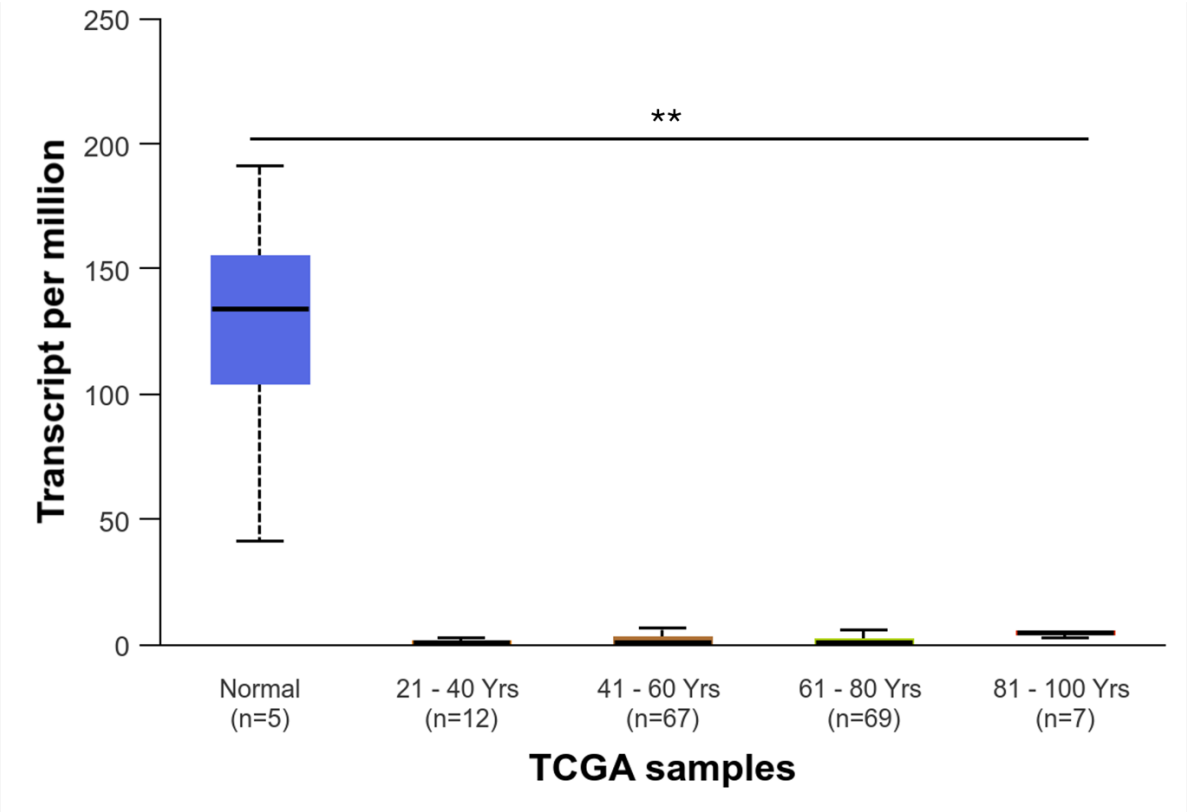


Figure 38. *SV2B* expression across different age groups in GB patients. All three GB age groups (21–40; 41-60; 61-80; 81-100 years) exhibited significantly lower median *SV2B* expression levels compared to their normal counterparts ($p<0.028$, $p<0.029$, $p<0.029$ and $p<0.032$, respectively). Additionally, a significant difference in *SV2B* expression was observed between the 21-40 years age group and the 41-60 years age group, with the latter exhibiting higher mRNA expression levels ($p<0.026$).

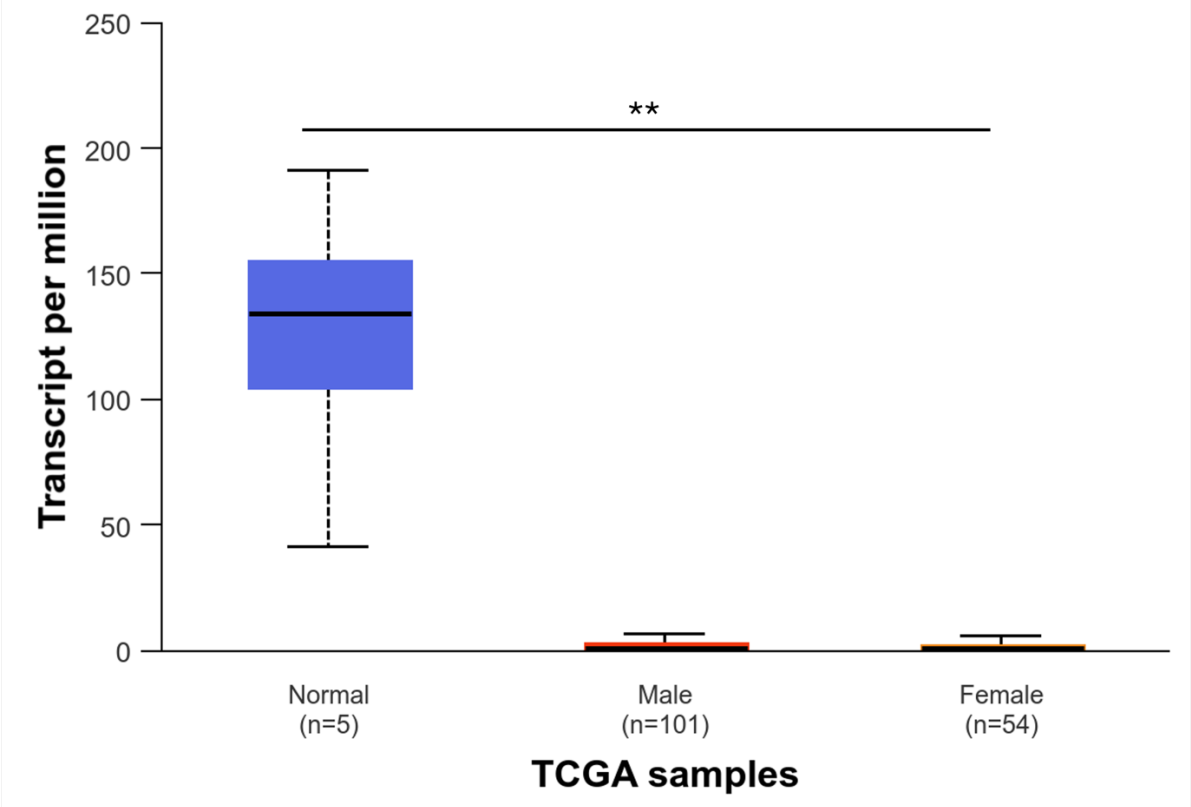


Figure 39. *SV2B* expression in male and female GB patients compared to normal controls. The analysis revealed that both males and females exhibit significantly lower median *SV2B* expression levels compared to their normal counterparts ($p<0.029$ and $p<0.028$, respectively).

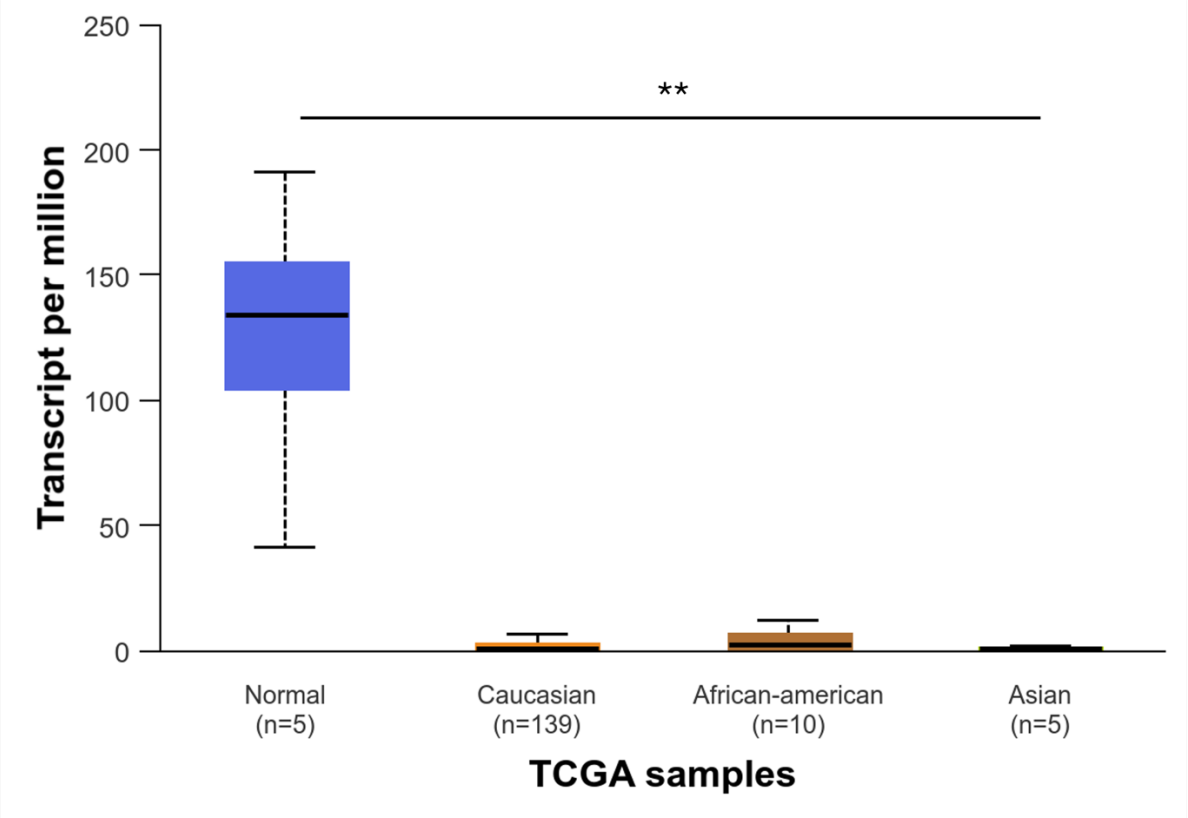


Figure 40. *SV2B* mRNA expression across different racial groups in GB patients compared to controls. The analysis showed significantly lower *SV2B* expression levels across all racial groups when compared to the control group (Normal versus Caucasian, $p<0.029$; Normal versus African-American, $p<0.030$; Normal versus Asian, $p<0.030$).

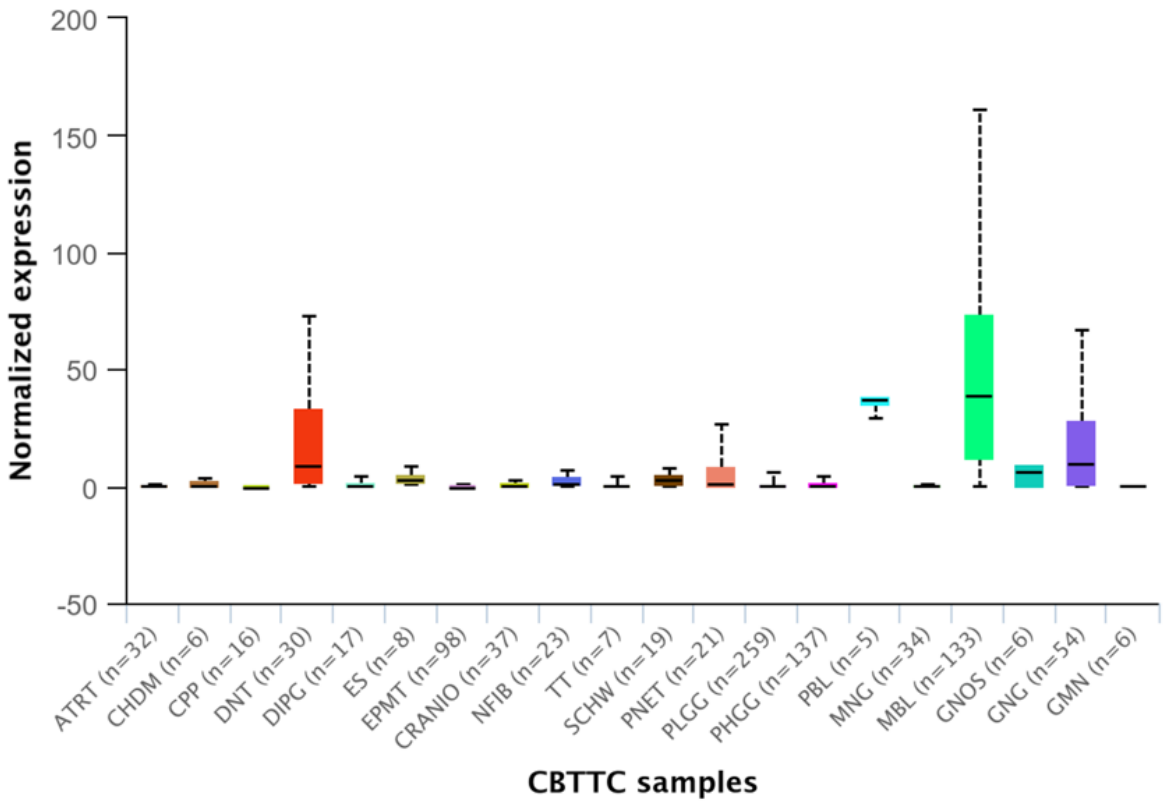


Figure 41. *SV2B* expression across different types of paediatric brain malignancies. The figure illustrated that the highest median *SV2B* expression was detected in MBs, followed by PBL, GNG and DNT. Medulloblastoma samples exhibited significantly higher *SV2B* expression compared to all other paediatric brain tumours analysed ($p<0.0001$). The CBTTC UALCAN analysis compares mean gene expression levels in paediatric brain tumour samples to those in normal tissues (not shown) or between different tumour subgroups.

2.3.12. *SV2B* mRNA expression analysis in GB cells

Figure 42a shows the tSNE heatmap with *SV2B* expression within some cells within the malignant cell cluster and oligodendrocyte cell cluster, with limited expression observed in the macrophage and T-cell clusters (lower panel). The median expression levels of *SV2B* ranged between logTPM of 1-1.5, with some cells expressing the mRNA at logTPM of 8. Further evaluation of SV2B expression was conducted via a two-dimensional representation of each cellular state. The heatmap of logTMP expression in Figure 42b revealed that *SV2B* was expressed mainly in the NPC-like cells with values of logTPM ranging between 7-8. Notably, the expression within the NPC-like state was slightly higher than in other cellular states (lower panel). *SV2B* expression within some parts of the paediatric cluster was higher than in others, ranging between logTPM of 1 and logTPM of 8 (Figure 42c). The same was observed within

the cluster composed of adult GB cells. However, the results indicated that adult cells expressed more *SV2B* in comparison to paediatric cells (lower panel).

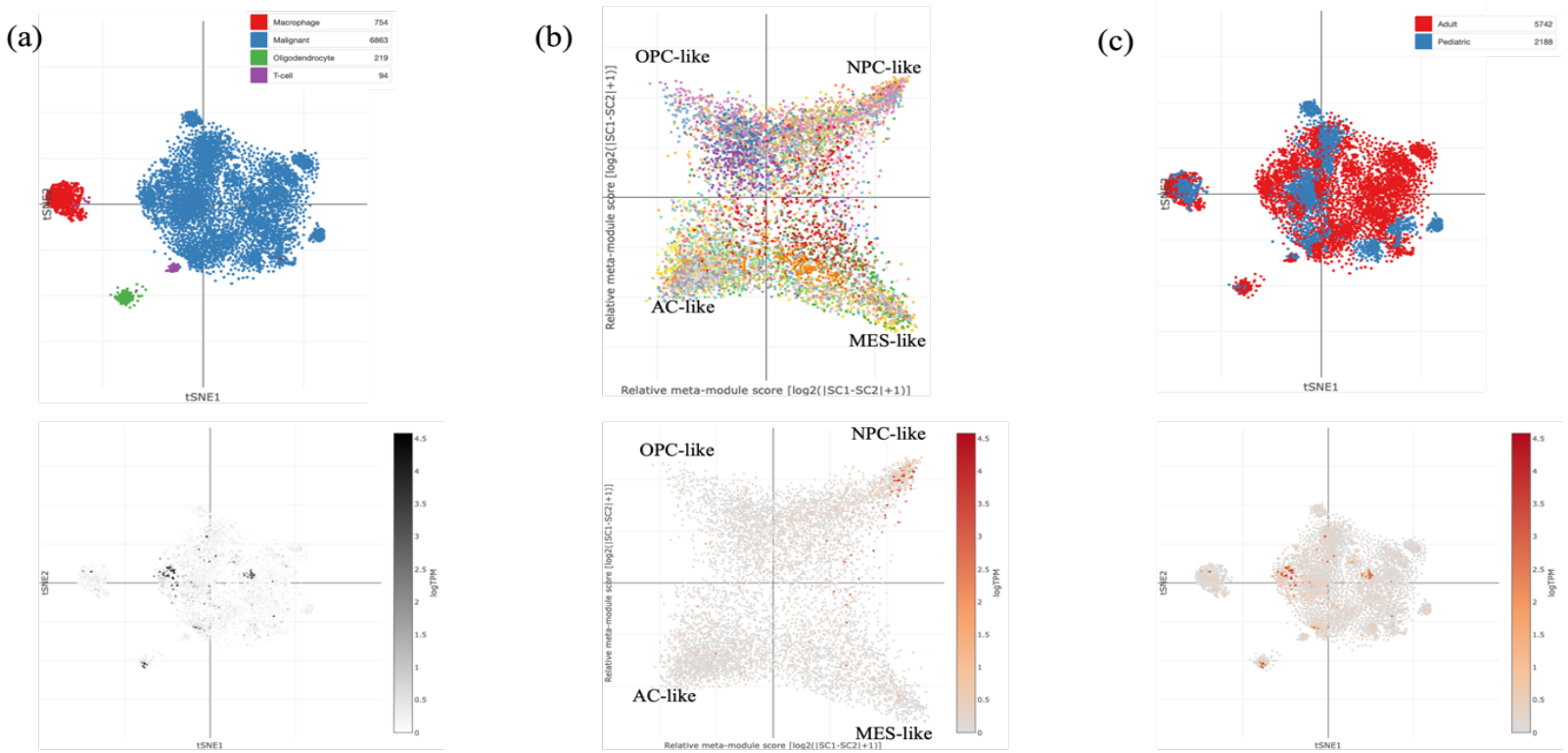


Figure 42. Single-cell *SV2B* analysis of GB cell clusters from paediatric and adult patients. (a) The tSNE heatmap displayed *SV2B* expression within few cells in the malignant cell cluster (blue) and oligodendrocyte cell cluster (green), with minimal expression observed in the macrophage (red) and T-cell clusters (purple). (b) Further analysis using a two-dimensional representation of cellular states revealed that *SV2B* expression was primarily observed in NPC-like cells, with logTPM values ranging between 7 and 8, which was higher than in other cellular states. (c) *SV2B* expression was higher in some parts of the paediatric cluster compared to others, with values ranging between logTPM 1 and logTPM 8. Similarly, within the cluster of adult GB cells, *SV2B* expression was generally higher, indicating that adult cells express more *SV2B* compared to paediatric cells.

2.3.13. *SV2B* survival analysis in GB cases

Survival analysis of primary GB samples revealed that patients with higher *SV2B* expression had significantly shorter OS and disease-specific survival compared to those with lower expression levels ($p < 0.01119$ and $p < 0.02197$, respectively) (Figures 43a and 43b). However, differences in *SV2B* expression profiles within the PFS analysis of GB were not statistically significant (Figure 43c).

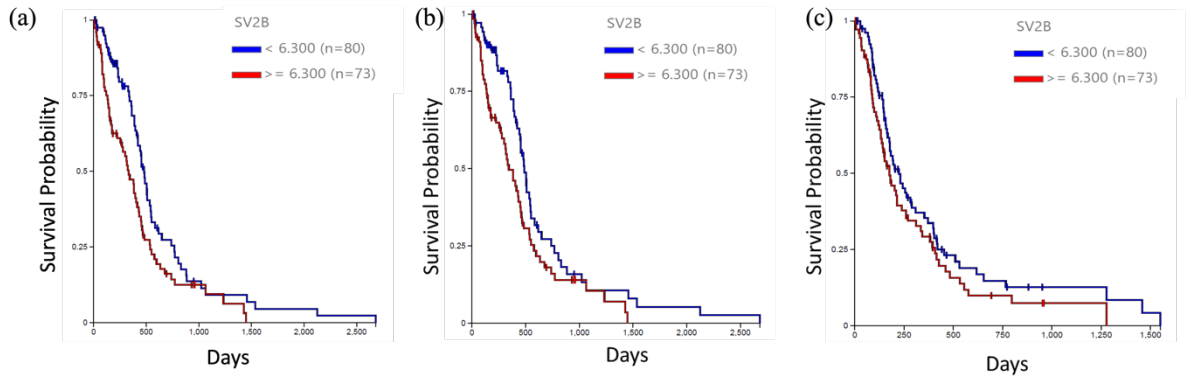


Figure 43. Survival analysis of *SV2B* expression in glioblastoma cases. (a) Survival analysis showed that elevated *SV2B* levels were significantly associated with shorter OS ($p<0.01119$). (b) Disease-specific survival analysis revealed that high *SV2B* expression correlated with reduced disease-specific survival ($p<0.02197$). (c) Progression-free survival analysis in GB did not demonstrate statistically significant differences.

2.3.14. SV2B pathway and protein analysis

The integrated KEGG pathway analysis (Figure 44a) revealed that members of the SV2 protein family, including SV2B, function as proteoglycans involved in ECM–receptor interactions, particularly with laminins. SV2B was found to closely interact with SYT1, emphasising its role in ECM-receptor signalling pathways (Figure 44b). The STRING analysis of SV2B revealed significant physical interactions with other members of the SV2 protein family, specifically SV2A and SV2C, as well as with SYT1 and glycoprotein 2 (GP2) (Figure 45a). Further investigation using the GeneMANIA database identified additional physical interactions between SV2B and a broader network of proteins, including C6orf15, SCTR, SYT1, SV2C, CA10, SV2A, and SLC17A7 (Figure 45b).

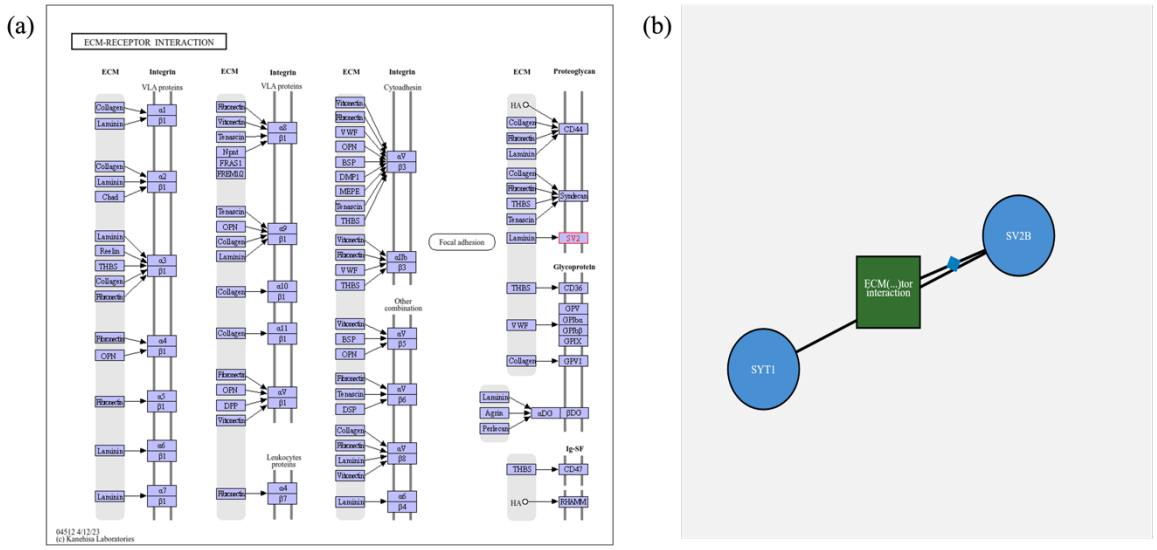


Figure 44. Integrated KEGG pathway analysis of SV2B. (a) The diagram showed that the SV2 protein family members, including SV2B, function as proteoglycans involved in ECM–receptor interactions, particularly with laminins. (b) Further analysis highlighted the close interaction between SV2B and SYT1, emphasising SV2B's role in ECM-receptor signalling pathways.

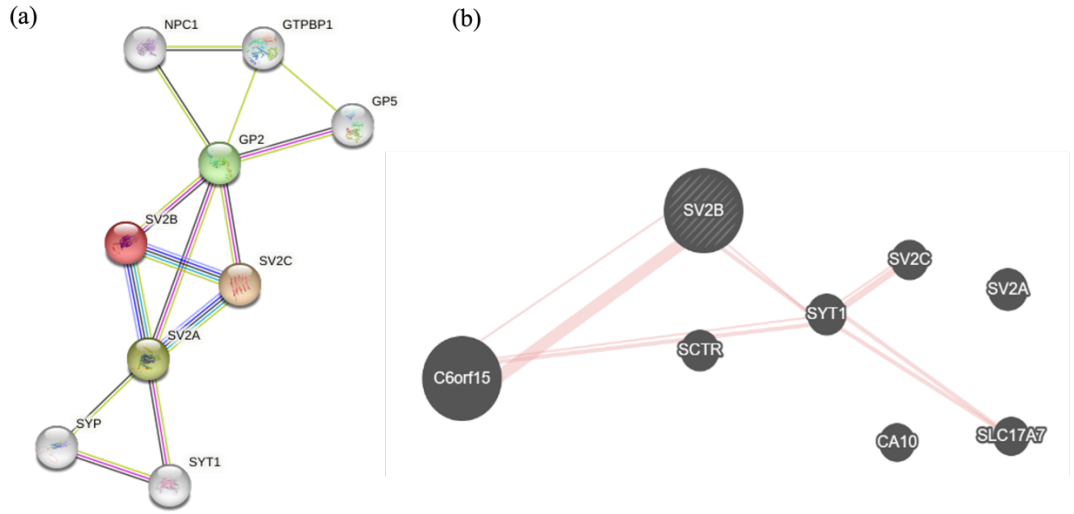


Figure 45. SV2B protein interaction network. (a) SV2B demonstrated physical interactions with other SV2 protein family members, specifically SV2A, SV2C, SYT1 and GP2. (b) GeneMANIA database analysis revealed additional physical interactions between SV2B and an expanded network of proteins, including C6orf15, SCTR, SYT1, SV2C, CA10, SV2A, and SLC17A7.

2.4. Discussion

The limited success in achieving favourable clinical outcomes for primary brain malignancies has encouraged increased efforts to understand the role of miRNAs in their pathogenesis. Our *in silico* investigation aimed to elucidate the roles of the identified miR-21, miR-34a, miR-128a, miR-206, and miR-383, and their effects on their target genes, *CORO1C* and *SV2B*.

Specifically, our *in silico* analysis revealed that miR-21 was overexpressed in GB tumours, whereas miR-128a, miR-34a, miR-206, and miR-383 were downregulated. These findings were supported by KEGG pathway analysis, which also indicated the upregulation of miR-21 functioning as an oncogene and the downregulation of miR-34a and miR-128a, suggesting that they manifest tumour suppressive roles.

MiR-21 plays a pivotal role in the pathogenesis of GB. Recent studies have demonstrated that miR-21 is significantly overexpressed in GB and contributes to tumour growth, proliferation, invasion, and resistance to therapy (Charbit & Lavon, 2024; Shaikh, *et al.,* 2024). One of the mechanisms through which miR-21 exerts its critical role in GB pathogenesis is through the regulation of tumour suppressor genes. MiR-21 targets several tumour suppressor genes, including *PTEN*, the reversion-inducing cysteine-rich protein with kazal motifs (*RECK*), and the programmed cell death 4 gene (*PDCD4*) (Bautista-Sánchez, *et al.,* 2020). By downregulating these genes, miR-21 promotes cell proliferation, invasion, and survival. For instance, *PTEN* is a critical regulator of the PI3K/Akt pathway, and its inhibition by miR-21 led to enhanced Akt signalling, promoting cell survival and growth (Ghafouri-Fard, *et al.,* 2021). Furthermore, miR-21 exhibited anti-apoptotic properties by targeting and downregulating pro-apoptotic genes such as the Fas ligand and Bcl-2 interacting mediator of cell death (*BIM*). This resulted in reduced caspase activation and decreased apoptotic cell death, contributing to the survival and proliferation of GB cells (Carneiro & El-Deiry, 2020). MiR-21 is also implicated in the regulation of angiogenesis, a crucial process for tumour growth and metastasis. It modulates the expression of *VEGF* and other angiogenic factors. Hermansen and colleagues demonstrated that miR-21 influenced GB angiogenesis by targeting the hypoxia-inducible factor-1α (*HIF-1α*) and *PTEN*, thereby enhancing the angiogenic potential of GB cells (Hermansen, Nielsen, Aaberg-Jessen & Kristensen, 2016). Additionally, miR-21 has been shown to interact with several key signalling pathways involved in GB pathogenesis, including the MAPK, STAT3, and TGF-β/Smad pathways. By modulating these pathways, miR-21 enhances the oncogenic potential of GB cells. For example, it has been shown to activate the

TGF-β/Smad3 signalling pathway, which is involved in cell proliferation, differentiation, and survival (Zhang, Alexander & Wang, 2017). Given its crucial role in GB pathogenesis, miR-21 has emerged as a potential biomarker for diagnosis, prognosis, and therapy. The elevated levels of miR-21 in GB tissues and exosomes suggested its value as a non-invasive diagnostic marker. Studies have demonstrated that miR-21 expression levels correlated with tumour grade and patient prognosis, suggesting its potential as a valuable prognostic biomarker (Bautista-Sánchez, *et al.,* 2020; Beylerli, Gareev, Sufianov, Ilyasova & Zhang, 2022). Several therapeutic strategies targeting miR-21 are being explored. These include the use of anti-miR-21 oligonucleotides, miR-21 sponges, and small molecule inhibitors that block miR-21 biogenesis and function (Wen, Danquah, Chaudhary & Mahato, 2015). For instance, AC1MMYR2 is a small molecule that inhibits the maturation of miR-21, thereby reducing its oncogenic effects (Zhao, Fu, Zhu, Chen & Liu, 2022b). Nevertheless, obstacles such as potential off-target effects, compromised tissue-specific delivery, poor cellular uptake, and *in vivo* instability are commonly associated with newly developed miRNA therapies (Segal & Slack, 2020). Thus, further research into miR-21 inhibitors and their integration with existing treatments could pave the way for more effective GB therapies and improved patient outcomes.

MiR-34a has also been found to play a significant role in the pathogenesis and progression of GB. Recognised as a tumour suppressor, miR-34a exerts its effects by targeting multiple genes involved in cell cycle regulation, apoptosis, and differentiation (Kalfert, *et al.,* 2020). One of the key pathways influenced by miR-34a is the p53 pathway, a crucial regulator of the cell cycle and apoptosis. MiR-34a is directly regulated by p53, and its expression is often reduced in p53-mutated tumours, including GB (Li, *et al.,* 2021). Previous research has observed that miR-34a suppressed the expression of oncogenes such as the high mobility group AT-hook 2 (*HMGA2*) and the MET proto-oncogene, receptor tyrosine kinase (*c-Met*) (Ma, Fu, Zhao & Gao, 2019; Li, *et al.,* 2009). *HMGA2* is involved in promoting cell proliferation and metastasis, while *c-Met* is associated with cell survival and motility. By downregulating these oncogenes, miR-34a inhibited tumour growth and induced apoptosis, which is a key mechanism for eliminating GB cancer cells (Li, *et al.,* 2009). Additionally, the involvement of miR-34a in promoting apoptosis was further supported by its ability to enhance the expression of pro-apoptotic proteins like BCL2 associated X, apoptosis regulator (BAX) while inhibiting anti-apoptotic proteins such as BCL2, promoting cell death of GB cells (Beylerli, Gareev, Sufianov, Ilyasova & Zhang, 2022). Furthermore, in GB, miR-34a targeted and suppressed genes, such as *Notch1* and *Jagged1* involved in the epithelial-mesenchymal transition (EMT), thereby

reducing the invasive potential of cancer cells (Imani, *et al.,* 2017). Vaitkiene and colleagues reported that lower miR-34a expression was linked to larger tumour volumes, reduced physical functioning, and lower Karnofsky Performance Status (KPS) scores in patients with GB (Vaitkiene, *et al.,* 2019). However, these findings are considered preliminary due to the small sample size used in the study. Additionally, miR-34a was significantly downregulated in patients' serum samples, indicating its potential as a promising non-invasive biomarker for GB. Nevertheless, larger studies are needed to validate its clinical significance (Vojdani, *et al.,* 2021). MiR-34a has also shown potential in overcoming chemoresistance, which is considered one of the most significant challenges in GB treatment. By targeting genes associated with drug resistance, such as sirtuin 1 (*SIRT1*), miR-34a enhances the sensitivity of GB cells to chemotherapeutic agents like TMZ (Singh, Mondal, Janjua, Popat & Kulshreshtha, 2023). These findings suggested that miR-34a-based therapies could be a viable strategy for treating GB. Clinical trials are exploring the use of miR-34a mimics as a novel therapeutic approach, aiming to harness its tumour-suppressive properties to combat GB more effectively (Hong, *et al.,* 2020). Its significant roles make miR-34a a promising target for developing new therapeutic strategies to improve outcomes for GB patients.

MiR-128a is an intronic miRNA primarily found in the brain and has been linked to normal brain development (Franzoni, *et al.,* 2015). However, miRNA assays, RT-qPCR, and western blot analyses have shown that miR-128a is expressed at lower levels in aggressive solid brain tumours, including GB (Roth, *et al.,* 2011). Our *in silico* analysis revealed that miR-128a was downregulated in GB patient samples, suggesting its tumour-suppressive properties. These findings align with previous evidence that identified low miR-128 levels in both serum and tissue samples from GB patients (Sun, *et al.,* 2015). MiR-128 is generally considered a tumour suppressor miRNA in GB, as its downregulation is associated with increased tumour growth and aggressiveness. It has been observed that miR-128 targets p70S6K1 (Shi, *et al.,* 2012). By targeting this protein, miR-128 can reduce *VEGF* and *HIF-1α* expression, which are crucial for tumour angiogenesis and survival under hypoxic conditions (Shi, *et al.,* 2012). Bmi-1, a protein regulating stem cell renewal, is downregulated by miR-128, resulting in reduced self-renewal of GB stem cells (Shan, *et al.,* 2016). Additionally, miR-128 targets *RhoE* to suppress GB cell proliferation and induce apoptosis (Budi, *et al.,* 2023). Furthermore, Budi and colleagues outlined that miR-128 increases GB cells' sensitivity to TMZ by targeting genes involved in drug resistance and modulating the c-Met/EMT pathway and RUNX1/MRP1 axis, crucial for drug resistance mechanisms (Budi, *et al.,* 2023). In terms of metabolic regulation, miR-128

affected GB cell metabolism by targeting the pyruvate dehydrogenase kinase 1 gene (*PDK1*), involved in the Warburg effect which is prevalent in cancer cells. This targeting led to reduced lactate production, increased reactive oxygen species (ROS), and mitochondrial dysfunction, thereby inhibiting tumour cell growth and survival (Qu, *et al.,* 2020). Furthermore, overexpression of miR-128 induced apoptosis and caused cell cycle arrest in the G0/G1 phase in GB cells by increasing the expression of apoptotic proteins such as caspase-3 and Bax while decreasing anti-apoptotic proteins like BCL2 (Budi, *et al.,* 2023). Given its wide range of regulatory functions and tumour-suppressive effects, miR-128 is considered a promising therapeutic target for GB treatment. Strategies to upregulate miR-128 or mimic its function could potentially improve GB outcomes by inhibiting tumour growth and enhancing the efficacy of existing therapies.

Even though miR-206 and its relation to GB has been less studied, there is evidence that it functions predominantly as a tumour suppressor miRNA. Several studies highlighted that miR-206 is notably downregulated in GB tissues compared to normal brain tissues (Hao, *et al.,* 2016; Zhou, *et al.,* 2019a). This downregulation is associated with higher glioma grades and poorer overall survival rates in patients (Zhou, *et al.,* 2019a). The differential expression of miR-206 serves as a potential biomarker for distinguishing GB from non-cancerous tissues and possibly predicting patient prognosis (Hosein Yazdi, Zarrinpour, Moslemi & Forghanifard, 2022). MiR-206 exerts its tumour-suppressive effects primarily through the regulation of cell cycle-related proteins and pathways. One of the critical targets of miR-206 is cyclin D2, a protein involved in cell cycle regulation. By directly binding to the 3'UTR of cyclin D2 mRNA, miR-206 inhibited its expression. This suppression led to G1/S phase arrest in the cell cycle, thereby reducing cell proliferation (Yang, *et al.,* 2015b). Transfection of glioma cells with miR-206 mimics resulted in a significant reduction in cyclin D2 levels, which correlated with decreased cell proliferation and colony formation (Yang, *et al.,* 2015b). Moreover, cell cycle analysis revealed an increased percentage of cells in the G0/G1 phase and a corresponding decrease in the S and G2 phases upon miR-206 overexpression, confirming its role in cell cycle arrest (Yang, *et al.,* 2015b). The inverse correlation between miR-206 and cyclin D2 levels further emphasised its role in glioma prognosis, as higher cyclin D2 levels were associated with higher tumour grades and poorer survival rates (Juric & Murphy, 2020). Given its tumour-suppressive functions, miR-206 presents a promising target for therapeutic interventions in GB. Strategies to upregulate miR-206 or mimic its function could potentially inhibit glioma

progression and improve patient outcomes. However, further research is needed to fully elucidate the molecular mechanisms by which miR-206 exerts its effects in GB cells.

MiR-383 was also depicted as GB-relevant miRNA throughout our *in silico* analysis. Previous research has shown that this miRNA plays a tumour suppressor role through various mechanisms that inhibit glioma cell proliferation, migration, invasion, and angiogenesis. MiR-383 was observed to be downregulated in glioma tissues compared to normal brain tissues, with its expression inversely correlating with glioma pathological grades (He, *et al.,* 2013). This suggested that miR-383 could serve as a useful diagnostic marker and potentially as a therapeutic target for gliomas (He, *et al.,* 2013). MiR-383 has been shown to significantly inhibit glioma cell growth by inducing cell cycle arrest at the G0/G1 phase. This tumour-suppressive effect was mediated through the direct targeting and downregulation of cyclin D1 (*CCND1*), a crucial regulator of cell cycle progression (Yi, Xie, Sun, Sun & Liao, 2022). Overexpression of miR-383 in glioma cell lines such as U251 and U87 resulted in a substantial decrease in *CCND1* levels, leading to reduced cell proliferation and anchorage-independent growth (Yi, *et al.,* 2022). Upregulation of miR-383 led to a reduction in the migration and invasion capabilities of GB cells. This effect was partly due to miR-383-dependent regulation of the insulin-like growth factor 1 receptor (IGF1R) pathway. MiR-383 directly targeted *IGF1R*, reducing its expression and subsequently inhibiting the downstream AKT signalling pathway and matrix metallopeptidase 2 (*MMP2*) expression, both of which are critical for cell invasion (Jafarzadeh, *et al.,* 2022; Liu, Wang, Tang, Fu & Wang, 2024). MiR-383 also significantly inhibited the angiogenic potential of glioma-exposed endothelial cells (GECs). This inhibition is mediated through the VEGF signalling pathway (Zhao, *et al.,* 2017). miR-383 downregulated *VEGF* and its receptor VEGFR2, as well as associated signalling molecules such as focal adhesion kinase (FAK) and Src. The suppression of these pathways resulted in decreased endothelial cell proliferation, migration, and tube formation, which are essential steps in angiogenesis (Zhao, *et al.,* 2017). Considering its tumour suppressive role in glioma progression through the regulation of cell proliferation, invasion, and angiogenesis, miR-383 holds great potential as a therapeutic target for GB patients.

Our interactome analysis identifying key miRNAs involved in the regulation of *CORO1C* and its co-expressed genes depicted miR-34a-5p, miR-128-3p, and miR-206-5p as significant regulators within this gene network. This suggested that these miRNAs play a crucial role in modulating the expression of *CORO1C* and its associated genes, potentially impacting various

cellular processes governed by these genes. The results of the Sfold analysis identified a single binding site for miR-34a-5p at the 3'UTR of *CORO1C*. The binding interaction, described as an 8mer, indicated strong binding affinity and full complementarity. This suggested that miR-34a-5p might effectively downregulate *CORO1C* expression, potentially impacting cellular processes where *CORO1C* is involved, such as actin cytoskeleton organisation and cell motility. There is no previous evidence suggesting the binding interaction between miR-34a-5p and *CORO1C* in GB. Nevertheless, there is evidence that miR-34/449 promoted the assembly of an apical actin network, required for proper basal bodies anchoring in human and *Xenopus* vertebrate multiciliated cells (MCCs). Thus, miR-34/449 promoted re-localisation of the actin binding protein Filamin-A near basal bodies in MCCs **(**Chevalier, *et al.,* 2015**)**. Given the role of *CORO1C* in cytoskeletal rearrangements suggests that miR-34a-5p could modulate the expression of the *CORO1C* mRNA. For miR-128a-3p, the analysis revealed a single binding site at the 3'UTR of *CORO1C*, characterised as a 7mer-A1. This partial complementarity binding suggested a moderate regulatory effect of miR-128a-3p on *CORO1C*, which could modulate the gene's expression levels without completely silencing it. There is previous evidence that has suggested the interaction between miR-128a-3p and *CORO1C* in GB (Yang, *et al.,* 2015a). A luciferase assay validated that 11 of 13 selected genes were potential targets of miR-128, and a mutagenesis experiment confirmed that core-binding factor subunit beta (*CBFB*)*, CORO1C,* glycolipid transfer protein (*GLTP*)*,* heterogeneous nuclear ribonucleoprotein F (*HnRNPF*)*,* and TROVE domain family member 2 (*TROVE2*) as the target genes for the miRNA **(**Yang, *et al.,* 2015a**).** To the best of our knowledge, this is the only study that has previously identified an association between miR-128 and *CORO1C* by screening only a limited number of GB patients. We further investigated the interactions between miR-206-5p and *CORO1C*. MiR-206-5p has several important functions in the brain, particularly related to neurogenesis, synaptic plasticity, and neuroprotection (Williams, *et al.,* 2009). Its target, *CORO1C*, has been shown to regulate the formation and maintenance of lamellipodia: sheet-like cell protrusions involved in cell migration, which could directly impact tumour cell migration (King, *et al.,* 2022). Based on our results, miR-206 was targeting *CORO1C* in an 8mer manner, suggesting a stable binding between the miRNA and the mRNA followed by a complete degradation of the target mRNA. The presence of multiple binding sites suggested a robust regulatory influence of miR-206-5p on *CORO1C*, potentially leading to a significant downregulation of the gene. To the best of our knowledge, *CORO1C* has not been previously associated with GB. The link between miR-206 and *CORO1C* has been demonstrated in non-small lung cell carcinomas and triple-negative breast cancer, where deletion or inhibition of

CORO1C rescued the expression levels of miR-206 and led to suppressed metastasis (Liao & Peng, 2020; Wang, *et al.,* 2014). Zhou and colleagues suggested that miR-206 could potentially influence the β-catenin growth-dependent mechanism within the Wnt/β-catenin signalling pathway via targeting *CORO1C* (Zhou, *et al.,* 2019b). Nevertheless, to the best of our knowledge, the link between miR-206 and *CORO1C* in GB has not been previously demonstrated.

Our analysis identified miR-34a-5p, miR-128-3p, and miR-206-5p as regulators of SV2B and its co-expressed genes, including *C6orf15, SCTR, SYT1, SV2C, CA10, SV2A,* and *SLC17A7*. The binding interaction between miR-34a-5p and *SV2B* as a 7mer-A1, indicating a strong but partially complementary binding. This interaction may contribute to the regulation of *SV2B*, which is involved in synaptic vesicle trafficking, suggesting the role of miR-34a-5p in neuronal function and synaptic plasticity. To the best of our knowledge, the interaction between miR-34a and SV2B has not been demonstrated before. However, miR-34a-5p was found to play a crucial role in neurodevelopment, influencing various aspects of neurogenesis and synaptogenesis (Mollinari, *et al.,* 2015). Mollinari *et al.* identified that overexpression of miR-34a promoted neural precursor proliferation, altered neuron morphology and synaptic function, and improved response to synaptic stimuli. Furthermore, their *in vivo* experiments showed that miR-34a-5p affected neural progenitor proliferation, neuroblast migration, and the development of neuron complexity (Mollinari, *et al.,* 2015). Additionally, this miRNA plays a role in neuronal differentiation and brain aging by targeting key genes such as *CCND1*, *SIRT1*, and *Bcl-2*, suggesting that miR-34a possesses the potential to influence the expression of *SV2B* as well (Modi, Jaiswal & Sharma, 2015). Given that SV2B is involved in synaptic vesicle function and neuronal communication, miR-34a could regulate its expression, thereby affecting synaptic plasticity and neuronal aging processes. MiR-128a-3p showed three binding sites on *SV2B's* 3'UTR. The seed type interactions varied between 7mer-A1 and 6mer, indicating partial complementarity and suggesting a moderate regulatory effect. This multi-site interaction highlighted a potential cumulative impact on *SV2B* expression, which could influence neurotransmitter release and synaptic function. MiR-128 has emerged as an important player in the regulation of synaptic properties. Specifically, miR-128 has been shown to regulate the expression of *SNAP-25* and *SYT1*, two proteins essential for synaptic transmission (Shvarts-Serebro, *et al.,* 2021). Additionally, *SYT1* was strongly co-expressed with *SV2B*, another protein that plays a critical role in synaptic vesicle trafficking and neurotransmitter release (Courtney, Bao, Briguglio & Chapman, 2019). Considering the

potential co-expression of *SV2B* and *SYT1*, it is likely that miR-128 could also regulate *SV2B*, either directly or indirectly. By modulating the levels of both *SYT1* and *SV2B*, miR-128 could play a critical role in modulating synaptic activity, particularly in conditions where a synaptic function is compromised, such as in neurodegenerative diseases like Alzheimer's or brain malignancies (Shvarts-Serebro, *et al.,* 2021). The interaction between miR-383-5p and the 3'UTR of *SV2B* was observed as an 8mer. This strong binding suggested that miR-383-5p may effectively downregulate *SV2B*, implicating a role in the modulation of synaptic vesicle exocytosis and neurotransmission by the complete degradation of the target mRNA. The significantly higher expression of miR-383 observed in the marginal division (MrD) compared to the hippocampus of Sprague-Dawley rats suggested that miR-383 might play an important role in the learning and memory functions associated with the MrD in the normal brain (Shu, *et al.,* 2013). Previous research has also demonstrated that miR-383 protects against propofol-induced cognitive impairment by preventing hippocampal neuron apoptosis and the dysregulation of associated signalling pathways (Wang, Ding, Lai, Liu & Shuai, 2018). Thus, we could hypothesise that miR-383 plays a significant role in brain and synaptic functions, hence its involvement in learning and its direct *SV2B* gene target.

Actin dynamics regulation is crucial in cell metabolism and processes, such as cell migration, polarity, signal transduction, and intracellular trafficking. Coronins, a highly conserved protein family, play a crucial role in cell motility and vesicle trafficking. *CORO1C* is a serum-induced gene, and external factors like serum and growth factors can enhance its transcriptional activation (Roadcap, Clemen & Bear, 2013). However, the precise molecular mechanisms driving this transcriptional upregulation remain unclear. The gene product is pivotal in actin rearrangement and cofilin dynamics through its influence on the assembly of actin-related proteins 2/3 (Arp2/3) (Chan, Roadcap, Holoweckyj & Bear, 2012).

Our findings indicated that *CORO1C* is predominantly distributed in the brain's white matter, medulla oblongata, and hippocampal formation. *CORO1C* was also detected in neuronal cells, oligodendrocytes, oligodendrocyte precursor cells, and microglial cells. Analysis of the regional distribution of *CORO1C* using the Allen Brain Atlas suggested that its overexpression in normal brain tissue is mainly concentrated in the hippocampal formation, particularly the CA1-CA4 fields. During murine brain development, hippocampal pyramidal neurons and Purkinje cells maintain high levels of *CORO1C*, which supports synaptic plasticity, a process crucial for learning and memory (Hasse, *et al.,* 2015). Our results also suggested that *CORO1C*

expression was also linked to myelination, as evidenced by high mRNA expression in the white matter, followed by the medulla oblongata and hippocampal formation. The localised expression of *CORO1C* suggested its significant role in differentiation, migration, neurite formation, and myelin sheath development in oligodendrocytes (Martorella, Barford, Winkler & Deppmann, 2017). Hasse and colleagues conducted *in vitro* experiments with neuro-2a and PC-12 cells transfected with GFP-tagged CORO1C, demonstrating that the full-length protein supported neurite outgrowth, while truncated versions of it inhibited that process. Thus, they concluded that CORO1C plays a crucial role in neuronal cell morphogenesis (Hasse, *et al.,* 2005). Glioblastomas are mostly found in the supratentorial region, encompassing the frontal, temporal, parietal, and occipital lobes. The frontal lobe exhibits the highest incidence, followed by tumours that span multiple lobes, and then the temporal and parietal lobes (Chakrabarti, Cockburn, Cozen, Wang & Preston-Martin, 2005). Our results also suggested elevated *CORO1C* expression in regions adjacent to the supratentorial area, near the cornu ammonis **(**CA) fields. The elevated *CORO1C* expression in regions adjacent to the supratentorial area, near the CA fields, suggested a spatial correlation between the areas where GBs are mostly found and where *CORO1C* expression is increased. Consequently, we could suggest that CORO1C may play a role in the tumorigenesis or progression of GBs in these specific brain regions.

Previous research has shown that CORO1C mediates its effects through F-actin turnover during neurite outgrowth and brain tumour cell migration (Rosentreter, *et al.,* 2007). The oncogenic potential of *CORO1C* has been reported in various cancer types, including gastric cancer, NSCLC, and melanomas (Cheng, *et al.,* 2019; Zhang, *et al.,* 2022; Tagliatela, *et al.,* 2020). The expression of *CORO1C* in astroglial and tumour cells is associated with migratory and proliferative phenotypes, with higher protein levels correlating with increased malignancy grades (Roadcap, *et al.,* 2013).

We also observed *CORO1C* overexpression in glioma cases, consistent with previous findings, which reported high *CORO1C* expression in diffuse gliomas (Thal, *et al.,* 2008). It has been observed that normal brain tissue exhibited significantly reduced CORO1C expression in cortical neurons, while high-grade benign brain tumours showed increased protein levels. This indicated that CORO1C expression may be dependent on tumour type and grade (Thal, *et al.,* 2008). CORO1C overexpression in aggressive solid tumours, such as GBs and head and neck cancers, is often linked to its metastatic capabilities (Shen, *et al.,* 2022). Among 17 cancer

types, *CORO1C* has shown the highest expression in head and neck cancers and gliomas. However, the exact mechanisms by which CORO1C enhances the metastatic and proliferative properties of GB remain unclear. Similar expression profiles have been observed in other malignancies. For example, high *CORO1C* expression has been found in melanomas compared to normal skin tissue, with increased mRNA levels in *BRAF* mutant melanomas with high phospho-Erk levels (Molinie, *et al.,* 2019). As a member of a conserved protein family, the actin-binding *CORO1C* has been shown to interact with trophoblast cell surface protein 2 (Trop2) in colorectal cancer (CRC) (Wang, *et al.,* 2021d). Trop2 is an oncogenic protein that plays a crucial role in promoting CRC's aggressive behaviour. The same study also suggested that CORO1C overexpression in CRC patients is associated with lymphatic and distant metastasis, venous invasion, and perineuronal invasion. These findings imply that elevated *CORO1C* levels may serve as a prognostic marker for early metastasis events in various neoplasms and could be clinically valuable for early detection of metastatic formations.

The UALCAN analysis revealed that *CORO1C* was significantly overexpressed in patient groups compared to their normal counterparts, except for the 81–100 years age group, in which the sample size was limited. Comparisons of *CORO1C* expression levels between males and females, and between different GB patient ethnicities showed significantly increased expression of the GB samples in comparison to their normal counterparts. However, there were no statistical differences in *CORO1C* expression between males and females and between different patient populations. Furthermore, a CBTTC dataset analysing *CORO1C* expression in different paediatric brain tumours based on histologic subtype was also incorporated. Our results showed that neurofibromas had the highest median *CORO1C* expression compared to paediatric high-grade gliomas (PHGG). Neurofibromas are benign nerve sheath brain tumours that form soft lumps under the skin (Hasse, *et al.,* 2005). However, these benign tumours can metastasise across the head, neck, and skin regions (Neftel, *et al.,* 2019). As previously mentioned, CORO1C levels were elevated in regions associated with myelination and differentiation. This finding is consistent with The Cancer Atlas dataset, which also showed the highest *CORO1C* expression in head and neck cancers, followed by gliomas and melanomas. The presence of *CORO1C* in these neoplasms suggests its potential role as a poor prognostic biomarker associated with the tumour’s metastatic capacity. Other paediatric histological neoplasms, such as low-grade gliomas (LGG), craniopharyngiomas, DNET, and choroid plexus papillomas (CPP), are examples of lower-grade brain tumours that are slow-growing and generally benign. *CORO1C* mRNA expression in these malignancies was

significantly lower compared to highly malignant HGG tumours, further supporting the evidence that CORO1C is highly expressed in tumours with malignant and invasive properties and could serve as a biomarker for unfavourable prognosis. Additionally, the increased *CORO1C* levels in highly malignant paediatric GB cases align with its expression in brain regions with high synaptic plasticity. Factors related to brain development and plasticity during childhood may explain why *CORO1C* levels are elevated in paediatric patients. These findings could potentially aid in the early identification of highly malignant tumours and improve patient prognosis. Further to that, large-scale molecular profiling studies have previously highlighted distinct molecular differences between paediatric and adult GBs (ICGC/TCGA Pan-Cancer Analysis of Whole Genomes Consortium, 2020; Michaeli & Tabori, 2018). The prominent expression of *CORO1C* in paediatric patients may be due to the high degree of neuronal plasticity in children's developing brains. Another contributing factor could be the high tumour mutational burden typical in children with mismatch repair deficiency syndrome (CMMRD) (Michaeli, *et al.,* 2018). Such paediatric patients often benefit from immune therapies, underscoring the urgent need for early diagnostic and prognostic biomarkers.

The *in silico* single-cell RNA sequencing dataset allowed the detection of *CORO1C* across different cell clusters from both adult and paediatric patient cohorts (Neftel, *et al.,* 2019). *CORO1C* expression was evaluated in intra-tumoral, heterogenic malignant cells from all patients, with limited expression observed in the T-cell cluster. Glioblastoma tumours are known to suppress the innate and adaptive immune systems (Borst, Dumas & Prinz, 2021). The absence of *CORO1C* in the T-cell cluster may be due to GB's ability to suppress T-cells, allowing neoplastic cells to evade immune checkpoints and proliferate further. Given the role of CORO1C in normal cell migration and proliferation, particularly through its actin-binding properties and involvement in neuronal lamellipodia formation, increased *CORO1C* expression in migrating malignant GB cells is anticipated and was observed in our findings. Glial cell subtypes, such as microglial cells, are also involved in constant screening of the brain's parenchyma (Wang, *et al.,* 2019b). This dynamic action requires frequent cytoskeletal rearrangements, partially facilitated by CORO1C, thus, its increased expression in brain microglial cells is expected and was observed in our findings. When the cell clusters were filtered to distinguish between adult and paediatric cell populations, it became apparent that paediatric cells predominantly occupied the left side of the malignant cell cluster, including nearly the entire macrophage cluster and the centre of the oligodendrocyte cell cluster. This observation aligns with the increased log2 expression of *CORO1C* in these regions, particularly

within the paediatric clusters. The higher expression of CORO1C during brain development, as demonstrated by specific expression patterns, supports our findings of elevated protein levels in paediatric patients.

When evaluating *CORO1C* expression across various cellular states, including AC-like, OPC-like, MES-like, and NPC-like, the heatmap of log2 expression revealed that *CORO1C* was expressed globally across all states, with an expression level exceeding 4 logTPM. Notably, the expression was slightly higher in NPC-like cells compared to other cellular states. This increased expression in NPC-like cells is consistent with their ability to differentiate into various glial and neuronal cells throughout the CNS. Evidence has suggested that GB cells can influence the migration of NPC-like cells toward the tumour site, enhancing the expression of transformed phenotypes (Pan, *et al.,* 2022).

The survival analysis of primary GB samples in relation to *CORO1C* expression levels revealed a notable association between higher *CORO1C* expression and improved patient outcomes. However, the analysis of progression-free survival did not show statistically significant differences in *CORO1C* expression profiles, indicating that while *CORO1C* may influence overall survival, it may not significantly impact the time to tumour recurrence or progression. This discrepancy suggests that *CORO1C*'s role in GB might be more complex, potentially involving mechanisms that affect long-term survival but not necessarily the early stages of cancer progression. Further research is needed to elucidate the precise function of *CORO1C* in GB biology and its potential as a prognostic marker or therapeutic target.

Our protein *in silico* analysis demonstrated that CORO1C had the highest degree of interaction with CORO1B at a protein level. CORO1C and CORO1B are both members of the Coronin family. At the protein level, CORO1C and CORO1B interact primarily through their shared structural domains and functions related to actin dynamics. Both CORO1C and CORO1B contain the amino acids tryptophan and aspartic acid (WD repeat domains), which allows protein-protein interaction motifs (Xavier, *et al.,* 2013). These domains facilitate the interaction between the two proteins, as well as their binding to actin filaments. The WD repeat domains allow CORO1C and CORO1B to form multi-protein complexes with actin and other actin-associated proteins contributing to the regulation of cytoskeletal rearrangements (Rybaki, & Clemen, 2005). The beta-propeller structure of WD repeats acts as a scaffold allowing these Coronin proteins to bind and recruit other molecules involved in cytoskeletal regulation (Hudson & Cooley, 2013). Additionally, both proteins are involved in the turnover and

remodelling of actin filaments. Their interaction could potentially influence the rate at which actin filaments are disassembled and reassembled, which is critical for cell migration and proliferation. By modulating actin dynamics via polymerisation and depolymerisation, CORO1C and CORO1B can affect various cellular processes, including migration, invasion, and intracellular trafficking (King, *et al.,* 2022). Thus, the interaction between CORO1C and CORO1B at the protein level is essential for the organisation of the actin cytoskeleton and could be crucial for the development and progression of GB. Further investigation using the GeneMANIA database revealed that CORO1C physically interacted with a diverse set of proteins, including WDR1, ETF1, CYB5B, and others, suggesting its involvement in various cellular processes. These interactions indicated that CORO1C played a significant role in actin dynamics, vesicle trafficking, and cellular signalling pathways. The interaction with proteins such as ACTB (beta-actin) and TCP1 further supports its role in the cytoskeletal organisation (Chan, Creed & Bear, 2011). Additionally, the association with proteins involved in metabolic processes and stress responses, like RIPK3 and DNAJB11, highlights CORO1C's potential influence on cell survival and stress adaptation, contributing to its role in tumorigenesis (Morgan & Kim, 2022; Sun, *et al.,* 2021).

As a prominent member of the SV2 family, SV2B has been widely distributed across the brain, where it is predominantly expressed within glutamatergic neurons (Grønborg, *et al.,* 2010). The primary function of SV2B involves storing neurotransmitters and releasing them upon neuronal excitation (Bao, *et al.,* 2023). Immunohistochemical analyses have detected this synaptic protein in the cerebellum, basal ganglia, and hippocampus (Morgans, *et al.,* 2009). These findings align with our results, which demonstrated that *SV2B* is primarily expressed in synaptically active brain regions, including the frontal cortex, cortex, cerebellar hemisphere, anterior cingulate cortex, and cerebellum. Our Allen Brain Atlas analysis further confirmed the high expression of *SV2B* in the hippocampal formation, cerebral cortex, frontal lobe, temporal lobe, claustrum, and parietal lobe. When examining other tissues, *SV2B* expression was considerably lower, further highlighting the brain-specific nature of *SV2B*. Through our single-cell analysis, we observed that *SV2B* was predominantly expressed in excitatory neuronal cells within the brain, whereas its expression in glial cells, including astrocytes, oligodendrocytes, oligodendrocyte precursor cells, and microglial cells, was notably low. This differential expression pattern highlighted the specific involvement of *SV2B* in neurons, particularly in regions known for their excitatory functions, which are crucial for cognitive processes and other high-order brain functions (Pazarlar, *et al.,* 2022). *SV2B* encodes a type of synaptic

vesicle protein which is involved in neurogenesis and neurological functions. Recent research demonstrated that in spinal cord injury (SCI) models, *SV2B* was seen as highly expressed in the regions in close proximity to nerve regeneration sites. *SV2B* was more expressed in areas associated with synaptic activity and neurogenesis, highlighting its potential role in nerve regeneration processes (Li, Zhu, Lee, Wu & Cheng, 2020).

Our TCGA and CBTCC analyses provided a comprehensive overview of *SV2B* expression across various cancer types, age groups, gender, and racial demographics, as well as in different types of paediatric brain malignancies. The analysis revealed that *SV2B* expression is particularly elevated in pancreatic cancer and gliomas among the 17 cancer types analysed. Previous bioinformatics studies have indicated that *SV2B* expression may correlate with glioma grade and poor prognosis, suggesting its oncogenic properties (Wang, Liu & Yang, 2019a; Zhang, *et al.,* 2020b). Furthermore, *SV2B* has been found to be overexpressed in breast cancer tissue compared to normal tissue (Bandala, *et al.,* 2012). SV2B has also been associated with energy metabolism, as the substantial energy demands within tumours may rely heavily on SV2B for regulating transporter protein activity, glucose transport, and other functions (Liu, *et al.,* 2023). Given the high expression of *SV2B* in specific brain regions, it could be indicative or causative of GB through several mechanisms. The high synaptic activity in these areas could create an environment that facilitates the overexpression or dysregulation of *SV2B*, leading to abnormal neurotransmitter release and heightened excitatory signalling. Such conditions could promote the proliferation and survival of glioma cells, particularly in the context of excessive calcium signalling and glutamate release, which have been associated with glioma progression (Sharma, Aaroe, Liang & Puduvalli, 2023). Moreover, the specific involvement of *SV2B* in excitatory neurons and its low expression in glial cells might indicate a shift towards a more aggressive, neuron-like phenotype in GB cells, contributing to the tumour malignant phenotype and resistance to treatment (Nowack, Yao, Custer & Bajjalieh, 2010).

Age-based analysis of SV2B expression decreases significantly in GB patients across all age groups when compared to normal controls. Gender-based analysis further supported the finding of reduced SV2B expression in GB patients. Additionally, ethnicity-based analysis confirmed that SV2B expression was significantly lower in all patient population groups screened. However, the survival analysis of primary GB samples revealed a significant correlation between elevated *SV2B* expression levels and poorer patient outcomes. Specifically, patients with higher *SV2B* expression exhibited significantly shorter overall survival and disease-

specific survival compared to those with lower *SV2B* expression. This suggested that *SV2B* overexpression is associated with a more aggressive disease course, potentially contributing to the rapid progression and increased lethality observed in these patients. However, the analysis of PFS did not reveal statistically significant differences between the groups with varying *SV2B* expression levels, suggesting that while *SV2B* expression is a strong predictor of overall survival and disease-specific survival, it may not be closely associated with the early phases of tumour progression or the initial response to therapy. The lack of significance might suggest that *SV2B*'s influence becomes more pronounced during later stages of tumour progression, leading to poorer long-term outcomes rather than immediate disease progression. Furthermore, the elevated expression of *SV2B* in normal, synoptically active brain regions could predispose these areas to tumorigenesis due to its role in synaptic vesicle function, which is critical for neurotransmitter release and neuronal communication. High *SV2B* expression may lead to an environment with increased synaptic activity, potentially promoting abnormal cell growth and survival signals that could contribute to the initiation of tumours. Alternatively, the elevated expression of *SV2B* might reflect a compensatory mechanism in response to early oncogenic events. If the brain is already undergoing early tumorigenic changes, the increased *SV2B* expression could be an attempt by the neural cells to maintain synaptic function and neuronal communication in the face of these disruptions. This compensatory upregulation could be a response to the stress or damage caused by oncogenic processes, where the brain tries to preserve normal function despite the onset of malignancy.

In paediatric brain malignancies, the highest median expression of *SV2B* was detected in MBs, with significantly elevated levels compared to other paediatric brain tumours. Furthermore, as illustrated on the tSNE heatmaps, the highest cellular distribution of *SV2B* expression within was found in NPC-like cells, with logTPM values between 7-8, indicating that *SV2B* might play a critical role in this specific cellular state. Medulloblastomas arise in the cerebellum, a region of the brain that is crucial for motor control and cognitive functions, which undergoes significant development during childhood (Sheng, *et al.,* 2024). The high expression of SV2B in these tumours might be reflective of the underlying biology of the developing cerebellum, where synaptic vesicle proteins like SV2B are essential for neurotransmitter release and synaptic function (Rossi, Arjmand, Bærentzen, Gjedde & Landau, 2022). In the context of the developing brain, this overexpression could be linked to the increased plasticity and rapid cell division characteristic of early brain development, which might consequently contribute to tumorigenesis when dysregulated (Qin, *et al.,* 2020). The tSNE heatmaps showing the highest

cellular distribution of SV2B expression in NPC-like cells further highlighted the potential role of SV2B in early neural development. Neural progenitor cells are crucial for generating the diverse cell types in the brain during development (Arai & Taverna, 2017). The elevated SV2B expression in these cells might indicate that SV2B plays a role in maintaining the proliferative and undifferentiated state of these cells, which could be recognised by tumour cells to promote growth and survival. The cell cluster expression of SV2B also revealed that there might be age-dependent differences in SV2B expression, with adult GB cells showing higher levels than paediatric cells. These differences could reflect changes in the brain's cellular environment and gene regulation mechanisms as it matures. Genes aligning with GB's spatial distribution are linked to neuroactive ligand–receptor interactions and biological processes such as synapse organisation, modulation of synaptic transmission, and interactions involving neuroactive ligands and receptors (Bao, *et al.,* 2023). Additionally, genes associated with synapses, particularly those with postsynaptic structures and glutamate receptors like SV2B, have shown elevated expression levels in various subtypes of malignant gliomas (Venkatesh, *et al.,* 2019). Glioma cells exposed to high Ca^{2+} levels increase glutamate release into the TME, leading to excessive glutamatergic and calcium signalling, which in turn promotes glioma cell proliferation (Masui, Onizuka, Cavenee, Mischel & Shibata, 2019). The increased energy conductivity observed in gliomas might reflect intensified information transmission, but it's noteworthy that this abnormal activity could reduce normal physiological conductivity. Thus, the expression of SV2B within NPCs and its differential expression across different age groups highlighted the complexity of how SV2B may contribute to both normal brain development and tumorigenesis. Understanding these dynamics, could influence the development of age-specific therapeutic strategies targeting SV2B, particularly in treating paediatric brain tumours like MBs.

SV2 proteins are primarily recognised for their role in vesicular processes, including neurotransmission, regulation of vesicular calcium sensitivity, and vesicular recycling. However, emerging evidence has suggested that SV2 proteins also play a significant role in interacting with the extracellular matrix (ECM), which aligns with our observations. Notably, SV2 proteins have been shown to directly bind to laminin-1, a key ECM component, with high affinity (Rossi, *et al.,* 2022). This interaction appears to be activity-dependent, occurring when SV2 proteins temporarily become part of the plasma membrane following vesicular fusion. The ability of SV2 proteins to act as laminin receptors may be crucial for processes such as axonal regeneration and activity-dependent synaptic adhesion, highlighting a potential link between

SV2 proteins and the ECM in regulating neural function and repair (Rossi, *et al.,* 2022). Additionally, SV2 proteins may facilitate the vesicular entry of neurotoxins and potentially have a mitochondrial function, further highlighting their diverse roles in cellular processes (Bartholome, *et al.,* 2017). Our STRING analysis also showed that SV2B is significantly co-expressed with genes involved in ECM-receptor interactions, making it a critical hub gene in signal transduction. SV2B demonstrated physical interactions with other SV2 protein family members, including SV2A, SV2C, and GP2, highlighting its role in synaptic vesicle function and neurotransmission. Previous studies suggested that PAK-1 and SV2B might jointly serve as GB prognostic biomarkers (Long, *et al.,* 2017). In addition, our KEGG pathway and GeneMania analyses revealed a strong interaction and co-expression between SV2B and SYT1, which is located on the vesicular membrane of nerve and endocrine cells. SYT1 acts as a primary Ca^{2+} sensor in neurotransmission and hormone secretion, playing a crucial role in Ca^{2+}-triggered secretion processes (Banerjee, Lee, Nemcova, Liu & Kaeser, 2020). Due to SYT1's involvement and its calcium-binding protein product, it has emerged as a GB hub oncogene alongside SV2B (Polisetty, *et al.,* 2012; Losada-Pérez, Hernández García-Moreno, García-Ricote & Casas-Tintó, 2022). Further large-scale analysis of GB and normal brain tissues from the TCGA and GEO databases identified SYT1 as one of the core genes linked to GB progression among the 552 differentially expressed genes (Zhou, *et al.,* 2019b). Additional analysis revealed physical interactions of SV2B with proteins such as C6orf15, SCTR, CA10, and SLC17A7. These findings suggested that SV2B is integrated into a complex network of proteins involved in synaptic vesicle trafficking, signalling pathways, and cellular communication, which may play a crucial role in maintaining synaptic function. These findings, along with our results, suggested that SV2B and SYT1 could serve as potential prognostic biomarkers for GB, as both are associated with shorter overall survival. However, we have not verified this finding. Further research is needed to better understand their precise role in GB. Techniques such as co-immunoprecipitation and mass spectrometry could confirm these protein-protein interactions, while CRISPR-Cas9 gene editing and RNA interference (RNAi) could be used to study the functional impacts of SV2B and SYT1 knockdown or overexpression in GB animal models.

In summary, our *in silico* study demonstrated that miR-21 was upregulated in GB, whilst miR-34a and miR-128a were identified as downregulated in GB confirming their oncogenic and tumour-suppressive roles, respectively. MiR-34a and miR-128a commonly target *CORO1C* and *SV2B*, which were upregulated in GB indicating their oncogenic potential. The differential

expression of these biomarkers across paediatric brain tumour patients and adult GB patients suggested their value as diagnostic biomarkers for high grade brain malignancies. Furthermore, the strong interactions observed between miR-206 and miR-383 and their target genes, *CORO1C* and *SV2B,* respectively, suggested that these miRNAs could be potentially used for targeted GB therapies using miRNA mimics. Our *in silico* data highlighted the important roles of CORO1C and SV2B in GB showing distinct expression patterns that could impact tumour behaviour and prognosis. The elevated expression of CORO1C, particularly in paediatric patients with high synaptic plasticity, suggested its potential as a diagnostic biomarker for aggressive brain tumours. High levels of SV2B were significant for predicting shorter overall survival, particularly in the later stages of GB influencing long-term outcomes. Further research is necessary to understand how CORO1C and SV2B contribute to tumour progression and metastasis and how they interact with other elements of the TME. This understanding could lead to more effective treatments for GB. Moreover, further research is needed to investigate whether CORO1C and SV2B act collectively or independently in contributing to GB progression.

Chapter 3. *In vitro* validations

3.1. Introduction

Up until the 4th edition of the WHO classification of CNS tumours published in 2007, the classification of CNS tumours primarily relied on histological characteristics and their resemblance to the presumed cell of origin (Louis, *et al.,* 2007). This approach incorporated the use of immunohistochemical markers that provided information about tumour differentiation and proliferation. Even though these microscopy-based diagnoses were considered reliable, significant diagnostic inter-observer variation was noticed (Kros, *et al.,* 2007). In turn, this led to unfavourable outcomes for patients, highlighting the need for more robust diagnostic markers. Since the update of the WHO classification in 2016, molecular alternations were recognised as a key feature in defining specific brain tumour entities (Louis, *et al.,* 2016). This shift in diagnostic methodology was seen in the classification of diffuse gliomas, MBs and other embryonal tumours, highlighting the growing importance of molecular profiling in CNS tumour diagnosis. Additionally, the integration of molecular biomarkers with traditional immunohistochemical analyses allows for a more comprehensive and accurate diagnosis of CNS tumours, which is increasingly required in the clinical setting (Zhou, *et al.,* 2024). For instance, the molecular profiling of GB now distinguishes between adult-type and paediatric-type diffuse gliomas, each with distinct molecular drivers. Adult-type gliomas are categorised into three types based on isocitrate dehydrogenase (IDH) mutations and other key molecular features, while paediatric-type gliomas are differentiated by alterations such as MAP kinase pathway mutations and H3K27M alterations (Antonelli & Poliani, 2022).

Similarly, the molecular classification of MB has led to the identification of distinct prognostic groups, such as those with WNT pathway alterations, which may benefit from reduced radiotherapy doses, and groups with sonic hedgehog (SHH) pathway alterations, which may respond to specific inhibitors (Kijima & Kanemura, 2016). Medulloblastoma, the most common paediatric brain tumour, accounts for 6.4% of all CNS tumours in children and adolescents (Cohen, 2022). This malignancy originates from neural precursor cells in specific regions of the rhombic lip, with maturation occurring in the cerebellum or brainstem during embryonic development (Richard, 2024). Classified as WHO grade 4 embryonal tumours, MBs are divided into four molecular subgroups (Cavalli, *et al.,* 2017). Our current understanding of MB is primarily informed by this molecular categorisation, identifying the tumours as WNT-

activated, SHH-activated, group 3, or group 4 medulloblastomas (Peterson, *et al.,* 2024). Despite this detailed molecular classification, the primary treatment for MB remains maximal safe surgical resection, adjuvant multi-agent chemotherapy, and, except in infants, risk-adapted craniospinal irradiation (Suk, Gwynne, Burns, Venugopal & Singh, 2022). However, these aggressive treatments are associated with significant short- and long-term adverse effects that can severely impact the patient's quality of life (Braoudaki, *et al.,* 2015). Moreover, despite intensive therapy, recurrence of the disease is common, and the emergence of treatment resistance remains a significant challenge (Slika, *et al.,* 2024).

The utilisation of molecular profiling in CNS tumour classification has largely impacted the current understanding of these tumours, their prognosis and optimal therapy (Porter, Wen & Polley, 2023). Furthermore, it has been suggested that conducting clinical trials with more homogeneous patient populations could improve the evaluation of new therapies and increase the potential for discovering new molecular targets (Husain & Srijithesh, 2016). The identification and application of such biomarkers within the clinical setting represents an advancement of precision oncology, which aims to deliver the most effective cancer treatments to the right patients at the optimal time (Hoeben, Joosten & van den Beuken-van Everdingen, 2021). In neuro-oncology, where brain tumours like GB and MB present significant clinical challenges, miRNAs have emerged as promising candidates for biomarkers. Due to their stability in biological fluids, tissue-specific expression, and ability to reflect the molecular state of tumours, miRNAs could serve as ideal biomarkers for diagnosing brain tumours, predicting patient outcomes, and guiding treatment strategies (Nikolova, *et al.,* 2023). Beyond their role as biomarkers, miRNAs are also being investigated as an alternative therapeutic approach for GB and MB, where they have the potential to modulate gene expression, inhibit tumour growth, or enhance the efficacy of existing treatments (Chakrabortty, Patton, Smith & Agarwal, 2023). However, despite the therapeutic promise of miRNAs and their potential as biomarkers, the identification of clinically significant miRNAs remains limited due to the heterogeneity of brain tumours and challenges in assay standardisation, which contribute to their insufficient clinical translation as effective therapies and diagnostic tools (Condrat, *et al.,* 2020).

In this context, RT-qPCR has emerged as a highly standardised technique for biomarker detection (Grätz, *et al.,* 2022). This technique offers several advantages over other methods for measuring miRNA and mRNA levels, including its simplicity, sensitivity, specificity, and reproducibility. Additionally, RT-qPCR is highly sensitive, allowing the detection of very low

levels of miRNA or mRNA expression (Khoury & Tran, 2020). As a result, this technique has come to major use in current biomarker research, providing reliable quantification of miRNA and gene transcripts. However, the accuracy of RT-qPCR results depends on the correct selection of reference genes that exhibit high stability and minimal variability in expression, regardless of tissue type, tumour stage, experimental conditions, or treatment (González-Bermúdez, Anglada, Genescà, Martín & Terradas, 2019). MiR-RNU-44 is one of the most commonly used reference miRNAs (Gu, *et al.,* 2022). Its expression remains stable across different tissue types and experimental conditions. The consistent expression miR-RNU-44 makes it an ideal internal control for normalising miRNA quantification, ensuring accurate and reliable results in comparative studies (Gu, *et al.,* 2022). On the other hand, *GAPDH* is one of the most widely used reference genes in gene expression assays (Kozera & Rapacz, 2013). This is due to its stable and consistent expression across various cell types and experimental conditions, alongside its involvement in cellular processes, such as glycolysis, making it an ideal internal control for normalising gene expression data, ensuring accuracy and reliability (Lazarev, Guzhova & Margulis, 2020).

Following RT-qPCR, western blotting is commonly employed in biomarker discovery to confirm the changes in protein expression levels, providing a functional verification of the molecular alterations observed at the RNA level (Bass, *et al.,* 2017). While the specificity of western blot results is generally high, exceptions can occur due to the presence of multiple protein antigens with similar molecular weights or nonspecific antibody binding, which can lead to false-positive results (Pillai-Kastoori, *et al.,* 2020). Thus, other techniques such as immunofluorescence (IF), could be further utilised in the molecular characterisation of tumours, allowing for the visualisation of expressed biomarkers and their localisation within specific tumour cells or tissues. This method has been widely used in brain tumour studies as it can provide spatial context, showing not only the presence of molecular markers but also their distribution within different cellular compartments or tissue regions (Tan, *et al.,* 2020b). Additionally, this technique could be used to co-localise multiple markers within the same sample, offering insights into the interactions and co-expression patterns of different molecules (Sheng, *et al.,* 2023). Thus, IF could contribute to a more specific understanding of brain tumour heterogeneity and possess the potential as a useful approach in identifying new therapeutic targets.

Additionally, transfections in miRNA research are essential not only for validating miRNAs as biomarkers but also for exploring their therapeutic potential, particularly in GB and MB (Chakrabortty, *et al.,* 2023). By transfecting miRNA mimics or inhibitors into cell lines or primary cells, the functional roles of specific miRNAs in tumour biology can be investigated (Wang, *et al.,* 2023b). These transfections allow the observation of changes in gene expression targets, cellular behaviour, and tumour characteristics, helping to validate specific miRNAs as biomarkers and therapeutics by demonstrating their impact on molecular pathways relevant to tumour progression (Reda El Sayed, *et al.,* 2021). Moreover, transfection studies can evaluate the therapeutic potential of miRNAs by assessing how altering miRNA expression may inhibit tumour growth via targeting specific gene targets. Techniques such as 3-(4,5-dimethylthiazol-2-yl)-2,5-diphenyltetrazolium bromide (MTT) and colony-forming assays are often incorporated in such studies, as they allow the effective measurement of the effects of miRNA transfections on cell viability and proliferative capacity (Cervena, *et al.,* 2021). Thus, the use of transfections with miRNA mimics or inhibitors, combined with MTT and colony-forming assays, is an important aspect of validating miRNAs as biomarkers and exploring their potential as targeted therapies for GB and MB.

Based on the introduced techniques above, it is essential to use the appropriate cell models to perform validations on, especially for the identification and testing of new biomarkers for GB and MB. The U87MG and U251MG are two of the most commonly used cell lines in GB research due to their well-characterised molecular profiles. The U87MB GB model, first established in 1968 by Ponten and colleagues at the University of Uppsala in Sweden, remains the most widely used GB cell model to date (Pontén & Macintyre, 1968). U87MG cells are known for forming large, highly vascularised tumours with minimal necrosis at their core (Radaelli, *et al.,* 2009). These cells also exhibit key genetic characteristics associated with GB, including mutations in *PTEN, PI3K*, and *Akt* (Pore, Liu, Haas-Kogan, O'Rourke & Maity, 2003). Despite their glial origin, U87MG cells lack the expression of two typical astrocytic markers, GFAP and S100β. However, GBs often exhibit GFAP staining at the tumour borders due to reactive astrocyte infiltration (Candolfi, *et al.,* 2007). A couple of years later, in 1973, the U251MG cell line was established by Bengt Westermark's laboratory at the University of Uppsala from a GB tumour in a 75-year-old male patient, and it is now the second most frequently used GB cell line (Westermark, Pontén & Hugosson, 1973). Unlike U87MG cells, U251MG cells replicate many of the hallmark characteristics of GB. In mouse models, U251MG tumours exhibit highly infiltrative and invasive growth patterns, small central tumour

cores, edema, haemorrhage, and regions of vascular proliferation (Radaelli, *et al.,* 2009). U251MG cells also display a wide range of genetic alterations, including mutations in *PTEN*, upregulation of *PI3K* and *Akt*, a non-functional p53 protein, and aberrant expression of various cell cycle-related proteins (Ishii, *et al.,* 1999). Due to their astrocytic origin, U251MG cells and tumours stain positive for the astrocytic markers GFAP, S100β, and vimentin (Radaelli, *et al.,* 2009). Similarly, the DAOY cell line is essential in MB research. The DAOY cell line was originally derived from a desmoplastic MB, a 4-year-old boy, in 1985 by Jacobsen at the Royal Perth Hospital in Western Australia (Jacobsen, Jenkyn & Papadimitriou, 1985). DAOY cells exhibit a colony growth pattern and high expression of the E-cadherin adhesion molecule, which plays a role in maintaining cell-to-cell contact (Bonfim-Silva, *et al.,* 2019). They are also characterised by a low CD146 expression, associated with higher proliferation, migration, and tumorigenic potential (Bonfim-Silva, *et al.,* 2019). Additionally, DAOY cells display a CD44+/CD24− profile, which may indicate a more aggressive phenotype (Casciati, *et al.,* 2020). Furthermore, DAOY cells exhibit the expression of markers implicated in tumour initiation and progression (Casciati, *et al.,* 2020). This cell line is often used to investigate signalling pathways involved in MB pathogenesis, such as the WNT and SHH pathways, and to explore new therapeutic approaches for this highly aggressive paediatric tumour.

Incorporating normal astrocytes alongside GB and MB cells in biomarker validation studies is essential for the distinguishment of cancer-specific alterations from normal cellular functions, thus ensuring that potential biomarkers and therapeutic targets are accurately validated. Astrocytes are the most abundant glial cells in the CNS, playing essential roles in maintaining the blood-brain barrier, providing structural support to neurons, regulating the extracellular environment, and modulating synaptic activity (Gradisnik & Velnar, 2023). These cells are non-transformed cells that retain these physiological functions, making them one of the most suitable models to represent the non-cancerous brain environment (Catalano, Limatola & Trettel, 2024). Astrocytes typically exhibit low proliferation rates, lack the invasive properties seen in tumour cells, and do not form tumours when implanted *in vivo*, reflecting their non-malignant nature (O'Brien, Howarth & Sibson, 2013). Thus, the comparison between normal astrocytes and cancer cells supports the identification of abnormal growth properties and metastatic potential of brain tumour cells. Normal astrocytes serve as a baseline for studying dysregulated molecular pathways in brain tumours. For example, in GB research, they could be used to assess the differences in signalling pathways like PI3K/AKT, MAPK, and p53 between normal and cancerous cells (Khabibov, *et al.,* 2022). In MB studies, astrocytes could

provide insight on the alterations in developmental pathways like SHH and WNT, which are often dysregulated in DAOY cells (Duarte, Teixeira, Gonzalez-Reyes & Reis, 2021).

One of the main advantages of human GB and MB cell models is their human origin, which ensures the direct translation of research findings into clinically relevant information. This in turn aids in the understanding of tumour-specific signalling pathways and the identification of new therapeutic targets. However, it is important to note that this human origin is also a limitation, as it may not fully capture the complexity of tumour interactions within the natural microenvironment and can lead to challenges in replicating the diverse conditions present *in vivo* (Idrisova, Simon & Gomzikova, 2022). Additionally, like many other human tumour cell lines, U87MG, U251MG, and DAOY cell lines have been in use for several decades, increasing the potential for alterations in their genetic and biological characteristics due to long-term culture (Idrisova, *et al.*, 2022). Despite their limitations, cell lines remain a widely used and valuable approach in the identification of new biomarkers, providing a practical and controlled environment for early-stage research (Mirabelli, Coppola & Salvatore, 2019).

3.1.1. Aims and research questions

3.1.1.1. Aims

The aim of this chapter was to validate our bioinformatics findings *in vitro* by performing RT-qPCR validations, western blotting, and immunofluorescence using cancerous GB and MB cell lines, with normal human astrocytes serving as controls. We also aimed to validate selected biomarkers and assess their effects on target genes and tumour biology via transfection assays.

3.1.1.2. Research Questions

1. Can the bioinformatically predicted biomarkers be confirmed at the miRNA and mRNA levels in GB and MB cell lines using RT-qPCR, compared to normal human astrocytes?
2. Are the protein expression levels of selected biomarkers in GB and MB cells consistent with the bioinformatics predictions when validated through western blotting?
3. Do immunofluorescence experiments reveal differential localisation or expression of the selected biomarkers between GB and MB cell lines and normal human astrocytes, and are these findings further validated by western blotting?
4. Can transfections with miRNA mimics support the selected biomarkers, reveal their effects on target gene expression, and demonstrate their influence on tumour growth or suppression in GB and MB cell lines?

3.2. Materials and Methods

3.2.1. Cell culture

The study utilised two commercially available human GB cell lines, U251MG and U87MG, along with one MB cell line, DAOY (ATCC, Manassas, VA, USA). These cell lines were cultured in Minimum Essential Medium (MEM; Gibco™, Bleiswijk, NL) enriched with 10% fetal bovine serum (FBS; Gibco™, Bleiswijk, NL) and 1% penicillin-streptomycin (10,000 U/mL) (Gibco™, Bleiswijk, NL) to support cellular growth. Human astrocyte cells isolated from the brain stem (HA-bs) served as the control cell line (CliniSciences, UK). The HA-bs cells were maintained in astrocyte medium supplemented with FBS, penicillin-streptomycin, and astrocyte growth supplements (CliniSciences, UK). All cell lines were cultured at 37°C in a 5% CO_2 environment. All cell lines used for subsequent experimental work were utilised once they reached 90% confluency.

3.2.2. Total RNA extraction

The protocol used for total RNA extraction was previously described by Braoudaki *et al.* (Braoudaki, *et al.,* 2014). In summary, 400µl of Trizol reagent (Ambion Life Technology, Auckland, New Zealand) were used to homogenise the pellets of HA-bs/U251MG/U87MG/DAOY cells from T75 flasks in 15ml falcon tubes. A syringe with a needle was used for the homogenisation process of each pellet. After homogenisation, the cell suspensions were incubated in Trizol for 5min at room temperature (RT). The Trizol cell homogenates were then transferred to 1.5ml RNase-free eppendorf tubes, and 80µl of chloroform was added to each of them (Sigma-AldrichTM, Dorset, UK). The contents were mixed thoroughly by vortexing at medium speed and incubated at RT for 2-3min. Subsequently, the samples were centrifuged (Biofuge Fresco, Germany) at 12,000g for 15min at 4°C. After centrifugation, the samples were separated into three distinct layers: an aqueous phase containing RNA, an interphase containing DNA, and an organic phase containing proteins and lipids. The upper RNA-containing layers were carefully pipetted into a new RNase-free 1.5ml eppendorf tubes, and 200µl of isopropanol was added to each. The samples were incubated for 30min at -20°C to allow RNA precipitation and then centrifuged for 10min at 12,000g at 4°C. Following centrifugation, a clear pellet was visible at the bottom of the eppendorf tubes. The isopropanol was carefully removed, and two wash steps with 400µl of 75% ethanol were performed. Each wash step involved resuspending the pellets with 75% ethanol by reverse pipetting and vortexing, followed by centrifugation at 7,500g at 4°C. Once the washes were completed, the ethanol was carefully removed, and the tubes were left open to air dry for 10min.

After air drying, 20µl of RNase-free water was added to the eppendorf tubes, and the samples were incubated on a heat block at 58°C for 15min. The samples' quantity and quality were assessed using a Nanodrop (Nanodrop ND1000 Spectrophotometer, Virginia, USA). All samples were adjusted to a final volume of 87.5µL by adding RNase-free water. DNase treatment was carried out after the initial quantification using the QIAGEN RNase-Free DNase Set (Qiagen, UK). Specifically, 10µL of RNase-free Buffer RDD and 2.5µL of RNase-free DNase I were added to the reaction tubes containing the samples, followed by incubation for 10 minutes at room temperature. After incubation, the samples were re-quantified using the Nanodrop ND1000. The samples were then stored at -20°C until further organic extraction or subsequent gene expression analysis.

3.2.3. Organic miRNA extraction

After the total RNA samples were quantitatively and qualitatively assessed using the Nanodrop (Nanodrop ND1000 Spectrophotometer, Virginia, USA), the purification and organic extraction process was initiated. A total of 10µl of homogenate additive was added to 100µl of each sample. The eppendorf tubes were vortexed and incubated on ice for 10min. Subsequently, an equal volume of Acid-Phenol-Chloroform (Ambion, Texas, USA), in this case, 100µl, was added to the eppendorf tubes. The acid-phenol-chloroform was taken from the lower phase of the bottle, as the upper phase contains buffer. The samples were vortexed and then centrifuged at 10,000g for 5min at RT, resulting in the formation of two layers: an aqueous phase and an organic phase. The upper aqueous layer of each sample was carefully removed, transferred to a new RNase-free 1.5ml eppendorf tube, and its volume was recorded. Following this, 1.25 volumes of 100% ethanol at RT were added to the aqueous phase. A filter cartridge was applied onto a collection tube provided in the mirVana isolation kit (ThermoFisher, Vilnius, Lithuania), and the lysate was applied directly onto the filter cartridge, avoiding contact with its sides. The collection tubes were centrifuged for 15-30sec at 10,000g to allow the lysate to pass through the filter cartridge. The flow-through was discarded, and the collection tube was centrifuged again under the same conditions to ensure complete removal of the lysate/ethanol mixture from the filter cartridge. The same collection tube was reused for the washing steps, where wash solution 1 and wash solution 2/3 were used. To make up wash solution 1, 21mL of 100% ethanol was added to the bottle from the kit labelled wash solution 1 designed to remove proteins, salts, and other contaminants from the RNA bound to the filter during the first wash step. To make up wash solution 2/3, 40 mL of 100% ethanol was added to the bottle from the kit labelled wash solution 2/3 designed to further clean the RNA by removing remaining

impurities and ensuring the RNA is as pure as possible before elution. For the first wash step, 700µl of solution 1 from the mirVana isolation kit was pipetted directly onto the centre of the filter cartridge. The collection tubes were centrifuged for 15-30sec at 10,000g to allow the wash solution to pass through, and the flow-through was discarded. The tubes were centrifuged again under the same conditions to ensure complete removal of the wash solution 1. The second wash step was performed by pipetting 500µl of wash solution 2/3 from the mirVana isolation kit onto the centre of the filter cartridge. The collection tubes were centrifuged twice for 15-30sec at 10,000g to ensure all the wash solution passed through, with the second centrifugation lasting 1min. The filter cartridges were then transferred to new collection tubes, and 75µl of preheated eluent buffer was pipetted onto the centre of each filter. The collection tubes were centrifuged at maximum speed for 30sec to recover the RNA from the filter. Finally, the eluent containing RNA was collected, and quantitative and qualitative analysis was performed using the Nanodrop.

3.2.4. cDNA synthesis

All cDNA synthesis reactions were conducted using a Thermal Cycler (Eppendorf, Mastercycler Nexus Gradient) (Applied Biosystems, Foster City, California, USA). Each cDNA experiment for gene expression analysis was performed in triplicate, using the TaqMan™ High-Capacity cDNA Reverse Transcription Kit (Applied Biosystems ThermoFisher, Pleasanton, CA) with three independent biological samples per cell line. Each sample contained 20ng/µL of RNA. The reaction mixture of each cDNA reaction included 2µL of 10X Reverse Transcription (RT) Buffer, 0.8µL of 25X Deoxynucleotide Triphosphate mix (dNTP) Mix (100mM), 2µL of RT Random Primers, 1µL MultiScribe™ Reverse Transcriptase, 4.2µL of nuclease-free water (Applied Biosystems ThermoFisher, Pleasanton, CA), and 10µL of RNA sample. The thermal cycler program was set at 25°C for 10min, followed by 37°C for 120min, and 85°C for 5min. After the reaction, samples were stored at -20°C until RT-qPCR analysis. Each cDNA experiment for miRNA expression analysis was performed in triplicate, using the TaqMan™ MicroRNA Reverse transcription kit (Applied Biosystems ThermoFisher, Pleasanton, CA) with three independent biological samples per cell line. Each sample contained 10ng/µL of miRNA. The reaction mixture of each cDNA reaction included 1.5µL of 10X RT Buffer, 0.15µL of dNTP Mix (100mM), 3µL of 5xRT miRNA Primer, 1µL MultiScribe™ Reverse Transcriptase, 0.19µL RNase Inhibitor (20U/µL), 4.16µL of nuclease-free water, and 5µL of miRNA sample. For miRNA profiling, the thermal cycler

program was set to 16°C for 30min, followed by 42°C for 30min, and 85°C for 5min. After the reaction, samples were stored at -20°C until RT-qPCR analysis.

3.2.5. RT-qPCR

All RT-qPCR experiments were conducted using the QuantStudio™ Real-Time PCR System (QuantStudio 7 Flex) (Applied Biosystems, Foster City, California, USA). The assay IDs used for the RT-qPCR gene expression analyses are listed in Table 9. Each RT-qPCR experiment for gene expression analysis was performed in triplicate with TaqMan Fast Advanced Master Mix (Applied Biosystems ThermoFisher, Pleasanton, CA) using three independent biological samples per cell line on 96-well PCR plates. GAPDH was used as an internal control. The reaction mixture in each well contained 1.00µL of primer TaqMan™ Small RNA Assay (20X) (Applied Biosystems ThermoFisher, Pleasanton, CA), 10.00µL of PCR Fast Advanced Master Mix (Applied Biosystems ThermoFisher, Pleasanton, CA), 7.67µL of nuclease-free water, and 1.33µL of cDNA template. A non-template control and no Master Mix control were included on each plate. The no-template control (NTC) served as the negative control for the PCR. The PCR cycling conditions were set to 95°C for 20sec (enzyme activation), followed by 40 cycles of 95°C for 1sec (denaturation) and 60°C for 20sec (annealing). The assay IDs used for the RT-qPCR miRNA expression analyses are listed in Table 10. Each RT-qPCR experiment for miRNA expression analysis was performed in triplicate with TaqMan Universal PCR Master Mix (no UNG) (Applied Biosystems ThermoFisher, Pleasanton, CA) using three independent biological samples per cell line on 96-well PCR plates. MiR-RNU-44 (mature sequence: CCTGGATGATGATAGCAAATGC) was used as an internal control. The reaction mixture in each well contained 1.00µL of primer TaqMan™ Small RNA Assay (20X) (Applied Biosystems ThermoFisher, Pleasanton, CA), 10.00µL of PCR Universal Master Mix (Applied Biosystems ThermoFisher, Pleasanton, CA), 7.67µL of nuclease-free water, and 1.33µL of cDNA template. A non-template control and no Master Mix control were included on each plate. The PCR cycles involved an initial step at 95°C for 10min (enzyme activation), followed by 40 cycles of 95°C for 15sec (denaturation) and 60°C for 1min (annealing).

Table 9. Assay IDs for gene expression analysis.

Gene name	Assay ID
CORO1C	Hs00902568_m1
SV2B	Hs00208178_m1

Table 10. Assay IDs for miRNA expression analysis.

miRNA name	Assay ID
hsa-miR-21	000397
hsa-miR-34a	000425
hsa-miR-128a	002216
hsa-miR-206	000510
hsa-miR-383	000573

3.2.6. Protein quantification via western blotting

Total protein extraction from HA-bs/U251MG/U87MG/DAOY cell lines was carried out using RIPA buffer and a protease inhibitor cocktail (Applied Biosystems ThermoFisher, Pleasanton, CA). The cells were washed twice with ice-cold phosphate-buffered saline (PBS) for 3min and 2.97mL of RIPA buffer, and 30µL protease inhibitor were added to each flask. A scraper was used to gently detach the cells from the flask surface. The extraction buffer containing cells was then transferred 1.5mL eppendorf tubes and vortexed for 20min at 4°C. The eppendorfs were then centrifuged at 12,000rpm at 4°C for 15mn. Following centrifugation, the sample supernatant was transferred to a fresh eppendorf tube. Following this, a BCA assay using a standard set of albumin concentrations, was used to determine the protein concentration of each sample (Applied Biosystems ThermoFisher, Pleasanton, CA). The BCA assay was performed on a 96-well plate by adding 200µL of working reagent to each well containing a sample. This was performed in mechanical triplicates. The BCA assay plate was covered with foil and incubated for 30min at 37°C. The absorbance readings were measured at 562nm via the CalrioStar microplate reader (BMG Labtech, Aylesbury, UK). The unknown concentrations were then calculated based on the standard curve produced by the set of standard samples. Each sample of protein was made to 50µg/µL for further western blotting analysis. The protein samples were then separated by electrophoresis on 10% SDS polyacrylamide gels under reducing conditions, followed by semi-dry transfer to nitrocellulose membranes (Amersham Biosciences, Upsala, Sweden). The gels were run for 100min at 100V. The semi-dry transfer was performed for 18min at 25V. The membranes were blocked with 5% BSA (Applied Biosystems ThermoFisher, Pleasanton, CA) in TBST solution for 1h at RT and then washed three times with TBS-0.1% Tween-20. Then, the nitrocellulose membranes were incubated overnight at 4°C in BSA-TBST with the appropriate primary antibodies against CORO1C (1:200 dilution), SV2B (1:200 dilution), and β-actin (1:1000 dilution). The membranes were

subsequently washed three times with TBST and incubated for 1h in the dark with an HRP-conjugated anti-rabbit secondary antibody at dilution 1:2000. Band quantification was performed using the iBright Imaging Systems iBright Analysis Software (Applied Biosystems ThermoFisher, Pleasanton, CA) through chemiluminescent detection and visualisation of proteins using the Novex™ ECL chemiluminescent substrate reagent kit (Applied Biosystems ThermoFisher, Pleasanton, CA). β-Actin was used as a housekeeping protein. All antibodies were obtained from ProteinTech, Manchester, UK.

3.2.7. Immunofluorescence

HA-bs/U251MG/U87MG/DAOY cells were seeded onto round coverslips placed in a 12-well plate at a density of 2.5×10^5 cells per well. The cells were cultured in their respective media for 24h, after which they were fixed with 4% paraformaldehyde (PFA) (Sigma-Aldrich™, Dorset, UK) for 45min. Following fixation, the cells were washed twice with PBS (ThermoFisher™, CA, USA) for 5min each. The coverslips were then blocked with 5% bovine serum albumin (BSA) (Sigma-Aldrich™, Dorset, UK) for 1h. After blocking, the solution was removed, and the cells were incubated overnight at 4°C with gentle agitation in primary antibodies diluted in 5% BSA. The dilutions for the CORO1C and SV2B were 1:200, whilst the dilution for the β-actin primary antibody was 1:1000. The following day, the antibody solution was removed, and the cells were washed three times with PBS for 5min each. For controls, cells were incubated in the blocking solution without primary antibody. Subsequently, all cells were incubated with Alexa Fluor 488 Phalloidin (Applied Biosystems ThermoFisher, Pleasanton, CA) secondary antibody at a 1:2000 dilution for 1h at room temperature with gentle agitation. The cells were then washed three times with PBS for 5min each. The coverslips were removed from the 12-well plate, and excess liquid was gently blotted off with tissue paper. A few drops of 4′,6-diamidino-2-phenylindole (DAPI) were added to each slide, and the coverslips were gently placed at a 45° angle. The coverslips were sealed with nail varnish, protected from light, and stored at 4°C overnight to allow the nail varnish to dry. Fluorescent images were captured using a Zeiss Axioimager M2 microscope equipped with an Axiocam 503 imaging device and Zeiss ZEN software (Zeiss Microscopy, ×40 magnification). Cell fluorescence was visualised using an EC Plan-Neofluar 63× (1.25) oil objective. The following channels were used for the fluorophores: DAPI (Ex. 353nm, Em. 465nm) and Alexa Fluor 488 (Ex. 493nm, Em. 517nm). Image acquisition was performed using ZenBlue (Zeiss) software. Fluorescence quantification analysis was performed by first splitting the image into its

respective channels using the "Split Channels" function in ImageJ to separate the blue (DAPI) and green (protein) fluorescence. The green channel was then analysed for overall fluorescence intensity across the entire image, with regions of interest (ROIs) drawn around high-power fields (HPFs) identified through thresholding, and the fluorescence intensity within these ROIs was quantified using the "Analyse Particles" tool in ImageJ. Mean fluorescence intensity (MFI) was calculated based on these ROIs and is reported in arbitrary units (AU). Unstained cells were used to establish baseline fluorescence levels, which served as background for assessing non-specific staining.

3.2.8. Transient transfections

U251MG, U87MG, and DAOY cell lines were transfected with negative control miRNA #1, positive control miR-1, and miR-206 and miR-383 mimics (Applied Biosystems ThermoFisher, Pleasanton, CA) using the Lipofectamine RNAiMAX reagent (Applied Biosystems ThermoFisher, Pleasanton, CA) (Table 11). Cells for RNA, miRNA, and protein extractions were seeded in 6-well plates at a density of $2.5x10^5$ cells/well. After reaching a confluence of between 60-80%, the cells were transfected with the siRNAs at final concertation 30pmol. This was achieved by performing the following dilutions: 9µL of Lipofectamine RNAiMAX mixed 150µL of Opti-MEM medium (Applied Biosystems ThermoFisher, Pleasanton, CA); and 18µL of siRNA stock solution (5nmol) mixed with 150µL of Opti-MEM medium. After the dilution was made, both mixtures were added together and incubated for 10min at RT. Following the incubation, 250µL of the mixtures were added to their respective wells. The cells were incubated at 37°C for 48h. Post that period, the cells were harvested for RNA, miRNA, and protein extraction for the analysis of miR-206, miR-383, *CORO1C*, *SV2B*, CORO1C, and SV2B via RT-qPCR and western blotting as described above.

Table 11. Assay IDs for siRNA transient transfections assays.

siRNA name	Assay ID
Negative control miRNA #1 (mature sequence: UCACAACCUCCUAGAAAGAGUAGA)	4464076
Positive control miR-1 (mature sequence: ACAUACUUCUUUAUAUGCCCAU)	MH10617
miR-206 mimic	MH10409
miR-383 mimic	MH10353

3.2.9. Cell viability assay

The cell viability of transfected U251MG, U87MG, and DAOY cells was assessed by an MTT assay. GB and MB cells were seeded in 96-well plates at a cell density of 1.5×10^4 per well and subsequently transfected with negative control miRNA #1, positive control miR-1, and miR-206 and miR-383 mimics using the Lipofectamine RNAiMAX reagent as described above. Following a 48h incubation with the siRNAs, 5mg/mL MTT dye (GibcoTM, Bleiswijk, NL) was added in each well. The plates were then incubated for 2h at 37°C in 5% CO_2. Following the incubation, the MTT solution was removed, and 100% isopropanol (Sigma-Aldrich™, Dorset, UK) was added to dissolve the formazan crystals, with the plates left on a rocking platform for 30min. The absorbance values were measured at 590nm using a CLARIOstar microplate reader (BMG Labtech, Aylesbury, UK). Cellular viability was quantified based on these readings.

3.2.10. Colony forming assay

To assess the ability of GB and MB cells to form colonies, cells were seeded at a density of 500 cells/well on 12-well plates and transfected with negative control miRNA #1, positive control miR-1, and miR-206 and miR-383 mimics using the Lipofectamine RNAiMAX reagent as described above. Post four days of incubation at 37°C, the colonies were washed twice with phosphate-buffered saline (PBS), fixed with 4% paraformaldehyde (PFA) (Sigma-AldrichTM, Dorset, UK) for 25min, and stained with 0.1% crystal violet (Sigma-AldrichTM, Dorset, UK) for 20min. Colonies with more than 30 cells were microscopically photographed and quantitatively assessed under a light microscope (Olympus Life Science Solutions, Stansted, UK).

3.2.11. Statistics

Statistical analysis and graphical representations were performed using GraphPad Prism 9.4.1 software (GraphPad Software, San Diego, USA). Results were obtained from three independent experiments (n=3). For comparing RT-qPCR expression levels between normal human astrocytes and GB cells, an ordinary one-way ANOVA was conducted, followed by Dunnett's multiple comparisons test to identify significant differences. For RT-qPCR comparisons between normal human astrocytes and MB cells, an unpaired t-test was used to determine significant differences in expression. Both western blotting and IF results were analysed using ordinary one-way ANOVA, followed by Dunnett's multiple comparisons test to assess significant differences among normal human astrocytes, GB, and MB cells. A p-value of <0.05 was considered statistically significant.

3.3. Results

3.3.1. RT-qPCR validations of miRNA expression profiles in GB cells

Through our bioinformatics analysis in Chapter 2, we observed that miR-21 was upregulated in GB, while miR-34a and miR-128a were both downregulated. Additionally, we identified that miR-206 and miR-383 directly target *CORO1C* and *SV2B*, respectively, suggesting their downregulation in GB. RT-qPCR validations confirmed that miR-21 expression was significantly upregulated in U87MG and U251MG GB cells compared to HA-bs cells (Figure 46a). Separately, miR-34a was significantly downregulated in GB cells, and miR-128a also showed decreased expression (Figures 46b and 46c). Furthermore, miR-206 was significantly downregulated in U87MG and U251MG GB cells compared to HA-bs cells (Figure 46d). The expression of miR-383 was significantly reduced in both GB cell lines when compared to normal human astrocytes (Figure 46e).

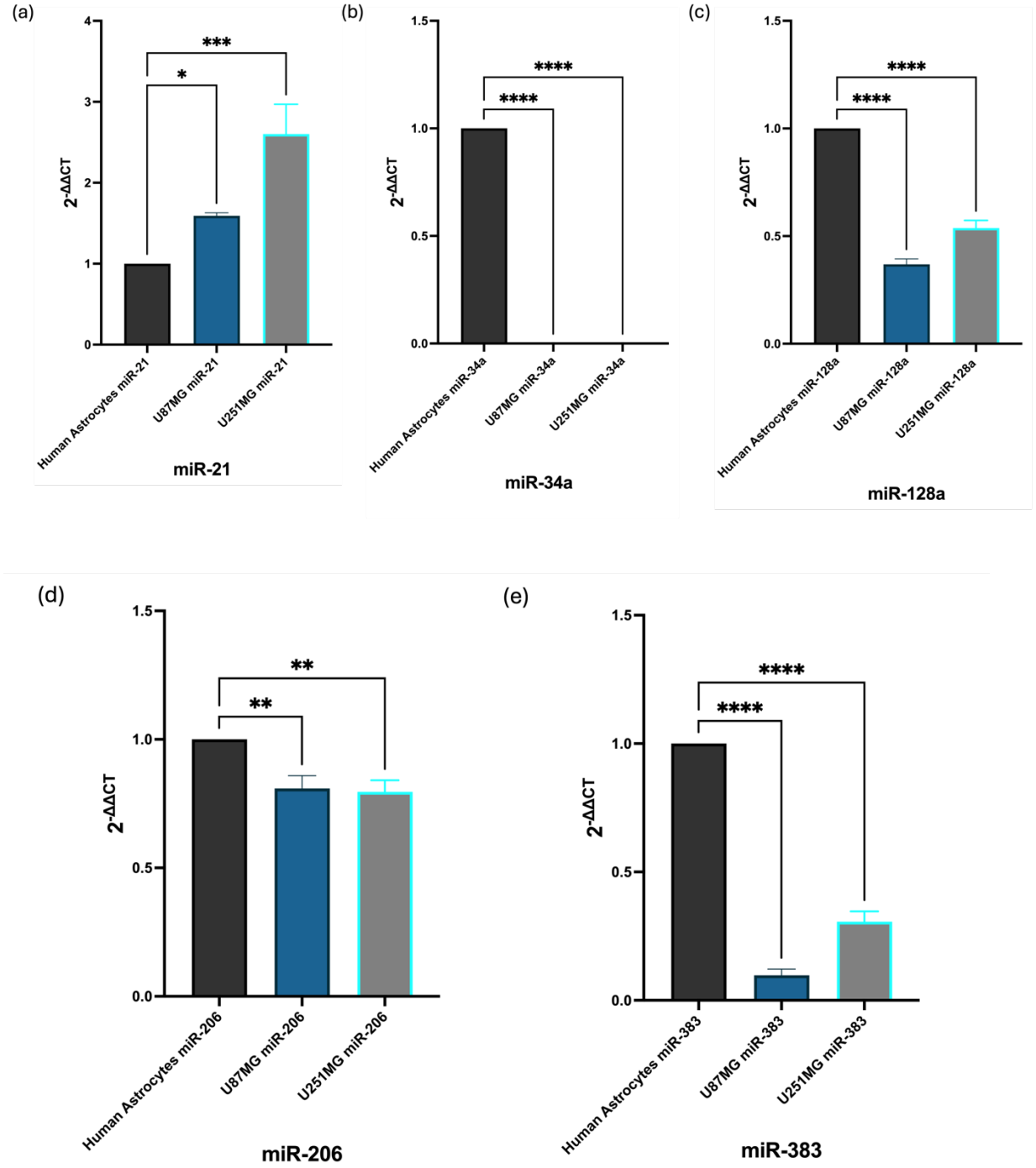


Figure 46. MiRNA RT-qPCR expression analyses in GB cells. (a) MiR-21 expression was significantly higher in both GB cell lines when compared to human astrocytes (U87MG, $p<0.02$; U251MG, $p<0.0002$). (b) MiR-34a showed reduced expression within U87MG and U251MG cells when compared to normal human astrocytes (U87MG, $p<0.0001$; U251MG, $p<0.0001$). (c) Similarly, MiR-128a was significantly downregulated within GB cells when compared to human astrocytes (U87MG, $p<0.0001$; U251MG, $p<0.0001$). (d) MiR-206 expression was also significantly reduced in U87MG and U251MG GB cells compared to normal human astrocytes (U87MG, $p<0.0017$; U251MG, $p<0.0012$). (e) Similarly, miR-383 was markedly downregulated in GB cells relative to normal human astrocytes (U87MG,

p<0.0002; U251MG, p<0.0009). Results are based on three independent experiments, n=3. All statistical analyses were conducted using ordinary one-way ANOVA, followed by Dunnett's multiple comparisons test to determine the significant differences in expression between normal human astrocytes and GB cells.

3.3.2. RT-qPCR validations of gene expression profiles in GB cells

In Chapter 2, we also observed the upregulation of *CORO1C* and *SV2B* in different cell cluster types and GB patients. When validated via RT-qPCR, the *CORO1C* gene exhibited significant upregulation in GB cells compared to HA-bs cells (Figure 47a). Similarly, *SV2B* expression was notably higher in GB cells compared to normal human astrocytes (Figure 47b). To further interpret the significance of these findings, we expanded the bioinformatics analyses to explore gene expression validation in GB and MB cell lines. These analyses revealed that miR-206 and miR-383, which are significantly downregulated in GB and MB, directly targeting *CORO1C* and *SV2B*, respectively. This suggests that the downregulation of miR-206 and miR-383 may contribute to the observed upregulation of their target genes, *CORO1C* and *SV2B*, thereby playing a crucial role in GB pathophysiology.

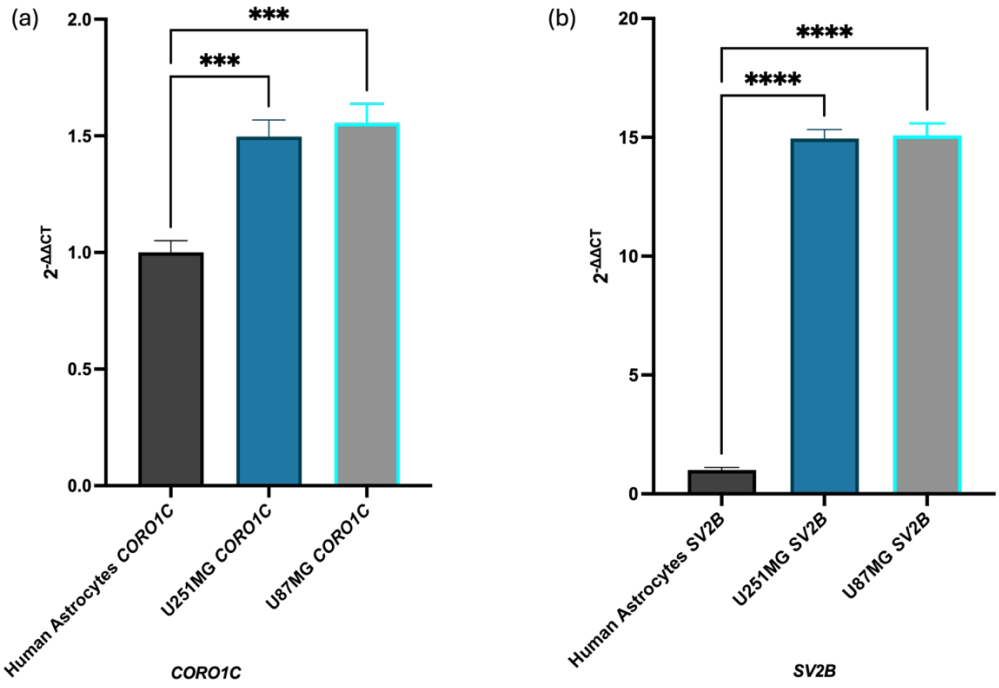


Figure 47. Gene RT-qPCR expression analyses in GB cells. (a) *CORO1C* expression was significantly elevated in GB cells when compared to normal human astrocytes (U251MG, p<0.0002; U87MG, p<0.0001). (b) Likewise, *SV2B* was observed to be upregulated in GB cells relative to normal human astrocytes (U251MG, p<0.0001; U87MG, p<0.0001). Results are based on three independent experiments, n=3. All statistical analyses were conducted using ordinary one-way ANOVA, followed by Dunnett's multiple comparisons test to determine the significant differences in expression between normal human astrocytes and GB cells.

3.3.3. RT-qPCR validations of miRNA expression profiles in MB cells

In addition to the bioinformatics analysis conducted on GB, we aimed to determine whether the expression patterns of these miRNAs were comparable in MB. RT-qPCR validations depicted that miR-21 expression was significantly higher in DAOY MB cells compared to HA-bs cells (Figure 48a). Separately, miR-34a was significantly downregulated in MB cells (Figures 48b). However, miR-128a showed no significant difference in expression in MB cells (Figure 48c). Furthermore, miR-206 was significantly downregulated in MB cells compared to HA-bs cells (Figure 48d). The expression of miR-383 was significantly reduced in the DAOY MB cell line when compared to normal human astrocytes (Figure 48e).

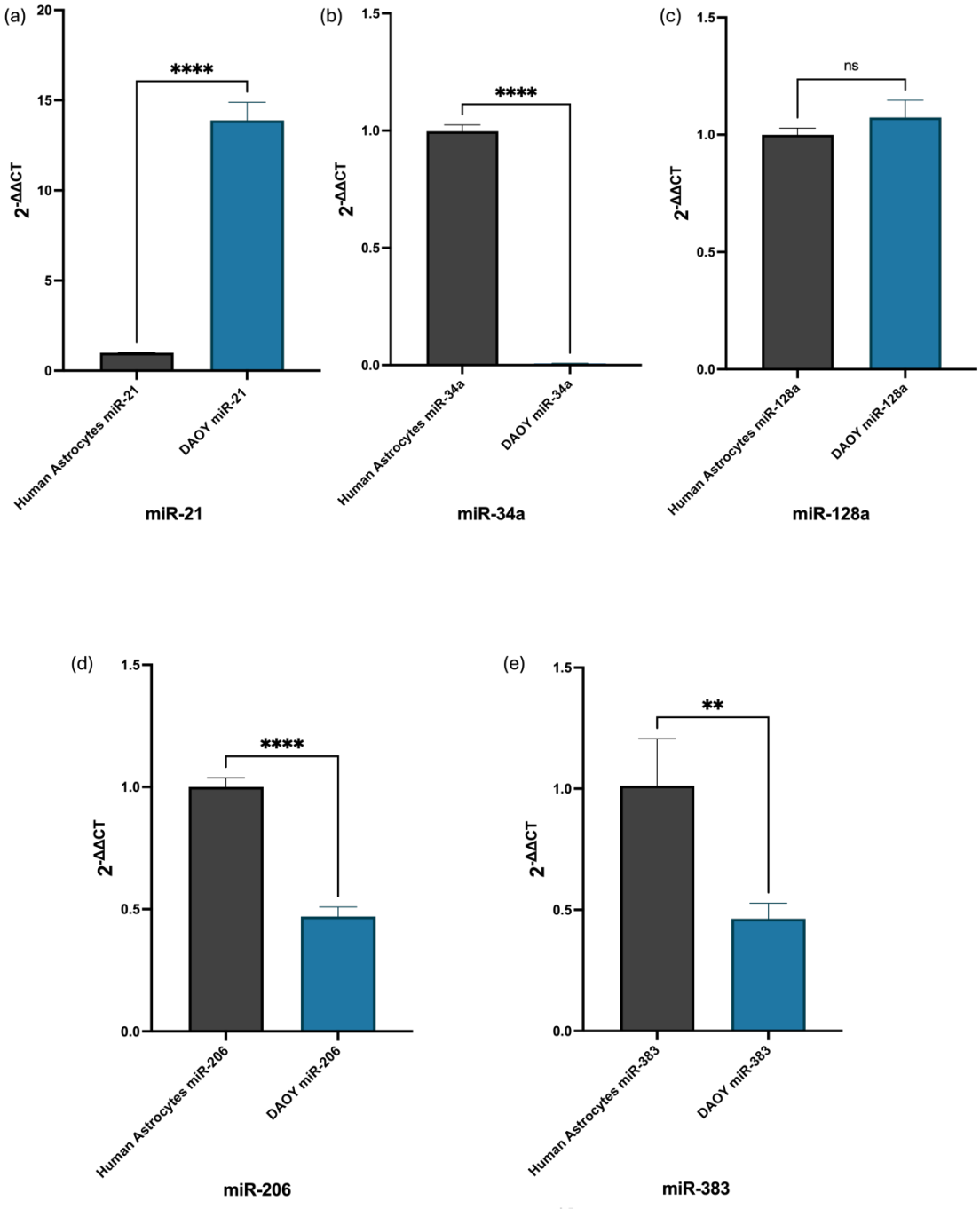


Figure 48. MiRNA RT-qPCR expression analyses in MB cells. (a) MiR-21 expression was significantly elevated within DAOY cells compared to human astrocytes ($p<0.0001$). (b) MiR-34a showed significantly reduced expression within MB cells when compared to normal human astrocytes ($p<0.0001$). (c) There was no significant difference of miR-128a expression observed between MB cells and human astrocytes ($p<0.1815$). (d) MiR-206 expression was significantly reduced in MB cells compared to normal human astrocytes ($p<0.0001$). (e) Similarly, miR-383 was observed to be downregulated in DAOY cells relative to normal human astrocytes ($p<0.0096$). Results are based on three independent experiments, n=3. All statistical analyses were conducted using the Unpaired t-test to determine the significant differences in expression between normal human astrocytes and MB cells.

3.3.4. RT-qPCR validations of gene expression profiles in MB cells

In Chapter 2, we also observed the expression of *CORO1C* and *SV2B* in MB paediatric patients. Therefore, we sought to investigate their expression within MB cells. The results showed that *CORO1C* was significantly upregulated in MB cells compared to HA-bs cells (Figure 49a). Similarly, *SV2B* exhibited a notable increase in expression in MB cells compared to normal human astrocytes (Figure 49b).

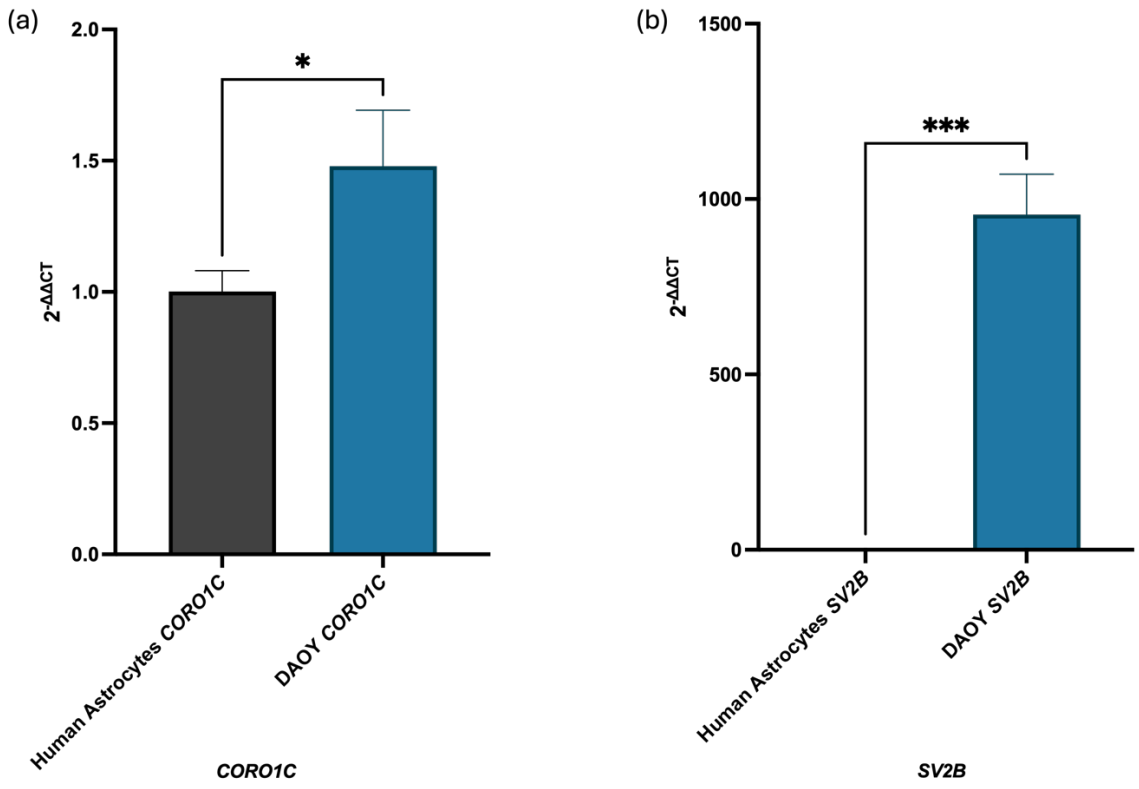


Figure 49. Gene RT-qPCR expression analyses in MB cells. (a) *CORO1C* expression was significantly elevated in MB cells compared to normal human astrocytes ($p<0.0218$). (b) Additionally, *SV2B* expression was significantly increased in MB cells relative to normal human astrocytes ($p<0.0001$). Results are based on three independent experiments, n=3. All statistical analyses were conducted using the Unpaired t-test to determine the significant differences in expression between normal human astrocytes and MB cells.

3.3.5. Protein quantification via western blotting

Western blot analysis was performed to assess the expression levels of CORO1C and SV2B across HA-bs, U251MG, U87MG, and DAOY cells (Figure 50a). The results revealed that CORO1C protein expression was significantly upregulated in both GB cell lines as well as in the MB cell line when compared to HA-bs cells (Figure 50b). Similarly, SV2B protein

expression showed a significant increase in U251MG, U87MG, and DAOY cells relative to HA-bs cells (Figure 50c). In contrast, β-actin protein expression remained consistent across normal astrocytes and both GB and MB cells, with no significant differences observed, confirming its role as a reliable loading control (Figure 50d).

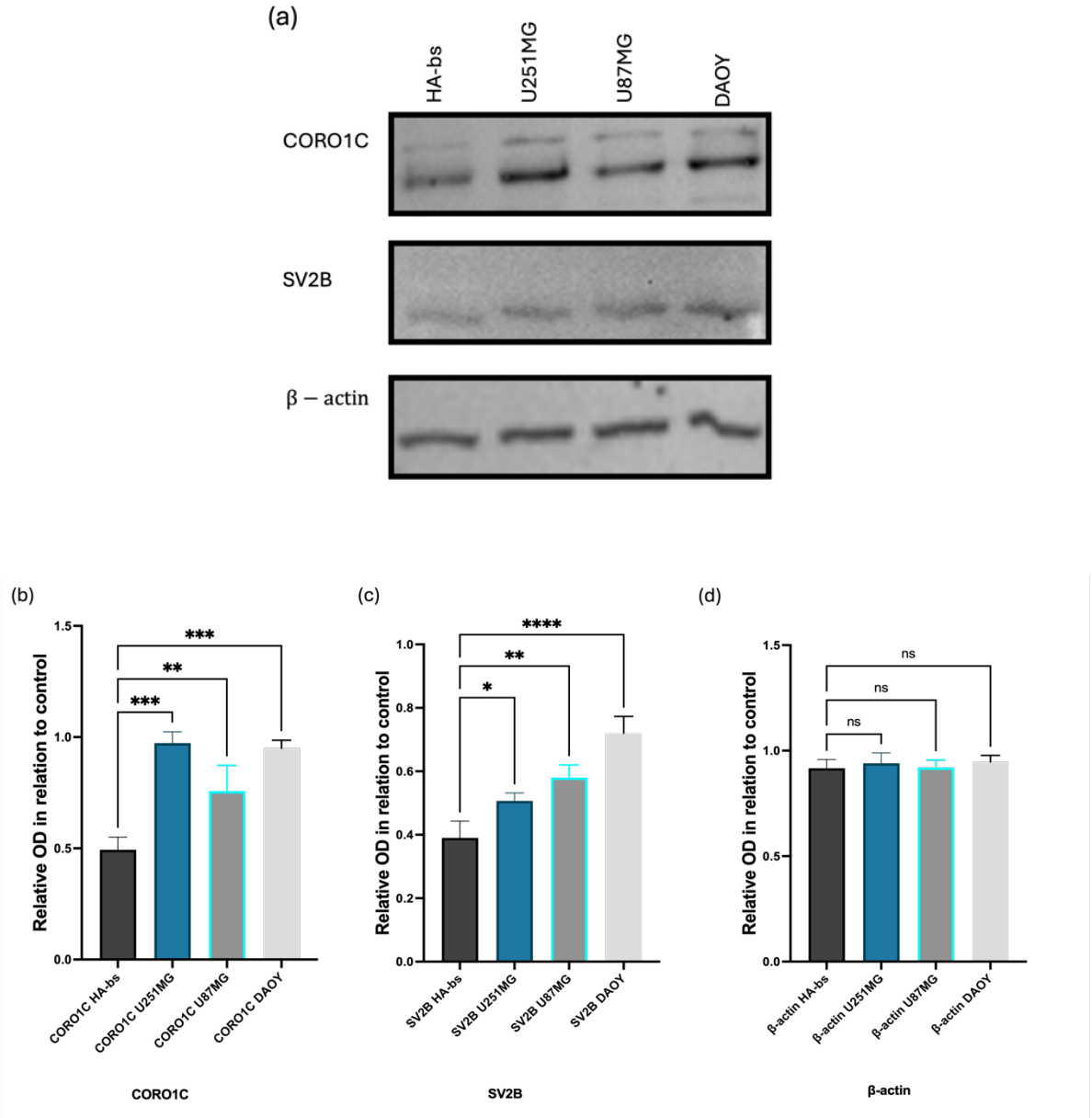


Figure 50. Western blotting protein quantification analyses. (a) Chemiluminescent images depicted the expression levels of CORO1C, SV2B, and β-actin in HA-bs, U251MG, U87MG, and DAOY cells. (b) CORO1C protein expression was significantly elevated in all GB and MB cell lines compared to normal HA-bs cells (U251MG, $p<0.0001$; U87MG, $p<0.003$; DAOY, $p<0.0002$). (c) SV2B protein expression was significantly upregulated in U251MG, U87MG, and DAOY cells relative to HA-bs cells (U251MG, $p<0.037$; U87MG, $p<0.003$; DAOY, $p<0.0001$). (d) β-actin protein expression showed no significant difference between normal astrocytes and GB or MB cells. Results are based on three independent experiments, n=3. All

statistical analyses were conducted using ordinary one-way ANOVA, followed by Dunnett's multiple comparisons test to determine the significant differences in expression between normal human astrocytes, GB and MB cells.

3.3.6. Immunofluorescence protein visualisation

The IF analyses revealed distinct localisation patterns and expression levels of CORO1C and SV2B across different cell lines. Immunofluorescence staining of HA-bs cells demonstrated that CORO1C was primarily localised in the cytoplasm, with a notable concentration in the perinuclear region, suggesting potential association with areas surrounding organelles (Figure 51). Meanwhile, SV2B also appeared to be cytoplasmic; however, unlike CORO1C, its distribution was more diffuse across the cytoplasm rather than predominantly perinuclear, indicating its presence across various cytoplasmic regions (Figure 52). In U251MG and U87MG GB cells, IF staining revealed significantly increased fluorescence of CORO1C compared to HA-bs cells, with a similar diffuse distribution across the cytoplasm (Figure 51). In DAOY cells, CORO1C was also significantly overexpressed in comparison to human astrocyte cells and localised in the cytoplasm, with a noticeable perinuclear concentration (Figure 51). In GB cells, SV2B showed a specific cytoplasmic localisation, particularly enriched around the nucleus, potentially indicating its concentration in cytoplasmic regions proximal to organelles (Figure 52). In DAOY MB cells, IF staining revealed a significant increase in SV2B fluorescence compared to HA-bs cells, indicating higher expression levels spread mainly across the cytoplasm (Figure 52). ACTB was used as an internal control and demonstrated uniform staining across U251MG, U87MG, DAOY, and HA-bs cell lines (Figure 53).

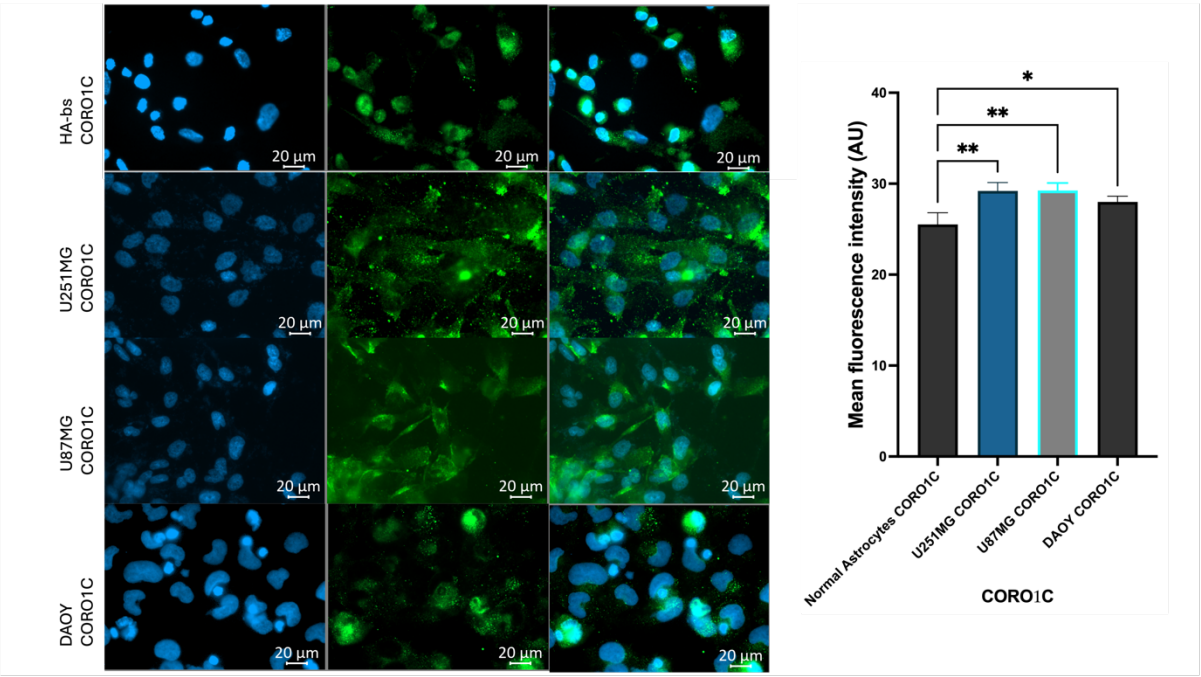


Figure 51. IF analysis of CORO1C localisation and quantification in HA-bs, U251MG, U87MG, and DAOY cells. IF staining for CORO1C of HA-bs cells revealed cytoplasmic localisation, with enhanced concentration in the perinuclear region. U251MG and U87MG GB cells exhibited significantly increased fluorescence intensity of CORO1C compared to HA-bs cells with a more diffuse distribution across the cytoplasm (HA-b versus U251MG, $p<0.0037$; HA-bs versus U87MG, $p<0.0035$). DAOY cells also showed a significant increase of CORO1C compared to HA-bs cells, with similar cytoplasmic localisation and perinuclear enrichment ($p<0.0321$). All images were taken at x40 magnification. Results are based on three independent experiments, n=3. All statistical analyses were conducted using ordinary one-way ANOVA, followed by Dunnett's multiple comparisons test to determine the significant differences in expression between normal human astrocytes, GB, and MB cells.

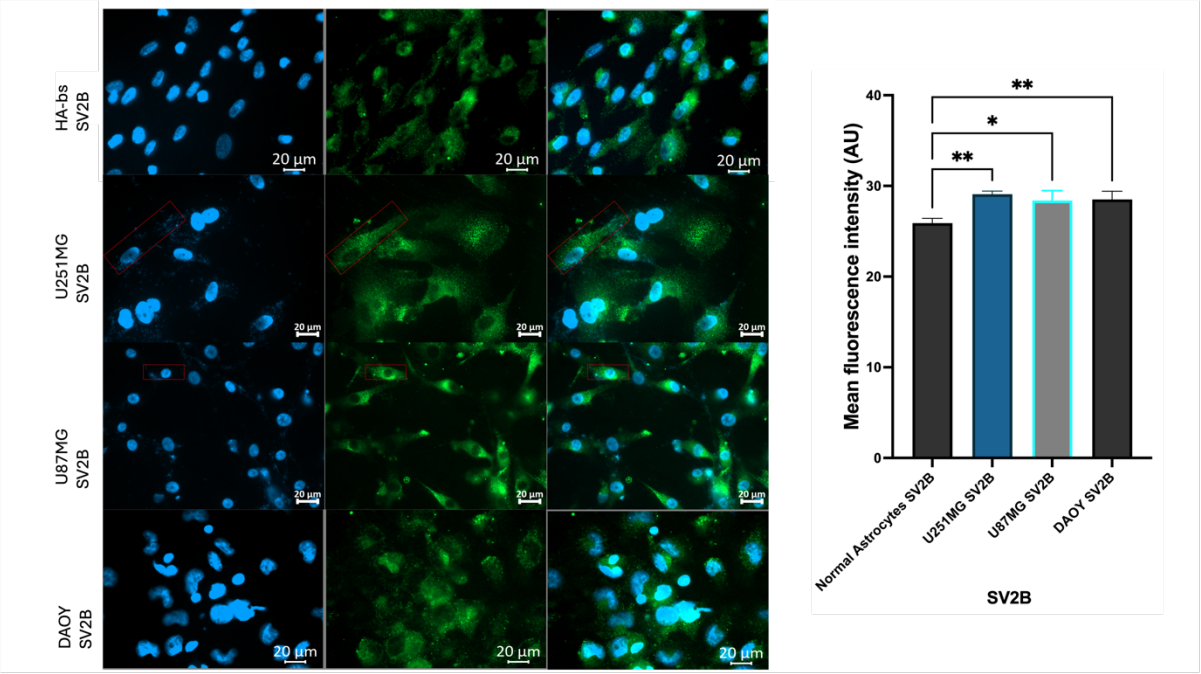


Figure 52. IF analysis of SV2B localisation and quantification in HA-bs, U251MG, U87MG, and DAOY cells. IF staining demonstrates that SV2B was predominantly localised in the cytoplasm across all cell lines. In HA-bs cells, SV2B displayed a diffuse cytoplasmic distribution. In GB cells, SV2B was specifically enriched around the nucleus and had a significantly higher expression in comparison to HA-bs cells (HA-bs versus U251MG, $P<0.0026$; HA-bs versus U87MG, $p<0.0110$). MB cells showed an increased SV2B fluorescence compared to HA-bs cells, with high expression levels distributed throughout the cytoplasm ($p<0.0085$). All images were taken at x40 magnification. Results are based on three independent experiments, n=3. All statistical analyses were conducted using ordinary one-way ANOVA, followed by Dunnett's multiple comparisons test to determine the significant differences in expression between normal human astrocytes, GB and MB cells.

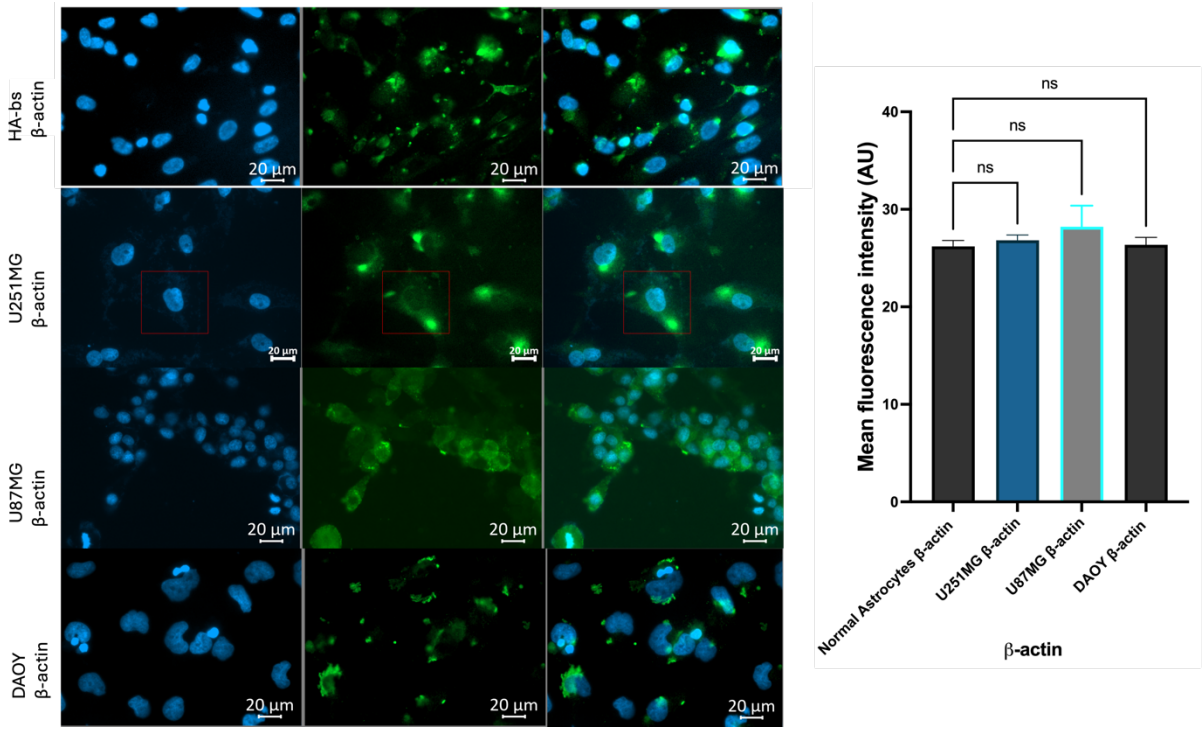


Figure 53. IF analysis of β-actin localisation and quantification in HA-bs, U251MG, U87MG, and DAOY cells. The internal control showed uniform staining across U251MG, U87MG, DAOY, and HA-bs cell lines, confirming consistent expression and serving as an internal control for comparing the expression levels of CORO1C and SV2B (HA-bs versus U251MG, $p<0.8642$; HA-bs versus U87MG, $p<0.1741$; HA-bs versus DAOY, $p<0.9960$). All images were taken at x40 magnification. Results are based on three independent experiments, n=3. All statistical analyses were conducted using ordinary one-way ANOVA, followed by Dunnett's multiple comparisons test to determine the significant differences in expression between normal human astrocytes, GB and MB cells.

3.3.7. Transient transfections of GB cells

Figures 54a and 54b illustrated the increased expression levels of miR-206 and miR-383 following transfection of U251MG and U87MG GB cells. Following transfection with miR-206 mimics, a significant downregulation of *CORO1C* was observed in both GB cell lines (Figure 55a). Additionally, transfection with miR-383 mimics led to a significant reduction in *SV2B* expression (Figure 55b). The transfection of GB cells with miR-206 and miR-383 mimics also resulted in a significant decrease in cell viability within both cell lines (Figures 56a and 56b). Additionally, GB cells exhibited a reduced colony-forming potential post-transfection with these miRNA mimics (Figures 57a, 57b, and 57c). Microscopic images (Figure 57c) of colony formation in GB cells post-transfection with miR-206 and miR-383 mimics (at x40 magnification) visually confirmed the loss of colony-forming ability. Western blotting analysis in U251MG cells showed a significant decrease in CORO1C protein levels following transfection with the miR-206 mimic compared to the negative control condition. However,

CORO1C levels were slightly reduced, but not significantly, when transfected with the miR-383 mimic (Figures 58a and 58b). The protein levels of SV2B were significantly reduced post-transfection with the miR-383 mimic compared to the negative control condition (Figures 58a and 58b). Additionally, SV2B levels were also downregulated in the miR-206 mimic condition (Figure 58b). In U87MG cells, CORO1C protein levels significantly decreased following transfection with the miR-383 mimic, while CORO1C levels remained unaffected by the miR-206 mimic (Figures 59a and 59b). SV2B protein levels were significantly reduced in the miR-383 mimic condition compared to the negative control. In contrast, SV2B levels were not affected by the miR-206 mimic in U87MG cells (Figure 59b). Chemiluminescent images displayed the expression levels of β-actin, CORO1C, and SV2B in U251MG and U87MG cells post-transfection with negative control miRNA #1, positive control miR-1, and the miR-206 and miR-383 mimics (Figures 58a and 59a). β-actin was consistently expressed across all samples, serving as a loading control. The images revealed the western blot findings, showing decreased CORO1C expression in U251MG with miR-206 and in U87MG with miR-383, as well as reduced SV2B expression in U251MG with both miR-206 and miR-383, and in U87MG with miR-383.

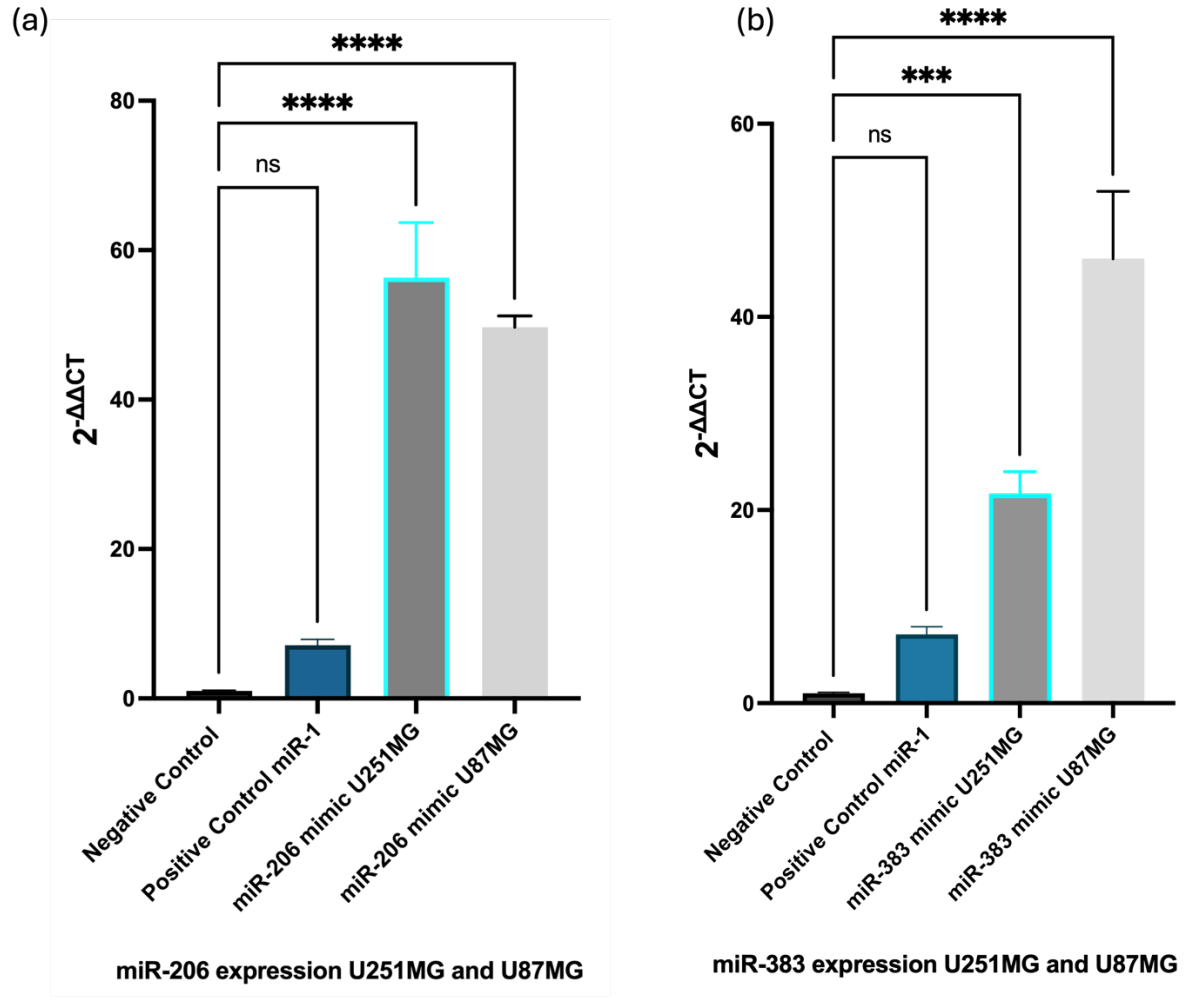


Figure 54. RT-qPCR of miRNA expression in GB cells post-transfection. (a) MiR-206 was significantly upregulated after transfection with miR-206 mimic within both GB cell lines (U251MG, $p<0.0001$; U87MG, $p<0.0034$). (b) MiR-383 was significantly upregulated after transfection with miR-383 mimic within both GB cell lines (U251MG, $p<0.0031$; U87MG, $p<0.0001$). Results are based on three independent experiments, n=3. All statistical analyses were conducted using ordinary one-way ANOVA, followed by Dunnett's multiple comparisons test to determine the significant differences of miRNA expressions post-transfection in U251MG and U87MG GB cells.

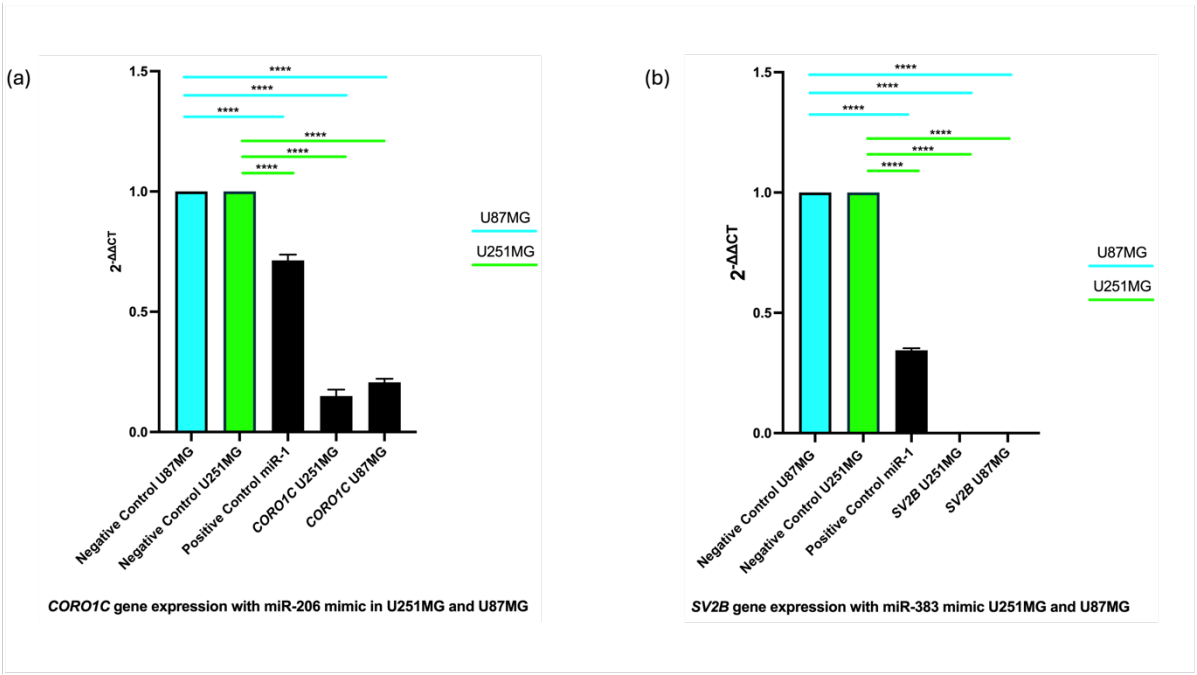


Figure 55. RT-qPCR of gene expression in GB cells post-transfection. (a) *CORO1C* was significantly downregulated post-transfection with miR-206 mimic in U251MG and U87MG cells (U251MG, $p<0.0001$; U87MG, $P<0.0001$). (b) *SV2B* was significantly downregulated post-transfection with miR-383 mimic with both GB cell lines (U251MG, $p<0.0001$; U87MG, $p<0.0001$). Results are based on three independent experiments, n=3. All statistical analyses were conducted using ordinary one-way ANOVA, followed by Dunnett's multiple comparisons test to determine the significant differences of gene expressions post-transfection in U251MG and U87MG GB cells.

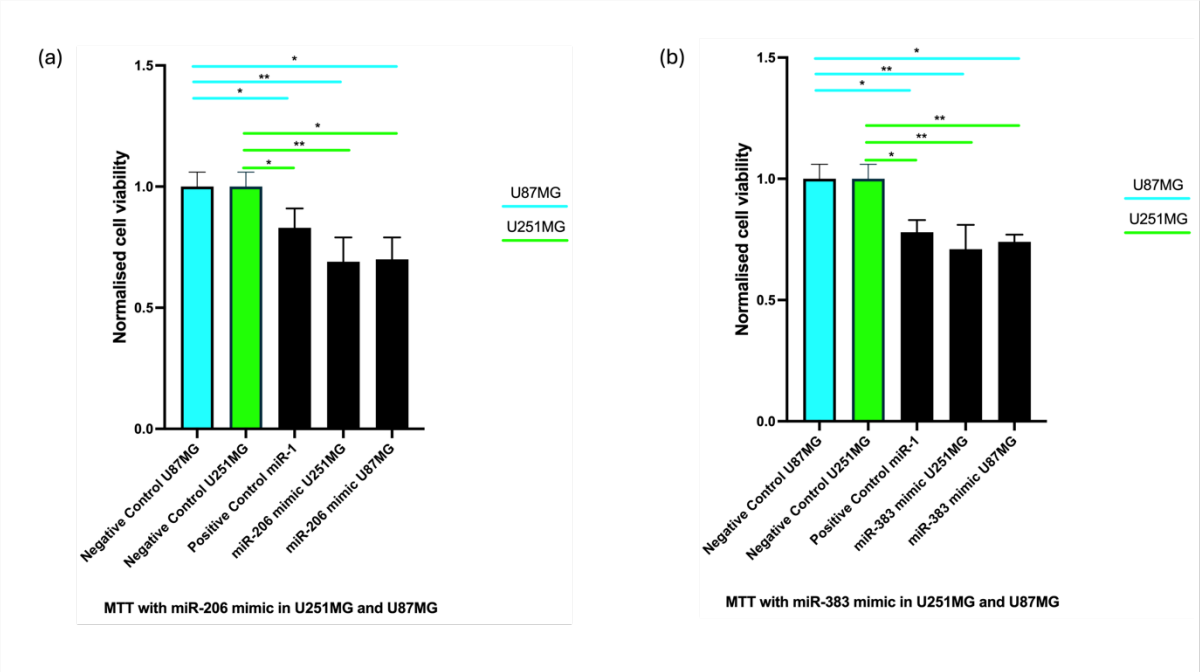


Figure 56. MTT assays in GB cells post-transfection with miR-206 or miR-383 mimics. (a) GB cell viability was significantly decreased post-transfection with miR-206 mimic in both, U251MG and U87MG cells (U251MG, $p<0.0039$; U87MG, $p<0.04$). (b) GB cell viability was significantly decreased post-transfection with miR-383 mimic in both U251MG and U87MG cells (U251MG, $p<0.002$; U87MG, $p<0.001$). Results are based on three independent experiments, n=3. All statistical analyses were conducted using ordinary one-way ANOVA, followed by Dunnett's multiple comparisons test to determine the significant differences of cell viability post-transfection in U251MG and U87MG GB cells.

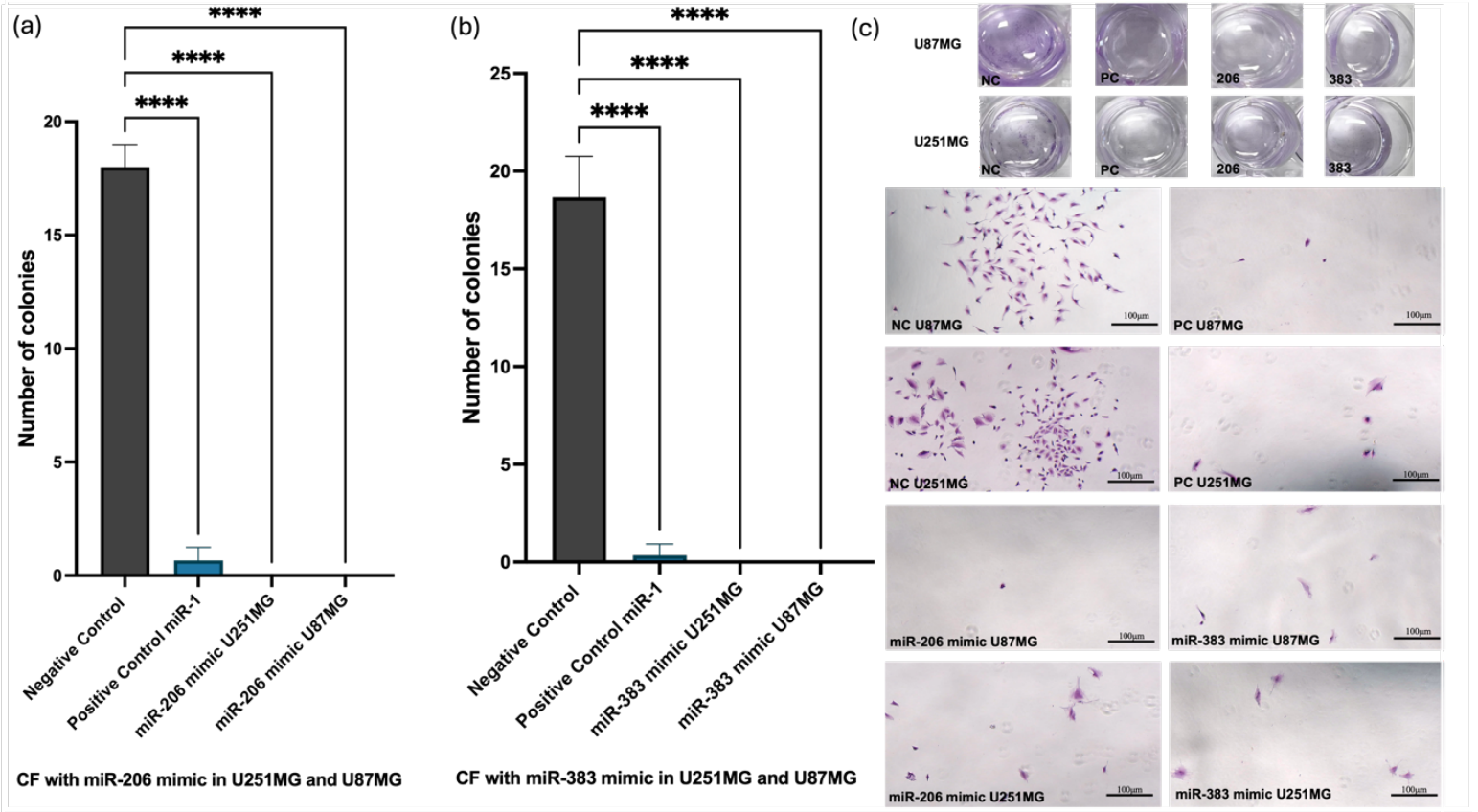


Figure 57. Colony-forming assays in GB cells post-transfection with miR-206 or miR-383 mimics. (a) Both GB cell lines lost their colony forming ability post-transfection with miR-206 mimic ($p<0.0001$). (b) Similarly, both GB cell lines lost their colony forming ability post-transfection with miR-383 mimic ($p<0.0001$). (c) Microscopic images of CF within GB cells post-exposure to miR-206 and miR-383 mimics (x40 magnification). Results are based on three independent experiments, n=3. All statistical analyses were conducted using ordinary one-way ANOVA, followed by Dunnett's multiple comparisons test to determine the significant differences of colony formation post-transfection in U251MG and U87MG GB cells.

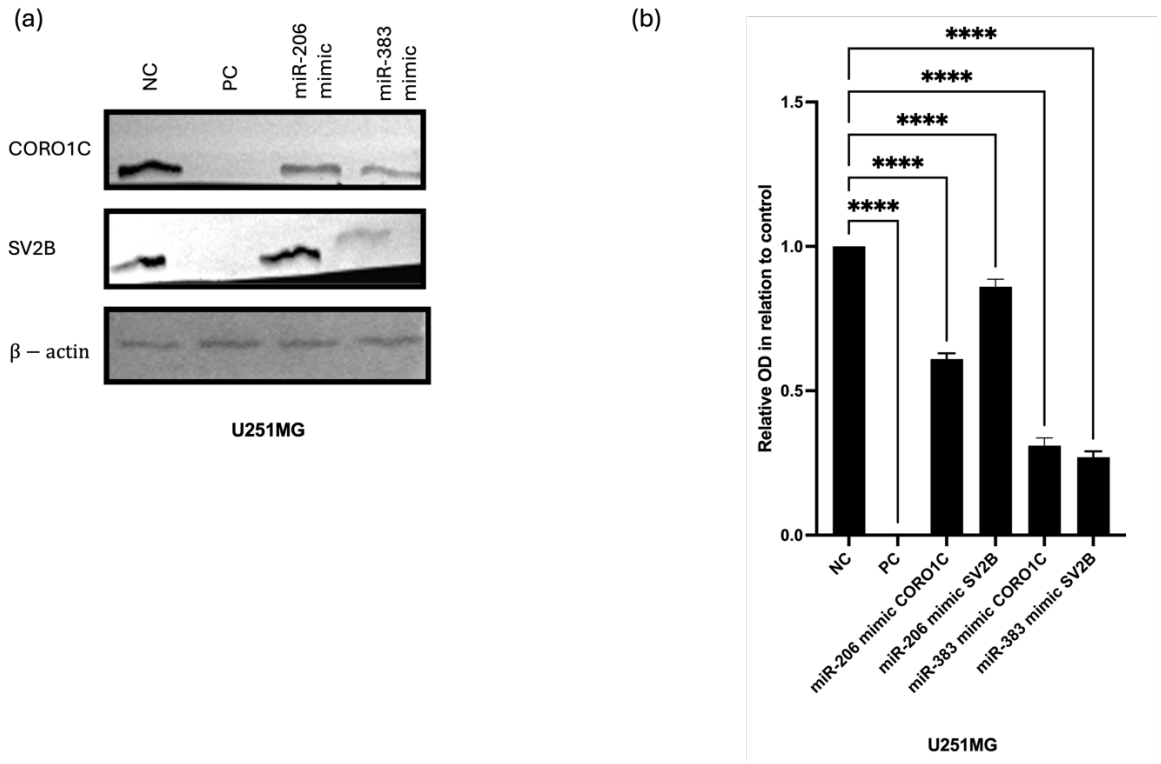


Figure 58. Western blotting of U251MG GB cells post-transfection with miR-206 or miR-383 mimics. (a) Chemiluminescent images illustrate the expression of β-actin, CORO1C, and SV2B within U251MG cells after exposure to various miRNA conditions, specifically negative control miRNA #1, positive control miR-1, and the miR-206 and miR-383 mimics. Negative control miRNA #1 was used to establish a baseline protein expression level for CORO1C and SV2B, providing a reference point for comparison to assess the effects of the miRNA mimics. This control ensures that any observed changes in protein levels are due to the specific action of the miRNA mimics rather than non-specific experimental effects. The positive control, miR-1, was included as a standard known to induce a measurable response in similar experimental setups, thus validating the experimental conditions and confirming the assay's sensitivity. (b) Western blotting analysis in U251MG showed that the protein levels of CORO1C were significantly decreased in comparison to the negative control condition post-exposure to the miR-206 mimic ($p<0.0001$), whilst the levels of CORO1C were unaffected in the miR-383 mimic condition $p<0.0993$). The protein levels of SV2B were also significantly reduced in comparison to the negative control condition post-exposure to miR-383 mimic ($p<0.0001$). Additionally, the levels of SV2B were also downregulated in the miR-206 mimic condition ($p<0.0001$). Results are based on three independent experiments, n=3. All statistical analyses were conducted using ordinary one-way ANOVA, followed by Dunnett's multiple comparisons test to determine the significant differences in protein expression post-transfection in U251MG GB cells.

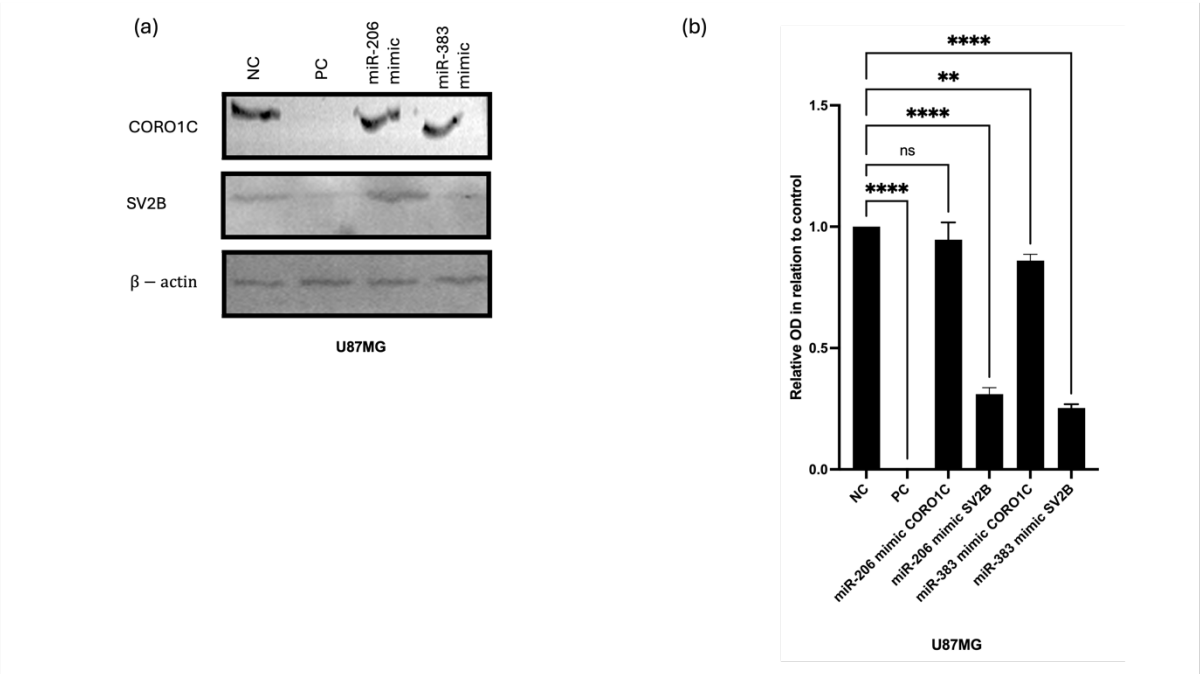


Figure 59. Western blotting of U87MG GB cells post-transfection with miR-206 ormiR-383 mimics. (a) Chemiluminescent images showing the expression of β-actin, CORO1C, and SV2B within U87MG cells post-exposure to negative control miRNA #1, positive control miR-1, and miR-206 and miR-383 mimics. Negative control miRNA #1 was used to establish a baseline protein expression level for CORO1C and SV2B, providing a reference point for comparison to assess the effects of the miRNA mimics. This control ensures that any observed changes in protein levels are due to the specific action of the miRNA mimics rather than non-specific experimental effects. The positive control, miR-1, was included as a standard known to induce a measurable response in similar experimental setups, thus validating the experimental conditions and confirming the assay's sensitivity. (b) Western blotting analysis in U87MG showed that the protein levels of CORO1C were not significantly decreased in comparison to the negative control condition post-exposure to miR-206 mimic ($p<0.9922$) and miR-383 ($p<0.7833$). The protein levels of SV2B were significantly reduced in comparison to the negative control condition post-exposure to miR-383 mimic ($p<0.0001$). Additionally, the levels of SV2B were also significantly reduced in the miR-206 mimic condition ($p<0.0032$). Results are based on three independent experiments, n=3. All statistical analyses were conducted using ordinary one-way ANOVA, followed by Dunnett's multiple comparisons test to determine the significant differences in protein expression post-transfection in U87MG GB cells.

3.3.8. Transient transfections of MB cells

Transient transfections of MB cells with miR-206 or miR-383 mimics resulted in significant upregulation of these miRNAs. Figures 60a and 60b illustrated the increased expression levels of miR-206 and miR-383 following transfection, confirming the effectiveness of the mimics. Following the transfection of MB cells with miR-206 mimics, a significant downregulation of *CORO1C* was observed (Figure 61a). Similarly, transfection with miR-383 mimics led to a significant reduction in *SV2B* expression (Figure 61b). Post-transfection with miR-206 and miR-383 mimics, there was a significant decrease in MB cell viability (Figures 62a and 62b). MB cells transfected with miR-206 or miR-383 mimics also demonstrated a significant loss of colony-forming abilities (Figures 63a, 63b, and 63c). Microscopic images (Figure 63c) of colony formation within MB cells post-transfection with miR-206 or miR-383 mimics (at x40 magnification) visually confirmed the loss of colony-forming ability. Western blotting analysis revealed that the protein levels of CORO1C were significantly decreased following transfection with the miR-206 mimic compared to the negative control condition (Figures 64a and 64b). Similarly, the protein levels of SV2B were significantly reduced after transfection with the miR-383 mimic compared to the negative control condition (Figures 64a and 64b). Chemiluminescent images showed the expression levels of β-actin, CORO1C, and SV2B across different conditions, including the negative control miRNA #1, positive control miR-1, and the miR-206 and miR-383 mimics (Figure 64a). β-actin was consistently expressed across all samples, confirming equal protein loading. CORO1C expression was visibly decreased in the miR-206 mimic condition, and SV2B expression was reduced in the miR-383 mimic condition.

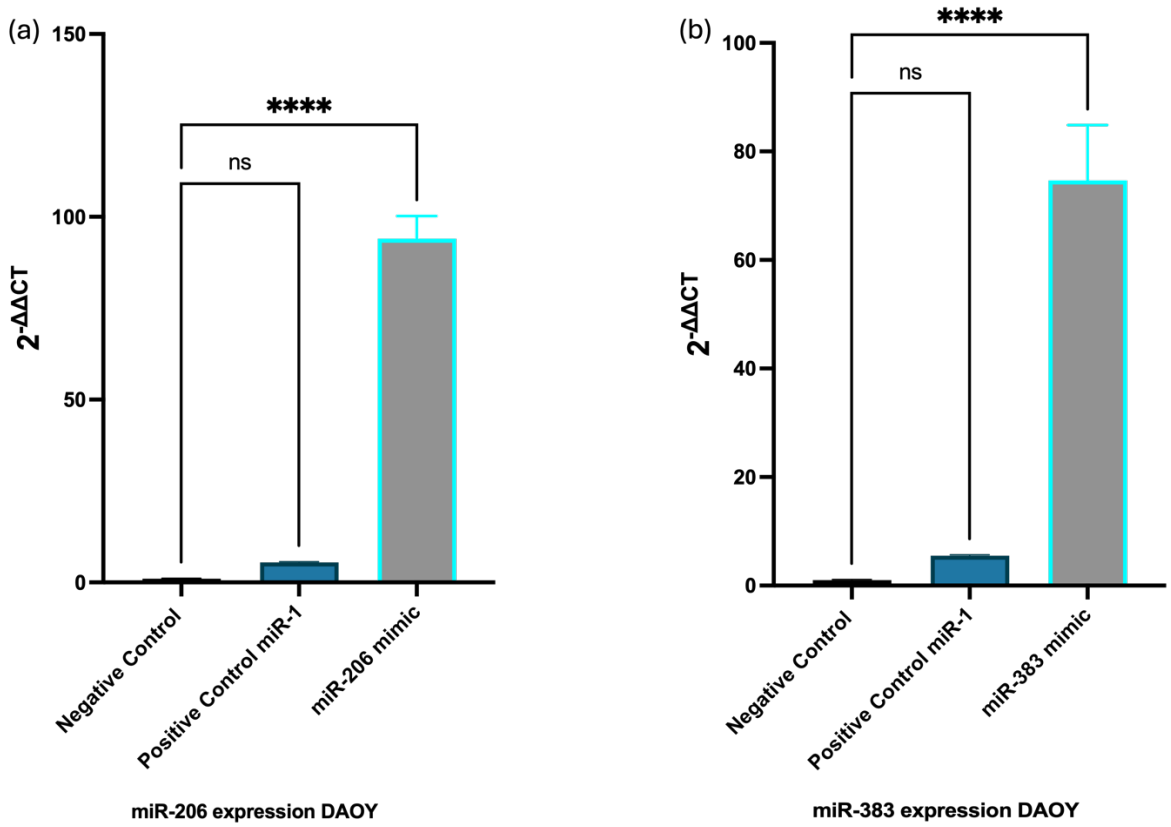


Figure 60. RT-qPCR of miRNA expressions in MB cells post-transfection. (a) MiR-206 was significantly upregulated after transfection with miR-206 mimic ($p<0.0001$). (b) MiR-383 was significantly upregulated after transfection with miR-383 mimic ($p<0.0001$). Results are based on three independent experiments, n=3. All statistical analyses were conducted using ordinary one-way ANOVA, followed by Dunnett's multiple comparisons test to determine the significant differences of miRNA expressions post-transfection in DAOY MB cells.

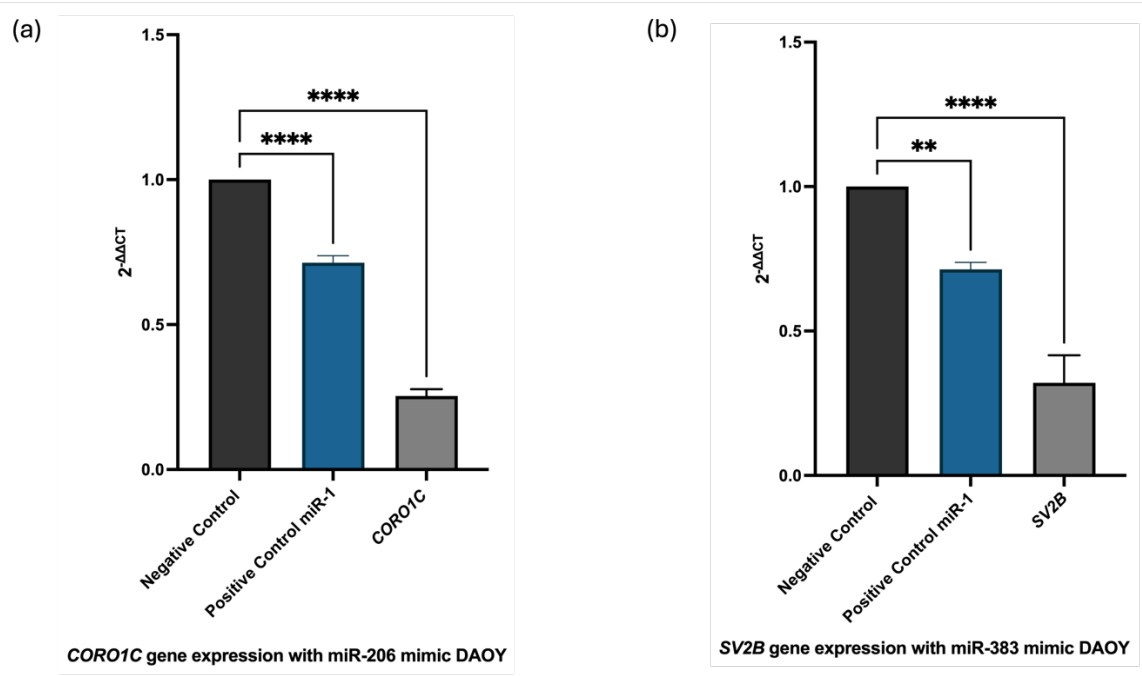


Figure 61. RT-qPCR of gene expressions in MB cells post-transfection. (a) *CORO1C* was significantly downregulated post-transfection with miR-206 mimic ($p<0.0009$). (d) *SV2B* was significantly downregulated post-transfection with miR-383 mimic ($p<0004$). Results are based on three independent experiments, n=3. All statistical analyses were conducted using ordinary one-way ANOVA, followed by Dunnett's multiple comparisons test to determine the significant differences of gene expressions post-transfection in DAOY MB cells.

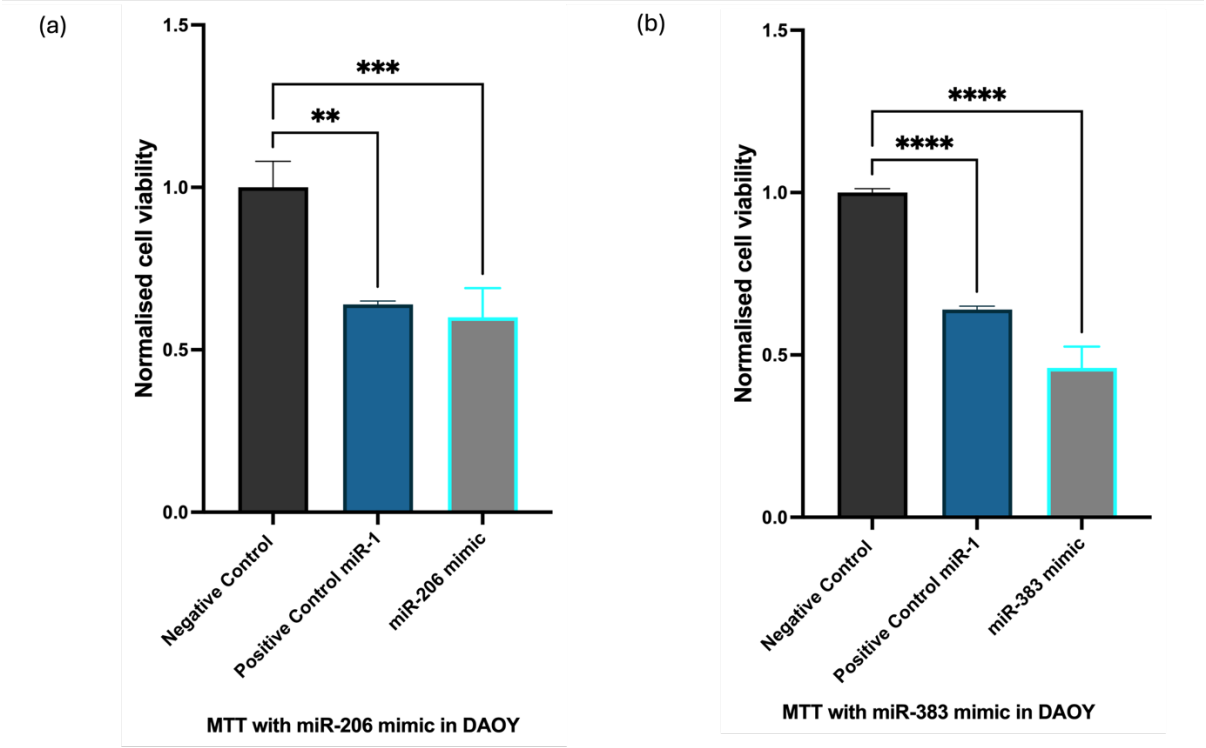


Figure 62. MTT assays in MB cells post-transfection with miR-206 or miR-383 mimics. (a) MB cell viability was significantly decreased post-transfection with miR-206 mimic ($p<0.0032$). (b) MB cell viability was significantly decreased post-transfection with miR-383 mimic ($p<0.009$). Results are based on three independent experiments, n=3. All statistical analyses were conducted using ordinary one-way ANOVA, followed by Dunnett's multiple comparisons test to determine the significant differences of cell viability post-transfection in DAOY MB cells.

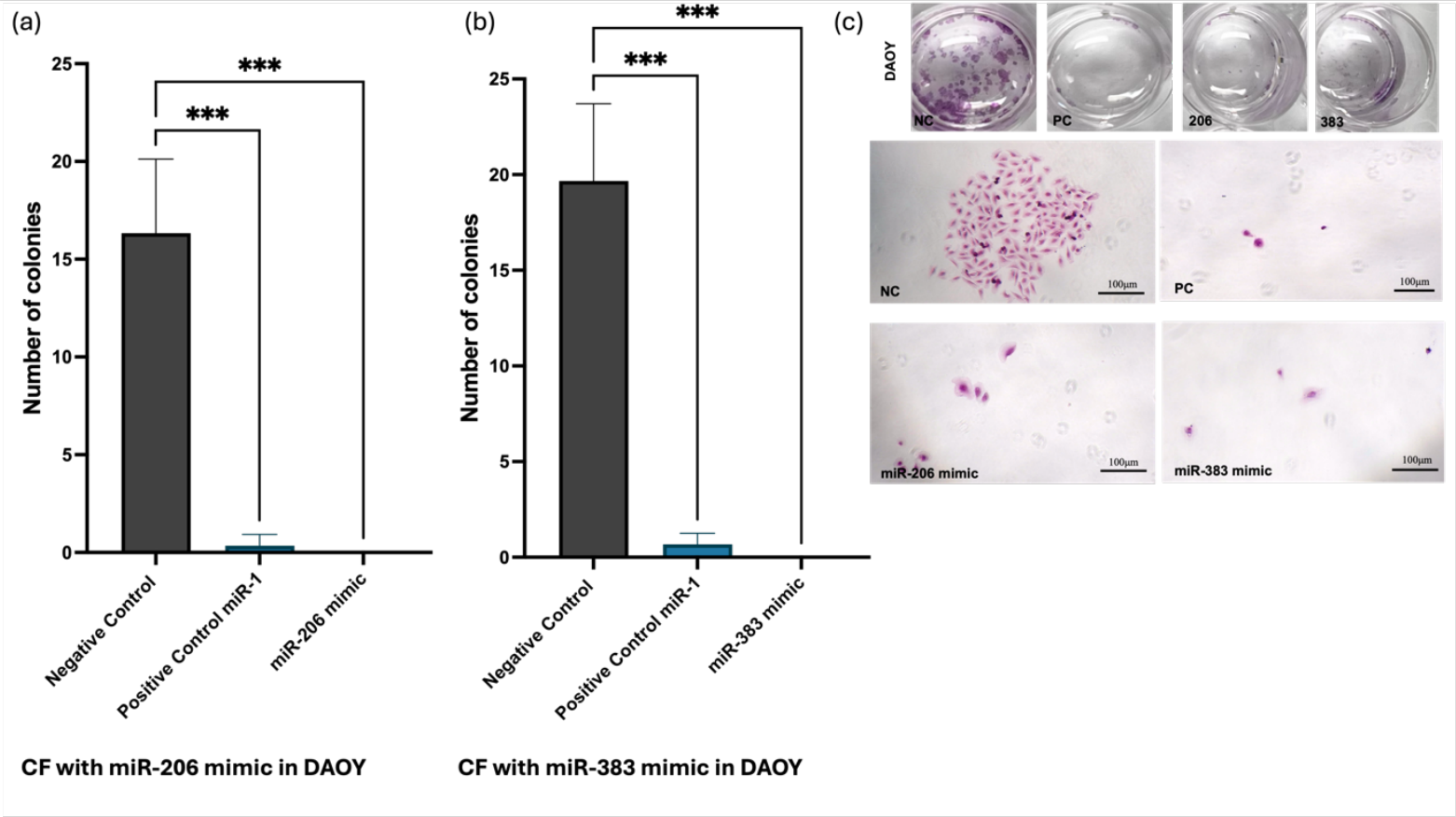


Figure 63. Colony-forming assays in MB cells post-transfection with miR-206 or miR-383 mimics. (a) MB cells lost their colony forming abilities post-transfection with miR-206 mimic ($p<0.001$). (b) Similarly, MB cells lost their colony forming abilities post-transfection with miR-383 mimic ($p<0.001$). (c) Microscopic images of CF within MB cells post-exposure to miR-206 and miR-383 mimics (x40 magnification). Results are based on three independent experiments, n=3. All statistical analyses were conducted using ordinary one-way ANOVA, followed by Dunnett's multiple comparisons test to determine the significant differences of colony formation post-transfection in DAOY MB cells.

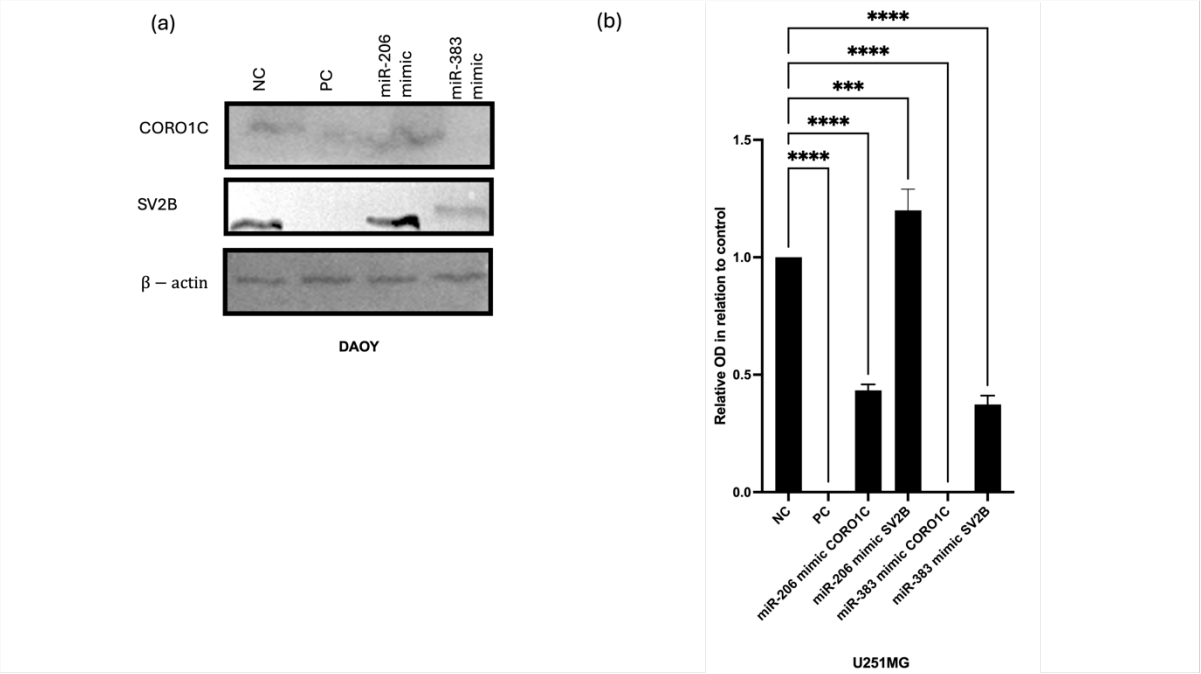


Figure 64. Western blotting of DAOY MB cells post-transfection with miR-206 or miR-383 mimics. (a) Chemiluminescent images showing the expression of β-actin, CORO1C, and SV2B within negative control miRNA #1, positive control miR-1, and miR-206 and miR-383 mimics. Negative control miRNA #1 was used to establish a baseline protein expression level for CORO1C and SV2B, providing a reference point for comparison to assess the effects of the miRNA mimics. This control ensures that any observed changes in protein levels are due to the specific action of the miRNA mimics rather than non-specific experimental effects. The positive control, miR-1, was included as a standard known to induce a measurable response in similar experimental setups, thus validating the experimental conditions and confirming the assay's sensitivity. (b) Western blotting analysis showed that the protein levels of CORO1C were significantly decreased in comparison to the negative control condition post-exposure to miR-206 mimic ($p<0.0001$). The protein levels of SV2B were also significantly reduced in comparison to the negative control condition post-exposure to miR-383 mimic ($p<0.0009$). Results are based on three independent experiments, n=3. All statistical analyses were conducted using ordinary one-way ANOVA, followed by Dunnett's multiple comparisons test to determine the significant differences of protein expression post-transfection in DAOY MB cells.

3.4. Discussion

The results of our bioinformatics analyses in Chapter 2 and the subsequent RT-qPCR validation provided valuable insights into the dysregulation of selected miRNAs in GB. The *in silico* analysis revealed that miR-21 was significantly upregulated in GB, which was further confirmed through RT-qPCR in U87MG and U251MG GB cell lines. This finding is consistent with the role of miR-21 as an oncomiR. As already mentioned in Chapter 2, in GB, miR-21 contributes to tumour pathogenesis by targeting multiple tumour suppressor genes and altering key signalling pathways. It primarily suppresses apoptosis by downregulating pro-apoptotic proteins like Bax and upregulating anti-apoptotic proteins such as Bcl2, thus promoting tumour growth (Bautista-Sánchez, *et al.,* 2020). Another important aspect of the role of miR-21 in GB is its involvement in the regulation of the TME. There is evidence that miR-21 is transferred from GB cells to adjacent non-malignant cells, such as microglia, via EVs (Abels, *et al.,* 2019). This transfer results in the re-programming of microglia, promoting a pro-tumorigenic environment that supports GB cell survival and invasion. Our RT-qPCR analysis also depicted that miR-21 was overexpressed in MB cells. Even though miR-21 is less studied in MB, there is evidence that it is similarly upregulated, playing a critical role in promoting cancer cell migration and metastasis (Grunder, *et al.,* 2011). Given its consistent upregulation in GB, miR-21 has been investigated as a potential biomarker for the diagnosis of GB. Numerous studies have demonstrated elevated levels of miR-21 in both tissue samples and biofluids such as CSF and serum of GB patients (Shi, *et al.,* 2015; Ivo D'Urso, *et al.,* 2015; Wang, *et al.,* 2012; Petrescu, Sabo, Torsin, Calin & Dragomir, 2019). The high specificity and sensitivity of miR-21 detection in these biological fluids makes it a promising non-invasive biomarker for GB diagnosis (Zhao, *et al.,* 2021). For instance, miR-21 levels in CSF have been shown to distinguish GB patients from healthy controls, providing a valuable tool for early detection and monitoring (Petrescu, *et al.*, 2019). In MB, miR-21 has also shown potential as a diagnostic biomarker. A highly sensitive electrochemical biosensor has been developed to detect miR-21 in CSF, with promising results for distinguishing MB from non-cancer controls (Wang, *et al.,* 2022). This suggests that miR-21 could serve as a reliable biomarker for MB diagnosis and monitoring. Considering the critical role of miR-21 in both GB and MB pathogenesis, targeting miR-21 has emerged as a potential therapeutic strategy as discussed in Chapter 2. We confirmed the dysregulated expression of miR-21 in both GB and MB cells, consistent with its known role in tumour biology. However, after further investigation, we found that miR-21 does

not target the key genes we identified and selected for deeper analysis related to our study. As a result, we decided to focus on other miRNAs that aligned with our gene targets.

Our bioinformatics analysis also identified miR-34a as downregulated in GB cases, suggesting its tumour-suppressive properties. Furthermore, our results suggested that miR-34a was acting as a tumour suppressor in MB. Our subsequent RT-qPCR expression analysis confirmed the downregulation of miR-34a in both GB cell lines and MB cells. Its downregulation in these malignancies suggested that the miRNA plays role in tumour pathogenesis and could potentially be utilised as a diagnostic biomarker for grade 4 malignancies. This downregulation usually leads to the loss of its tumour-suppressive functions, allowing the upregulation of oncogenes like *c-Met*, *Notch-1*, and *Notch-2*, which have been proven essential for GB tumorigenesis (Fu, Imani, Wu & Wu, 2023). Furthermore, in GB, miR-34a levels could help distinguish between normal and malignant tissue, particularly in the context of *p53* mutations and other genetic alterations (Navarro & Lieberman, 2015). Similarly, in MB, the downregulation of miR-34a and its effects on tumour growth and differentiation could serve as a diagnostic biomarker, particularly in cases with specific genetic mutations like *MYCN* and *SIRT1* overexpression (Thor, *et al.,* 2015). Additionally, miR-34a possesses potential as a therapeutic agent against both GB and MB. In GB, miR-34a could simultaneously target multiple oncogenic pathways such as c-Met and Notch suggesting its broad anti-tumour effect and overcoming the limitations of therapies that target a single molecule (Guessous, *et al.,* 2010). In our bioinformatic analyses, we identified that miR-34 was downregulated while targeting both the *CORO1C* and *SV2B* genes, both of which were upregulated in GB cells. This correlation suggested a potential diagnostic approach for GB patients, as the dysregulation of miR-34 and its target genes may play a role in the GB tumorigenesis. Furthermore, given that we observed a similar downregulation of miR-34 and upregulation of these target genes in MB cells during our *in vitro* experiments, we could suggest that this diagnostic option could also be relevant for MB patients, indicating a broader diagnostic implication. However, despite the ability of miR-34a to target *CORO1C* and *SV2B*, the strength of the miRNA interaction was weaker compared to other miRNAs selected for further study, as discussed in detail later in this section. Subsequently, we chose to focus on miRNAs with stronger binding interactions for further therapeutic exploration.

Our bioinformatics analyses and subsequent RT-qPCR validations revealed that miR-128a was significantly downregulated in GB cells suggesting its tumour suppressive properties. In GB,

miR-128a inhibited tumour growth by targeting several oncogenic pathways. One of its primary mechanisms, as mentioned in Chapter 2, is the downregulation of the *Bmi-1* gene, which is crucial for glioma stem cell self-renewal. By inhibiting *Bmi-1*, miR-128a reduces glioma cell proliferation and tumour growth, both *in vitro* and *in vivo* (Shan, *et al.,* 2016). The reduction in miR-128a levels in GB contributes to enhanced proliferation, invasion, and maintenance of glioma stem cells, which are central to the tumour's aggressive behaviour and resistance to therapy (Makowska, Smolarz & Romanowicz, 2023). Our RT-qPCR analysis depicted miR-128a as not significantly dysregulated in MB cells. Opposing our observation, previous evidence has suggested that in MB, miR-128a similarly acted as a tumour suppressor by targeting the *Bmi-1* oncogene (Venkataraman, *et al.,* 2010). The loss of miR-128a in MB led to unchecked *Bmi-1* activity promoting tumour growth and resistance to therapy (Venkataraman, *et al.,* 2010). However, only one study found on miR-128a in MB, indicating a gap in this research area. Further investigation is needed to precisely elucidate its function and role in the progression of this cancer type. Nevertheless, the consistent downregulation of miR-128a in GB suggested its potential as a diagnostic biomarker for high grade brain neoplams. In GB, miR-128a levels could be used to distinguish between normal and malignant brain tissue, particularly in identifying aggressive subtypes of the tumour (Buruiană, *et al.,* 2020). In our bioinformatic analyses, we found that miR-128a was downregulated in GB cases and targeted *CORO1C* and *SV2B*, suggesting a potential diagnostic axis in GB. Despite this, the strength of the miRNA interaction with the two target genes was relatively weaker compared to other miRNAs we studied, which is why we did not assess the function of miR-128a further via *in vitro* analysis.

Furthermore, our bioinformatics predictions indicated that miR-206 targeted *CORO1C* with greater affinity when compared to the previously discussed miRNAs suggesting that the miRNA possesses tumour suppressive properties in GB. When validated through RT-qPCR, our results demonstrated that this miRNA was downregulated in both GB and MB cells. Our findings also depicted that following transfection of the U251MG and U87MG cells with miR-206 mimics, a notable downregulation of the *CORO1C* gene was observed in both cell lines indicating that miR-206 effectively targeted and reduced the expression of *CORO1C* at the mRNA level. In GB, miR-206 expression was observed to be downregulated, particularly in high-grade gliomas (HGGs) compared to low-grade gliomas (LGGs) and normal brain tissues (Zhou, *et al.,* 2019a). We also demonstrated that after transfection of the U251MG and U87MG GB cells with miR-206 mimics, a significant upregulation of the miRNA was observed in both

GB and MB cell lines suggesting its potential application as a therapeutic against GB. In support of our findings, it has been demonstrated that normalised expression of miR-206 suppressed glioma cell proliferation, induced cell cycle arrest, and decreased the invasiveness of GB cells (Zhou, *et al.,* 2019a). Our transfections results were in line with these observations as we showed that transfections with miR-206 mimics resulted in a significant decrease in cell viability in both U251 and U87MG cell lines suggesting that miR-206 acted effectively as a tumour suppressor when overexpressed. In addition, miR-206 transfections led to a significant reduction in the colony-forming potential of GB cells, indicating an inhibited proliferative capacity post-transfection. The significant downregulation of miR-206 in GB, particularly in more aggressive stages of the tumour, suggested its potential use as a biomarker for tumour grading and prognosis, as lower levels correlated with higher tumour grades and poorer patient survival outcomes (Hosein Yazdi, Zarrinpour, Moslemi & Forghanifard, 2022). Similarly, it has been observed that miR-206 plays an important role in MB in all four molecular subgroups exhibiting decreased miR-206 expression (Panwalkar, *et al.,* 2015). Clinically, miR-206 was significantly downregulated in MB tissues compared to adjacent non-tumour tissues, and this low expression was associated with aggressive tumour features, such as anaplastic histology, highlighting its potential as a diagnostic and prognostic biomarker (Pan, Wang, Wan & Zheng, 2017). Although restoring miR-206 expression alone may not be sufficient to inhibit tumour growth, overexpression of miR-206 has been shown to reduce MB cell viability, migration, and invasion (Pan, *et al.,* 2017). Our transfection of MB cells with miR-206 mimics led to a significant increase in the expression levels of miR-206, confirming the role of the miRNA as a tumour suppressor and offering a potential therapeutic against MB. Our results also depicted a decrease in cell viability, suggesting that miR-206 could reduce the overall survival of MB cells. Moreover, a significant reduction in the colony-forming potential of MB cells was observed through our functional assays. The upregulation of miR-206 in both GB and MB, along with the subsequent downregulation of *CORO1C*, suggested a potential alternative therapeutic axis. Thus, restoring miR-206 levels in aggressive tumours, such as GB and MB, could offer a promising therapeutic strategy against these brain malignancies.

Our bioinformatics analysis also depicted that miR-383 targeted *SV2B* in a stronger manner when compared to miR-34a and miR-128a suggesting that it possesses tumour suppressive properties in GB. When tested via RT-qPCR, our results demonstrated that this miRNA was downregulated in both GB and MB cells. We also showed that transfections with miR-383 significantly downregulated the expression of *SV2B* in both GB and MB cells. In GB cells,

transfection with miR-383 mimics led to a marked reduction in SV2B at both the mRNA and protein levels. It has been reported that miR-383 plays an important role in the pathogenesis of both GB and MB. In GB, miR-383 expression was observed significantly downregulated, contributing to the malignant phenotype observed in GB cells (Xu, *et al.,* 2015). One of the primary mechanisms through which miR-383 exerted its tumour-suppressive effects was by directly targeting the oncogene *CIP2A*. CIP2A promotes cell proliferation, invasion, and migration in GB cells by inhibiting protein phosphatase 2A (PP2A) activity, subsequently leading to the activation of oncogenic pathways, including those involving c-Myc and Akt (Chen, Hu & Chen, 2023). It has also been observed that miR-383 exerted tumour-suppressive effects in MB by targeting and downregulating oncogenes involved in tumour proliferation, migration, and invasion, specifically the forkhead box M1 (*FOXM1*) gene (Wang, *et al.,* 2020b). *FOXM1* is overexpressed in MB and is known to play a significant role in promoting cell proliferation and survival (Liao, *et al.,* 2018). The depletion of miR-383 led to enhanced malignant behaviour of MB cells by regulating the expression of genes involved in the cell cycle, apoptosis resistance, and metastasis (Liao, *et al.,* 2018). In line with this evidence, our transfections of GB and MB cells with miR-383 mimics led to a significant upregulation of miR-383. Consequently, we observed a decrease in cell viability, suggesting that miR-383 plays an essential role in reducing the survival of both GB and MB cells. Moreover, the colony-forming ability of these cells was significantly impaired following transfection with miR-383 mimics, highlighting the impact of miR-383 on the proliferative capacity of these cancer cells. The upregulation of miR-383 and its role in downregulating *SV2B* suggested a potential therapeutic axis. Hence, restoring miR-383 levels or targeting its regulatory pathways could offer a promising therapeutic strategy against these aggressive malignancies, especially in cases resistant to conventional treatments.

The bioinformatics analysis also depicted that *CORO1C* was particularly upregulated in gliomas and paediatric brain malignancies, including MB. Our RT-qPCR validation expression assays depicted the upregulation of the gene within both GB and MB cell lines. The expression of *CORO1C* in diffuse gliomas has been previously noted (Thal, *et al.,* 2008). Specifically, the elevated expression of the mRNA in GB correlated with the increased malignancy by which these types of tumours are characterised (Thal, *et al.,* 2008). It also has been observed that *CORO1C* plays a distinctive role in the pathogenesis of colorectal cancer by contributing to cell migration, proliferation, and invasion (Wang, *et al.,* 2021d). These processes are essential for the aggressive behaviour of malignant cells, such as GB cells, including their ability to

infiltrate surrounding brain tissues, making the tumour difficult to treat surgically. CORO1C is involved in bundling and crosslinking actin filaments, which strengthens the actin cytoskeleton and supports the formation of cellular protrusions like lamellipodia (Xavier, *et al.,* 2012). In GB, these structures are crucial for the motility of tumour cells as they allow them to migrate through the brain tissue, which is a hallmark of GB invasiveness (Seker-Polat, Pinarbasi Degirmenci, Solaroglu & Bagci-Onder, 2022). Further to the formation of lamellipodia, CORO1C is also involved in the formation of invadopodia in triple-negative breast cancer (Castagnino, *et al.,* 2018). These are actin-rich protrusions that penetrate and degrade the ECM. This degradation is mediated by matrix metalloproteinases (MMPs), which are enzymes commonly secreted by GB cells that break down the ECM, allowing the tumour cells to invade surrounding healthy tissue (Hagemann, Anacker, Ernestus & Vince, 2012). Hence, it could be suggested that the presence of invadopodia formation and ECM invasion might be crucial for the invasive behaviour of GB cells. Additionally, it has been observed that the MMP-2 (gelatinase A) matrix metalloproteinase was largely implicated in GB cell invasion (Yu, Chen, Lu, Hong & Chiang, 2017). The knockdown of *CORO1C* in A172 GB cells resulted in reduced MMP activity suggesting that *CORO1C* was involved in the regulation of proteases necessary for ECM degradation, aiding GB pathogenesis (Solga, *et al.,* 2019). Our *in-silico* analysis also depicted the expression of *CORO1C* in normal astrocytes and microglial cells within the tumour microenvironment. These non-malignant cells, which could become activated in response to the tumour as discussed in the Introduction Chapter, can contribute to the overall malignancy by promoting inflammation and creating a supportive niche for tumour growth, highlighting the role of CORO1C in GB development (Sharma, Aaroe, Liang & Puduvalli, 2023). The bioinformatics analysis and the subsequent RT-qPCR analysis demonstrated the overexpression of *CORO1C* in MB patient tissues and cell lines. Furthermore, following transfection, there was a significant downregulation of *CORO1C* in MB cells suggesting that miR-206 effectively targeted and suppressed *CORO1C*, suggesting its oncogenic nature. To the best of our knowledge, the association between this gene and its protein product within MB have not been previously investigated. In our results, we depicted that *CORO1C* was effectively downregulated in GB and MB cells post-transfection with miR-206 mimics indicating that miR-206 and CORO1C might play a significant role in brain tumour pathogenies. Furthermore, in MB cells, miR-206 transfection resulted in a decreased CORO1C expression, both at the mRNA and protein levels. Thus, we might hypothesise that in MB, CORO1C might play a similar role in contributing to tumour aggressiveness by promoting cell proliferation and metastasis, features associated with highly malignant paediatric brain

tumours. The higher expression levels detected in high-grade brain malignancies potentially suggest that CORO1C could serve as a useful diagnostic biomarker. Furthermore, the involvement of CORO1C in key processes such as cell proliferation, migration, and invasion make it a putative promising therapeutic target.

Our bioinformatics analyses also revealed that patients with high expression of *SV2B* were associated with significantly lower overall survival when compared to patients with decreased expression. Notably, we saw that *SV2B* was particularly expressed in MB cases. Our subsequent RT-qPCR expression analysis indicated that *SV2B* was overexpressed in both GB and MB cell lines. We also observed that *SV2B* was significantly downregulated when GB and MB cells were transfected with the miR-383 mimic confirming the strong interaction between the miRNA and the mRNA. This downregulation was associated with a decrease in cell viability and a reduction in colony-forming ability, indicating that miR-383 and *SV2B* may play an important role in inhibiting the growth and survival of GB and MB cells. These findings could suggest that miR-383 consistently targets and suppresses SV2B across different types of brain tumours, including both GB and MB, contributing to reduced cell proliferation and survival in these cancer cells. To the best of our knowledge, there are no previous studies illustrating the role of SV2B within GB and MB cell lines. Interestingly, recent bioinformatics research identified *SV2B* as a gene of interest due to its association with poor prognosis in gliomas (Zhang, *et al.,* 2020b). This is in line with our results, which suggested that SV2B might play a role in the aggressive behaviour of GB, contributing to the progression of the malignancy. It has been observed that SV2B is implicated in promoting tumour progression through several mechanisms. The link of the protein to energy metabolism and the regulation of transporter proteins is necessitated for maintaining the high metabolic demands of rapidly proliferating tumour cells, such as GB and MB (Rossi, Arjmand, Bærentzen, Gjedde & Landau, 2022). Additionally, it has been observed that SV2B is involved in ECM interactions, which are critical for tumour invasion and metastasis. By facilitating the transport of nutrients and signalling molecules, SV2B may support the invasive and metastatic potential of GB cells (Bartholome, *et al.,* 2017). There is also evidence implicating SV2B in brain metastases, particularly in cases of metastatic colorectal cancer (Michl, *et al.,* 2024). Currently, although there is no direct evidence linking SV2B with MB, the role of SV2B in synaptic vesicle regulation and neuroendocrine processes suggests that it could be involved in the progression of paediatric brain tumours as well. Its expression in neuroendocrine tumours indicates that similar mechanisms might be involved in paediatric malignancies with neurodevelopmental

components (Castle, Levy & Chauhan, 2022). Given its overexpression in high-grade brain malignancies, SV2B could serve as a potential prognostic biomarker. Its expression levels could influence the decision-making process for patients based on the aggressiveness of their tumours and guide therapeutic decisions. Furthermore, targeting SV2B or its related pathways may disrupt key processes like vesicle trafficking, neuroendocrine signalling, and tumour cell metabolism, offering new treatment options for these aggressive malignancies.

The western blotting and IF analyses provided insights into the expression and localisation patterns of both CORO1C and SV2B across the HA-bs, U251MG, U87MG, and DAOY cell lines. As a member of the coronin protein family, the function of CORO1C is associated with the regulation of cytoskeletal dynamics, particularly in actin filament organisation, which is essential for cellular processes such as migration, adhesion, and intracellular trafficking (King, *et al.,* 2022). Previous research demonstrated that CORO1C plays a crucial role in the ER-associated fission of actin-dependent cargo-sorting domains on endosomes, highlighting its key role in coordinating endosome fission and cargo sorting (Hoyer, *et al.,* 2018). Our IF staining of HA-bs cells demonstrated that CORO1C was mainly localised in the cytoplasm with a significant concentration in the perinuclear region, often associated with organelles such as the ER or Golgi apparatus. In contrast, GB cells showed significantly increased fluorescence of CORO1C compared to HA-bs cells, with a more diffuse distribution throughout the cytoplasm. The western blotting analysis further supported this observation, revealing that the CORO1C protein was significantly overexpressed in both GB cell lines compared to HA-bs cells. This indicated that CORO1C may play a more extensive role in cytoskeletal reorganisation in GB cells, potentially facilitating their enhanced migratory and invasive capabilities. Previous evidence identified that CORO1C was also overexpressed in CRC tissues and that it was localised mostly in the cytoplasm (Wang, *et al.,* 2021d). These findings were in line with our observations regarding the cytoplasmic localisation of CORO1C and suggested that it may have potential oncogenic effects in GB, similar to its role in other cancers. Similarly, in DAOY cells, CORO1C was shown to be significantly overexpressed compared to HA-bs cells, with a noticeable concentration in the perinuclear region, as revealed by IF staining. This was corroborated by the subsequent western blotting analysis, which verified the elevated CORO1C expression in DAOY cells relative to HA-bs cells. There is no existing evidence regarding the expression of CORO1C in paediatric brain malignancies. However, in primary effusion lymphoma (PEL), CORO1C was overexpressed due to amplification at the 12q24.11 chromosomal region, suggesting that it contributed to the pathogenesis of PEL by enhancing

cell migration and invasion, promoting the aggressive behaviour of the lymphoma cells (Luan, *et al.,* 2010). The consistent pattern of increased CORO1C expression across GB and MB cells suggested that this protein may be a key contributor to the malignant phenotype of these cancers, potentially through its role in regulating cytoskeletal dynamics. Furthermore, the overexpression of CORO1C in high grade brain malignancies makes it a potential therapeutic target for inhibiting the aggressive behaviour of these tumours.

The expression and quantification analyses of the SV2B protein revealed its significant upregulation in both U251MG and U87MG GB cell lines, as well as in DAOY cells, compared to HA-bs cells. SV2B is typically associated with synaptic vesicles in neurons and our IF results showed that it exhibited a diffuse cytoplasmic distribution, indicating its presence in various cytoplasmic structures or organelles. Currently, there is no evidence regarding the localisation and expression of SV2B within brain tumour cells or tissues. However, it has been shown that synaptic vesicles in GB could drive tumour progression by facilitating communication between GB cells and neurons through the formation of synaptic connections (Losada-Pérez, Hernández García-Moreno, García-Ricote & Casas-Tintó, 2022). Subsequently, GB cells interacted with neurons by forming functional synapses, allowing for the exchange of signalling molecules that promoted tumour growth, invasion, and neurodegeneration (Sharma, Aaroe, Liang & Puduvalli, 2023). This synaptic activity enhanced calcium signalling and activated pathways, such as the c-Jun NH2-terminal Kinase (JNK) pathway, enhancing proliferation and the formation of tumour microtubes, thereby contributing to the aggressiveness of the tumour (Losada-Pérez, *et al.,* 2022). In GB cells, SV2B demonstrated specific cytoplasmic localisation, particularly enriched around the nucleus, suggesting that SV2B may be involved in processes related to protein trafficking, secretion, or organelle function near the nucleus, such as within the ER or Golgi apparatus. Furthermore, SV2B was overexpressed in other types of aggressive cancer, such as breast cancer, aligning with our observations of its overexpression in aggressive brain malignancies (Bandala, *et al.,* 2012). The high SV2B accumulation in brain malignancies may be due to its role in neurotransmitter distribution, leading to increased intracellular Ca^{2+} levels, which could promote cell proliferation and migration (Pei, Lee, Khan, Erisnor & Wang, 2020). Additionally, SV2B was linked to energy metabolism, essential for tumour growth by regulating transporter protein activity and glucose transport (Liu, *et al.,* 2023). This increased expression, coupled with its specific localisation around the nucleus, suggested that SV2B may be involved in processes such as vesicle trafficking, membrane fusion, and protein secretion, all of which are essential for cancer cell growth and invasion. In DAOY cells, the IF staining

indicated that SV2B was significantly overexpressed compared to HA-bs cells, with its expression spread mainly across the cytoplasm. This observation aligned with the western blotting results, which also showed elevated SV2B expression in DAOY cells. The widespread cytoplasmic distribution of SV2B in MB cells may reflect its involvement in processes essential for maintaining the malignant phenotype of these cells, similar to the processes involved in GB tumorigenesis. Thus, SV2B could serve as a potential drug target in GB and MB due to its overexpression in these high-grade brain malignancies.

The results of our *in vitro* validations provided strong evidence for the dysregulation of miRNAs and their associated targets in GB and MB. RT-qPCR analysis confirmed the upregulation of miR-21 and the downregulation of miR-34a and miR-128a GB cells, highlighting their roles as oncogenic and tumour-suppressive miRNAs, respectively. MiR-21 and miR-34a were also dysregulated in MB cells showing similar expression patterns to GB. Additionally, miR-206 and miR-383, identified as potential tumour suppressors, were downregulated in both GB and MB cells, targeting *CORO1C* and *SV2B*. Furthermore, miR-206 effectively targeted and downregulated *CORO1C*, subsequently leading to decreased cell viability and impaired colony-forming ability in both GB and MB cells. Similarly, miR-383 consistently suppressed *SV2B* expression, resulting in significant reductions in cell viability and colony formation across these brain tumour cell line models. The significant downregulation of *CORO1C* by miR-206 and *SV2B* by miR-383 highlighted their utilisation as therapeutics against these oncogenes. Moreover, western blotting and IF analyses provided further validation of these findings by demonstrating the upregulation and localisation of CORO1C and SV2B proteins across different GB and MB cell lines. The localisation patterns observed through IF revealed that both CORO1C and SV2B were not only upregulated but also localised within the cells to support their roles in tumour progression. This overexpression was consistent with results based on the bioinformatics predictions, RT-qPCR, and functional assays, indicating the potential of CORO1C and SV2B as promising therapeutic targets in these malignancies. Our study is the first to highlight the clinical significance of the miR-206/*CORO1C* and miR-383/*SV2B* axes as potential therapeutic targets for adult GB and paediatric MB. Notably, while these axes are present in both malignancies, they seem to operate independently and do not synergise. This finding could open new avenues for shared targeted treatment strategies in adults and children diagnosed with aggressive brain malignancies.

Chapter 4: Patient tissue and liquid biopsy-based biomarkers

4.1. Introduction

Glioblastoma and MB are highly complex and diverse malignancies that possess significant challenges in diagnosis, prognosis, and treatment. An in-depth understanding of their molecular and genetic aspects is essential for developing more effective clinical strategies for their management and better patients' outcomes (Veliz, *et al.,* 2015). Current technological advancements have revolutionised the study of complex tumours like GB and MB, providing researchers with the tools to perform detailed biological analyses with high accuracy. Since the beginning of high-throughput sequencing in 2005, these techniques have become an essential part of cancer research as they allow the study of life processes at the molecular level, enabling detailed investigation of the genome and transcriptome of brain tumours (Margulies, *et al.,* 2005). Total RNA sequencing (RNA-seq) and small RNA-sequencing (sRNA-seq), key components of high-throughput sequencing, offer insights into the diverse molecular landscapes of cancer cells, enabling the identification of gene and regulatory small RNA expression patterns (Sheng, *et al.,* 2017).

Total RNA-seq, also called bulk RNA-seq, is a technique that has the potential to detect early mutations alongside high-risk molecular mutations, enabling the identification of new cancer biomarkers and therapeutic targets (Hong, *et al.,* 2020). RNA-sequencing has been used to evaluate the tumour mutation burden in GB. Previous RNA-seq research has established that *IDH* mutations serve as a favourable prognostic marker in gliomas (Wang, *et al.,* 2020a). Moreover, this technique has identified *MET* exon 14 and *IDH1* mutations as promising therapeutic targets in patients with lung adenocarcinoma and chondrosarcoma, respectively (Seo, *et al.,* 2012; Nakagawa, *et al.,* 2019). It has been demonstrated that RNA-seq improves the detection rate beyond that of DNA sequencing, providing more comprehensive diagnostic results and achieving better outcomes in targeted therapies (Postel, Culver, Ricker & Craig, 2022). Furthermore, with advances in RNA-seq, international collaborative efforts to sequence the MB genome have discovered new driver alterations for the malignancy (Funakoshi, Sugihara, Uneda, Nakashima & Suzuki, 2023). While SHH MBs were previously thought to be well-characterised due to their frequent genetic alterations in the canonical SHH signalling pathway, unidentified recurrent mutations have been observed. These include mutations in the

U1 small nuclear RNA (snRNA) and *ELP1* within the SHH MB subtype (Suzuki, et al., 2019; Waszak, et al., 2020). Thus, RNA-seq is a valuable technique for identifying new gene functions and potential molecular mechanisms, aiding in the discovery of unreported mutations and therapeutic targets.

In addition to total RNA-seq, sRNA-seq plays an important role in the detection of miRNAs in GB and MB due to its ability to detect small RNAs with differentially expressed profiles. In GB and MB, miRNAs have been implicated in tumour initiation, progression, and therapy resistance (Ordóñez-Rubiano, *et al.,* 2024; Mollashahi, Aghamaleki & Movafagh, 2019; Gareev, *et al.,* 2021). Small RNA-seq allows for the comprehensive identification and quantification of miRNAs, including novel and low-abundance miRNAs, which may not be detectable through traditional methods (Benesova, Kubista & Valihrach, 2021). This is of high importance in brain malignancies where specific miRNA expression profiles can serve as diagnostic biomarkers, prognostic indicators, or potential therapeutic targets. For example, one sRNA-seq study analysing EVs from GB cell lines revealed the presence of 712 non-coding RNA sequences, many of which had not been previously associated with GB-derived EVs. These included various RNA species alongside the more well-known miRNAs like miR-21-5p and let-7b-5p (de Mooij, Peterson, Evans, McCutcheon & Parney, 2020). Furthermore, a pilot study exploring the EVs cargo from MB and diffuse infiltrative pontine glioma (DIPG) patient-derived cell lines identified distinct non-coding RNA (ncRNA) profiles, with a notable depletion of miRNAs (Magaña, *et al.,* 2022). Novel miRNAs, not previously associated with MB or DIPG, were identified, along with dysregulated miRNAs targeting genes involved in cancer-related pathways. Thus, dysregulated miRNAs have been linked to aberrant signalling pathways in GB and MB, and their modulation could offer new avenues for targeted therapies.

Total RNA-seq and sRNA-seq are currently regarded as gold standard techniques in modern sequencing. Several RNA sequencing platforms, including Illumina, Ion Torrent/Proton, and Oxford Nanopore, have been employed for gene expression profiling in human cancers (Lahens, *et al.,* 2017; Kono & Arakawa, 2019). These platforms incorporate distinct equipment and physical principles for signal detection, as well as varying library preparation protocols, using different enzymes and numbers of PCR cycles (Borisov, *et al.,* 2017). Therefore, this variation causes significant differences and incompatibilities between outputs generated from different platforms, reagents, and kits. Consequently, gene expression profiles are typically compared only within datasets produced by the same platform (Borisov & Buzdin, 2022). Even

though there are variations between the different sequencing platforms used in various studies, the overall findings often highlight key molecular patterns and pathways involved in tumorigenesis, thus emphasising the potential for these discoveries to guide future diagnostic and therapeutic strategies.

In addition to the techniques designed to assess the tumour's acellular content, tissues also contain various microscopic features which are essential for determining the identity of brain tumours (Azzarelli, Simons & Philpott, 2018). Immunohistochemistry plays an important role in this process, as it is a key technique for both the classification and diagnosis of CNS malignancies (Jaiswal, 2016). It allows the identification of specific molecular protein markers that help distinguish between different tumour types and guide clinical decision-making (Painter, Clayton & Herbert, 2010). Over time, the use of IHC has expanded to assess predictive and prognostic biomarkers in a variety of malignancies, including GB and MB. Brain tumours are characterised by unique histological complexity. Primary brain tumours, such as gliomas and neuroembryonal tumours, often have histological features that are hardly resembling normal brain tissue (Torp, Solheim & Skjulsvik, 2022). For instance, GB shows glial features, while neuroembryonal tumours, such as MB, mimic parts of the developing brain (Torp, *et al.,* 2022). In the clinical setting, IHC has been successfully integrated into practice for brain tumour diagnosis. However, there is a growing effort to move away from tissue biopsies, as they are invasive and can pose risks to patients (Pulumati, Pulumati, Dwarakanath, Verma & Papineni, 2023). As a result, alternative approaches, such as liquid biopsies and proteomics, are being explored to provide non-invasive, high-throughput molecular insights, allowing for more comprehensive and less invasive diagnostic methods in the management of brain tumours. Moreover, in mammalian cells, mRNA and protein levels for known genes are highly correlated, with mRNA levels accounting for up to 84% of the variation in protein expression (Liu, Beyer & Aebersold, 2016). Thus, while genomic and transcriptomic alterations drive tumorigenesis, the proteins they encode regulate nearly all cellular processes, making them essential to consider when studying GB and MB heterogeneity.

Proteomics, the large-scale study of proteins and their functions, has become a valuable tool for understanding brain tumours at the molecular level. By analysing changes in protein expression, modifications, interactions, and cellular localisation, researchers have gained an essential understanding of the molecular mechanisms driving brain tumours (Chandramouli & Qian, 2009). Proteomics is also utilised in identifying biomarkers for early detection, predicting

patient outcomes, and developing targeted therapies (Kwon, *et al.,* 2021). Even though there are variations between different platforms and methodologies, the detection of protein dynamics in brain tumours via proteomics provides alternative avenues for clinical advancements. Differential proteomic profiling of brain tumours compared to disease-free states enables the detection and monitoring of pathological changes by identifying potential biomarkers for diagnosing, prognosing, or assessing treatment response in CNS neoplasms (Pirlog, Susman, Iuga & Florian, 2019). Moreover, proteomic analysis of biological fluids offers a less invasive alternative to tissue biopsies while providing information about the underlying causes and progression of brain tumour pathologies (Saenz-Antoñanzas, *et al.,* 2019).

In general, -omics techniques, such as transcriptomics and proteomics, are facilitating a shift from traditional tissue-based approaches to blood-based diagnostics by revealing molecular signatures in the blood that reflect those in tumour tissues. The development of less invasive blood-based biopsy tests aims to identify novel biomarkers to enhance early detection, patient stratification, and treatment monitoring, thus improving patient outcomes (Alexandrou, *et al.,* 2023). One promising source of blood-based biomarkers is EVs, which offer several advantages over other analytes like blood proteins, circulating nucleic acids, and circulating cells due to their stability and relative abundance in the peripheral circulation (Pink, Beaman, Samuel, Brooks & Carter, 2022). Extracellular vesicles are lipid bilayer-enclosed particles released by all living cells as a means of intercellular communication (van Niel, D'Angelo & Raposo, 2018). They include subtypes such as exosomes (50-150nm) and microvesicles (50-500nm), which are distinguished by their biogenesis (van Niel, *et al.,* 2018). Initially, exosomes were believed to serve as a cellular mechanism for removing unwanted materials. However, current research has shown that exosomes can transfer membrane proteins and cytosolic contents between cells, activating signalling pathways in recipient cells, with their function being determined by their composition (Kalluri & LeBleu, 2020). These vesicles carry lipids, proteins, DNA, miRNA, mRNA, long non-coding RNA, and genetic material from their cellular origin to their intended target (Tetta, Ghigo, Silengo, Deregibus & Camussi, 2013). Exosomes, released by various cell types, including neurons, play a key role in the nervous system by regulating synaptic communication and nerve regeneration (Liu, *et al.,* 2019). They are increasingly recognised as means of intercellular communication, contributing not only to normal neuronal function but also to the spread of pathogenic proteins (Aheget, *et al.,* 2020). In brain tumours, exosomes are crucial for packaging and transporting proteins, potentially

influencing both tumour development and progression (Ciregia, Urbani & Palmisano, 2017). Given their significant role in intercellular communication and tumour dynamics, studying exosomes is essential for understanding the underlying mechanisms of brain tumours, which could lead to the identification of new therapeutic targets and biomarkers for GB and MB.

4.1.2. Aims and research questions

4.1.2.1. Aims

Herein, we aimed to determine whether our *in vitro* findings were reflected in GB and MB tissues through IHC. Additionally, we sought to investigate whether these results were mirrored in paediatric MB tissues by performing sRNA-seq and transcriptomics. Finally, we aimed to assess if the findings were reflected in GB liquid biopsy samples derived from exosomes by conducting sRNA-seq and proteomic analyses.

4.1.2.2. Research questions

1. Are the *in vitro* findings reflected in GB and MB tissues when analysed through IHC?
2. Are the *in vitro* results mirrored in paediatric MB tissues, as evaluated through sRNA-seq and transcriptomics?
3. Can the *in vitro* findings be detected in GB liquid biopsy samples from exosomes using sRNA-seq and proteomic analyses?

4.2. Materials and Methods

4.2.1. Patient's samples

For the sRNA-seq and bulk RNA-seq of MB paediatric samples, resected brain tumours from children diagnosed with MB (n=9) according to the 2007 WHO criteria were analysed (Louis, *et al.,* 2007). The control sample was obtained from one deceased male child who had undergone autopsy and exhibited no brain abnormalities. This control sample was taken from the medulla oblongata. The patient cohort included four males and five females, aged between 4.02 and 12.05 years, with a median age of 9 years for the non-malignant cohort. For the sRNA-seq and proteomics of GB patient samples, plasma from five controls and six GB patients was obtained. The control samples were obtained from healthy individuals who had no brain abnormalities. The patient samples cohort comprised of four males and two females, aged between 21 and 74 years, with a median age of 48 years. The control cohort comprised of five male individuals aged between 25 and 48 years, with a median age of 34 years. All samples were snap-frozen at the time of resection or collection and stored at -80°C until further use. The study received approval from the University of Hertfordshire Ethics Committee (Protocol No. aLMS/PGR/UH/05146(1)).

For the IHC experiments with CORO1C, a total of 376 biopsy cores of malignant and adjacent control tissue were screened, encompassing samples from various brain tumours (GL2082, GL2083c, GL803c, GL631). Specifically, the analysis included astrocytoma (n=192), aged between 19 and 70 years; IDH-wild type astrocytic tumours (n=8), aged between 29 and 66 years; ependymoma (n=19), aged between 26 and 81 years; oligodendroglioma (n=29), aged between 30 and 67 years; medulloblastoma (n=23), aged between 4 and 47 years; glioblastoma (n=73), aged between 9 and 80 years; normal tissues (n=19), aged between 20 and 72 years; and adjacent normal tissue (n=13), aged between 30 and 67 years. The cohort of patients included 213 males and 163 females, with a median age of 41 years for the control cohort.

For the IHC experiments with SV2B, a total of 169 biopsy cores of malignant and adjacent control tissues were screened, encompassing samples from various brain tumours (GL631, GL803c, GL2082a). Specifically, the analysis included astrocytoma (n=62), aged between 20 and 68 years; IDH-wild type astrocytic tumours (n=4), aged between 28 and 54 years; ependymoma (n=4), aged between 33 and 55 years; oligodendroglioma (n=10), aged between 28 and 72 years; medulloblastoma (n=23), aged between 4 and 47 years; glioblastoma (n=50),

aged between 9 and 80 years; normal tissue (n=11), aged between 30 and 67 years; and adjacent normal tissue (n=5), aged between 30 and 67 years. The cohort of patients included 73 males and 96 females, with a median age of 37 years for the control cohort.

4.2.2. Immunohistochemistry

Commercially available paraffin-embedded brain tumour tissue slides (US Biomax Inc., London, UK; GL2082, GL2083c, GL631, GL803c, GL2082a) were obtained in accordance with the Health Insurance Portability and Accountability Act (HIPAA)-approved protocols to ensure ethical compliance. The protocol used was previously described by Filipe *et al.* (Filipe, *et al.,* 2022). To begin with, all slides were deparaffinised by performing the following washes in coplin jars: histoclear (Applied Biosystems ThermoFisher, Pleasanton, CA, USA) twice for 5min each time, followed by histoclear:ethanol in a 1:1 ration for 3min, 100% ethanol for 3min, 95% ethanol for 3min, 70% ethanol for 3min, 50% ethanol for 3min, and running tap water for 1min. Ethanol was diluted in distilled water. The slides were blotted gently with a tissue to soak excess liquid in between washes. The total volume for each step mentioned above was 50mL. Following deparaffinisation, antigen retrieval was performed by incubating the slides with sodium citrate for 10min at 70°C. The slides were then allowed to cool and placed in water for 5min. This was followed by two wash steps for 5min in PBS 0.025% Triton-X. Then, the slides were incubated in 3% H_2O_2 for 15min. Thereafter, the slides were washed three times for 5min in PBS 0.025% Triton-X. Following the washes, the slides were blocked with 5% BSA in PBS for 1h at RT in a humidity chamber. Once blocked, the slides were incubated with their respective primary antibodies (CORO1C, 1:200 dilution in 5% BSA; SV2B, 1:200 dilution in 5% BSA (ProteinTech, Manchester, UK) and incubated in the humidity chamber at 4°C overnight. Following the overnight incubation with primary antibodies, the slides were washed three times for 5min in PBS 0.025% Triton-X. Following the washes, the slides were treated with a secondary anti-rabbit antibody from the Zytochem Plus HRP-DAB Kit (HRP008DAB-RB; Zytomed Systems, Berlin, Germany) for 1h at RT. Then again, the slides were washed three times for 5min in PBS 0.025% Triton-X. This was followed by the addition of streptavidin-HRP conjugate and a 45min incubation. After three washes as described above, staining and counterstaining were performed with diaminobenzidine (DAB; Vector Laboratories, Newark, CA, USA) and hematoxylin (Applied Biosystems ThermoFisher, Pleasanton, CA), respectively. Then, the slides were stained in 0.1% sodium bicarbonate for

1min and rinsed with water. Dehydration of the slides was then performed in the following order: 50% ethanol for 3min, 70% ethanol for 3min, 95% ethanol for 3min, 100% ethanol for 3min, histoclear: ethanol (1:1) for 3min, and histoclear for 3min. A coverslip was placed on each slide after the addition of a few drops of distrene, plasticizer, and xylene (DPX; Applied Biosystems ThermoFisher, Pleasanton, CA, USA). The slides were placed in the fridge and dried overnight at 4°C. Immunoreactivity was evaluated by three independent observers using a light microscope (Zeiss Microscopy, Oberkochen, Germany), with brown staining extent scored based on the percentage of positively stained cells. Staining intensity was defined as follows: no staining (score 0), low (score 1), moderate (score 2), high (score 3). Staining proportion was defined as follows: 0% (score 0), <10% (score 1), 10-29% (score 2), 30-59% (score 3), 60-100% (score 4). The final score was determined by averaging the scores from the three independent assessments.

4.2.3. Small RNA-sequencing

MiRNAs from MB patients were extracted following the mirVana isolation protocol described in Chapter 3, method section 3.2.3. MiRNAs from GB patients were extracted following the total exosome RNA and protein extraction kit protocol described in method section 4.2.14. The concentration of each sample was measured with a Nanodrop bioanalyzer (Nanodrop ND1000 Spectrophotometer, Virginia, USA), and RNA integrity was assessed using the Agilent Bioanalyzer 2100 (Agilent, Manchester, UK), with only samples having RIN numbers above seven qualifying for sRNA-seq (Biomarker Technologies, Berlin, Germany). A total of 1.5µg of RNA per sample was used as input material for preparation. Sequencing libraries were generated using the NEBNext® Ultra™ Small RNA Sample Library Prep Kit for Illumina (New England Biolabs, Ipswich, UK) following the manufacturer's instructions, with index codes added to assign sequences to each sample. Firstly, the 3′ SR adaptor for Illumina was ligated by mixing it with RNA and nuclease-free water. The mixture was incubated for 2min at 70°C in a preheated thermal cycler and then transferred on ice. Next, the 3′ ligation reaction buffer (2x) and 3′ ligation enzyme mix were added for the ligation of the 3′ SR adaptor, and the mixture was incubated at 25°C for 1h. To prevent the formation of adaptor-dimers, the SR reverse transcription primer hybridised with excess 3′ SR adaptor remaining after the 3′ ligation reaction, converting the single-stranded DNA adaptor into a double-stranded DNA molecule. Next, the 5′ SR adaptor was ligated, followed by a reverse transcription synthetic chain reaction. Finally, PCR amplification and size selection were performed. Electrophoresis on a PAGE gel was used for fragment screening, and the resulting small RNA libraries were

extracted by rubber cutting recycling. The PCR products were purified using the AMPure XP system, and library quality was evaluated on the Agilent Bioanalyzer 2100 system.

4.2.4. Clustering and sequencing

Index-coded samples were clustered using a cBot Cluster Generation System with the TruSeq PE Cluster Kit v4-cBot-HS (Illumina, San Diego, CA, USA). After cluster generation, the libraries were sequenced on an Illumina Hiseq 2500 platform, generating paired-end reads.

4.2.5. Data analysis

Raw data (raw reads) in fastq format were initially processed with in-house Perl scripts (these in-house Perl scripts are not publicly available) (Biomarker Technologies, Berlin, Germany). Clean data (clean reads) were generated by removing reads containing adapters, poly-N, and low-quality sequences from the raw data. Reads shorter than 18 nucleotides or longer than 30 nucleotides were also filtered out. Quality metrics such as Q20, Q30, GC-content, and sequence duplication levels were calculated for the clean data. All subsequent analyses were based on these high-quality, clean data.

4.2.6. Comparative analysis

Bowtie tools software was used to align the clean reads with sequences from the Silva, GtRNAdb, Rfam, and Repbase databases to filter out ribosomal RNA (rRNA), transfer RNA (tRNA), small nuclear RNA (snRNA), small nucleolar RNA (snoRNA), and other ncRNAs and repeats. The remaining reads were used to identify known miRNAs and predict novel miRNAs by comparing them with known sequences from miRBase (https://www.mirbase.org). New miRNA secondary structures were predicted using Randfold tools (https://bio.tools/randfold).

4.2.7. Target gene functional annotation

Gene function was annotated using the following databases: Nr (NCBI non-redundant protein sequences, https://www.ncbi.nlm.nih.gov), Nt (NCBI non-redundant nucleotide sequences, https://www.ncbi.nlm.nih.gov), Pfam (Protein family, http://pfam.xfam.org), KOG/COG (Clusters of Orthologous Groups of proteins, https://mycocosm.jgi.doe.gov/help/kogbrowser.jsf#:~:text=EuKaryotic%20Orthologous%20Groups%20(KOG)%20is,by%20KOG%20classification%20or%20ID), Swiss-Prot (a

manually curated protein sequence database, https://www.expasy.org/resources/uniprotkb-swiss-prot), KO (KEGG Ortholog database, https://www.genome.jp/kegg/), and GO (Gene Ontology, https://geneontology.org).

4.2.8. Quantification of miRNA expression levels

MiRNA expression levels were quantified for each sample by mapping sRNAs back onto the precursor sequences, and the read count for each miRNA was calculated based on the mapping results.

4.2.9. Differential expression analysis

For samples with biological replicates, differential expression analysis between two conditions or groups was conducted using the DESeq R package (1.10.1) (Bioconductor, Boston, MA, USA), which uses a model based on the negative binomial distribution. P-values were adjusted using the Benjamini and Hochberg method to control the false discovery rate (Haynes, 2013). MiRNAs with an adjusted p-value <0.05 were considered differentially expressed. For samples without biological replicates, differential gene expression analysis between two samples was performed using IDEG6, with p-value adjustments made using the q-value (Storey & Tibshirani, 2003). A q-value <0.005 and |log2(fold change)| ≥ 1 were set as thresholds for significant differential expression.

4.2.10. GO enrichment and KEGG pathway enrichment analysis

Gene ontology enrichment analysis of differentially expressed genes (DEGs) was carried out using the GOseq R package, which employs Wallenius' non-central hypergeometric distribution. KEGG pathway enrichment analysis, a resource for understanding high-level biological functions from molecular data, was performed using KOBAS software (Bio Tools, London, UK) to assess the statistical enrichment of DEGs in KEGG pathways. Regarding proteomics, the enrichment factor represents the ratio of the proportion of proteins annotated to a specific GO term in the set of differential proteins to the proportion of proteins annotated to the pathway in all proteins. A larger enrichment factor indicates a more significant enrichment level of differential expression proteins in that pathway.

4.2.11. Transcriptomics

Total RNA from MB samples and controls was extracted using the Trizol method as described in Chapter 3, method section 3.2.2. Bulk RNA sequencing was performed at Biomarker Technologies (Berlin, Germany). The concentration of extracted nucleic acid was measured using the Nanodrop2000 (Applied Biosystems ThermoFisher, Pleasanton, CA, USA), and the integrity was assessed using the Agilent Bioanalyzer 2100 (Agilent, Manchester, UK) and LabChip GX (Perkin Elmer, model: LabChip GX). The VAHTS Universal V8 RNA-seq Library Prep Kit for Illumina NR605 was employed to construct the mRNA and strand-specific mRNA libraries, following the protocol provided by Vazyme (Xing, *et al.,* 2024). The prepared libraries were sequenced on the Illumina Novaseq X platform (Illumina, San Diego, CA, USA), and sequencing reads were generated. Follow up data analysis, enrichment analysis, and differential expression analysis were performed as described above.

4.2.12. Extracellular vesicles extractions

The extraction of EVs and their subsequent characterisation was performed as described by Robinson *et al.* (Robinson, *et al.,* 2024). For all experiments with EVs derived exosomes, 1mL of plasma was used. Samples were thawed on ice and centrifuged at 1500g for 10min at RT. The supernatant was then centrifuged at 10,000g for 10min at RT to remove cellular debris. The cleared supernatant was collected and adjusted to a final volume of 1mL with sterile-filtered PBS. New size exclusion chromatography (SEC) columns (IZON qEV1/35nm) were prepared by draining and flushing with sterile-filtered PBS. The sample was loaded onto the column, followed by the addition of 3mL of sterile-filtered PBS, and the first 4mL of buffer was collected. Seven additional 700µL SEC fractions were collected after adding 700µL of sterile-filtered PBS to the column. Following this, SEC fractions 2–5 were combined to balance EV recovery with sample purity. The combined sample was then concentrated to 100µL using a 100kDa molecular weight ultrafiltration filter (Vivaspin 6, Sartorius, Epsom, UK) and centrifuged at 4000g (Mega Star 1.6R, VWR, Leicestershire, UK). The concentrated SEC fraction samples were stored at -80°C for further use.

4.2.13. Nanoparticle tracking analysis

Particle concentration and size distribution were measured using a NanoSight NS300 with a blue laser (488nm) and analysed with Nanosight NTA 3.2 software (Malvern Technologies, Malvern, UK). Samples were diluted 1:100 to 1:1000 in sterile-filtered PBS, and five 30-

second videos were recorded per sample. The camera level was set close to the maximum (15 or 16), and a threshold of 5 was applied for the analysis.

4.2.14. Western blotting

Protein expression of known EV markers and common contaminants was assessed via western blotting, following standard protocols as previously described in Chapter 3. Equal amounts of EVs (5µg) were lysed in 5× Laemmli sample buffer (containing 1.5M Tris-HCl, glycerol, 20% sodium dodecyl sulfate (SDS), 0.25% bromophenol blue, and 1M dithiothreitol), boiled at 95°C for 10min, and separated on SDS/PAGE gradient gels (4–12%). Proteins were transferred using the iBlot 2 system (Invitrogen, Paisley, UK). Primary antibodies used included: anti-CD9 (1:1000, System Biosciences, Palo Alto, CA, USA), anti-CD81 (1:1000, System Biosciences EXOAB-KIT-1), anti-GM130 (1:1000, Cell Signaling Technology, Danvers, MA, USA), and anti-apolipoprotein B (1:1000, St John's Laboratory, London, UK). Secondary antibodies used were Anti-rabbit IgG HRP linked (1:5000, Cell Signaling, Danvers, MA, USA) and Anti-mouse IgG HRP linked (1:5000, Cell Signaling, Danvers, MA, USA). Membranes were developed using SuperSignal West Pico PLUS Chemiluminescent Substrate (Thermo Scientific, Pleasanton, CA, USA) and imaged with a UVP ChemStudio instrument (Analytik Jena, London, UK) and VisionWorks software (LTF Labortechnik, Wasserburg, Germany).

4.2.15. Protein and miRNA extractions from exosomes

Protein and miRNA extractions from exosomes were performed using the total exosome RNA and protein isolation kit (Applied Biosystems ThermoFisher, Pleasanton, CA, USA). For protein analysis, exosome resuspension buffer was added in equal volumes to the sample (e.g. 40µL of buffer added to 40µL of the sample). The sample was incubated for 10min at RT and gently pipetted up and down to ensure thorough mixing. Protein samples were then frozen at -80°C and shipped for proteomics analysis described in methods sections 4.2.16-4.2.18, or protein isolation was then performed for subsequent western blotting analysis as described in 4.2.14. For RNA isolation, 1x PBS was added to the exosome sample in an RNase-free tube to reach a total volume of 200µL. Then 200µL of pre-warmed 2x denaturing solution (37°C) was added to the sample and mixed thoroughly. The mixture was incubated on ice for 5min, followed by the addition of 400µL of acid-phenol chloroform. The acid-phenol chloroform was added to match the total volume of the sample plus the 2x denaturing solution. Samples were vortexed for 1min and centrifuged at 10,000g for 5min at RT to separate the aqueous and organic phases. The aqueous (upper) phase was carefully removed and transferred to a fresh

tube, and its volume was noted. Next, the one-third volume of 100% ethanol was added to the aqueous phase and mixed thoroughly. A filter cartridge was placed into a collection tube, and up to 700µL of the lysate/ethanol mixture was added to the filter cartridge. The mixture was centrifuged for approximately 30sec or until it passed through the filter. The flow-through containing the small RNA was collected. To the flow-through containing the small RNA, two-thirds volume of 100% ethanol was added and mixed thoroughly. A new filter cartridge was placed into a collection tube, and up to 700µL of the flow-through/ethanol mixture was added to the filter cartridge. The mixture was centrifuged for approximately 30sec or until it passed through the filter, and the flow-through was discarded. Following that, 700µL of miRNA wash solution 1 was added to the filter cartridge. The mixture was centrifuged for approximately 15sec, and the flow-through was discarded. The filter cartridge was replaced with the same collection tube. Then, 500µL of wash solution 2/3 was applied, centrifuged for 15sec, and the flow-through was discarded. This step was repeated one more time. After discarding the flow-through from the final wash, the filter cartridge was replaced in the same collection tube and spun for 1min to remove residual fluid from the filter. The filter cartridge was then transferred into a fresh collection tube. A volume of 50µL of preheated (95°C) elution solution was added to the centre of the filter. The mixture was centrifuged for approximately 30sec to recover the small RNA. This step was performed twice. The eluate containing the small RNA was collected and stored at -80°C before being shipped to Biomarker Technologies (Berlin, Germany) for sRNA-seq analysis.

4.2.16. Proteomics of GB exosomes

Protein concentration was measured using the BCA method as described in Chapter 3, method section 3.2.6. Dithiothreitol (DTT) (VWR, Leicestershire, UK) was added to the protein solution at a final concentration of 5mM, followed by incubation at 37°C for 1h using an electric constant temperature water bath (Beijing Yongguangming Medical Instruments Co., Ltd., Beijing, China). The solution was equilibrated to RT before iodoacetamide (IAM) (VWR, Leicestershire, UK) was added to a final concentration of 10mM and incubated in the dark for 45min. The sample was then diluted fourfold with 25mM ammonium bicarbonate (Sigma-Aldrich, Dorset, UK), and trypsin (Promega, V5280/100ug) was added at a 50:1 protein-to-enzyme ratio. Digestion was performed overnight at 37°C in the water bath. The next day, formic acid (Sigma-Aldrich, Dorset, UK) was added to adjust the pH to below 3, terminating the reaction. Desalting was carried out using a C18 Ziptip desalting column (Millipore Sigma, Massachusetts, USA). The column was activated with 100% acetonitrile (VWR, Leicestershire,

UK), equilibrated with 0.1% formic acid (Sigma-Aldrich, Dorset, UK), and the sample was loaded onto the column. The column was washed with 0.1% formic acid to remove impurities, and elution was performed with 70% acetonitrile. The flow-through was collected and lyophilised using a vacuum centrifugal concentrator (Beijing Jiaimu Technology Co., Ltd., Beijing, China).

4.2.17. Mass spectrometry analysis

For mass spectrometry, mobile phase A (100% water, 0.1% formic acid) and mobile phase B (80% acetonitrile, 0.1% formic acid) were prepared. The lyophilised samples were dissolved in 10μL of mobile phase A and centrifuged at 14,000g at 4°C for 20min using a centrifuge (Eppendorf, Stevenage, UK). The supernatant (1μg) was used for liquid chromatography-mass spectrometry (LC-MS) analysis on a RIGOL L-3000 high-performance liquid chromatography system (Beijing RIGOL Technology Co., Ltd., Beijing, China). The mass spectrometry was performed using an ORBITRAP ECLIPSE mass spectrometer equipped with the FAIMS Pro™ Interface (Applied Biosystems ThermoFisher, Pleasanton, CA, USA). The compensating voltage (CV) alternated between -45 and -65 every 1sec. The Nanospray Flex™ ion source (Applied Biosystems ThermoFisher, Pleasanton, CA, USA) was used with an ion spray voltage of 2.0kV and an ion transfer tube temperature of 320°C. The full-scan range was m/z 350-1500, with a primary mass resolution of 120,000 (m/z) and AGC set to 4×10^5. Secondary mass spectrometry was performed using "Top Speed" mode, with a resolution of 15,000 (200m/z), AGC of 5×10^4, and a maximum injection time of 22ms. The peptide fragmentation was carried out at 33% collision energy. The raw data files (.raw) were acquired for further analysis.

4.2.18. Database search and bioinformatics analyses

The *Homo sapiens*_ SP database (https://www.uniprot.org/proteomes/UP000005640) was used for protein identification, and the search was performed using Proteome Discoverer 2.4 software (ThermoFisher, Pleasanton, CA, USA). Statistical analysis, including differential expression analysis, was performed as described in method section 4.2.9.

4.2.19. Data availability

The sRNA-seq data and the mRNA sequencing data of the MB patient samples were uploaded on Mendeley Data DOI: 10.17632/yrryf4btst.1.

4.2.20. Statistics

Statistical analysis and graphical representations were performed using GraphPad Prism 9.4.1 software (GraphPad Software, San Diego, USA). For comparing the IHC expression levels CORO1C and SV2B, an ordinary one-way ANOVA was conducted, followed by Dunnett's multiple comparisons test to identify significant differences. A p-value of <0.05 was considered statistically significant. For sRNA-seq, p-values were adjusted using the Benjamini and Hochberg method to control the false discovery rate (Haynes, 2013). MiRNAs with an adjusted p-value <0.05 were considered differentially expressed. For samples without biological replicates, differential gene expression analysis between two samples was performed using IDEG6, with p-value adjustments made using the q-value (Storey & Tibshirani, 2003). A q-value <0.005 and $|\log2(\text{fold change})| \geq 1$ were set as thresholds for significant differential expression. The log2 fold change >1 threshold was selected to identify genes with meaningful expression changes that may still be biologically relevant, even if they do not meet the higher fold change threshold of >2. Regarding proteomics, the selection criteria for up-regulated proteins are $FC \geq 1.80$ and a p-value ≤ 0.03. Similarly, for down-regulated proteins, the criteria are $FC \leq 1/1.80$ and a p-value ≤ 0.03.

4.3 Results

4.3.1. Immunohistochemistry for CORO1C

Immunohistochemical analysis of CORO1C was conducted on patient cohorts and normal brain samples, revealing higher protein expression in patients across all age groups compared to normal and adjacent normal brain tissues. Notably, significant differences in protein expression were observed in all age groups, with the highest significance being within the 0-20 years age groups when compared to their normal counterparts (Figure 65a). Figure 65b demonstrates varying CORO1C expression patterns across different tumour types. The highest significant increase in CORO1C levels was observed in MB and GB in comparison to their normal counterparts. Malignant brain tumours, in general, expressed higher CORO1C levels than normal and adjacent normal tissues, with these differences reaching statistical significance. A significant increase in CORO1C expression was also observed with advancing tumour grade (Figure 65c). Significant differences in CORO1C levels were observed between all grades, with grade 4 tumours exhibiting much higher CORO1C levels than lower-grade tumours. Microscopic images in Figure 65d show increased brown staining intensity in high-grade tumours, including medulloblastoma and glioblastoma, illustrating the elevated CORO1C expression. Figure 65e panels display different patient samples at various tumour stages, further emphasising the progression-related increase in CORO1C expression.

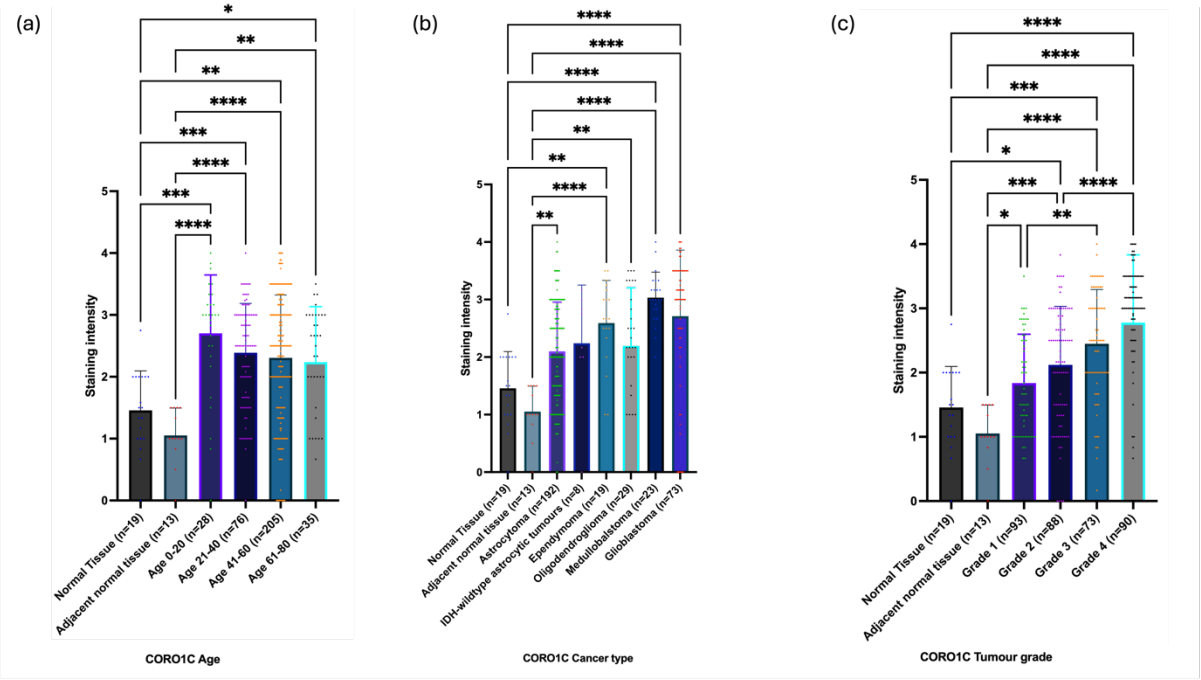


Figure 65. Immunohistochemistry analyses of CORO1C. (a) All age groups showed significantly increased levels of CORO1C in comparison to their normal counterparts. The age groups of 0–20 years showed the most significantly increased levels of CORO1C in comparison to normal and normal adjacent tissues controls (Normal Tissue versus Age 0-20, $p<0.0001$; Adjacent brain tissue versus Age 0-20, $p<0.0001$; Normal Tissue versus Age 21-40, $p<0.0009$; Adjacent Brain Tissue versus Age 21-40, $p<0.0001$; Normal Tissue versus Age 41-60, $p<0.0019$; Adjacent Brain Tissue versus Age 41-60, $p<0.0001$; Normal Tissue versus Age 61-80, $p<0.0360$; Adjacent Brain Tissue versus Age 61-80, $p<0.0012$). (b) Significantly higher levels of the CORO1C protein were observed in medulloblastoma and glioblastoma in comparison to the rest of the malignancies and their normal counterparts (Adjacent Brain Tissue versus Astrocytoma, $p<0.0014$; Normal Tissue versus Ependymoma, $p<0.0027$; Adjacent Brain Tissue versus Ependymoma, $p<0.0001$; Adjacent Brain Tissue versus Oligodendroglioma, $p<0.0037$; Normal Tissue versus Medulloblastoma, $p<0.0001$; Adjacent Brain Tissue versus Medulloblastoma, $p<0.0001$; Normal Tissue versus Glioblastoma, $p<0.0001$; Adjacent Tissue versus Glioblastoma, $p<0.0001$). (c) Significant differences between tumour grades 2, 3 and 4 in comparison to normal brain tissue were observed. Grade 1 tumours showed significantly higher expression in comparison to normal adjacent tissue. Significant differences between grades 3 and 4 and grades 1 and 2 (Adjacent Brain Tissue versus Grade 1, $p<0.0460$; Normal Tissue versus Grade 2, $p<0.0395$; Adjacent Brain Tissue versus Grade 2, $p<0.0009$; Normal Tissue versus Grade 3, $p<0.0003$; Adjacent Brain Tissue versus Grade 3, $p<0.0001$; Normal Tissue versus Grade 4, $p<0.0001$; Adjacent Brain Tissue versus Grade 4, $p<0.0001$; Grade 1 versus Grade 3, $p<0.0012$; Grade 1 versus Grade 4, $p<0.0001$; Grade 2 versus Grade 4, $p<0.0001$).

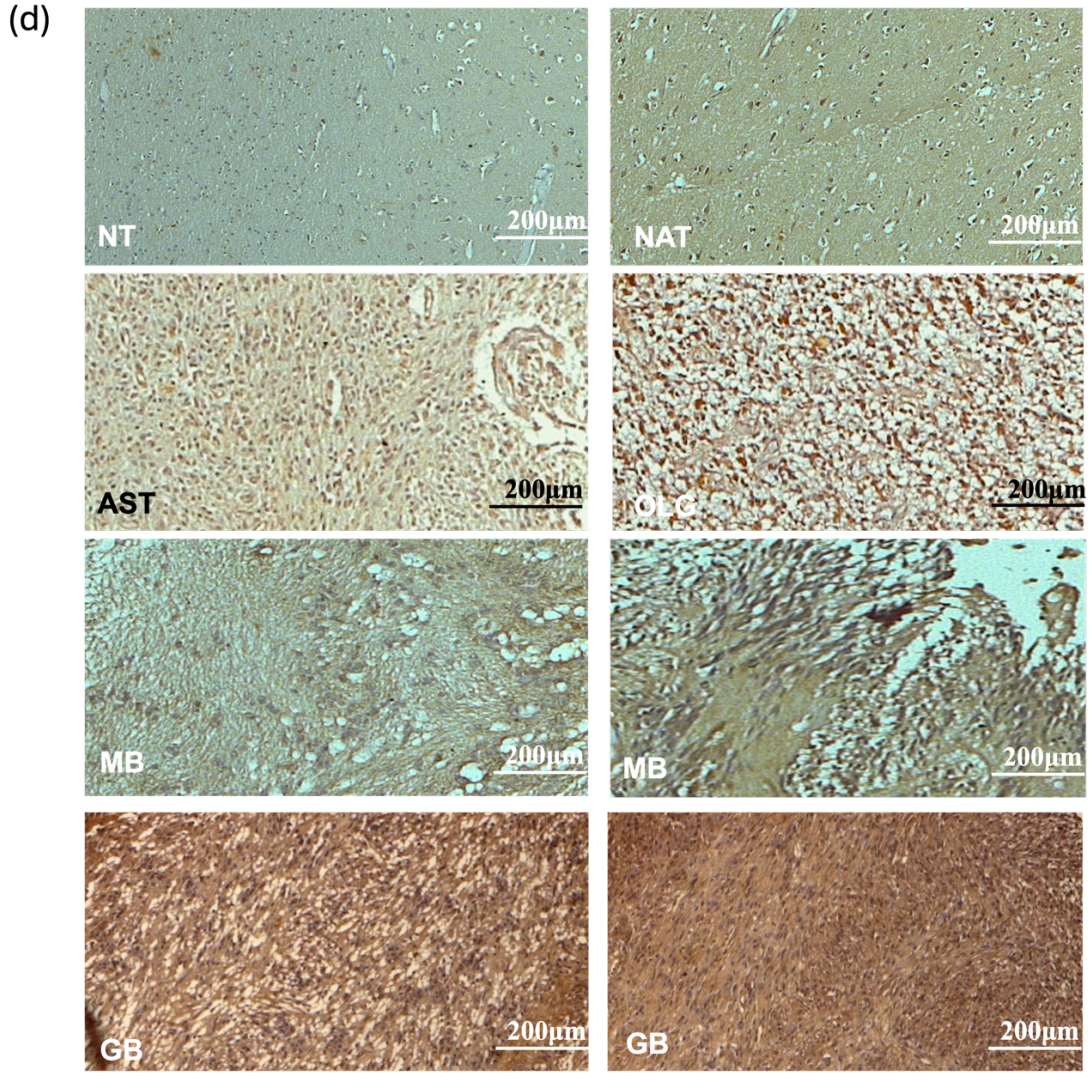


Figure 65 (continued). (d) Microscopic images of CORO1C stained tissue sections illustrating the staining intensity within normal brain tissue, tumour adjacent tissue, astrocytoma, oligodendroglioma, medulloblastoma and glioblastoma tissues at ×100 magnification. *NT* normal tissue, *NAT* normal adjacent tissue, *AST* astrocytoma, *OLG* oligodendroglioma, *MB* medulloblastoma, *GB* glioblastoma.

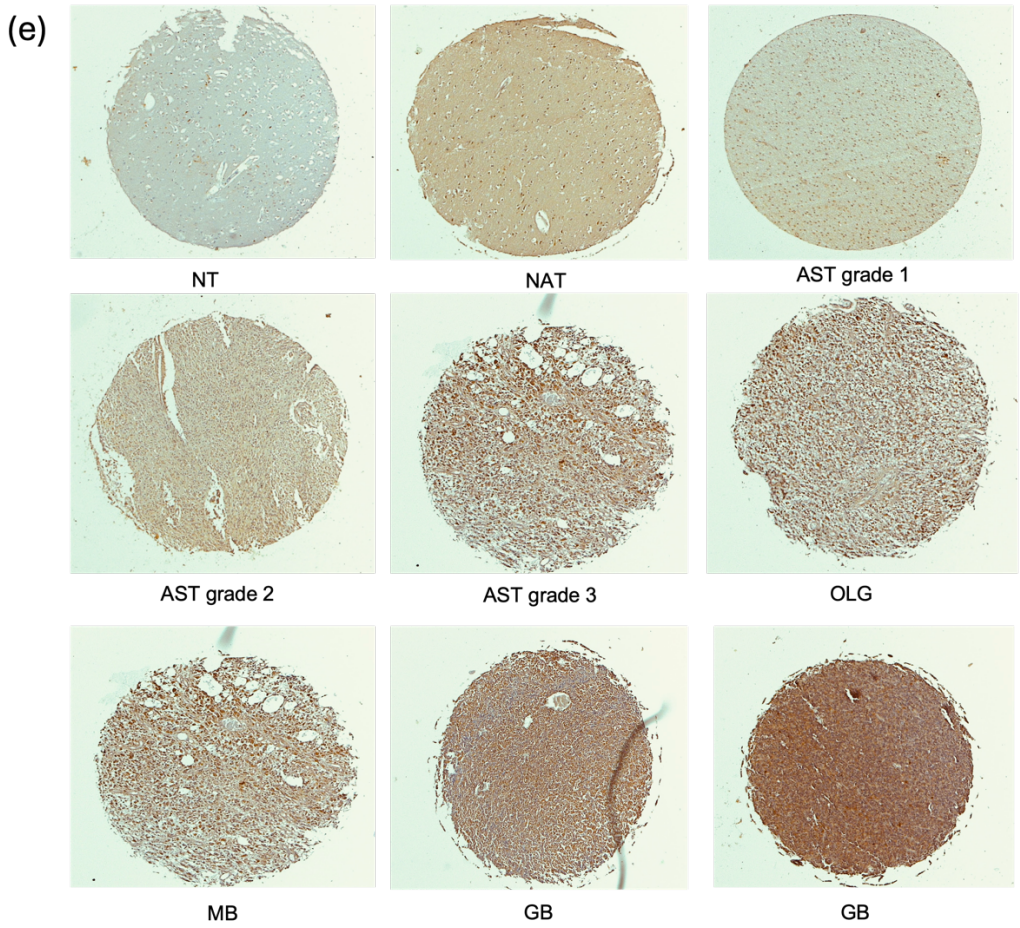


Figure 65 (continued). (e) Microscopic images of CORO1C stained tissue cores of normal brain tissue, tumour adjacent tissue, and different brain malignancies at ×40 magnification. *NT* normal tissue, *NAT* normal adjacent tissue, *AST* astrocytoma, *OLG* oligodendroglioma, *MB* medulloblastoma, *GB* glioblastoma. Results are based on three independent scoring assessments, n=3. All statistical analyses were conducted using ordinary one-way ANOVA, followed by Dunnett's multiple comparisons test to determine the significant differences in CORO1C expression.

4.3.2. Immunohistochemistry for SV2B

The immunohistochemical analysis of SV2B performed within patient cohorts and normal brain samples revealed higher expression of the protein in all age patient groups in comparison to normal and normal adjacent brain tissue samples. However, only the age groups of 0-20 years and 61-80 years reached a significant difference regarding protein expression when compared to its normal counterparts (Figure 66a). Figure 66b illustrates the different patterns of SV2B expression within different tumour types. The analysis depicted significant differences of SV2B levels between astrocytomas, IDH-wild-type diffuse astrocytic tumours, and oligodendrogliomas when compared to glioblastomas, the latter expressing higher protein

abundance within patient samples. Medulloblastomas also possessed a significantly higher abundance of SV2B in comparison to astrocytomas. Malignant brain tumours evidently expressed higher levels of SV2B when compared to normal and normal adjacent tissue samples, reaching significance. Figure 66c depicted a significant increase in SV2B expression with increasing tumour grade. Significant differences in measured SV2B levels were seen between grades 1 and 2 in comparison to grade 4 brain tumour samples. Furthermore, the differences between grades 2 and 3 we also denoted with significance. Grades 3 and 4 were shown to express much higher levels of SV2B in comparison to lower tumour grades. As illustrated in the panel of microscopic images in Figure 66d, the intensity of the brown colourised tissues section increased within high grade tumours. The panels in Figure 66e showed different patient samples with progressing tumour stages.

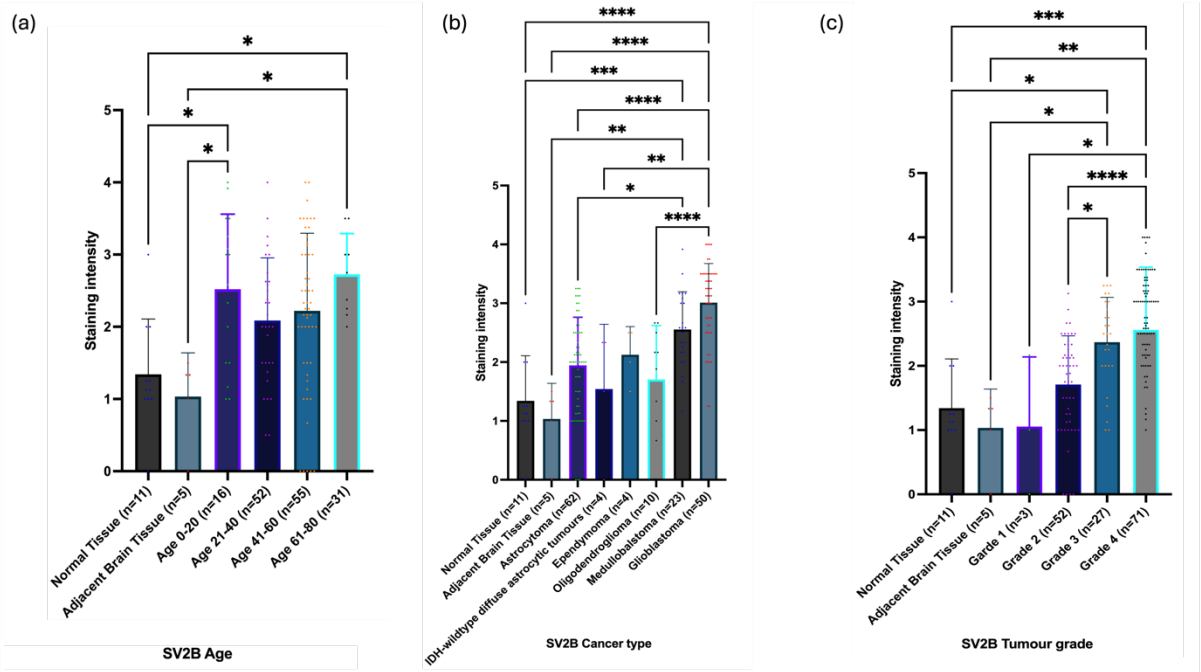


Figure 66. Immunohistochemistry analyses of SV2B. (a) The age groups of 0–20 years and 61–80 years reached significant differences in expression of SV2B when compared to their normal counterparts (Normal Tissue versus Age 0–20, $p<0.0249$; Adjacent Brain Tissue versus Age 0–20, $p<0.0344$; Normal Tissue versus Age 61–80, $p<0.0200$; Adjacent Brain Tissue versus Age 61–80, $p<0.0231$). (b) Significantly higher levels of the protein were observed within glioblastomas when compared to astrocytoma, IDH-wild-type diffuse astrocytic tumours, and oligodendrogliomas ($p<0.0001$, $p<0.0056$, and $p<0.0001$, respectively). Medulloblastoma samples also reached statistical significance of high abundance of SV2B in comparison to astrocytoma ($p<0.0245$). Both medulloblastoma and glioblastoma expressed significantly higher levels of SV2B in comparison to normal and adjacent brain tissues (Normal Tissue versus Medulloblastoma, $p<0.0005$; Adjacent Brain Tissue versus Medulloblastoma, $p<0.0016$; Normal Tissue versus Glioblastoma, $p<0.0001$; Adjacent Brain Tissue versus Glioblastoma, $p<0.0001$). (c) Significant differences between tumour grades 3 and 4 in comparison to normal brain tissue were observed ($p<0.0133$ and $p<0.0002$, respectively).

Significant differences between grades 1 and 2 in comparison to grade 4 and grades 2 and 3 we also depicted (Grade 1 versus Grade 4, $p<0.0390$; Grade 2 versus Grade 4, $p<0.0001$; Grade 2 versus Grade 3, $p<0.0184$).

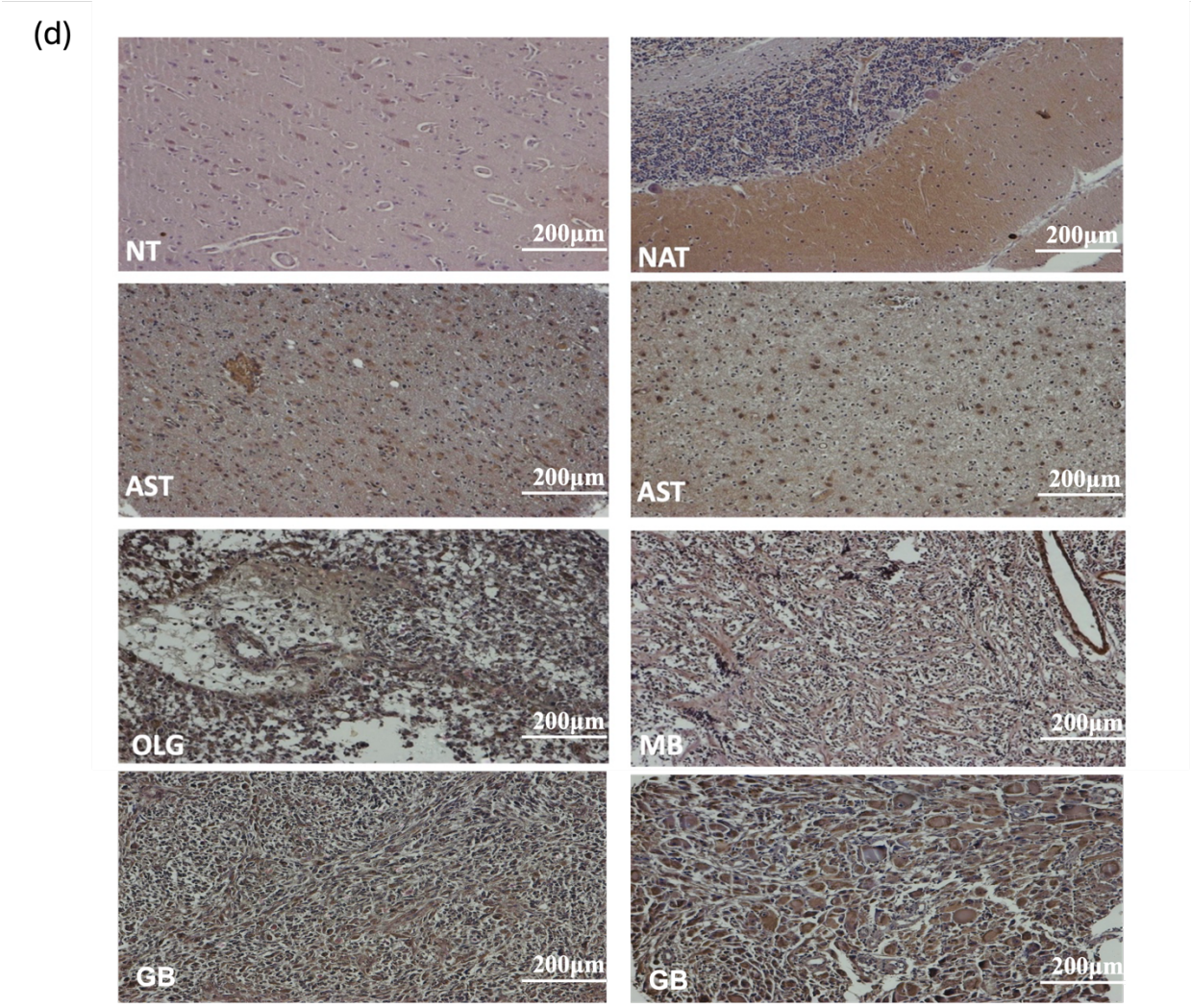


Figure 66 (continued). (d) Microscopic images of SV2B stained tissue sections illustrating the staining intensity within normal brain tissue, tumour adjacent tissue, and different brain malignancies at ×100 magnification. *NT* normal tissue, *NAT* normal adjacent tissue, *AST* astrocytoma, *OLG* oligodendroglioma, *MB* medulloblastoma, *GB* glioblastoma.

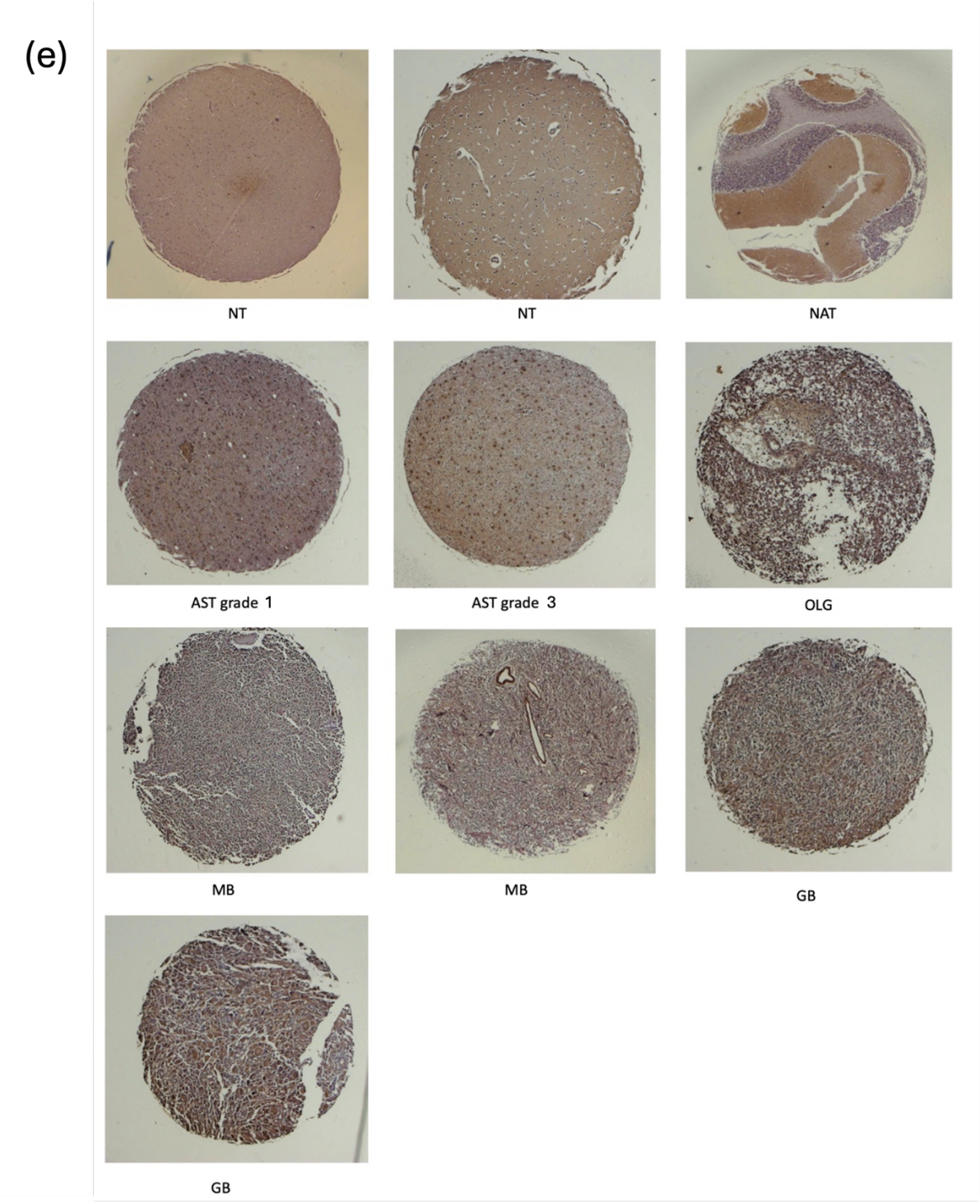


Figure 66 (continued). (e) Microscopic images of SV2B stained tissue cores of normal brain tissue, tumour adjacent tissue, and different brain malignancies at ×40 magnification. *NT* normal tissue, *NAT* normal adjacent tissue, *AST* astrocytoma, *OLG* oligodendroglioma, *MB* medulloblastoma, *GB* glioblastoma. Results are based on three independent scoring assessments, n=3. All statistical analyses were conducted using ordinary one-way ANOVA, followed by Dunnett's multiple comparisons test to determine the significant differences in SV2B expression.

4.3.3. sRNA-seq analysis of MB tissue profiles

Our sRNA-seq analysis identified significant dysegulation of miRNAs in MB tissue compared to controls. The heatmap in Figure 67a highlights a distinct expression pattern, with clear segregation between the control (D) and MB (C1-C9) samples, indicating widespread miRNA dysregulation in MB tissues. Further quantification of miRNA dysregulation is illustrated on the volcano plot in Figure 67b. The results revealed a total of 328 miRNAs with altered expression levels. Of these, 57 miRNAs were significantly downregulated, while 271 miRNAs were upregulated in MB tissues. MiR-206 and miR-383 were amongst the most significantly downregulated miRNAs across all MB samples. Pathway analysis using KEGG highlighted that the dysregulated miRNAs were predominantly associated with critical cellular pathways (Figure 68). Notably, the dysregulated miRNAs were linked to lysosomal pathways, axon guidance, natural killer cell-mediated cytotoxicity, and various cancer-related pathways. Molecular function analysis indicated that the identified dysregulated miRNAs are involved in essential cellular functions, such as metal ion binding and nucleic acid binding activities (Figure 69). Biological process analysis revealed that most dysregulated miRNAs are implicated in key regulatory mechanisms, such as the regulation of transcription and intracellular signal transduction (Figure 70).

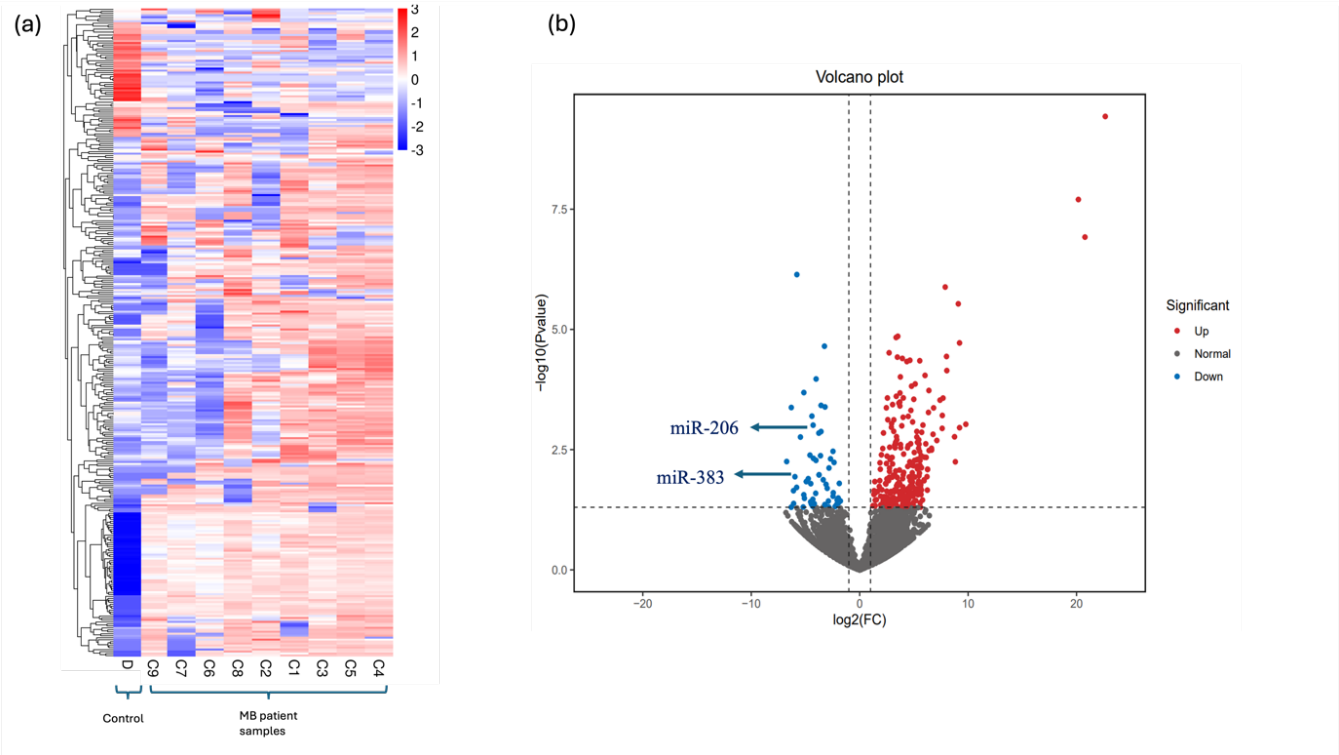


Figure 67. Comprehensive sRNA-seq analysis of MB tissue miRNA profiles. (a) Heatmap of deregulated miRNAs (control group D (D); MB group C (C1-C9). (b) Volcano plot of miRNA expression revealed 328 deregulated miRNAs: 57 downregulated and 271 upregulated. MiR-206 and miR-383 showed significant downregulation in all MB samples ($p<0.04$ and $p<0.01$, respectively).

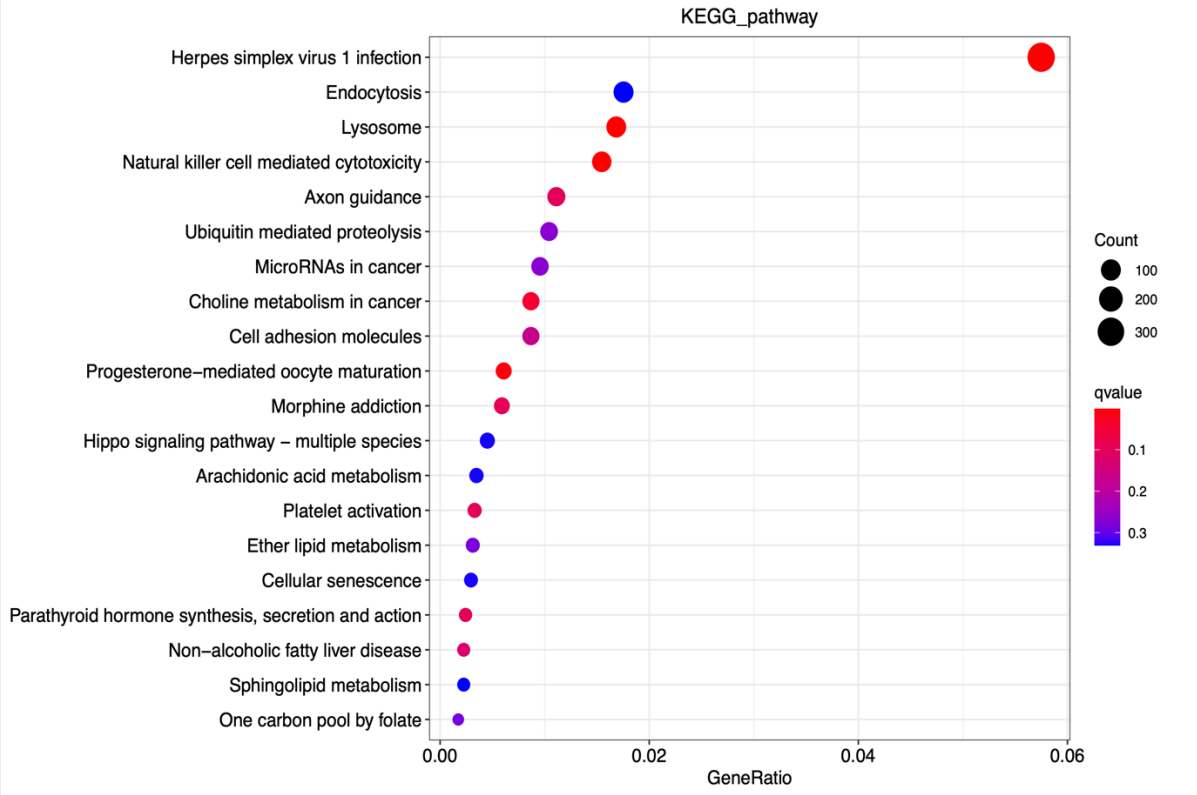


Figure 68. KEGG pathway analysis. KEGG pathway analysis revealed that dysregulated miRNAs were primarily associated with lysosome pathways, axon guidance, natural killer cell mediated cytotoxicity, and pathways in cancer (red boxes).

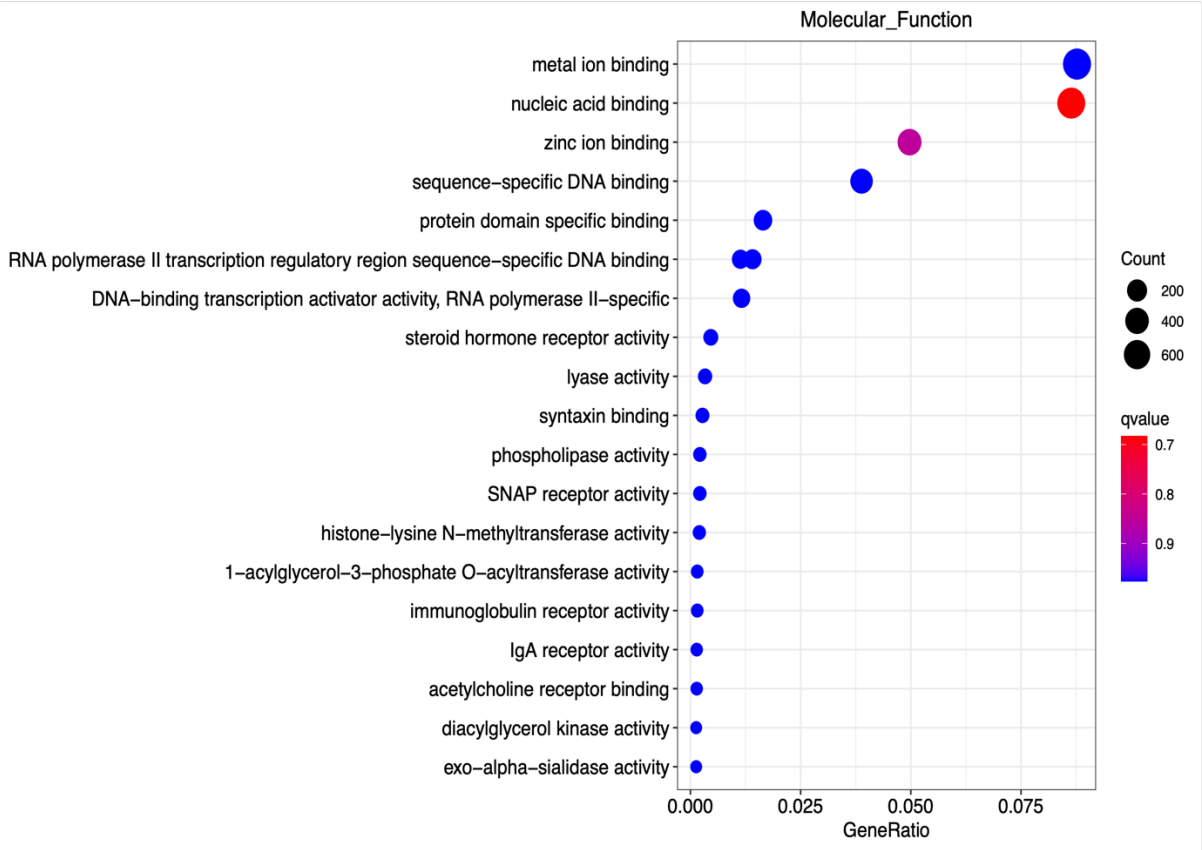


Figure 69. Molecular function analysis. Molecular function analysis of dysregulated miRNAs showed that they took part mainly in metal ion binding and nucleic acid binding (red boxes).

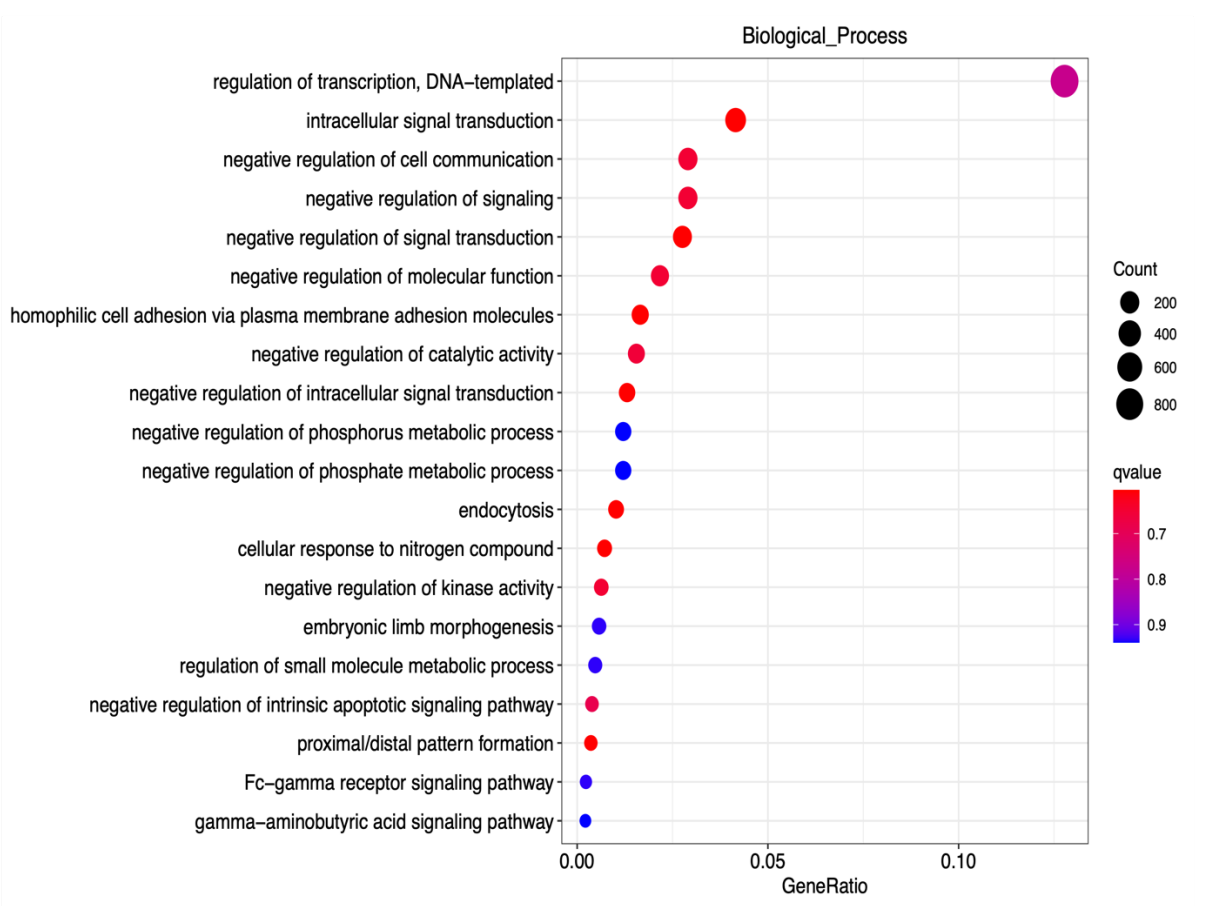


Figure 70. Biological process analysis. Biological process analysis showed that most dysregulated miRNAs were involved in processes such as the regulation of transcription and intracellular signal transduction (red boxes).

4.3.4. Transcriptomics analysis of MB tissue profiles

The comprehensive transcriptomics analysis of MB tissues revealed significant dysregulation in gene expression patterns when compared to control tissues. The heatmap illustrated in Figure 71a exhibited distinct gene expression profiles between the MB group (C1-C9) and the control (D), indicating substantial differences in transcriptomic landscapes between normal and cancerous tissues. The volcano plot analysis (Figure 71b) identified a total of 1013 genes with significantly altered expression levels in MB tissues. Of these, 415 genes were downregulated, while 598 genes were upregulated. *CORO1C* and *SV2B* genes were amongst the upregulated genes in MB samples. The pathway enrichment analysis of the differentially expressed genes (DEG) revealed their association with several biological pathways, including the cell cycle, synaptic vesicle cycle, axon guidance, and miRNAs in cancer (Figure 72). Further analysis into the molecular functions of the DEG showed a significant involvement in microtubule motor activity and binding, ATP binding, and nucleic acid binding processes (Figure 73). Biological process analysis highlighted that the dysregulated genes were predominantly associated with cell division, cellular response to DNA damage, regulation of neuronal synaptic plasticity, and mitotic cell cycle checkpoints (Figure 74).

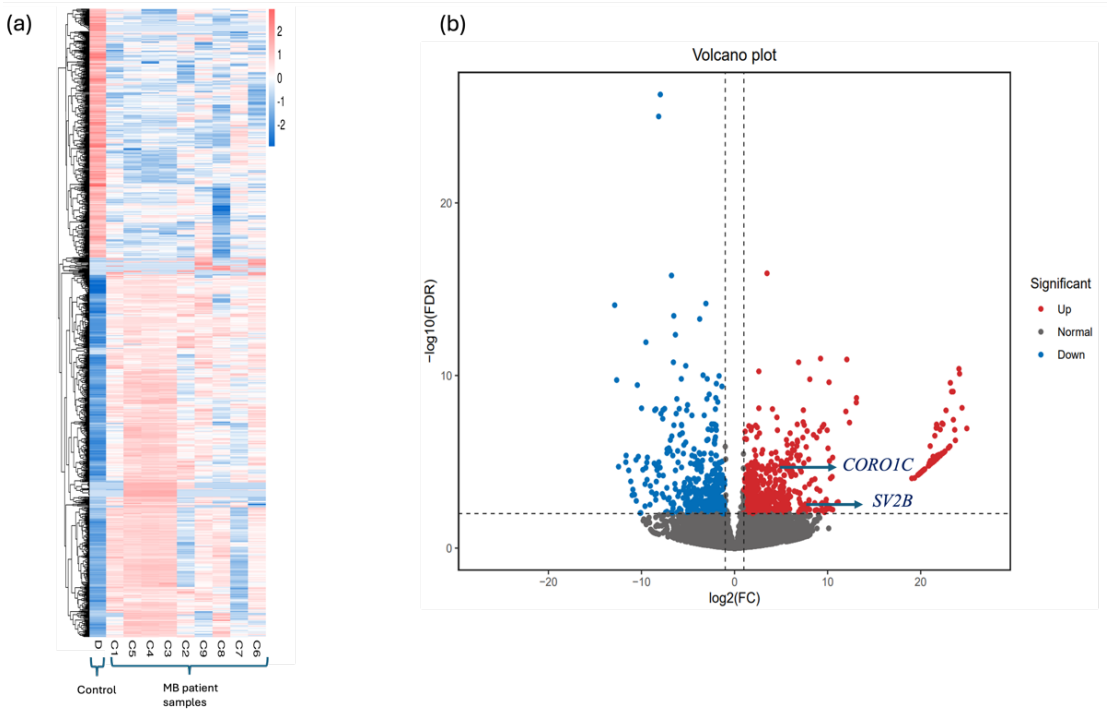


Figure 71. Comprehensive transcriptomics analysis of MB tissue profiles. (a) Heatmap of deregulated genes (control group D (D); MB group C (C1-C9). (b) Volcano plot of gene expression revealed 1013 deregulated genes: 415 downregulated and 598 upregulated. *CORO1C* and *SV2B* were identified as upregulated in the patient sample cohort ($p<0.005$).

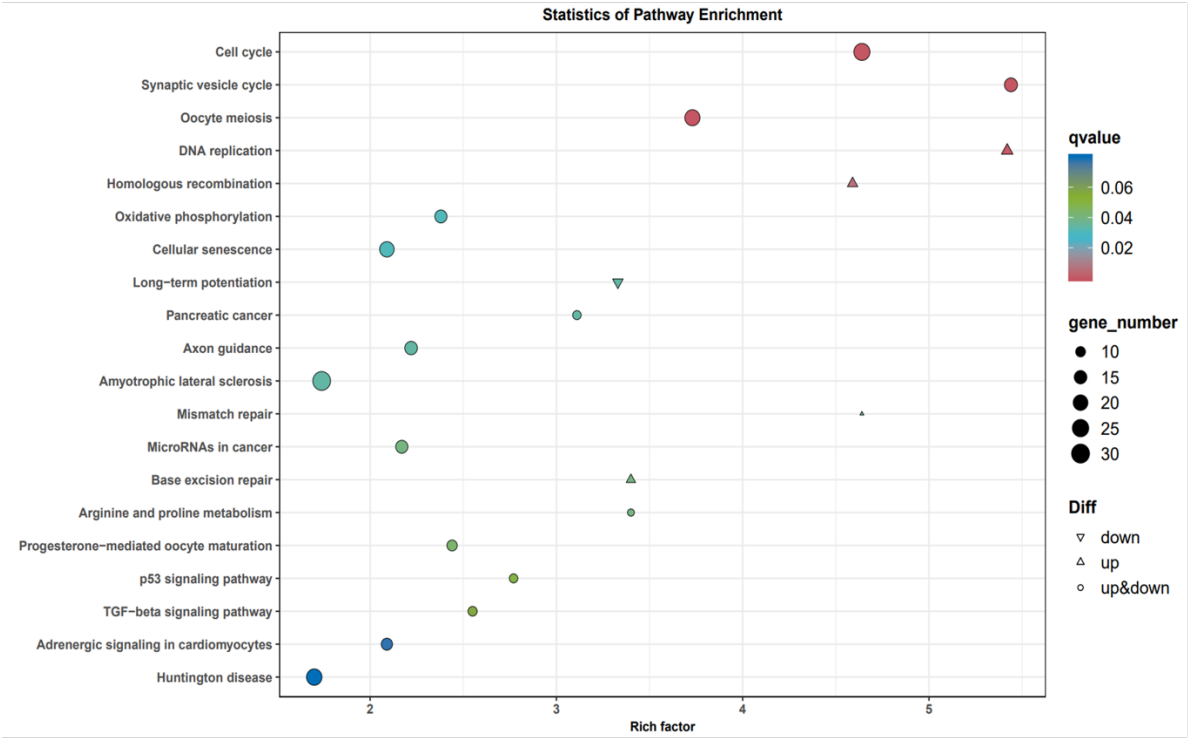


Figure 72. Pathway enrichment analysis. Pathway enrichment analysis revealed that DEGs were primarily associated with the regulation of the cell cycle, synaptic vesicle cycle, axon guidance, and miRNAs in cancer (red boxes).

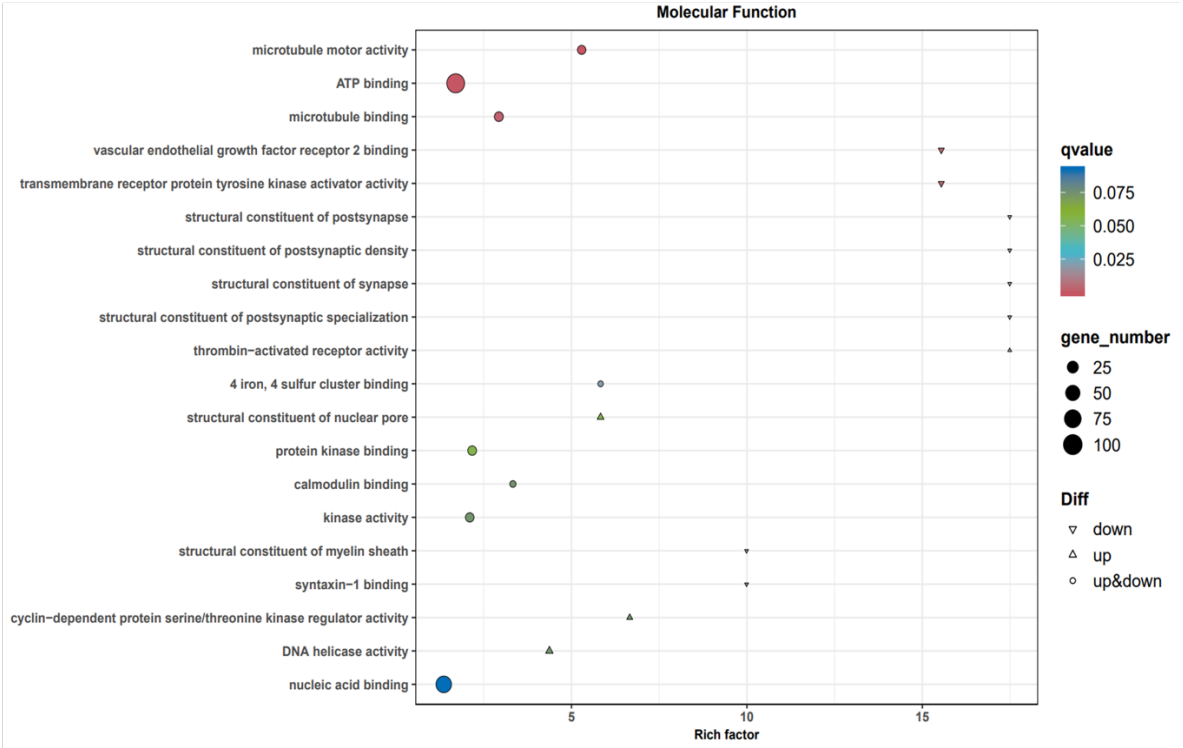


Figure 73. Molecular function analysis. The molecular function analysis showed that the vast majority of DEGs were involved in processes such as microtubule activity and binding, ATP binding, and nucleic acid binding (red boxes).

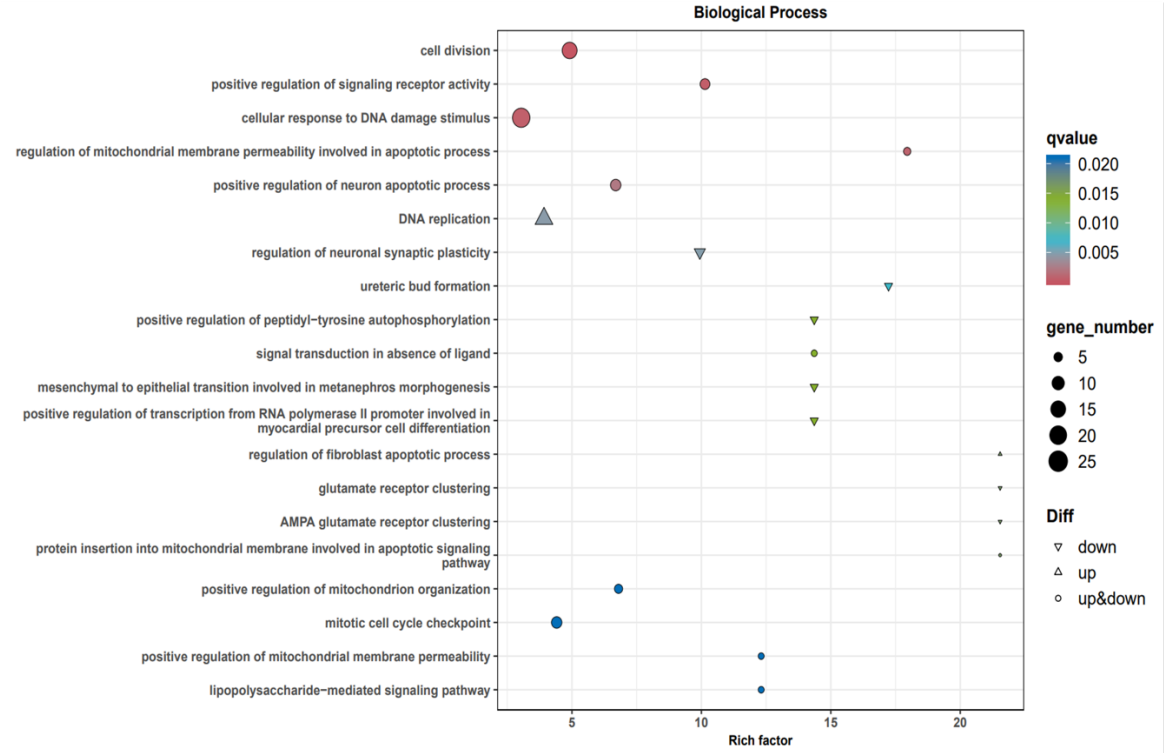


Figure 74. Biological process analysis. Biological process analysis showed that most dysregulated genes were involved cell division, cellular response to DNA damage, regulation of neuronal synaptic plasticity, and mitotic cell cycle checkpoints (red boxes).

4.3.5. Exosome extraction and validation

The nanoparticle tracking analysis (NTA) size and protein concentration of control (C1–C5) and patient (P1–P6) samples were analysed (Table 12). In control samples, the average NTA particle size was 91.24nm, with a standard deviation (SD) of 15.27nm. The protein concentration, measured in terms of the amount from 1mL plasma, averaged 430.83µg, with a standard deviation of 119.34µg. Control samples also had an average particle-to-protein ratio of 2.05^{11} particles/µg. In patient samples, the average NTA particle size was larger, measuring 113.47nm with a standard deviation of 13.21nm. The average protein concentration from 1mL plasma was lower, averaging 360.40µg, with a standard deviation of 92.53µg. The particle-to-protein ratio in patient samples was slightly higher than in controls, averaging 2.61^{11} particles/µg. Furthermore, TEM visualised EVs isolated from human plasma at magnifications of x10,000 and x30,000, with a white arrow indicating representative EVs (Figures 75a and 75b). Additionally, ponceau staining and western blotting confirmed the presence of EV-specific surface markers, including CD81 and CD9, in both control and patient samples, indicating successful isolation of EVs (Figures 76a and 76b). Apolipoprotein B (APOB) was absent in the western blot images, indicating an effective enrichment for EVs while minimising lipoprotein contamination.

Table 12. Comparison of protein concentration and NTA size in control and patient extracellular vesicle samples.

		Protein content			NTA conc.	NTA size	
	Volume eluted (µl)	Conc, µg/µl	Amount ug in MS sample	Total ug from 1mL plasma			Particles/ µg protein
C1	100	3.929625446	314.370	392.963	1.01E+12	102.4	2.57E+11
C2	100	3.673174926	293.854	367.317	8.89E+11	111	2.42E+11
C3	100	2.659808932	212.785	265.981	5.29E+11	95.8	1.99E+11
C4	100	6.034473604	482.758	603.447	9.90E+11	74.2	1.64E+11
C5	100	5.244490428	419.559	524.449	8.68E+11	72.8	1.66E+11
	Average	4.308	344.665	430.831	8.57E+11	91.240	2.05E+11
	SD	1.193	95.468	119.335	1.73E+11	15.272	3.83E+10
	SEM	0.534	42.695	53.368	7.74E+10	6.830	1.71E+10
P1	100	3.364141924	269.131	336.414	9.28E+11	103.5	2.76E+11
P2	100	4.845381886	387.631	484.538	1.37E+12	119.6	2.83E+11
P3	100	3.388297404	271.064	338.830	9.35E+11	119.7	2.76E+11
P4	100	4.483345322	358.668	448.335	8.41E+11	123.8	1.88E+11
P5	100	3.588065486	287.045	358.807	8.54E+11	125.6	2.38E+11
P6	100	1.955145966	156.412	195.515	5.96E+11	88.6	3.05E+11
	Average	3.604	288.325	360.406	9.21E+11	113.467	2.61E+11
	SD	0.925	74.026	92.532	2.30E+11	13.217	3.82E+10
	SEM	0.378	30.221	37.776	9.40E+10	5.396	1.56E+10

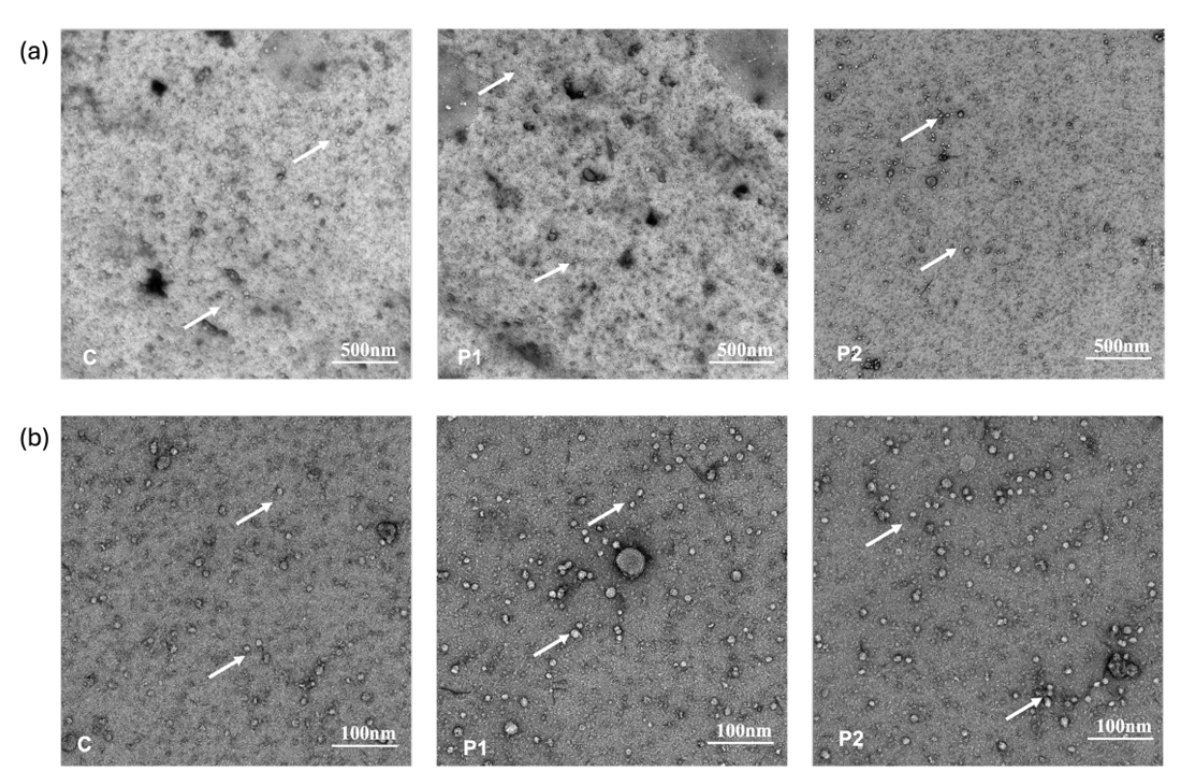


Figure 75. Assessment of EV enrichment and purity. (a) Transmission electron microscopy (TEM) was used to visualise EVs isolated from human plasma at two magnifications: x10,000 (scale bar 500nm) and (b) x30,000 (scale bar 100nm), with a white arrow indicating a representative EV. The letter C indicates control samples, while P1 and P2 stand for two patient samples.

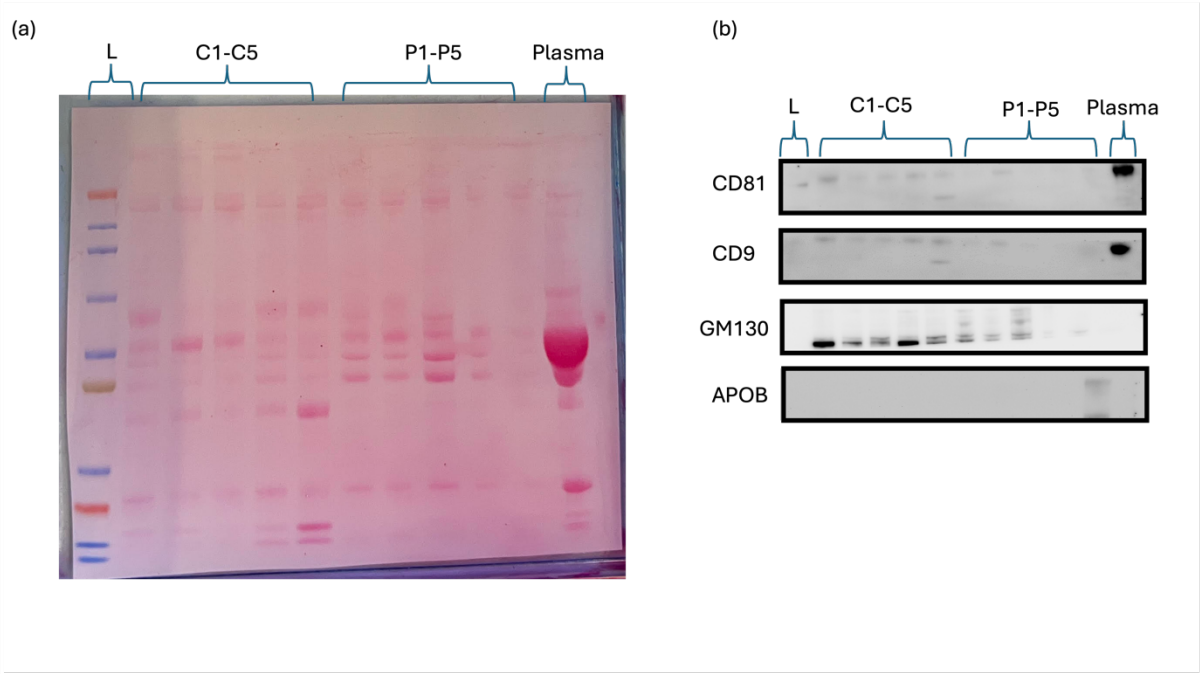


Figure 76. Ponceau staining and western blotting. (a) Ponceau staining. (b) Western blotting showed that the control and patient samples expressed EV surface specific markers (CD81 and CD9). Additionally, the most common co-isolated contaminants, including GM130, albumin, and Apolipoprotein B, and were examined using 5µg of sample from each separation method and unprocessed plasma. The letter L stand for protein ladder, C1-C5 indicated the five control samples, while P1-P5 indicated the five patient samples.

3.4.6. sRNA-seq of GB exosome profiles

The sRNA-seq analysis of exosomal miRNA profiles in GB revealed significant dysregulation in miRNA expression between the control (A1-A5) and GB (B1-B6) groups. A heatmap depicting dysregulated miRNAs showed an altered miRNA expression pattern between the two groups (Figure 77a). A volcano plot of miRNA expression identified 78 dysregulated miRNAs, with 36 miRNAs downregulated and 42 miRNAs upregulated in the GB group compared to controls (Figure 77b). MiR-206 and miR-383 were identified amongst the dysregulated miRNAs within the exosome analysis. KEGG pathway analysis indicated that the dysregulated miRNAs were predominantly associated with lysosomal and cancer pathways, emphasising their potential role in tumour progression and malignancy (Figure 78). Molecular function analysis revealed that the identified miRNAs participated in critical cellular functions, including protein, nucleic acid, and enzyme binding (Figure 79). Biological process analysis demonstrated that most dysregulated miRNAs were involved in essential biological processes, particularly those regulating phosphorus and phosphate metabolism, alongside the regulation of phosphorylation (Figure 80).

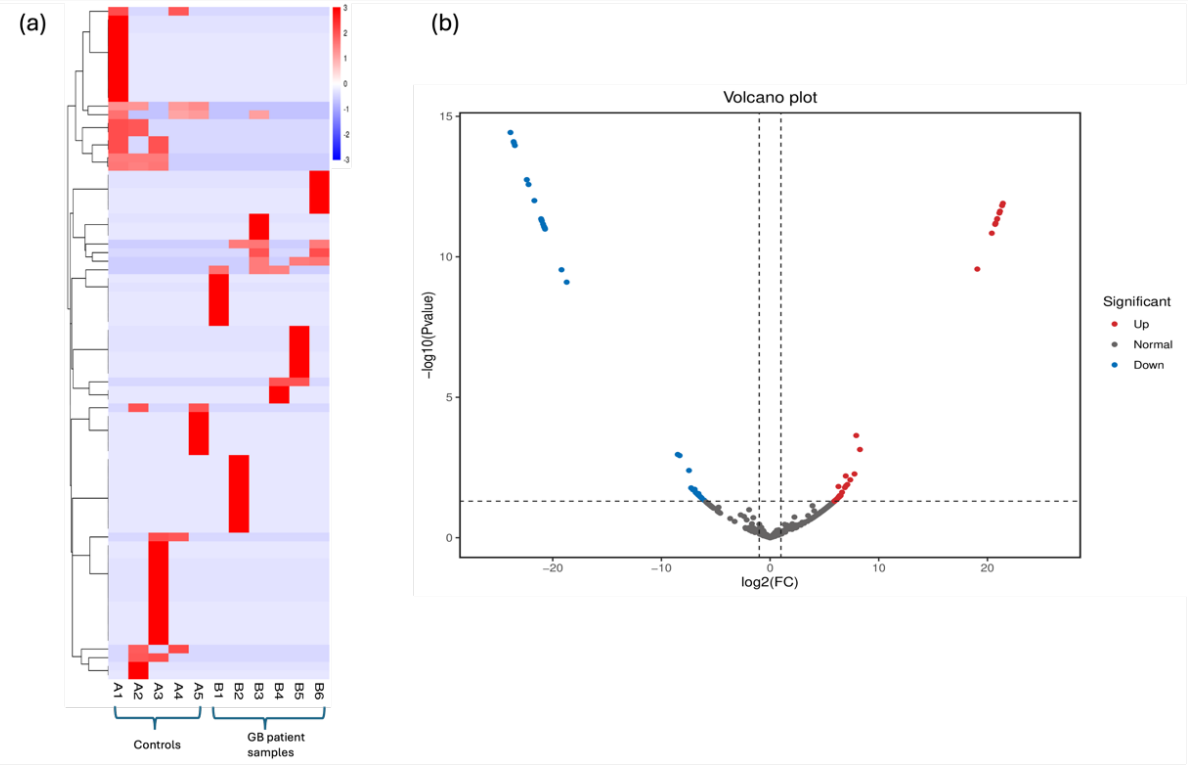


Figure 77. Comprehensive sRNA-seq analysis of GB exosomal miRNA profiles. (a) Heatmap of dysregulated miRNAs (control group A (A1-A5); GB group B (B1-B6). (b) Volcano plot of miRNA expression revealed 78 deregulated miRNAs: 36 downregulated and 42 upregulated. MiR-206 and miR-383 were not identified amongst the significantly dysregulated miRNAs from the exosome sequencing analysis.

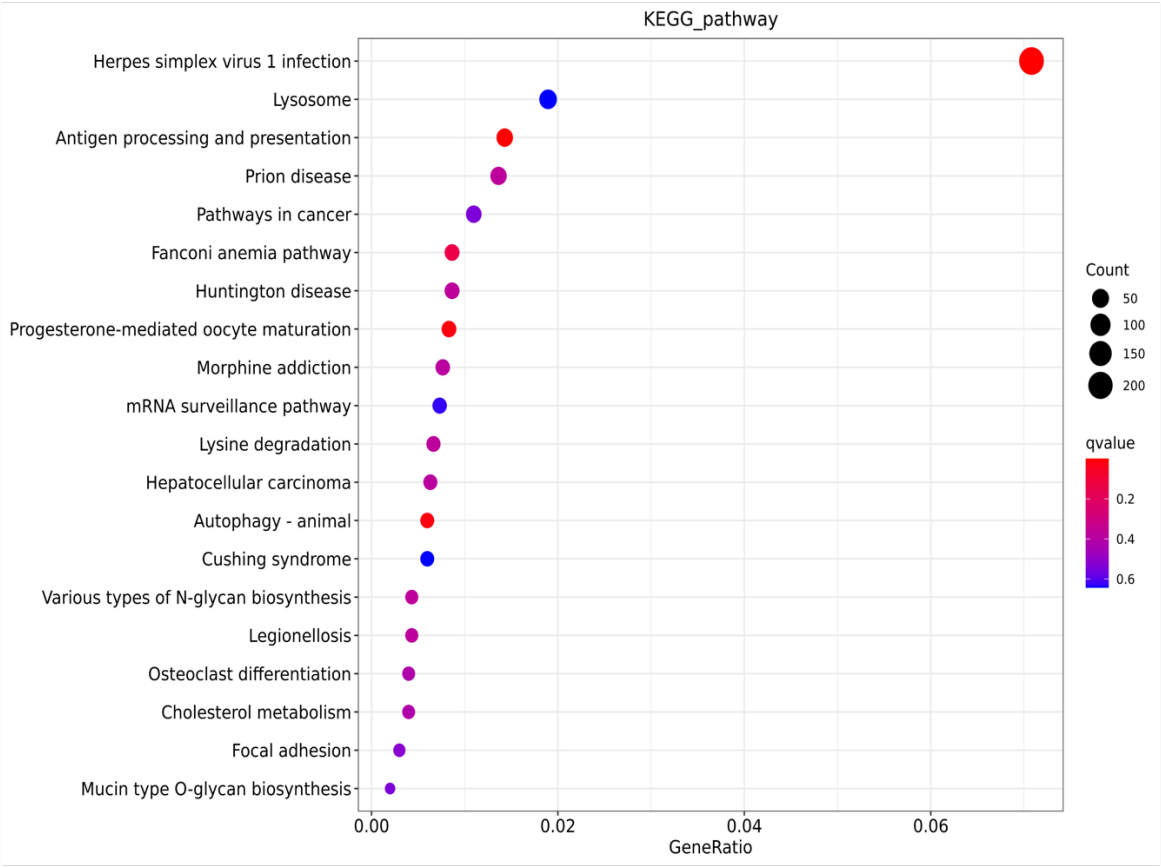


Figure 78. KEGG pathway analysis. KEGG pathway analysis revealed that dysregulated miRNAs were primarily associated with lysosomal pathways and pathways in cancer (red boxes).

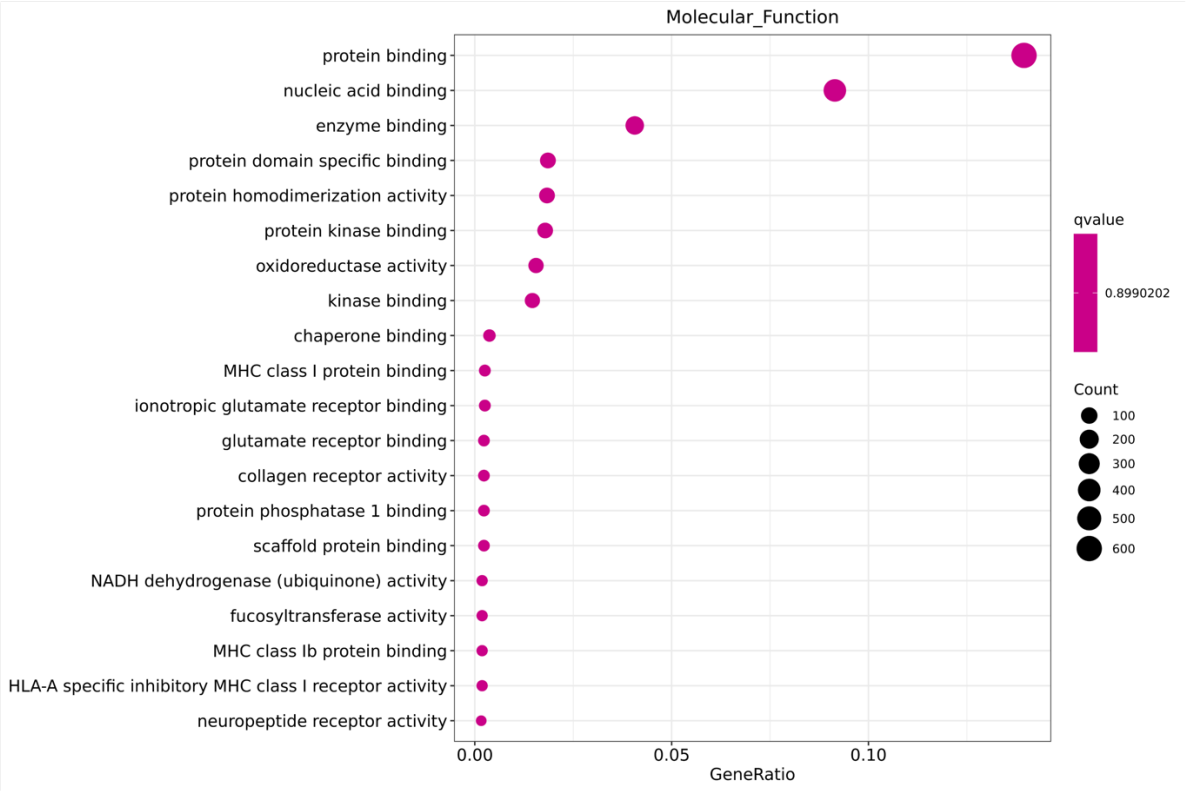


Figure 79. Molecular function analysis. Molecular function analysis of dysregulated miRNAs showed that most identified miRNAs took part in protein, nucleic acid, and enzyme binding (red boxes).

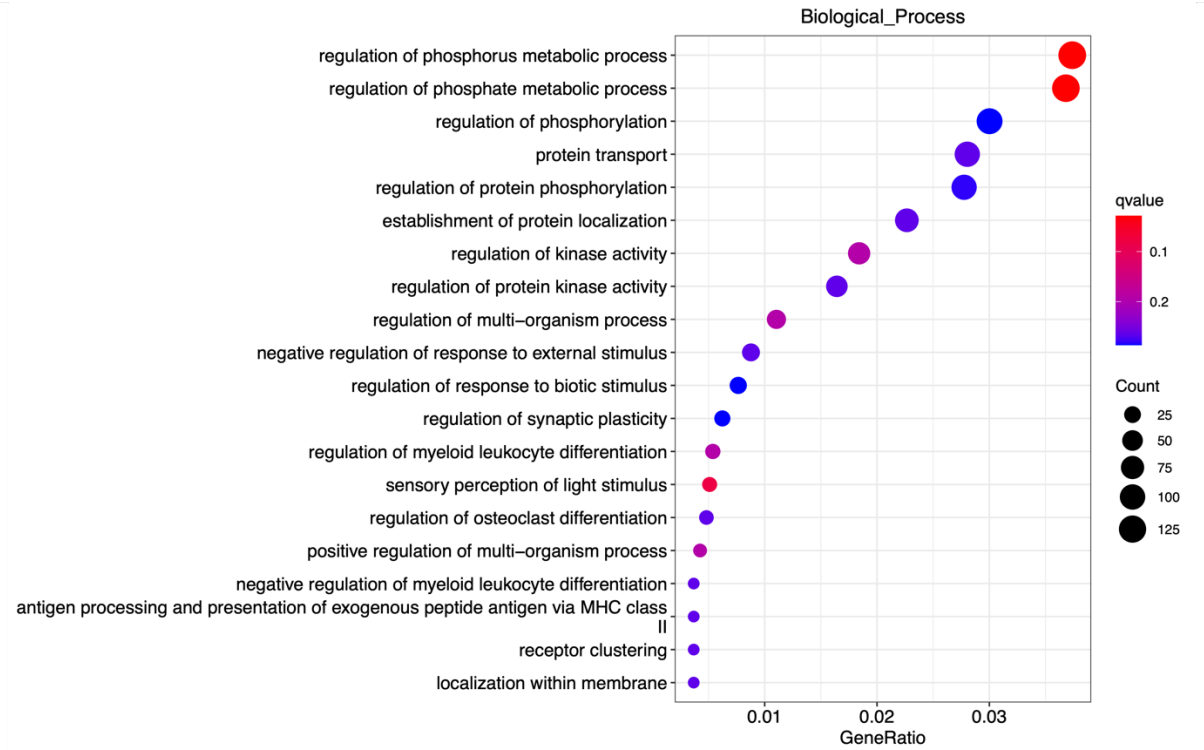


Figure 80. Biological process analysis. Biological process analysis showed that most dysregulated miRNAs were involved in processes such as phosphorus and phosphate metabolic regulation, and the regulation of phosphorylation (red boxes).

3.4.7. Proteomics analysis of GB exosome profiles

The proteomics analysis of exosome samples from GB patients, conducted using mass spectrometry, identified alterations in protein expression between the control and GB groups. A heatmap of dysregulated proteins revealed distinct expression patterns between the control group (A1-A5) and the GB group (B1-B6), showing the differential protein expression (Figure 81a). A volcano plot of protein expression identified 11 dysregulated proteins, with 8 proteins downregulated and 3 proteins upregulated in the GB group compared to controls (Figure 81b). CORO1C and SV2B were not identified in the group of dysregulated proteins from the exosome analysis. KEGG pathway analysis indicated that the differentially expressed proteins were primarily associated with the regulation of the actin cytoskeleton and the complement and coagulation cascades (Figure 82). Reactome pathway analysis revealed that most of the dysregulated proteins were involved in key biological processes, such as signal transduction and immune system regulation (Figure 83). Gene ontology analysis indicated that the dysregulated proteins were primarily involved in lipase inhibitor activity and actin binding (Figure 84).

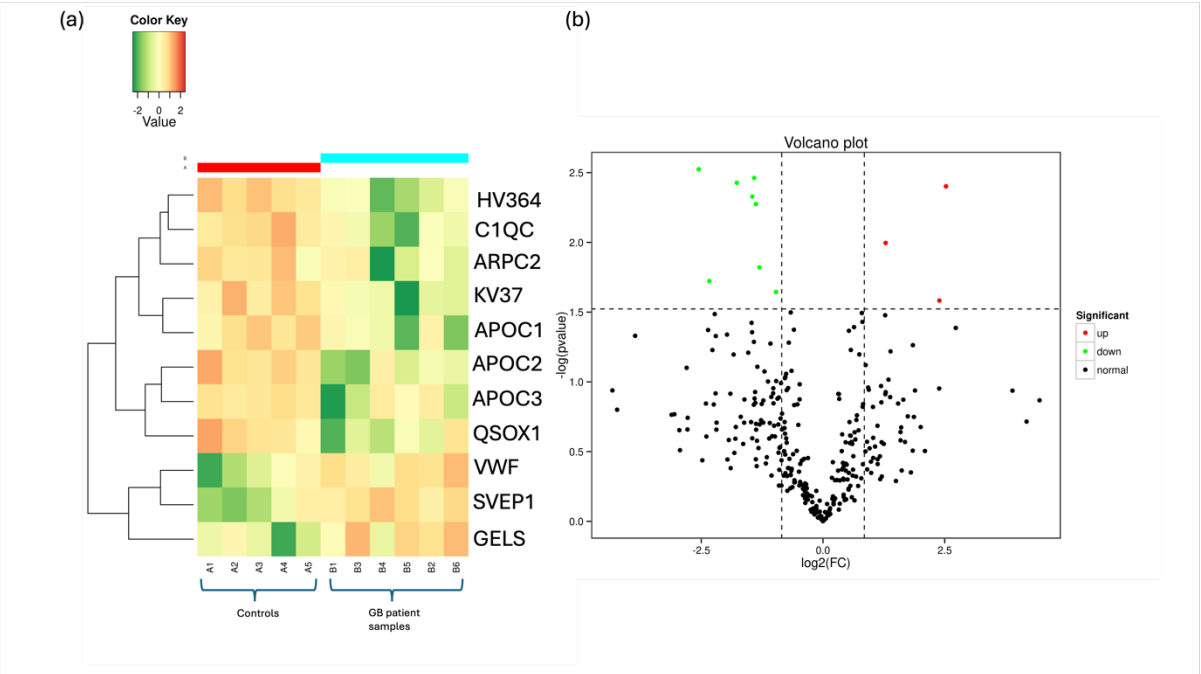


Figure 81. Comprehensive proteomics analysis of GB exosome samples. (a) Heatmap of dysregulated proteins (control group A (A1-A5); GB group B (B1-B6). (b) Volcano plot of protein expression revealed 11 deregulated proteins: 8 downregulated and 3 upregulated. CORO1C and SV2B were not identified throughout the proteomics analysis of GB exosomes. The selection criteria for up-regulated proteins are FC ≥ 1.80 and a p-value ≤ 0.03. Similarly, for down-regulated proteins, the criteria are FC ≤ 1/1.80 and a p-value ≤ 0.03.

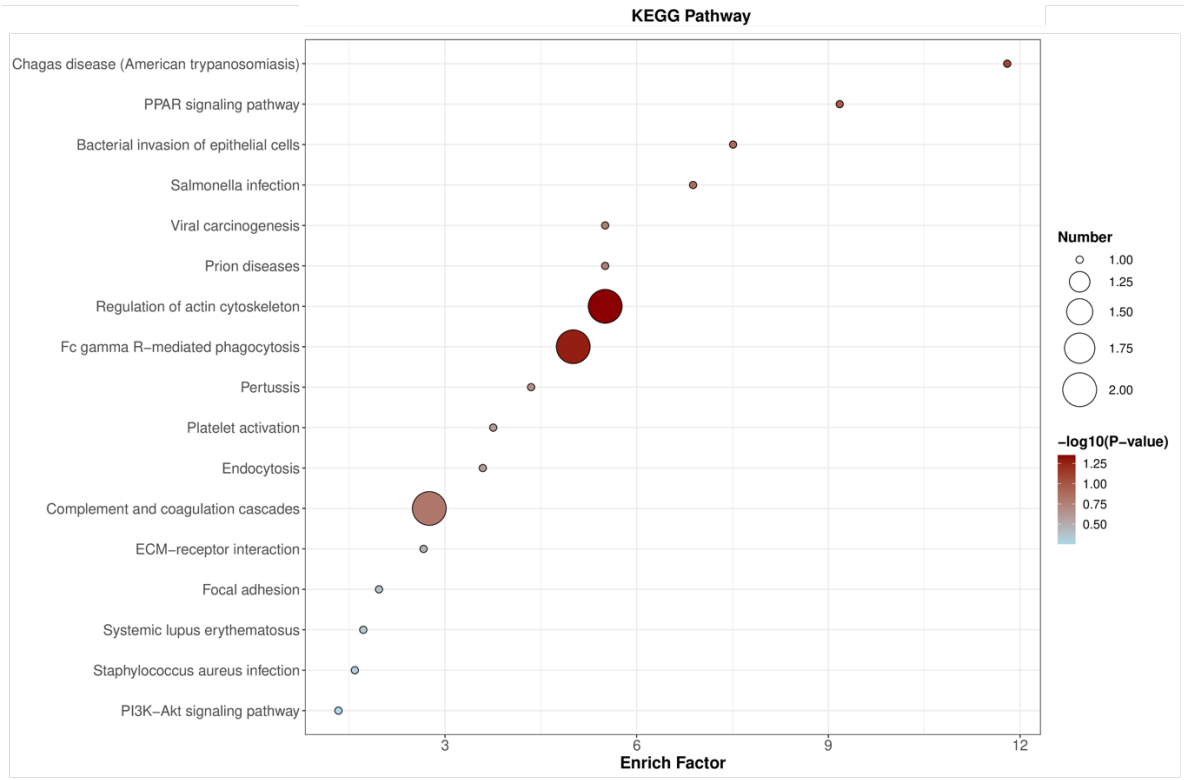


Figure 82. KEGG pathway analysis. KEGG pathway analysis revealed that most of the dysregulated proteins were primarily associated with the regulation of the actin cytoskeleton, the complement and coagulation cascades (red boxes).

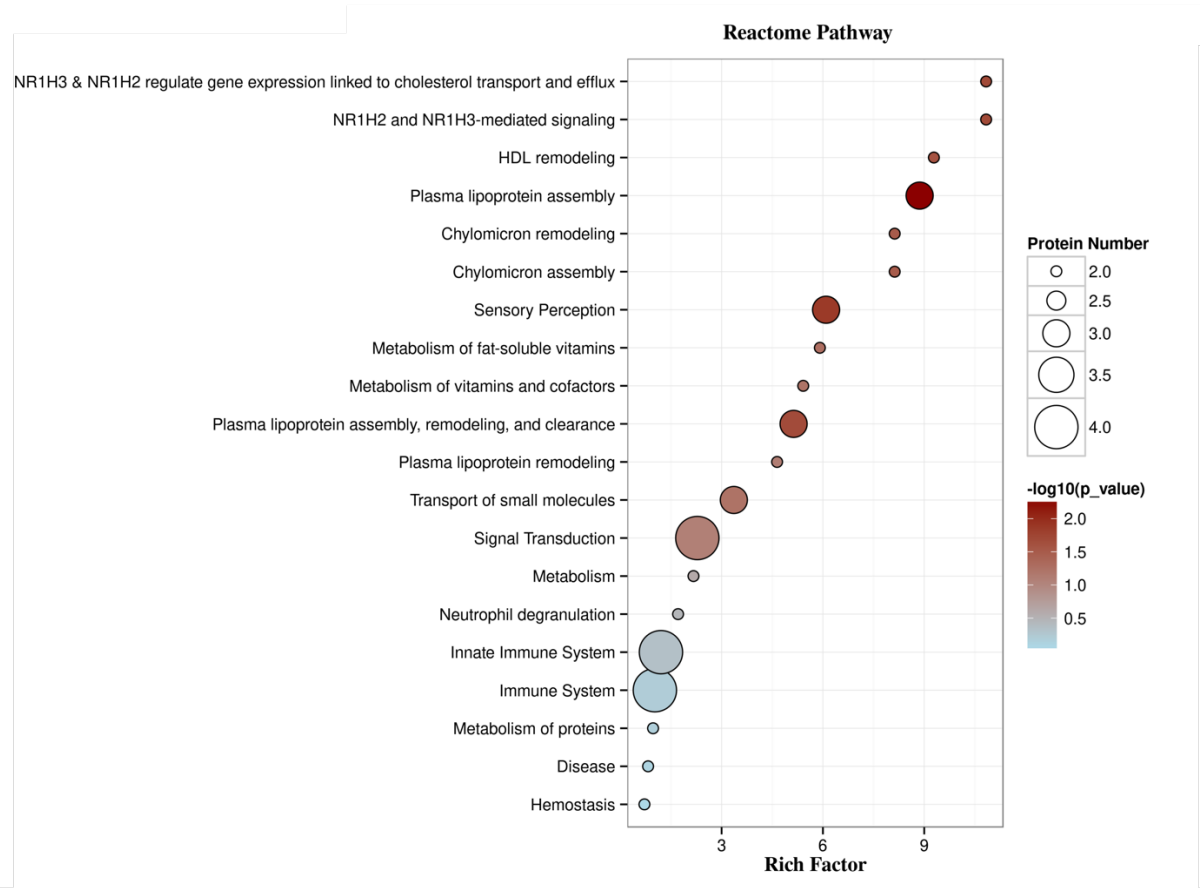


Figure 83. Reactome protein analysis. The reactome pathway analysis showed that most dysregulated proteins were involved in processes such as signal transduction and the immune system (red boxes).

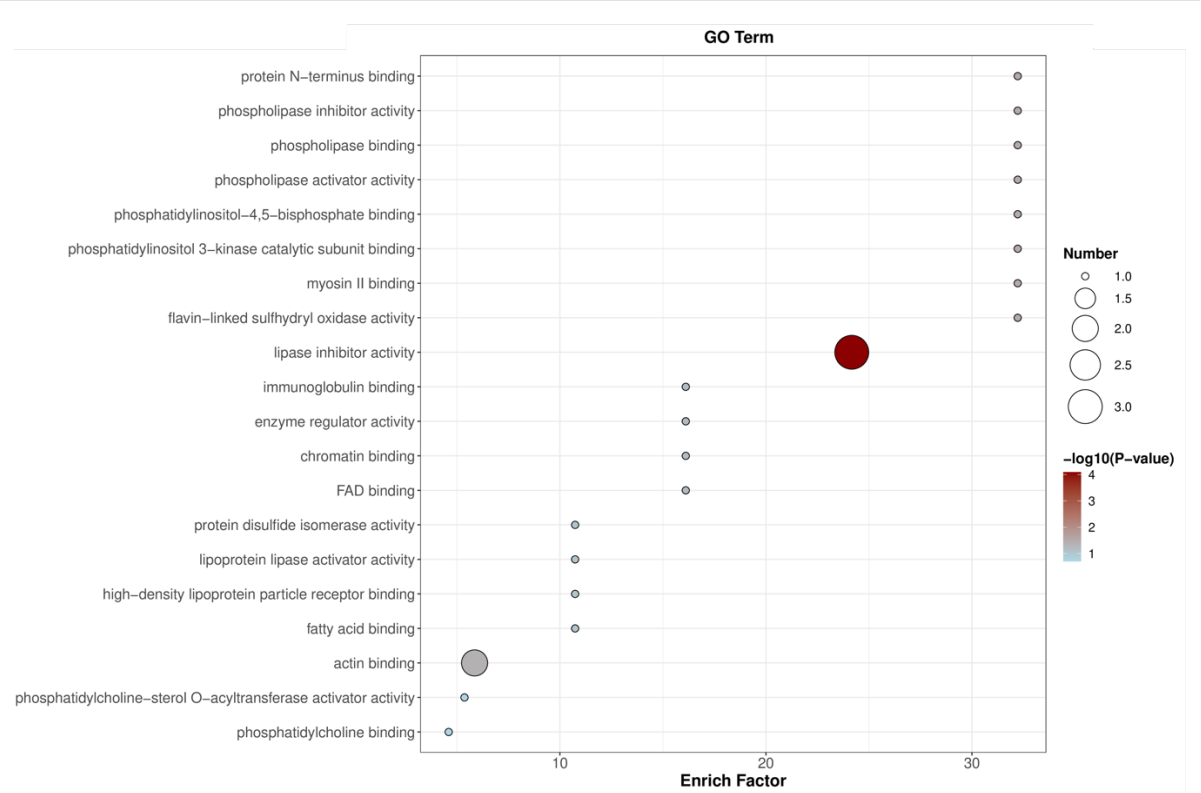


Figure 84. Gene ontology analysis. GO analysis revealed that most dysregulated proteins were primarily involved in lipase inhibitor activity and actin binding (red boxes).

4.4. Discussion

Medulloblastomas and GBs are the most aggressive brain tumours found in children and adults, respectively. Limited effective treatments face challenges such as tumour recurrence, resistance, and significant side effects (Aldape, *et al.,* 2019). The potential use of miRNAs in targeting specific gene targets is regarded as a promising therapeutic approach because miRNAs can regulate gene expression involved in tumour growth and resistance (Balachandran, Larcher, Chen & Veedu, 2020). Thus, targeting specific miRNAs could provide a new, less invasive, and more precise therapeutic approach for the management of aggressive brain malignancies, such as GB and MB.

As previously discussed in Chapters 2 and 3, we identified that miR-206 directly targeted *CORO1C*, while miR-383 targeted *SV2B*. We also showed that CORO1C and SV2B were upregulated in GB and MB cell lines, both the mRNA and protein levels. To check whether these protein biomarkers were expressed in GB and MB patients, we further performed an IHC analysis of brain tumour tissues. Immunohistochemistry of CORO1C revealed its overexpression in GB and MB tissues when compared to normal brain tissues and tumour adjacent tissue. The strong significant increase between the GB/MB and control groups observed through IHC suggested that CORO1C possessed oncogenic properties and that it could serve as a potential therapeutic target. Our IHC findings also revealed that CORO1C expression increased with tumour grade, suggesting that highly metabolically active malignancies, such as both GB and MB, might require increased expression of this protein for proliferation and metastasis. Our findings are in line with previous observations, which showed that high-grade gliomas, such as GB, had a significantly higher number of CORO1C-positive tumour cells compared to low-grade gliomas (Thal, *et al.,* 2008). Furthermore, in high-grade gliomas, CORO1C expression varies within different regions of the tumour. For instance, tumour cells located near proliferating microvessels in the tumour periphery showed higher CORO1C expression compared to those adjacent to necrotic areas (Thal, *et al.,* 2008). This regional variation in expression may reflect the dynamic needs of tumour cells in different microenvironments, with higher CORO1C expression supporting active proliferation and invasion in areas of vascular proliferation (Fukuda, *et al.,* 2023). Our results also showed significantly higher CORO1C expression in patients aged 0-20 compared to their normal counterparts, indicating its clinical relevance in paediatric brain malignancies, such as MB. Moreover, the elevated levels of CORO1C in highly malignant paediatric brain malignancies could be associated with its role in influencing cell migration and proliferation. The significant

overexpression of CORO1C in the 61–80 age group also suggested its high expression in adult brain malignancies, such as GB. Thus, the elevated expression levels of CORO1C proposed that it could serve as a putative prognostic biomarker or therapeutic target, enhancing its clinical relevance in the fight against highly malignant brain tumours like GB and MB.

Previous bioinformatics studies have suggested that SV2B expression may correlate with glioma grade and poor prognosis, implying its potential oncogenic function (Wang *et al.,* 2019; Zhang *et al.,* 2020). SV2B has been previously found overexpressed in breast cancer tissue compared to normal tissue (Bandala *et al.,* 2012). These findings are consistent with our IHC data, which demonstrated significantly higher SV2B protein expression in high-grade brain malignancies, such as GB and MB. To date, no immunohistochemical evidence of SV2B expression has been reported in brain tumour patient cohorts. One possible explanation for the elevated SV2B accumulation in high-grade brain malignancies is its role as a widely distributed neurotransmitter in the brain, which raises intracellular Ca^{2+} levels, promoting cell proliferation and migration, and thus demonstrating tumorigenic properties in GB and MB (Pei, Lee, Khan, Erisnor & Wang, 2020). Additionally, SV2B has been associated with energy metabolism, suggesting that tumours with high energy requirements might depend on SV2B to regulate transporter protein activity and glucose transport (Liu, *et al.,* 2023). Our IHC analysis demonstrated that SV2B expression increased with tumour grade, suggesting that highly metabolically active malignancies may require higher SV2B levels for proliferation and metastasis. Glioblastomas and MBs represent advanced brain malignancies characterised by differential gene expression. Notably, half of the newly diagnosed high-grade brain tumours occur in patients over 65 years old (Renovanz, *et al.,* 2020). Our results showed significantly elevated SV2B expression in patients aged 61-80 years compared to normal tissue, highlighting its prognostic significance in high-grade brain cancers. High SV2B expression in the 0-20 age group also indicated its relevance in paediatric brain malignancies, possibly linked to regions of the brain exhibiting high synaptic plasticity. This suggested that SV2B may function as an oncogene, given its prevalence in highly malignant brain tumours. Moreover, the expression pattern of SV2B indicated its potential as a prognostic marker and therapeutic target, emphasising its clinical importance in addressing highly malignant brain tumours like GB and MB.

It is important to mention that the use of whole tissue microarray staining as a basis for scoring, rather than a tumour-specific assessment, presents limitations in accuracy by potentially

incorporating signals from stromal components and non-neoplastic cells into the analysis. This broader approach may lead to an overestimation or misinterpretation of staining intensity and distribution within tumour regions. Consequently, the results may reflect a composite signal that does not exclusively represent the tumour cell population, potentially impacting the specificity and reliability of data derived from TMA-based assessments.

Our sRNA-seq results depicted that a total of 328 miRNAs were significantly dysregulated in MB patient samples when compared to normal brain tissue. Both miR-206 and miR-383 were amongst the most significantly downregulated miRNAs in the patient cohort, supporting our *in vitro* observations made in Chapter 3. Previous studies also depicted the dysregulated expression of miR-206 and miR-383 in paediatric brain tumours compared to normal tissue. Both miR-206 and miR-383 were identified as being consistently downregulated in tumour samples, suggesting potential tumour-suppressive roles (Braoudaki, *et al.,* 2014; Lambrou, Zaravinos & Braoudaki, 2021). Our results in MB patients align with these results and indicate that these miRNAs may contribute to MB tumorigenesis. Furthermore, these observations may offer insights into their potential interactions with their targets, *CORO1C* and *SV2B*, respectively. Both CORO1C and SV2B have been implicated in tumour progression and cellular processes such as cell migration, invasion, and energy metabolism, which are essential for GB and MB. MiR-206, known to regulate several oncogenic pathways like the EGF/EGFR/MAPK and TGF-β pathways, might influence the activity of *CORO1C*, which plays roles in cancer proliferation, motility, and extracellular matrix invasion (Adams, Cowee & White, 2009; Yin, *et al.,* 2016). Furthermore, *CORO1C* has been previously linked to cytoskeletal dynamics and cell motility, which may be supported by miR-206-regulated pathways such as PI3K/AKT/mTOR and Wnt/β-catenin (Tang, *et al.,* 2017; Zhou, *et al.,* 2019a). Additionally, miR-383 also plays a significant role in inhibiting cell growth and promoting apoptosis in various cancers by regulating key oncogenic pathways. In particular, miR-383 has been shown to suppress tumour cell proliferation and invasion by targeting specific proteins and pathways, such as the PI3K/AKT/mTOR and STAT3 signalling pathways (Wang, *et al.,* 2019c; Wang, Xu, Jin, Li & Li, 2021a). Given the role of SV2B in brain malignancies and its involvement in energy metabolism and intracellular calcium regulation, it could be suggested that the under-expression of miR-383 in cancer could influence the overexpression of *SV2B.* Thus, miR-383-regulated pathways, such as the PI3K/AKT/mTOR pathway, could potentially contribute to enhanced cell metabolism and signalling in GB and

MB. These interactions emphasise the importance of adopting miRNA-based therapies, which may potentially disrupt key oncogenic pathways, including those regulated by the two miRNAs, providing an alternative avenue for therapeutic approaches in highly malignant brain tumours.

Furthermore, in the KEGG pathway analysis, the involvement of dysregulated miRNAs in MB was linked to key cancer-related pathways, including natural killer cell-mediated cytotoxicity, axon guidance, and lysosome function. These pathways are important for tumour progression, immune evasion, and the invasion capabilities of cancer cells (Yu, 2023b; Kim & Kim, 2020b; Tang, *et al.,* 2020). Regarding molecular functions, dysregulated miRNAs were involved in metal ion binding and nucleic acid binding, which are essential for enzymatic activity and the regulation of transcription (Sinha, Sangani, Kehr, Rule & Jen-Jacobson, 2016). Metal ions, such as zinc, play roles in the structural integrity of proteins involved in DNA repair and cell division, which miRNAs can regulate, thereby influencing tumour progression (Li, Tong, Liu & Lou, 2022). In the biological process analysis, regulation of transcription, DNA-templated and intracellular signal transduction were the processes affected by most dysregulated miRNAs identified. MiRNAs regulate transcription factors and signalling molecules, controlling cellular responses to external stimuli, cell cycle progression, and apoptosis (O'Brien, *et al.,* 2018). This further emphasises the role of miRNAs in maintaining cellular homeostasis and suggests that their dysregulation could contribute to tumorigenesis.

Further transcriptomics analysis of the MB patient samples identified 1013 dysregulated genes, with *CORO1C* being amongst the upregulated genes in MB patients, suggesting its oncogenic capacity. To the best of our knowledge, *CORO1C* has not been associated with MB previously. The association between miR-206 and *CORO1C* has been demonstrated in non-small lung cell carcinomas, where deletion or inhibition of *CORO1C* rescued the expression levels of miR-206 and led to suppressed metastasis (Liao & Peng, 2020). Our team also showed that miR-206 potentially targeted *CORO1C* in paediatric and adult tumours, such as MB and GB. Zhou and colleagues suggested that miR-206 could potentially influence the β-catenin growth-dependent mechanism within the Wnt/β-catenin signalling pathway (Zhou, *et al.,* 2019a). Nevertheless, to the best of our knowledge, the link between miR-206 and *CORO1C* in MB or GB has not been previously demonstrated. Factors related to brain development and plasticity during childhood might explain why *CORO1C* levels are elevated in MB paediatric patients. We further identified the upregulation of *CORO1C* in MB and GB cell lines, suggesting that its

overexpression could enhance the early identification of paediatric and adult brain tumours and serve as therapeutic targets for their management. Our transcriptomics analysis also showed that *SV2B* was among the upregulated genes in MB patient samples. We also demonstrated that the SV2B protein was highly expressed within GB and MB tissues. Given SV2B's role in synaptically active regions and its involvement in glioma progression, its expression and function might have implications in paediatric MB. Since *SV2B* is expressed in the cerebellum, where medulloblastomas commonly arise, it could play a role in its tumorigenesis (Pazarlar, *et al.,* 2022). We also showed that *SV2B* in MB and GB cells was overexpressed, suggesting that *SV2B* could also serve as a therapeutic target in MB and GB patients. To the best of our knowledge, there is no existing evidence regarding the association between *SV2B* and its newly proposed regulatory miRNA, miR-383.

The dysregulated genes identified in MB were primarily involved in the regulation of the cell cycle, synaptic vesicle cycle, axon guidance, and miRNAs in cancer, highlighting their crucial role in cellular proliferation, communication, and structural integrity, all of which are essential in the context of MB development and progression and correlate the functions of the selected oncogenes, *CORO1C* and *SV2B.* The dysregulation of the cell cycle and axon guidance are important processes that could drive uncontrolled cell proliferation and neuronal signalling, respectively, both of which are associated with the aggressive nature of MB (Kumar, Liu & Northcott, 2020a). The synaptic vesicle cycle may also play a role in the neural origin of MB, as it involves neurotransmitter release, which could be potentially aided by *SV2B* and lead to a tumorigenic behaviour of the tumour cells (Li, *et al.,* 2022). The dysregulated genes in MB were also associated with ATP binding, microtubule motor activity, and nucleic acid binding, which are important for cellular energy regulation, intracellular transport, and transcriptional control. These molecular functions are key to maintaining cell division and proliferation in MB. Disruption in microtubule motor activity could affect the structural dynamics of the cell and, when potentially aided by *CORO1C*, could lead to increased migration and invasion, which is commonly associated with high-grade brain tumours (Dubey, Ratnakaran & Koushika, 2015). Key biological processes impacted by the dysregulated genes include cell division, DNA replication, cellular response to DNA damage, and mitotic cell cycle checkpoint. Alterations in these processes lead to genomic instability, allowing MB cells to proliferate uncontrollably and resist therapeutic interventions (Skowron, Ramaswamy & Taylor, 2015). The role of DEGs in the regulation of neuronal synaptic plasticity further

suggested that MB cells may exhibit neural signalling mechanisms that promote tumour survival and progression, which could be potentially driven by *SV2B*.

As indicated by our previous analyses and *in vitro* work, miR-206 and miR-383 were also seen downregulated in GB cells. However, our liquid biopsy analysis and the subsequent exosomal sRNA-seq did not demonstrate that these miRNAs were dysregulated in GB patient samples. The downregulation of certain miRNAs in GB cell lines but not in exosomal sRNA-seq can result from selective export mechanisms (Cha, *et al.,* 2015). GB cells package specific miRNAs into exosomes to modulate the tumour microenvironment, influencing processes like immune evasion and angiogenesis (Nail, *et al.,* 2023). Additionally, miRNA functions can differ between intracellular and extracellular contexts (Finn & Searles, 2012). Thus, miR-206 and miR-383, which regulate *CORO1C* and *SV2B*, respectively, might not be found in exosomes due to their roles within the cell. *CORO1C*, involved in cytoskeleton organisation and cell motility, requires internal regulation by miRNAs to maintain intracellular processes, such as cell motility (Gerasymchuk, Hubiernatorova & Domanskyi, 2020). Therefore, exporting these miRNAs in exosomes would limit their availability for these functions. Similarly, *SV2B*, located in synaptic vesicles and essential for neurotransmitter release, also relies on internal miRNA regulation for proper synaptic function (Kumar & Reddy, 2020b). Thus, miRNAs, such as miR-383 are likely retained within the cell to ensure the proper regulation of genes involved in synaptic processes.

In our sRNA-seq exosome analysis, a few miRNAs were significantly dysregulated, including miR-196b-5p and miR-92b-5p. Additionally, our analyses showed that most dysregulated miRNAs carried by exosomes regulated critical pathways such as lysosomal function, cancer-related pathways, protein binding, nucleic acid binding, and metabolic processes. The lysosome pathway, which plays a crucial role in autophagy and the degradation of cellular waste, is exploited by GB cells to survive under stress, as discussed earlier (Kumar, *et al.,* 2021). Both, miR-92b-5p and miR-196b-5p were seen upregulated in exosomes, potentially contributing to tumorigenic processes, enabling GB survival and proliferation. These miRNAs were previously reported as oncomiRs in GB and also targeted oncogenic pathways involved in proliferation, invasion, and metastasis. In GB, miR-92b-5p was seen targeting tumour suppressor genes such as *PTEN*, activating the PI3K/Akt pathway, which is essential for cell survival and proliferation (Song, *et al.,* 2016). Moreover, miR-92b was also observed to regulate the Wnt/β-catenin pathway through *DKK3*, which contributed to tumour growth and

poor prognosis (Li, *et al.,* 2013). Furthermore, miR-92b-5p was previously observed in the GB exosomal cargo, proposing its involvement in the communication between tumour cells and their microenvironment (Xu, *et al.,* 2019). Additionally, miR-196b-5p plays a significant oncogenic role in GB. When upregulated in GB, it leads to an unfavourable prognosis (Ma, *et al.,* 2012). Studies have reported that miR-196b promotes tumour cell proliferation, invasion, and migration by targeting key tumour suppressor pathways (Ma, *et al.,* 2012; Xu & Xu, 2020b). A further functional study indicated that miR-196b-5p suppressed apoptosis and enhanced GB growth through pathways like PTEN/Akt and NF-kB signalling (Yang, *et al.,* 2014b). Moreover, miR-196b-5p has been detected in the exosomal cargo of colorectal cancer, suggesting its role in facilitating intercellular communication and modulating the tumour microenvironment (Ren, *et al.,* 2019). These findings support our observations regarding the upregulation of miR-92b-5p and miR-196b-5p in GB exosomes and suggest their potential utilisation as a liquid biopsy biomarker for the malignancy.

Our proteomics exosome analysis did not identify the dysregulation of CORO1C and SV2B in GB patients. However, our western blotting, IF and IHC analysis pointed out that the proteins were overexpressed in GB and MB cell lines and patients. The discrepancy between exosome proteomics and western blotting, IF, and IHC results could be due to exosomal selectivity and heterogeneity (Hu, *et al.,* 2022). Exosomes selectively package certain proteins, so CORO1C and SV2B, while overexpressed in GB and MB cells, might not be included in exosomes. Furthermore, the overexpression of CORO1C and SV2B seen in GB and MB cells could be more relevant to intracellular processes rather than being exosome-bound. Proteins like CORO1C and SV2B function primarily within the cells themselves, regulating cytoskeletal organisation and synaptic vesicle activity, respectively, making their presence in exosomes less likely.

The proteomics analysis of GB exosomes revealed that most dysregulated proteins played part in key processes involved in tumour progression, particularly in pathways related to the actin cytoskeleton, coagulation cascades, immune modulation, and lipid metabolism. In our GB cohort, the most significantly dysregulated exosomal proteins included the von Willebrand factor (VWF), fibrinogen subunit beta (FGB), and Hemicentin 1 (HMCN1). VWF and FGB, both found upregulated in our analysis, play part in coagulation and support the formation of a pro-thrombotic environment. By promoting blood clotting and platelet adhesion, these proteins facilitate tumour vascularisation, which is crucial for maintaining an adequate blood supply to

the tumour (Liao, *et al.,* 2023). Furthermore, HMCN1, involved in extracellular matrix (ECM) organisation, enhances cell adhesion, migration, and invasion (Welcker, *et al.,* 2021). Its upregulation in exosomes could allow GB cells to manipulate their microenvironment, making it easier for tumour cells to invade surrounding tissues. This increased motility and invasive potential, supported by exosome-mediated ECM remodelling, is a hallmark of the aggressive behaviour of GB (Wortzel, Dror, Kenific & Lyden, 2019). Together, these dysregulated proteins potentially influence the coagulation pathways and ECM remodelling of GB to promote vascular growth and rapid progression of the malignancy, making them putative diagnostic biomarkers and/or therapeutic targets for GB.

In summary, our IHC results supported the *in vitro* findings of elevated protein expression of CORO1C and SV2B in GB and MB. Furthermore, sRNA-seq of paediatric MB patient samples showed the downregulation of miR-206 and miR-383, which target these genes, aligning with the observed downregulation of both miRNAs in MB and GB cells *in vitro*. Transcriptomics analysis of MB patient tissues also revealed upregulation of *CORO1C* and *SV2B* mRNAs, further confirming their oncogenic potential in paediatric brain malignancies. However, our exosomal GB sRNA-seq and proteomics analysis did not show these miRNAs or proteins as dysregulated, likely due to the fact that CORO1C and SV2B have more specialised roles in intracellular processes rather than being associated with exosome-mediated communication. These findings emphasised the clinical relevance of CORO1C and SV2B in high grade brain cancers, particularly as potential therapeutic targets.

Chapter 5. New GB therapies

5.1. Introduction

The complexity of GB, characterised by its highly infiltrative nature, microenvironment heterogeneity, and intrinsic repair capabilities, poses significant challenges to current treatment strategies (Karve, *et al.,* 2024). This necessitates the development of innovative therapies, drawing attention to new classes of synthetic compounds as promising alternative treatment options for this aggressive malignancy.

The β-amino carbonyl (β-AC) compounds, a class of synthetic molecules, have gained attention in cancer therapy due to their broad-spectrum activity and enhanced pharmacokinetic properties (Rambabu, *et al.,* 2022). These compounds have emerged as potential candidates in cancer therapy due to their ability to modulate various cellular pathways important for cancer progression. They often target key enzymes and proteins involved in cell proliferation, apoptosis, and metastasis (Andrés, Pérez de la Lastra, Bustamante Munguira, Andrés Juan & Pérez-Lebeña, 2024). For instance, some β-AC derivatives inhibit histone deacetylases (HDACs), leading to altered gene expression and suppression of tumour growth (Monneret, 2005). Others have been shown to interact with topoisomerases, disrupting DNA replication in rapidly dividing cancer cells. An example is the β-AC-based inhibitor of carbonic anhydrase IX (CAIX), an enzyme overexpressed in hypoxic tumour microenvironments, which is crucial for maintaining the acidic pH favourable to cancer cell survival (Mahon, Pinard & McKenna, 2015). Additionally, these compounds exhibit antineoplastic properties by interfering with mitochondrial structures, decreasing membrane potential, and generating reactive oxygen species (ROS), leading to programmed cell death (Lesgards, *et al.,* 2011). The versatility and bioactivity of β-AC compounds make them promising tools in the development of alternative GB therapies. Furthermore, their impact on the miRNome of GB cancer cells remains largely unexplored, presenting an alternative avenue for research that could reveal new mechanisms by which these compounds influence cancer cell behaviour and potentially enhance GB therapeutic strategies.

On the other hand, chalcones, a class of unsaturated ketones in the flavonoid family, have also shown promising anticancer properties through various mechanisms. These compounds are known to target multiple cellular pathways, making them effective against a wide range of

cancers, including those resistant to traditional therapies, such as GB (Constantinescu & Lungu, 2021). Their simple chemistry, ease of synthesis, and modifiable structure make them attractive for cancer treatment. One of the key anticancer activities of chalcones is their ability to inhibit tubulin polymerisation, which is essential for microtubule formation during cell division (Liu, He, Li, Peng & Wang, 2022). By interfering with microtubule dynamics, chalcones induce cell cycle arrest, particularly at the G2/M phase, leading to apoptosis (Ouyang, *et al.,* 2021). This mechanism is further enhanced in chalcones with trimethoxyphenyl or quinoline/quinazoline residues, which bind strongly to the colchicine binding site on tubulin (Constantinescu, *et al.*, 2021). Moreover, chalcones exert their anticancer effects by modulating signalling pathways such as PI3K/AKT, NF-kB, and MAPK (Michalkova, *et al.,* 2023). For instance, licochalcone A has been shown to suppress hexokinase-2-mediated glycolysis in gastric cancer cells and to inhibit the PI3K/Akt/mTOR pathway in breast cancer, resulting in reduced cell proliferation and increased apoptosis (Wu, *et al.,* 2018a; Xue, Zhang, Fan & Wang, 2018). Chalcones also impact apoptosis regulation by modulating the expression of pro-apoptotic and anti-apoptotic proteins (Zhu, *et al.,* 2019). For example, xanthohumol, a prenylated chalcone, has been shown to induce apoptosis in cancer cells by upregulating p53 and Bax while downregulating Bcl-2 and Bcl-xL, thereby promoting caspase activation and cell death (Harish, *et al.,* 2021). Furthermore, this chalcone was also evaluated for its effectiveness against GB using T98G cells. It was demonstrated that xanthohumol significantly reduced cell viability and promoted apoptosis, involving the cleavage of poly (ADP-ribose) polymerase (PARP) and the activation of both caspase-3 and caspase-9 in a concentration- and time-dependent manner (Festa, *et al.,* 2013). A recent study also demonstrated that the chalcone derivative 3',4',5'-trimethoxychalcone possessed significant antiproliferative and anti-invasion activities against GB cells (Alves, *et al.,* 2024). Nevertheless, research on how chalcone derivatives regulate the miRNome in GB cells is limited. It has been shown that a chalcone derivative from hops, Xanthohumol (XN), could kill GB cells by triggering cell death and targeting miR-204-3p, a tumour suppressor in GB (Chen, *et al.,* 2016). Given the prominent anticancer properties of chalcones and the largely unexplored potential of their effects on the miRNome within cancer cells, these compounds could offer alternative strategies for targeting GB cancer cells.

In the exploration of new cancer therapeutics, cellular functional assays are essential tools for the early-stage evaluation of their biological properties. These assays mimic the complex cellular processes *in vitro* and provide important information about the pharmacodynamics, efficacy, and mechanism of action of new therapeutics (Gordon, Brown & Reynolds, 2018).

Functional assays are designed to measure specific cellular responses to drug compounds, such as proliferation, colony formation, migration, and apoptosis. By quantifying these responses, the potency, efficacy, and potential toxicity of a new compound can be determined (Barba-Ostria, *et al.,* 2022). For example, cell proliferation assays, such as the MTT or bromodeoxyuridine (BrdU) assays, are widely used to assess the ability of a drug to inhibit or promote cell viability (Isobe, Yanagisawa & Michikawa,2001; Crane & Bhattacharya, 2013). These assays are valuable in cancer research, where the inhibition of uncontrolled cell proliferation is a primary therapeutic target. Furthermore, colony formation and migration assays are employed to study the effects of therapeutic compounds on the proliferative and migratory capabilities of cells, respectively (Gordon, *et al.,* 2018). These assays are relevant in cancer research, where the ability of cancer cells to form colonies and migrate is a key factor in tumour growth and metastasis. Additionally, the ROS assay is a biochemical assay used to detect and measure the levels of reactive oxygen species within cells or biological samples (Katerji, Filippova & Duerksen-Hughes, 2019). ROS assays are used in drug development to evaluate the effects of new compounds on ROS production. This is essential for determining whether a compound induces oxidative stress, which could lead to cellular damage or apoptosis, or if it has antioxidant properties that could be therapeutically beneficial. Furthermore, apoptosis assays, such as the DAPI and acridine orange and propidium iodide (AO/PI) staining assays, are techniques commonly used to assess cell morphology and apoptosis. DAPI is a fluorescent stain that binds strongly to the adenine-thymine rich regions in DNA, making it an effective tool for assessing the nuclear morphology of cells and apoptosis. In apoptotic cells, DAPI staining can reveal condensed or fragmented nuclei, which are characteristic of cells undergoing programmed cell death (Tarnowski, Spinale & Nicholson, 1991). On the other hand, AO/PI staining can distinguish between live, apoptotic, and necrotic cells, which is useful for evaluating the extent of apoptosis or necrosis in cell populations following various drug treatments (Liu, Liu, Liu & Wu, 2015). Since many anticancer drugs promote their effects by inducing apoptosis in cancer cells, these assays could be used in the evaluation of the pro-apoptotic effects of new compounds under exploration.

Moreover, the use of molecular techniques, such as RT-qPCR, alongside sequencing methods, can be employed in determining the expression levels of drug targets. The use of sRNA-seq, introduced in Chapter 4, has enabled detailed analysis of changes in miRNA expression, which can reveal effects on gene regulation triggered by the tested drug (Chen, *et al.,* 2024). These changes can indicate the mechanisms of action, potential therapeutic targets, or adverse effects

of the examined compound. Furthermore, these molecular approaches enable the elucidation of key pathways and molecular targets affected by the compound, providing an enhanced understanding of its biological effects. Following the analysis of sRNA-seq data, molecular docking can be considered to predict the binding affinity and interaction sites between the drug and its target molecules (Agu, *et al.,* 2023). This computational technique allows the prediction of the potential mechanisms of action by simulating how the drug interacts at the molecular level, providing a more comprehensive understanding of its biological effects. Simultaneously, the absorption, distribution, metabolism, excretion, and toxicity (ADMET) bioinformatic tools are essential in evaluating the pharmacological properties of new compounds (Dulsat, López-Nieto, Estrada-Tejedor & Borrell, 2023). These databases simulate and predict how the compound behaves within a biological system, comparing the results against established profiles of FDA-approved drugs. Thus, ADMET analyses are useful in assessing the safety and efficacy of new molecules early in the drug development process (Guan, *et al.,* 2018). The incorporation of these techniques enhances the understanding of the drug's impact at a molecular level, offering a comprehensive approach to evaluating new compounds before clinical testing.

5.1.2. Aims and research questions

5.1.2.1. Aims

In this chapter we aimed to investigate the therapeutic potential and efficacy of the in-house synthesised compounds, b3-(4-bromophenyl)-1-phenyl-3-(phenylamino)propan-1-one (SHG-8) and (E)-1-(4-chlorophenyl)-3-(p-tolyl)prop-2-en-1-one (SHG-44), in pre-clinical U87MG and U251MG GB cell line models. We also sought to elucidate the cellular mechanisms of action of these compounds by employing an array of functional assays and performing sRNA-seq to assess their effects on miRNA regulation within GB cells.

5.1.2.2. Research questions

1. How did the therapeutic efficacy of the in-house synthesised β-AC compound SHG-8 and the synthetic chalcone compound SHG-44 affect U87MG and U251MG GB cell line models?
2. What are the cellular mechanisms of action of SHG-8 and SHG-44 in GB cells, as revealed by the functional assays?

3. How do SHG-8 and SHG-44 influence miRNA regulation in GB cells, as determined by sRNA-seq, and what implications do potential changes have in the therapeutic response against GB?

5.2. Materials and Methods

5.2.1. SHG-8 synthesis and characterisation

In alignment with the sustainable development goals (SDGs) of the United Nations (UN) 2030 Agenda, a sustainable catalytic strategy was adopted in the synthesis of the β-AC SHG-8 compound (Weiland, Hickmann, Lederer, Marquardt & Schwindenhammer, 2021). Specifically, propyl sulfonic groups were functionalised via organosilylation-sulfonation on well-ordered silica nanospheres, resulting in the sulfonic acid-functionalised silica nanospheres (SAFSNS) nanocatalyst (Ahmad, Shagufta, Dhar, Hisaindee & Hasan, 2021). This SAFSNS nanocatalyst was efficiently utilised in the synthesis of SHG-8 through a three-component, one-pot Mannich reaction. The reaction involved a simple, efficient, and green catalytic process for the one-pot condensation of aromatic ketone, aromatic aldehyde, and aromatic amine using the environmentally benign solid acid SAFSNS nanocatalyst, leading to the production of a β-amino carbonyl compound. The catalytic reaction was conducted at ambient temperature using ethanol as the solvent. All starting materials, reagents, and solvents were obtained from Merck and Spectrochem and used without further purification unless otherwise stated (Merck, Feltham, UK; Specrochem, Mumbai, India). In the reaction procedure, acetophenone (1.1mmol), benzaldehyde (1mmol), and 4-bromobenzaldehyde (1mmol) were stirred in 2mL of ethanol at RT, with 0.04g of SAFSNS nanocatalyst added. The reaction mixture was stirred for 4h at RT. Upon completion, as indicated by thin-layer chromatography (TLC), the reaction mixture was allowed to evaporate at ambient temperature, yielding a yellow solid. This solid was dissolved in 10mL of dichloromethane at 35°C and filtered to remove the catalyst. The crude product was purified by recrystallisation in ethanol, resulting in the corresponding pure compound SHG-8, which was obtained as a light yellow solid. The progress of the reactions was monitored by TLC on silica gel plates, with spots visualised under ultraviolet (UV) light at 254nm. IR spectra were recorded on a PerkinElmer FTIR spectrophotometer (PerkinElmer, Massachusetts, USA), and mass spectra were measured using electrospray ionization mass spectrometry (ESI-MS) on a Shimadzu LCMS spectrophotometer (Shimadzu, Kyoto, Japan). The ^{1}H and ^{13}C NMR spectra of all synthesised compounds were recorded using a Bruker AV-400 spectrometer (Bruker, Massachusetts, USA) with tetramethylsilane as the internal standard. High-resolution mass spectrometry (HRMS) was performed on an Agilent 6540 HD Accurate Mass QTOF/LC/MS with electrospray ionisation (ESI) (Agilent, Manchester, UK). Notably, those experiments were performed at AURAK.

5.2.2. SHG-44 synthesis and characterisation

The reagents and solvents were obtained from Merck and Spectrochem and were used without further purification unless otherwise specified (Merck, Feltham, UK; Specrochem, Mumbai, India). The 10% NaOH solution (2.0mL) was added to a stirring mixture of 4-chloroacetophenone (1mol) and 4-methylbenzaldehyde (1mol) in 10 mL of ethanol at RT. The reaction mixture was stirred at RT for 15min. Upon completion, as indicated by TLC, the reaction mixture was poured into crushed ice under mildly acidic conditions to neutralise the sodium hydroxide. The resulting chalcone (SHG-44) precipitated as a solid, which was then filtered, washed with water, dried, and recrystallised from ethanol to yield the pure compound SHG-44 as a light yellow crystalline solid with an 85% yield. The reaction progress was monitored using TLC on silica gel plates, with spots visualised under UV light at 254nm. Infrared (IR) spectra were recorded on a PerkinElmer FTIR spectrophotometer (PerkinElmer, Massachusetts, USA) in ATR mode, with data reported in wave numbers ($cm^{-}1$). The melting points of the synthesised compound were determined using a Stuart (SMP 11) melting point apparatus (Sigma-Aldrich, Dorset, UK) with capillary tubes. High-resolution mass spectrometry was performed on an Agilent 6540 HD Accurate Mass QTOF/LC/MS with ESI (Agilent, Manchester, UK). ^{1}H NMR and ^{13}C NMR spectra were recorded using a Bruker Avance III HD 500 MHz NMR spectrometer (Bruker, Massachusetts, USA). Proton chemical shifts were reported in ppm (δ) relative to internal tetramethylsilane (TMS, δ 0.00) or with solvent reference relative to TMS (CDCl3, δ 7.26 ppm), with data presented as chemical shift multiplicity (singlet (s) and doublet (d), coupling constants (Hz), and integration. Carbon chemical shifts were reported in ppm (δ) relative to TMS, with the solvent resonance as the internal standard (CDCl3, δ 77.0 ppm). Notably, those experiments were performed at AURAK.

5.2.3. Cell culture

Two commercially available human GB cell lines, U87MG and U251MG (ATCC, Manassas, VA, USA) were cultured in MEM (Gibco™, Bleiswijk, NL) supplemented with 10% FBS (Gibco™, Bleiswijk, NL) and 1% penicillin-streptomycin (10,000 U/mL) (Gibco™, Bleiswijk, NL) to support cell growth. The cells were maintained at 37°C in an atmosphere of 5% CO_2. To evaluate the cytotoxic profiles of SHG-8 and SHG-44 on GB cells *in vitro*, the compounds were dissolved in sterile dimethyl sulfoxide (DMSO) (Thermofisher™, CA, USA) suitable for cell culture at a final concentration of 10mM.

5.2.4. Cell viability assay

To determine the cytotoxic effects of SHG-8 and SHG-44 on U251MG and U87MG GB cells, MTT assays were conducted (Gibco™, Bleiswijk, NL). Both U251MG and U87MG cells were seeded in 96-well plates at a density of 1.5×10^4 cells per well. The concentrations of SHG-8 and SHG-44 used for treating U87MG and U251MG cells are summarised in Table 13 below. All drugs were prepared using dimethyl sulfoxide (DMSO) as the solvent before treatment (Sigma-Aldrich™, Dorset, UK). DMSO alone (<1%) was used as a negative control, while cis-platin (200µM; Sigma-Aldrich™, Dorset, UK) served as a positive control for both cell lines. After a 24h incubation period under the treatment conditions, 5mg/mL of MTT dye was added to each treated well. The plates were then incubated for 2h at 37°C in 5% CO_2. Following the incubation, the MTT solution was removed, and 100% isopropanol (Sigma-Aldrich™, Dorset, UK) was added to dissolve the formazan crystals, with the plates left on a rocking platform for 30min. The absorbance values were measured at 590nm using a CLARIOstar microplate reader (BMG Labtech, Aylesbury, UK). Cellular viability was quantified based on these readings.

Table 13. Treatment concentrations of SHG-8 and SHG-44 in U87MG and U251MG cells (Cell viability assay). The table summarises the concentrations of SHG-8 and SHG-44 used for treating U87MG and U251MG GB cell lines. Control wells received either <1% DMSO as a negative control or 200µM cis-platin as a positive control, which served as reference points for evaluating the effects of the treatments.

Treatment	Cell line	Concentrations (µM)	Control conditions
SHG-8	U87MG	20, 40, 60, 80, 100, 120, 140	<1% DMSO (negative control), 200µM cis-platin (positive control)
SHG-8	U251MG	50, 100, 150, 200, 250, 300	<1% DMSO (negative control), 200µM cis-platin (positive control)
SHG-44	U87MG	10, 20, 40, 60, 80, 100	<1% DMSO (negative control), 200µM cis-platin (positive control)
SHG-44	U251MG	10, 20, 40, 60, 80, 100	<1% DMSO (negative control), 200µM cis-platin (positive control)

5.2.5. Colony formation assay

To assess the colony formation potential of U87MG and U251MG cells, both cell lines were seeded at a density of 500 cells per well in triplicate on 12-well plates. The specific treatment concentrations and control conditions for SHG-8 and SHG-44 in U87MG and U251MG cells are shown in Table 14 below. After 24h of treatment in complete media, the drug-supplemented media were removed and replaced with fresh media, and the cells were further incubated for five days at 37°C and 5% CO_2 in a humidified incubator to allow colony formation. Control wells were treated with <1% DMSO as a negative control and 200 µM cis-platin as a positive

control. After the incubation period, colonies were fixed with 4% paraformaldehyde (PFA; Sigma-Aldrich™, Dorset, UK) for 25min, followed by staining with 0.1% crystal violet for 20min (Sigma-Aldrich™, Dorset, UK). The stained colonies were washed with distilled water and allowed to air dry overnight. Colonies containing more than 30 cells were photographed and quantitatively assessed using a light microscope (Olympus Life Science Solutions, Stansted, UK).

Table 14. Treatment concentrations of SHG-8 and SHG-44 in U87MG and U251MG cells (Colony formation assay). The table presents the concentrations of SHG-8 and SHG-44 used for treating U87MG and U251MG cells, and the corresponding control conditions.

Treatment	Cell line	Concentrations (µM)	Control conditions
SHG-8	U87MG	50, 100	<1% DMSO (negative control), 200µM cis-platin (positive control)
SHG-8	U251MG	50, 100	<1% DMSO (negative control), 200µM cis-platin (positive control)
SHG-44	U87MG	70, 100	<1% DMSO (negative control), 200µM cis-platin (positive control)
SHG-44	U251MG	50, 100	<1% DMSO (negative control), 200µM cis-platin (positive control)

5.2.6. Scratch assay

A wound healing assay was conducted to assess the migration ability of U87MG and U251MG cells. Both cell lines were seeded in a 12-well plate at a density of 2.5×10^5 cells per well. Once the cells had been attached, a linear scratch was made across the cell monolayer using a 2µL pipette tip. The wells were washed twice with PBS to remove any debris created during the scratching process. The treatment concentrations of SHG-8 and SHG-44 for U87MG and U251MG cells are outlined in Table 15. In both cell lines, <1% DMSO was used as a negative control, and 200µM cis-platin served as a positive control. Microscopic images of the scratch midlines were captured at 0h, 24h, and 48h post-treatment using a light-phase microscope. The migration of cells into the scratch area was analysed using ImageJ (Java, Redwood Shores, CA, USA) software with the wound healing plugin (Schneider, Rasband & Eliceiri, 2012; Suarez-Arnedo, *et al.,* 2020). The percentage of the healed area at 24h and 48h was normalised to the initial scratch size at 0h (t0) to facilitate comparison across different treatment conditions.

Table 15. Treatment concentrations of SHG-8 and SHG-44 in U87MG and U251MG cells (Scratch assay). The table presents the concentrations of SHG-8 and SHG-44 used for treating U87MG and U251MG GB cell lines. Control wells were treated with DMSO at less than 1% (negative control) and 200µM cis-platin (positive control) providing reference conditions to evaluate the effects of the treatments.

Treatment	Cell line	Concentrations (µM)	Control conditions
SHG-8	U87MG	20, 40	DMSO (<1% as negative control), 200µM cis-platin (positive control)
SHG-8	U251MG	50, 100	DMSO (<1% as negative control), 200µM cis-platin (positive control)
SHG-44	U87MG	70, 100	DMSO (<1% as negative control), 200µM cis-platin (positive control)
SHG-44	U251MG	50, 100	DMSO (<1% as negative control), 200µM cis-platin (positive control)

5.2.7. Reactive oxygen species assay

A ROS assay kit (CellROX® Deep Red Reagent, Abcam, Cambridge, UK) was used to evaluate ROS release in U87MG and U251MG GB cell lines post-exposure to SHG-8 and SHG-44. Both cell lines were seeded in 96-well plates at a density of 1.5×10^4 cells per well. Following seeding, cells were pre-treated with 20µL of red ROS dye stock solution, specifically designed to detect superoxide and hydroxyl radicals, diluted in 10mL of assay buffer according to the manufacturer's instructions and incubated for 1h at 37°C and 5% CO_2. After dye incubation, cells were treated with increasing concentrations of either SHG-8 or SHG-44 as outlined in Table 16. PBS was used as a negative control, and 1mM H_2O_2 (Sigma-Aldrich™, Dorset, UK) served as a positive control for both treatments. In this assay, the drug dilutions were performed in PBS, and 20µL was added to each well. Fluorescence intensity, representing ROS levels, was measured at an excitation wavelength of 520nm and an emission wavelength of 605nm using a CLARIOstar microplate reader (BMG Labtech, Aylesbury, UK). Measurements were taken at multiple time points: 0min, 15min, 30min, 45min, 60min, 75min, 90min, 105min, and 120min.

Table 16. Treatment concentrations of SHG-8 and SHG-44 in U87MG and U251MG cells (ROS assay). The table summarises the treatment concentrations of SHG-8 and SHG-44 used for both U87MG and U251MG GB cell lines. PBS was used as a negative control, while 1mM H_2O_2 served as the positive control for both treatments.

Treatment	Cell line	Concentrations (µM)	Control conditions
SHG-8	U87MG and U251MG	50, 100	PBS (negative control), 1 mM H_2O_2 (positive control)
SHG-44	U87MG and U251MG	40, 60, 80, 100	PBS (negative control), 1 mM H_2O_2 (positive control)

5.2.8. 4′,6-diamidino-2-phenylindole, dihydrochloride staining

U87MG and U251MG cells were seeded at a density of 3×10^4 cells per well. After an overnight incubation, cells were treated as outlined in Table 17 for 24h. Following treatment, the culture media were aspirated, and the cells were washed twice with PBS for 1min. The cells were then fixed with 4% PFA for 25min at RT, followed by two additional PBS washes for 3min each. To visualise the nuclei, cells were counterstained with DAPI (ThermoFisher™, CA, USA) in mounting media, and coverslips were mounted onto the slides. Immunofluorescence images were captured using a 40x objective on an EVOS fluorescent microscope (Life Technologies, CA, USA) with a pre-set exposure of 30lx/s.

Table 17. Treatment concentrations of SHG-8 and SHG-44 in U87MG and U251MG cells (DAPI assay). The table summarises the treatment compounds and the concentrations used for U87MG and U251MG cells. DMSO was used as a negative control (<1%), and cis-platin (200µM) as a positive control. SHG-8 and SHG-44 treatments were applied at the specified concentrations for each cell line, with control conditions consistent across all treatments.

Treatment	Cell line	Concentrations (µM)	Control conditions
SHG-8	U87MG	50, 100	DMSO (<1% as negative control), 200µM cis-platin (positive control)
SHG-8	U251MG	50, 100	DMSO (<1% as negative control), 200µM cis-platin (positive control)
SHG-44	U87MG	70, 100	DMSO (<1% as negative control), 200µM cis-platin (positive control)
SHG-44	U251MG	50, 100	DMSO (<1% as negative control), 200µM cis-platin (positive control)

5.2.9. Acridine Orange/Ethidium bromide staining

U87MG and U251MG cells were seeded at a density of 5×10^5 cells per well in six-well chambers and treated as outlined in Table 18 for 24h. Following treatment, the media were removed, and the cells were washed twice with PBS for 1min. The cells were then trypsinised

and pelleted by centrifugation at 200g for 5min. The pellets were resuspended in 1mL of ice-cold PBS and centrifuged again under the same conditions. After the second centrifugation, the pellets were resuspended in 20µL of ice-cold PBS and stained with 2µL of acridine orange (100µg/mL) and ethidium bromide (100µg/mL) (ThermoFisher, CA, USA) for 3min at RT. The stain mix was prepared by adding 1µl of AO and 1µl of EB into 25µl of PBS. The stained cell suspension was then mounted on glass slides, covered with coverslips, and immunofluorescence images were captured using a 40× objective on an EVOS fluorescent microscope with a preset exposure of 30lx/s. Viable cells exhibit green fluorescence due to AO binding to double-stranded DNA, indicating intact cell membranes. Early apoptotic cells show green fluorescence with some orange/red fluorescence as AO binds to both DNA and RNA, reflecting early membrane alterations. Late apoptotic or necrotic cells display prominent red fluorescence as EtBr binds to DNA upon membrane compromise, indicating loss of cell integrity. This combination enables precise identification of cell viability stages.

Table 18. Treatment concentrations of SHG-8 and SHG-44 in U87MG and U251MG cells (acridine orange/ethidium bromide staining assay). The table summarises the treatment compounds and the concentrations used for U87MG and U251MG cells. DMSO was used as a negative control (<1%), and cis-platin (200µM) was used as a positive control.

Treatment	Cell line	Concentrations (µM)	Control conditions
SHG-8	U87MG and U251MG	50, 100	DMSO (<1% as negative control), 200µM cis-platin (positive control)
SHG-44	U87MG and U251MG	70, 100	DMSO (<1% as negative control), 200µM cis-platin (positive control)

5.2.10. RNA isolation, preparation of samples for sRNA-seq, and sRNA-seq

U87MG RNA samples were extracted from SHG-8/SHG-44 treated cells and DMSO control samples, as described in Chapter 3. In brief, total RNA was extracted with Trizol reagent (Ambion Life Technology, Aukland, New Zealand). A nanodrop bioanalyzer was used to detect the concentration of each sample (Nanodrop ND1000 Spectrophotometer, Marshall Scientific, Hampton, USA). RNA integrity was assessed as described in Chapter 4 using the RNA Screen Tape Kit in the Agilent Bioanalyzer 2100 system (Agilent Technologies, CA, USA). Samples with RIN numbers greater than seven were sent off for external sRNA-seq to Biomarker Technologies (Biomarker Technologies, Berlin, Germany). Small RNA library preparation was performed using 1.5µg RNA per sample via the NEBNext® Ultra™ Illumina kit (New England

Biolabs, Ipswich, UK). This involved 3' and 5' adapter ligation and reverse transcription. Finally, PCR amplification and size selection enriched the samples for small RNA libraries. Libraries were then clustered and sequenced on an Illumina HiSeq platform. Raw data was processed to remove low-quality reads and filter for lengths of the RNA between 18-30 nucleotides. Clean reads were used for downstream analyses. Reads were aligned against databases to remove rRNA, tRNA, and other non-coding RNAs. Known and novel miRNAs were identified. Differential expression analysis was performed to compare miRNA levels between the DMSO and SHG-8/SHG-44 groups.

5.2.11. TaqMan Expression Assays

RT-qPCR was performed as described in Chapter 3. In brief, total RNA and miRNAs were extracted using the Trizol reagent (Ambion Life Technology, Auckland, New Zealand) and the mirVana isolation kit (ThermoFisher, Vilnius, Lithuania), respectively. The quantity and quality of the samples were assessed with a Nanodrop spectrophotometer (Nanodrop ND1000, Marshall Scientific, Hampton, USA). cDNA synthesis for genes was carried out using a Thermal cycler (Eppendorf Mastercycler Nexus Gradient, ThermoFisher, CA, USA) and the High-Capacity cDNA Reverse Transcription Kit (Applied Biosystems ThermoFisher, Pleasanton, CA). cDNA synthesis for miRNAs was carried out using the MicroRNA Reverse transcription kit (Applied Biosystems ThermoFisher, Pleasanton, CA). RT-qPCR experiments were conducted using the QuantStudio™ Real-Time PCR system (Quant Studio 7 Flex, Applied Biosystems, Massachusetts, USA). The thermal cycler settings used for cDNA synthesis and RT-qPCR during mRNA and miRNA profiling are outlined in Table 19 and Table 20, respectively. Expression analysis was performed using specific primers for each gene and miRNA, and the $2^{-\Delta\Delta Ct}$ method was applied to compare the relative differences between SHG-8/SHG-44 treated U87MG samples and U87MG DMSO control samples.

Table 19. Thermal cycler settings for cDNA synthesis. The table shows the cDNA synthesis settings used for mRNA and miRNA profiling.

Profiling type	Step	Temperature (°C)	Time
mRNA profiling	Annealing	25	10min
	DNA polymerisation	37	120min
	Enzyme deactivation	85	5min
miRNA profiling	Annealing	16	30min
	DNA polymerisation	42	30min
	Enzyme deactivation	85	5min

Table 20. Settings for RT-qPCR. This table shows the RT-qPCR steps for mRNA and miRNA profiling.

Profiling type	Step	Temperature (°C)	Time	Cycles
mRNA profiling	Enzyme activation	95	20sec	1
	Denaturation	95	1sec	40
	Annealing	60	20sec	
miRNA profiling	Enzyme activation	95	10min	1
	Denaturation	95	15sec	40
	Annealing	60	1min	

5.2.12. Molecular docking

The crystal structures of human CORO1C were obtained from the Protein Data Bank (https://www.rcsb.org), whereas the crystal structure for human SV2B was obtained from the AlphaFold protein structure database (https://alphafold.ebi.ac.uk). Docking analysis was conducted using CB-DOCK2 (https://cadd.labshare.cn/cb-dock2/index.php) to predict the stable binding configurations and molecular interactions between the receptors (CORO1C and SV2B) and the ligands SHG-8 and SHG-44. SDF files of the ligands were uploaded to CB-DOCK2, and blind docking was performed. The molecular docking outcomes for both SHG-8 and SHG-44 with the target proteins were visualised using BioLip (version of 2021.09.15) (Yang, Roy & Zhang, 2013).

5.2.13. *In silico* analysis of SHG-8 and SHG-44 and their metabolites

The metabolites of SHG-8 and SHG-44 were predicted using Biotransformer 3.1.0 with the canonical simplified molecular-input line-entry system (SMILES) (Wishart, *et al.,* 2022). For both compounds, the "Human and Human Gut" metabolic transformations set was selected with one reaction iteration and the "combined CYP450 mode." Following metabolite prediction, the absorption, distribution, metabolism, excretion, and toxicity (ADMET) properties of SHG-8, SHG-44, and their respective metabolites were assessed using admetSAR 2.0 (Yang, *et al.,* 2019). The "ADMET properties for drug discovery" option was selected within admetSAR 2.0, a machine learning tool that utilises molecular similarity data from 96,000 compounds to predict ADMET properties tailored for drug discovery applications.

5.2.14. Data availability

The sRNA-seq data for the SHG-8 treatment of U87MG cells were uploaded on the Mendeley Data 10.17632/v5mcf8hpsz.1. Similarly, the sRNA-seq data for the SHG-44 experiments were uploaded on the same database 10.17632/4sg8c7xz8c.1.

5.2.15. Statistics

Statistical analysis and graphical representations were performed using GraphPad Prism 9.4.1 software (GraphPad Software, San Diego, USA). Results were obtained from three independent experiments (n=3). Statistical analysis of MTT cell viability, colony formation, and migration assays was performed using an ordinary one-way ANOVA followed by Dunnett's multiple comparison test. Quantitative ROS and AO/EB staining experiments were analysed using a two-way ANOVA, also followed by Dunnett's multiple comparison test. For comparing RT-qPCR expression levels between SHG-8/SHG-44 treated GB cells and DMSO controls, an ordinary one-way ANOVA was conducted, followed by Dunnett's multiple comparisons test to identify significant differences. A p-value of <0.05 was considered statistically significant. Differential expression analysis for sRNA-seq was conducted using the DESeq R package for samples with biological replicates, with statistical routines based on the negative binomial distribution and p-values adjusted via the Benjamini and Hochberg method, while for samples without biological replicates, IDEG6 was used with p-values adjusted using q-value, setting a threshold of q-value <0.005 and $|\log2(\text{fold change})| \geq 1$ for significant differential expression (Haynes, 2013; Storey & Tibshirani, 2003).

5.3. Results

5.3.1. Synthesis and characterisation of SHG-8

The sustainable SAFSNS nanocatalyst was synthesised and characterised following the procedure outlined by Ahmad and colleagues (Ahmad, *et al.*, 2021). A mixture of acetophenone (1.1mmol), benzaldehyde (1mmol), and 4-bromo benzaldehyde (1mmol) was stirred in 2mL of ethanol at RT. Then, the SAFSNS nanocatalyst (0.04g) was added to the solution, and the reaction mixture was stirred for 4h (Figure 85). The progress of the reaction was monitored by TLC and the product of the reaction was characterised using IR, ^{1}H-NMR, ^{13}C-NMR, and HRMS techniques (Figures 86-90). The synthesised compound, SHG-8 was obtained with a yield of 85%. It appeared as a light-yellow solid with a melting point of 122-126°C. The characterisation data were as follows: FT-IR (cm^{-1}): 3391 (NH), 1667 (CO), 1601, 1483, 1284, 744, 681 (Figure 86); ^{1}H NMR (400 MHz, $CDCl_3$): δ 3.41-3.45 (m, 2H, $COCH_2$), 4.56 (s, 1H, NH), 4.96 (t, 1H, NHCH), 6.53 (d, J = 8 Hz, 2H, ArH), 6.68 (t, 1H, ArH), 7.07-7.11 (m, 2H, ArH), 7.31 (d, J = 8 Hz, 2H, ArH), 7.42-7.57 (m, 4H, ArH), 7.55-7.57 (m, 1H, ArH), 7.79 (d, J = 8 Hz, 2H, ArH) (Figure 87); ^{13}C NMR (400 MHz, $CDCl_3$): δ 45.9, 54.1, 113.8, 118.6, 121.3, 128.2, 128.3, 128.8, 129.4, 132.0, 133.7, 136.7, 142.3, 146.3, 197.9 (Figure 88). MS (ESI): m/z 380 (M+1) (Figure 89). HRMS (ESI): m/z calculated for $C_{21}H_{19}BrNO$ $[M+H]^+$: 380.0645; found: 380.0639 (Figure 90) (Ahmad, *et al.,* 2023). The synthesis of the SHG-8 compound was conducted in collaboration with the University of Ras Al-Khaimah, UAE, as part of the broader research project.

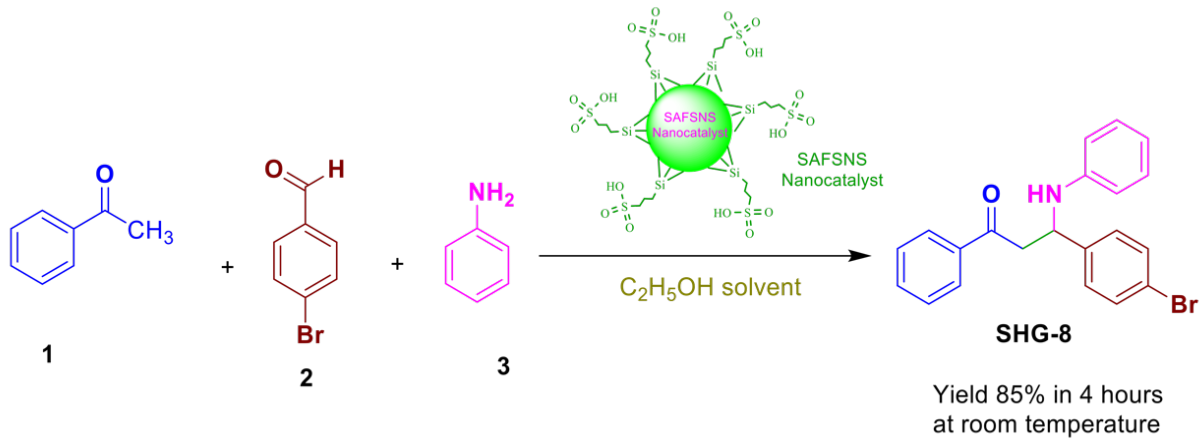


Figure 85. SHG-8 synthesis reaction. A three-component reaction involving acetophenone, 4-bromo benzaldehyde, and aniline, catalysed by SAFSNS was employed to synthesise the target compound SHG-8. The SAFSNS catalyst was effectively utilised in the synthesis of SHG-8 (4) via the Mannich reaction. This process involved a simple, efficient, and green catalytic method for the one-pot condensation of an aromatic ketone (1), aromatic aldehyde (2), and aromatic amine (3) using an environmentally friendly solid acid catalyst at RT. The synthesis of the SHG-8 compound was conducted in collaboration with the University of Ras Al-Khaimah, UAE, as part of the broader research project.

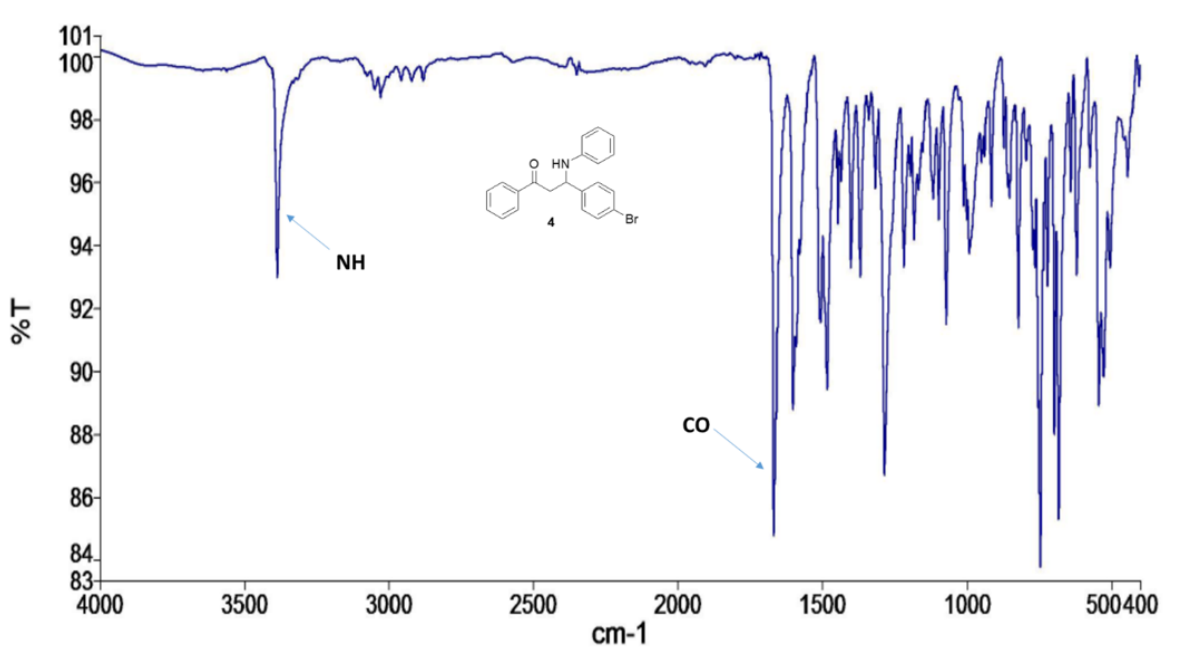


Figure 86. FT-IR spectrum of SHG-8. FT-IR spectrum of the synthesised compound SHG-8, showing characteristic absorption bands at 3391cm^{-1} (NH stretch) and 1667cm^{-1} (CO stretch). The image was obtained and modified from Ahmad, *et al.,* 2023. The synthesis of the SHG-8 compound was conducted in collaboration with the University of Ras Al-Khaimah, UAE, as part of the broader research project.

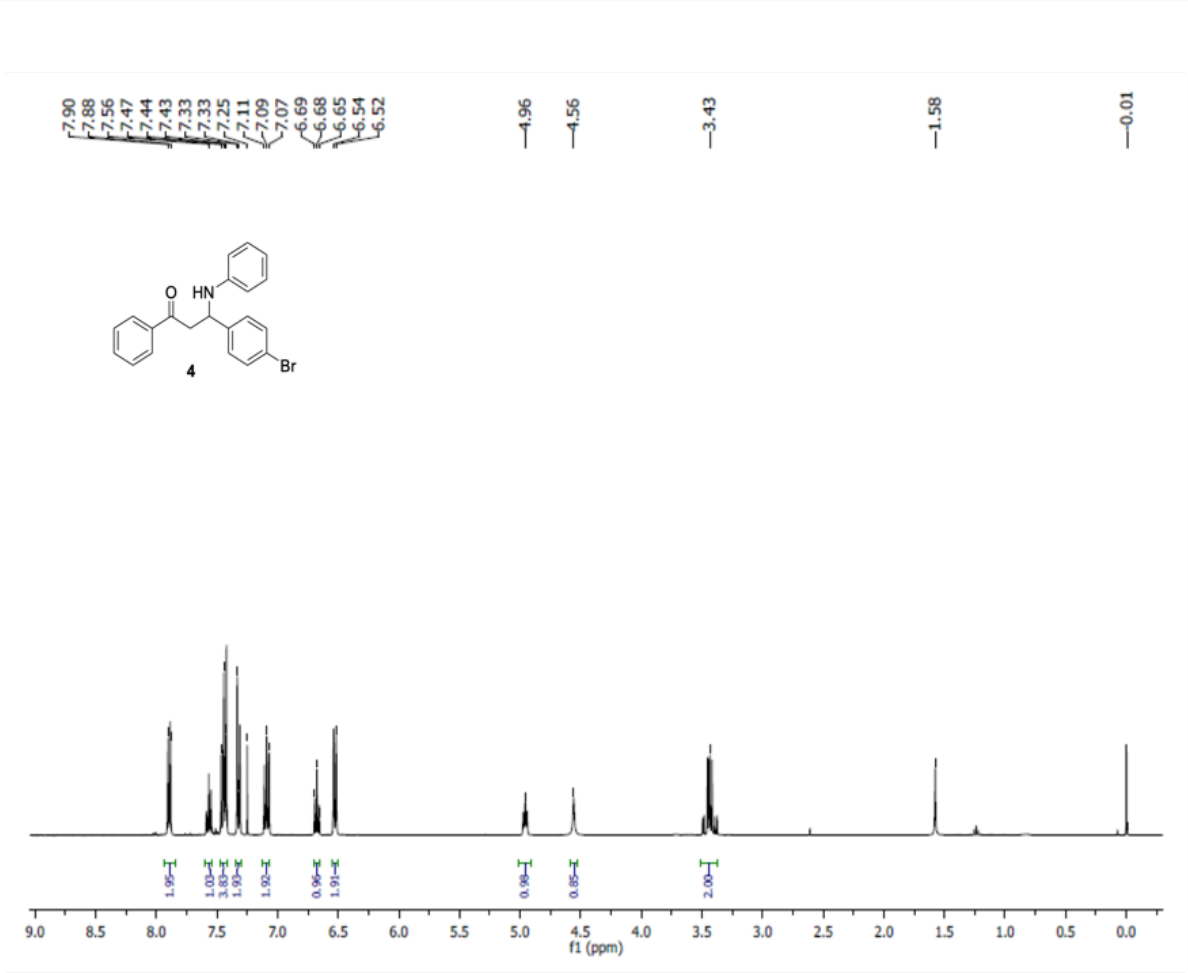


Figure 87. ^{1}H NMR spectrum of SHG-8 in $CDCl_3$. ^{1}H NMR spectrum (400 MHz, $CDCl_3$) of the synthesised compound SHG-8, displaying chemical shifts at δ 3.41-3.45 ppm (multiplet, 2H, $COCH_2$), 4.56 ppm (singlet, 1H, NH), 4.96 ppm (triplet, 1H, NHCH), 6.53 ppm (doublet, J = 8 Hz, 2H, ArH), 6.68 ppm (triplet, 1H, ArH), 7.07-7.11 ppm (multiplet, 2H, ArH), 7.31 ppm (doublet, J = 8 Hz, 2H, ArH), 7.42-7.57 ppm (multiplet, 4H, ArH), 7.55-7.57 ppm (multiplet, 1H, ArH), and 7.79 ppm (doublet, J = 8 Hz, 2H, ArH). The image was obtained and modified from Ahmad, *et al.,* 2023. The synthesis of the SHG-8 compound was conducted in collaboration with the University of Ras Al-Khaimah, UAE, as part of the broader research project.

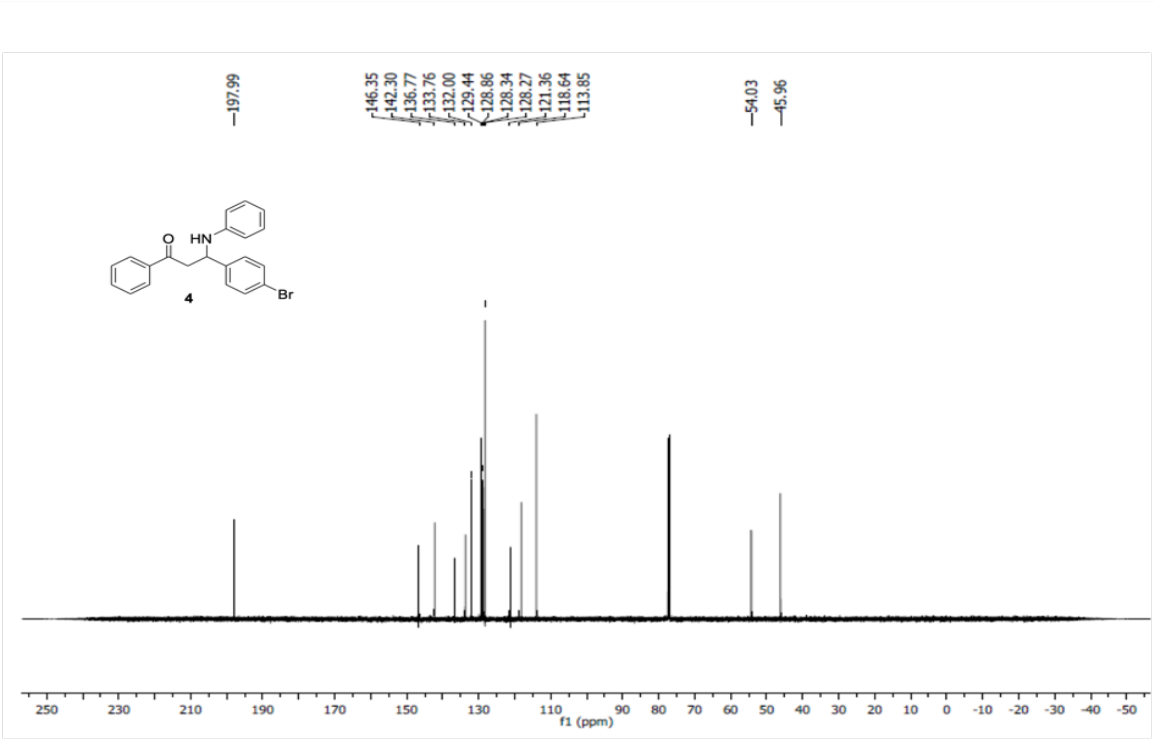


Figure 88. ^{13}C NMR spectrum of SHG-8 in $CDCl_3$. ^{13}C NMR spectrum (400 MHz, $CDCl_3$) of the synthesised compound SHG-8, showing chemical shifts at δ 45.9 ppm, 54.1 ppm, 113.8 ppm, 118.6 ppm, 121.3 ppm, 128.2 ppm, 128.3 ppm, 128.8 ppm, 129.4 ppm, 132.0 ppm, 133.7 ppm, 136.7 ppm, 142.3 ppm, 146.3 ppm, and 197.9 ppm. The image was obtained and modified from Ahmad, et al., 2023. The synthesis of the SHG-8 compound was conducted in collaboration with the University of Ras Al-Khaimah, UAE, as part of the broader research project.

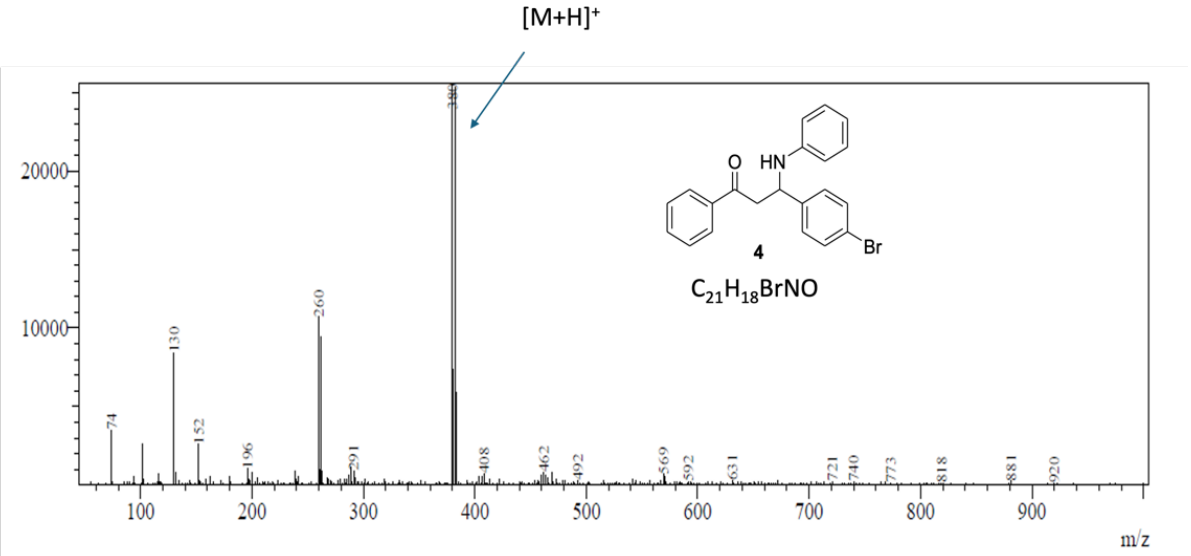


Figure 89. ESI-MS spectrum of SHG-8. Mass spectrum of the synthesised compound SHG-8 showing a molecular ion peak at m/z 380 ($[M^{+1}]^+$). The image was modified from Ahmad, et al., 2023. The synthesis of the SHG-8 compound was conducted in collaboration with the University of Ras Al-Khaimah, UAE, as part of the broader research project.

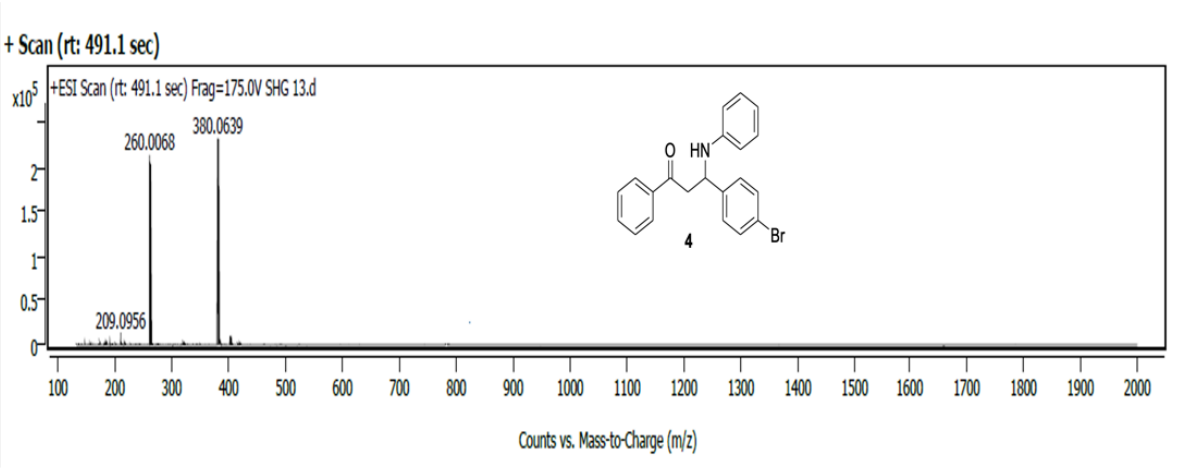


Figure 90. High-resolution mass spectrum of SHG-8. HRMS (ESI) confirmed the molecular ion with a calculated m/z for $C_{21}H_{19}BrNO$ $[M+H]^+$ of 380.0645 and a found m/z of 380.0639. The image was obtained and modified from Ahmad, *et al.,* 2023. The synthesis of the SHG-8 compound was conducted in collaboration with the University of Ras Al-Khaimah, UAE, as part of the broader research project.

5.3.2. Synthesis and characterisation of SHG-44

The SHG-44 compound was synthesised through the conventional Claisen-Schmidt condensation reaction (Firmino, *et al.,* 2022). In this method, 4-chloroacetophenone (1) and 4-methylbenzaldehyde (2) were reacted in the presence of sodium hydroxide as a catalyst at RT in ethanol, resulting in the formation of SHG-44 (Figure 91). The synthesised compound was characterised using various techniques, including melting point determination, FT-IR, HRMS, and ^{1}H-NMR and ^{13}C-NMR spectroscopy (Figures 92-95). The melting point of SHG-44 was recorded as 160-165°C. In the FT-IR spectrum of SHG-44, a sharp peak at 1657 cm^{-1} confirmed the presence of the C=O group. Additionally, very weak peaks at 3026 and 2918 cm^{-1} corresponded to sp^2 and sp^3 C–H bonds, respectively. The medium and strong peaks at 1599 cm^{-1} and 988 cm^{-1} were attributed to aromatic C=C and trans C=C vibrations, respectively (Figure 92). Analysis of the ^{1}H- and ^{13}C-NMR spectra revealed the following chemical shifts: ^{1}H-NMR (500 MHz, $CDCl_3$) δ/ppm: 2.40 (s, 3H, -CH_3), 7.23 (d, 2H, J = 10 Hz, Ar–H), 7.44 (d, 1H, J = 15 Hz, C=C trans), 7.47 (d, 2H, J = 10 Hz, Ar–H), 7.54 (d, 2H, J = 10 Hz, Ar–H), 7.80 (d, 1H, J = 15 Hz, C=C trans), 7.94 (d, 2H, J = 10 Hz, Ar–H) (Figure 93). ^{13}C-NMR ($CDCl_3$) δ/ppm: 21.58 (-CH_3), 120.5 & 145.4 (C=C trans), 189.3 (C=O), 128.5, 128.9, 129.7, 129.9, 131.9, 136.6, 139.1, 141.3 (aromatic carbons) (Figure 94). In the HRMS (ESI) spectrum, the observed m/z peak at 257.0711 corresponded closely with the calculated m/z value of 257.0733 for $C_{16}H_{14}ClO$ $[M+H]^+$, with a delta value of 0.0022 (Figure 95). The synthesis of the

SHG-44 compound was conducted in collaboration with the University of Ras Al-Khaimah, UAE, as part of the broader research project.

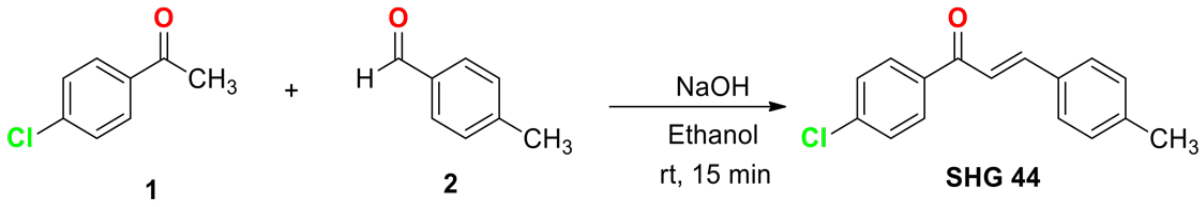


Figure 91. SHG-44 synthesis reaction. Synthesis of SHG-44 via the conventional Claisen-Schmidt condensation reaction where 4-chloroacetophenone (1) and 4-methylbenzaldehyde (2) were reacted in ethanol at RT using sodium hydroxide as a catalyst, leading to the formation of the target compound SHG-44. The synthesis of the SHG-44 compound was conducted in collaboration with the University of Ras Al-Khaimah, UAE, as part of the broader research project.

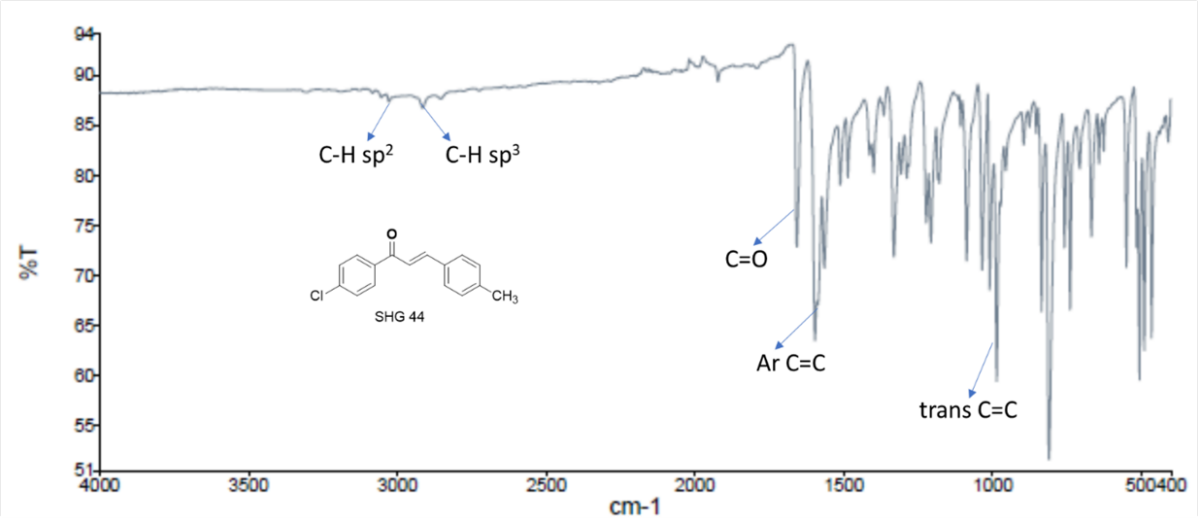


Figure 92. FT-IR spectrum of SHG-44. FT-IR spectrum of SHG-44 displayed a sharp peak at 1657 cm^{-1} confirming the presence of the C=O group. Weak peaks at 3026 cm^{-1} and 2918 cm^{-1} correspond to sp^2 and sp^3 C–H bonds, respectively. The medium and strong peaks at 1599 cm^{-1} and 988 cm^{-1} were associated with the aromatic C=C and trans C=C vibrations, respectively. The synthesis of the SHG-44 compound was conducted in collaboration with the University of Ras Al-Khaimah, UAE, as part of the broader research project.

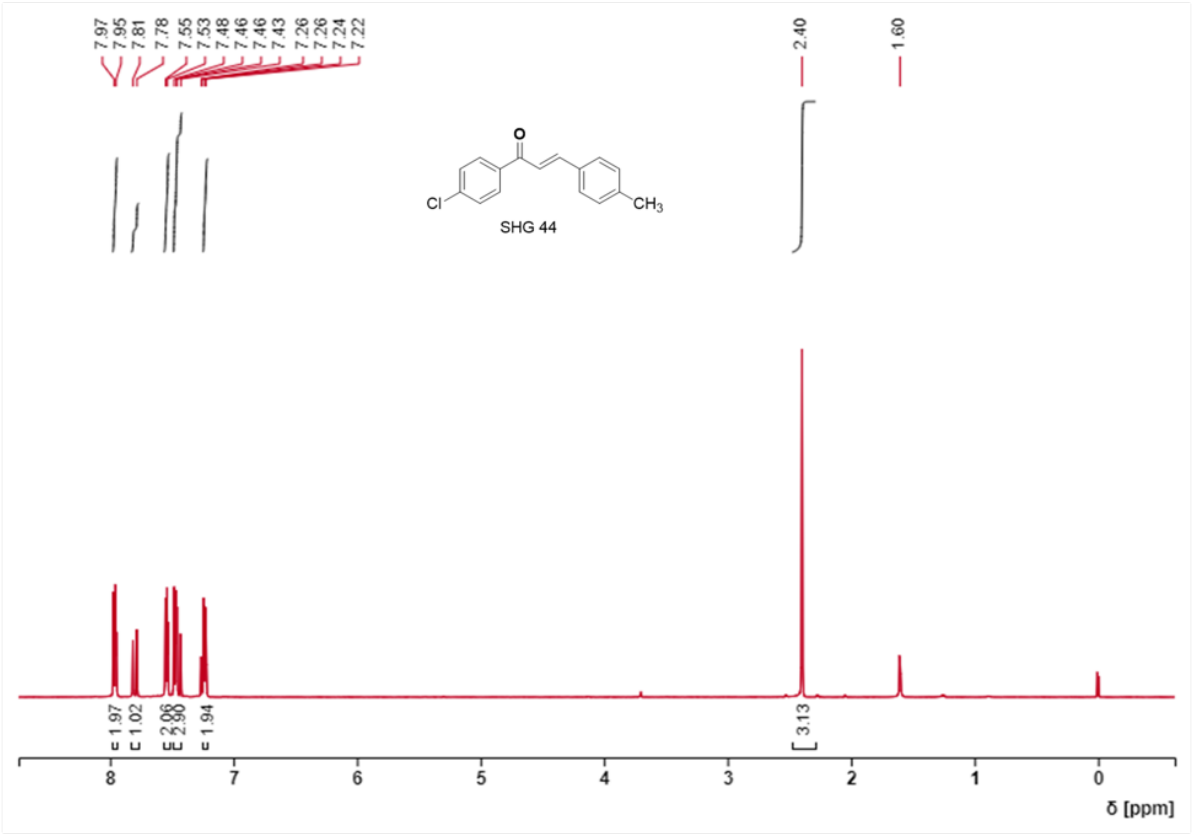


Figure 93. ^{1}H NMR spectrum of SHG-44 in $CDCl_3$. ^{1}H-NMR spectrum (500 MHz, $CDCl_3$) of SHG-44, showing chemical shifts at δ/ppm: 2.40 (singlet, 3H, -CH_3), 7.23 (doublet, 2H, J = 10 Hz, Ar–H), 7.44 (doublet, 1H, J = 15 Hz, C=C trans), 7.47 (doublet, 2H, J = 10 Hz, Ar–H), 7.54 (doublet, 2H, J = 10 Hz, Ar–H), 7.80 (doublet, 1H, J = 15 Hz, C=C trans), and 7.94 (doublet, 2H, J = 10 Hz, Ar–H). The synthesis of the SHG-44 compound was conducted in collaboration with the University of Ras Al-Khaimah, UAE, as part of the broader research project.

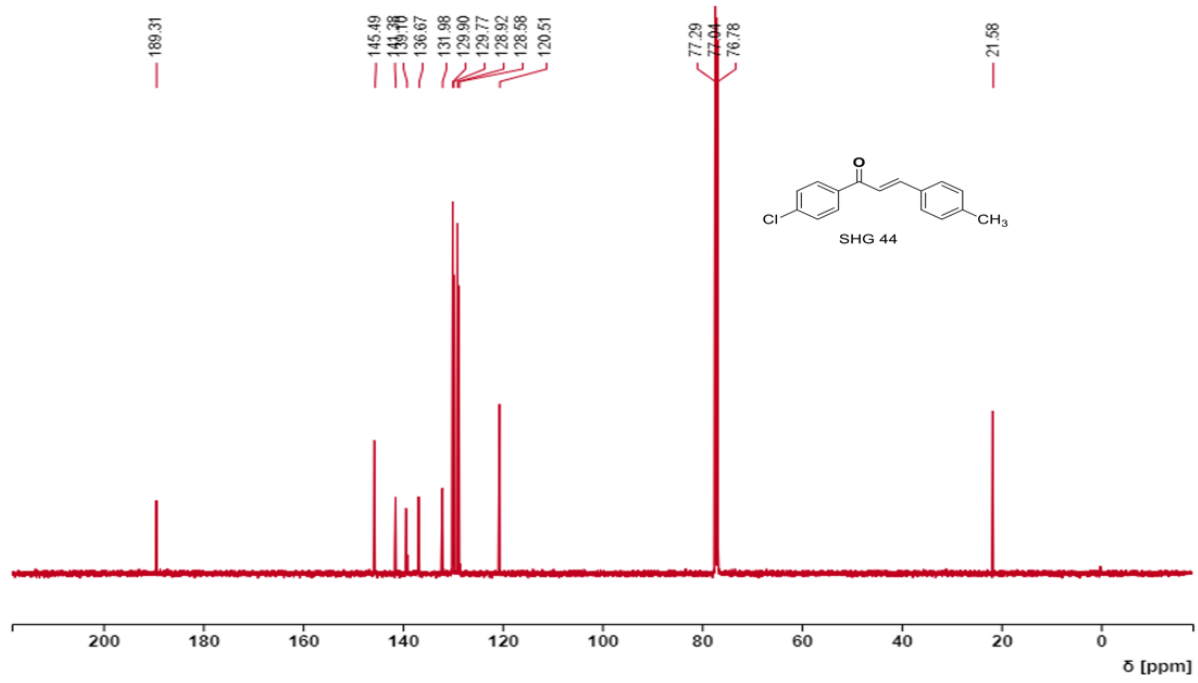


Figure 94. ^{13}C NMR spectrum of SHG-44 in $CDCl_3$. ^{13}C-NMR spectrum ($CDCl_3$) of SHG-44, displaying chemical shifts at δ/ppm: 21.58 (-CH_3), 120.5 and 145.4 (C=C trans), 189.3 (C=O), and 128.5, 128.9, 129.7, 129.9, 131.9, 136.6, 139.1, and 141.3 (aromatic carbons). The synthesis of the SHG-44 compound was conducted in collaboration with the University of Ras Al-Khaimah, UAE, as part of the broader research project.

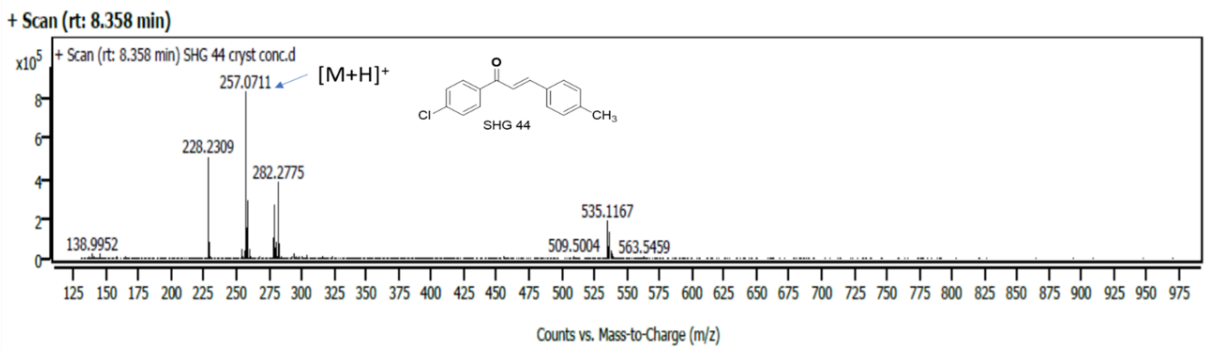


Figure 95. High-resolution mass spectrum of SHG-44. HRMS (ESI) spectrum of SHG-44, showing an observed m/z peak at 257.0711, which closely matched the calculated m/z value of 257.0733 for $C_{16}H_{14}ClO$ $[M+H]^+$, with a delta value of 0.0022, indicating high accuracy in the mass measurement. The synthesis of the SHG-44 compound was conducted in collaboration with the University of Ras Al-Khaimah, UAE, as part of the broader research project.

5.3.3. SHG-8 and SHG-44 cell viability assays

To evaluate the cytotoxic effects of SHG-8 and SHG-44 on GB cells, MTT cell viability assays were performed on U251MG and U87MG cell lines. After an incubation time of 24 hours for the drug treatments, the MTT assay results indicated a significant reduction in cell viability in U251MG cells treated with SHG-8 at concentrations ranging from 50µM to 300µM (Figure 96a). In U87MG cells, significant cytotoxicity was observed between SHG-8 concentrations of 80µM and 140µM (Figure 96b). SHG-44 also demonstrated significant cytotoxicity in both cell lines, with reductions in cell viability observed at all tested concentrations after 20µM treatments compared to the DMSO control (Figures 97a and 97b). The IC_{50} of SHG-8 in U251MG cells was estimated to be 100.00µM (Figure 96a, $p<0.0001$), while the IC_{50} in U87MG cells was 85.00µM (Figure 96b, $p<0.0001$). For SHG-44, the IC_{50} in U251MG cells was determined to be 64.19µM (Figure 97a, $p<0.05$), and in U87MG cells, it was 70.39µM (Figure 97b, $p<0.05$). Treatment with 200µM cis-platin significantly reduced cell viability in both U251MG and U87MG cells (Figure 98) (U251MG, $p<0.05$; U87MG, $p<0.0001$). The results demonstrated that the tested compounds exhibited significantly higher efficacy compared to the FDA-approved and widely used cis-platin.

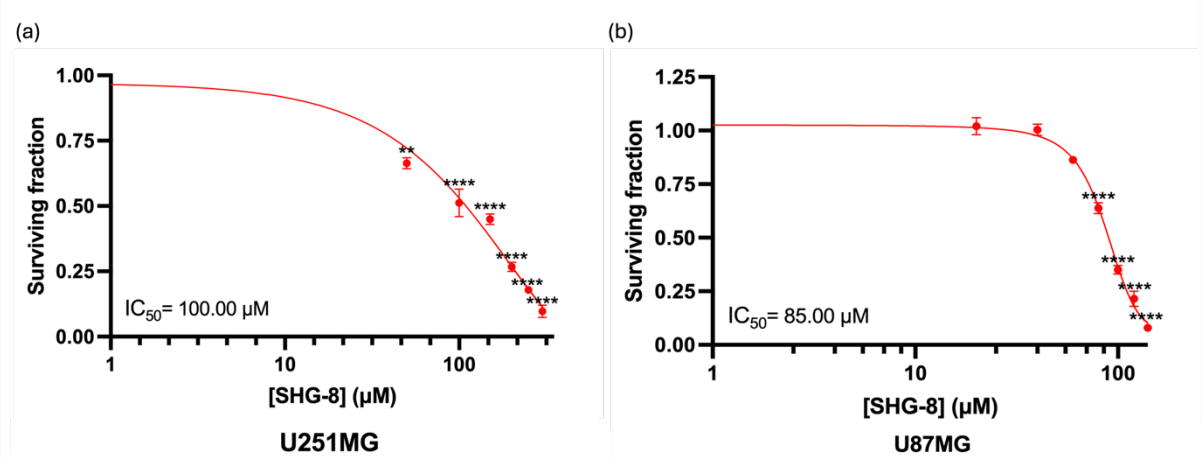


Figure 96. U251MG and U87MG glioma cell viability and proliferation in response to varying concentrations of SHG-8. (a) The MTT assay conducted on U251MG cells treated with SHG-8 at concentrations of 50µM, 100µM, 150µM, 200µM, 250µM, and 300µM revealed an IC_{50} of 100.00µM. (b) Similarly, the MTT assay on U87MG cells treated with SHG-8 at concentrations of 20µM, 40µM, 60µM, 80µM, 100µM, 120µM, and 140µM determined an IC_{50} of 85.00µM. Results are based on three independent experiments, n=3. All statistical analyses were conducted using ordinary one-way ANOVA, followed by Dunnett's multiple comparisons test to determine the significant differences between SHG-8 treated samples and DMSO control samples (legend: **p<0.01, ***p<0.001, ****p<0.0001).

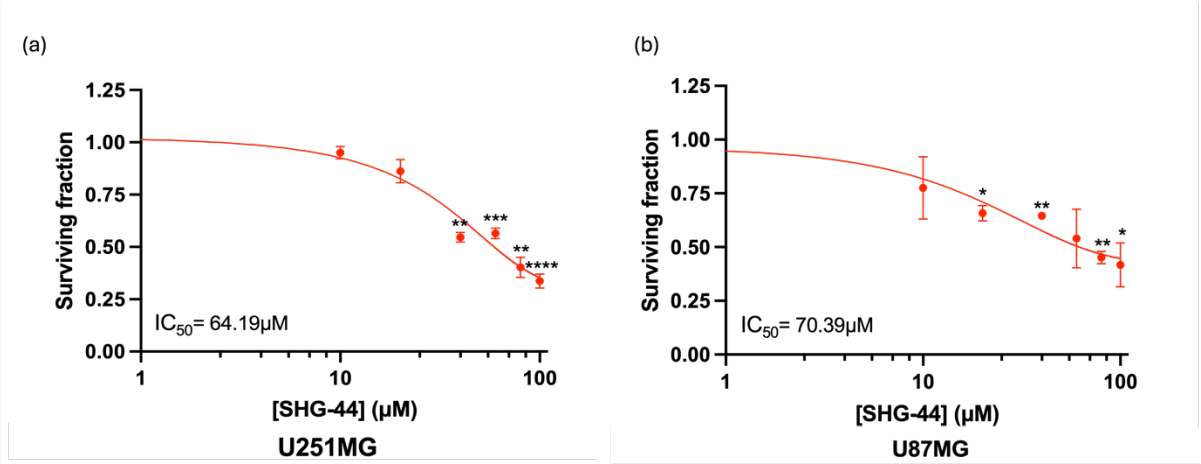


Figure 97. U251MG and U87MG glioma cell viability and proliferation in response to varying concentrations of SHG-44. (a) The MTT assay conducted on U251MG cells treated with SHG-44 at concentrations of 10µM, 20µM, 40µM, 60µM, 80µM, and 100µM revealed an IC_{50} of 64.19µM. (b) Similarly, the MTT assay on U87MG cells treated with SHG-4 at concentrations of 10µM, 20µM, 40µM, 60µM, 80µM, and 100µM determined an IC_{50} of 70.39µM. Results are based on three independent experiments, n=3. All statistical analyses were conducted using ordinary one-way ANOVA, followed by Dunnett's multiple comparisons test to determine the significant differences between SHG-44 treated samples and DMSO control samples (legend: *p<0.05, **p<0.01, ***p<0.001, ****p<0.0001).

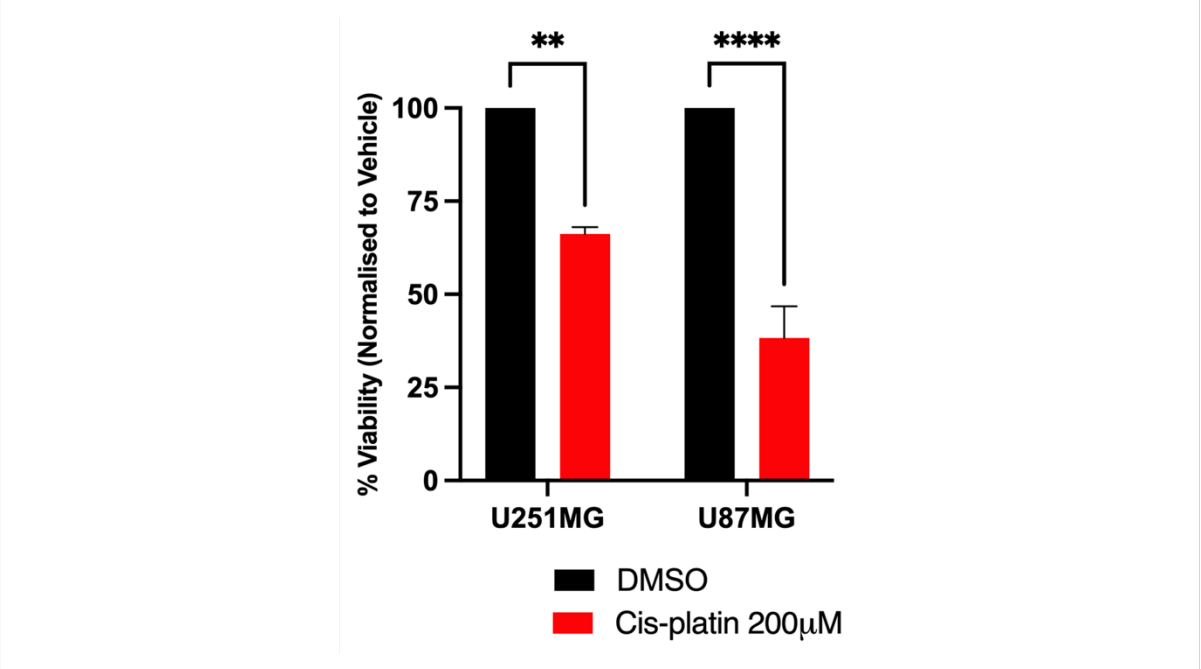


Figure 98. U251MG and U87MG glioma cell viability and proliferation in response to cis-platin treatment. Treatment with 200µM cis-platin (positive control) resulted in significantly reduced cell viability within both cell lines. Results are based on three independent experiments, n=3. All statistical analyses were conducted using ordinary one-way ANOVA, followed by Dunnett's multiple comparisons test to determine the significant differences between cis-platin treated samples and DMSO control samples (legend: **p<0.01, ****p<0.0001).

5.3.4. Small RNA-sequencing of SHG-8 and SHG-44 treated U87MG cells

The comprehensive sRNA-seq miRNA expression and pathway analysis revealed significant changes in miRNA profiles following 24 hours treatment with SHG-8 and SHG-44. In the 100μM SHG-8 treated sequencing of U87MG cells, the heat map revealed a distinct pattern of expression, with clear differences between the treated and DMSO control samples, indicating significant alterations in miRNA expression profiles between the two conditions (Figure 99a). The volcano plot further revealed that 771 miRNAs were significantly upregulated or downregulated compared to control samples, with 175 miRNAs downregulated and 596 upregulated (Figure 99b). Notably, miR-7974 was the most downregulated miRNA, while miR-3648 was the most upregulated. Additionally, miR-21-5p and miR-128a-3p were significantly downregulated, whereas miR-34a-5p, miR-206 and miR-383 showed no significant changes between the two tested groups. KEGG pathway analysis revealed that the differentially expressed miRNAs were primarily involved in lysosomal pathways, axon guidance and miRNAs in cancer (Figure 100). Molecular function analysis indicated that most differently expressed miRNAs played a part in processes such as nucleic acid binding, zinc ion binding, and sequence-specific DNA binding (Figure 101). Further biological processes analysis identified that most dysregulated miRNAs were associated with neuronal development, cell adhesion, and the regulation signal transduction (Figure 102). Figure 103 shows cellular component enrichment analysis, with significant gene enrichment observed in obsolete cell, nucleus, nucleoplasm, and components like integral component of plasma membrane and endoplasmic reticulum. Similarly, sRNA-seq data for U87MG cells treated with 100μM SHG-44 showed significant alterations in miRNA expression profiles with 254 miRNAs dysregulated, predominantly downregulated (231) compared to upregulated (23) (Figures 104a and 104b). The most notable changes included the downregulation of miR-122b-5p and miR-730 and the upregulation of miR-144-3p, miR-5009-5p, and miR-664b-3p (Figure 104b). MiRNAs, including miR-21, miR-34a, miR-128a, and miR-383, were not differentially expressed between the two conditions, whilst miR-206 was found downregulated in the presence of SHG-44. Further KEGG pathway analysis indicated that most dysregulated miRNAs in the presence of SHG-44 were involved in regulating pathways, such as lysosomal pathways and axon guidance (Figure 105). At the molecular level, they interacted with nucleic acids, zinc ions, and sequence-specific DNA binding processes (Figure 106). Further biological processes analysis revealed most dysregulated miRNAs were associated with the nervous

system, neurogenesis and regulation of neurogenesis (Figure 107). Figure 108 shows cellular component enrichment analysis, highlighting significant gene enrichment in components such as intracellular, cytosol, and nucleoplasm, as well as synaptic-related regions like postsynaptic density and glutamatergic synapse.

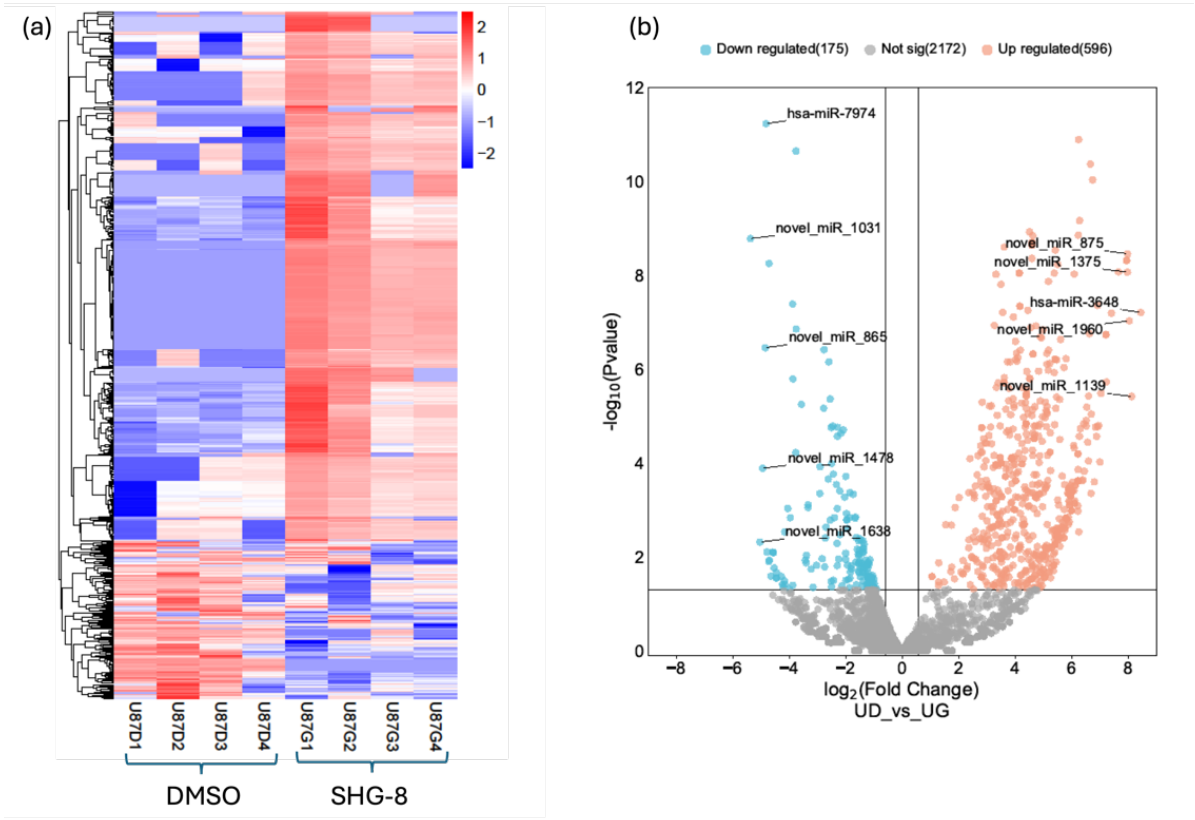


Figure 99. sRNA-seq of U87MG cells (SHG-8). (a) The heat map displayed a distinct pattern of miRNA expression, with clear differences between the treated and DMSO control samples, indicating significant alterations in miRNA expression profiles. (b) The volcano plot depicted that 771 miRNAs were significantly dysregulated under the influence of SHG-8, with 175 miRNAs downregulated and 596 upregulated. Notably, miR-7974 was the most downregulated miRNA, while miR-3648 was the most upregulated.

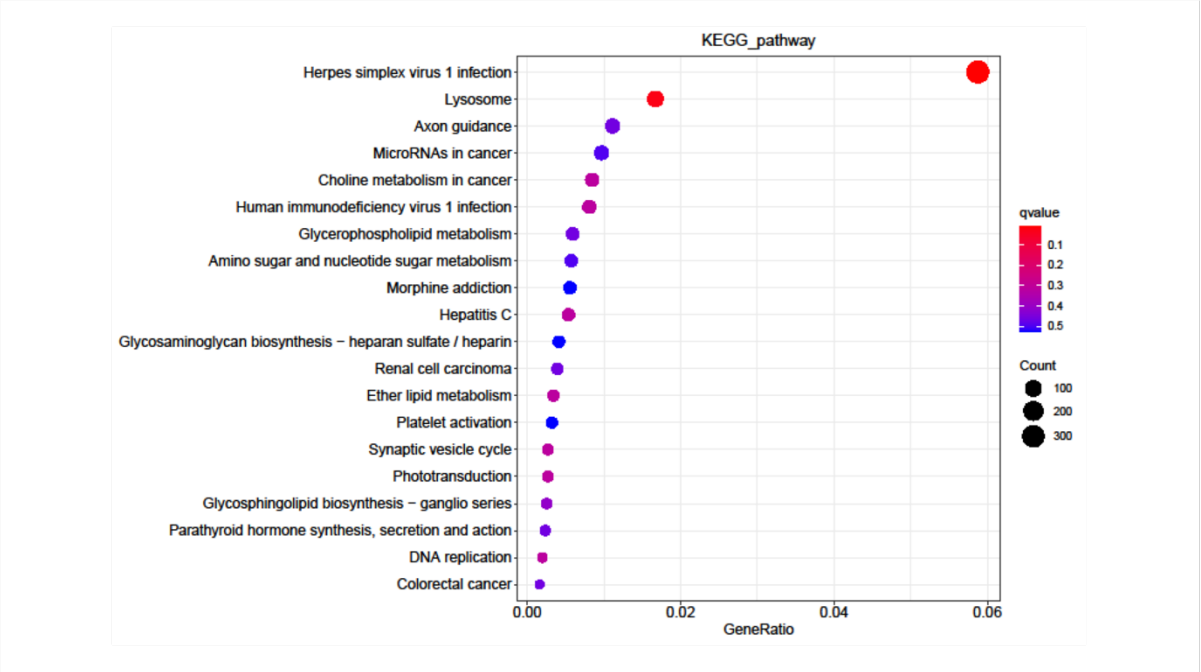


Figure 100. KEGG pathway analysis (SHG-8). KEGG pathway analysis of the differentially expressed miRNAs showed that they were primarily involved in lysosomal pathways, axon guidance, and miRNAs in cancer.

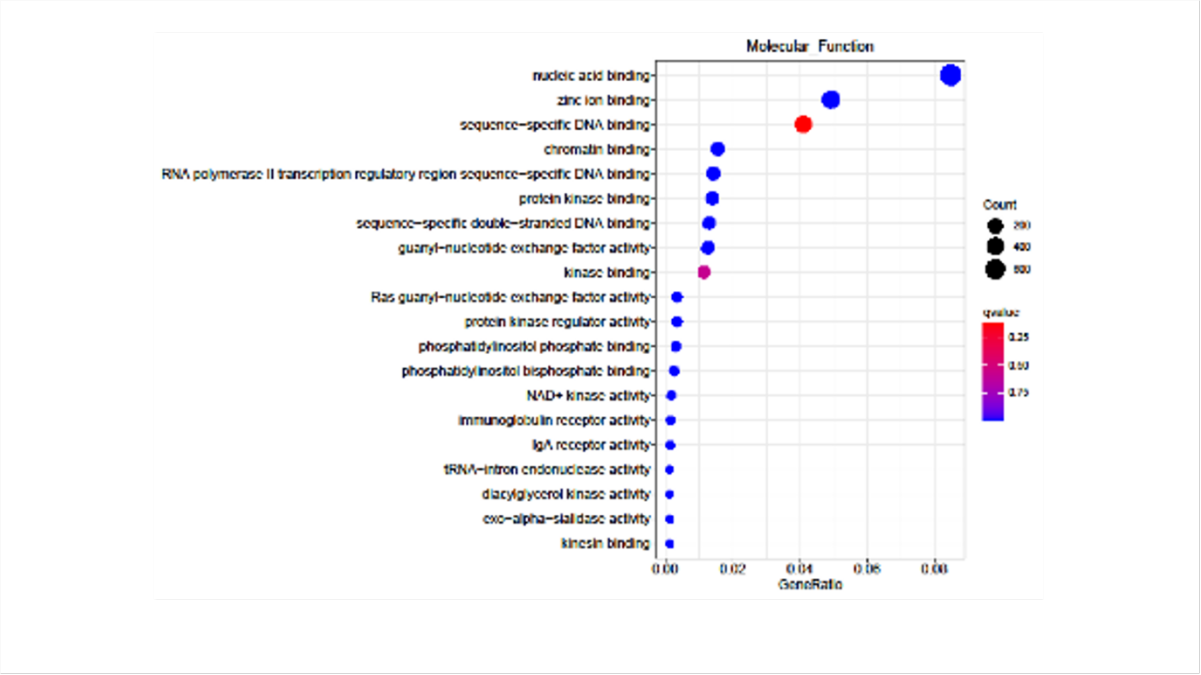


Figure 101. Molecular function analysis (SHG-8). Molecular function analysis of the differentially expressed miRNAs indicated that they predominantly participated in processes such as nucleic acid binding, zinc ion binding, and sequence-specific DNA binding.

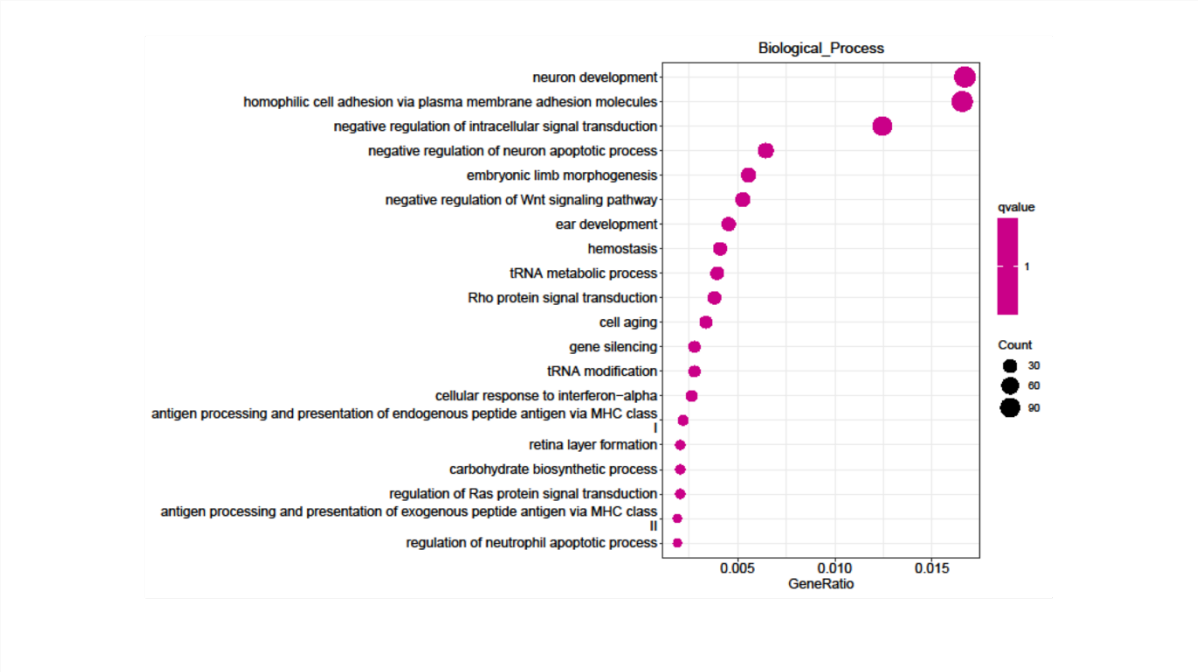


Figure 102. Biological process analysis (SHG-8). Biological process analysis revealed that most of dysregulated miRNAs were associated with neuronal development, cell adhesion, and the regulation of signal transduction.

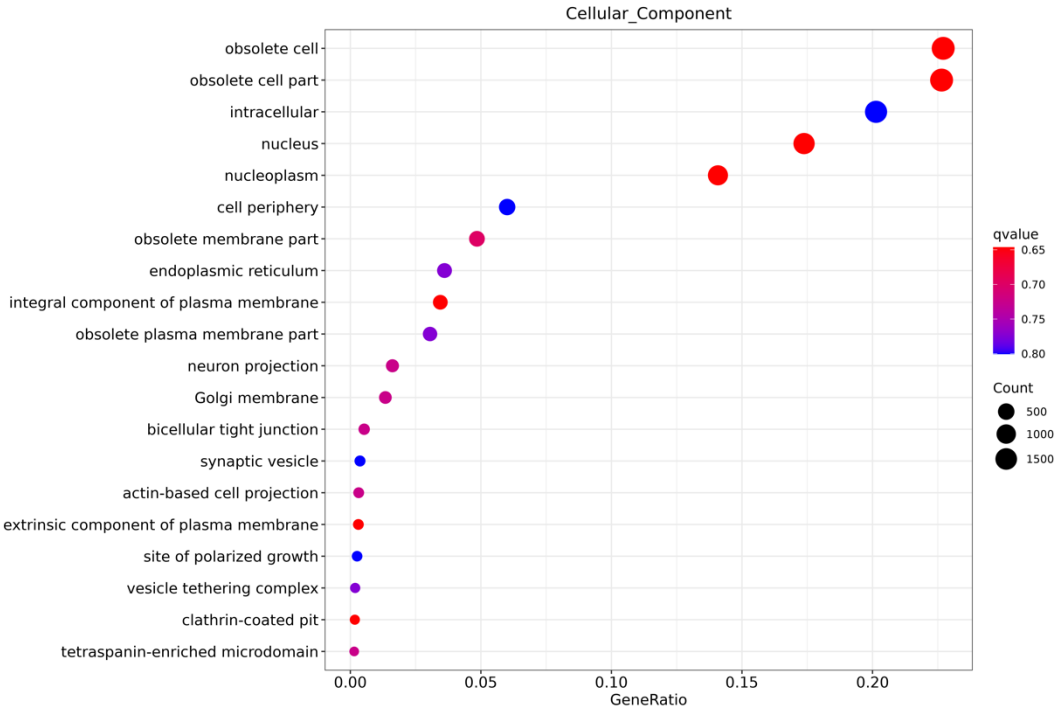


Figure 103. Cellular component enrichment analysis (SHG-8). Key components include obsolete cell, nucleus, and endoplasmic reticulum, highlighting significant gene enrichment in these cellular locations.

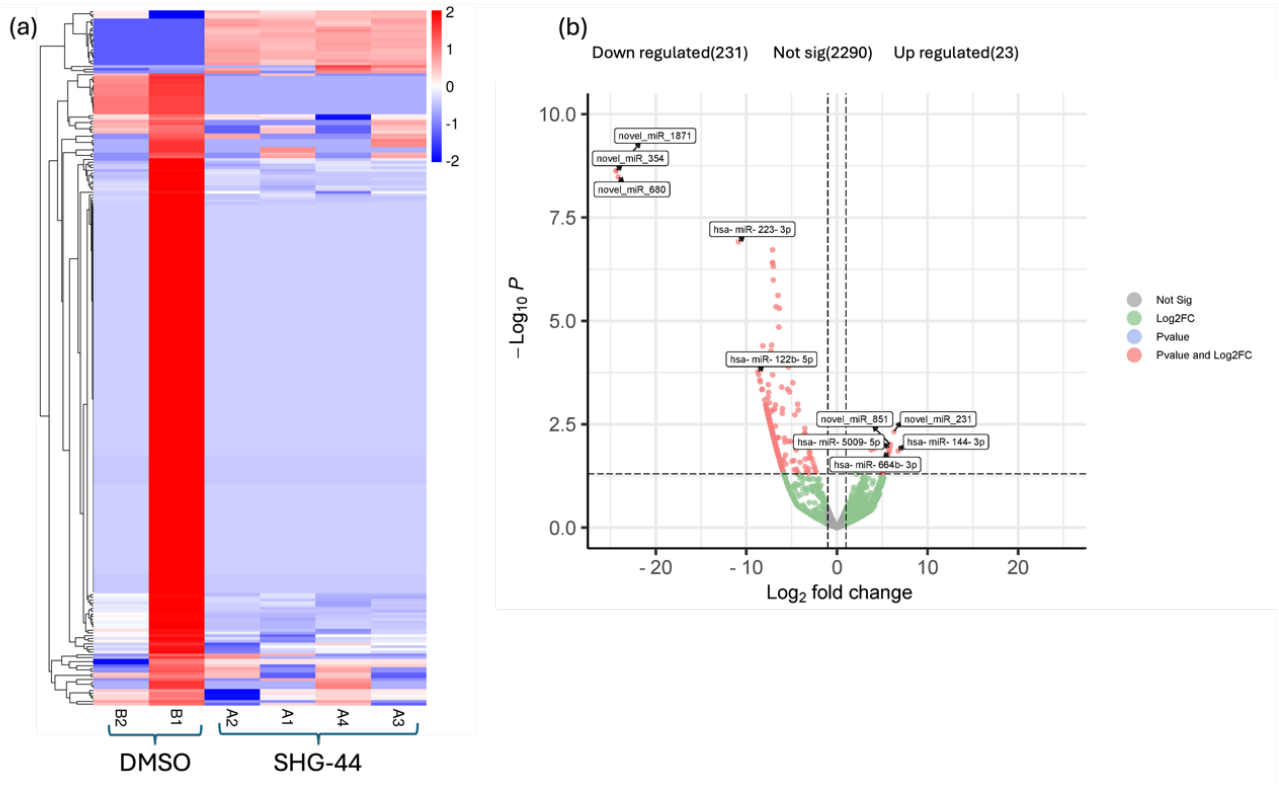


Figure 104. sRNA-seq of U87MG cells (SHG-44). (a) A heat map showing the pattern of miRNA expression between the treated and DMSO control samples. Notably, sample B1 appears to have an error, displaying uniform red expression across most genes. (b) The volcano plot depicted that 254 miRNAs were significantly dysregulated under the influence of SHG-44, with 231 miRNAs downregulated and 23 upregulated.

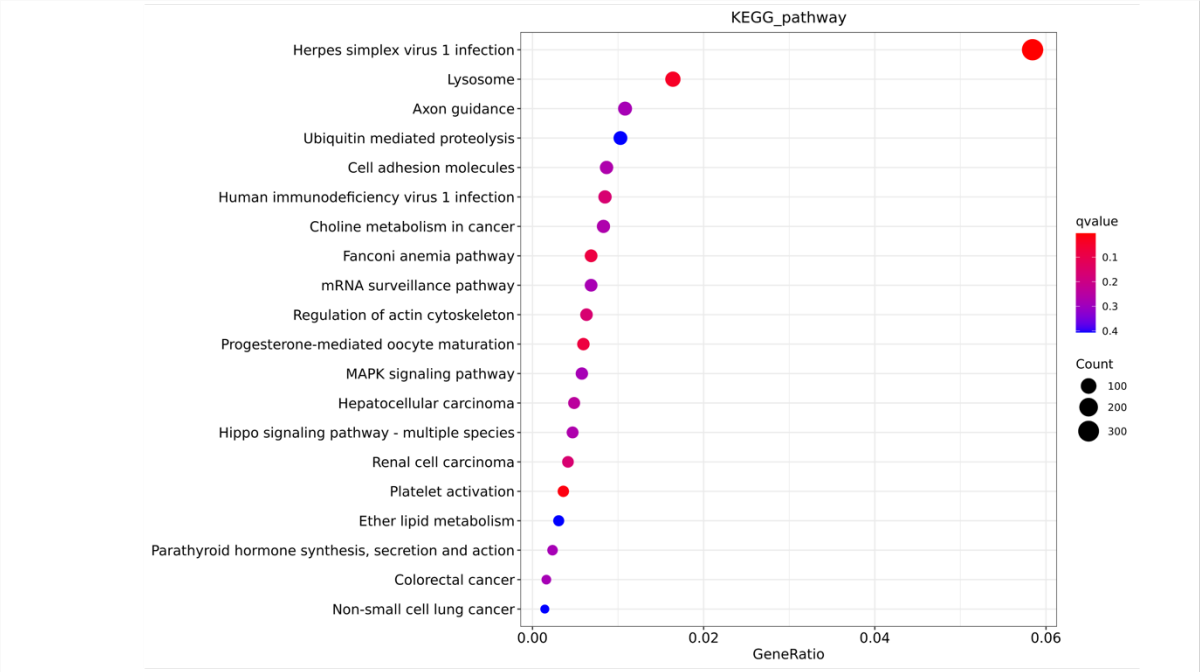


Figure 105. KEGG pathway analysis (SHG-44). KEGG pathway analysis of the differentially expressed miRNAs showed that they were primarily involved in lysosomal pathways and axon guidance.

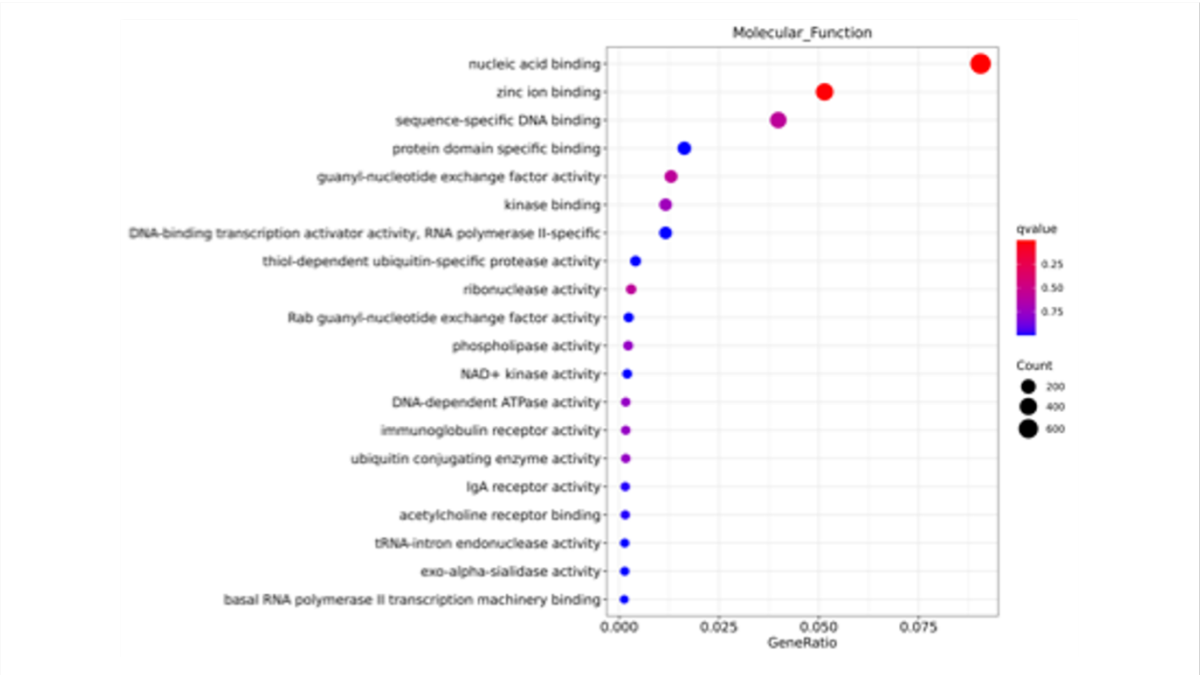


Figure 106. Molecular function analysis (SHG-44). Molecular function analysis of the differentially expressed miRNAs indicated that they predominantly participated in processes such as nucleic acid binding, zinc ion binding, and sequence-specific DNA binding.

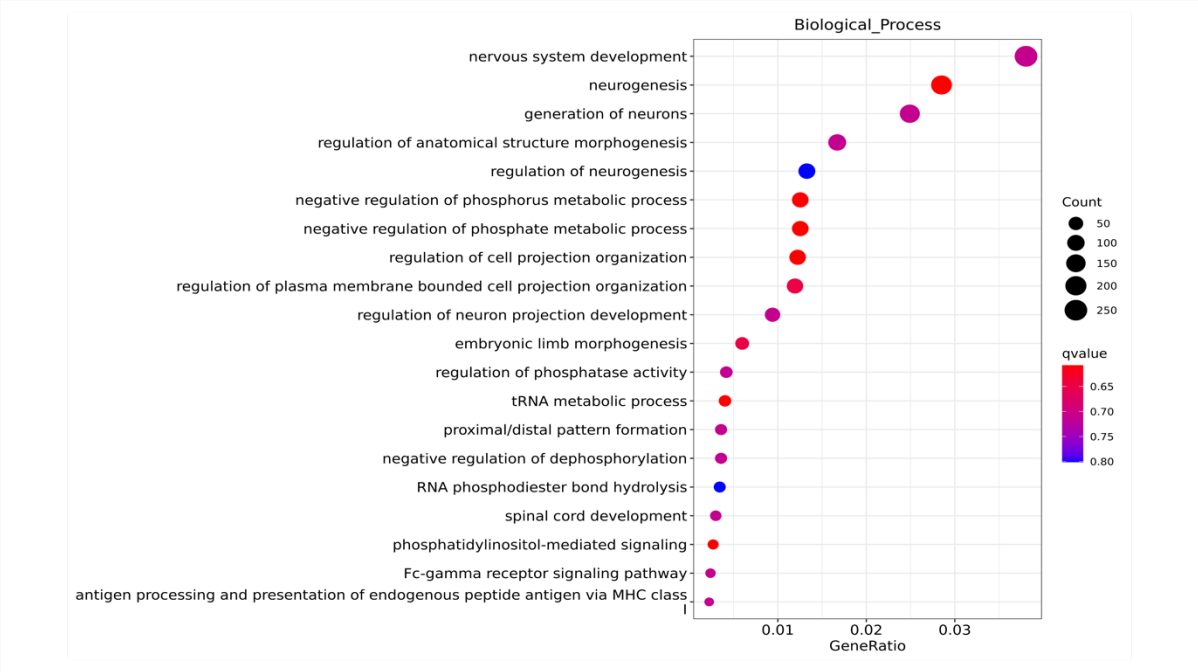


Figure 107. Biological process analysis (SHG-44). Biological process analysis revealed that most dysregulated miRNAs were associated with nervous system development, neurogenesis, generation of neurones, regulation of morphogenesis, and regulation of neurogenesis.

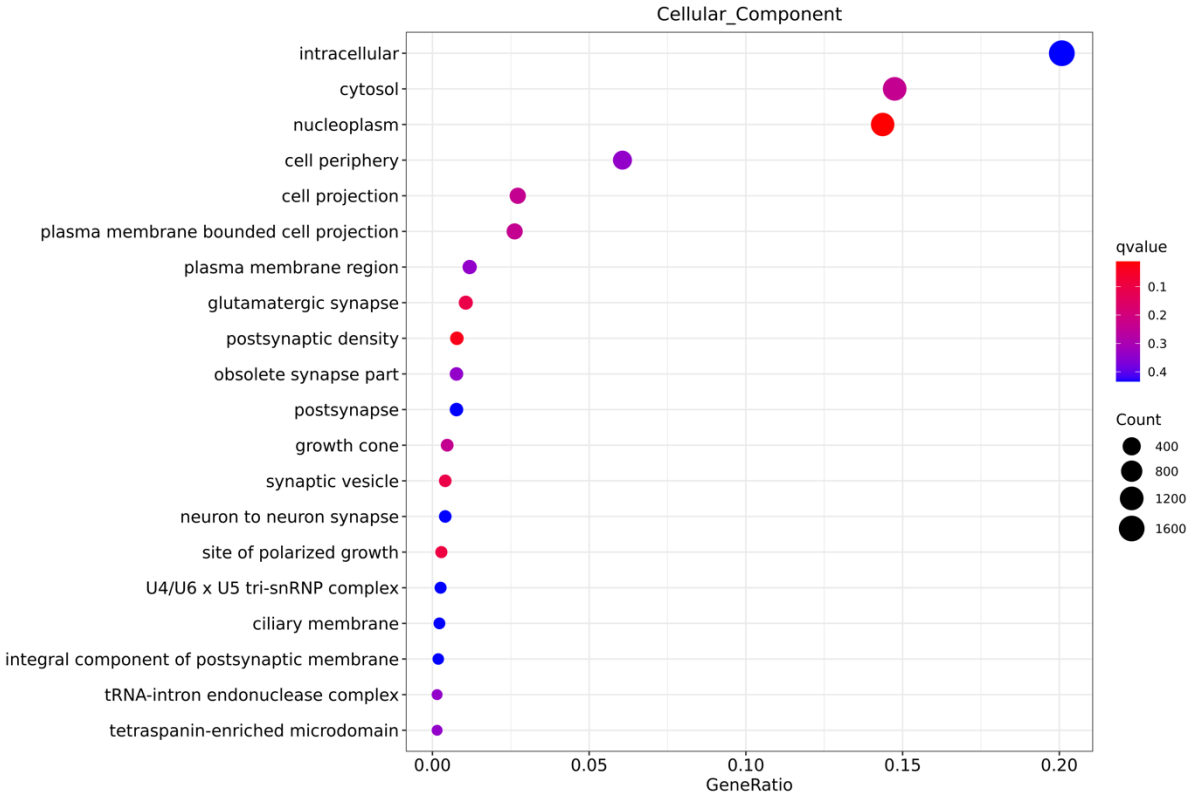


Figure 108. Cellular component enrichment analysis (SHG-44). Key enriched components include intracellular, cytosol, nucleoplasm, and synaptic regions such as postsynaptic density and glutamatergic synapse.

5.3.5. RT-qPCR validation

Following the sRNA-seq, RT-qPCR was employed to validate the sequencing results. The results demonstrated that miR-7974 was significantly downregulated in the presence of 50µM and 100µM SHG-8 within U87MG GB cells (Figure 109a). This was in line with the positive control condition (cis-platin 200µM), which also showed significant downregulation of miR-7974 in comparison to the DMSO control condition. The relative expression of miR-3648 was significantly upregulated in the presence of the compounds and cis-platin (Figure 109b). The expression of miR-21 was unaffected in the presence of SHG-8 within U87MG treated cells (Figure 109c). However, there was a significant elevation of miR-21 in the cis-platin condition in comparison to the DMSO control (Figure 109c).

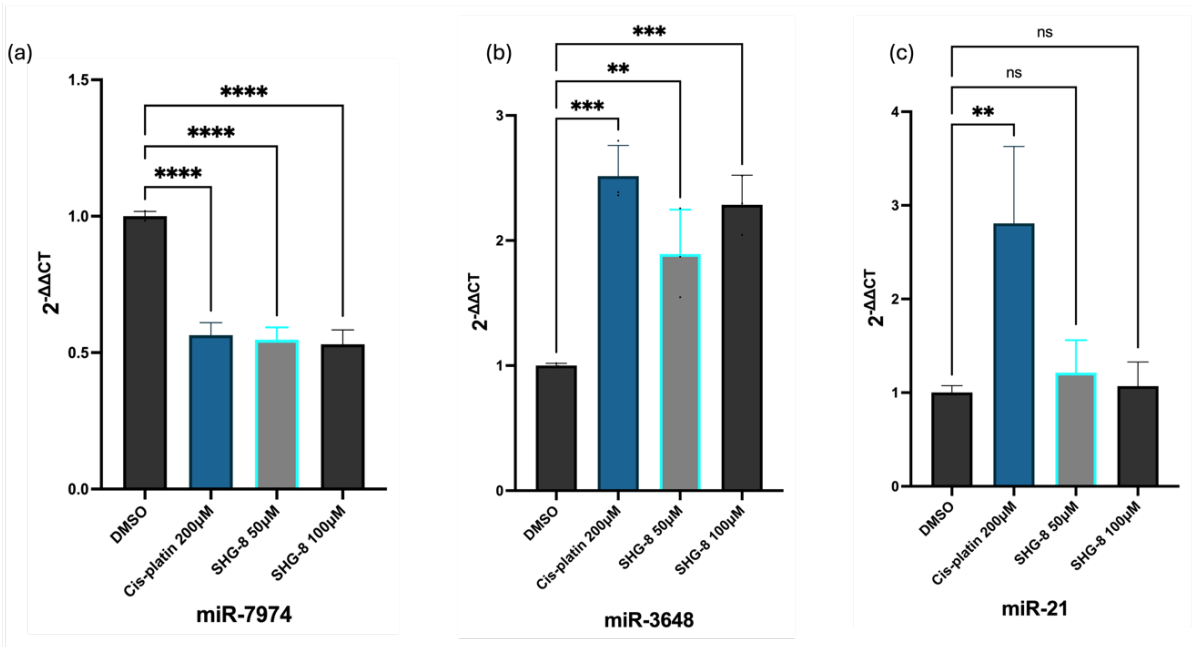


Figure 109. RT-qPCR validation. (a) MiR-7974 was significantly downregulated in U87MG cells post-SHG-8 treatment with 50μM and 100μM ($p<0.0001$ and $p<0.0001$, respectively). Cis-platin (200μM) also reduced the expression of miR-7974 significantly ($p<0.0001$). (b) MiR-3648 was significantly upregulated by both tested concentrations of SHG-8 and cis-platin (SHG-8 50μM, $p<0.0056$; SHG-8 100μM, $p<0.0006$; cis-platin (200μM, $p<0.0002$). (c) There was no significant difference in the expression of miR-21 post-exposure to SHG-8 (50μM, $p<0.8994$; 100μM, $p<0.9957$). However, cis-platin (200μM) significantly upregulated the expression of miR-21 in treated cells ($p<0.0037$). Results are based on three independent experiments, n=3. All statistical analyses were conducted using ordinary one-way ANOVA, followed by Dunnett's multiple comparisons test to determine the significant differences between SHG-8 treated cells, cis-platin treated cells, and DMSO control samples.

5.3.6. SHG-8 and SHG-44 impaired the colony formation within GB cells

Following the observed cytotoxic effects, the clonogenic capacity of U87MG and U251MG cells was further assessed after treatment with SHG-8 and SHG-44. For SHG-8, cells were treated with concentrations of 50µM and 100µM, leading to a significant reduction in clonogenic potential in both cell lines. In U87MG cells, SHG-8 treatment at 50µM and 100µM significantly reduced colony formation to 0% in both treatment conditions ($p<0.0001$) (Figure 110a). This was also observed in the microscopic images which showed no surviving cells and no colonies (Figures 110b and 110c). Similarly, in U251MG cells, SHG-8 treatment at 50µM and 100µM reduced the survival fraction to 0% (Figure 111a, $p<0.0001$). The microscopic images revealed no colony formation (Figures 111b and 111c). In parallel, SHG-44 treatment also demonstrated a significant decrease in clonogenic potential in both U87MG and U251MG cells. U87MG cells were treated with 70µM and 100µM SHG-44, while U251MG cells were treated with 50µM and 100µM SHG-44, considering their higher sensitivity to the compound as indicated by the cell viability assays. Specifically, in U87MG cells, SHG-44 treatment at 70µM and 100µM significantly reduced colony formation to 22% ($p<0.004$) and 5% ($p<0.0001$), respectively (Figure 112a). The microscopic images in Figures 112b and 112c further confirmed these results visually. Similarly, in U251MG cells, SHG-44 treatment at 50µM and 100µM reduced the survival fraction to 9% ($p<0.0001$) and 3% ($p<0.0001$), respectively (Figure 113a). The reduction of colony formation capacity under these concentrations was observed in the microscopic images in Figures 113b and 113c. Cis-platin treatment at 200µM further confirmed significantly lower survival rates in both cell lines compared to the DMSO control (Figures 110b, 110c, 111b, 111c, 112b, 112c, 113b, 113c, and 114).

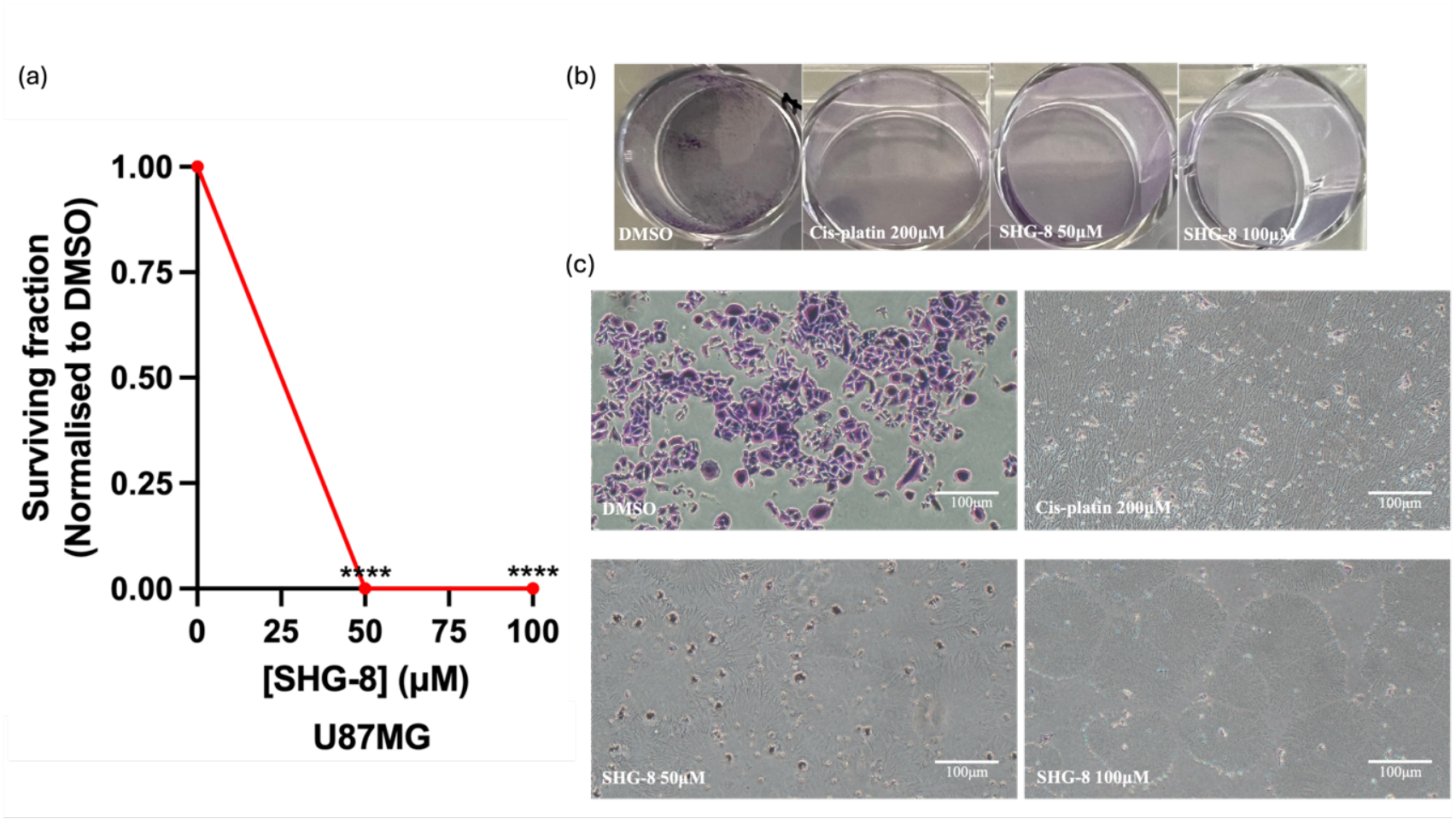


Figure 110. Colony formation of U87MG post-SHG-8 treatment. (a) A significant decrease in the proliferative clonal capacity of U87MG colonies was observed with 50μM and 100μM SHG-8 treatment. (b, c) This effect was also evident microscopically, where inhibition of colony formation was observed in U87MG cells treated with both SHG-8 concentrations**.** Microscopic images of colonies were taken at ×40 magnification. Results are based on three independent experiments, n=3. All statistical analyses were conducted using ordinary one-way ANOVA, followed by Dunnett's multiple comparisons test to determine the significant differences between SHG-8 treated samples and DMSO control samples (legend: ****p<0.0001).

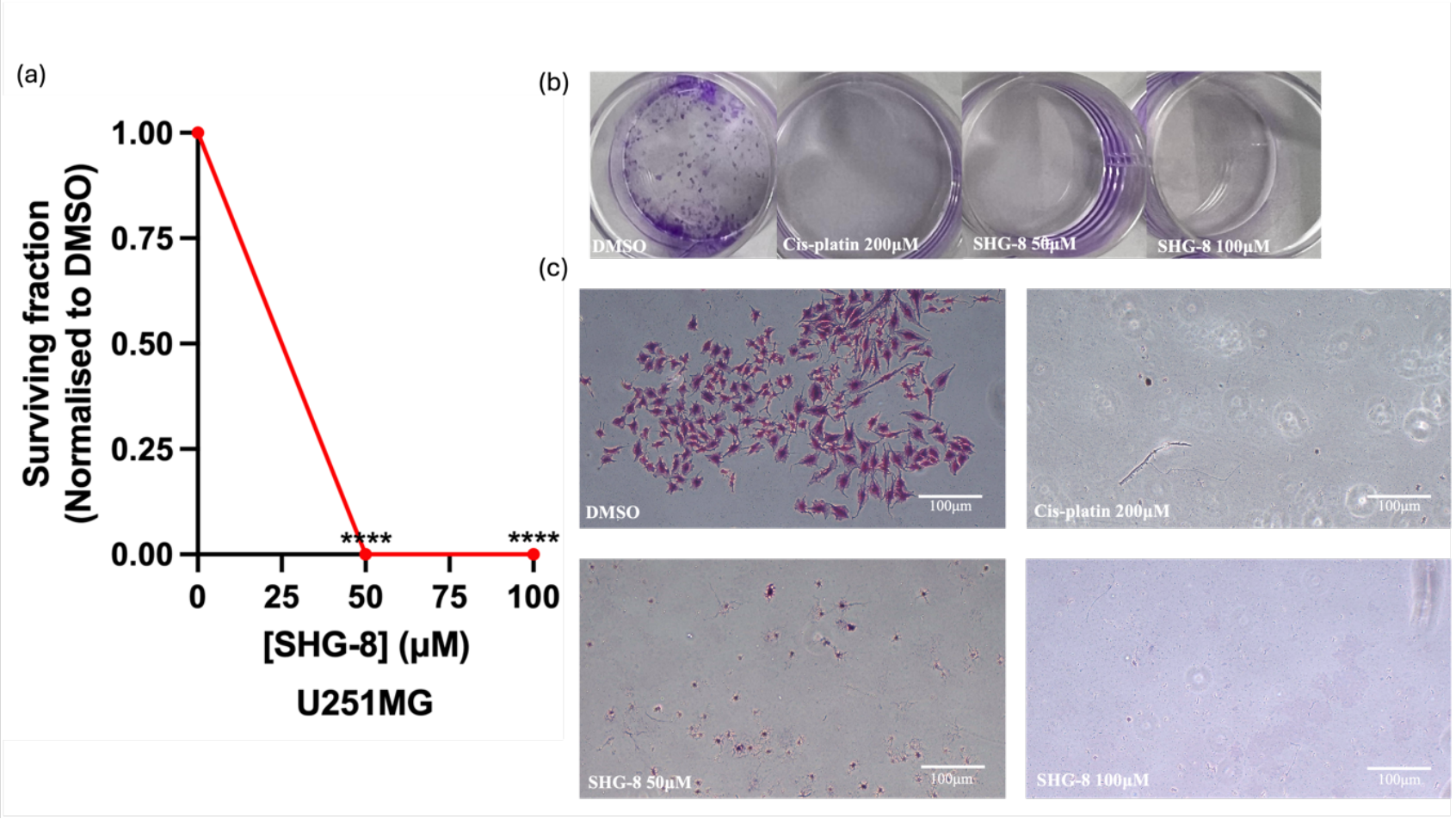


Figure 111. Colony formation of U251MG post-SHG-8 treatment. (a) A significant decrease in the clonal capacity of U251MG cells was observed with 50μM and 100μM SHG-8 treatment. (b, c) This effect was also observed microscopically, where inhibition of colony formation was seen post-treatment with both SHG-8 concentrations**.** Microscopic images of colonies were taken at ×40 magnification. Results are based on three independent experiments, n=3. All statistical analyses were conducted using ordinary one-way ANOVA, followed by Dunnett's multiple comparisons test to determine the significant differences between SHG-8 treated samples and DMSO control samples (legend: ****$p<0.0001$).

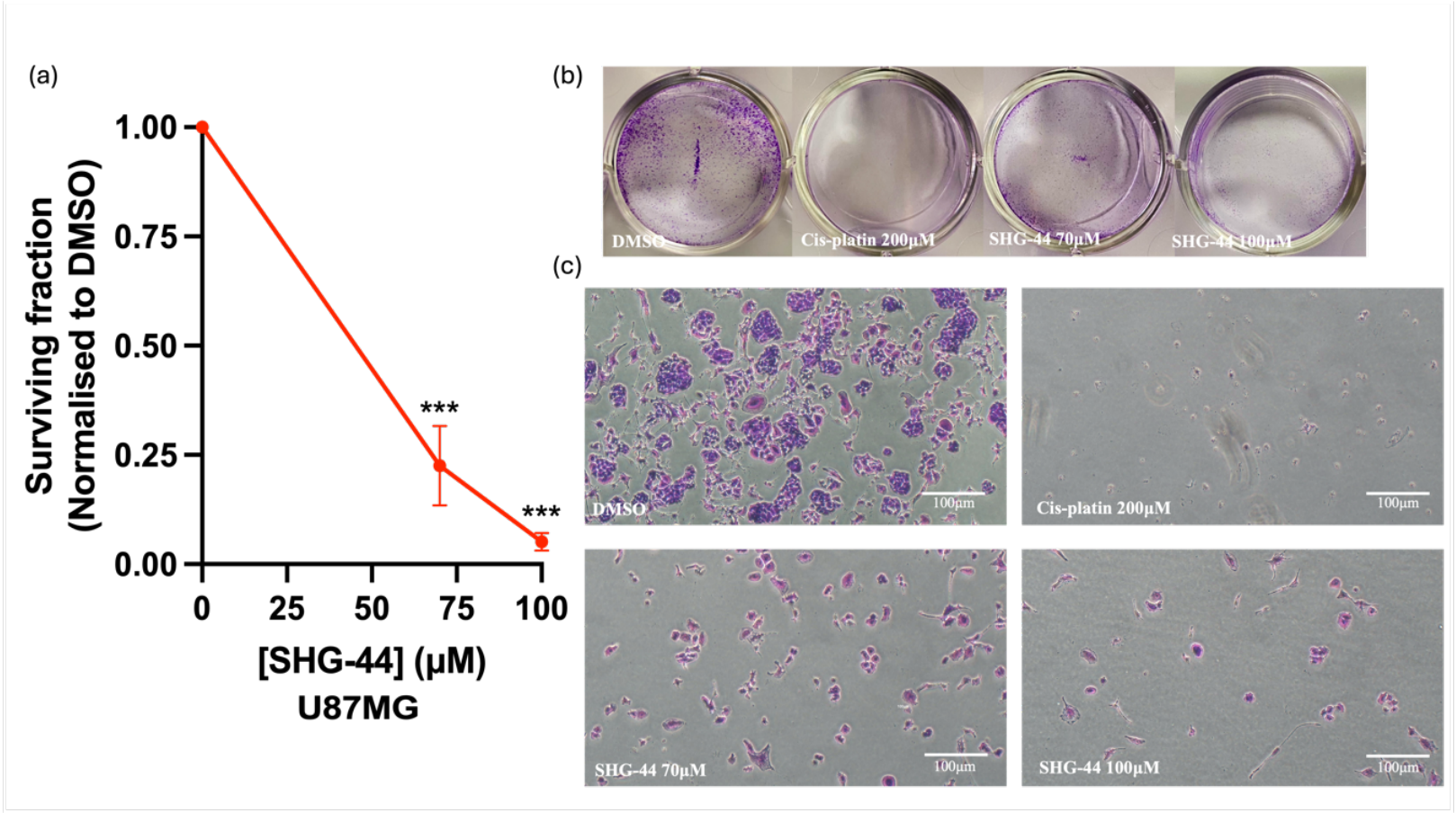


Figure 112. Colony formation of U87MG post-SHG-44 treatment. (a) A significant decrease in the proliferative clonal capacity of U87MG colonies was observed with 70μM and 100μM SHG-44 treatment. (b, c) This was also demonstrated microscopically, where no colony formation was observed post-treatment with both SHG-44 concentrations**.** Microscopic images of colonies were taken at ×40 magnification. Results are based on three independent experiments, n=3. All statistical analyses were conducted using ordinary one-way ANOVA, followed by Dunnett's multiple comparisons test to determine the significant differences between SHG-44 treated samples and DMSO control samples (legend: ***p<0.004).

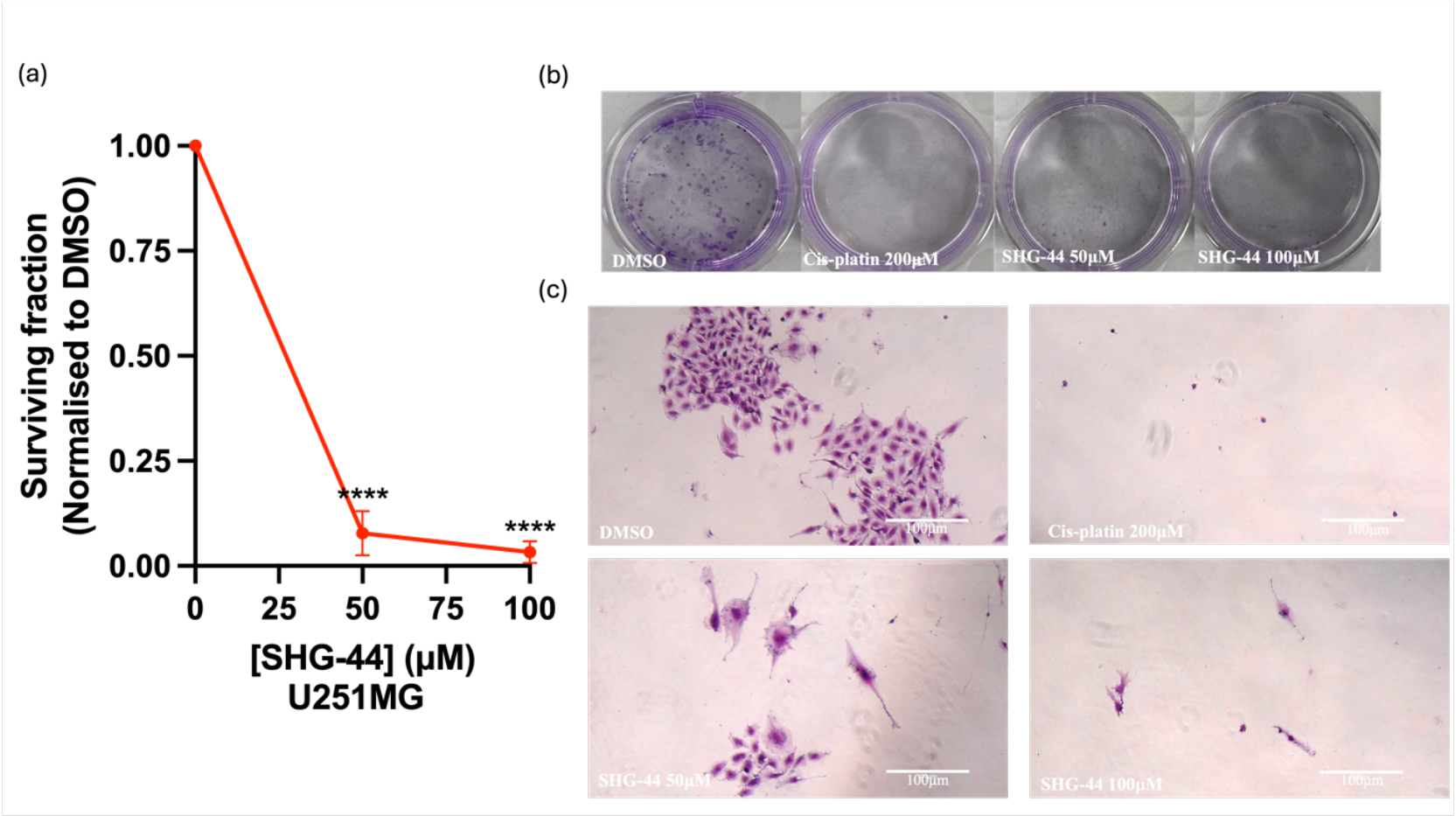


Figure 113. Colony formation of U251MG post-SHG-44 treatment. (a) A significant decrease in the colony formation abilities of U251MG was observed with 50μM and 100μM SHG-44 treatment. (b, c) This was also demonstrated microscopically, where no colony formation was observed post-treatment with both SHG-44 concentrations**.** Microscopic images of colonies were taken at ×40 magnification. Results are based on three independent experiments, n=3. All statistical analyses were conducted using ordinary one-way ANOVA, followed by Dunnett's multiple comparisons test to determine the significant differences between SHG-44 treated samples and DMSO control samples (legend: ****$p<0.0001$).

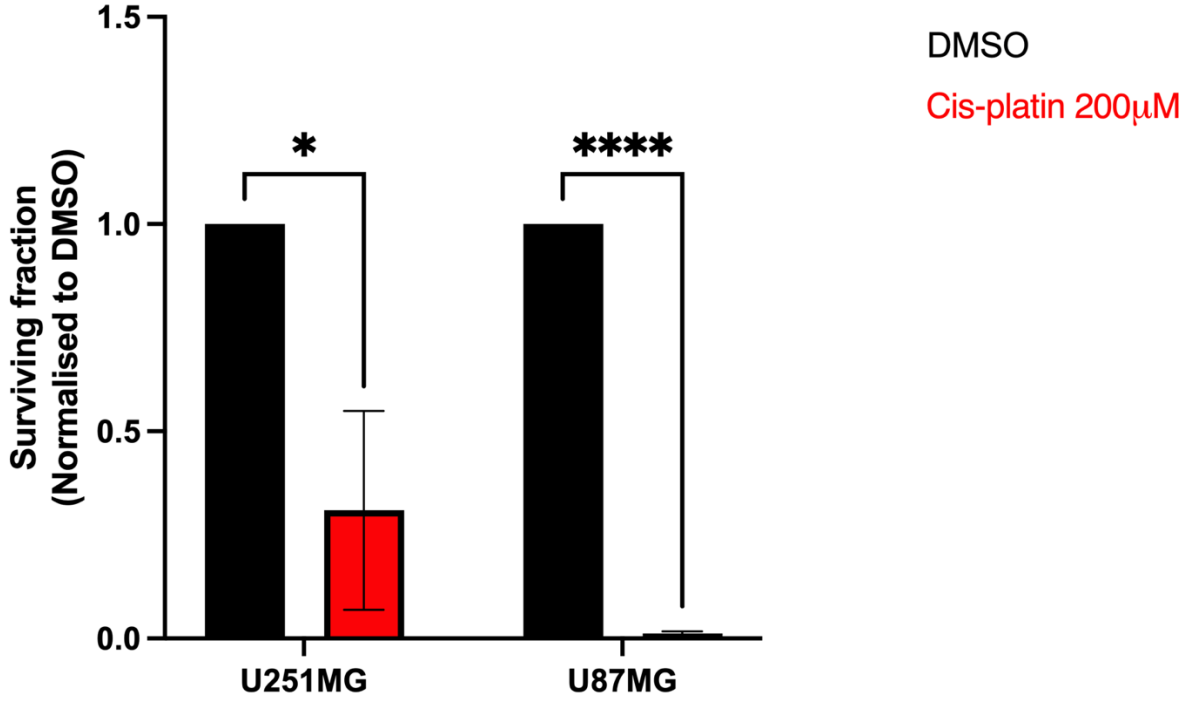


Figure 114. Colony formation of U251MG and U87MG post-cis-platin treatment. Cis-platin 200µM (positive control) also significantly inhibited the formation of colonies within both cell line models. Results are based on three independent experiments, n=3. All statistical analyses were conducted using ordinary one-way ANOVA, followed by Dunnett's multiple comparisons test to determine the significant differences between cis-platin treated samples and DMSO control samples (legend: *p<0.05, ****p<0.0001).

5.3.7. SHG-8 and SHG-44 disrupted the migratory abilities in both GB cell lines

The wound-healing assay results demonstrated that SHG-8 and SHG-44 had concentration-dependent effects on cell migration in both U87MG and U251MG cells. In U87MG cells, treatment with 20µM SHG-8 resulted in no significant migration impairment in comparison to the DMSO control (p<0.7633, Figures 115a and 115b). In contrast, 40µM SHG-8 exposure resulted in significantly impaired wound closure at 24h in comparison to the DMSO control (p<0.0001), whilst at 48h it led to a change in cell morphology and cell death, retaining the clear scratch area (p<0.0001), thus indicating a concentration-dependent inhibition of migration (Figures 115a and 115b). For U251MG cells, exposure to both 50µM and 100µM SHG-8 resulted in significantly impaired cell migration at 24h and 48h in comparison to the DMSO control (Figures 116a and 116b, p<0.0001). Additionally, 100µM SHG-8 led to cell death (Figure 116b). For SHG-44, treatment with 70µM showed wound closure rates similar to the DMSO control at 24h and 48h (p<0.0825 and p<0.7577, respectively), but 100µM

significantly impaired wound closure at both time points ($p<0.01$) (Figures 117a and 117b). Similarly, SHG-44 at 50μM showed no impairment of cell migration compared to DMSO at 24h and 48h ($p< 0.7655$ and $p<0.9981$, respectively), whereas 100μM significantly inhibited wound closure at both time points ($p<0.001$) (Figures 118a and 118b). Furthermore, cis-platin (200μM) treatment significantly inhibited wound closure in both U251MG and U87MG cell lines compared to the DMSO control (Figures 115-118, $p<0.0001$).

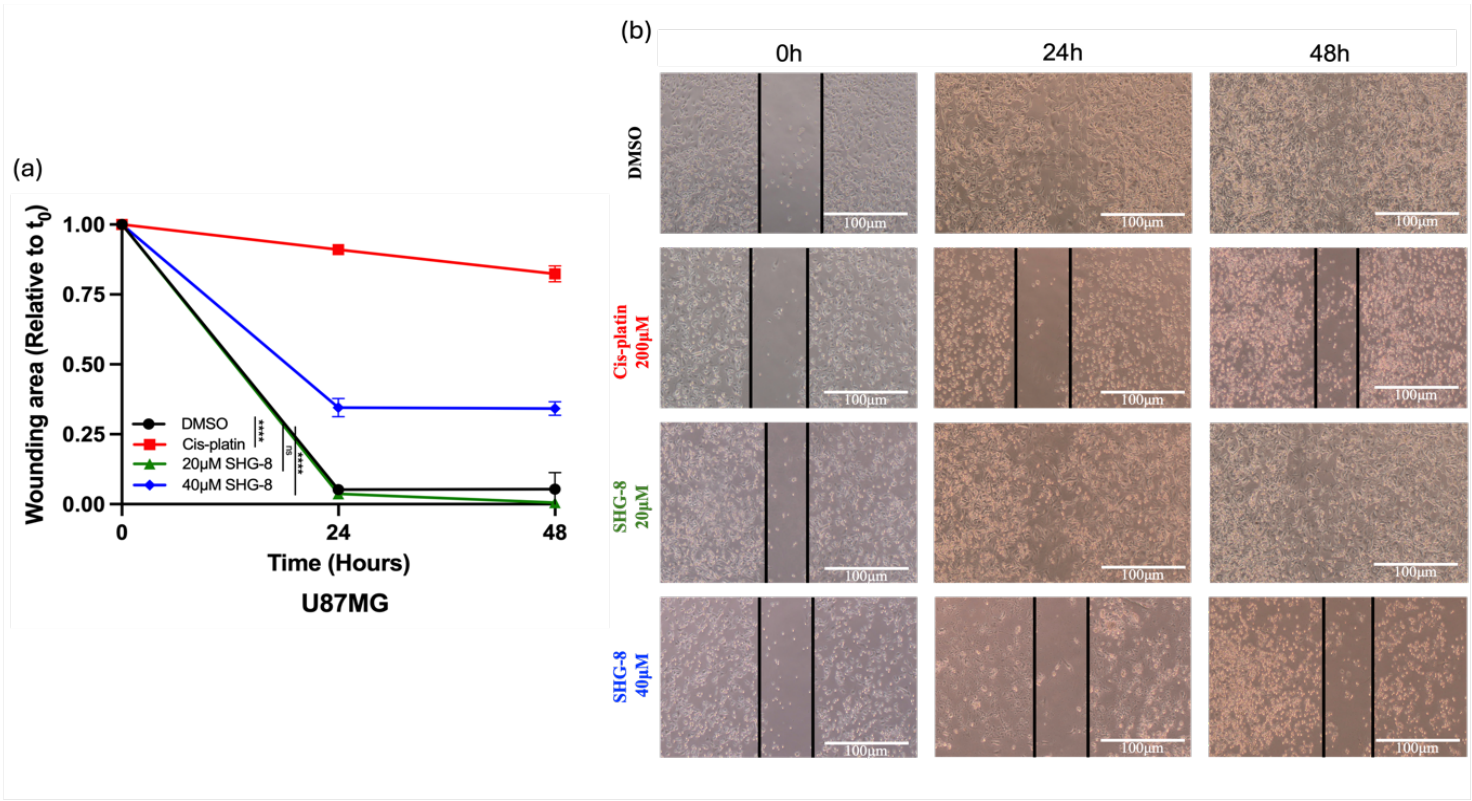


Figure 115. Cell migration of U87MG cells post-SHG-8 exposure. (a) Quantification of the wound-healing assay for U87MG cells following treatment with DMSO, cis-platin (200μM), and SHG-8 (20μM and 40μM) at various time points. Treatment with 20μM SHG-8 resulted in no significant impairment of cell migration compared to the DMSO control. Exposure to 40μM SHG-8 significantly impaired wound closure at 24h and 48h compared to the DMSO control. Cis-platin treatment resulted in significant inhibition of migration at 24h and 48h. (b) Scratch images were acquired at 0h, 24h, and 48h from U87MG cells treated as described above. At 48h, 40μM SHG-8 induced changes in cell morphology and cell death, maintaining a clear scratch area. Microscopic images of scratch areas were taken at ×40 magnification. Results are based on three independent experiments, n=3. All statistical analyses were conducted using ordinary one-way ANOVA, followed by Dunnett's multiple comparisons test to determine the significant differences between SHG-8 treated cells and DMSO control samples (legend: ns: non-significant, ****$p<0.0001$).

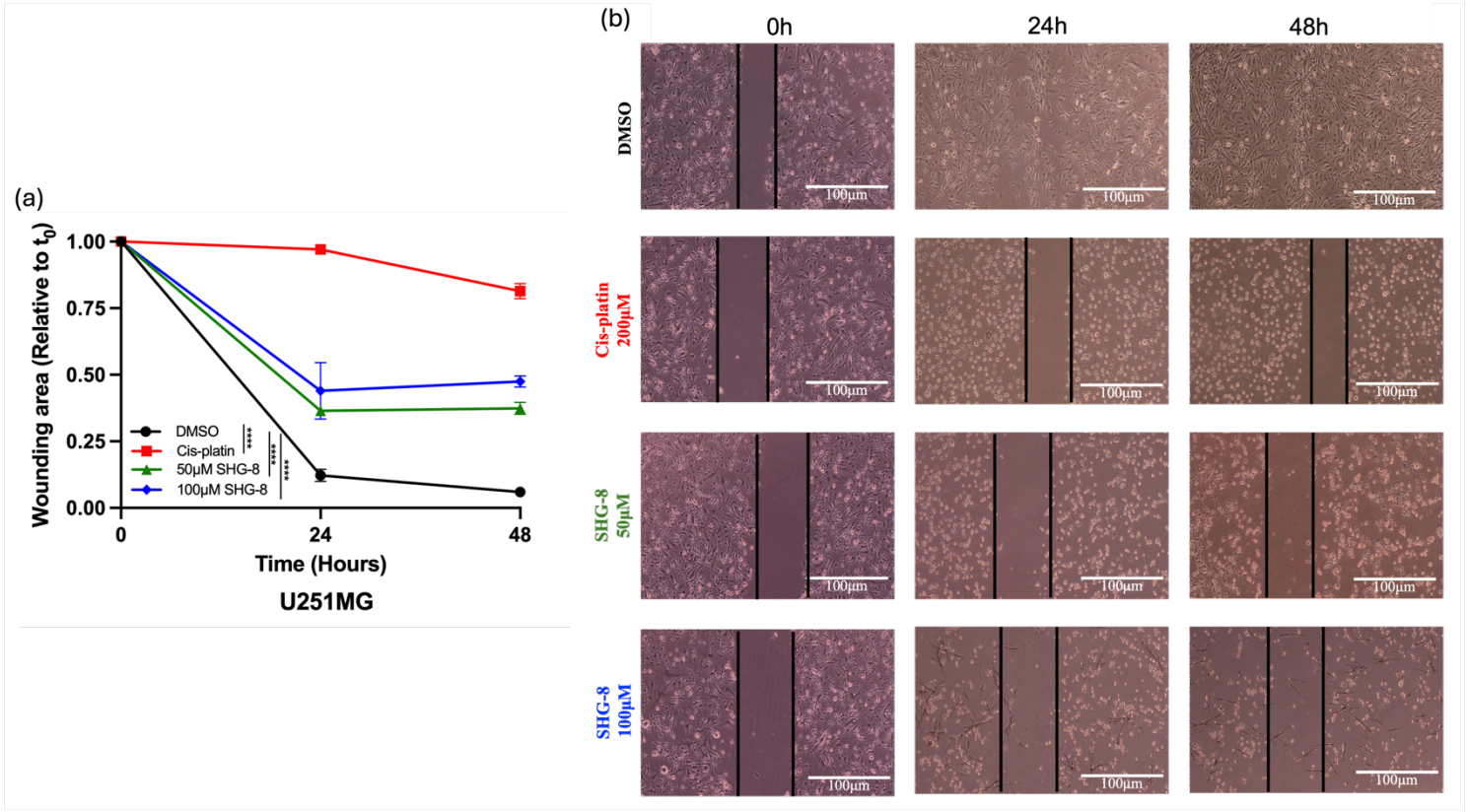


Figure 116. Cell migration of U251MG cells post-SHG-8 exposure. (a) Quantification of the wound-healing assay for U251MG cells following treatment with DMSO, cis-platin (200µM), and SHG-8 (50µM and 100µM) at various time points. Treatment with 50µM and 100µM SHG-8 resulted in significant impairment of cell migration compared to the DMSO control. Cis-platin treatment resulted in significant inhibition of migration at 24h and 48h. (b) Scratch images were acquired at 0h, 24h, and 48h from U251MG cells treated as described above. Both concentrations of SHG-8 induced changes in cell morphology, and 100µM SHG-8 exposure resulted in cell death. Microscopic images of scratch areas were taken at ×40 magnification. Results are based on three independent experiments, n=3. All statistical analyses were conducted using ordinary one-way ANOVA, followed by Dunnett's multiple comparisons test to determine the significant differences between SHG-8 treated cells and DMSO control samples (legend: ****$p<0.0001$).

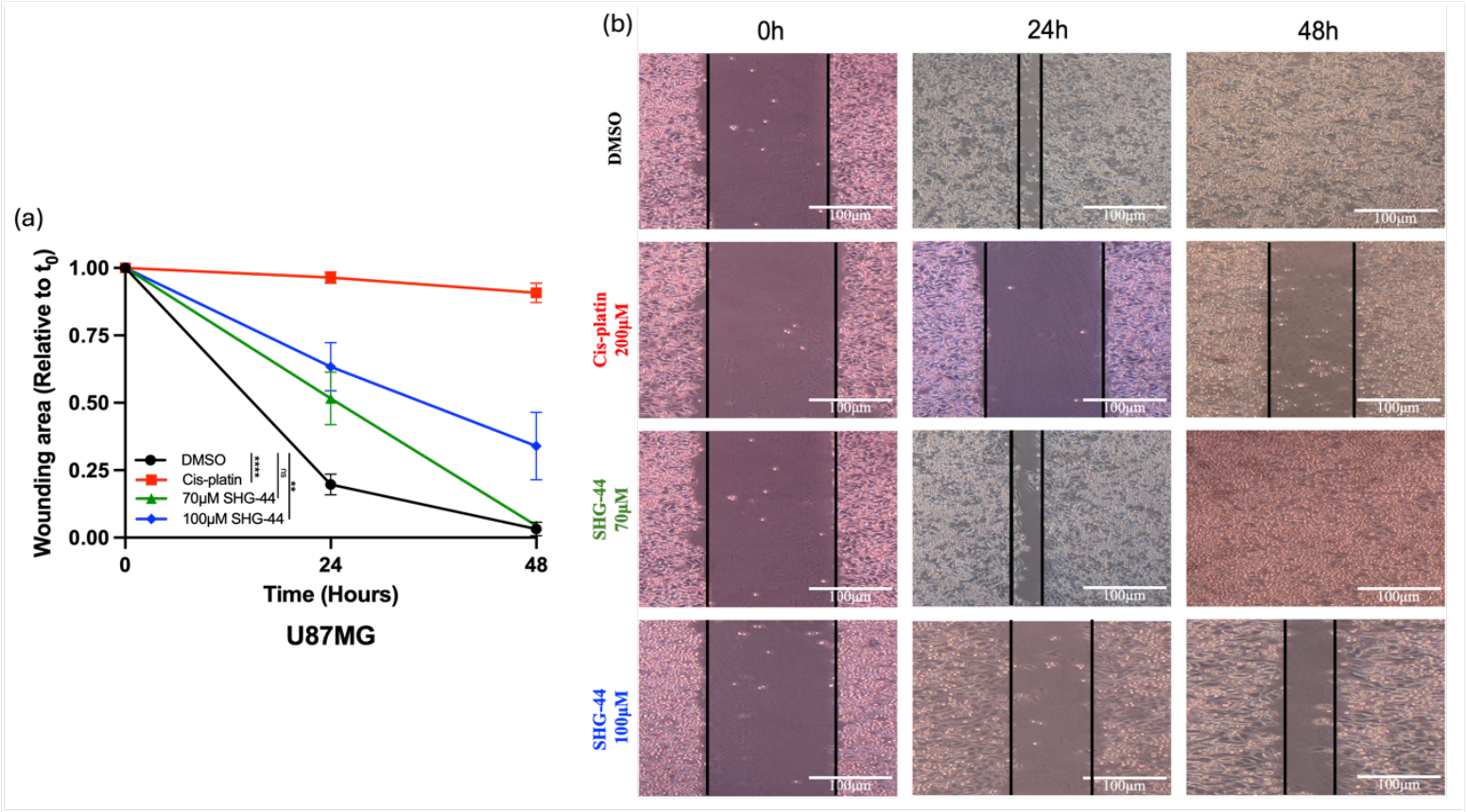


Figure 117. Cell migration of U87MG cells post-SHG-44 exposure. (a) Quantification of the wound-healing assay for U87MG cells following treatment with DMSO, cis-platin (200µM), and SHG-44 (70µM and 100µM) at various time points. Treatment with 70µM resulted in no significant impairment of cell migration compared to the DMSO control. Treatment with 100µM SHG-44 resulted in significant impairment of cell migration compared to the DMSO control. Cis-platin treatment resulted in significant inhibition of migration at 24h and 48h. (b) Scratch images were acquired at 0h, 24h, and 48h from U87MG cells treated as described above. At 48h, 100µM SHG-44 inhibited cell migration and maintained a clear scratch area. Microscopic images of scratch areas were taken at ×40 magnification. Results are based on three independent experiments, n=3. All statistical analyses were conducted using ordinary one-way ANOVA, followed by Dunnett's multiple comparisons test to determine the significant differences between SHG-44 treated cells and DMSO control samples (legend: ns: non-significant, ****p<0.0001).

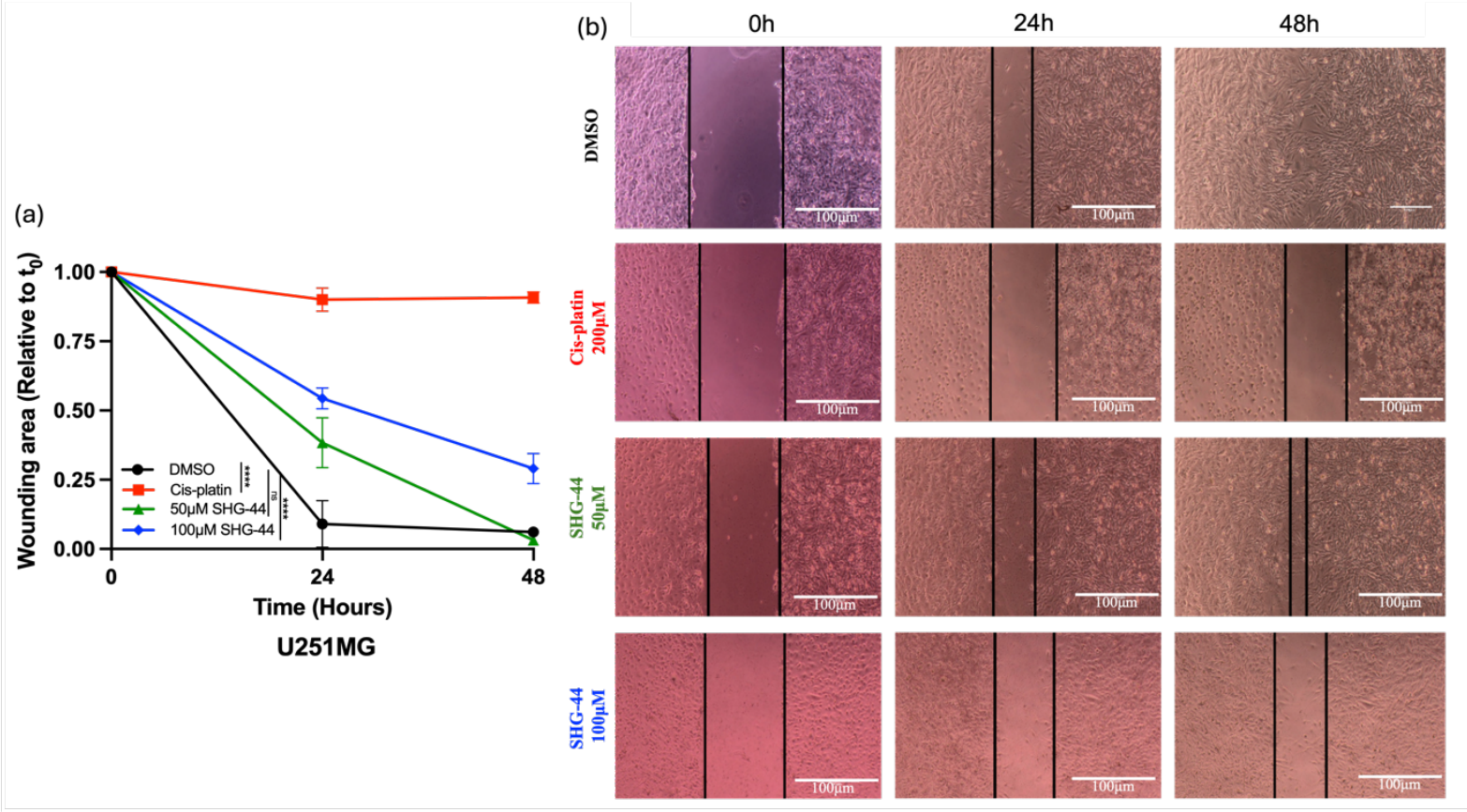


Figure 118. Cell migration of U251MG cells post-SHG-44 exposure. (a) Quantification of the wound-healing assay for U251MG cells following treatment with DMSO, cis-platin (200µM), and SHG-44 (50µM and 100µM) at various time points. Treatment with 50µM resulted in no significant impairment of cell migration compared to the DMSO control. Treatment with 100µM SHG-44 resulted in significant impairment of cell migration compared to the DMSO control. Cis-platin treatment resulted in significant inhibition of migration at 24h and 48h. (b) Scratch images were acquired at 0h, 24h, and 48h from U251MG cells treated as described above. At 48h, 100µM SHG-44 inhibited cell migration and maintained a clear scratch area. Microscopic images of scratch areas were taken at ×40 magnification. Results are based on three independent experiments, n=3. All statistical analyses were conducted using ordinary one-way ANOVA, followed by Dunnett's multiple comparisons test to determine the significant differences between SHG-44 treated cells and DMSO control samples (legend: ns: non-significant, ****$p<0.0001$).

5.3.8. Reactive oxygen species determination post-exposure to SHG-8 and SHG-44

A significant elevation of ROS was observed in U87MG cells after 30min treatment with 50μM SHG-8 compared to the PBS control condition (Figure 119). Additionally, SHG-8 at 100μM induced ROS cytotoxicity at 90min, with both concentrations (50μM and 100μM) showing significantly higher ROS levels at 120min, leading to oxidative damage in U87MG GB cells. The ROS release mechanism induced by SHG-8 in GB cells was found to be time-dependent. For U251MG cells, a significant elevation in ROS was seen at 105min with 50μM and 100μM SHG-8 treatment, but 100μM SHG-8 did not result in a significant ROS increase at 120min (Figure 120). To assess the effects of SHG-44 on ROS levels, U87MG and U251MG cells were treated with increasing concentrations of SHG-44 (40μM, 60μM, 80μM, and 100μM). Interestingly, in U87MG cells, high concentrations of SHG-44 (80μM, and 100μM) did not significantly affect ROS levels compared to the control, while 40μM and 60μM SHG-44 led to a significant increase in ROS post-90min incubation with the compound ($p<0.01$ and $p<0.001$, respectively) (Figure 121). In contrast, no significant elevation in ROS levels was observed in U251MG cells at any SHG-44 concentration (Figure 122).

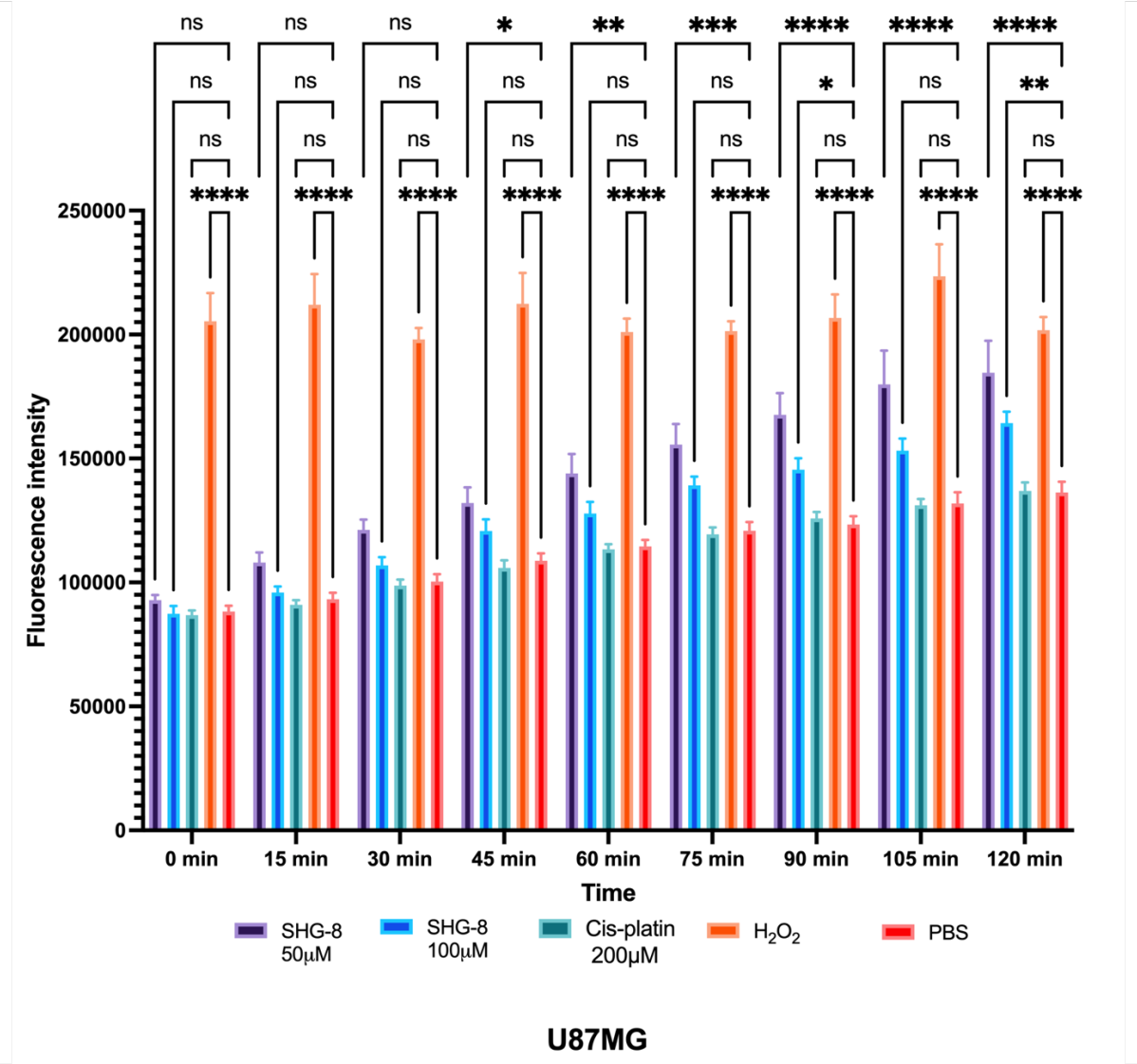


Figure 119. SHG-8 induced the release of ROS in U87MG treated cells. A significant but non-concentration-dependent increase in ROS levels was observed in U87MG cells after a 30min treatment with 50µM SHG-8 compared to the control. A 100µM concentration of SHG-8 caused ROS cytotoxicity at 90min. By 120 minutes, both 50µM and 100µM SHG-8 treatments resulted in significantly elevated ROS levels in U87MG cells. Results are based on three independent experiments, n=3. All statistical analyses were conducted using a two-way ANOVA, followed by Dunnett's multiple comparisons test to determine the significant differences in ROS production between SHG-8 samples and PBS control samples (legend: ns: non-significant, *p<0.05, **p<0.01, ***p<0.001, ****p<0.0001).

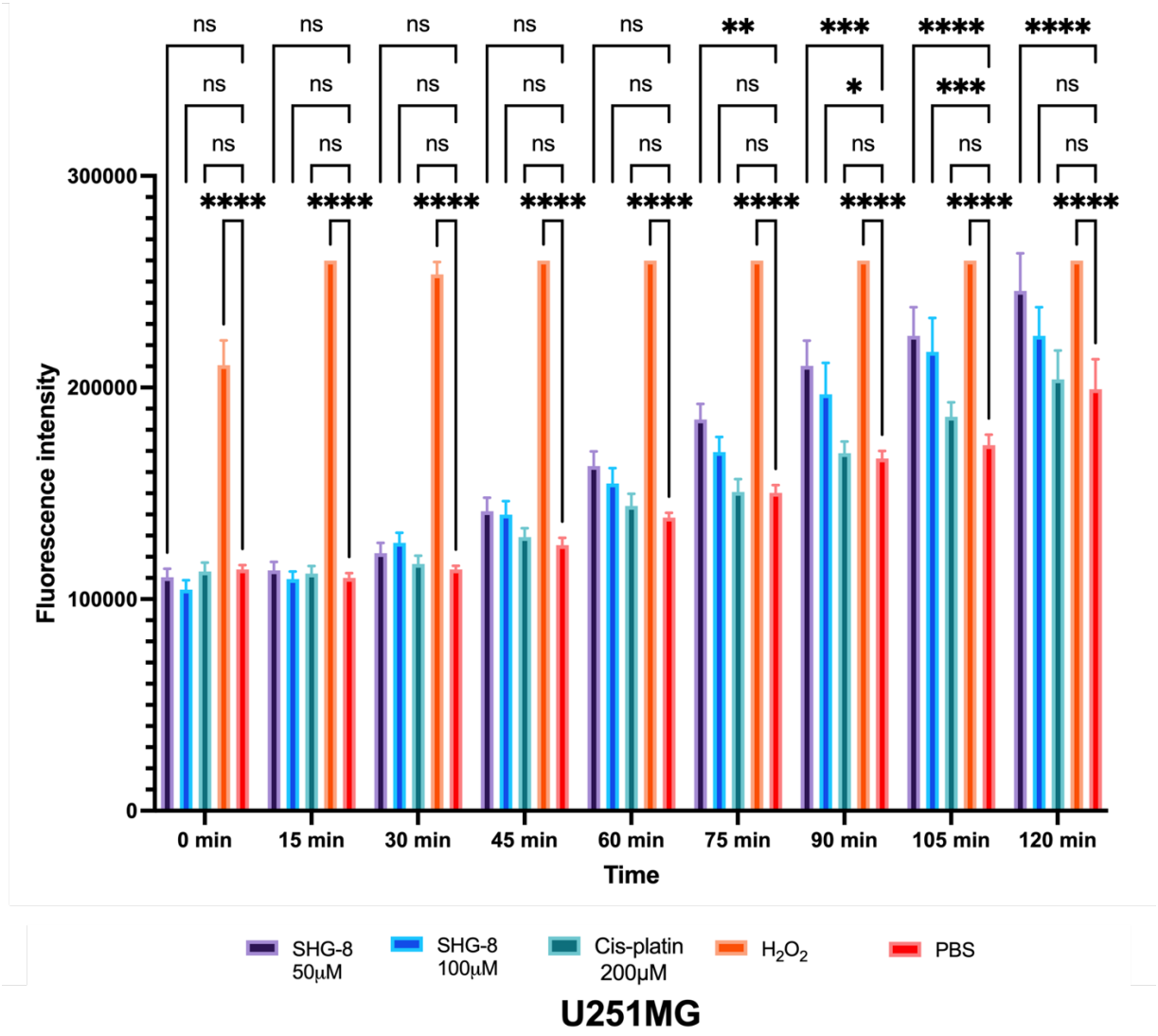


Figure 120. SHG-8 induced the release of ROS in U251MG treated cells. A significant but non-concentration-dependent increase in ROS levels was observed in U251MG cells after a 105min treatment with 50µM and 100µM SHG-8 compared to the control. The 100µM concentration of SHG-8 caused no ROS cytotoxicity at 120min. Results are based on three independent experiments, n=3. All statistical analyses were conducted using a two-way ANOVA, followed by Dunnett's multiple comparisons test to determine the significant differences of ROS production between SHG-8 samples and PBS control samples (legend: ns: non-significant, *p<0.05, **p<0.01, ***p<0.001, ****p<0.0001).

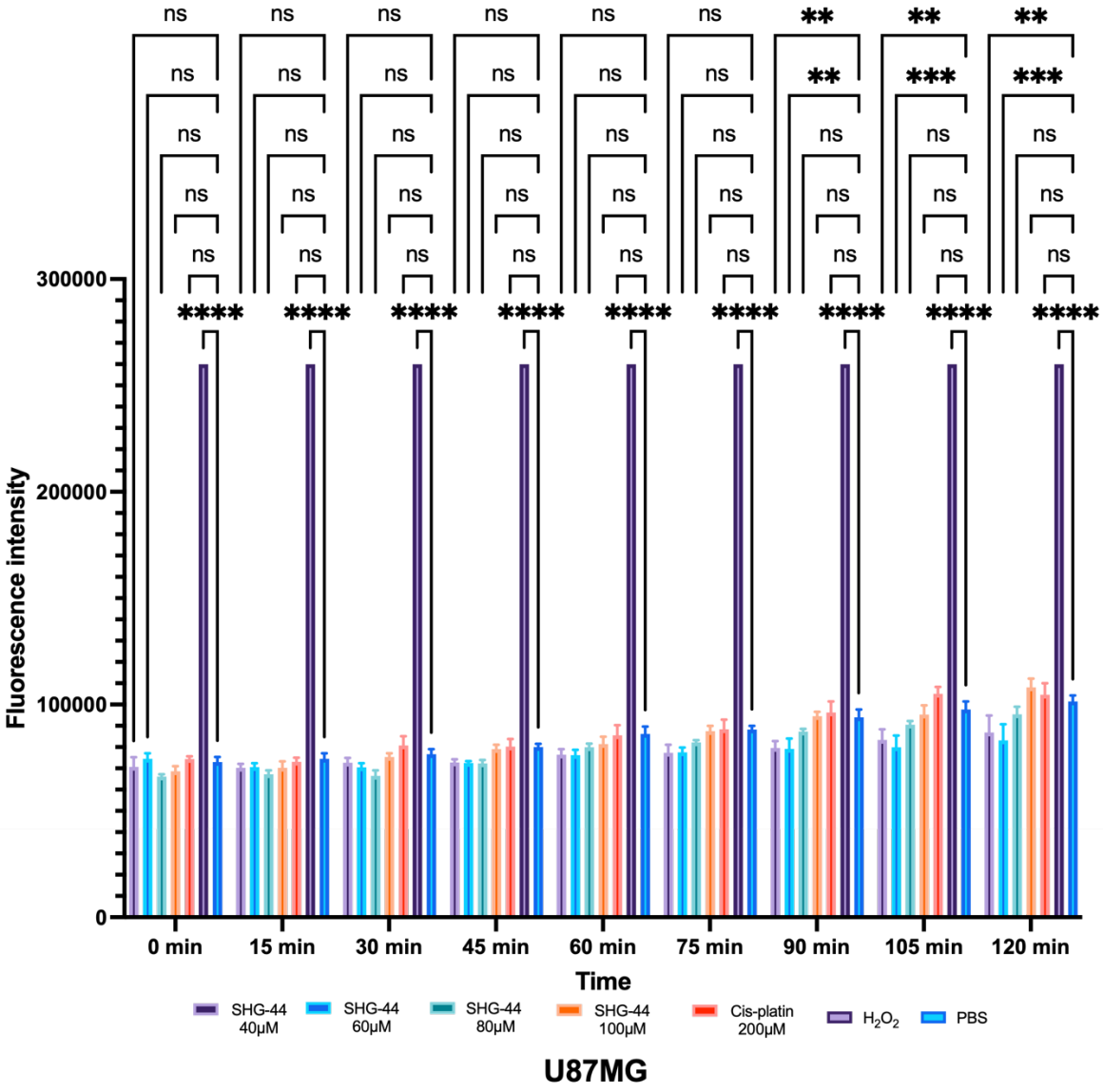


Figure 121. SHG-44 induced the release of ROS in U87MG treated cells. A significant but non-concentration-dependent increase in ROS levels was observed in U87MG cells after a 90min treatment with 40μM and 60μM SHG-44 compared to the control. The 80μM and 100μM concentrations of SHG-44 caused no ROS cytotoxicity. Results are based on three independent experiments, n=3. All statistical analyses were conducted using a two-way ANOVA, followed by Dunnett's multiple comparisons test to determine the significant differences in ROS production between SHG-44 samples and PBS control samples (legend: ns: non-significant, **p<0.01, ***p<0.001, ****p<0.0001).

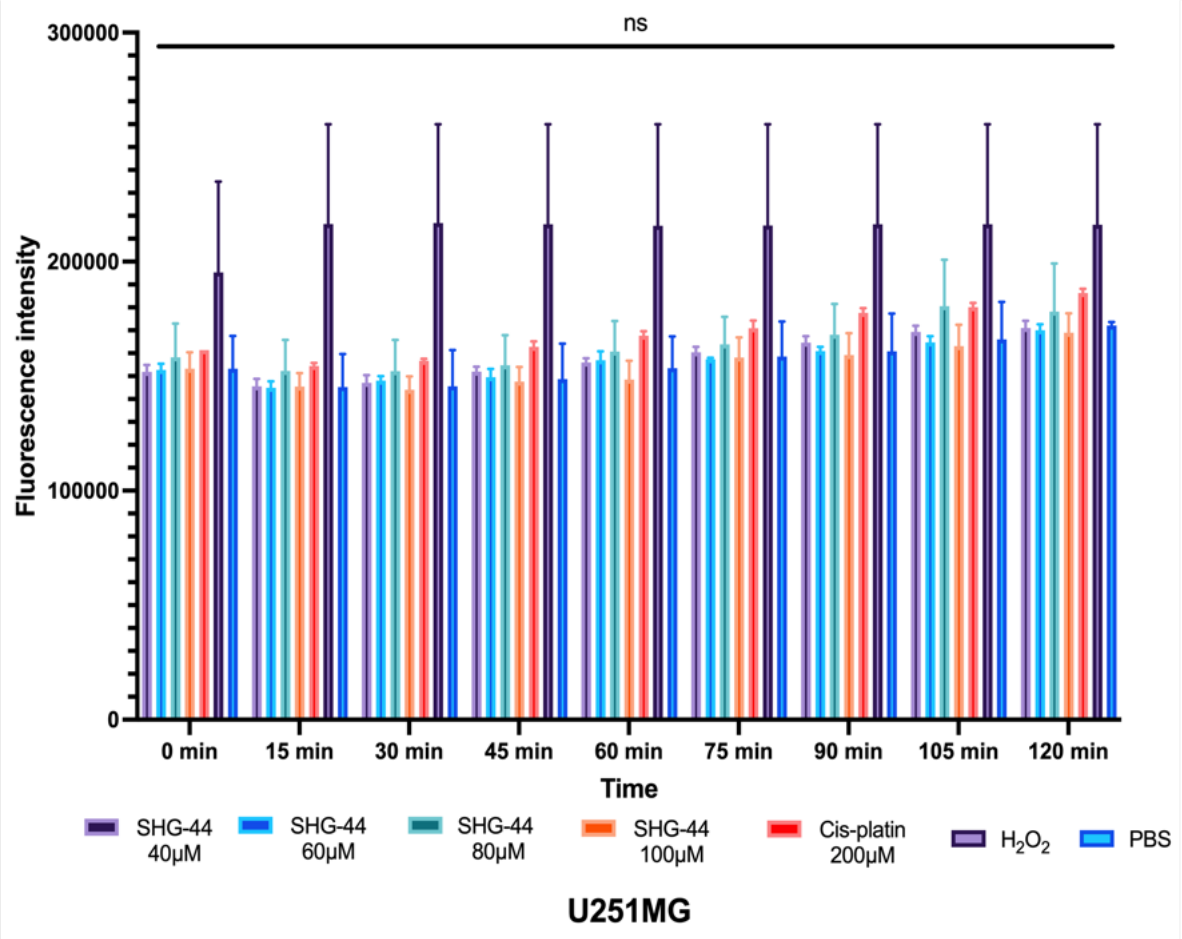


Figure 122. SHG-44 induced the release of ROS in U251MG treated cells. No significant elevation in ROS levels was observed in U251MG cells at any SHG-44 concentration. Results are based on three independent experiments, n=3. All statistical analyses were conducted using a two-way ANOVA, followed by Dunnett's multiple comparisons test to determine the significant differences in ROS production between SHG-44 samples and PBS control samples (legend: ns: non-significant).

5.3.9. SHG-8 and SHG-44 mediated apoptosis in U87MG and U251MG glioma cells

To investigate whether SHG-8 and SHG-44 induced loss in cellular integrity leading to apoptosis, after an incubation time of 24 hours for the drug treatments, DAPI and AO/EtBr staining were performed on U87MG and U251MG cells. DAPI staining revealed that treatment with 50µM and 100µM SHG-8 induced nuclear fragmentation in both cell lines (Figures 123a and 123b). However, the disintegration of the nuclear structure was more pronounced in U251MG cells under 50µM and 100µM SHG-8 treatment conditions, whereas U87MG cells exhibited minimal nuclear fragmentation at the 50µM concentration. In SHG-8-treated cells, high uptake of ethidium bromide was observed at 100µM concentrations, indicating a loss of membrane integrity and cell death (Figures 125a, 125b, 126a and 126b). Specifically, U251MG cells treated with 50µM SHG-8 exhibited more early apoptosis compared to U87MG cells.

Additionally, treatment with 200μM cis-platin also showed nuclear fragmentation alongside apoptotic and necrotic stages, with increased ethidium bromide uptake, particularly in U251MG cells. In contrast, the negative control (DMSO) condition showed no signs of cell death, with cells' nuclei appearing intact and maintaining regular shape (Figures 125 and 126). Similarly, SHG-44 treatment led to notable morphological changes. DAPI staining revealed that U87MG treated with cis-platin (200μM) or SHG-44 at either 70μM or 100μM displayed prominent nuclear fragmentation, characterised by multiple nuclear ruptures (Figures 124a). U251MG cells treated with cis-platin (200μM) or SHG-44 at either 50μM or 100μM also displayed nuclear fragmentation, with minimal nuclear fragmentation at the 50μM concentration (Figure 124b). AO/EtBr staining further confirmed that 100μM SHG-44 induced significant ethidium bromide uptake, indicating cell death, while 70μM SHG-44 caused more early apoptosis in U87MG in comparison to U251MG cells which were treated with 50μM SHG-44 as the lower end concertation (Figures 127a, 127b, 128a and 128b). Similar levels of apoptotic and necrotic cell death were observed with 200μM cis-platin treatment. The negative control (DMSO) showed no signs of drug-induced cell death, with cells retaining an intact and regular shape (Figures 127 and 128).

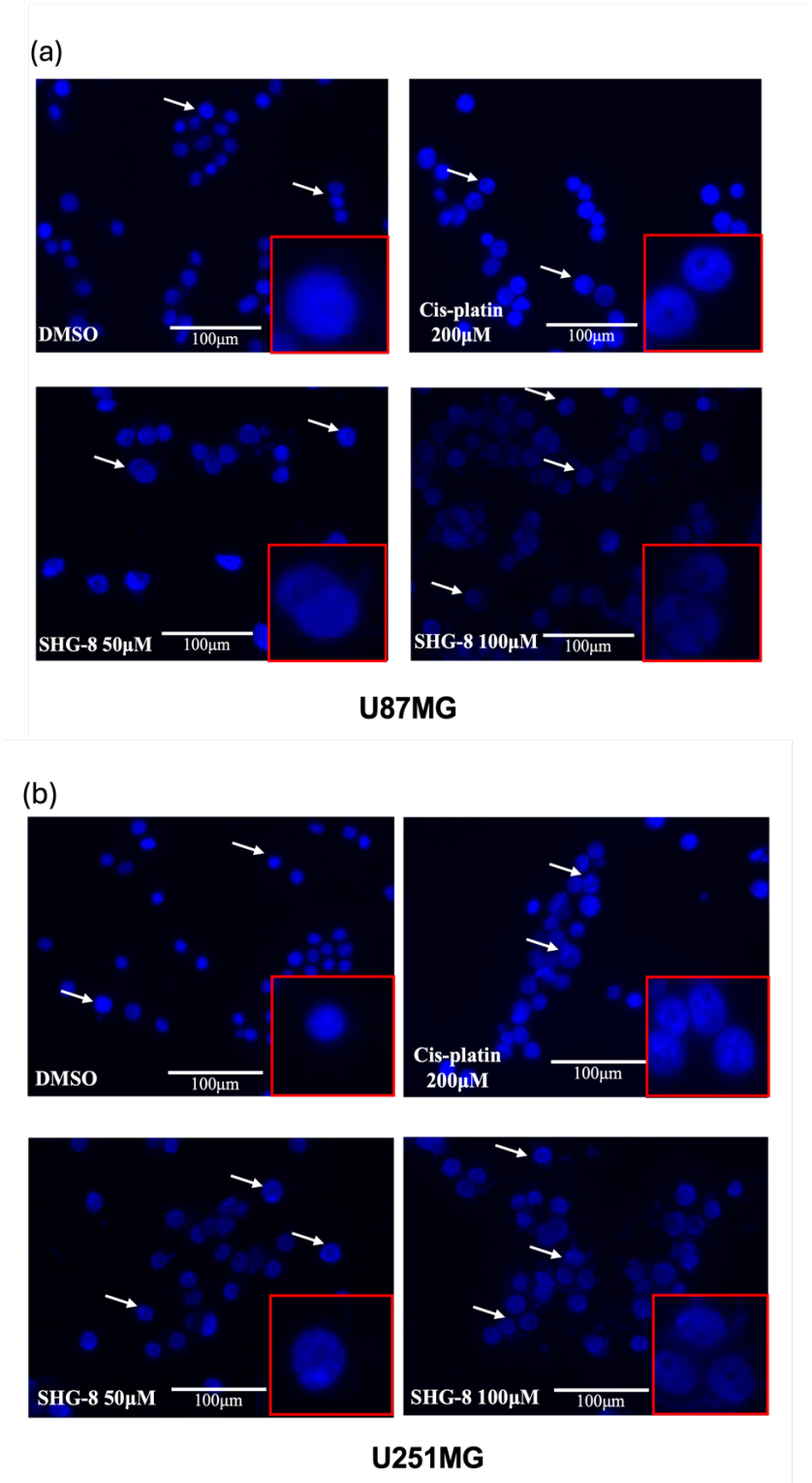


Figure 123. DAPI staining of U87MG and U251MG cells treated with SHG-8. (a) Treatment with 50µM and 100µM SHG-8 induced nuclear fragmentation in U87MG cells (white arrows). (b) Nuclear disintegration was more pronounced in U251MG cells at both concentrations. In both U87MG and U251MG cell lines, DMSO showed regular nuclei, whereas cis-platin treatment also resulted in nuclear fragmentation (white arrows). Results are based on three independent experiments, n=3.

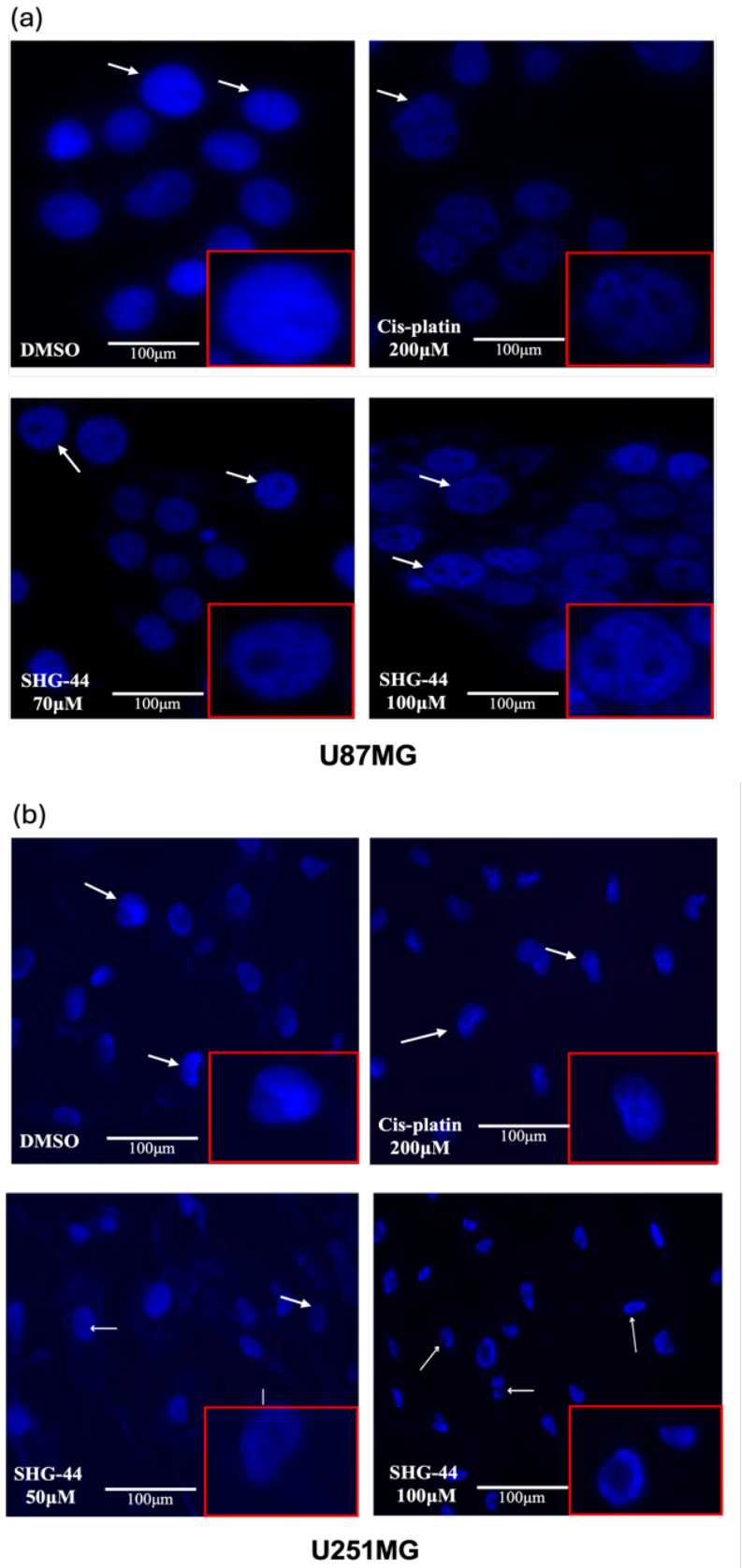


Figure 124. DAPI staining of U87MG and U251MG cells treated with SHG-44. (a) SHG-44 treatment of U87MG cells at 70µM or 100µM, as well as cis-platin treatment at 200µM, resulted in significant morphological changes, including obvious nuclear fragmentation characterised by multiple nuclear ruptures (white arrows). (b) Similarly, SHG-44 treatments of

U251MG cells at 50μM or 100μM, as well as cis-platin treatment also resulted in nuclear disintegration, with minimal nuclear fragmentation noticed at the 50μM concentration (white arrows). DMSO exposed cells showed regular nuclei and no signs of fragmentation in both cell lines. Results are based on three independent experiments, n=3.

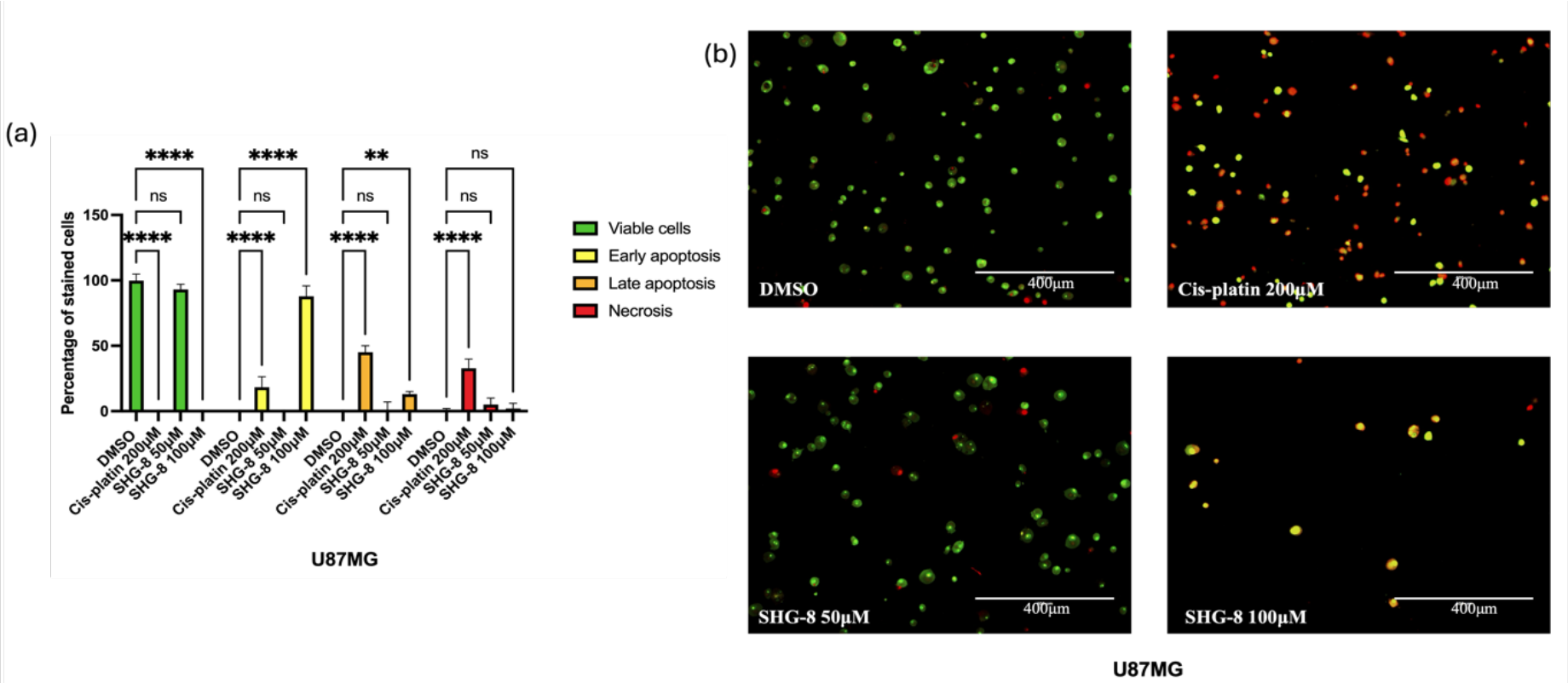


Figure 125. Acridine orange/ethidium bromide staining of U87MG cells post-SHG-8 treatment. (a) Quantification of apoptosis within U87MG cells post-exposure to DMSO, 200µM cis-platin, and 50µM and 100µM SHG-8. Treatment with 50µM SHG-8 did not lead to significant changes when compared to the DMSO control condition. The concentration of 100µM led to a significant increase in cells entering early apoptosis in comparison to the DSMO control. Cis-platin treatment showed a significantly high number of cells undergoing late apoptosis and necrosis. (b) Fluorescent microscopic images of U87MG cells treated with DMSO, 200µM cis-platin, and 50µM and 100µM SHG-8. Green cells indicate viability, yellow cells indicate early apoptosis, orange cells indicate late apoptosis, and red cells indicate necrosis. Results are based on three independent experiments, n=3. All statistical analyses were conducted using a two-way ANOVA, followed by Dunnett's multiple comparisons test to determine the significant differences between SHG-8 treated cells in early and late apoptosis, or necrosis with DMSO control samples (legend: ns: non-significant, **p<0.01, ****p<0.0001).

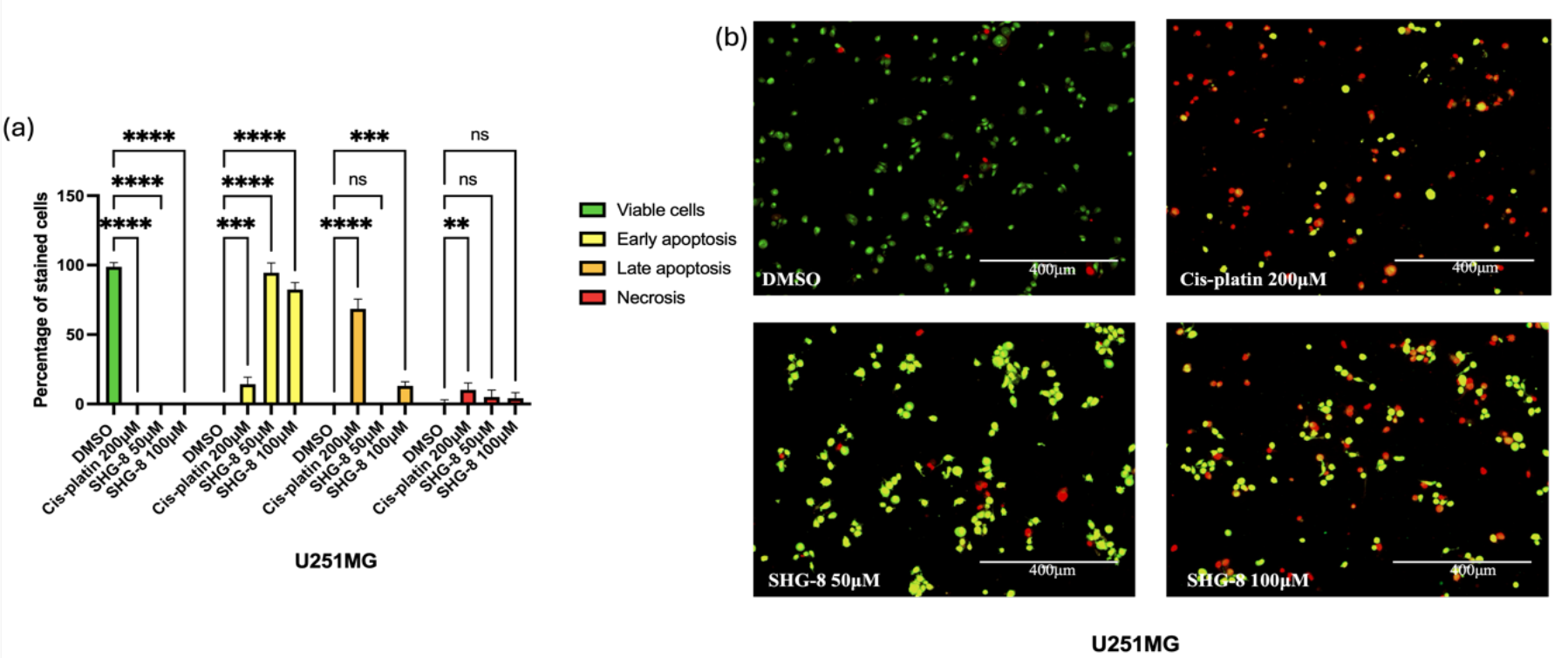


Figure 126. Acridine orange/ethidium bromide staining of U251MG cells post-SHG-8 treatment. (a) Quantification of apoptosis within U251MG cells post-exposure to DMSO, 200µM cis-platin, and 50µM and 100µM SHG-8. Both concentrations of 50µM and 100µM led to a significant increase of cells in early apoptosis in comparison to the DSMO control. The concentration of 100µM also led to a significant increase of cells in late apoptosis. Cis-platin treatment showed significantly high number of cells undergoing late apoptosis and necrosis. (b) Fluorescent microscopic images of U251MG cells treated with DMSO, 200µM cis-platin, and 50µM and 100µM SHG-8. Green cells indicate viability, yellow cells indicate early apoptosis, orange cells indicate late apoptosis, and red cells indicate necrosis. Results are based on three independent experiments, n=3. All statistical analyses were conducted using a two-way ANOVA, followed by Dunnett's multiple comparisons test to determine the significant differences between SHG-8 treated cells in early and late apoptosis or necrosis with DMSO control samples (legend: ns: non-significant, **p<0.01, ***p<0.001, ****p<0.0001).

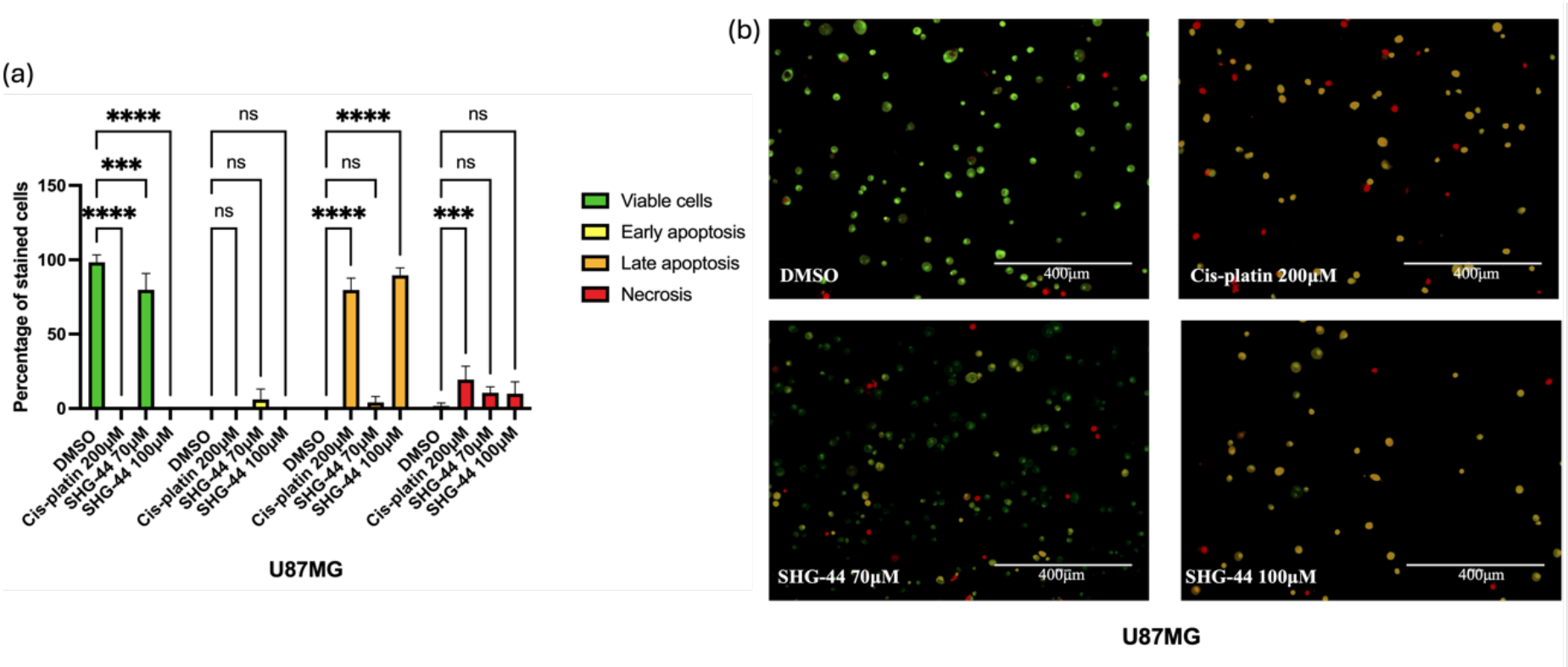


Figure 127. Acridine orange/ethidium bromide staining of U87MG cells post-SHG-44 treatment. (a) Quantification of apoptosis within U87MG cells post-exposure to DMSO, 200µM cis-platin, and 70µM and 100µM SHG-44. Treatment with 100µM SHG-44 led to a significant increase of cells in late apoptosis in comparison to the DSMO control. The concentration of 50µM did not lead a significant increase of cells in early or late apoptosis. Cis-platin treatment showed significantly high number of cells undergoing late apoptosis and necrosis. (b) Fluorescent microscopic images of U87MG cells treated with DMSO, 200µM cis-platin, and 70µM and 100µM SHG-44. Green cells indicate viability, yellow cells indicate early apoptosis, orange cells indicate late apoptosis, and red cells indicate necrosis. Results are based on three independent experiments, n=3. All statistical analyses were conducted using a two-way ANOVA, followed by Dunnett's multiple comparisons test to determine the significant differences between SHG-44 treated cells in early and late apoptosis or necrosis with DMSO control samples (legend: ns: non-significant, ***$p<0.001$, ****$p<0.0001$).

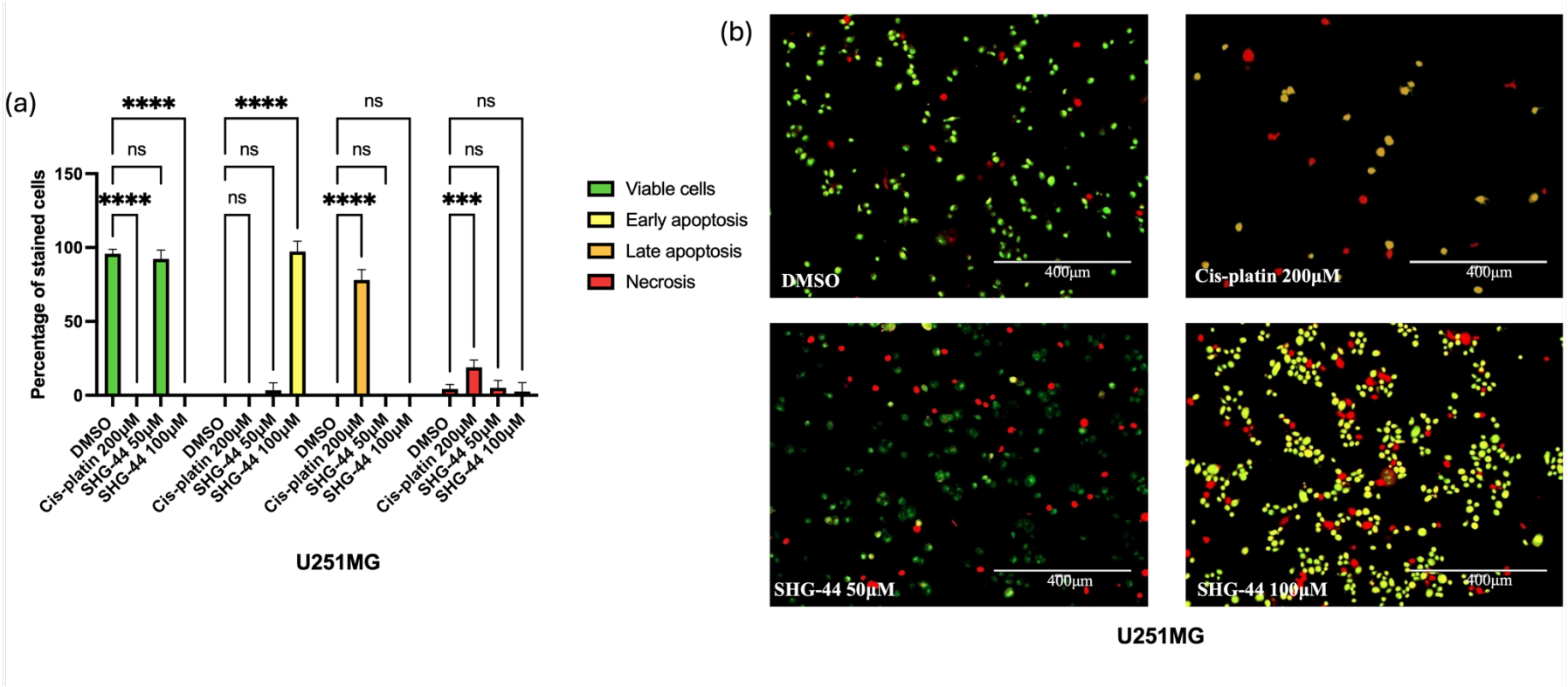


Figure 128. Acridine orange/ethidium bromide staining of U251MG cells post-SHG-44 treatment. (a) Quantification of apoptosis within U251MG cells post-exposure to DMSO, 200µM cis-platin, and 50µM and 100µM SHG-44. Treatment with 50µM SHG-44 did not lead a significant increase of cells in early or late apoptosis. Treatment with 100µM SHG-44 led to a significant increase of cells in early apoptosis in comparison to the DSMO control. Cis-platin treatment showed significantly high number of cells undergoing late apoptosis and necrosis. (b) Fluorescent microscopic images of U251MG cells treated with DMSO, 200µM cis-platin, and 50µM and 100µM SHG-44. Green cells indicate viability, yellow cells indicate early apoptosis, orange cells indicate late apoptosis, and red cells indicate necrosis. Results are based on three independent experiments, n=3. All statistical analyses were conducted using a two-way ANOVA, followed by Dunnett's multiple comparisons test to determine the significant differences between SHG-44 treated cells in early and late apoptosis or necrosis with DMSO control samples (legend: ns: non-significant, ***p<0.001, ****p<0.0001).

5.3.10. Molecular docking

Molecular docking analysis was performed to explore the interaction between SHG-8 and SHG-44 and CORO1C and SV2B. Figure 129a illustrates the spatial configuration of the five binding sites identified between SHG-8 and CORO1C, depicted in a spacefill model. Among these, the binding site at position C1 demonstrated the strongest interaction, characterised by the lowest binding energy of -8.1kcal/mol, as indicated by the Vina score (Table 21, Figure 129b). Similarly, SHG-8 possessed five binding sites for SV2B as well, with lowest binding site energy being -8.6kcal/mol at position C1 (Table 22, Figure 130a and 130b). SHG-44 showed five binding sites with lower affinities towards both, CORO1C and SV2B (Table 23, Table 24, Figure 131a, and 132a). The highest affinity binding between SHG-44 and CORO1C was at position C1 with Vina score of -7.3kcal/mol (Figure 131b). The highest affinity binding between SHG-44 and SV2B was at position C1 with Vina score of -7.2kcal/mol (Figure 132b).

Table 21. Molecular docking sites and binding affinities between the large molecule receptor protein CORO1C and the small molecule ligand SHG-8.

CurPocket ID	Vina score	Cavity volume (Å3)	Center (x, y, z)	Docking size (x, y, z)
C1	-8.1	3858	54, 18, 9	22, 35, 34
C5	-7.6	132	49, 21, -23	22, 22, 22
C2	-7.2	196	74, 2, -5	22, 22, 22
C3	-6.5	178	39, 4, -2	22, 22, 22
C4	-6.3	139	70, 9, -10	22, 22, 22

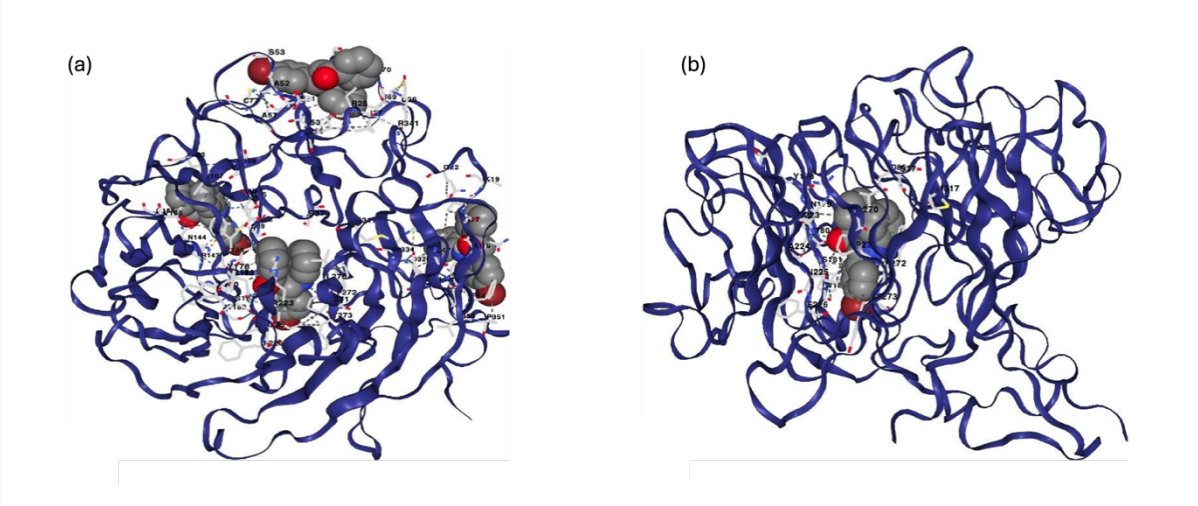


Figure 129. Molecular docking between SHG-8 and CORO1C. (a) The illustration depicted the five binding sites between CORO1C and SHG-8 using a spacefill model. (b) The strongest binding interaction between CORO1C and SHG-8 was observed at position C1, characterised by the lowest binding energy of -8.1 (Vina score).

Table 22. Molecular docking sites and binding affinities between the large molecule receptor protein SV2B and the small molecule ligand SHG-8.

CurPocket ID	Vina score	Cavity volume (Å3)	Center (x, y, z)	Docking size (x, y, z)
C1	-8.6	7672	17, 8, -10	35, 35, 35
C2	-7.3	2626	-29, -11, 15	22, 22, 22
C4	-6.4	377	-24, -28, -2	22, 22, 22
C5	-6.0	265	1, 14, 14	22, 22, 22
C3	-5.9	385	23, -9, -13	22, 22, 22

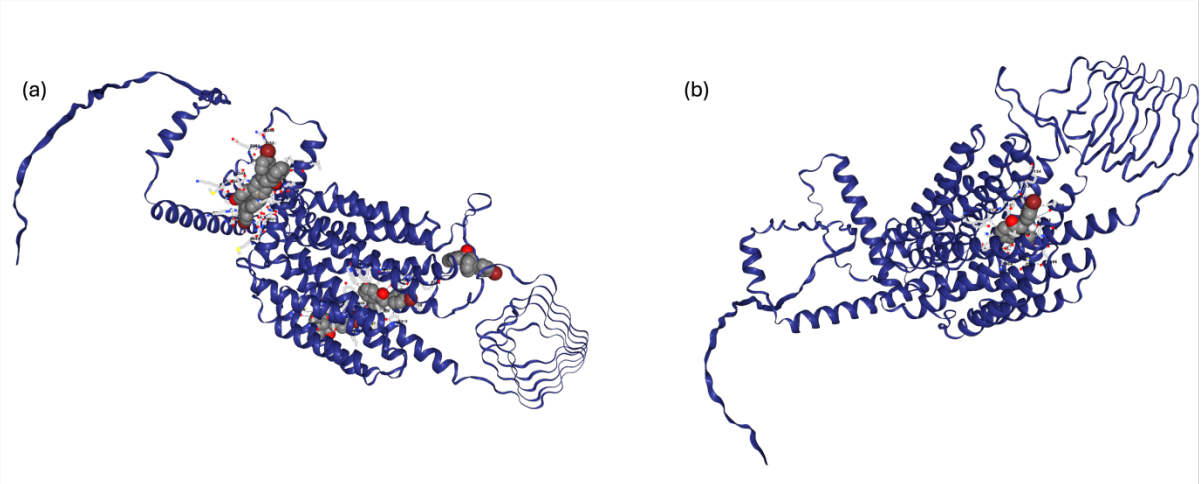


Figure 130. Molecular docking between SHG-8 and SV2B. (a) The illustration depicted the five binding sites between SV2B and SHG-8 using a spacefill model. (b) The strongest binding interaction between SV2B and SHG-8 was observed at position C1, characterised by the lowest binding energy of -8.6 (Vina score).

Table 23. Molecular docking sites and binding affinities between the large molecule receptor protein CORO1C and the small molecule ligand SHG-44.

CurPocket ID	Vina score	Cavity volume (Å3)	Center (x, y, z)	Docking size (x, y, z)
C1	-7.3	3858	54, 18, 9	22, 35, 34
C2	-6.5	196	74, 2, -5	22, 22, 22
C4	-6.5	139	70, 9, -10	22, 22, 22
C5	-6.4	132	49, 21, -23	22, 22, 22
C3	-5.5	178	39, 4, -2	22, 22, 22

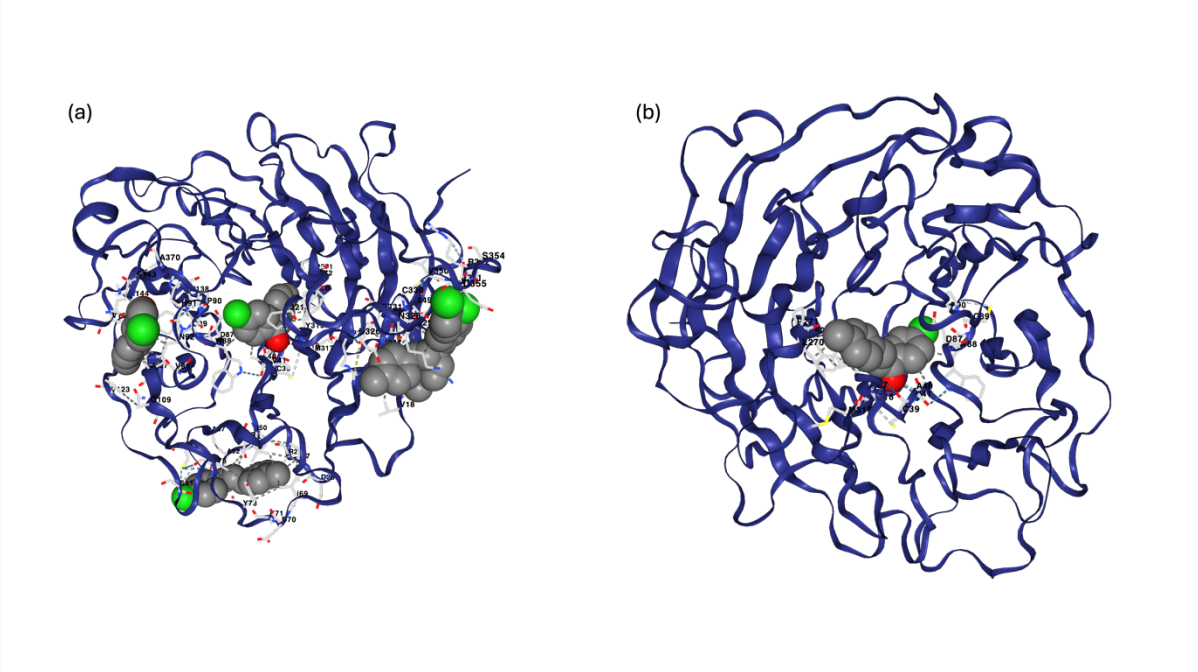


Figure 131. Molecular docking between SHG-44 and CORO1C. (a) The illustration depicted the five binding sites between CORO1C and SHG-44 using a spacefill model. (b) The strongest binding interaction between CORO1C and SHG-44 was observed at position C1, characterised by the lowest binding energy of -7.3 (Vina score).

Table 24. Molecular docking sites and binding affinities between the large molecule receptor protein SV2B and the small molecule ligand SHG-44.

CurPocket ID	Vina score	Cavity volume (Å3)	Center (x, y, z)	Docking size (x, y, z)
C1	-7.2	7672	17, 8, -10	35, 35, 35
C2	-6.7	2626	-29, -11, 15	22, 22, 22
C4	-6.3	377	-24, -28, -2	22, 22, 22
C3	-6.0	385	23, -9, -13	22, 22, 22
C5	-6.0	265	1, 14, 14	22, 22, 22

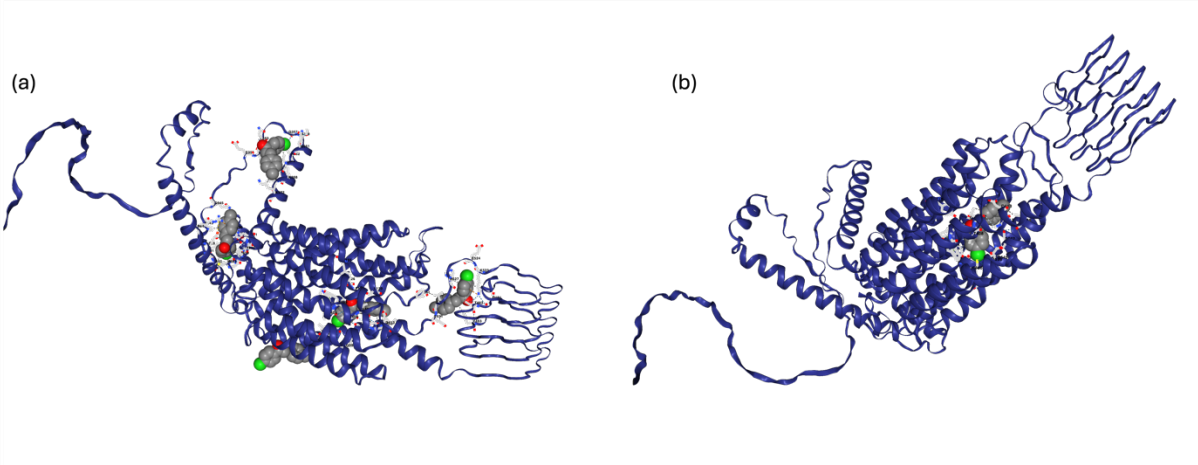


Figure 132. Molecular docking between SHG-44 and SV2B. (a) The illustration depicted the five binding sites between SV2B and SHG-44 using a spacefill model. (b) The strongest binding interaction between SV2B and SHG-44 was observed at position C1, characterised by the lowest binding energy of -7.2 (Vina score).

5.3.11. RT-qPCR gene analysis following molecular docking

RT-qPCR of treated U87MG cells was subsequently performed. The results revealed a significant downregulation of *CORO1C* within U87MG cells when exposed to 100µM SHG-8 treatments (Figure 133a). RT-qPCR of U87MG treated with 50µM of SHG-8 showed a significant increase of *SV2B* expression, followed by decreased expression of *SV2B* at 100µM (Figure 133b). Treatment with SHG-44 demonstrated no significant differences in *CORO1C* and *SV2B* expression levels in comparison to the DSMO control (Figures 133c and 133d).

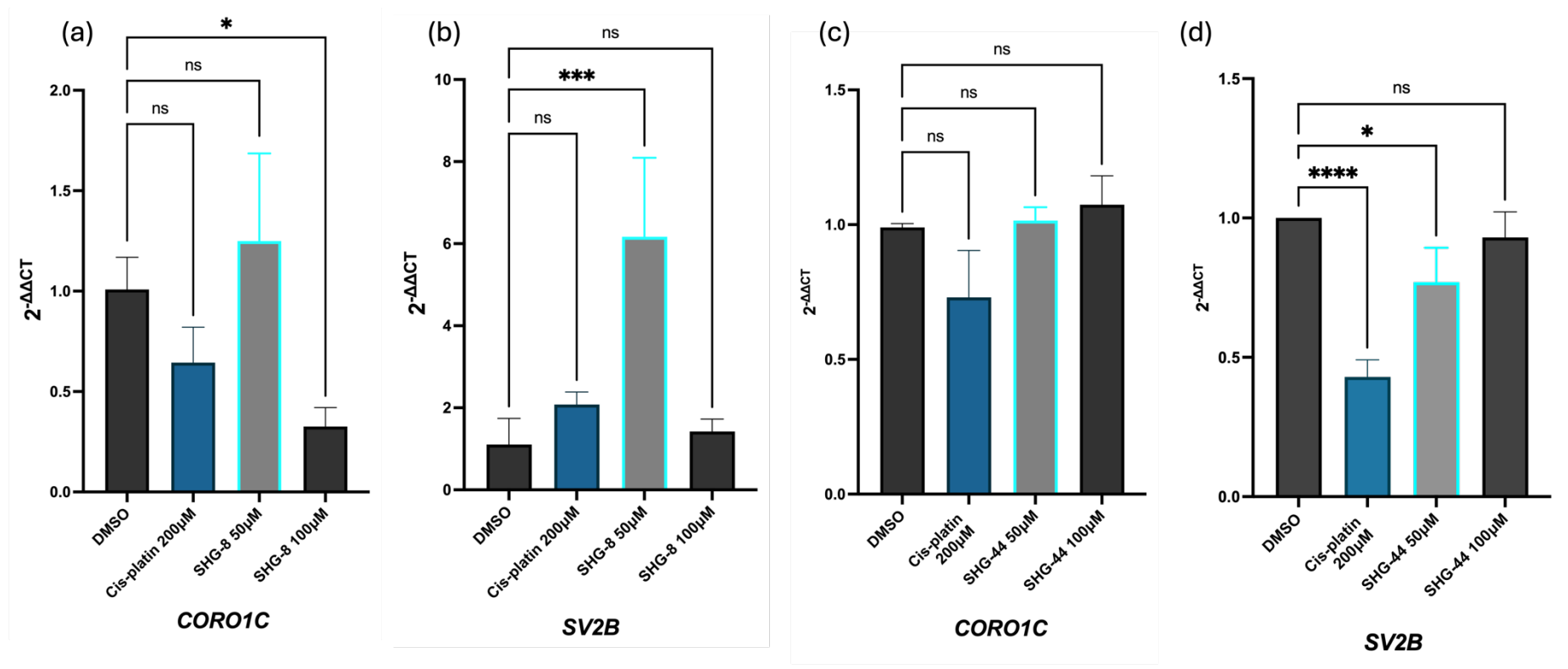


Figure 133. RT-qPCR analysis of gene expression following SHG-8 and SHG-44 treatments. (a) *CORO1C* was significantly downregulated in U87MG cells post-treatment with 100µM SHG-8 ($p<0.0270$). (b) *SVB2* was significantly upregulated by 50µM SHG-8 ($p<0.0009$). (c) There was no significant difference in the expression of *CORO1C* post-exposure to SHG-44 (50µM, $p<0.9930$; 100µM, $p<0.8297$). (d) There was no significant difference in the expression of *SV2B* post-SHG-44 treatment (50µM, $p<0.05$; 100µM, $p<0.3585$). Results are based on three independent experiments, n=3. All statistical analyses were conducted using ordinary one-way ANOVA, followed by Dunnett's multiple comparisons test to determine the significant differences between SHG-8/SHG-44 treated cells, cis-platin treated cells, and DMSO control samples.

5.3.12. *In silico* analysis of the pharmacokinetic and pharmacodynamic characteristics of SHG-8 and SHG-44

The nine predicted metabolites of SHG-8 (SHG-8-1 to SHG-8-9), shown in Figure 134 were based on one reduction of the parent compound by carbonyl reductase, with additional hydroxylations and dealkylations predicted by cytochrome P450 1A2 (CYP1A2). Similarly, two predicted metabolites of SHG-44 (SHG-44-1 and SHG-44-2), shown in Figure 135 were obtained through carbonyl reductase reduction and reduction of an alpha, beta-unsaturated carbon-carbon double bond. Selected absorption, distribution, and toxicity properties of SHG-8 and SHG-44, along with their metabolites, were predicted using admetSAR 2.0 and compared to over-the-counter painkillers ibuprofen and aspirin (Table 25 and Table 26). SHG-8 and SHG-44 exhibited absorption and distribution profiles similar to ibuprofen and aspirin, respectively. Furthermore, both compounds were predicted to pass the blood-brain barrier. The results also showed that neither SHG-8 nor SHG-44 were substrates or inhibitors of P-glycoprotein. Toxicity predictions revealed that both SHG-8 and SHG-44, along with their metabolites, fell into acute oral toxicity class III (medium), similar to ibuprofen and aspirin. However, SHG-8 and several metabolites were predicted to be positive for the micronucleus test, while SHG-44 was negative in this test. Both compounds were not predicted to be mutagenic in the Ames test. Notably, SHG-44 displayed nephrotoxicity and mitochondrial toxicity profiles similar to aspirin and ibuprofen, while SHG-8 showed potential hERG inhibition, usually associated with cardiac issues. Several SHG-44 metabolites were also predicted to inhibit hERG. Neither SHG-8 nor SHG-44, nor their metabolites were predicted to be carcinogenic.

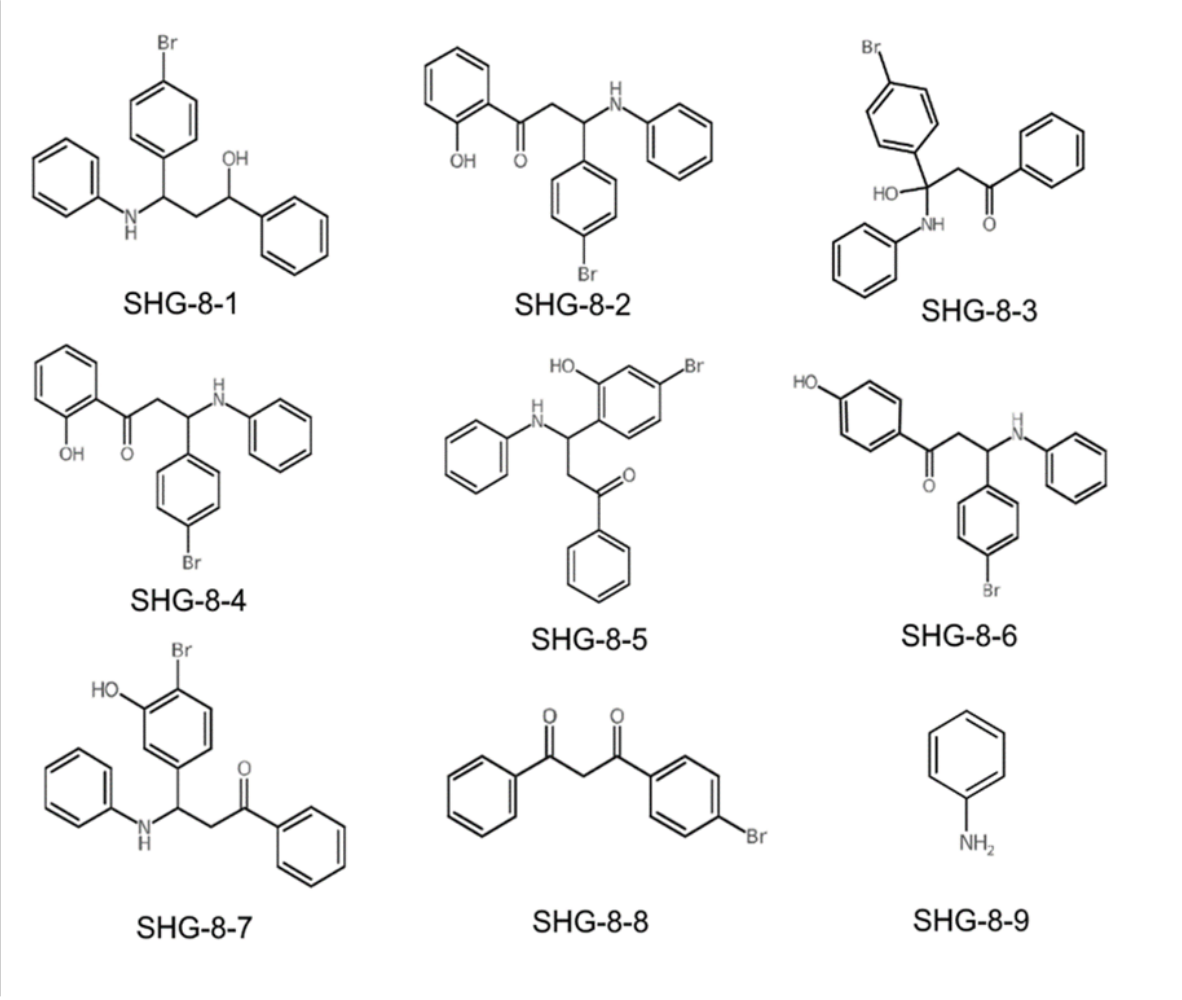


Figure 134. Metabolites of SHG-8 predicted by Biotransformer 3.1. The nine predicted metabolites of SHG-8 (SHG-8-1 to SHG-8-9), derived from a single reduction of the parent compound by carbonyl reductase, followed by further hydroxylation and dealkylation reactions predicted by cytochrome P450 1A2 (CYP1A2).

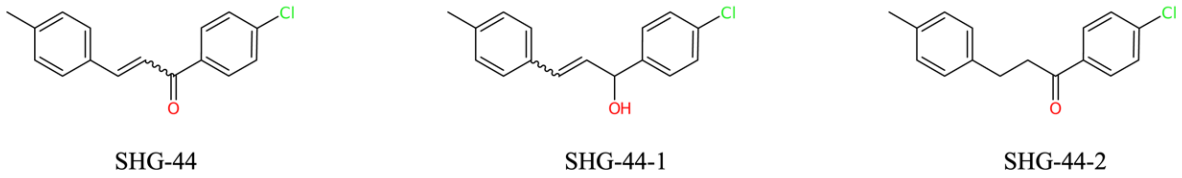


Figure 135. Metabolites of SHG-44 predicted by Biotransformer 3.1. The two predicted metabolites of SHG-44 (SHG-44-1 and SHG-44-2), derived from carbonyl reductase reduction and the reduction of an alpha, beta-unsaturated carbon-carbon double bond.

Table 25. Prediction of absorption, distribution, and toxicity properties of SHG-8 and its metabolites, alongside aspirin and ibuprofen analysis. A '+' symbol indicates a positive prediction, while a '-' symbol signifies a negative prediction or the absence of a feature. The numbers represent fractions between 0 and 1. Toxicity classes are categorised from IV to I, with class IV representing the lowest level of toxicity.

	Compound										
Feature[1]	**SHG-8**	**SHG-8-1**	**SHG-8-2**	**SHG-8-3**	**SHG-8-4**	**SHG-8-5**	**SHG-8-6**	**SHG-8-7**	**SHG-8-8**	**Aspirin**	**Ibuprofen**
Caco-2 permeability	+	+	-	+	-	+	-	+	+	-	+
Human Intestinal Absorption	+	+	+	+	+	+	+	+	+	+	+
Human oral bioavailability	+	+	+	+	+	+	-	+	+	+	+
Blood Brain Barrier	+	+	+	+	+	+	+	+	+	-	+
P-glycoprotein inhibitior	-	-	-	-	-	-	-	-	-	-	-
P-glycoprotein substrate	-	-	-	-	-	-	-	-	-	-	-
Plasma protein binding[2]	0.791	0.725	0.972	0.918	0.972	0.821	0.649	0.897	0.760	0.583	0.751
Ames mutagenesis	-	-	-	-	-	-	-	-	-	-	-
Acute Oral Toxicity[3]	III	III	III	III	III	III	III	III	III	II	III
Carcinogenicity (binary)	-	-	-	-	-	-	-	-	-	-	-
Hepatotoxicity	+	-	+	+	+	+	+	+	+	+	+
hERG inhibition	+	+	-	-	-	+	+	-	-	-	-
Mitochondrial toxicity	-	+	+	+	+	+	-	+	-	+	+
Micronucleus test	-	-	+	+	+	+	+	+	-	+	-
Nephrotoxicity	-	-	-	+	-	-	-	-	-	+	-
Reproductive toxicity	-	-	+	-	+	+	+	+	-	+	+
Respiratory toxicity	-	+	+	-	+	-	-	-	-	+	+

Table 26. Prediction of absorption, distribution, and toxicity properties of SHG-44 and its metabolites, alongside aspirin and ibuprofen analysis. A '+' symbol indicates a positive prediction, while a '-' symbol signifies a negative prediction or the absence of a feature. The numbers represent fractions between 0 and 1. Toxicity classes are categorised from IV to I, with class IV representing the lowest level of toxicity.

	Compound				
Feature[1]	**SHG-44**	**SHG-44-1**	**SHG-44-2**	**Aspirin**	**Ibuprofen**
Caco-2 permeability	+	+	+	-	+
Human Intestinal Absorption	+	+	+	+	+
Human oral bioavailability	+	+	+	+	+
Blood Brain Barrier	+	+	+	-	+
P-glycoprotein inhibitior	+	+	-	-	-
P-glycoprotein substrate	-	-	-	-	-
Plasma protein binding[2]	100%	100%	92%	58%	75%
Ames mutagenesis	+	+	-	-	-
Acute Oral Toxicity[3]	III	III	III	II	III
Carcinogenicity (binary)	-	-	-	-	-
Micronucleus test	-	-	-	+	-
hERG inhibition	+	-	+	-	-
Mitochondrial toxicity	-	+	+	+	+
Nephrotoxicity	+	+	+	+	-
Reproductive toxicity	-	-	+	+	+
Respiratory toxicity	-	-	+	+	+

5.4. Discussion

Combination therapies for GB often show promising efficacy in overcoming resistant tumour clones (Rong, Li & Zhang, 2022). However, their clinical application is frequently limited by severe side effects and substantial financial costs. This has led to an increased interest in natural and biosynthetic compounds, which are reported to have low toxicity and versatile pharmaceutical properties, though their mechanisms of action are not yet fully understood (Atanasov, *et al.,* 2021). Within the class of synthetic compounds, β-AC derivatives are particularly noteworthy. These compounds contain both an amino group (-NH) and a carbonyl group (C=O) in close proximity, typically with the amino group positioned adjacent to a carbon-oxygen bond (Kaur & Kumar, 2020). They have shown significant potential in medicinal chemistry and cancer therapy due to their diverse biological activities, mainly their ability to induce apoptosis in cancer cells (Ahmad, *et al.,* 2023). Additionally, chalcones, a class of unsaturated ketones in the flavonoid family, have also gained attention as potential anticancer agents. They exhibit a 1,3-diaryl-2-propen-1-one skeleton and a range of biological functions, including the induction of apoptosis, modulation of cell cycle progression, and inhibition of angiogenesis (Li, *et al.,* 2019). *In vitro* studies have demonstrated significant cytotoxic effects of chalcones against various cancer cell lines, such as those from breast, colon, and lung cancers (Ouyang, *et al.,* 2021). Given these promising results, due to the unique properties that these compounds possess, it is essential to investigate their potential role in GB therapy by examining the underlying molecular processes through which they function and thus assess their therapeutic efficacies and safety profiles. Herein, we aimed to elucidate the *in vitro* cytotoxic effects of the synthetic compounds SHG-8 and SHG-44 on GB cell models while simultaneously investigating their mechanisms of action upon the miRNome of these cells and the molecular processes that take place during GB pathogenesis.

The evaluation of the metabolic effects of SHG-8 and SHG-44 on GB cells revealed significant cytotoxic properties that limit the growth, proliferation, and spread of cancer cells. SHG-8 demonstrated a dose-dependent decrease in cell viability and proliferation, with concentrations below 100μM being sufficient to induce substantial cytotoxicity, thus suggesting that SHG-8 can act effectively against brain tumour cells at relatively low doses. The reduction in clonogenic potential indicated impaired immortalisation and proliferation of U87MG and U251MG cells, aligning with similar effects observed in other β-AC compounds tested on prostate and colorectal cancer cells (Zhang, *et al.,* 2014b; Ahmad, *et al.,* 2023). Similarly, SHG-44 also exhibited dose-dependent cytotoxicity, significantly reducing cell viability, colony

formation, and migration in both U87MG and U251MG cells. The reduction in cell viability observed with SHG-44 was consistent with previous studies on chalcone derivatives, which have been shown to induce cell death across various cancer types, such as breast and colon cancer cells (Bustos, *et al.,* 2022; Hba, *et al.,* 2023; Ahmad, *et al.,* 2023). Furthermore, SHG-44 significantly impaired the colony-forming potential of both cell lines, disrupting not only cell proliferation but also the ability of GB cells to form new colonies, thus seizing tumour growth. Additionally, SHG-44 treatment inhibited cell migration, suggesting that the compound may target crucial cellular processes involved in tumour metastasis. Therefore, by disrupting the migratory and proliferative abilities of GB cancer cells, SHG-8 and SHG-44 possess potential therapeutic properties that could improve patient outcomes by preventing tumour spread and recurrence.

We also observed that SHG-8 was more effective in U87MG cells, whilst SHG-44 had a lower IC_{50} in U251MG cells. The differential toxicity observed between the chalcone compound and β-AC compound towards GB cells could be attributed to both the distinct chemical properties of the compounds and the biological differences between the cell lines. U87MG and U251MG cells, although both derived from GB, exhibit significant differences in their molecular profiles and biological behaviour. U87MG cells are known for their higher proliferative and migratory capacity compared to U251MG cells (Kałuzińska-Kołat, Kołat, Kośla, Płuciennik & Bednarek, 2023). This cell line also exhibits greater expression of proteins involved in RNA processing, splicing, and intracellular signalling, which are essential for maintaining rapid cell division and migration (Motaln, *et al.,* 2015). Thus, the SHG-8 compound could have targeted these processes, disrupting critical pathways that U87MG cells depend on for their aggressive growth and proliferation. On the other hand, U251MG cells were more sensitive to the SHG-44 chalcone compound. These cells have a lower proliferative capacity and increased expression of proteins associated with metabolic pathways such as glycolysis and purine metabolism (Martins, van der Kellen, Gonçalves & Serpa, 2023). Chalcones are known to modulate oxidative stress, apoptosis, and other cellular processes (Michalkova, Mirossay, Gazdova, Kello & Mojzis, 2021). The increased toxicity of the chalcone in U251MG cells may be a result from its ability to disrupt these metabolic pathways, particularly glycolysis, which U251MG cells rely on more heavily. Additionally, U251MG cells exhibit higher expression of extracellular components, which could make them more vulnerable to the actions of chalcones, which often interact with cell surface receptors or extracellular enzymes (Michalkova, *et al.,* 2021). In contrast, U87MG cells, which depend more on intracellular processes were more

susceptible to the β-AC compound's interference with RNA processing and signalling pathways.

Through our wound healing assays, we also observed that SHG-8 led to an apparent cell death at the high-end concentrations tested within both cell lines at 48h. For the U87MG cells the high concentration used in the wound healing assay was lower than the determined IC_{50} for the compound. In the MTT assay, which measures overall cell viability based on metabolic activity, cells were exposed to the drug for only 24h. During this shorter exposure time, cells often have a certain threshold of damage they can withstand before their metabolic activity decreases significantly (Ghasemi, Turnbull, Sebastian & Kempson, 2021). Thus, lower concentrations of the treatment might potentially cause damage to the cells that does not directly reduce metabolic activity below the detection threshold within this 24-hour period. Consequently, significant cell death may not be observed in the MTT assay until higher concentrations are used. In contrast, during the wound healing assay, cells were exposed to the drug for 48h, allowing more time for cumulative damage to occur, which could have resulted in the observed cell death even at lower concentrations.

During our ROS determination experiments, we observed an increase in ROS levels induced by both SHG-8 and SHG-44 in both GB cells. Disrupting genomic integrity is a well-known cytotoxic mechanism of many genotoxic therapies (Sies & Jones, 2020). High levels of ROS have been previously detected in multiple neurodegenerative disorders, such as Alzheimer's and Parkinson's disease (Houldsworth, 2024). Reactive oxygen species have a complex and dual role in GB cells. For instance, ROS are primarily generated as byproducts of cellular metabolism, particularly through mitochondrial activity, and can influence various signalling pathways crucial for tumour growth and survival (Zhao, *et al.,* 2023b). However, the excessive accumulation of ROS can induce oxidative stress, leading to cellular damage and triggering cell death pathways such as apoptosis and autophagy (Schieber & Chandel, 2014). Another key mechanism of ROS involves the inactivation of protein tyrosine phosphatases (PTPs) through the oxidation of their catalytic cysteine residues (Ray, Huang & Tsuji, 2012). This oxidative modification can result in the formation of sulfenic acid, sulfinic acid, or sulfonic acid, which are relatively irreversible, disrupting PTP function and altering downstream signalling pathways (Paulsen & Carroll, 2013). Additionally, ROS are known to inflict direct damage on cellular macromolecules, including DNA, RNA, lipids, and proteins (Jena, Samal, Bhol & Duttaroy, 2023). Lipid peroxidation caused by ROS affects the integrity of cellular membranes,

disrupting normal cell function (Su, *et al.,* 2019). Protein oxidation can modify amino acid side chains, altering protein structure and function, while oxidative deactivation of specific enzymes further disrupts cellular homeostasis (Cecarini, *et al.,* 2007). Reactive oxygen species could also modulate signal transduction pathways by activating kinases such as p38 mitogen-activated protein kinase (MAPK) and extracellular signal-related kinases (ERK) (Son, *et al.,* 2011). These kinases can modify the function of ion channels and other key proteins influencing cellular responses to external stimuli. ROS-mediated signalling pathways can lead to deviating outcomes, including the activation of cell survival mechanisms or the initiation of proapoptotic pathways (Villalpando-Rodriguez & Gibson, 2021). The balance between these opposing pathways determines whether a cell survives or undergoes apoptosis. This dual nature of ROS is commonly observed in GB resistance to conventional therapies like chemotherapy and radiotherapy, which often rely on inducing lethal levels of ROS to kill cancer cells (Wang, *et al.,* 2021c). Thus, we evaluated the therapeutic potential of SHG-8 and SHG-44 induced ROS as a possible GB hallmark. During our ROS determination experiments, we depicted differential effects of SHG-8 and SHG-44 on ROS generation in U87MG and U251MG GB cell lines, suggesting cell line-specific responses to these treatments. U87MG cells exhibited a significant increase in ROS levels shortly after SHG-8 treatment, with oxidative stress becoming evident within 30min and intensifying over time. This early and constant ROS production indicated that SHG-8 could effectively disrupt the cellular redox balance, leading to oxidative damage and contributing to the cytotoxic effects observed in the U87MG cells. In contrast, U251MG cells displayed a delayed response to SHG-8, with an observed increase in ROS only after a longer exposure to the treatment. Interestingly, the ROS levels did not continue to rise significantly at later time points, suggesting that U251MG cells might have activated antioxidant defences or other compensatory mechanisms that protect the cells from oxidative stress. Furthermore, this could also be the reason why ROS production was higher in the lower concentrations of the compound in comparison to the higher concentrations tested. When testing the effects of SHG-44, U87MG cells showed a concentration-dependent response. Lower concentrations of SHG-44 significantly increased ROS levels, whereas higher concentrations did not, suggesting that at higher doses, SHG-44 might have activated protective mechanisms that limit ROS production. U251MG cells, however, did not exhibit a significant ROS increase at any concentration of SHG-44, indicating a resistance to ROS-mediated effects.

Moreover, low to moderate levels of ROS have been seen to contribute to tumour progression by promoting cell proliferation, survival, and resistance to therapies (Nakamura & Takada,

2021). They achieve this by activating redox-sensitive signalling pathways, including those involving nuclear factor-kappa B (NF-κB) and hypoxia-inducible factors (HIFs), which support the aggressive nature of GB and its resistance to treatment (Olivier, Oliver, Lalier & Vallette, 2021). Therefore, when these low to moderate levels of ROS are increased, as in the case of U87MG cells treated by SHG-8 and SHG-44, this could lead to increased oxidative stress. U87MG cells have a higher proliferation and migration capacity compared to U251MG cells, which results in more active metabolic processes (Demircan, Yavuz, Kaya, Akgül & Altuntaş, 2021). This increased activity could lead to higher baseline ROS levels, making U87MG cells more susceptible to ROS-induced damage. In contrast, U251MG cells demonstrated upregulation of glycolysis and other metabolic pathways associated with enhanced resistance to oxidative stress (Bhardwaj & He, 2020). These pathways promote a stronger antioxidant system, enabling U251MG cells to manage ROS more effectively and thus reducing their susceptibility to ROS-induced cytotoxicity, which is in line with our observations. Even though chalcone compounds are known for their induction of ROS in different cancer types, it is important to note that ROS production might not be a universal effect of chalcones on GB cells given their biological characteristics (Jin, *et al.,* 2019; Gin, *et al.,* 2019). We did not further investigate ROS mechanisms under our treatment conditions in GB cells. To better understand the impact of ROS on cellular processes, especially under various treatment conditions, several specific assays and experimental approaches can be employed to quantify ROS production and assess oxidative stress levels in cells. The Dichlorofluorescein diacetate (DCFH-DA) assay is a widely used fluorescent probe for detecting ROS in cells (Kim & Xue, 2020a). Dichlorofluorescein diacetate is oxidised by ROS into a fluorescent compound allowing for quantification of ROS levels through fluorescence intensity. Furthermore, the Amplex Red assay could be used to detect H_2O_2 production offering a direct measurement of its levels in cell culture media (Karakuzu, Cruz, Liu & Garsin, 2019). Electron spin resonance (ESR) spectroscopy is another highly sensitive technique that can directly detect and quantify free radicals, including ROS providing real-time data on ROS production dynamics within cells (He, Liu, Wamer & Yin, 2014). These assays, combined with mechanistic studies could further elucidate the roles of ROS under our treatment conditions, providing more information regarding their dual role in promoting cell survival or death.

Even though we observed higher ROS production in the low treatment concentrations of SHG-8 and SHG-44, this does not necessarily imply that apoptosis was induced solely through ROS-related mechanisms, given the dual effects of ROS in GB as previously discussed. Our DAPI

and apoptosis assays demonstrated that apoptosis occurred with both compounds at higher concentrations, potentially attributed to mechanisms other than ROS, such as the inhibition of the PI3K/AKT signalling pathway or down-regulation of the AKT and c-MYC pathway (Neophytou, Trougakos, Erin & Papageorgis, 2021). Previous research has demonstrated the pro-apoptotic potential of both β-AC compounds and chalcones in different cancers (Bazzaro, *et al.,* 2011; Merve Aydin, *et al.,* 2023). Furthermore, there is exciting evidence that synthetic chalcones have the potential to lead to cell death via apoptosis within GB cells (Mendanha, *et al.,* 2021; Wu, *et al.,* 2022a). These observations were in line with our results from the DAPI and AO/EtBr staining experiments, which revealed that SHG-8 and SHG-44 induce distinct loss in cellular integrity associated with apoptosis in U87MG and U251MG GB cell lines. DAPI staining demonstrated that treatment with SHG-8 led to nuclear fragmentation in both U87MG and U251MG cells. However, the fragmentation was more noticeable in U251MG cells, particularly at higher concentrations, indicating a greater susceptibility to SHG-8-induced nuclear damage. Similarly, AO/EtBr staining confirmed that SHG-8 treatment at higher concentrations led to significant ethidium bromide uptake, indicating a loss of membrane integrity and cell death, especially in U251MG cells. The differential sensitivity to SHG-8 of U87MG and U251MG GB cells could be influenced by the *p53* status of these cells. U251MG cells, with mutated *p53* showed increased sensitivity to the compound, leading to obvious nuclear fragmentation and apoptosis due to impaired DNA damage response (Djuzenova, *et al.,* 2015). In contrast, U87MG cells possessing wild-type *p53* demonstrated greater resistance to early apoptosis, likely due to effective stress management and repair mechanisms. However, prolonged exposure or higher drug concentrations were seen to overcome these defences, resulting in significant cellular damage (Djuzenova, *et al.,* 2015). When examining the effects of SHG-44, both cell lines showed nuclear fragmentation, but U87MG cells treated with higher concentrations of SHG-44 exhibited more prominent nuclear ruptures. This difference suggested that U87MG cells might experience more severe nuclear damage under SHG-44 treatment, possibly due to their higher metabolic activity, which could potentially worsen the effects of the drug.

MiRNAs play an important role in influencing various cellular pathways and protein production mechanisms. Their involvement in tumour development, including GB, is well-established (Chen, Medarova & Moore, 2021). Differences in miRNA expression between normal tissues and tumours emphasise their role in processes like tumour stem cell differentiation and the initiation of CNS-originating tumours (Sati & Parhar, 2021). The loss

or overexpression of specific miRNAs can contribute to cancer survival pathways by disrupting cell cycle control, enabling escape from apoptosis, or deregulating the DNA damage response (Banelli, *et al.,* 2017). As a result, miRNAs have emerged as promising therapeutic targets for GB. Their small size and stability provide advantages over targeting protein-coding genes, making them attractive candidates for therapeutic interventions. However, miRNA-based therapies are not yet feasible due to their diverse binding capabilities, which can lead to varied responses to a given drug, as a single miRNA can regulate multiple targets (Seyhan, 2024).

The role of β-AC compounds in the regulation of miRNAs remains largely unexplored and is an area that requires further investigation. To investigate the impact of SHG-8 on miRNA regulation in U87MG cells, sRNA-seq was performed, revealing a wide array of dysregulated miRNAs. The observed shifts in miRNA expression profiles indicated that SHG-8 had significant effects on their regulation. This was further supported by the KEGG pathway, molecular function and biological process analyses which showed that a substantial number of miRNA-regulated processes were affected in the presence of SHG-8. Our analysis identified that SHG-8 strongly influenced the expression of several miRNAs potentially involved in cancer progression and GB pathogenesis, including miR-7974, miR-335-3p, miR-663a, miR-3648, and miR-21.

In cancer, miR-7974 was seen to play an important role in regulating cancer metabolism, particularly in multicellular tumour spheroids (Muciño-Olmos, *et al.,* 2020). This study found that miR-7974 was involved in the regulation of lipid metabolism, especially glycerophospholipid metabolism, during the progression of breast cancer multicellular tumour spheroids, suggesting its oncogenic potential (Muciño-Olmos, *et al.,* 2020). These pathways are crucial for the synthesis of lipids required by cancer cells to maintain their rapid growth and sustain the cell membrane structure, especially in conditions where nutrient supply may be limited (Baenke, Peck, Miess & Schulze, 2013). Furthermore, increased expression of miR-7974 within gastric cancer influenced tumour cell proliferation, confirming its potential oncogenic properties (Sexton, *et al.,* 2021). The ability of miR-7974 to influence lipid metabolism suggested that this miRNA might play an important role in supporting the metabolic flexibility of cancer cells, enabling them to adapt to the varying conditions within the tumour microenvironment. This regulatory function of miR-7974 suggested its potential as a therapeutic target in brain cancer. Manipulating its expression could disrupt the metabolic processes that tumours rely on for survival, particularly under hypoxic and nutrient-deprived

conditions commonly found within solid tumours, such as GB. The biological actions of miR-7974 within GB cells are yet to be elucidated; however, we can hypothesise that miR-7974 could act as an oncomiR within GB cells, supporting tumour growth and metabolism. Thus, its downregulation by SHG-8 has a potential anti-tumour effect against GB, making the compound a putative agent against miRNAs that promote tumorigenesis. We also validated our sequencing results via RT-qPCR and identified that miR-7974 was significantly downregulated in U87MG cells treated with SHG-8.

MiR-335-3p was also downregulated in our results, a change that could contribute to the inhibition of GB progression. There is existing evidence that in GB miR-335 functions as an oncomiR, contributing to its aggressive nature (Chen, Medarova & Moore, 2021). This miRNA has been seen upregulated in GB, where it played an antiapoptotic role, thus promoting tumour growth, invasion, and survival of cancer cells (Shea, *et al.,* 2016). Additionally, in astrocytoma cells, miR-335 targeted and downregulated Disheveled-associated activator of morphogenesis 1 (*DAAM1*), a tumour suppressor. The suppression of *DAAM1* by miR-335 enhanced the proliferative and invasive capabilities of these cells (Shu, *et al.,* 2021). Furthermore, miR-335 was reported to be involved in regulating the retinoblastoma protein 1 (RB1), an important cell cycle regulator, thereby promoting cell proliferation in a p53-dependent manner (Scarola, Schoeftner, Schneider & Benetti, 2010). This regulation is essential as it allows GB cells to bypass normal growth control mechanisms, contributing to their uncontrolled growth. Experimental inhibition of miR-335 has demonstrated potential therapeutic benefits expressed in inducing apoptosis and reducing cell proliferation of GB cells (Diana, Gaido, Maxia & Murtas, 2020). These effects suggested that miR-335 plays a vital role in GB progression and apoptotic mechanism, making it a promising target for therapeutic intervention. Therefore, we can suggest that the SHG-8 could successfully downregulate miR-335-5p and promote apoptosis in GB cells, revealing a potential molecular mechanism of action for the compound.

MiR-663a has also been extensively studied in GB where it functions as a tumour suppressor. MiR-663a was reported to be significantly downregulated in GB tissues, and its reduced expression was correlated with poorer overall patient survival (Wang, Lang, Zhou, Ma & Hu, 2021). Functionally, miR-663a inhibited the proliferation, migration, invasion, and stem cell-like properties of GB cells. Furthermore, when overexpressed, miR-663a exerted its tumour-suppressive effects by targeting key genes involved in tumorigenesis, such as *KDM2A*, a lysine demethylase that modulates the TGF-β/SMAD signalling pathway (Wang, *et al.,* 2021b). By

repressing *KDM2A*, miR-663a disrupted the oncogenic signalling associated with glioma cell survival and proliferation. Thus, SHG-8 could have affected this regulatory pathway via the overexpression of miR-663a seen in our results, leading to restricted GB cell survival and proliferation.

Our results also showed that miR-21 was significantly downregulated in the presence of SHG-8. MiR-21, as discussed in previous chapters, it is known to be upregulated in GB, contributing to enhanced tumour cell survival, invasiveness, and resistance to treatments such as chemotherapy and radiotherapy (Aloizou, *et al.,* 2020). The consistently elevated levels of miR-21 in GB cells and malignant brain tissues have suggested its role as an oncomiR. In our sRNA-seq analysis, miR-21 was significantly downregulated by SHG-8, suggesting that reduced migratory and clonogenic abilities of glioma cells might have resulted from the inhibition of miR-21. Furthermore, the sensitisation of the treated cells to apoptosis could also be aided by the downregulation of miR-21. However, subsequent RT-qPCR analysis did not show significant changes in miR-21 levels between control and treatment conditions, which could be due to the differences between the more targeted approach of RT-qPCR and the broader transcriptomic capture of sRNA-seq. Nonetheless, potential downregulation or inhibition of miR-21 by SHG-8 might be beneficial for suppressing tumour growth and metastasis in GB.

MiR-3648 has been associated with the inactivation of the Wnt/β-catenin signalling pathway in gastric cancer (Tang, *et al.,* 2022b). Tang and colleagues observed that miR-3648 acted as a tumour-suppressive miRNA via a negative miR-3648/FRAT1-FRAT2/c-Myc feedback loop (ref?). Even though the exact mechanism of action of miR-3648 within GB is not fully understood, its potential association with the Wnt/β-catenin signalling pathway suggested possible implications as a therapeutic target. The Wnt/β-catenin pathway plays a crucial role in controlling cancer progression. It is transduced through Frizzled receptors and LRP5/LRP6 co-receptors, leading to a β-catenin signalling cascade (MacDonald, Tamai & He, 2009). Given that the Wnt/β-catenin pathway is also implicated in GB for maintaining the self-renewal and survival of glioma stem cells, miR-3648 might serve as a promising therapeutic target in GB as well (Guan, Zhang & Guo, 2020). Targeting this pathway could potentially disrupt the malignant properties of GB cells, thereby inhibiting tumour growth and improving treatment outcomes. The therapeutic potential of targeting miR-3648 in GB was also demonstrated via the use of SHG-8 in our results. SHG-8 facilitated the overexpression of miR-3648 in GB cells.

Hence, we could hypothesise that by enhancing the expression of miR-3648, SHG-8 could effectively suppress the Wnt/β-catenin signalling pathway, consequently inducing tumour cell apoptosis, reducing proliferation, and potentially overcoming the resistance mechanisms associated with GB. We also validated the expression of this miRNA in U87MG treated cells via RT-qPCR and found that it was significantly upregulated in the presence of SHG-8, which further validated our sequencing results.

We further wanted to examine the effects of SHG-44 on the miRNA regulatory network within GB cells, as previous research has demonstrated that chalcone compounds could modulate miRNA activity in cancer (Komoto, *et al.,* 2023). TChal, a small molecule trans-chalcone, has been shown to have antitumor effects in breast cancer (Komoto, *et al.,* 2023). Treatment with TChal altered the expression of several miRNAs, such as miR-27a-3p, miR-449a, miR-25-5p, miR-4485, and miR-891a-5p. Specifically, miR-27a-3p and miR-449a were found to inhibit genes related to metastasis and proliferation, while miR-4485 targeted a gene linked to mitochondrial function and apoptosis (Komoto, *et al.,* 2023).

Our sRNA-seq analysis revealed that the two most downregulated miRNAs in the presence of SHG-44 were miR-122b-5p and miR-223-3p, whilst the three most upregulated were miR-144-3p, miR-5009-5p and miR-664b-3p. In the SHG-44 treated GB cells, we did not observe dysregulation of the commonly affected miRNAs by SHG-8, suggesting the chalcone could exhibit its properties through the dysregulation of other miRNAs involved in cancer progression.

To the best of our knowledge, the role of miR-122b-5p has not been previously associated with GB or other types of brain tumours. A recent study has demonstrated that miR-122b-5p had an important implication in the development of oropharyngeal squamous cell carcinoma (OPSCC) (Carron, *et al.,* 2022). Patients who carried more than three copies of the inherited pseudogenes *ADAM3A* and *ADAM5* on chromosome 8p11.23–22 presented higher expression of the *ADAM9* gene, which is involved in tumour formation and progression. These pseudogenes and *ADAM9* shared a common homologous sequence to which miR-122b-5p binds. The pseudogenes and *ADAM9* compete for miR-122b-5p binding, generating a higher expression of *ADAM9* and a higher risk of developing OPSCC. Thus, we could hypothesise that miR-122b-5p acted as a potential oncomiR in GB cells as well, and its downregulation by SHG-44 had tumour suppressive effects upon GB cells. The potential benefits of SHG-44 in this scenario included its capacity to reduce the expression of oncogenes like *ADAM9*, which is associated with

tumour proliferation, invasion, and metastasis (Sarkar, Zemp, Senger, Robbins & Yong, 2015). By downregulating miR-122b-5p, SHG-44 may effectively reduce the oncogenic signalling pathways and aggressive nature of GB cells.

On the other hand, one of the most significantly downregulated miRNAs in the presence of SHG-44 was miR-223-3p, which has been previously linked to GB. It has been shown that downregulation of miR-223-3p by the long non-coding RNA SNHG29 resulted in increased expression of *CTNND1*, a gene involved in the Wnt/β-catenin signalling pathway in GB, consequently promoting tumour progression (Han, Li, Jiang, Jiang & Tang, 2019). This suggested that miR-223-3p may have tumour-suppressive properties in GB. However, more recent research has identified miR-223-3p as one of the most upregulated miRNAs in GB stem-like cells, indicating its potential oncogenic role (Evers, *et al.,* 2023). This dual expression of miR-223-3p highlights the complexity of its function in GB, which requires further investigation. The ability of SHG-44 to downregulate miR-223-3p could suggest its potential as a drug that can modulate this miRNA's expression, possibly inhibiting its oncogenic effects and contributing to GB suppression.

Among the miRNAs significantly upregulated by SHG-44 was miR-144-3p. Existing evidence has shown that when miR-144-3p is downregulated in GB, the expression of c-Met, a gene involved in tumour proliferation and invasiveness, is increased (Lan, Yu, Hu, Xia & Yue, 2015). This indicated that miR-144-3p functioned as a tumour-suppressive miRNA in GB, and its downregulation was associated with poor patient prognosis (Li, *et al.,* 2015). Furthermore, overexpression of miR-144-3p has been observed to inhibit cell proliferation and invasion in human cytomegalovirus (HCMV)-positive GB by targeting *TOP2A*, an important biomarker in cancer therapy (Song, *et al.,* 2018). The upregulation of miR-144-3p by SHG-44 suggested that the chalcone can restore miR-144-3p levels, thus re-establishing its tumour-suppressive properties and leading to the inhibition of GB cell proliferation and invasion.

MiR-5009-5p was another miRNA that was significantly upregulated in the presence of SHG-44. Although miR-5009-5p has not previously been associated with cancer, its downregulation has been observed in sepsis, where it was explored as a potential therapeutic target within the *RUNX3, MAPK14,* miR-19b-1-5p, and miR-5009-5p axis (Luo, *et al.,* 2022). Given these findings, we could hypothesise that miR-5009-5p could have tumour-suppressive properties in GB, and its upregulation by SHG-44 may contribute to inhibiting GB cell growth and progression, demonstrating the potential efficacy of the drug in cancer treatment.

Additionally, our sequencing analysis identified miR-664b-3p as one of the top three miRNAs upregulated by SHG-44, indicating its potential tumour-suppressive role in GB. Research has shown that miR-664b-3p directly targets *Rheb* in the Rheb/mTOR/c-MYC pathway, mediating glycolysis in osteosarcoma (OS) cells (Yu, *et al.,* 2023a). The increased expression of this miRNA was found to inhibit OS growth and progression, suggesting its capacity to suppress tumours. Furthermore, miR-664b-3p has been found to be downregulated in colon cancer, where it played a tumour-suppressive role by negatively regulating the progression of colon cell carcinoma through suppression of BUB3, a protein involved in the kinetochore complex (Zhao, *et al.,* 2022a). While the role of miR-664b-3p in GB has not been previously described, the observed upregulation of miR-664b-3p in GB cells treated with SHG-44 suggested that this miRNA might also exhibit tumour-suppressive properties in GB. Thus, the ability of SHG-44 to upregulate miR-664b-3p could contribute to the inhibition of GB cells, enhancing its potential as a therapeutic agent in treating GB.

Our findings suggested that SHG-8 and SHG-44 have significant potential to broadly influence cellular functions through their effects on miRNA expression. Furthermore, we identified that the dysregulated miRNAs were also affecting lysosome dynamics in U87MG treated cells. It has been demonstrated that lysosomal membrane permeabilization (LMP) could lead to the release of hydrolases like cathepsins into the cytosol, triggering cell death through apoptosis, necrosis, or a combination of both, depending on the extent of lysosomal disruption (Aits, Jäättelä & Nylandsted, 2015). Furthermore, lysosomal dysfunction, particularly in GSCs, disrupted critical signalling pathways such as mTOR, which are essential for cell growth, proliferation, and survival (Divé, *et al.,* 2022). This evidence supports our findings, which suggested that SHG-8 and SHG-44 played roles in apoptosis, as discussed earlier. The connection between miRNA regulation, lysosomal function, and apoptosis highlighted a potential mechanism by which these compounds exert their anti-tumour effects. The involvement of lysosomal pathways could also explain the absence of ROS in our treatment conditions with high concentrations, as lysosomes may be efficiently managing cellular debris and oxidative stress (de Almeida, *et al.,* 2022). Moreover, the altered expression of miRNAs in our sequencing suggested a potential impact on various biological processes, such as axon guidance, which is essential for proper neuronal connectivity and communication, especially in malignancies such as GB (Chokshi, *et al.,* 2024). Thus, disruption of neuronal signalling aided by SHG-8 and SHG-44 could have contributed to potential neurological deficits and inhibition of tumour development in GB cells.

Subsequent docking analysis indicated that SHG-8 exhibited strong binding affinities for both CORO1C and SV2B, suggesting its potential in targeting these proteins. This computational prediction was followed by RT-qPCR analysis revealed that only CORO1C was significantly downregulated in the presence of SHG-8, while SV2B expression remained unaffected. The negative effects of SHG-8 upon this oncogene supported the findings that SHG-8 exerted negative regulation upon *de novo* neurone overgrowth and the Wnt pathway, thus limiting the proliferative and migratory abilities of U87MG GB cells. In contrast, docking analysis for SHG-44 revealed relatively weaker binding affinities for both CORO1C and SV2B, indicating a reduced potential for these interactions. This suggested that SHG-44 might be less effective in modulating these targets and it potentially exerted its mode of action through different mechanisms.

Cytotoxicity presents significant challenges in GB treatment due to the selectivity of the BBB, which restricts the entry of many therapeutic agents into the brain, limiting their efficacy against GB cells while potentially causing toxicity to healthy brain tissue (Arvanitis, Ferraro & Jain, 2020). As predicted via our *in-silico* analysis, SHG-8 and SHG-44 can pass freely through the BBB, overcoming cytotoxicity-related challenges in GB treatment. The complex tumour microenvironment of GB, combined with the rigid protection by the BBB, often hinders the delivery and effectiveness of cytotoxic treatments (Karmur, *et al.,* 2020). Our research demonstrated that SHG-8 and SHG-44 could regulate neuronal processes, potentially weakening the BBB and thus exerting direct cytotoxic effects on GB cells. In the case of SHG-8, it could be affecting these processes by targeting genes such as *GFAP*, which encodes for the glial fibrillary acidic protein, a key component of the intermediate filament protein family that regulates the shape, movement, and function of glial cells (Yang & Wang, 2015c). The negative regulation exerted by SHG-8 on *GFAP* could disturb glial balance and enhance BBB permeability, allowing SHG-8 molecules to pass through and directly target GB. Recent evidence has also demonstrated that trans chalcones could safely cross the BBB and inhibit VEGFR-2 in GB *in vivo* (Senrung, *et al.,* 2023). This is in line with our *in-silico* analysis, which predicted that SHG-44 could also pass freely through the BBB, addressing cytotoxicity-related challenges in GB treatment. Additionally, the low oral toxicity the compounds and their metabolites could prove beneficial for patient comfort and quality of life during therapy. Consequently, they could be combined with other chemotherapeutic agents with low oral toxicity to enhance therapeutic effectiveness among GB patients. Moreover, several SHG-8 metabolites were predicted to act as potential genotoxicity effectors, supporting the findings

observed in our *in vitro* investigations. On the other hand, toxicological assessments of different chalcones have revealed very low genotoxicity (Maronpot 2015). Our *in-silico* results also indicated that SHG-44 was not genotoxic. Furthermore, SHG-44 was not associated with carcinogenicity, and none of its metabolites were predicted to be carcinogenic in the Ames test, suggesting its safer clinical application in GB therapy.

In summary, both SHG-8 and SHG-44 have shown potential as alternative therapeutic agents against GB, exhibiting similar inhibitory effects on cell viability, migration, and proliferation. These compounds also induced apoptosis, in part, through the release of ROS, and via influencing various miRNAs involved in GB apoptotic pathways. Furthermore, SHG-8 downregulated the expression of *CORO1C* and inhibited Wnt pathway, hence suggesting a possible mode of action for the compound. SHG-44 similarly modulated the levels of GB-associated oncomiRs and tumour suppressor miRNAs, further emphasising its potential as therapeutic agent for GB management.

Chapter 6. Final Discussion

Early detection of brain tumours, such as GB and MB, is of main importance for improving patients' outcomes and survival rates. These aggressive tumours often remain asymptomatic until they reach an advanced stage, making timely diagnosis a challenging task. The early identification of brain neoplasms allows for more effective tumour management, which can slow the growth and progression of the malignancies, improve treatment efficacy, and enhance quality of life. Despite advancements in imaging techniques, current diagnostic methods rely heavily on invasive tissue biopsies, which present risks and limitations, such as difficulty accessing tumour sites and the potential for severe side effects. As a result, we have turned our attention to miRNAs as non-invasive biomarkers for brain tumour diagnosis and treatment. MiRNAs have emerged as promising biomarkers as they are small, non-coding RNA molecules that regulate gene expression and are often dysregulated in cancer (Mustafov, Ahmad, Serrano, Braoudaki & Siddiqui, 2024a). Their stability in bodily fluids, such as blood, plasma and CSF, and their ability to reflect tumour-specific changes make them ideal candidates for non-invasive biomarkers. Moreover, miRNAs offer a means of detecting GB and MB at a molecular level, potentially providing insights into tumour origin, progression, and response to therapy. By analysing circulating miRNAs in bodily fluids, liquid biopsies provide a less invasive and more dynamic method for monitoring these molecular changes. The transition from traditional tissue biopsies to liquid biopsies represents an important advancement in cancer diagnostics. Liquid biopsies, which analyse circulating biomarkers such as miRNAs, offer several advantages, including minimal invasiveness, easier accessibility, and the ability to monitor tumour dynamics in real-time. This transition holds promise for more accurate, personalised approaches to managing GB and MB, ultimately advancing early detection and improving treatment outcomes.

Our research focused on investigating miRNAs as key molecular biomarkers in GB and MB due to their important role in gene regulation and their potential as both diagnostic and therapeutic targets. Our goal was to bridge the gap in knowledge about how specific miRNAs and their target genes contribute to the oncogenic processes in GB and MB, ultimately aiming to improve diagnostic precision and identify more effective treatment strategies. We also aimed to evaluate the effects of new therapeutic agents against GB, specifically focusing on their impact on miRNA regulation and tumour progression.

In our *in-silico* analyses, we focused on identifying differentially expressed miRNAs and their target genes in GB patients. We found that miR-21 was upregulated, whilst miR-34a and miR-128a were downregulated, confirming their putative roles as oncomiRs and tumour suppressors, respectively (Mustafov, Siddiqui, Klena, Karteris & Braoudaki, 2024c). We also demonstrated that the downregulated miRNAs were targeting the *CORO1C* and *SV2B* genes, found upregulated in GB, suggesting that they may act as oncogenes. However, we further analysed the interactive miRNA networks for both genes, and we identified that miR-206 and miR-383 were directly targeting *CORO1C* and *SV2B*, respectively, in a stronger manner in comparison to the other miRNAs detected through this analysis (Mustafov, Lambrou, Siddiqui & Braoudaki, 2024b, in press). Furthermore, in our bioinformatics analyses we also demonstrated that *CORO1C* and *SV2B* were significantly upregulated in paediatric brain malignancies, in particular MB, suggesting their general role as oncogenes in highly malignant brain neoplasms (Mustafov, Karteris & Braoudaki, 2023; Mustafov, *et al.,* 2024c). These findings highlighted the potential of miRNAs and their target genes as valuable tools for both the diagnosis and treatment of specifically aggressive brain cancers. Despite the promising insights gained from *in-silico* methods, the predictions required experimental validation through *in vitro* experiments to confirm their clinical relevance.

The results of our *in vitro* validations (Mustafov, *et al.,* 2024b, in press) provided evidence for the dysregulation of the aforementioned miRNAs and their associated target genes in GB and MB cell lines. We used the U87MG and U251MG cell lines for GB and the DAOY cell line for MB. Our *in-silico* analysis was fully supported by our *in vitro* experiments in GB cells, demonstrating consistent findings in miRNA expression. Similar expression patterns were observed in MB cells with miR-21 being upregulated and miR-34a downregulated. Moreover, miR-206 and miR-383, identified as potential tumour suppressors, were consistently downregulated in both GB and MB cells. These miRNAs targeted *CORO1C* and *SV2B*, suggesting their possible use as therapeutic agents to counteract the oncogenic effects of these genes. Western blotting and IF analyses further validated these findings at a protein level, exhibiting upregulation and specific cellular localisation of CORO1C and SV2B across GB and MB cell lines. The IF staining analysis revealed that these proteins were not only overexpressed but also localised in a manner consistent with their oncogenic roles in supporting tumour progression. However, while the observed localisation is consistent with their hypothesised functional roles, it is important to note that IF staining provides a static snapshot

of protein distribution. Therefore, further validation using complementary techniques, such as live-cell imaging or co-localisation studies with known markers, is necessary to definitively confirm the subcellular localisation and its functional implications.

Our study also investigated the effects of transient transfections of GB and MB cells with miR-206 and miR-383 mimics. Firstly, we observed that the transfections with miR-206 and miR-383 mimics resulted in significant upregulation of these miRNAs, suggesting their utilisation as potential therapeutics against MB and GB. Furthermore, we observed that *CORO1C* was significantly downregulated post-transfection with the miR-206 mimic, suggesting the direct effects of miR-206 upon *CORO1C*. Similarly, *SV2B* was significantly downregulated following transfection with the miR-383 mimic. Downregulation of these genes suggested a possible decrease in the aggressive characteristics of GB and MB cells, thereby rescuing the malignant phenotype in these neoplasms. The observed *in-silico* and *in vitro* interaction between miR-206 and miR-383 with *CORO1C* and *SV2B*, respectively, suggested a potential clinical implication of these findings in the development of miRNA-based therapies that could provide more personalised and less invasive treatment options for patients with aggressive brain cancers. The impact of miR-206 and miR-383 mimics on GB and MB cell viability and colony-forming abilities revealed a significantly decreased cell viability, highlighting their potential as therapeutic agents in reducing tumour cell survival. Moreover, the loss of colony-forming abilities in these cells post-transfection further supported the likelihood that these miRNAs can inhibit tumorigenicity. Taken together, these findings provided an essential understanding of the potential therapeutic applications of these miRNAs in GB and MB treatment. The overexpression of CORO1C and SV2B proteins observed through western blotting and IF aligns with our bioinformatics predictions and RT-qPCR results, emphasising the potential of these proteins as therapeutic targets in GB and MB. These findings suggested that targeting miRNAs and their downstream oncogenic proteins could offer an alternative approach to the management of these aggressive brain malignancies.

Building on this, our findings further demonstrated the oncogenic role of CORO1C and SV2B in both GB and MB, with elevated protein expression in patient tissue samples confirmed through IHC analysis (Mustafov, *et al.,* 2024c; Mustafov, *et al.,* 2024b, in press). We detected the overexpression of the proteins in highly malignant brain tumours, particularly GB and MB. Furthermore, we noticed that the abundance of the proteins was increasing with tumour grade, suggesting their potential prognostic value within GB and MB. Additionally, our sRNA-seq

data from paediatric MB tissue samples revealed the downregulation of miR-206 and miR-383, aligning with their dysregulation observed *in vitro*. Transcriptomics analysis further validated the oncogenic roles of these genes, as *CORO1C* and *SV2B* were significantly upregulated at the mRNA level in MB patient tissues. These results collectively highlighted the potential of CORO1C and SV2B as diagnostic markers and therapeutic targets in high-grade brain malignancies, especially in paediatric cases. An important finding was the absence of miR-206, miR-383, CORO1C, and SV2B in our GB exosome sRNA-seq and proteomics analysis. This suggested that, unlike several other miRNA and protein biomarkers, these molecules may have a more specialised function within the tumour cells, focusing on intracellular regulatory mechanisms rather than exosome-mediated intercellular communication and transport. This distinction highlighted their potential as targets for intracellular therapeutic strategies rather than for use in exosome-based diagnostics. While they may not be ideal for non-invasive diagnostic techniques such as liquid biopsies, which rely on exosomal cargo, their essential role within tumour cells presented valuable opportunities for targeted therapies that focus on disrupting internal tumour processes and pathways.

We also aimed to assess the effects of newly in-house synthesised compounds as potential therapeutics for GB and to evaluate their impact on the miRNome in GB cells. Our study found that both SHG-8 and SHG-44 demonstrated significant potential as alternative therapeutic agents against GB. These compounds exhibited similar inhibitory effects on key factors involved in tumour growth and progression, such as cell viability, migration, and proliferation. In addition to their anti-tumour activities, both SHG-8 and SHG-44 induced apoptosis, in part through the release of ROS and, more importantly, through the modulation of miRNAs implicated in apoptotic pathways specific to GB. These compounds were shown to affect the expression of miRNAs, reshaping the molecular landscape of GB cells and altering the regulatory networks involved in cell survival and apoptosis. This mechanism emphasised the potential of these compounds in GB therapy. SHG-8 demonstrated an inhibitory effect by downregulating the expression of *CORO1C*, which we found to be upregulated in GB and linked to tumour invasiveness and metastasis. Hence, we could suggest that by downregulating *CORO1C*, SHG-8 could directly interfere with the mechanisms that allow GB cells to invade surrounding tissues and spread to other parts of the brain. In addition to the suppression of *CORO1C*, SHG-8 inhibited the Wnt signalling pathway, suggesting its potential to disrupt the self-renewal capabilities of GB stem cells, making the tumour more susceptible to apoptosis and reducing its ability to grow and invade new tissue (Mustafov, *et al.,* 2024d). On the other

hand, SHG-44 was also seen effective in the modulation of miRNA profiles by targeting both GB-associated oncomiRs and tumour-suppressor miRNAs (Mustafov, *et al.,* 2024e, in press). This modulation of miRNAs by SHG-44 included the suppression of oncomiRs, which promote tumour growth and resistance to apoptosis. Additionally, SHG-44 upregulated tumour-suppressor miRNAs, which are often downregulated in aggressive cancers like GB. Even though SHG-44 did not affect the expression of *CORO1C* in GB cells, its mode of action via disrupting critical pathways involved in GB progression suggested that the compound possess promising features for future therapeutic development. By targeting both miRNA expression profiles and essential tumorigenic pathways, these compounds offer a promising, multi-targeted approach to the management of aggressive brain malignancies like GB. Further investigation into their efficacy and safety in *in vivo* models is necessitated to promote the utilisation of these compounds in the clinical setting.

While the use of cell line models, including U87MG, U251MG, and DAOY has been helpful for the initial studies in biomarker discovery, they do not fully represent the complexity and heterogeneity of brain tumours found in patients. As such, further validation in more biologically representative models is needed to ensure that our findings translate effectively to clinical settings. Similarly, while the *in vitro* experiments are highly valuable for the detection of cellular mechanisms, they do not entirely replicate the full tumour microenvironment. Factors such as immune system interactions and extracellular matrix involvement are not present in these controlled settings. To better understand the role of miRNAs and their targets in tumour progression, *in vivo* studies using animal models or patient-derived xenografts will be essential to provide a more comprehensive context. Although our focus on miRNAs generated significant insights, it is important to recognise that tumour biology is influenced by a broader spectrum of regulatory elements, including long non-coding RNAs, circular RNAs, and epigenetic factors. Expanding the scope of future research could reveal additional mechanisms driving GB and MB progression, offering new opportunities for therapeutic development. Despite their absence in exosomal analysis, miR-206/*CORO1C* and miR-383/*SV2B* axes remain important in the clinical setting due to their significant roles noted within GB and MB tumour cells. These biomarkers remain valuable targets for therapeutic interventions, as their regulation of particular oncogenic pathways makes them potential candidates for intracellular therapies. Additionally, their expression within tumours may still serve as useful diagnostic or prognostic biomarkers through tissue biopsies or other targeted diagnostic methods. This absence in exosomes could potentially be overcome by exploring

alternative non-invasive diagnostic techniques, such as CTCs or analysing other biofluids like CSF, which may contain these biomarkers and provide a clearer representation of their clinical relevance. Subsequently, given the importance of non-invasive diagnostic techniques, further exploration of their role in different cancer contexts may be beneficial. Increasing the patient sample cohorts could also lead to an improved understanding of the variability and robustness of our findings. Additionally, expanding the cohort could reveal correlations between specific miRNA profiles, target gene expression, and clinical outcomes such as patient survival and treatment response, which will be ideal for the identification of putative prognostic biomarkers. This, in turn, would strengthen the clinical applicability of our biomarkers and therapeutic targets, providing a way for more personalised and effective treatment strategies. Lastly, while the *in vitro* results of SHG-8 and SHG-44 are promising, their efficacy has not yet been tested *in vivo*. Conducting *in vivo* studies will be essential for evaluating their pharmacokinetics, ensuring that the compounds are adequately absorbed, distributed, metabolised, and excreted in living organisms. Additionally, assessing their bioavailability will help determine how effectively these compounds reach the tumour site and maintain therapeutic concentrations over time. Investigating the potential toxicity is crucial to ensure that these compounds selectively target tumour cells without causing significant harm to healthy tissues, thereby promoting their safety before advancing to clinical trials.

Additional research on miRNAs in GB and MB could further validate our findings and enhance the therapeutic potential of the identified miRNAs and their targets. Firstly, *in vivo* validation is essential to confirm the therapeutic efficacy of miR-206 and miR-383 in more biologically relevant settings. Animal models should be used to assess the effectiveness of the miRNA mimics in targeting the oncogenes *CORO1C* and *SV2B*. This would provide a more accurate understanding of how these therapies would function in a real tumour environment. In addition to animal studies, utilising patient-derived models, including GB and MB cells or organoids, would allow for more accurate testing of miRNA-based therapies by reflecting the genetic diversity and heterogeneity of actual tumours, thus enhancing the translational potential of our findings. Moreover, conducting functional studies, such as gene knockdown or overexpression assays, would allow us to precisely identify the roles of these miR-206 and miR-383 and their targets in tumour progression. The role of CORO1C and SV2B in exosome-mediated communication should also be further explored in other brain tumour subtypes or stages of cancer, as their involvement in exosomal pathways may vary depending on the cancer context. Given the heterogeneity of GB and MB, patient-specific approaches should be considered,

where patients are stratified based on molecular subtypes or specific miRNA profiles to tailor therapeutic interventions more effectively. In terms of SHG-8 and SHG-44, *in vivo* validation is again crucial to determine the effectiveness, bioavailability, and safety of these compounds in GB animal models. This would provide a more comprehensive understanding of how SHG-8 and SHG-44 interact with the tumour microenvironment and whether they hold real clinical promise. Investigating combination therapy is another key area of future research, as combining these compounds with existing GB therapies, such as radiotherapy, chemotherapy, or immunotherapy, might enhance efficacy or overcome resistance mechanisms. Finally, conducting detailed mechanistic studies of SHG-8 and SHG-44 is important for understanding how they modulate miRNAs and interact with key regulatory pathways in GB, enabling the optimisation of these compounds for better therapeutic targeting.

In summary, our research demonstrated the role of the miR-206/*CORO1C* and miR-383/*SV2B* axes in GB and MB malignancies, highlighting their potential for diagnostic and therapeutic applications (Figure 136). Through *in silico* and *in vitro* analyses, we revealed that both miRNAs may function as tumour suppressors by directly targeting oncogenes and that increased expression of both could potentially rescue the tumour phenotype. Additionally, we demonstrated the efficacy of two in-house synthesised compounds, SHG-8 and SHG-44, against GB, underscoring their potential as new therapies for aggressive brain tumours (Figure 136). Overall, our findings enhance scientific knowledge by identifying miRNAs and their targets as putative diagnostic biomarkers and by uncovering miRNA-based therapeutic strategies, thereby providing alternative avenues for more personalised approaches in brain cancer treatment.

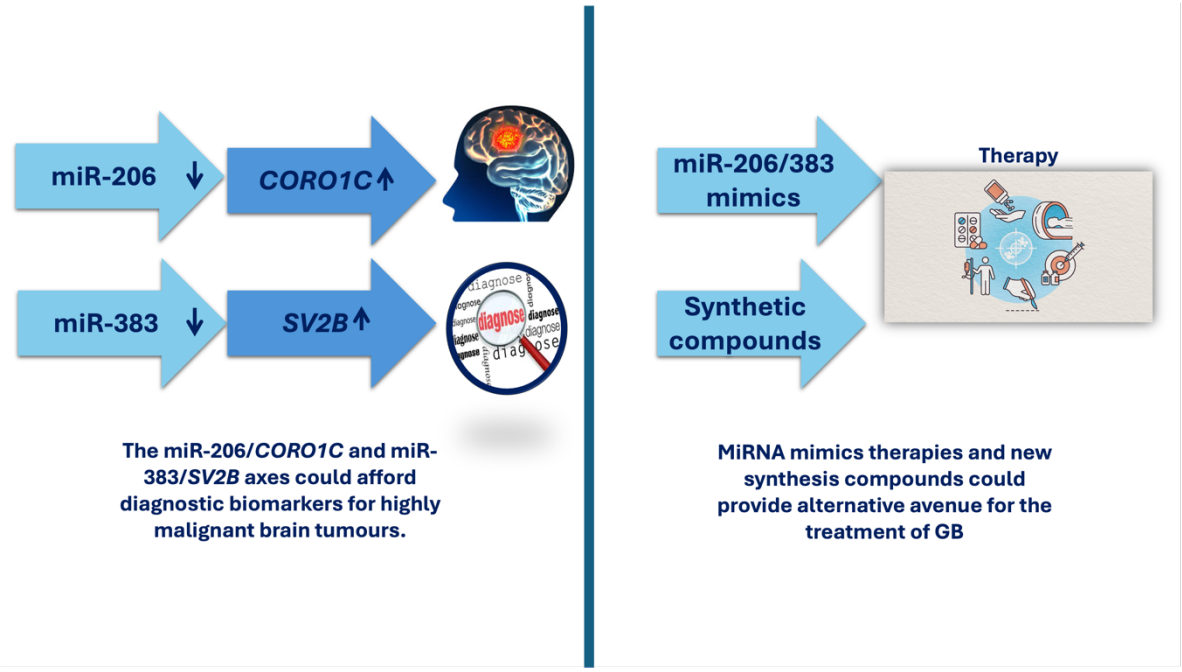


Figure 136. MiRNA axes and therapeutics in high grade brain malignancies. Summary of the roles of the miR-206/*CORO1C* and miR-383/*SV2B* axes in GB and MB. MiR-206 and miR-383 act as tumour suppressors by targeting oncogenes, with their restoration potentially reversing tumour phenotypes. The in-house compounds SHG-8 and SHG-44 showed efficacy against GB, highlighting their therapeutic potential. These findings underscore miRNAs and small molecules as promising diagnostic and therapeutic tools for brain neoplasms.

References

Abbosh, C., Birkbak, N. J., Wilson, G. A., Jamal-Hanjani, M., Constantin, T., Salari, R., Le Quesne, J., Moore, D. A., Veeriah, S., Rosenthal, R., Marafioti, T., Kirkizlar, E., Watkins, T. B. K., McGranahan, N., Ward, S., Martinson, L., Riley, J., Fraioli, F., Al Bakir, M., Grönroos, E., … Swanton, C. (2017). Phylogenetic ctDNA analysis depicts early-stage lung cancer evolution. *Nature, 545*(7655), 446–451. https://doi.org/10.1038/nature22364

Abdullah, K. G., Lubelski, D., Nucifora, P. G., & Brem, S. (2013). Use of diffusion tensor imaging in glioma resection. *Neurosurgical Focus, 34*(4), E1. https://doi.org/10.3171/2013.1.FOCUS12412

Abels, E. R., Maas, S. L. N., Nieland, L., Wei, Z., Cheah, P. S., Tai, E., Kolsteeg, C. J., Dusoswa, S. A., Ting, D. T., Hickman, S., El Khoury, J., Krichevsky, A. M., Broekman, M. L. D., & Breakefield, X. O. (2019). Glioblastoma-associated microglia reprogramming is mediated by functional transfer of extracellular miR-21. *Cell Reports, 28*(12), 3105–3119.e7. https://doi.org/10.1016/j.celrep.2019.08.036

Adams, B. D., Cowee, D. M., & White, B. A. (2009). The role of miR-206 in the epidermal growth factor (EGF) induced repression of estrogen receptor-alpha (ERalpha) signaling and a luminal phenotype in MCF-7 breast cancer cells. *Molecular Endocrinology (Baltimore, Md.)*, 23(8), 1215–1230. https://doi.org/10.1210/me.2009-0062

Agarwal, V., Bell, G. W., Nam, J. W., & Bartel, D. P. (2015). Predicting effective microRNA target sites in mammalian mRNAs. *eLife, 4*, e05005. https://doi.org/10.7554/eLife.05005

Agu, P. C., Afiukwa, C. A., Orji, O. U., Ezeh, E. M., Ofoke, I. H., Ogbu, C. O., Ugwuja, E. I., & Aja, P. M. (2023). Molecular docking as a tool for the discovery of molecular targets of nutraceuticals in diseases management. *Scientific Reports, 13*(1), 13398. https://doi.org/10.1038/s41598-023-40160-2

Aheget, H., Mazini, L., Martin, F., Belqat, B., Marchal, J. A., & Benabdellah, K. (2020). Exosomes: Their Role in Pathogenesis, Diagnosis and Treatment of Diseases. *Cancers*, 13(1), 84. https://doi.org/10.3390/cancers13010084

Ahmad, I., Shagufta, Dhar, R., Hisaindee, S., & Hasan, K. (2021). An environmentally benign solid acid nanocatalyst for the green synthesis of carboxylic acid ester. *ChemistrySelect, 6*(36), 9645-9652. https://doi.org/10.1002/slct.202102230

Ahmad, M. S., Braoudaki, M., Patel, H., Ahmad, I., Shagufta, & Siddiqui, S. S. (2023). Novel Siglec-15-Sia axis inhibitor leads to colorectal cancer cell death by targeting miR-6715b-3p and oncogenes. *Frontiers in Immunology, 14*, 1254911. https://doi.org/10.3389/fimmu.2023.1254911

Ahmed, S. P., Castresana, J. S., & Shahi, M. H. (2021). Glioblastoma and miRNAs. *Cancers, 13*(7), 1581. https://doi.org/10.3390/cancers13071581

Ahn, S. J., Shin, H. J., Chang, J. H., & Lee, S. K. (2014). Differentiation between primary cerebral lymphoma and glioblastoma using the apparent diffusion coefficient: Comparison of

three different ROI methods. *PloS One, 9*(11), e112948. https://doi.org/10.1371/journal.pone.0112948

Aits, S., Jäättelä, M., & Nylandsted, J. (2015). Methods for the quantification of lysosomal membrane permeabilization: A hallmark of lysosomal cell death. *Methods in Cell Biology, 126*, 261–285. https://doi.org/10.1016/bs.mcb.2014.10.032

Akdemir, E. S., Huang, A. Y., & Deneen, B. (2020). Astrocytogenesis: Where, when, and how. *F1000Research, 9*, F1000 Faculty Rev-233. https://doi.org/10.12688/f1000research.22405.1

Aldape, K., Brindle, K. M., Chesler, L., Chopra, R., Gajjar, A., Gilbert, M. R., Gottardo, N., Gutmann, D. H., Hargrave, D., Holland, E. C., Jones, D. T. W., Joyce, J. A., Kearns, P., Kieran, M. W., Mellinghoff, I. K., Merchant, M., Pfister, S. M., Pollard, S. M., Ramaswamy, V., Rich, J. N., … Gilbertson, R. J. (2019). Challenges to curing primary brain tumours. *Nature Reviews. Clinical Oncology*, 16(8), 509–520. https://doi.org/10.1038/s41571-019-0177-5

Alexander, B. M., & Cloughesy, T. F. (2017). Adult glioblastoma. *Journal of Clinical Oncology, 35*(21), 2402–2409. https://doi.org/10.1200/JCO.2017.73.0119

Alexandrou, G., Mantikas, K. T., Allsopp, R., Yapeter, C. A., Jahin, M., Melnick, T., Ali, S., Coombes, R. C., Toumazou, C., Shaw, J. A., & Kalofonou, M. (2023). The Evolution of Affordable Technologies in Liquid Biopsy Diagnostics: The Key to Clinical Implementation. *Cancers*, 15(22), 5434. https://doi.org/10.3390/cancers15225434

Alieva, M., van Rheenen, J., & Broekman, M. L. D. (2018). Potential impact of invasive surgical procedures on primary tumor growth and metastasis. *Clinical & Experimental Metastasis, 35*(4), 319–331. https://doi.org/10.1007/s10585-018-9896-8

Aloizou, A. M., Pateraki, G., Siokas, V., Mentis, A. A., Liampas, I., Lazopoulos, G., Kovatsi, L., Mitsias, P. D., Bogdanos, D. P., Paterakis, K., & Dardiotis, E. (2020). The role of MiRNA-21 in gliomas: Hope for a novel therapeutic intervention? *Toxicology Reports, 7*, 1514–1530. https://doi.org/10.1016/j.toxrep.2020.11.001

Alves, A., Silva, A. M., Moreira, J., Nunes, C., Reis, S., Pinto, M., Cidade, H., Rodrigues, F., Ferreira, D., Costa, P. C., & Correia-da-Silva, M. (2024). Polymersomes for sustained delivery of a chalcone derivative targeting glioblastoma cells. *Brain Sciences, 14*(1), 82. https://doi.org/10.3390/brainsci14010082

Amjad, M. T., Chidharla, A., & Kasi, A. (2023). Cancer chemotherapy. In *StatPearls* (Accessed: 20th August 2024). StatPearls Publishing. https://www.ncbi.nlm.nih.gov/books/NBK564367/

Anastasiadou, E., Seto, A. G., Beatty, X., Hermreck, M., Gilles, M. E., Stroopinsky, D., Pinter-Brown, L. C., Pestano, L., Marchese, C., Avigan, D., Trivedi, P., Escolar, D. M., Jackson, A. L., & Slack, F. J. (2021). Cobomarsen, an oligonucleotide inhibitor of miR-155, slows DLBCL tumor cell growth in vitro and in vivo. *Clinical Cancer Research, 27*(4), 1139–1149. https://doi.org/10.1158/1078-0432.CCR-20-3139

Andrés, C. M. C., Pérez de la Lastra, J. M., Bustamante Munguira, E., Andrés Juan, C., & Pérez-Lebeña, E. (2024). Michael acceptors as anti-cancer compounds: Coincidence or causality? *International Journal of Molecular Sciences, 25*(11), 6099. https://doi.org/10.3390/ijms25116099

Annese, T., Tamma, R., De Giorgis, M., & Ribatti, D. (2020). microRNAs biogenesis, functions and role in tumor angiogenesis. *Frontiers in Oncology, 10*, 581007. https://doi.org/10.3389/fonc.2020.581007

Antonelli, M., & Poliani, P. L. (2022). Adult type diffuse gliomas in the new 2021 WHO Classification. *Pathologica, 114*(6), 397–409. https://doi.org/10.32074/1591-951X-823

Arai, Y., & Taverna, E. (2017). Neural progenitor cell polarity and cortical development. *Frontiers in Cellular Neuroscience, 11*, 384. https://doi.org/10.3389/fncel.2017.00384

Arif, K. M. T., Elliott, E. K., Haupt, L. M., & Griffiths, L. R. (2020). Regulatory mechanisms of epigenetic miRNA relationships in human cancer and potential as therapeutic targets. *Cancers, 12*(10), 2922. https://doi.org/10.3390/cancers12102922

Armakolas, A., Kotsari, M., & Koskinas, J. (2023). Liquid biopsies, novel approaches and future directions. *Cancers, 15*(5), 1579. https://doi.org/10.3390/cancers15051579

Arora, S., Rana, R., Chhabra, A., Jaiswal, A., & Rani, V. (2013). miRNA-transcription factor interactions: A combinatorial regulation of gene expression. *Molecular Genetics and Genomics (MGG), 288*(3-4), 77–87. https://doi.org/10.1007/s00438-013-0734-z

Arvanitis, C. D., Ferraro, G. B., & Jain, R. K. (2020). The blood-brain barrier and blood-tumor barrier in brain tumors and metastases. *Nature Reviews Cancer, 20*(1), 26–41. https://doi.org/10.1038/s41568-019-0205-x

Asija, S., Chatterjee, A., Goda, J. S., Yadav, S., Chekuri, G., & Purwar, R. (2023). Oncolytic immunovirotherapy for high-grade gliomas: A novel and an evolving therapeutic option. *Frontiers in Immunology, 14*, 1118246. https://doi.org/10.3389/fimmu.2023.1118246

Atanasov, A. G., Zotchev, S. B., Dirsch, V. M., International Natural Product Sciences Taskforce, & Supuran, C. T. (2021). Natural products in drug discovery: Advances and opportunities. *Nature Reviews Drug Discovery, 20*(3), 200–216. https://doi.org/10.1038/s41573-020-00114-z

Auffinger, B., Spencer, D., Pytel, P., Ahmed, A. U., & Lesniak, M. S. (2015). The role of glioma stem cells in chemotherapy resistance and glioblastoma multiforme recurrence. *Expert Review of Neurotherapeutics, 15*(7), 741–752. https://doi.org/10.1586/14737175.2015.1051968

Azzarelli, R., Simons, B. D., & Philpott, A. (2018). The developmental origin of brain tumours: a cellular and molecular framework. *Development (Cambridge, England), 145*(10), dev162693. https://doi.org/10.1242/dev.162693

Baenke, F., Peck, B., Miess, H., & Schulze, A. (2013). Hooked on fat: The role of lipid synthesis in cancer metabolism and tumour development. *Disease Models & Mechanisms, 6*(6), 1353–1363. https://doi.org/10.1242/dmm.011338

Balachandran, A. A., Larcher, L. M., Chen, S., & Veedu, R. N. (2020). Therapeutically Significant MicroRNAs in Primary and Metastatic Brain Malignancies. *Cancers*, 12(9), 2534. https://doi.org/10.3390/cancers12092534

Bandala, C., Miliar-García, A., Mejía-Barradas, C. M., Anaya-Ruiz, M., Luna-Arias, J. P., Bazán-Méndez, C. I., Gómez-López, M., Juárez-Méndez, S., & Lara-Padilla, E. (2012). Synaptic vesicle protein 2 (SV2) isoforms. *Asian Pacific Journal of Cancer Prevention: APJCP, 13*(10), 5063–5067. https://doi.org/10.7314/apjcp.2012.13.10.5063

Banelli, B., Forlani, A., Allemanni, G., Morabito, A., Pistillo, M. P., & Romani, M. (2017). MicroRNA in glioblastoma: An overview. *International Journal of Genomics, 2017*, 7639084. https://doi.org/10.1155/2017/7639084

Banerjee, A., Lee, J., Nemcova, P., Liu, C., & Kaeser, P. S. (2020). Synaptotagmin-1 is the Ca2+ sensor for fast striatal dopamine release. *eLife, 9*, e58359. https://doi.org/10.7554/eLife.58359

Bao, H., Ren, P., Yi, L., Lv, Z., Ding, W., Li, C., Li, S., Li, Z., Yang, X., Liang, X., & Liang, P. (2023). New insights into glioma frequency maps: From genetic and transcriptomic correlate to survival prediction. *International Journal of Cancer, 152*(5), 998–1012. https://doi.org/10.1002/ijc.34336

Barba-Ostria, C., Carrera-Pacheco, S. E., Gonzalez-Pastor, R., Heredia-Moya, J., Mayorga-Ramos, A., Rodríguez-Pólit, C., Zúñiga-Miranda, J., Arias-Almeida, B., & Guamán, L. P. (2022). Evaluation of biological activity of natural compounds: Current trends and methods. *Molecules (Basel, Switzerland), 27*(14), 4490. https://doi.org/10.3390/molecules27144490

Bartholome, O., Van den Ackerveken, P., Sánchez Gil, J., de la Brassinne Bonardeaux, O., Leprince, P., Franzen, R., & Rogister, B. (2017). Puzzling out synaptic vesicle 2 family members functions. *Frontiers in Molecular Neuroscience, 10*, 148. https://doi.org/10.3389/fnmol.2017.00148

Bass, J. J., Wilkinson, D. J., Rankin, D., Phillips, B. E., Szewczyk, N. J., Smith, K., & Atherton, P. J. (2017). An overview of technical considerations for Western blotting applications to physiological research. *Scandinavian Journal of Medicine & Science in Sports, 27*(1), 4–25. https://doi.org/10.1111/sms.12702

Bautista-Sánchez, D., Arriaga-Canon, C., Pedroza-Torres, A., De La Rosa-Velázquez, I. A., González-Barrios, R., Contreras-Espinosa, L., Montiel-Manríquez, R., Castro-Hernández, C., Fragoso-Ontiveros, V., Álvarez-Gómez, R. M., & Herrera, L. A. (2020). The promising role of miR-21 as a cancer biomarker and its importance in RNA-based therapeutics. *Molecular Therapy. Nucleic Acids, 20*, 409–420. https://doi.org/10.1016/j.omtn.2020.03.003

Bayat Mokhtari, R., Homayouni, T. S., Baluch, N., Morgatskaya, E., Kumar, S., Das, B., & Yeger, H. (2017). Combination therapy in combating cancer. *Oncotarget, 8*(23), 38022–38043. https://doi.org/10.18632/oncotarget.16723

Bazzaro, M., Anchoori, R. K., Mudiam, M. K., Issaenko, O., Kumar, S., Karanam, B., Lin, Z., Isaksson Vogel, R., Gavioli, R., Destro, F., Ferretti, V., Roden, R. B., & Khan, S. R. (2011). α,β-Unsaturated carbonyl system of chalcone-based derivatives is responsible for broad inhibition of proteasomal activity and preferential killing of human papilloma virus (HPV) positive cervical cancer cells. *Journal of Medicinal Chemistry, 54*(2), 449–456. https://doi.org/10.1021/jm100589p

Benesova, S., Kubista, M., & Valihrach, L. (2021). Small RNA-Sequencing: Approaches and Considerations for miRNA Analysis. *Diagnostics (Basel, Switzerland), 11*(6), 964. https://doi.org/10.3390/diagnostics11060964

Berghoff, A. S., Kiesel, B., Widhalm, G., Rajky, O., Ricken, G., Wöhrer, A., Dieckmann, K., Filipits, M., Brandstetter, A., Weller, M., Kurscheid, S., Hegi, M. E., Zielinski, C. C., Marosi, C., Hainfellner, J. A., Preusser, M., & Wick, W. (2015). Programmed death ligand 1 expression and tumor-infiltrating lymphocytes in glioblastoma. *Neuro-Oncology, 17*(8), 1064–1075. https://doi.org/10.1093/neuonc/nou307

Bernstock, J. D., Gary, S. E., Klinger, N., Valdes, P. A., Ibn Essayed, W., Olsen, H. E., Chagoya, G., Elsayed, G., Yamashita, D., Schuss, P., Gessler, F. A., Paolo Peruzzi, P., Bag, A. K., & Friedman, G. K. (2022). Standard clinical approaches and emerging modalities for glioblastoma imaging. *Neuro-Oncology Advances*, *4*(1), vdac080. https://doi.org/10.1093/noajnl/vdac080

Beylerli, O., Gareev, I., Sufianov, A., Ilyasova, T., & Zhang, F. (2022). The role of microRNA in the pathogenesis of glial brain tumors. *Non-Coding RNA Research, 7*(2), 71–76. https://doi.org/10.1016/j.ncrna.2022.02.005

Bhardwaj, V., & He, J. (2020). Reactive oxygen species, metabolic plasticity, and drug resistance in cancer. *International Journal of Molecular Sciences, 21*(10), 3412. https://doi.org/10.3390/ijms21103412

Bizzi, A., Blasi, V., Falini, A., Ferroli, P., Cadioli, M., Danesi, U., Aquino, D., Marras, C., Caldiroli, D., & Broggi, G. (2008). Presurgical functional MR imaging of language and motor functions: Validation with intraoperative electrocortical mapping. *Radiology, 248*(2), 579–589. https://doi.org/10.1148/radiol.2482071214

Bofill-De Ros, X., & Vang Ørom, U. A. (2024). Recent progress in miRNA biogenesis and decay. *RNA Biology, 21*(1), 1–8. https://doi.org/10.1080/15476286.2023.2288741

Bonfim-Silva, R., Salomão, K. B., Pimentel, T. V. C. A., Menezes, C. C. B. O., Palma, P. V. B., & Fontes, A. M. (2019). Biological characterization of the UW402, UW473, ONS-76 and DAOY pediatric medulloblastoma cell lines. *Cytotechnology, 71*(5), 893–903. https://doi.org/10.1007/s10616-019-00332-3

Borchert, G. M., Lanier, W., & Davidson, B. L. (2006). RNA polymerase III transcribes human microRNAs. *Nature Structural & Molecular Biology, 13*(12), 1097–1101. https://doi.org/10.1038/nsmb1167

Borisov, N., & Buzdin, A. (2022). Transcriptomic Harmonization as the Way for Suppressing Cross-Platform Bias and Batch Effect. *Biomedicines, 10*(9), 2318. https://doi.org/10.3390/biomedicines10092318

Borisov, N., Suntsova, M., Sorokin, M., Garazha, A., Kovalchuk, O., Aliper, A., Ilnitskaya, E., Lezhnina, K., Korzinkin, M., Tkachev, V., Saenko, V., Saenko, Y., Sokov, D. G., Gaifullin, N. M., Kashintsev, K., Shirokorad, V., Shabalina, I., Zhavoronkov, A., Mishra, B., Cantor, C. R., … Buzdin, A. (2017). Data aggregation at the level of molecular pathways improves stability of experimental transcriptomic and proteomic data. *Cell Cycle, 16*(19), 1810–1823. https://doi.org/10.1080/15384101.2017.1361068

Borst, K., Dumas, A. A., & Prinz, M. (2021). Microglia: Immune and non-immune functions. *Immunity, 54*(10), 2194–2208. https://doi.org/10.1016/j.immuni.2021.09.014

Braoudaki, M., & Lambrou, G. I. (2015). MicroRNAs in pediatric central nervous system embryonal neoplasms: the known unknown. *Journal of Hematology & Oncology, 8*, 6. https://doi.org/10.1186/s13045-014-0101-5

Braoudaki, M., Lambrou, G. I., Giannikou, K., Milionis, V., Stefanaki, K., Birks, D. K., Prodromou, N., Kolialexi, A., Kattamis, A., Spiliopoulou, C. A., Tzortzatou-Stathopoulou, F., & Kanavakis, E. (2014). Microrna expression signatures predict patient progression and disease outcome in pediatric embryonal central nervous system neoplasms. *Journal of Hematology & Oncology, 7*, 96. https://doi.org/10.1186/s13045-014-0096-y

Brennan, P. M., Borchert, R., Coulter, C., Critchley, G. R., Hall, B., Holliman, D., Phang, I., Jefferies, S. J., Keni, S., Lee, L., Liaquat, I., Marcus, H. J., Thomson, S., Thorne, L., Vintu, M., Wiggins, A. N., Jenkinson, M. D., & Erridge, S. (2021). Second surgery for progressive glioblastoma: a multi-centre questionnaire and cohort-based review of clinical decision-making and patient outcomes in current practice. *Journal of Neuro-Oncology, 153*(1), 99–107. https://doi.org/10.1007/s11060-021-03748-0

Brown, N. F., Ng, S. M., Brooks, C., Coutts, T., Holmes, J., Roberts, C., Elhussein, L., Hoskin, P., Maughan, T., Blagden, S., & Mulholland, P. (2020). A phase II open label, randomized study of ipilimumab with temozolomide versus temozolomide alone after surgery and chemoradiotherapy in patients with recently diagnosed glioblastoma: The Ipi-Glio trial protocol. *BMC Cancer, 20*(1), 198. https://doi.org/10.1186/s12885-020-6624-y

Brümmer, A., & Hausser, J. (2014). MicroRNA binding sites in the coding region of mRNAs: Extending the repertoire of post-transcriptional gene regulation. *BioEssays, 36*(6), 617–626. https://doi.org/10.1002/bies.201300104

Buchbinder, E. I., & Desai, A. (2016). CTLA-4 and PD-1 pathways: Similarities, differences, and implications of their inhibition. *American Journal of Clinical Oncology, 39*(1), 98–106. https://doi.org/10.1097/COC.0000000000000239

Budi, H. S., Younus, L. A., Lafta, M. H., Parveen, S., Mohammad, H. J., Al-Qaim, Z. H., Jawad, M. A., Parra, R. M. R., Mustafa, Y. F., Alhachami, F. R., Karampoor, S., & Mirzaei, R. (2023). The role of miR-128 in cancer development, prevention, drug resistance, and immunotherapy. *Frontiers in Oncology, 12*, 1067974. https://doi.org/10.3389/fonc.2022.1067974

Buruiană, A., Florian, Ș. I., Florian, A. I., Timiș, T. L., Mihu, C. M., Miclăuș, M., Oșan, S., Hrapșa, I., Cataniciu, R. C., Farcaș, M., & Șușman, S. (2020). The roles of miRNA in glioblastoma tumor cell communication: Diplomatic and aggressive negotiations. *International Journal of Molecular Sciences, 21*(6), 1950. https://doi.org/10.3390/ijms21061950

Bustos, L., Echiburú-Chau, C., Castro-Alvarez, A., Bradshaw, B., Simirgiotis, M. J., Mellado, M., Parra, C., & Cuellar, M. (2022). Cytotoxic effects on breast cancer cell lines of chalcones derived from a natural precursor and their molecular docking analysis. *Molecules, 27*(14), 4387. https://doi.org/10.3390/molecules27144387

Cai, X., Hagedorn, C. H., & Cullen, B. R. (2004). Human microRNAs are processed from capped, polyadenylated transcripts that can also function as mRNAs. *RNA, 10*(12), 1957–1966. https://doi.org/10.1261/rna.7135204

Cancer Genome Atlas Research Network. (2008). Comprehensive genomic characterization defines human glioblastoma genes and core pathways. *Nature, 455*(7216), 1061–1068. https://doi.org/10.1038/nature07385

Candolfi, M., Curtin, J. F., Nichols, W. S., Muhammad, A. G., King, G. D., Pluhar, G. E., McNiel, E. A., Ohlfest, J. R., Freese, A. B., Moore, P. F., Lerner, J., Lowenstein, P. R., & Castro, M. G. (2007). Intracranial glioblastoma models in preclinical neuro-oncology: Neuropathological characterization and tumor progression. *Journal of Neuro-Oncology, 85*(2), 133–148. https://doi.org/10.1007/s11060-007-9400-9

Cao, H., Liu, X., Chen, Y., Yang, P., Huang, T., Song, L., & Xu, R. (2020). Circulating tumor DNA is capable of monitoring the therapeutic response and resistance in advanced colorectal cancer patients undergoing combined target and chemotherapy. *Frontiers in Oncology, 10*, 466. https://doi.org/10.3389/fonc.2020.00466

Carneiro, B. A., & El-Deiry, W. S. (2020). Targeting apoptosis in cancer therapy. *Nature Reviews Clinical Oncology, 17*(7), 395–417. https://doi.org/10.1038/s41571-020-0341-y

Carrano, A., Juarez, J. J., Incontri, D., Ibarra, A., & Guerrero Cazares, H. (2021). Sex-specific differences in glioblastoma. *Cells, 10*(7), 1783. https://doi.org/10.3390/cells10071783

Carron, J., Torricelli, C., Silva, J. K., Liu, Y., Pellegrino, R., Lima, C. S. P., & Lourenço, G. J. (2022). Association of inherited copy number variation in ADAM3A and ADAM5 pseudogenes with oropharynx cancer risk and outcome. *Genes, 13*(12), 2408. https://doi.org/10.3390/genes13122408

Casciati, A., Tanori, M., Manczak, R., Saada, S., Tanno, B., Giardullo, P., Porcù, E., Rampazzo, E., Persano, L., Viola, G., Dalmay, C., Lalloué, F., Pothier, A., Merla, C., & Mancuso, M.

(2020). Human medulloblastoma cell lines: Investigating on cancer stem cell-like phenotype. *Cancers, 12*(1), 226. https://doi.org/10.3390/cancers12010226

Castagnino, A., Castro-Castro, A., Irondelle, M., Guichard, A., Lodillinsky, C., Fuhrmann, L., Vacher, S., Agüera-González, S., Zagryazhskaya-Masson, A., Romao, M., El Kesrouani, C., Noegel, A. A., Dubois, T., Raposo, G., Bear, J. E., Clemen, C. S., Vincent-Salomon, A., Bièche, I., & Chavrier, P. (2018). Coronin 1C promotes triple-negative breast cancer invasiveness through regulation of MT1-MMP traffic and invadopodia function. *Oncogene, 37*(50), 6425–6441. https://doi.org/10.1038/s41388-018-0422-x

Castle, J. T., Levy, B. E., & Chauhan, A. (2022). Pediatric Neuroendocrine Neoplasms: Rare Malignancies with Incredible Variability. *Cancers, 14*(20), 5049. https://doi.org/10.3390/cancers14205049

Catalano, M., Limatola, C., & Trettel, F. (2024). Non-neoplastic astrocytes: Key players for brain tumor progression. *Frontiers in Cellular Neuroscience, 17*, 1352130. https://doi.org/10.3389/fncel.2023.1352130

Cavalli, F. M. G., Remke, M., Rampasek, L., Peacock, J., Shih, D. J. H., Luu, B., Garzia, L., Torchia, J., Nor, C., Morrissy, A. S., Agnihotri, S., Thompson, Y. Y., Kuzan-Fischer, C. M., Farooq, H., Isaev, K., Daniels, C., Cho, B. K., Kim, S. K., Wang, K. C., Lee, J. Y., … Taylor, M. D. (2017). Intertumoral heterogeneity within medulloblastoma subgroups. *Cancer Cell, 31*(6), 737–754.e6. https://doi.org/10.1016/j.ccell.2017.05.005

Cecarini, V., Gee, J., Fioretti, E., Amici, M., Angeletti, M., Eleuteri, A. M., & Keller, J. N. (2007). Protein oxidation and cellular homeostasis: Emphasis on metabolism. *Biochimica et Biophysica Acta, 1773*(2), 93–104. https://doi.org/10.1016/j.bbamcr.2006.08.039

Cervena, K., Novosadova, V., Pardini, B., Naccarati, A., Opattova, A., Horak, J., Vodenkova, S., Buchler, T., Skrobanek, P., Levy, M., Vodicka, P., & Vymetalkova, V. (2021). Analysis of microRNA expression changes during the course of therapy in rectal cancer patients. *Frontiers in Oncology, 11*, 702258. https://doi.org/10.3389/fonc.2021.702258

Cha, D. J., Franklin, J. L., Dou, Y., Liu, Q., Higginbotham, J. N., Demory Beckler, M., Weaver, A. M., Vickers, K., Prasad, N., Levy, S., Zhang, B., Coffey, R. J., & Patton, J. G. (2015). KRAS-dependent sorting of miRNA to exosomes. *eLife*, 4, e07197. https://doi.org/10.7554/eLife.07197

Chakrabarti, I., Cockburn, M., Cozen, W., Wang, Y. P., & Preston-Martin, S. (2005). A population-based description of glioblastoma multiforme in Los Angeles County, 1974-1999. *Cancer, 104*(12), 2798–2806. https://doi.org/10.1002/cncr.21539

Chakrabortty, A., Patton, D. J., Smith, B. F., & Agarwal, P. (2023). miRNAs: Potential as Biomarkers and Therapeutic Targets for Cancer. *Genes, 14*(7), 1375. https://doi.org/10.3390/genes14071375

Chan, K. T., Creed, S. J., & Bear, J. E. (2011). Unraveling the enigma: Progress towards understanding the coronin family of actin regulators. *Trends in Cell Biology, 21*(8), 481–488. https://doi.org/10.1016/j.tcb.2011.04.004

Chan, K. T., Roadcap, D. W., Holoweckyj, N., & Bear, J. E. (2012). Coronin 1C harbours a second actin-binding site that confers co-operative binding to F-actin. *The Biochemical Journal, 444*(1), 89–96. https://doi.org/10.1042/BJ20120209

Chan, R. W., Chen, H., Myrehaug, S., Atenafu, E. G., Stanisz, G. J., Stewart, J., Maralani, P. J., Chan, A. K. M., Daghighi, S., Ruschin, M., Das, S., Perry, J., Czarnota, G. J., Sahgal, A., & Lau, A. Z. (2021). Quantitative CEST and MT at 1.5T for monitoring treatment response in glioblastoma: Early and late tumor progression during chemoradiation. *Journal of Neuro-Oncology, 151*(2), 267–278. https://doi.org/10.1007/s11060-020-03661-y

Chandramouli, K., & Qian, P. Y. (2009). Proteomics: challenges, techniques and possibilities to overcome biological sample complexity. *Human Genomics and Proteomics : HGP*, 2009, 239204. https://doi.org/10.4061/2009/239204

Chandrashekar, D. S., Karthikeyan, S. K., Korla, P. K., Patel, H., Shovon, A. R., Athar, M., Netto, G. J., Qin, Z. S., Kumar, S., Manne, U., Creighton, C. J., & Varambally, S. (2022). UALCAN: An update to the integrated cancer data analysis platform. *Neoplasia (New York, N.Y.)*, *25*, 18–27. https://doi.org/10.1016/j.neo.2022.01.001

Charbit, H., & Lavon, I. (2024). Investigating expression dynamics of miR-21 and miR-10b in glioblastoma cells in vitro: Insights into responses to hypoxia and secretion mechanisms. *International Journal of Molecular Sciences*, *25*(14), 7984. https://doi.org/10.3390/ijms25147984

Chen, B., Hu, H., & Chen, X. (2023). From basic science to clinical practice: The role of Cancerous Inhibitor of Protein Phosphatase 2A (CIP2A)/p90 in cancer. *Frontiers in Genetics, 14*, 1110656. https://doi.org/10.3389/fgene.2023.1110656

Chen, H., Judkins, J., Thomas, C., Wu, M., Khoury, L., Benjamin, C. G., Pacione, D., Golfinos, J. G., Kumthekar, P., Ghamsari, F., Chen, L., Lein, P., Chetkovich, D. M., Snuderl, M., & Horbinski, C. (2017). Mutant IDH1 and seizures in patients with glioma. *Neurology, 88*(19), 1805–1813. https://doi.org/10.1212/WNL.0000000000003911

Chen, L., Heikkinen, L., Wang, C., Yang, Y., Sun, H., & Wong, G. (2019). Trends in the development of miRNA bioinformatics tools. *Briefings in Bioinformatics*, *20*(5), 1836–1852. https://doi.org/10.1093/bib/bby054

Chen, M., Medarova, Z., & Moore, A. (2021). Role of microRNAs in glioblastoma. *Oncotarget, 12*(17), 1707–1723. https://doi.org/10.18632/oncotarget.28039

Chen, P. H., Chang, C. K., Shih, C. M., Cheng, C. H., Lin, C. W., Lee, C. C., Liu, A. J., Ho, K. H., & Chen, K. C. (2016). The miR-204-3p-targeted IGFBP2 pathway is involved in xanthohumol-induced glioma cell apoptotic death. *Neuropharmacology, 110*(Pt A), 362–375. https://doi.org/10.1016/j.neuropharm.2016.07.038

Chen, S., Cai, Y., Yang, H., Zhang, B., Li, N., & Ren, G. (2024). PBOX-sRNA-seq uncovers novel features of miRNA modification and identifies selected 5'-tRNA fragments bearing 2'-O-modification. *Nucleic Acids Research, 52*(14), e65. https://doi.org/10.1093/nar/gkae537

Cheng, X., Wang, X., Wu, Z., Tan, S., Zhu, T., & Ding, K. (2019). CORO1C expression is associated with poor survival rates in gastric cancer and promotes metastasis in vitro. *FEBS Open Bio, 9*(6), 1097–1108. https://doi.org/10.1002/2211-5463.12639

Cheng, Y., & Zhang, C. (2010). MicroRNA-21 in cardiovascular disease. *Journal of Cardiovascular Translational Research, 3*(3), 251–255. https://doi.org/10.1007/s12265-010-9169-7

Chevalier, B., Adamiok, A., Mercey, O., Revinski, D. R., Zaragosi, L. E., Pasini, A., Kodjabachian, L., Barbry, P., & Marcet, B. (2015). miR-34/449 control apical actin network formation during multiciliogenesis through small GTPase pathways. *Nature Communications, 6*, 8386. https://doi.org/10.1038/ncomms9386

Chiarella, E., Aloisio, A., Scicchitano, S., Bond, H. M., & Mesuraca, M. (2021). Regulatory role of microRNAs targeting the transcription co-factor ZNF521 in normal tissues and cancers. *International Journal of Molecular Sciences, 22*(16), 8461. https://doi.org/10.3390/ijms22168461

Chinot, O. L., Wick, W., Mason, W., Henriksson, R., Saran, F., Nishikawa, R., Carpentier, A. F., Hoang-Xuan, K., Kavan, P., Cernea, D., Brandes, A. A., Hilton, M., Abrey, L., & Cloughesy, T. (2014). Bevacizumab plus radiotherapy-temozolomide for newly diagnosed glioblastoma. *The New England Journal of Medicine, 370*(8), 709–722. https://doi.org/10.1056/NEJMoa1308345

Chokshi, C. R., Shaikh, M. V., Brakel, B., Rossotti, M. A., Tieu, D., Maich, W., Anand, A., Chafe, S. C., Zhai, K., Suk, Y., Kieliszek, A. M., Miletic, P., Mikolajewicz, N., Chen, D., McNicol, J. D., Chan, K., Tong, A. H. Y., Kuhlmann, L., Liu, L., Alizada, Z., … Singh, S. K. (2024). Targeting axonal guidance dependencies in glioblastoma with ROBO1 CAR T cells. *Nature Medicine*. Advance online publication. https://doi.org/10.1038/s41591-024-03138-9

Chou, C. H., Shrestha, S., Yang, C. D., Chang, N. W., Lin, Y. L., Liao, K. W., Huang, W. C., Sun, T. H., Tu, S. J., Lee, W. H., Chiew, M. Y., Tai, C. S., Wei, T. Y., Tsai, T. R., Huang, H. T., Wang, C. Y., Wu, H. Y., Ho, S. Y., Chen, P. R., Chuang, C. H., … Huang, H. D. (2018). miRTarBase update 2018: A resource for experimentally validated microRNA-target interactions. *Nucleic Acids Research*, *46*(D1), D296–D302. https://doi.org/10.1093/nar/gkx1067

Chuang, J., & Jones, P. (2007). Epigenetics and microRNAs. *Pediatric Research, 61*, 24–29. https://doi.org/10.1203/pdr.0b013e3180457684

Chudasama, D., Katopodis, P., Stone, N., Haskell, J., Sheridan, H., Gardner, B., Urnovitz, H., Schuetz, E., Beck, J., Hall, M., Barr, J., Sisu, C., Rice, A., Polychronis, A., Anikin, V., & Karteris, E. (2019). Liquid biopsies in lung cancer: four emerging technologies and potential clinical applications. *Cancers, 11*(3), 331. https://doi.org/10.3390/cancers11030331

Ciregia, F., Urbani, A., & Palmisano, G. (2017). Extracellular Vesicles in Brain Tumors and Neurodegenerative Diseases. *Frontiers in Molecular Neuroscience*, 10, 276. https://doi.org/10.3389/fnmol.2017.00276

Ciruelas, K., Marcotulli, D., & Bajjalieh, S. M. (2019). Synaptic vesicle protein 2: A multi-faceted regulator of secretion. *Seminars in Cell & Developmental Biology, 95*, 130–141. https://doi.org/10.1016/j.semcdb.2019.02.003

Clegg, N., Ferguson, C., True, L. D., Arnold, H., Moorman, A., Quinn, J. E., Vessella, R. L., & Nelson, P. S. (2003). Molecular characterization of prostatic small-cell neuroendocrine carcinoma. *The Prostate, 55*(1), 55–64. https://doi.org/10.1002/pros.10217

Cohen, A. R. (2022). Brain Tumors in Children. *The New England Journal of Medicine, 386*(20), 1922–1931. https://doi.org/10.1056/NEJMra2116344

Condrat, C. E., Thompson, D. C., Barbu, M. G., Bugnar, O. L., Boboc, A., Cretoiu, D., Suciu, N., Cretoiu, S. M., & Voinea, S. C. (2020). miRNAs as biomarkers in disease: Latest findings regarding their role in diagnosis and prognosis. *Cells, 9*(2), 276. https://doi.org/10.3390/cells9020276

Connal, S., Cameron, J. M., Sala, A., Brennan, P. M., Palmer, D. S., Palmer, J. D., Perlow, H., & Baker, M. J. (2023). Liquid biopsies: the future of cancer early detection. *Journal of Translational Medicine, 21*(1), 118. https://doi.org/10.1186/s12967-023-03960-8

Connolly, J. L., Schnitt, S. J., Wang, H. H., et al. (2003). Role of the surgical pathologist in the diagnosis and management of the cancer patient. In Kufe, D. W., Pollock, R. E., Weichselbaum, R. R., et al. (Eds.), *Holland-Frei Cancer Medicine* (6th ed.). BC Decker. https://www.ncbi.nlm.nih.gov/books/NBK13237/

Constantinescu, T., & Lungu, C. N. (2021). Anticancer activity of natural and synthetic chalcones. *International Journal of Molecular Sciences, 22*(21), 11306. https://doi.org/10.3390/ijms222111306

Courtney, N. A., Bao, H., Briguglio, J. S., & Chapman, E. R. (2019). Synaptotagmin 1 clamps synaptic vesicle fusion in mammalian neurons independent of complexin. *Nature Communications, 10*(1), 4076. https://doi.org/10.1038/s41467-019-12015-w

Crane, A. M., & Bhattacharya, S. K. (2013). The use of bromodeoxyuridine incorporation assays to assess corneal stem cell proliferation. *Methods in Molecular Biology (Clifton, N.J.), 1014*, 65–70. https://doi.org/10.1007/978-1-62703-432-6_4

Crivii, C. B., Boșca, A. B., Melincovici, C. S., Constantin, A. M., Mărginean, M., Dronca, E., Suflețel, R., Gonciar, D., Bungărdean, M., & Șovrea, A. (2022). Glioblastoma microenvironment and cellular interactions. *Cancers, 14*(4), 1092. https://doi.org/10.3390/cancers14041092

Cui, M., Zorrilla-Veloz, R. I., Hu, J., Guan, B., & Ma, X. (2021). Diagnostic accuracy of PET for differentiating true glioma progression from post-treatment-related changes: A systematic review and meta-analysis. *Frontiers in Neurology, 12*, 671867. https://doi.org/10.3389/fneur.2021.671867

D'Urso, P. I., D'Urso, O. F., Gianfreda, C. D., Mezzolla, V., Storelli, C., & Marsigliante, S. (2015). miR-15b and miR-21 as circulating biomarkers for diagnosis of glioma. *Current Genomics, 16*(5), 304–311. https://doi.org/10.2174/1389202916666150707155610

Dasgupta, I., & Chatterjee, A. (2021). Recent advances in miRNA delivery systems. *Methods and Protocols, 4*(1), 10. https://doi.org/10.3390/mps4010010

de Almeida, A. J. P. O., de Oliveira, J. C. P. L., da Silva Pontes, L. V., de Souza Júnior, J. F., Gonçalves, T. A. F., Dantas, S. H., de Almeida Feitosa, M. S., Silva, A. O., & de Medeiros, I. A. (2022). ROS: Basic concepts, sources, cellular signaling, and its implications in aging pathways. *Oxidative Medicine and Cellular Longevity, 2022*, 1225578. https://doi.org/10.1155/2022/1225578

de Mooij, T., Peterson, T. E., Evans, J., McCutcheon, B., & Parney, I. F. (2020). Short non-coding RNA sequencing of glioblastoma extracellular vesicles. *Journal of Neuro-Oncology, 146*(2), 253–263. https://doi.org/10.1007/s11060-019-03384-9

de Rooij, L. A., Mastebroek, D. J., Ten Voorde, N., van der Wall, E., van Diest, P. J., & Moelans, C. B. (2022). The microRNA lifecycle in health and cancer. *Cancers, 14*(23), 5748. https://doi.org/10.3390/cancers14235748

Delgado-Martín, B., & Medina, M. Á. (2020). Advances in the knowledge of the molecular biology of glioblastoma and its impact in patient diagnosis, stratification, and treatment. *Advanced Science (Weinheim, Baden-Wurttemberg, Germany)*, *7*(9), 1902971. https://doi.org/10.1002/advs.201902971

Demircan, T., Yavuz, M., Kaya, E., Akgül, S., & Altuntaş, E. (2021). Cellular and molecular comparison of glioblastoma multiform cell lines. *Cureus, 13*(6), e16043. https://doi.org/10.7759/cureus.16043

Di Martino, M. T., Arbitrio, M., Caracciolo, D., Cordua, A., Cuomo, O., Grillone, K., Riillo, C., Caridà, G., Scionti, F., Labanca, C., Romeo, C., Siciliano, M. A., D'Apolito, M., Napoli, C., Montesano, M., Farenza, V., Uppolo, V., Tafuni, M., Falcone, F., D'Aquino, G., … Tassone, P. (2022). miR-221/222 as biomarkers and targets for therapeutic intervention on cancer and other diseases: A systematic review. *Molecular Therapy. Nucleic Acids, 27*, 1191–1224. https://doi.org/10.1016/j.omtn.2022.02.005

Diana, A., Gaido, G., Maxia, C., & Murtas, D. (2020). MicroRNAs at the crossroad of the dichotomic pathway cell death vs. stemness in neural somatic and cancer stem cells: Implications and therapeutic strategies. *International Journal of Molecular Sciences, 21*(24), 9630. https://doi.org/10.3390/ijms21249630

Ding, Y., Chan, C. Y., & Lawrence, C. E. (2004). Sfold web server for statistical folding and rational design of nucleic acids. *Nucleic Acids Research*, *32*(Web Server issue), W135–W141. https://doi.org/10.1093/nar/gkh449

Ding, Z., Wang, N., Ji, N., & Chen, Z. S. (2022). Proteomics technologies for cancer liquid biopsies. *Molecular Cancer, 21*(1), 53. https://doi.org/10.1186/s12943-022-01526-8

Divé, I., Klann, K., Michaelis, J. B., Heinzen, D., Steinbach, J. P., Münch, C., & Ronellenfitsch, M. W. (2022). Inhibition of mTOR signaling protects human glioma cells from hypoxia-induced cell death in an autophagy-independent manner. *Cell Death Discovery, 8*(1), 409. https://doi.org/10.1038/s41420-022-01195-y

Djuzenova, C. S., Fiedler, V., Memmel, S., Katzer, A., Hartmann, S., Krohne, G., Zimmermann, H., Scholz, C. J., Polat, B., Flentje, M., & Sukhorukov, V. L. (2015). Actin cytoskeleton organization, cell surface modification and invasion rate of 5 glioblastoma cell lines differing in PTEN and p53 status. *Experimental Cell Research, 330*(2), 346–357.

Duarte, T. T., Teixeira, S. A., Gonzalez-Reyes, L., & Reis, R. M. (2021). Decoding the roles of astrocytes and hedgehog signaling in medulloblastoma. *Current Oncology (Toronto, Ont.), 28*(4), 3058–3070. https://doi.org/10.3390/curroncol28040267

Dubey, J., Ratnakaran, N., & Koushika, S. P. (2015). Neurodegeneration and microtubule dynamics: death by a thousand cuts. *Frontiers in Cellular Neuroscience*, 9, 343. https://doi.org/10.3389/fncel.2015.00343

Dulsat, J., López-Nieto, B., Estrada-Tejedor, R., & Borrell, J. I. (2023). Evaluation of free online ADMET tools for academic or small biotech environments. *Molecules, 28*(2), 776. https://doi.org/10.3390/molecules28020776

Egger, J. V., Lane, M. V., Antonucci, L. A., Dedi, B., & Krucher, N. A. (2016). Dephosphorylation of the retinoblastoma protein (Rb) inhibits cancer cell EMT via Zeb. *Cancer Biology & Therapy, 17*(11), 1197–1205. https://doi.org/10.1080/15384047.2016.1235668

Ehara, T., Ohka, F., Motomura, K., & Saito, R. (2024). Epilepsy in patients with gliomas. *Neurologia Medico-Chirurgica, 64*(7), 253–260. https://doi.org/10.2176/jns-nmc.2023-0299

Eibl, R. H., & Schneemann, M. (2023). Liquid biopsy and glioblastoma. *Exploration of Targeted Anti-Tumor Therapy, 4*(1), 28–41. https://doi.org/10.37349/etat.2023.00121

Englot, D. J., Chang, E. F., & Vecht, C. J. (2016). Epilepsy and brain tumors. *Handbook of Clinical Neurology, 134*, 267–285. https://doi.org/10.1016/B978-0-12-802997-8.00016-5

Erices, J. I., Bizama, C., Niechi, I., Uribe, D., Rosales, A., Fabres, K., Navarro-Martínez, G., Torres, Á., San Martín, R., Roa, J. C., & Quezada-Monrás, C. (2023). Glioblastoma Microenvironment and Invasiveness: New Insights and Therapeutic Targets. *International journal of molecular sciences*, *24*(8), 7047. https://doi.org/10.3390/ijms24087047

Essig, M., Shiroishi, M. S., Nguyen, T. B., Saake, M., Provenzale, J. M., Enterline, D., Anzalone, N., Dörfler, A., Rovira, A., Wintermark, M., & Law, M. (2013). Perfusion MRI: The five most frequently asked technical questions. *AJR. American Journal of Roentgenology, 200*(1), 24–34. https://doi.org/10.2214/AJR.12.9543

Estevez-Ordonez, D., Stein, J., Maleknia, P., Gallegos, C., Atchley, T., Laskay, N., Clements, J., Lobbous, M., Leavenworth, J., Riley, K., Aban, I., Sorace, A., Chkheidze, R., Nabors, B., & Markert, J. (2023). Phase I clinical trial of oncolytic HSV-1 M032, a second-generation virus armed to express IL-12, for the treatment of adult patients with recurrent or progressive malignant glioma. *Neuro-Oncology, 25*(Suppl_5), v64. https://doi.org/10.1093/neuonc/noad179.0253

Evers, L., Schäfer, A., Pini, R., Zhao, K., Stei, S., Nimsky, C., & Bartsch, J. W. (2023). Identification of dysregulated microRNAs in glioblastoma stem-like cells. *Brain Sciences, 13*(2), 350. https://doi.org/10.3390/brainsci13020350

Fan, Y., Siklenka, K., Arora, S. K., Ribeiro, P., Kimmins, S., & Xia, J. (2016). miRNet—dissecting miRNA-target interactions and functional associations through network-based visual analysis. *Nucleic Acids Research*, *44*(W1), W135–W141. https://doi.org/10.1093/nar/gkw288

Fasoulakis, Z., Psarommati, M. Z., Papapanagiotou, A., Pergialiotis, V., Koutras, A., Douligeris, A., Mortaki, A., Mihail, A., Theodora, M., Stavros, S., Karakalpakis, D., Papamihail, M., Kontomanolis, E. N., Daskalakis, G., & Antsaklis, P. (2023). MicroRNAs can influence ovarian cancer progression by dysregulating integrin activity. *Cancers, 15*(18), 4449. https://doi.org/10.3390/cancers15184449

Feng, F., Wu, J., Gao, Z., Yu, S., & Cui, Y. (2017). Screening the key microRNAs and transcription factors in prostate cancer based on microRNA functional synergistic relationships. *Medicine, 96*(1), e5679. https://doi.org/10.1097/MD.0000000000005679

Fernandes, C., Costa, A., Osório, L., Lago, R. C., Linhares, P., Carvalho, B., & Caeiro, C. (2017). Current Standards of Care in Glioblastoma Therapy. In S. De Vleeschouwer (Ed.), *Glioblastoma*. Codon Publications. doi:10.15586/codon.glioblastoma.2017.ch11

Festa, M., Caputo, M., Cipolla, C., D'Acunto, C., Rossi, A., Tecce, M., & Capasso, A. (2013). The involvement of xanthohumol in the expression of annexin in human malignant glioblastoma cells. *The Open Biochemistry Journal, 7*, 1–10. https://doi.org/10.2174/1874091X01307010001

Filipe, A., Katopodis, P., Chudasama, D., Kerslake, R., Jeyaneethi, J., Anikin, V., Silva, E., Kyrou, I., Randeva, H. S., Sisu, C., Hall, M., & Karteris, E. (2022). Differential Expression of RAD51AP1 in Ovarian Cancer: Effects of siRNA In Vitro. *Journal of Personalized Medicine, 12*(2), 201. https://doi.org/10.3390/jpm12020201

Finn, N. A., & Searles, C. D. (2012). Intracellular and Extracellular miRNAs in Regulation of Angiogenesis Signaling. *Current Angiogenesis*, 4(102), 299–307. https://doi.org/10.2174/2211552811201040299

Franzoni, E., Booker, S. A., Parthasarathy, S., Rehfeld, F., Grosser, S., Srivatsa, S., Fuchs, H. R., Tarabykin, V., Vida, I., & Wulczyn, F. G. (2015). miR-128 regulates neuronal migration, outgrowth and intrinsic excitability via the intellectual disability gene Phf6. *eLife, 4*, e04263. https://doi.org/10.7554/eLife.04263

Friedman, J. S., Hertz, C. A. J., Karajannis, M. A., & Miller, A. M. (2022). Tapping into the genome: the role of CSF ctDNA liquid biopsy in glioma. *Neuro-Oncology Advances, 4*(Suppl 2), ii33–ii40. https://doi.org/10.1093/noajnl/vdac034

Friedman, R. C., Farh, K. K., Burge, C. B., & Bartel, D. P. (2009). Most mammalian mRNAs are conserved targets of microRNAs. *Genome Research, 19*(1), 92–105. https://doi.org/10.1101/gr.082701.108

Fu, J., Imani, S., Wu, M. Y., & Wu, R. C. (2023). MicroRNA-34 family in cancers: Role, mechanism, and therapeutic potential. *Cancers, 15*(19), 4723. https://doi.org/10.3390/cancers15194723

Fukuda, K., Seki, N., Yasudome, R., Mitsueda, R., Asai, S., Kato, M., Idichi, T., Kurahara, H., & Ohtsuka, T. (2023). Coronin 1C, Regulated by Multiple microRNAs, Facilitates Cancer Cell Aggressiveness in Pancreatic Ductal Adenocarcinoma. *Genes*, 14(5), 995. https://doi.org/10.3390/genes14050995

Funakoshi, Y., Sugihara, Y., Uneda, A., Nakashima, T., & Suzuki, H. (2023). Recent advances in the molecular understanding of medulloblastoma. *Cancer Science, 114*(3), 741–749. https://doi.org/10.1111/cas.15691

Furnari, F., Cloughesy, T., Cavenee, W., & Mischel, P. S. (2015). Heterogeneity of epidermal growth factor receptor signalling networks in glioblastoma. *Nature Reviews Cancer, 15*, 302–310. https://doi.org/10.1038/nrc3918

Galka-Marciniak, P., Urbanek-Trzeciak, M. O., Nawrocka, P. M., Dutkiewicz, A., Giefing, M., Lewandowska, M. A., & Kozlowski, P. (2019). Somatic mutations in miRNA genes in lung cancer—Potential functional consequences of non-coding sequence variants. *Cancers, 11*(6), 793. https://doi.org/10.3390/cancers11060793

Gao, H., Zhao, H., & Xiang, W. (2013). Expression level of human miR-34a correlates with glioma grade and prognosis. *Journal of Neuro-Oncology, 113*(2), 221–228. https://doi.org/10.1007/s11060-013-1119-1

Garcia, C. M., & Toms, S. A. (2020). The role of circulating microRNA in glioblastoma liquid biopsy. *World Neurosurgery, 138*, 425–435. https://doi.org/10.1016/j.wneu.2020.03.128

Gareev, I., Beylerli, O., Liang, Y., Xiang, H., Liu, C., Xu, X., Yuan, C., Ahmad, A., & Yang, G. (2021). The Role of MicroRNAs in Therapeutic Resistance of Malignant Primary Brain Tumors. *Frontiers in Cell and Developmental Biology, 9*, 740303. https://doi.org/10.3389/fcell.2021.740303

Gerasymchuk, D., Hubiernatorova, A., & Domanskyi, A. (2020). MicroRNAs Regulating Cytoskeleton Dynamics, Endocytosis, and Cell Motility-A Link Between Neurodegeneration and Cancer? *Frontiers in Neurology*, 11, 549006. https://doi.org/10.3389/fneur.2020.549006

Gerritsen, J. K. W., Klimek, M., Dirven, C. M. F., Hoop, E. O., Wagemakers, M., Rutten, G. J. M., Kloet, A., Hallaert, G. G., & Vincent, A. J. P. E. (2020). The SAFE-trial: Safe surgery for glioblastoma multiforme: Awake craniotomy versus surgery under general anesthesia. Study protocol for a multicenter prospective randomized controlled trial. *Contemporary Clinical Trials, 88*, 105876. https://doi.org/10.1016/j.cct.2019.105876

Gerson, S. L. (2004). MGMT: Its role in cancer aetiology and cancer therapeutics. *Nature Reviews Cancer, 4*(4), 296–307. https://doi.org/10.1038/nrc1319

Ghafouri-Fard, S., Abak, A., Shoorei, H., Mohaqiq, M., Majidpoor, J., Sayad, A., & Taheri, M. (2021). Regulatory role of microRNAs on PTEN signaling. *Biomedicine & pharmacotherapy*

= *Biomedecine & pharmacotherapie*, *133*, 110986. https://doi.org/10.1016/j.biopha.2020.110986

Ghasemi, M., Turnbull, T., Sebastian, S., & Kempson, I. (2021). The MTT assay: Utility, limitations, pitfalls, and interpretation in bulk and single-cell analysis. *International Journal of Molecular Sciences, 22*(23), 12827. https://doi.org/10.3390/ijms222312827

Ghatol, D., & Widrich, J. (2023). Intraoperative neurophysiological monitoring. In *StatPearls*. StatPearls Publishing. https://www.ncbi.nlm.nih.gov/books/NBK563203/

Ghosh, D., Nandi, S., & Bhattacharjee, S. (2018). Combination therapy to checkmate glioblastoma: Clinical challenges and advances. *Clinical and Translational Medicine, 7*(1), 33. https://doi.org/10.1186/s40169-018-0211-8

Ghosh, S., Lazarus, D., Robertson, N., Crosier, E., Liu, P., & Medarova, Z. (2023). The microRNA-10b targeted therapeutic, TTX-MC138, is effective in preclinical pancreatic adenocarcinoma. *Cancer Research, 83*(7_Suppl), 548. https://doi.org/10.1158/1538-7445.AM2023-548

Gibson, D., Vo, A. H., Lambing, H., Bhattacharya, P., Tahir, P., Chehab, F. F., & Butowski, N. (2024). A systematic review of high impact CpG sites and regions for MGMT methylation in glioblastoma. *BMC Neurology, 24*(1), 103. https://doi.org/10.1186/s12883-024-03605-3

Gil, H. N., Jung, E., Koh, D., Lim, Y., Lee, Y. H., & Shin, S. Y. (2019). A synthetic chalcone derivative, 2-hydroxy-3',5,5'-trimethoxychalcone (DK-139), triggers reactive oxygen species-induced apoptosis independently of p53 in A549 lung cancer cells. *Chemico-Biological Interactions, 298*, 72–79. https://doi.org/10.1016/j.cbi.2018.11.003

Gilbert, M. R., Dignam, J. J., Armstrong, T. S., Wefel, J. S., Blumenthal, D. T., Vogelbaum, M. A., Colman, H., Chakravarti, A., Pugh, S., Won, M., Jeraj, R., Brown, P. D., Jaeckle, K. A., Schiff, D., Stieber, V. W., Brachman, D. G., Werner-Wasik, M., Tremont-Lukats, I. W., Sulman, E. P., Aldape, K. D., … Mehta, M. P. (2014). A randomized trial of bevacizumab for newly diagnosed glioblastoma. *The New England Journal of Medicine, 370*(8), 699–708. https://doi.org/10.1056/NEJMoa1308573

Gilbert, T. L. (2018). The Allen Brain Atlas as a resource for teaching undergraduate neuroscience. *Journal of Undergraduate Neuroscience Education : JUNE : A Publication of FUN, Faculty for Undergraduate Neuroscience*, *16*(3), A261–A267.

Gillespie, C. S., Bligh, E. R., Poon, M. T. C., Solomou, G., Islim, A. I., Mustafa, M. A., Rominiyi, O., Williams, S. T., Kalra, N., Mathew, R. K., Booth, T. C., Thompson, G., Brennan, P. M., Jenkinson, M. D., INTERVAL-GB Collaborative, British Neurosurgical Trainee Research Collaborative (BNTRC), & Neurology and Neurosurgery Interest Group (NANSIG). (2022). Imaging timing after glioblastoma surgery (INTERVAL-GB): Protocol for a UK and Ireland, multicentre retrospective cohort study. *BMJ Open, 12*(9), e063043. https://doi.org/10.1136/bmjopen-2022-063043

Gilson, P., Merlin, J. L., & Harlé, A. (2022). Deciphering tumour heterogeneity: From tissue to liquid biopsy. *Cancers, 14*(6), 1384. https://doi.org/10.3390/cancers14061384

Giza, D. E., Vasilescu, C., & Calin, G. A. (2014). Key principles of miRNA involvement in human diseases. *Discoveries (Craiova, Romania), 2*(4), e34. https://doi.org/10.15190/d.2014.26

Goldman, M. J., Craft, B., Hastie, M., Repečka, K., McDade, F., Kamath, A., Banerjee, A., Luo, Y., Rogers, D., Brooks, A. N., Zhu, J., & Haussler, D. (2020). Visualizing and interpreting cancer genomics data via the Xena platform. *Nature Biotechnology*, *38*(6), 675–678. https://doi.org/10.1038/s41587-020-0546-8

González-Bermúdez, L., Anglada, T., Genescà, A., Martín, M., & Terradas, M. (2019). Identification of reference genes for RT-qPCR data normalisation in aging studies. *Scientific Reports, 9*(1), 13970. https://doi.org/10.1038/s41598-019-50035-0

Gordon, J. L., Brown, M. A., & Reynolds, M. M. (2018). Cell-based methods for determination of efficacy for candidate therapeutics in the clinical management of cancer. *Diseases (Basel, Switzerland), 6*(4), 85. https://doi.org/10.3390/diseases6040085

Gradisnik, L., & Velnar, T. (2023). Astrocytes in the central nervous system and their functions in health and disease: A review. *World Journal of Clinical Cases, 11*(15), 3385–3394. https://doi.org/10.12998/wjcc.v11.i15.3385

Grätz, C., Bui, M. L. U., Thaqi, G., Kirchner, B., Loewe, R. P., & Pfaffl, M. W. (2022). Obtaining reliable RT-qPCR results in molecular diagnostics—MIQE goals and pitfalls for transcriptional biomarker discovery. *Life (Basel, Switzerland), 12*(3), 386. https://doi.org/10.3390/life12030386

Green, K., Panagopoulou, P., D'Arco, F., O'Hare, P., Bowman, R., Walters, B., Dahl, C., Jorgensen, M., Patel, P., Slater, O., Ahmed, R., Bailey, S., Carceller, F., Collins, R., Corley, E., English, M., Howells, L., Kamal, A., Kilday, J. J., Lowis, S., … Opocher, E. (2023). A nationwide evaluation of bevacizumab-based treatments in pediatric low-grade glioma in the UK: Safety, efficacy, visual morbidity, and outcomes. *Neuro-Oncology, 25*(4), 774–785. https://doi.org/10.1093/neuonc/noac223

Greuter, L., Guzman, R., & Soleman, J. (2021). Typical pediatric brain tumors occurring in adults—Differences in management and outcome. *Biomedicines, 9*(4), 356. https://doi.org/10.3390/biomedicines9040356

Griffin, M., Khan, R., Basu, S., & Smith, S. (2020). Ion channels as therapeutic targets in high grade gliomas. *Cancers, 12*(10), 3068. https://doi.org/10.3390/cancers12103068

Grochans, S., Cybulska, A. M., Simińska, D., Korbecki, J., Kojder, K., Chlubek, D., & Baranowska-Bosiacka, I. (2022). Epidemiology of glioblastoma multiforme—Literature review. *Cancers, 14*(10), 2412. https://doi.org/10.3390/cancers14102412

Grønborg, M., Pavlos, N. J., Brunk, I., Chua, J. J., Münster-Wandowski, A., Riedel, D., Ahnert-Hilger, G., Urlaub, H., & Jahn, R. (2010). Quantitative comparison of glutamatergic and GABAergic synaptic vesicles unveils selectivity for few proteins including MAL2, a novel synaptic vesicle protein. *The Journal of Neuroscience: The Official Journal of the Society for Neuroscience, 30*(1), 2–12. https://doi.org/10.1523/JNEUROSCI.4074-09.2010

Grunder, E., D'Ambrosio, R., Fiaschetti, G., Abela, L., Arcaro, A., Zuzak, T., Ohgaki, H., Lv, S. Q., Shalaby, T., & Grotzer, M. (2011). MicroRNA-21 suppression impedes medulloblastoma cell migration. *European Journal of Cancer (Oxford, England: 1990), 47*(16), 2479–2490. https://doi.org/10.1016/j.ejca.2011.06.041

GTEx Consortium. (2013). The Genotype-Tissue Expression (GTEx) project. *Nature Genetics*, *45*(6), 580–585. https://doi.org/10.1038/ng.2653

Gu, W., Tu, X., Lu, W., Yin, Y., Meng, Q., Wang, X., Zhang, F., & Fu, Y. (2022). Identification of RNU44 as an endogenous reference gene for normalizing cell-free RNA in tuberculosis. *Open Forum Infectious Diseases, 9*(12), ofac540. https://doi.org/10.1093/ofid/ofac540

Guan, L., Yang, H., Cai, Y., Sun, L., Di, P., Li, W., Liu, G., & Tang, Y. (2018). ADMET-score - a comprehensive scoring function for evaluation of chemical drug-likeness. *MedChemComm, 10*(1), 148–157. https://doi.org/10.1039/c8md00472b

Guan, R., Zhang, X., & Guo, M. (2020). Glioblastoma stem cells and Wnt signaling pathway: Molecular mechanisms and therapeutic targets. *Chinese Neurosurgical Journal, 6*, 25. https://doi.org/10.1186/s41016-020-00207-z

Guessous, F., Zhang, Y., Kofman, A., Catania, A., Li, Y., Schiff, D., Purow, B., & Abounader, R. (2010). microRNA-34a is tumor suppressive in brain tumors and glioma stem cells. *Cell Cycle (Georgetown, Tex.), 9*(6), 1031–1036. https://doi.org/10.4161/cc.9.6.10987

Ha, M., & Kim, V. N. (2014). Regulation of microRNA biogenesis. *Nature Reviews Molecular Cell Biology, 15*(8), 509–524. https://doi.org/10.1038/nrm3838

Hagemann, C., Anacker, J., Ernestus, R. I., & Vince, G. H. (2012). A complete compilation of matrix metalloproteinase expression in human malignant gliomas. *World Journal of Clinical Oncology, 3*(5), 67–79. https://doi.org/10.5306/wjco.v3.i5.67

Hai, L., Liu, P., Yu, S., Yi, L., Tao, Z., Zhang, C., Abeysekera, I. R., Li, T., Tong, L., Ma, H., Liu, B., Xie, Y., Zhou, X., Lin, Y., Zhu, M., Zhang, K., Ren, B., Ming, H., Huang, Y., & Yang, X. (2018). Jagged1 is clinically prognostic and promotes invasion of glioma-initiating cells by activating NF-κB(p65) signaling. *Cellular Physiology and Biochemistry, 51*(6), 2925–2937. https://doi.org/10.1159/000496044

Hamad, A., Yusubalieva, G. M., Baklaushev, V. P., Chumakov, P. M., & Lipatova, A. V. (2023). Recent developments in glioblastoma therapy: Oncolytic viruses and emerging future strategies. *Viruses, 15*(2), 547. https://doi.org/10.3390/v15020547

Han, J., & Puri, R. K. (2018). Analysis of the cancer genome atlas (TCGA) database identifies an inverse relationship between interleukin-13 receptor α1 and α2 gene expression and poor prognosis and drug resistance in subjects with glioblastoma multiforme. *Journal of Neuro-Oncology*, *136*(3), 463–474. https://doi.org/10.1007/s11060-017-2680-9

Han, L., Li, Z., Jiang, Y., Jiang, Z., & Tang, L. (2019). SNHG29 regulates miR-223-3p/CTNND1 axis to promote glioblastoma progression via Wnt/β-catenin signaling pathway. *Cancer Cell International, 19*(1). https://doi.org/10.1186/s12935-019-1057-x

Han, S., Liu, Y., Cai, S. J., Qian, M., Ding, J., Larion, M., Gilbert, M. R., & Yang, C. (2020). IDH mutation in glioma: Molecular mechanisms and potential therapeutic targets. *British Journal of Cancer, 122*(11), 1580–1589. https://doi.org/10.1038/s41416-020-0814-x

Hanif, F., Muzaffar, K., Perveen, K., Malhi, S. M., & Simjee, S. hU. (2017). Glioblastoma multiforme: A review of its epidemiology and pathogenesis through clinical presentation and treatment. *Asian Pacific Journal of Cancer Prevention, 18*(1), 3–9. https://doi.org/10.22034/APJCP.2017.18.1.3

Hao, W., Luo, W., Bai, M., Li, J., Bai, X., Guo, J., Wu, J., & Wang, M. (2016). MicroRNA-206 Inhibited the Progression of Glioblastoma Through BCL-2. *Journal of Molecular Neuroscience: MN, 60*(4), 531–538. https://doi.org/10.1007/s12031-016-0824-6

Harish, V., Haque, E., Śmiech, M., Taniguchi, H., Jamieson, S., Tewari, D., & Bishayee, A. (2021). Xanthohumol for human malignancies: Chemistry, pharmacokinetics and molecular targets. *International Journal of Molecular Sciences, 22*(9), 4478. https://doi.org/10.3390/ijms22094478

Hasse, A., Rosentreter, A., Spoerl, Z., Stumpf, M., Noegel, A. A., & Clemen, C. S. (2005). Coronin 3 and its role in murine brain morphogenesis. *The European Journal of Neuroscience, 21*(5), 1155–1168. https://doi.org/10.1111/j.1460-9568.2005.03917.x

Haumann, R., Videira, J. C., Kaspers, G. J. L., van Vuurden, D. G., & Hulleman, E. (2020). Overview of current drug delivery methods across the blood-brain barrier for the treatment of primary brain tumors. *CNS Drugs, 34*(11), 1121–1131. https://doi.org/10.1007/s40263-020-00766-w

Haynes, W. (2013). Benjamini–Hochberg Method. In: Dubitzky, W., Wolkenhauer, O., Cho, KH., Yokota, H. (eds) *Encyclopedia of Systems Biology*. Springer, New York, NY. https://doi.org/10.1007/978-1-4419-9863-7_1215

Hba, S., Ghaddar, S., Wahnou, H., Pinon, A., El Kebbaj, R., Pouget, C., Sol, V., Liagre, B., Oudghiri, M., & Limami, Y. (2023). Natural chalcones and derivatives in colon cancer: Pre-clinical challenges and the promise of chalcone-based nanoparticles. *Pharmaceutics, 15*(12), 2718. https://doi.org/10.3390/pharmaceutics15122718

He, J., Jiang, Y., Liu, L., Zuo, Z., & Zeng, C. (2021). Circulating microRNAs as promising diagnostic biomarkers for patients with glioma: A meta-analysis. *Frontiers in Neurology, 11*, 610163. https://doi.org/10.3389/fneur.2020.610163

He, W., Liu, Y., Wamer, W. G., & Yin, J. J. (2014). Electron spin resonance spectroscopy for the study of nanomaterial-mediated generation of reactive oxygen species. *Journal of Food and Drug Analysis, 22*(1), 49–63. https://doi.org/10.1016/j.jfda.2014.01.004

He, Z., Cen, D., Luo, X., Li, D., Li, P., Liang, L., & Meng, Z. (2013). Downregulation of miR-383 promotes glioma cell invasion by targeting insulin-like growth factor 1 receptor. *Medical Oncology (Northwood, London, England), 30*(2), 557. https://doi.org/10.1007/s12032-013-0557-0

He, Z., Wilson, A., Rich, F., Kenwright, D., Stevens, A., Low, Y. S., & Thunders, M. (2023). Chromosomal instability and its effect on cell lines. *Cancer Reports (Hoboken, N.J.), 6*(6), e1822. https://doi.org/10.1002/cnr2.1822

HeadSmart Be Brain Tumour Aware. (2016). A new clinical guideline from the Royal College of Paediatrics and Child Health with a national awareness campaign accelerates brain tumor diagnosis in UK children—"HeadSmart: Be Brain Tumour Aware". *Neuro-Oncology, 18*(3), 445–454. https://doi.org/10.1093/neuonc/nov187

Hegi, M. E., Diserens, A. C., Gorlia, T., Hamou, M. F., de Tribolet, N., Weller, M., Kros, J. M., Hainfellner, J. A., Mason, W., Mariani, L., Bromberg, J. E., Hau, P., Mirimanoff, R. O., Cairncross, J. G., Janzer, R. C., & Stupp, R. (2005). MGMT gene silencing and benefit from temozolomide in glioblastoma. *The New England Journal of Medicine, 352*(10), 997–1003. https://doi.org/10.1056/NEJMoa043331

Herholz, K. (2017). Brain tumors: An update on clinical PET research in gliomas. *Seminars in Nuclear Medicine, 47*(1), 5–17. https://doi.org/10.1053/j.semnuclmed.2016.09.004

Hermansen, S. K., Nielsen, B. S., Aaberg-Jessen, C., & Kristensen, B. W. (2016). miR-21 is linked to glioma angiogenesis: A co-localization study. *The Journal of Histochemistry and Cytochemistry, 64*(2), 138–148. https://doi.org/10.1369/0022155415623515

Herrlinger, U., Tzaridis, T., Mack, F., Steinbach, J. P., Schlegel, U., Sabel, M., Hau, P., Kortmann, R. D., Krex, D., Grauer, O., Goldbrunner, R., Schnell, O., Bähr, O., Uhl, M., Seidel, C., Tabatabai, G., Kowalski, T., Ringel, F., Schmidt-Graf, F., Suchorska, B., … Neurooncology Working Group of the German Cancer Society. (2019). Lomustine-temozolomide combination therapy versus standard temozolomide therapy in patients with newly diagnosed glioblastoma with methylated MGMT promoter (CeTeG/NOA-09): A randomised, open-label, phase 3 trial. *The Lancet, 393*(10172), 678–688. https://doi.org/10.1016/S0140-6736(18)31791-4

Hickman, R. A., Miller, A. M., & Arcila, M. E. (2023). Cerebrospinal fluid: a unique source of circulating tumor DNA with broad clinical applications. *Translational Oncology, 33*, 101688. https://doi.org/10.1016/j.tranon.2023.101688

Hide, T., Komohara, Y., Miyasato, Y., Nakamura, H., Makino, K., Takeya, M., Kuratsu, J. I., Mukasa, A., & Yano, S. (2018). Oligodendrocyte progenitor cells and macrophages/microglia produce glioma stem cell niches at the tumor border. *EBioMedicine, 30*, 94–104. https://doi.org/10.1016/j.ebiom.2018.02.024

Ho, P. T. B., Clark, I. M., & Le, L. T. T. (2022). MicroRNA-based diagnosis and therapy. *International Journal of Molecular Sciences, 23*(13), 7167. https://doi.org/10.3390/ijms23137167

Hoeben, A., Joosten, E. A. J., & van den Beuken-van Everdingen, M. H. J. (2021). Personalized Medicine: Recent Progress in Cancer Therapy. *Cancers, 13*(2), 242. https://doi.org/10.3390/cancers13020242

Hoggarth, A. R., Muthukumar, S., Thomas, S. M., Crowley, J., Kiser, J., & Witcher, M. R. (2024). Clinical theranostics in recurrent gliomas: A review. *Cancers, 16*(9), 1715. https://doi.org/10.3390/cancers16091715

Hölzl, D., Hutarew, G., Zellinger, B., Schlicker, H. U., Schwartz, C., Winkler, P. A., Sotlar, K., & Kraus, T. F. J. (2021). Integrated analysis of programmed cell death ligand 1 expression reveals increased levels in high-grade glioma. *Journal of Cancer Research and Clinical Oncology, 147*(8), 2271–2280. https://doi.org/10.1007/s00432-021-03656-w

Hong, D. S., Kang, Y. K., Borad, M., Sachdev, J., Ejadi, S., Lim, H. Y., Brenner, A. J., Park, K., Lee, J. L., Kim, T. Y., Shin, S., Becerra, C. R., Falchook, G., Stoudemire, J., Martin, D., Kelnar, K., Peltier, H., Bonato, V., Bader, A. G., Smith, S., … Beg, M. S. (2020). Phase 1 study of MRX34, a liposomal miR-34a mimic, in patients with advanced solid tumours. *British Journal of Cancer, 122*(11), 1630–1637. https://doi.org/10.1038/s41416-020-0802-1

Hong, M., Tao, S., Zhang, L., Diao, L. T., Huang, X., Huang, S., Xie, S. J., Xiao, Z. D., & Zhang, H. (2020). RNA sequencing: new technologies and applications in cancer research. *Journal of Hematology & Oncology, 13*(1), 166. https://doi.org/10.1186/s13045-020-01005-x

Hosein Yazdi, A., Zarrinpour, V., Moslemi, E., & Forghanifard, M. M. (2022). A Signature of Three microRNAs Is a Potential Diagnostic Biomarker for Glioblastoma. *Iranian Biomedical Journal, 26*(4), 301–312. https://doi.org/10.52547/ibj.3671

Hou, J., Lv, A., Deng, Q., Zhang, G., Hu, X., & Cui, H. (2019). TROP2 promotes the proliferation and metastasis of glioblastoma cells by activating the JAK2/STAT3 signaling pathway. *Oncology Reports, 41*(2), 753–764. https://doi.org/10.3892/or.2018.6859

Houldsworth, A. (2024). Role of oxidative stress in neurodegenerative disorders: A review of reactive oxygen species and prevention by antioxidants. *Brain Communications, 6*(1), fcad356. https://doi.org/10.1093/braincomms/fcad356

Hoyer, M. J., Chitwood, P. J., Ebmeier, C. C., Striepen, J. F., Qi, R. Z., Old, W. M., & Voeltz, G. K. (2018). A Novel Class of ER Membrane Proteins Regulates ER-Associated Endosome Fission. *Cell, 175*(1), 254–265.e14. https://doi.org/10.1016/j.cell.2018.08.030

Hsu, K., Middlemiss, S., Saletta, F., & Haber, M. (2021). Chimeric antigen receptor-modified T cells targeting EphA2 for the immunotherapy of paediatric bone tumours. *Cancer Gene Therapy, 28*(4), 321–334. https://doi.org/10.1038/s41417-020-00221-4

Hu, C., Jiang, W., Lv, M., Fan, S., Lu, Y., Wu, Q., & Pi, J. (2022). Potentiality of Exosomal Proteins as Novel Cancer Biomarkers for Liquid Biopsy. *Frontiers in Immunology*, 13, 792046. https://doi.org/10.3389/fimmu.2022.792046

Huang, L. E. (2022). Impact of CDKN2A/B homozygous deletion on the prognosis and biology of IDH-mutant glioma. *Biomedicines, 10*(2), 246. https://doi.org/10.3390/biomedicines10020246

Huang, S. W., Ali, N. D., Zhong, L., & Shi, J. (2018). MicroRNAs as biomarkers for human glioblastoma: Progress and potential. *Acta Pharmacologica Sinica, 39*(9), 1405–1413. https://doi.org/10.1038/aps.2017.173

Huang, Y., Hoffman, C., Rajappa, P., Kim, J. H., Hu, W., Huse, J., Tang, Z., Li, X., Weksler, B., Bromberg, J., Lyden, D. C., & Greenfield, J. P. (2014). Oligodendrocyte progenitor cells promote neovascularization in glioma by disrupting the blood-brain barrier. *Cancer Research, 74*(4), 1011–1021. https://doi.org/10.1158/0008-5472.CAN-13-1072

Hudson, A. M., & Cooley, L (2013). Phylogenetic, structural and functional relationships between WD-and Kelch-repeat proteins. In *Madame Curie Bioscience Database*. Austin (TX): Landes Bioscience; Available from: https://www.ncbi.nlm.nih.gov/books/NBK6031/

Husain, S., & Srijithesh, P. R. (2016). Homogeneity and the outcome of clinical trials: An appraisal of the outcome of recent clinical trials on endovascular intervention in acute ischemic stroke. *Annals of Indian Academy of Neurology, 19*(1), 21–24. https://doi.org/10.4103/0972-2327.173308

Hwang, H., Chang, H. R., & Baek, D. (2023). Determinants of functional microRNA targeting. *Molecules and Cells, 46*(1), 21–32. https://doi.org/10.14348/molcells.2023.2157

ICGC/TCGA Pan-Cancer Analysis of Whole Genomes Consortium (2020). Pan-cancer analysis of whole genomes. *Nature, 578*(7793), 82–93. https://doi.org/10.1038/s41586-020-1969-6

Idrisova, K. F., Simon, H. U., & Gomzikova, M. O. (2022). Role of patient-derived models of cancer in translational oncology. *Cancers, 15*(1), 139. https://doi.org/10.3390/cancers15010139

Ikeda, Y., Morikawa, S., Nakashima, M., Yoshikawa, S., Taniguchi, K., Sawamura, H., Suga, N., Tsuji, A., & Matsuda, S. (2023). CircRNAs and RNA-binding proteins involved in the pathogenesis of cancers or central nervous system disorders. *Non-Coding RNA, 9*(2), 23. https://doi.org/10.3390/ncrna9020023

Ilic, I., & Ilic, M. (2023). International patterns and trends in brain cancer incidence and mortality: An observational study based on the global burden of disease. *Heliyon, 9*(7), e18222. https://doi.org/10.1016/j.heliyon.2023.e18222

Imani, S., Wei, C., Cheng, J., Khan, M. A., Fu, S., Yang, L., Tania, M., Zhang, X., Xiao, X., Zhang, X., & Fu, J. (2017). MicroRNA-34a targets epithelial to mesenchymal transition-inducing transcription factors (EMT-TFs) and inhibits breast cancer cell migration and invasion. *Oncotarget, 8*(13), 21362–21379. https://doi.org/10.18632/oncotarget.15214

Incekara, F., Smits, M., Dirven, L., Bos, E. M., Balvers, R. K., Haitsma, I. K., Schouten, J. W., & Vincent, A. J. P. E. (2021). Intraoperative B-Mode ultrasound-guided surgery and the extent of glioblastoma resection: A randomized controlled trial. *Frontiers in Oncology, 11*, 649797. https://doi.org/10.3389/fonc.2021.649797

Iorio, M. V., & Croce, C. M. (2012). Causes and consequences of microRNA dysregulation. *Cancer Journal (Sudbury, Mass.), 18*(3), 215–222. https://doi.org/10.1097/PPO.0b013e318250c001

Irmer, B., Chandrabalan, S., Maas, L., Bleckmann, A., & Menck, K. (2023). Extracellular vesicles in liquid biopsies as biomarkers for solid tumors. *Cancers, 15*(4), 1307. https://doi.org/10.3390/cancers15041307

Ishii, N., Maier, D., Merlo, A., Tada, M., Sawamura, Y., Diserens, A. C., & Van Meir, E. G. (1999). Frequent co-alterations of TP53, p16/CDKN2A, p14ARF, PTEN tumor suppressor genes in human glioma cell lines. *Brain Pathology (Zurich, Switzerland), 9*(3), 469–479. https://doi.org/10.1111/j.1750-3639.1999.tb00536.x

Isobe, I., Yanagisawa, K., & Michikawa, M. (2001). 3-(4,5-Dimethylthiazol-2-yl)-2,5-diphenyltetrazolium bromide (MTT) causes Akt phosphorylation and morphological changes in intracellular organellae in cultured rat astrocytes. *Journal of Neurochemistry, 77*(1), 274–280. https://doi.org/10.1046/j.1471-4159.2001.t01-1-00237.x

Ius, T., Sabatino, G., Panciani, P. P., Fontanella, M. M., Rudà, R., Castellano, A., Barbagallo, G. M. V., Belotti, F., Boccaletti, R., Catapano, G., Costantino, G., Della Puppa, A., Di Meco, F., Gagliardi, F., Garbossa, D., Germanò, A. F., Iacoangeli, M., Mortini, P., Olivi, A., Pessina, F., … Esposito, V. (2023). Surgical management of Glioma Grade 4: Technical update from the neuro-oncology section of the Italian Society of Neurosurgery (SINch®): A systematic review. *Journal of Neuro-Oncology, 162*(2), 267–293. https://doi.org/10.1007/s11060-023-04274-x

Ivo D'Urso, P., Fernando D'Urso, O., Damiano Gianfreda, C., Mezzolla, V., Storelli, C., & Marsigliante, S. (2015). miR-15b and miR-21 as circulating biomarkers for diagnosis of glioma. *Current Genomics, 16*(5), 304–311. https://doi.org/10.2174/1389202916666150707155610

Jacobsen, P. F., Jenkyn, D. J., & Papadimitriou, J. M. (1985). Establishment of a human medulloblastoma cell line and its heterotransplantation into nude mice. *Journal of Neuropathology and Experimental Neurology, 44*(5), 472–485. https://doi.org/10.1097/00005072-198509000-00003

Jafarzadeh, A., Noori, M., Sarrafzadeh, S., Tamehri Zadeh, S. S., Nemati, M., Chatrabnous, N., Jafarzadeh, S., Hamblin, M. R., Jafari Najaf Abadi, M. H., & Mirzaei, H. (2022). MicroRNA-383: A tumor suppressor miRNA in human cancer. *Frontiers in Cell and Developmental Biology, 10*, 955486. https://doi.org/10.3389/fcell.2022.955486

Jaiswal, S. (2016). Role of immunohistochemistry in the diagnosis of central nervous system tumors. *Neurology India, 64*(3), 502–512. https://doi.org/10.4103/0028-3886.181547

Jee, J., Lebow, E. S., Yeh, R., Das, J. P., Namakydoust, A., Paik, P. K., Chaft, J. E., Jayakumaran, G., Rose Brannon, A., Benayed, R., Zehir, A., Donoghue, M., Schultz, N., Chakravarty, D., Kundra, R., Madupuri, R., Murciano-Goroff, Y. R., Tu, H. Y., Xu, C. R., Martinez, A., … Li, B. T. (2022). Overall survival with circulating tumor DNA-guided therapy in advanced non-small-cell lung cancer. *Nature Medicine, 28*(11), 2353–2363. https://doi.org/10.1038/s41591-022-02047-z

Jena, A. B., Samal, R. R., Bhol, N. K., & Duttaroy, A. K. (2023). Cellular red-ox system in health and disease: The latest update. *Biomedicine & Pharmacotherapy, 162*, 114606. https://doi.org/10.1016/j.biopha.2023.114606

Jermyn, M., Mok, K., Mercier, J., Desroches, J., Pichette, J., Saint-Arnaud, K., Bernstein, L., Guiot, M. C., Petrecca, K., & Leblond, F. (2015). Intraoperative brain cancer detection with Raman spectroscopy in humans. *Science Translational Medicine, 7*(274), 274ra19. https://doi.org/10.1126/scitranslmed.aaa2384

Jin, J., Qiu, S., Wang, P., Liang, X., Huang, F., Wu, H., Zhang, B., Zhang, W., Tian, X., Xu, R., Shi, H., & Wu, X. (2019). Cardamonin inhibits breast cancer growth by repressing HIF-1α-dependent metabolic reprogramming. *Journal of Experimental & Clinical Cancer Research, 38*(1), 377. https://doi.org/10.1186/s13046-019-1351-4

Ju, S., Chen, C., Zhang, J., Xu, L., Zhang, X., Li, Z., Chen, Y., Zhou, J., Ji, F., & Wang, L. (2022). Detection of circulating tumour cells: opportunities and challenges. *Biomarker Research, 10*(1), 58. https://doi.org/10.1186/s40364-022-00403-2

Juric, V., & Murphy, B. (2020). Cyclin-dependent kinase inhibitors in brain cancer: current state and future directions. *Cancer Drug Resistance (Alhambra, Calif.), 3*(1), 48–62. https://doi.org/10.20517/cdr.2019.105

Kalfert, D., Ludvikova, M., Pesta, M., Ludvik, J., Dostalova, L., & Kholová, I. (2020). Multifunctional roles of miR-34a in cancer: A review with the emphasis on head and neck squamous cell carcinoma and thyroid cancer with clinical implications. *Diagnostics, 10*(8), 563. https://doi.org/10.3390/diagnostics10080563

Kalluri, R., & LeBleu, V. S. (2020). The biology, function, and biomedical applications of exosomes. *Science (New York, N.Y.)*, 367(6478), eaau6977. https://doi.org/10.1126/science.aau6977

Kałuzińska-Kołat, Ż., Kołat, D., Kośla, K., Płuciennik, E., & Bednarek, A. K. (2023). Molecular landscapes of glioblastoma cell lines revealed a group of patients that do not benefit from WWOX tumor suppressor expression. *Frontiers in Neuroscience, 17*, 1260409. https://doi.org/10.3389/fnins.2023.1260409

Kamiya-Matsuoka, C., & Gilbert, M. R. (2015). Treating recurrent glioblastoma: An update. *CNS Oncology, 4*(2), 91–104. https://doi.org/10.2217/cns.14.55

Kanderi, T., Munakomi, S., & Gupta, V. (2024). Glioblastoma multiforme. In *StatPearls*. Treasure Island (FL): StatPearls Publishing. Available from https://www.ncbi.nlm.nih.gov/books/NBK553201/

Kanehisa, M., Furumichi, M., Tanabe, M., Sato, Y., & Morishima, K. (2017). KEGG: New perspectives on genomes, pathways, diseases and drugs. *Nucleic Acids Research*, *45*(D1), D353–D361. https://doi.org/10.1093/nar/gkw1092

Karakuzu, O., Cruz, M. R., Liu, Y., & Garsin, D. A. (2019). Amplex Red assay for measuring hydrogen peroxide production from Caenorhabditis elegans. *Bio-protocol, 9*(21), e3409. https://doi.org/10.21769/BioProtoc.3409

Kariuki, D., Asam, K., Aouizerat, B. E., Lewis, K. A., Florez, J. C., & Flowers, E. (2023). Review of databases for experimentally validated human microRNA-mRNA

interactions. *Database: The Journal of Biological Databases and Curation*, 2023, baad014. https://doi.org/10.1093/database/baad014

Karmur, B. S., Philteos, J., Abbasian, A., Zacharia, B. E., Lipsman, N., Levin, V., Grossman, S., & Mansouri, A. (2020). Blood-brain barrier disruption in neuro-oncology: Strategies, failures, and challenges to overcome. *Frontiers in Oncology, 10*, 563840. https://doi.org/10.3389/fonc.2020.563840

Karve, A. S., Desai, J. M., Gadgil, S. N., Dave, N., Wise-Draper, T. M., Gudelsky, G. A., Phoenix, T. N., DasGupta, B., Yogendran, L., Sengupta, S., Plas, D. R., & Desai, P. B. (2024). A review of approaches to potentiate the activity of temozolomide against glioblastoma to overcome resistance. *International Journal of Molecular Sciences, 25*(6), 3217. https://doi.org/10.3390/ijms25063217

Katerji, M., Filippova, M., & Duerksen-Hughes, P. (2019). Approaches and methods to measure oxidative stress in clinical samples: Research applications in the cancer field. *Oxidative Medicine and Cellular Longevity, 2019*, 1279250. https://doi.org/10.1155/2019/1279250

Kaur, B., & Kumar, H. (2020). Ultrasound-promoted one-pot three-component synthesis of β-amino carbonyl compounds using manganese perchlorate. *Organic Preparations and Procedures International, 52*(5), 474–477. https://doi.org/10.1080/00304948.2020.1805995

Khabibov, M., Garifullin, A., Boumber, Y., Khaddour, K., Fernandez, M., Khamitov, F., Khalikova, L., Kuznetsova, N., Kit, O., & Kharin, L. (2022). Signaling pathways and therapeutic approaches in glioblastoma multiforme (Review). *International Journal of Oncology, 60*(6), 69. https://doi.org/10.3892/ijo.2022.5359

Khan, I., Mahfooz, S., Karacam, B., Elbasan, E. B., Akdur, K., Karimi, H., Sakarcan, A., & Hatiboglu, M. A. (2022). Glioma cancer stem cells modulating the local tumor immune environment. *Frontiers in Molecular Neuroscience, 15*, 1029657. https://doi.org/10.3389/fnmol.2022.1029657

Khoury, S., & Tran, N. (2020). qPCR multiplex detection of microRNA and messenger RNA in a single reaction. *PeerJ, 8*, e9004. https://doi.org/10.7717/peerj.9004

Kijima, N., & Kanemura, Y. (2016). Molecular Classification of Medulloblastoma. *Neurologia Medico-Chirurgica, 56*(11), 687–697. https://doi.org/10.2176/nmc.ra.2016-0016

Kim, H. J., Park, J. W., & Lee, J. H. (2021). Genetic architectures and cell-of-origin in glioblastoma. *Frontiers in Oncology, 10*, 615400. https://doi.org/10.3389/fonc.2020.615400

[a]Kim, H., & Xue, X. (2020). Detection of total reactive oxygen species in adherent cells by 2',7'-dichlorodihydrofluorescein diacetate staining. *Journal of Visualized Experiments, 160*, e60682. https://doi.org/10.3791/60682

Kim, K., Nguyen, T. D., Li, S., & Nguyen, T. A. (2018). SRSF3 recruits DROSHA to the basal junction of primary microRNAs. *RNA (New York, N.Y.), 24*(7), 892–898. https://doi.org/10.1261/rna.065862.118

[b]Kim, S. W., & Kim, K. T. (2020). Expression of Genes Involved in Axon Guidance: How Much Have We Learned?. *International Journal of Molecular Sciences*, 21(10), 3566. https://doi.org/10.3390/ijms21103566

Kim, T. M., Huang, W., Park, R., Park, P. J., & Johnson, M. D. (2011). A developmental taxonomy of glioblastoma defined and maintained by microRNAs. *Cancer Research, 71*(9), 3387–3399. https://doi.org/10.1158/0008-5472.CAN-10-4117

Kim, T., & Croce, C. M. (2023). MicroRNA: Trends in clinical trials of cancer diagnosis and therapy strategies. *Experimental & Molecular Medicine, 55*, 1314–1321. https://doi.org/10.1038/s12276-023-01050-9

King, Z. T., Butler, M. T., Hockenberry, M. A., Subramanian, B. C., Siesser, P. F., Graham, D. M., Legant, W. R., & Bear, J. E. (2022). Coro1B and Coro1C regulate lamellipodia dynamics and cell motility by tuning branched actin turnover. *The Journal of Cell Biology, 221*(8), e202111126. https://doi.org/10.1083/jcb.202111126

Kirchweger, P., Wundsam, H. V., & Rumpold, H. (2022). Circulating tumor DNA for diagnosis, prognosis and treatment of gastrointestinal malignancies. *World Journal of Clinical Oncology, 13*(6), 473–484. https://doi.org/10.5306/wjco.v13.i6.473

Kitange, G. J., Carlson, B. L., Schroeder, M. A., Grogan, P. T., Lamont, J. D., Decker, P. A., Wu, W., James, C. D., & Sarkaria, J. N. (2009). Induction of MGMT expression is associated with temozolomide resistance in glioblastoma xenografts. *Neuro-Oncology, 11*(3), 281–291. https://doi.org/10.1215/15228517-2008-090

Knudson, K. M., Hwang, S., McCann, M. S., Joshi, B. H., Husain, S. R., & Puri, R. K. (2022). Recent advances in IL-13Rα2-directed cancer immunotherapy. *Frontiers in Immunology, 13*, 878365. https://doi.org/10.3389/fimmu.2022.878365

Kokkinos, V., Chatzisotiriou, A., & Seimenis, I. (2023). Functional magnetic resonance imaging and diffusion tensor imaging-tractography in resective brain surgery: Lesion coverage strategies and patient outcomes. *Brain Sciences, 13*(11), 1574. https://doi.org/10.3390/brainsci13111574

Komoto, T. T., Nishimura, F. G., Evangelista, A. F., de Freitas, A. J. A., da Silva, G., Silva, W. A., Peronni, K., Marques, M. M. C., Marins, M., & Fachin, A. L. (2023). Exploring the therapeutic potential of trans-chalcone: Modulation of microRNAs linked to breast cancer progression in MCF-7 cells. *International Journal of Molecular Sciences, 24*(13), 10785. https://doi.org/10.3390/ijms241310785

Kono, N., & Arakawa, K. (2019). Nanopore sequencing: Review of potential applications in functional genomics. *Development, Growth & Differentiation, 61*(5), 316–326. https://doi.org/10.1111/dgd.12608

Kozera, B., & Rapacz, M. (2013). Reference genes in real-time PCR. *Journal of Applied Genetics, 54*(4), 391–406. https://doi.org/10.1007/s13353-013-0173-x

Krishna, S., Choudhury, A., Keough, M. B., Seo, K., Ni, L., Kakaizada, S., Lee, A., Aabedi, A., Popova, G., Lipkin, B., Cao, C., Nava Gonzales, C., Sudharshan, R., Egladyous, A., Almeida,

N., Zhang, Y., Molinaro, A. M., Venkatesh, H. S., Daniel, A. G. S., Shamardani, K., … Hervey-Jumper, S. L. (2023). Glioblastoma remodelling of human neural circuits decreases survival. *Nature, 617*(7961), 599–607. https://doi.org/10.1038/s41586-023-06036-1

Krol, J., Loedige, I., & Filipowicz, W. (2010). The widespread regulation of microRNA biogenesis, function, and decay. *Nature Reviews Genetics, 11*(9), 597–610. https://doi.org/10.1038/nrg2843

Królikowska, A., Filipska-Blejder, K., Jabłońska, R., Haor, B., Antczak-Komoterska, A., Biercewicz, M., Grzelak, L., Harat, M., & Ślusarz, R. (2022). Quality of life after surgical treatment of brain tumors. *Journal of Clinical Medicine, 11*(13), 3733. https://doi.org/10.3390/jcm11133733

Kros, J. M., Gorlia, T., Kouwenhoven, M. C., Zheng, P. P., Collins, V. P., Figarella-Branger, D., Giangaspero, F., Giannini, C., Mokhtari, K., Mørk, S. J., Paetau, A., Reifenberger, G., & van den Bent, M. J. (2007). Panel review of anaplastic oligodendroglioma from European Organization For Research and Treatment of Cancer Trial 26951: assessment of consensus in diagnosis, influence of 1p/19q loss, and correlations with outcome. *Journal of Neuropathology and Experimental Neurology, 66*(6), 545–551. https://doi.org/10.1097/01.jnen.0000263869.84188.72

Kubben, P. L., ter Meulen, K. J., Schijns, O. E., ter Laak-Poort, M. P., van Overbeeke, J. J., & van Santbrink, H. (2011). Intraoperative MRI-guided resection of glioblastoma multiforme: A systematic review. *The Lancet Oncology, 12*(11), 1062–1070. https://doi.org/10.1016/S1470-2045(11)70130-9

[a]Kumar, R., Liu, A. P. Y., & Northcott, P. A. (2020). Medulloblastoma genomics in the modern molecular era. *Brain Pathology (Zurich, Switzerland)*, 30(3), 679–690. https://doi.org/10.1111/bpa.12804

[b]Kumar, S., & Reddy, P. H. (2020). The role of synaptic microRNAs in Alzheimer's disease. *Biochimica et Biophysica Acta. Molecular Basis of Disease*, 1866(12), 165937. https://doi.org/10.1016/j.bbadis.2020.165937

Kumar, S., Sánchez-Álvarez, M., Lolo, F. N., Trionfetti, F., Strippoli, R., & Cordani, M. (2021). Autophagy and the Lysosomal System in Cancer. *Cells*, 10(10), 2752. https://doi.org/10.3390/cells10102752

Kung, C. P., & Weber, J. D. (2022). It's getting complicated—A fresh look at p53-MDM2-ARF triangle in tumorigenesis and cancer therapy. *Frontiers in Cell and Developmental Biology, 10*, 818744. https://doi.org/10.3389/fcell.2022.818744

Kwon, Y. W., Jo, H. S., Bae, S., Seo, Y., Song, P., Song, M., & Yoon, J. H. (2021). Application of Proteomics in Cancer: Recent Trends and Approaches for Biomarkers Discovery. *Frontiers in Medicine*, 8, 747333. https://doi.org/10.3389/fmed.2021.747333

Lahens, N. F., Ricciotti, E., Smirnova, O., Toorens, E., Kim, E. J., Baruzzo, G., Hayer, K. E., Ganguly, T., Schug, J., & Grant, G. R. (2017). A comparison of Illumina and Ion Torrent sequencing platforms in the context of differential gene expression. *BMC Genomics, 18*(1), 602. https://doi.org/10.1186/s12864-017-4011-0

Lam, J. K., Chow, M. Y., Zhang, Y., & Leung, S. W. (2015). siRNA versus miRNA as therapeutics for gene silencing. *Molecular Therapy. Nucleic Acids, 4*(9), e252. https://doi.org/10.1038/mtna.2015.23

Lambrou, G. I., Zaravinos, A., & Braoudaki, M. (2021). Co-Deregulated miRNA Signatures in Childhood Central Nervous System Tumors: In Search for Common Tumor miRNA-Related Mechanics. *Cancers, 13*(12), 3028. https://doi.org/10.3390/cancers13123028

Lan, F., Yu, H., Hu, M., Xia, T., & Yue, X. (2015). miR-144-3p exerts anti-tumor effects in glioblastoma by targeting c-Met. *Journal of Neurochemistry, 135*(2), 274-286. https://doi.org/10.1111/jnc.13272

Lan, Z., Li, X., & Zhang, X. (2024). Glioblastoma: An update in pathology, molecular mechanisms and biomarkers. *International Journal of Molecular Sciences, 25*(5), 3040. https://doi.org/10.3390/ijms25053040

Lanza, M., Cuzzocrea, S., Oddo, S., Esposito, E., & Casili, G. (2023). The role of miR-128 in neurodegenerative diseases. *International Journal of Molecular Sciences, 24*(7), 6024. https://doi.org/10.3390/ijms24076024

Lazarev, V. F., Guzhova, I. V., & Margulis, B. A. (2020). Glyceraldehyde-3-phosphate dehydrogenase is a multifaceted therapeutic target. *Pharmaceutics, 12*(5), 416. https://doi.org/10.3390/pharmaceutics12050416

Le, C. T., Nguyen, T. D., & Nguyen, T. A. (2024). Two-motif model illuminates DICER cleavage preferences. *Nucleic Acids Research, 52*(4), 1860–1877. https://doi.org/10.1093/nar/gkad1186

Lee, R. C., Feinbaum, R. L., & Ambros, V. (1993). The C. elegans heterochronic gene lin-4 encodes small RNAs with antisense complementarity to lin-14. *Cell, 75*(5), 843–854. https://doi.org/10.1016/0092-8674(93)90529-y

[a]Lee, S., Jee, D., Srivastava, S., Yang, A., Ramidi, A., Shang, R., Bortolamiol-Becet, D., Pfeffer, S., Gu, S., Wen, J., & Lai, E. C. (2023). Promiscuous splicing-derived hairpins are dominant substrates of tailing-mediated defense of miRNA biogenesis in mammals. *Cell Reports, 42*(2), 112111. https://doi.org/10.1016/j.celrep.2023.112111

[b]Lee, Y. Y., Kim, H., & Kim, V. N. (2023). Sequence determinant of small RNA production by DICER. *Nature, 615*(7951), 323–330. https://doi.org/10.1038/s41586-023-05722-4

[c]Lee, Y. Y., Lee, H., Kim, H., Kim, V. N., & Roh, S. H. (2023). Structure of the human DICER-pre-miRNA complex in a dicing state. *Nature, 615*(7951), 331–338. https://doi.org/10.1038/s41586-023-05723-3

Leon, S. A., Shapiro, B., Sklaroff, D. M., & Yaros, M. J. (1977). Free DNA in the serum of cancer patients and the effect of therapy. *Cancer Research, 37*(3), 646–650.

Lesgards, J. F., Gauthier, C., Iovanna, J., Vidal, N., Dolla, A., & Stocker, P. (2011). Effect of reactive oxygen and carbonyl species on crucial cellular antioxidant enzymes. *Chemico-Biological Interactions, 190*(1), 28–34. https://doi.org/10.1016/j.cbi.2010.12.028

Li, C., Zhu, X., Lee, C. M., Wu, Z., & Cheng, L. (2020). A mouse model of complete-crush transection spinal cord injury made by two operations. *Annals of Translational Medicine, 8*(5), 210. https://doi.org/10.21037/atm.2020.01.58

Li, J., Liang, R., Song, C., Xiang, Y., & Liu, Y. (2018). Prognostic significance of epidermal growth factor receptor expression in glioma patients. *OncoTargets and Therapy, 11*, 731–742. https://doi.org/10.2147/OTT.S155160

Li, J., Xu, Y., Zhu, H., Wang, Y., Li, P., & Wang, D. (2022). The dark side of synaptic proteins in tumours. *British Journal of Cancer*, 127(7), 1184–1192. https://doi.org/10.1038/s41416-022-01863-x

Li, M., Xiao, A., Floyd, D., Olmez, I., Lee, J., Godlewski, J., Bronisz, A., Bhat, K. P. L., Sulman, E. P., Nakano, I., & Purow, B. (2017). CDK4/6 inhibition is more active against the glioblastoma proneural subtype. *Oncotarget, 8*(33), 55319–55331. https://doi.org/10.18632/oncotarget.19429

Li, Q., Shen, K., Zhao, Y., Ma, C., Liu, J., & Ma, J. (2013). MiR-92b inhibitor promoted glioma cell apoptosis via targeting DKK3 and blocking the Wnt/beta-catenin signaling pathway. *Journal of Translational Medicine*, 11, 1-9.

Li, S., Lei, Z., & Sun, T. (2023). The role of microRNAs in neurodegenerative diseases: A review. *Cell Biology and Toxicology, 39*(1), 53–83. https://doi.org/10.1007/s10565-022-09761-x

Li, W. J., Wang, Y., Liu, R., Kasinski, A. L., Shen, H., Slack, F. J., & Tang, D. G. (2021). MicroRNA-34a: Potent tumor suppressor, cancer stem cell inhibitor, and potential anticancer therapeutic. *Frontiers in Cell and Developmental Biology, 9*, 640587. https://doi.org/10.3389/fcell.2021.640587

Li, W., Xu, F., Shuai, W., Sun, H., Yao, H., Ma, C., Xu, S., Yao, H., Zhu, Z., Yang, D. H., Chen, Z. S., & Xu, J. (2019). Discovery of novel quinoline-chalcone derivatives as potent antitumor agents with microtubule polymerization inhibitory activity. *Journal of Medicinal Chemistry, 62*(2), 993–1013. https://doi.org/10.1021/acs.jmedchem.8b01755

Li, X. J., Ren, Z. J., & Tang, J. H. (2014). MicroRNA-34a: A potential therapeutic target in human cancer. *Cell Death & Disease, 5*(7), e1327. https://doi.org/10.1038/cddis.2014.270

Li, X., Sun, S., Zhang, W., Liang, Z., Fang, Y., Sun, T., Wan, Y., Ma, X., Zhang, S., Xu, Y., & Tian, R. (2024). Identification of genetic modifiers enhancing B7-H3-targeting CAR T cell therapy against glioblastoma through large-scale CRISPRi screening. *Journal of Experimental & Clinical Cancer Research, 43*(1), 95. https://doi.org/10.1186/s13046-024-03027-6

Li, Y., Guessous, F., Zhang, Y., Dipierro, C., Kefas, B., Johnson, E., Marcinkiewicz, L., Jiang, J., Yang, Y., Schmittgen, T. D., Lopes, B., Schiff, D., Purow, B., & Abounader, R. (2009). MicroRNA-34a inhibits glioblastoma growth by targeting multiple oncogenes. *Cancer Research, 69*(19), 7569–7576. https://doi.org/10.1158/0008-5472.CAN-09-0529

Li, Y., Tong, Y., Liu, J., & Lou, J. (2022). The Role of MicroRNA in DNA Damage Response. *Frontiers in Genetics*, 13, 850038. https://doi.org/10.3389/fgene.2022.850038

Liang, T., Han, L., & Guo, L. (2020). Rewired functional regulatory networks among miRNA isoforms (isomiRs) from let-7 and miR-10 gene families in cancer. *Computational and Structural Biotechnology Journal, 18*, 1238–1248. https://doi.org/10.1016/j.csbj.2020.05.001

Liao, G. B., Li, X. Z., Zeng, S., Liu, C., Yang, S. M., Yang, L., Hu, C. J., & Bai, J. Y. (2018). Regulation of the master regulator FOXM1 in cancer. *Cell Communication and Signaling: CCS, 16*(1), 57. https://doi.org/10.1186/s12964-018-0266-6

Liao, K., Zhang, X., Liu, J., Teng, F., He, Y., Cheng, J., Yang, Q., Zhang, W., Xie, Y., Guo, D., Cao, G., Xu, Y., Huang, B., & Wang, X. (2023). The role of platelets in the regulation of tumor growth and metastasis: the mechanisms and targeted therapy. *MedComm*, 4(5), e350. https://doi.org/10.1002/mco2.350

Liao, M., & Peng, L. (2020). MiR-206 may suppress non-small lung cancer metastasis by targeting CORO1C. *Cellular & Molecular Biology Letters, 25*, 22. https://doi.org/10.1186/s11658-020-00216-x

Lim, D. H., Kim, S. Y., Na, Y. C., & Cho, J. M. (2023). Navigation guided biopsy is as effective as frame-based stereotactic biopsy. *Journal of Personalized Medicine, 13*(5), 708. https://doi.org/10.3390/jpm13050708

Lin, C., Wang, N., & Xu, C. (2023). Glioma-associated microglia/macrophages (GAMs) in glioblastoma: Immune function in the tumor microenvironment and implications for immunotherapy. *Frontiers in Immunology, 14*, 1123853. https://doi.org/10.3389/fimmu.2023.1123853

Lin, D., Shen, L., Luo, M., Zhang, K., Li, J., Yang, Q., Zhu, F., Zhou, D., Zheng, S., Chen, Y., & Zhou, J. (2021). Circulating tumor cells: biology and clinical significance. *Signal Transduction and Targeted Therapy, 6*(1), 404. https://doi.org/10.1038/s41392-021-00817-8

[a]Liu, F., Shi, Y., Liu, Z., Li, Z., & Xu, W. (2021). The emerging role of miR-10 family in gastric cancer. *Cell Cycle (Georgetown, Tex.), 20*(15), 1468–1476. https://doi.org/10.1080/15384101.2021.1949840

[b]Liu, J., Chen, Y., Pei, F., Zeng, C., Yao, Y., Liao, W., & Zhao, Z. (2021). Extracellular vesicles in liquid biopsies: potential for disease diagnosis. *BioMed Research International, 2021*, 6611244. https://doi.org/10.1155/2021/6611244

Liu, K., Liu, P. C., Liu, R., & Wu, X. (2015). Dual AO/EB staining to detect apoptosis in osteosarcoma cells compared with flow cytometry. *Medical Science Monitor Basic Research, 21*, 15–20. https://doi.org/10.12659/MSMBR.893327

Liu, W., Bai, X., Zhang, A., Huang, J., Xu, S., & Zhang, J. (2019). Role of Exosomes in Central Nervous System Diseases. *Frontiers in Molecular Neuroscience*, 12, 240. https://doi.org/10.3389/fnmol.2019.00240

Liu, W., He, M., Li, Y., Peng, Z., & Wang, G. (2022). A review on synthetic chalcone derivatives as tubulin polymerisation inhibitors. *Journal of Enzyme Inhibition and Medicinal Chemistry, 37*(1), 9–38. https://doi.org/10.1080/14756366.2021.1976772

Liu, Y., Beyer, A., & Aebersold, R. (2016). On the Dependency of Cellular Protein Levels on mRNA Abundance. *Cell, 165*(3), 535–550. https://doi.org/10.1016/j.cell.2016.03.014

Liu, Y., Wang, Z., Tang, Z., Fu, Y., & Wang, L. (2024). mirna-383-5p functions as an anti-oncogene in glioma through the Akt/mTOR signaling pathway by targeting VEGFA. *Current Cancer Drug Targets, 24*(4), 463–475. https://doi.org/10.2174/1568009623666230817102104

Liu, Z., Jiang, Z., Huang, J., Huang, S., Li, Y., Yu, S., Yu, S., & Liu, X. (2014). miR-7 inhibits glioblastoma growth by simultaneously interfering with the PI3K/ATK and Raf/MEK/ERK pathways. *International Journal of Oncology, 44*(5), 1571–1580. https://doi.org/10.3892/ijo.2014.2322

Liu, Z., Lee, P. G., Krez, N., Lam, K. H., Liu, H., Przykopanski, A., Chen, P., Yao, G., Zhang, S., Tremblay, J. M., Perry, K., Shoemaker, C. B., Rummel, A., Dong, M., & Jin, R. (2023). Structural basis for botulinum neurotoxin E recognition of synaptic vesicle protein 2. *Nature Communications, 14*(1), 2338. https://doi.org/10.1038/s41467-023-37860-8

Livermore, L. J., Isabelle, M., Bell, I. M., Edgar, O., Voets, N. L., Stacey, R., Ansorge, O., Vallance, C., & Plaha, P. (2020). Raman spectroscopy to differentiate between fresh tissue samples of glioma and normal brain: A comparison with 5-ALA-induced fluorescence-guided surgery. *Journal of Neurosurgery, 135*(2), 469–479. https://doi.org/10.3171/2020.5.JNS20376

Livermore, L. J., Isabelle, M., Bell, I. M., Scott, C., Walsby-Tickle, J., Gannon, J., Plaha, P., Vallance, C., & Ansorge, O. (2019). Rapid intraoperative molecular genetic classification of gliomas using Raman spectroscopy. *Neuro-Oncology Advances, 1*(1), vdz008. https://doi.org/10.1093/noajnl/vdz008

Lone, S. N., Nisar, S., Masoodi, T., Singh, M., Rizwan, A., Hashem, S., El-Rifai, W., Bedognetti, D., Batra, S. K., Haris, M., Bhat, A. A., & Macha, M. A. (2022). Liquid biopsy: a step closer to transform diagnosis, prognosis and future of cancer treatments. *Molecular Cancer, 21*(1), 79. https://doi.org/10.1186/s12943-022-01543-7

Long, D., Chan, C. Y., & Ding, Y. (2008). Analysis of microRNA-target interactions by a target structure-based hybridization model. *Pacific Symposium on Biocomputing. Pacific Symposium on Biocomputing*, 64–74.

Long, H., Liang, C., Zhang, X., Fang, L., Wang, G., Qi, S., Huo, H., & Song, Y. (2017). Prediction and analysis of key genes in glioblastoma based on bioinformatics. *BioMed Research International, 2017*, 7653101. https://doi.org/10.1155/2017/7653101

Losada-Pérez, M., Hernández García-Moreno, M., García-Ricote, I., & Casas-Tintó, S. (2022). Synaptic components are required for glioblastoma progression in Drosophila. *PLoS Genetics, 18*(7), e1010329. https://doi.org/10.1371/journal.pgen.1010329

Louis, D. N., Ohgaki, H., Wiestler, O. D., Cavenee, W. K., Burger, P. C., Jouvet, A., Scheithauer, B. W., & Kleihues, P. (2007). The 2007 WHO classification of tumours of the central nervous system. *Acta Neuropathologica, 114*(2), 97–109. https://doi.org/10.1007/s00401-007-0243-4

Louis, D. N., Perry, A., Reifenberger, G., von Deimling, A., Figarella-Branger, D., Cavenee, W. K., Ohgaki, H., Wiestler, O. D., Kleihues, P., & Ellison, D. W. (2016). The 2016 World Health Organization Classification of Tumors of the Central Nervous System: a summary. *Acta Neuropathologica, 131*(6), 803–820. https://doi.org/10.1007/s00401-016-1545-1

Louis, D. N., Perry, A., Wesseling, P., Brat, D. J., Cree, I. A., Figarella-Branger, D., Hawkins, C., Ng, H. K., Pfister, S. M., Reifenberger, G., Soffietti, R., von Deimling, A., & Ellison, D. W. (2021). The 2021 WHO classification of tumors of the central nervous system: A summary. *Neuro-Oncology, 23*(8), 1231–1251. https://doi.org/10.1093/neuonc/noab106

Lu, T. P., Lee, C. Y., Tsai, M. H., Chiu, Y. C., Hsiao, C. K., Lai, L. C., & Chuang, E. Y. (2012). miRSystem: An integrated system for characterizing enriched functions and pathways of microRNA targets. *PLoS ONE*, *7*(8), e42390. https://doi.org/10.1371/journal.pone.0042390

Luan, S. L., Boulanger, E., Ye, H., Chanudet, E., Johnson, N., Hamoudi, R. A., Bacon, C. M., Liu, H., Huang, Y., Said, J., Chu, P., Clemen, C. S., Cesarman, E., Chadburn, A., Isaacson, P. G., & Du, M. Q. (2010). Primary effusion lymphoma: genomic profiling revealed amplification of SELPLG and CORO1C encoding for proteins important for cell migration. *The Journal of Pathology, 222*(2), 166–179. https://doi.org/10.1002/path.2752

Luksik, A. S., Yazigi, E., Shah, P., & Jackson, C. M. (2023). CAR T cell therapy in glioblastoma: Overcoming challenges related to antigen expression. *Cancers, 15*(5), 1414. https://doi.org/10.3390/cancers15051414

Luo, X., Lu, W., Zhao, J., Hu, J., Chen, E., Fu, S., & Fu, Q. (2022). Identification of the TF-miRNA-mRNA co-regulatory networks involved in sepsis. *Functional & Integrative Genomics, 22*(4), 481-489. https://doi.org/10.1007/s10142-022-00843-x

Luo, Y., Na, Z., & Slavoff, S. A. (2018). P-Bodies: Composition, properties, and functions. *Biochemistry, 57*(17), 2424–2431. https://doi.org/10.1021/acs.biochem.7b01162

Ma, R., de Pennington, N., Hofer, M., Blesing, C., & Stacey, R. (2013). Diagnostic and prognostic markers in gliomas—An update. *British Journal of Neurosurgery, 27*(3), 311–315. https://doi.org/10.3109/02688697.2012.752432

Ma, R., Yan, W., Zhang, G., Lv, H., Liu, Z., Fang, F., ... & Kang, X. (2012). Upregulation of miR-196b confers a poor prognosis in glioblastoma patients via inducing a proliferative phenotype. *PloS One*, 7(6), e38096.

Ma, S., Fu, T., Zhao, S., & Gao, M. (2019). MicroRNA-34a-5p suppresses tumorigenesis and progression of glioma and potentiates temozolomide-induced cytotoxicity for glioma cells by targeting HMGA2. *European Journal of Pharmacology, 852*, 42–50. https://doi.org/10.1016/j.ejphar.2019.03.005

MacDonald, B. T., Tamai, K., & He, X. (2009). Wnt/beta-catenin signaling: Components, mechanisms, and diseases. *Developmental Cell, 17*(1), 9–26. https://doi.org/10.1016/j.devcel.2009.06.016

Magaña, S. M., Peterson, T. E., Evans, J. E., Decker, P. A., Simon, V., Eckel-Passow, J. E., Daniels, D. J., & Parney, I. F. (2022). Pediatric brain tumor cell lines exhibit miRNA-depleted, Y RNA-enriched extracellular vesicles. *Journal of Neuro-Oncology, 156*(2), 269–279. https://doi.org/10.1007/s11060-021-03914-4

Mahon, B. P., Pinard, M. A., & McKenna, R. (2015). Targeting carbonic anhydrase IX activity and expression. *Molecules, 20*(2), 2323-2348.

Mak, K. S., Agarwal, A., Qureshi, M. M., & Truong, M. T. (2017). Hypofractionated short-course radiotherapy in elderly patients with glioblastoma multiforme: An analysis of the National Cancer Database. *Cancer Medicine, 6*(6), 1192–1200. https://doi.org/10.1002/cam4.1070

Makowska, M., Smolarz, B., & Romanowicz, H. (2023). microRNAs (miRNAs) in glioblastoma multiforme (GBM)—Recent literature review. *International Journal of Molecular Sciences, 24*(4), 3521. https://doi.org/10.3390/ijms24043521

Malhotra, S., Miras, M. C. M., Pappolla, A., Montalban, X., & Comabella, M. (2023). Liquid biopsy in neurological diseases. *Cells, 12*(14), 1911. https://doi.org/10.3390/cells12141911

Malzkorn, B., Wolter, M., Liesenberg, F., Grzendowski, M., Stühler, K., Meyer, H. E., & Reifenberger, G. (2010). Identification and functional characterization of microRNAs involved in the malignant progression of gliomas. *Brain Pathology, 20*(3), 539–550. https://doi.org/10.1111/j.1750-3639.2009.00328.x

Mansouri, A., Hachem, L. D., Mansouri, S., Nassiri, F., Laperriere, N. J., Xia, D., Lindeman, N. I., Wen, P. Y., Chakravarti, A., Mehta, M. P., Hegi, M. E., Stupp, R., Aldape, K. D., & Zadeh, G. (2019). MGMT promoter methylation status testing to guide therapy for glioblastoma: Refining the approach based on emerging evidence and current challenges. *Neuro-Oncology, 21*(2), 167–178. https://doi.org/10.1093/neuonc/noy132

Margulies, M., Egholm, M., Altman, W. E., Attiya, S., Bader, J. S., Bemben, L. A., Berka, J., Braverman, M. S., Chen, Y. J., Chen, Z., Dewell, S. B., Du, L., Fierro, J. M., Gomes, X. V., Godwin, B. C., He, W., Helgesen, S., Ho, C. H., Irzyk, G. P., Jando, S. C., … Rothberg, J. M. (2005). Genome sequencing in microfabricated high-density picolitre reactors. *Nature, 437*(7057), 376–380. https://doi.org/10.1038/nature03959

Marino, S., Menna, G., Di Bonaventura, R., Lisi, L., Mattogno, P., Figà, F., Bilgin, L., D'Alessandris, Q. G., Olivi, A., & Della Pepa, G. M. (2023). The extracellular matrix in glioblastomas: A glance at its structural modifications in shaping the tumoral microenvironment—A systematic review. *Cancers, 15*(6), 1879. https://doi.org/10.3390/cancers15061879

Maronpot, R. R. (2015). Toxicological assessment of Ashitaba chalcone. *Food and Chemical Toxicology, 77*, 111–119. https://doi.org/10.1016/j.fct.2014.12.021

Martins, F., van der Kellen, D., Gonçalves, L. G., & Serpa, J. (2023). Metabolic profiles point out metabolic pathways pivotal in two glioblastoma (GBM) cell lines, U251 and U-87MG. *Biomedicines, 11*(7), 2041. https://doi.org/10.3390/biomedicines11072041

Martorella, M., Barford, K., Winkler, B., & Deppmann, C. D. (2017). Emergent role of Coronin-1a in neuronal signaling. *Vitamins and Hormones, 104*, 113–131. https://doi.org/10.1016/bs.vh.2016.10.002

Martucci, M., Russo, R., Giordano, C., Schiarelli, C., D'Apolito, G., Tuzza, L., Lisi, F., Ferrara, G., Schimperna, F., Vassalli, S., Calandrelli, R., & Gaudino, S. (2023). Advanced magnetic resonance imaging in the evaluation of treated glioblastoma: A pictorial essay. *Cancers, 15*(15), 3790. https://doi.org/10.3390/cancers15153790

Martuza, R. L., Malick, A., Markert, J. M., Ruffner, K. L., & Coen, D. M. (1991). Experimental therapy of human glioma by means of a genetically engineered virus mutant. *Science, 252*(5007), 854–856. https://doi.org/10.1126/science.1851332

Marusyk, A., & Polyak, K. (2010). Tumor heterogeneity: Causes and consequences. *Biochimica et Biophysica Acta, 1805*(1), 105–117. https://doi.org/10.1016/j.bbcan.2009.11.002

Masui, K., Onizuka, H., Cavenee, W. K., Mischel, P. S., & Shibata, N. (2019). Metabolic reprogramming in the pathogenesis of glioma: Update. *Neuropathology: Official Journal of the Japanese Society of Neuropathology, 39*(1), 3–13. https://doi.org/10.1111/neup.12535

McKinnon, C., Nandhabalan, M., Murray, S. A., & Plaha, P. (2021). Glioblastoma: Clinical presentation, diagnosis, and management. *BMJ, 374*.

Medley, J. C., Panzade, G., & Zinovyeva, A. Y. (2021). microRNA strand selection: Unwinding the rules. *Wiley Interdisciplinary Reviews. RNA, 12*(3), e1627. https://doi.org/10.1002/wrna.1627

Mendanha, D., Vieira de Castro, J., Moreira, J., Costa, B. M., Cidade, H., Pinto, M., Ferreira, H., & Neves, N. M. (2021). A new chalcone derivative with promising antiproliferative and anti-invasion activities in glioblastoma cells. *Molecules, 26*(11), 3383. https://doi.org/10.3390/molecules26113383

Mendiola-Soto, D. K., Bárcenas-López, D. A., Pérez-Amado, C. J., Cruz-Miranda, G. M., Mejía-Aranguré, J. M., Ramírez-Bello, J., Hidalgo-Miranda, A., & Jiménez-Morales, S. (2023). MiRNAs in hematopoiesis and acute lymphoblastic leukemia. *International Journal of Molecular Sciences, 24*(6), 5436. https://doi.org/10.3390/ijms24065436

Merve Aydin, E., Canıtez, İ. S., Colombo, E., Princiotto, S., Passarella, D., Dallavalle, S., Christodoulou, M. S., & Durmaz Şahin, I. (2023). Targeting ovarian cancer with chalcone derivatives: Cytotoxicity and apoptosis induction in HGSOC cells. *Molecules, 28*(23), 7777. https://doi.org/10.3390/molecules28237777

Mesfin, F. B., & Al-Dhahir, M. A. (2023). Gliomas. In *StatPearls*. StatPearls Publishing.
Mezzacappa, F. M., & Thorell, W. (2022). Neuronal brain tumors. In *StatPearls*. StatPearls Publishing. https://www.ncbi.nlm.nih.gov/books/NBK576406/

Michaeli, O., & Tabori, U. (2018). Pediatric high grade gliomas in the context of cancer predisposition syndromes. *Journal of Korean Neurosurgical Society, 61*(3), 319–332. https://doi.org/10.3340/jkns.2018.0031

Michalkova, R., Mirossay, L., Gazdova, M., Kello, M., & Mojzis, J. (2021). Molecular mechanisms of antiproliferative effects of natural chalcones. *Cancers, 13*(11), 2730. https://doi.org/10.3390/cancers13112730

Michalkova, R., Mirossay, L., Kello, M., Mojzisova, G., Baloghova, J., Podracka, A., & Mojzis, J. (2023). Anticancer potential of natural chalcones: In vitro and in vivo evidence. *International Journal of Molecular Sciences, 24*(12), 10354. https://doi.org/10.3390/ijms241210354

Michl, M., Taverna, F., Woischke, C., Li, P., Klauschen, F., Kirchner, T., Heinemann, V., von Bergwelt-Baildon, M., Stahler, A., Herold, T. M., Jurinovic, V., Engel, J., Kumbrink, J., & Neumann, J. (2024). Identification of a gene expression signature associated with brain metastasis in colorectal cancer. *Clinical & Translational Oncology, 26*(8), 1886–1895. https://doi.org/10.1007/s12094-024-03408-5

Microenvironment and Invasiveness: New Insights and Therapeutic Targets. (2023). *International Journal of Molecular Sciences, 24*(8), 7047. https://doi.org/10.3390/ijms24087047

Miguel, V., Cui, J. Y., Daimiel, L., Espinosa-Díez, C., Fernández-Hernando, C., Kavanagh, T. J., & Lamas, S. (2018). The role of microRNAs in environmental risk factors, noise-induced hearing loss, and mental stress. *Antioxidants & Redox Signaling, 28*(9), 773–796. https://doi.org/10.1089/ars.2017.7175

Mirabelli, P., Coppola, L., & Salvatore, M. (2019). Cancer cell lines are useful model systems for medical research. *Cancers, 11*(8), 1098. https://doi.org/10.3390/cancers11081098

Modi, P. K., Jaiswal, S., & Sharma, P. (2015). Regulation of Neuronal Cell Cycle and Apoptosis by MicroRNA 34a. *Molecular and Cellular Biology, 36*(1), 84–94. https://doi.org/10.1128/MCB.00589-15

Mohammed, S., Dinesan, M., & Ajayakumar, T. (2022). Survival and quality of life analysis in glioblastoma multiforme with adjuvant chemoradiotherapy: A retrospective study. *Reports of Practical Oncology and Radiotherapy, 27*(6), 1026–1036. https://doi.org/10.5603/RPOR.a2022.0113

Molinaro, A. M., Hervey-Jumper, S., Morshed, R. A., Young, J., Han, S. J., Chunduru, P., Zhang, Y., Phillips, J. J., Shai, A., Lafontaine, M., Crane, J., Chandra, A., Flanigan, P., Jahangiri, A., Cioffi, G., Ostrom, Q., Anderson, J. E., Badve, C., Barnholtz-Sloan, J., Sloan, A. E., … Berger, M. S. (2020). Association of maximal extent of resection of contrast-enhanced and non-contrast-enhanced tumor with survival within molecular subgroups of patients with newly diagnosed glioblastoma. *JAMA Oncology, 6*(4), 495–503. https://doi.org/10.1001/jamaoncol.2019.6143

Molinaro, A. M., Taylor, J. W., Wiencke, J. K., & Wrensch, M. R. (2019). Genetic and molecular epidemiology of adult diffuse glioma. *Nature Reviews Neurology, 15*(7), 405–417. https://doi.org/10.1038/s41582-019-0220-2

Molinie, N., Rubtsova, S. N., Fokin, A., Visweshwaran, S. P., Rocques, N., Polesskaya, A., Schnitzler, A., Vacher, S., Denisov, E. V., Tashireva, L. A., Perelmuter, V. M., Cherdyntseva, N. V., Bièche, I., & Gautreau, A. M. (2019). Cortical branched actin determines cell cycle progression. *Cell Research, 29*(6), 432–445. https://doi.org/10.1038/s41422-019-0160-9

Mollashahi, B., Aghamaleki, F. S., & Movafagh, A. (2019). The Roles of miRNAs in Medulloblastoma: A Systematic Review. *Journal of Cancer Prevention, 24*(2), 79–90. https://doi.org/10.15430/JCP.2019.24.2.79

Mollinari, C., Racaniello, M., Berry, A., Pieri, M., de Stefano, M. C., Cardinale, A., Zona, C., Cirulli, F., Garaci, E., & Merlo, D. (2015). miR-34a regulates cell proliferation, morphology and function of newborn neurons resulting in improved behavioural outcomes. *Cell Death & Disease, 6*(1), e1622. https://doi.org/10.1038/cddis.2014.589

Monneret, C. (2005). Histone deacetylase inhibitors. *European Journal of Medicinal Chemistry, 40*(1), 1-13.

Monteiro-Reis, S., Carvalho-Maia, C., Bart, G., Vainio, S. J., Pedro, J., Silva, E. R., Sales, G., Henrique, R., & Jerónimo, C. (2021). Secreted extracellular vesicle molecular cargo as a novel liquid biopsy diagnostics of central nervous system diseases. *International Journal of Molecular Sciences, 22*(6), 3267. https://doi.org/10.3390/ijms22063267

Morgan, M. J., & Kim, Y. S. (2022). Roles of RIPK3 in necroptosis, cell signaling, and disease. *Experimental & Molecular Medicine, 54*(10), 1695–1704. https://doi.org/10.1038/s12276-022-00868-z

Morgans, C. W., Kensel-Hammes, P., Hurley, J. B., Burton, K., Idzerda, R., McKnight, G. S., & Bajjalieh, S. M. (2009). Loss of the synaptic vesicle protein SV2B results in reduced neurotransmission and altered synaptic vesicle protein expression in the retina. *PLoS One, 4*(4), e5230. https://doi.org/10.1371/journal.pone.0005230

Motaln, H., Koren, A., Gruden, K., Ramšak, Ž., Schichor, C., & Lah, T. T. (2015). Heterogeneous glioblastoma cell cross-talk promotes phenotype alterations and enhanced drug resistance. *Oncotarget, 6*(38), 40998–41017. https://doi.org/10.18632/oncotarget.5701

Muciño-Olmos, E. A., Vázquez-Jiménez, A., López-Esparza, D. E., Maldonado, V., Valverde, M., & Resendis-Antonio, O. (2020). MicroRNAs regulate metabolic phenotypes during multicellular tumor spheroids progression. *Frontiers in Oncology, 10*, 582396. https://doi.org/10.3389/fonc.2020.582396

[a]Mustafov, D., Ahmad, M. S., Serrano, A., Braoudaki, M., & Siddiqui, S. S. (2024). MicroRNA:Siglec crosstalk in cancer progression. *Current opinion in chemical biology*, *81*, 102502. https://doi.org/10.1016/j.cbpa.2024.102502

Mustafov, D., Karteris, E., & Braoudaki, M. (2023). Deciphering the role of microRNA mediated regulation of Coronin 1C in glioblastoma development and metastasis. *Non-coding RNA, 9*(1), 4. https://doi.org/10.3390/ncrna9010004

[b]Mustafov, D., Lambrou, G. I., Siddiqui, S. S., & Braoudaki, M. (2024). New kinder miRNA-based therapies shared between medulloblastoma and glioblastoma. *In press*.

[c]Mustafov, D., Siddiqui, S. S., Klena, L., Karteris, E., & Braoudaki, M. (2024). SV2B/miR-34a/miR-128 axis as prognostic biomarker in glioblastoma multiforme. *Scientific Reports, 14*(1), 6647. https://doi.org/10.1038/s41598-024-55917-6

[d]Mustafov, D., Siddiqui, S. S., Kukol, A., Lambrou, G. I., Shagufta, Ahmad, I., & Braoudaki, M. (2024). MicroRNA-dependent mechanisms underlying the function of a β-amino carbonyl compound in glioblastoma cells. *ACS Omega, 9*(29), 31789–31802. https://doi.org/10.1021/acsomega.4c02991

[e]Mustafov, D., Siddiqui, S. S., Shagufta, Ahmad, I., Gkantalis, J., Rodriguez, P., & Braoudaki, M. (2024). New chalcone compound exhibits microRNA-mediated anticancer properties in glioblastoma. *In press.*

Nail, H. M., Chiu, C. C., Leung, C. H., Ahmed, M. M. M., & Wang, H. D. (2023). Exosomal miRNA-mediated intercellular communications and immunomodulatory effects in tumor microenvironments. *Journal of Biomedical Science*, 30(1), 69. https://doi.org/10.1186/s12929-023-00964-w

Nakagawa, M., Nakatani, F., Matsunaga, H. et al. (2019). Selective inhibition of mutant IDH1 by DS-1001b ameliorates aberrant histone modifications and impairs tumor activity in chondrosarcoma. *Oncogene, 38*, 6835–6849. https://doi.org/10.1038/s41388-019-0929-9

Nakamura, H., & Takada, K. (2021). Reactive oxygen species in cancer: Current findings and future directions. *Cancer Science, 112*(10), 3945–3952. https://doi.org/10.1111/cas.15068

Nakanishi, K. (2022). Anatomy of four human Argonaute proteins. *Nucleic Acids Research, 50*(12), 6618–6638. https://doi.org/10.1093/nar/gkac519

Navarro, F., & Lieberman, J. (2015). miR-34 and p53: New insights into a complex functional relationship. *PLOS ONE, 10*(7), e0132767. https://doi.org/10.1371/journal.pone.0132767

Neftel, C., Laffy, J., Filbin, M. G., Hara, T., Shore, M. E., Rahme, G. J., Richman, A. R., Silverbush, D., Shaw, M. L., Hebert, C. M., Dewitt, J., Gritsch, S., Perez, E. M., Gonzalez Castro, L. N., Lan, X., Druck, N., Rodman, C., Dionne, D., Kaplan, A., Bertalan, M. S., … Suvà, M. L. (2019). An integrative model of cellular states, plasticity, and genetics for glioblastoma. *Cell, 178*(4), 835–849.e21. https://doi.org/10.1016/j.cell.2019.06.024

Neophytou, C. M., Trougakos, I. P., Erin, N., & Papageorgis, P. (2021). Apoptosis deregulation and the development of cancer multi-drug resistance. *Cancers, 13*(17), 4363. https://doi.org/10.3390/cancers13174363

Nguyen, H. M., Nguyen, T. D., Nguyen, T. L., & Nguyen, T. A. (2019). Orientation of human microprocessor on primary microRNAs. *Biochemistry, 58*(4), 189–198. https://doi.org/10.1021/acs.biochem.8b00944

Nguyen, T. A., Park, J., Dang, T. L., Choi, Y. G., & Kim, V. N. (2018). Microprocessor depends on hemin to recognize the apical loop of primary microRNA. *Nucleic Acids Research, 46*(11), 5726–5736. https://doi.org/10.1093/nar/gky248

Nguyen, T. D., Trinh, T. A., Bao, S., & Nguyen, T. A. (2022). Secondary structure RNA elements control the cleavage activity of DICER. *Nature Communications, 13*(1), 2138. https://doi.org/10.1038/s41467-022-29822-3

Nguyen, T. L., Nguyen, T. D., & Nguyen, T. A. (2021). The conserved single-cleavage mechanism of animal DROSHA enzymes. *Communications Biology, 4*(1), 1332. https://doi.org/10.1038/s42003-021-02860-1

NHS England. (2023, September 6). Urgent GP direct access to diagnostic services for people with symptoms not meeting the threshold for an urgent suspected cancer referral. *NHS*. https://www.england.nhs.uk/long-read/urgent-gp-direct-access-to-diagnostic-services-for-people-with-symptoms-not-meeting-the-threshold-for-an-urgent-suspected-cancer-referral/

NHS England. (2024). NHS to roll out first targeted treatment for rare childhood brain tumours. *NHS*. Accessed: 15th July 2024, from https://www.england.nhs.uk/2024/04/nhs-to-roll-out-first-targeted-treatment-for-rare-childhood-brain-tumours/

NHS Scotland. (2024). Brain and central nervous system cancers. *Cancer Referral*. Accessed: 29th July 2024, from https://www.cancerreferral.scot.nhs.uk/brain-and-central-nervous-system-cancers/

Nie, Q. M., Lin, Y. Y., Yang, X., Shen, L., Guo, L. M., Que, S. L., Li, X. X., Ge, J. W., Wang, G. S., Xiong, W. H., Guo, P., & Qiu, Y. M. (2015). IDH1R^{132}H decreases the proliferation of U87 glioma cells through upregulation of microRNA-128a. *Molecular Medicine Reports, 12*(5), 6695–6701. https://doi.org/10.3892/mmr.2015.4241

Nikolova, E., Laleva, L., Milev, M., Spiriev, T., Stoyanov, S., Ferdinandov, D., Mitev, V., & Todorova, A. (2023). miRNAs and related genetic biomarkers according to the WHO glioma classification: From diagnosis to future therapeutic targets. *Non-coding RNA Research, 9*(1), 141–152. https://doi.org/10.1016/j.ncrna.2023.10.003

Novakova, J., Slaby, O., Vyzula, R., & Michalek, J. (2009). MicroRNA involvement in glioblastoma pathogenesis. *Biochemical and Biophysical Research Communications, 386*(1), 1–5. https://doi.org/10.1016/j.bbrc.2009.06.034

Nowack, A., Yao, J., Custer, K. L., & Bajjalieh, S. M. (2010). SV2 regulates neurotransmitter release via multiple mechanisms. *American Journal of Physiology. Cell Physiology, 299*(5), C960–C967. https://doi.org/10.1152/ajpcell.00259.2010

O'Brien, E. R., Howarth, C., & Sibson, N. R. (2013). The role of astrocytes in CNS tumors: Pre-clinical models and novel imaging approaches. *Frontiers in Cellular Neuroscience, 7*, 40. https://doi.org/10.3389/fncel.2013.00040

O'Brien, J., Hayder, H., Zayed, Y., & Peng, C. (2018). Overview of MicroRNA Biogenesis, Mechanisms of Actions, and Circulation. *Frontiers in Endocrinology*, 9, 402. https://doi.org/10.3389/fendo.2018.00402

Oliveros, J. C. (2007-2015). Venny. An interactive tool for comparing lists with Venn's diagrams. https://bioinfogp.cnb.csic.es/tools/venny/index.html

Olivier, C., Oliver, L., Lalier, L., & Vallette, F. M. (2021). Drug resistance in glioblastoma: The two faces of oxidative stress. *Frontiers in Molecular Biosciences, 7*, 620677. https://doi.org/10.3389/fmolb.2020.620677

Ontario Health (Quality). (2020). 5-Aminolevulinic acid hydrochloride (5-ALA)-guided surgical resection of high-grade gliomas: A health technology assessment. *Ontario Health Technology Assessment Series, 20*(9), 1–92. PMCID: PMC7077938.

Ordóñez-Rubiano, E. G., Rincón-Arias, N., Espinosa, S., Shelton, W. J., Salazar, A. F., Cómbita, A., Baldoncini, M., Luzzi, S., Payán-Gómez, C., Gómez-Amarillo, D. F., Hakim, F., Patiño-Gómez, J. G., & Parra-Medina, R. (2024). The potential of miRNA-based approaches in glioblastoma: An update in current advances and future perspectives. *Current Research in Pharmacology and Drug Discovery, 7*, 100193. https://doi.org/10.1016/j.crphar.2024.100193

Ørom, U. A., Nielsen, F. C., & Lund, A. H. (2008). MicroRNA-10a binds the 5'UTR of ribosomal protein mRNAs and enhances their translation. *Molecular Cell, 30*(4), 460–471. https://doi.org/10.1016/j.molcel.2008.05.001

Oronsky, B., Reid, T. R., Oronsky, A., Sandhu, N., & Knox, S. J. (2021). A review of newly diagnosed glioblastoma. *Frontiers in Oncology, 10*, 574012. https://doi.org/10.3389/fonc.2020.574012

Ortiz, R., Perazzoli, G., Cabeza, L., Jiménez-Luna, C., Luque, R., Prados, J., & Melguizo, C. (2021). Temozolomide: An updated overview of resistance mechanisms, nanotechnology advances and clinical applications. *Current Neuropharmacology, 19*(4), 513–537. https://doi.org/10.2174/1570159X18666200626204005

[a]Ostrom, Q. T., Bauchet, L., Davis, F. G., Deltour, I., Fisher, J. L., Langer, C. E., Pekmezci, M., Schwartzbaum, J. A., Turner, M. C., Walsh, K. M., Wrensch, M. R., & Barnholtz-Sloan, J. S. (2014). The epidemiology of glioma in adults: A "state of the science" review. *Neuro-Oncology, 16*(7), 896–913. https://doi.org/10.1093/neuonc/nou087

Ostrom, Q. T., Cioffi, G., Waite, K., Kruchko, C., & Barnholtz-Sloan, J. S. (2021). CBTRUS statistical report: Primary brain and other central nervous system tumors diagnosed in the United States in 2014-2018. *Neuro-Oncology, 23*(12 Suppl 2), iii1–iii105. https://doi.org/10.1093/neuonc/noab200

Ostrom, Q. T., Gittleman, H., Fulop, J., Liu, M., Blanda, R., Kromer, C., Wolinsky, Y., Kruchko, C., & Barnholtz-Sloan, J. S. (2015). CBTRUS Statistical Report: Primary brain and central nervous system tumors diagnosed in the United States in 2008-2012. *Neuro-Oncology, 17*(Suppl 4), iv1–iv62. https://doi.org/10.1093/neuonc/nov189

[b]Ostrom, Q. T., Gittleman, H., Liao, P., Rouse, C., Chen, Y., Dowling, J., Wolinsky, Y., Kruchko, C., & Barnholtz-Sloan, J. (2014). CBTRUS statistical report: Primary brain and central nervous system tumors diagnosed in the United States in 2007-2011. *Neuro-Oncology, 16*(Suppl 4), iv1–iv63. https://doi.org/10.1093/neuonc/nou223

Ouyang, Y., Li, J., Chen, X., Fu, X., Sun, S., & Wu, Q. (2021). Chalcone derivatives: Role in anticancer therapy. *Biomolecules, 11*(6), 894. https://doi.org/10.3390/biom11060894

Ozair, A., Bhat, V., Alisch, R. S., Khosla, A. A., Kotecha, R. R., Odia, Y., McDermott, M. W., & Ahluwalia, M. S. (2023). DNA methylation and histone modification in low-grade gliomas: Current understanding and potential clinical targets. *Cancers, 15*(4), 1342. https://doi.org/10.3390/cancers15041342

Ozawa, M., Brennan, P. M., Zienius, K., Kurian, K. M., Hollingworth, W., Weller, D., Grant, R., Hamilton, W., & Ben-Shlomo, Y. (2019). The usefulness of symptoms alone or combined for general practitioners in considering the diagnosis of a brain tumour: A case-control study using the clinical practice research database (CPRD) (2000-2014). *BMJ Open, 9*(8), e029686. https://doi.org/10.1136/bmjopen-2019-029686

Paech, D., Windschuh, J., Oberhollenzer, J., Dreher, C., Sahm, F., Meissner, J. E., Goerke, S., Schuenke, P., Zaiss, M., Regnery, S., Bickelhaupt, S., Bäumer, P., Bendszus, M., Wick, W., Unterberg, A., Bachert, P., Ladd, M. E., Schlemmer, H. P., & Radbruch, A. (2018). Assessing the predictability of IDH mutation and MGMT methylation status in glioma patients using relaxation-compensated multipool CEST MRI at 7.0 T. *Neuro-Oncology, 20*(12), 1661–1671. https://doi.org/10.1093/neuonc/noy073

Pagès, M., Rotem, D., Gydush, G., Reed, S., Rhoades, J., Ha, G., Lo, C., Fleharty, M., Duran, M., Jones, R., Becker, S., Haller, M., Sinai, C. E., Goumnerova, L., Golub, T. R., Love, J. C., Ligon, K. L., Wright, K. D., Adalsteinsson, V. A., Beroukhim, R., … Bandopadhayay, P. (2022). Liquid biopsy detection of genomic alterations in pediatric brain tumors from cell-free DNA in peripheral blood, CSF, and urine. *Neuro-Oncology, 24*(8), 1352–1363. https://doi.org/10.1093/neuonc/noab299

Painter, J. T., Clayton, N. P., & Herbert, R. A. (2010). Useful immunohistochemical markers of tumor differentiation. *Toxicologic Pathology, 38*(1), 131–141. https://doi.org/10.1177/0192623309356449

Pan, J., Sheng, S., Ye, L., Xu, X., Ma, Y., Feng, X., Qiu, L., Fan, Z., Wang, Y., Xia, X., & Zheng, J. C. (2022). Extracellular vesicles derived from glioblastoma promote proliferation and migration of neural progenitor cells via PI3K-Akt pathway. *Cell Communication and Signaling: CCS, 20*(1), 7. https://doi.org/10.1186/s12964-021-00760-9

Pan, X., Wang, Z., Wan, B., & Zheng, Z. (2017). MicroRNA-206 inhibits the viability and migration of medulloblastoma cells by targeting LIM and SH3 protein 1. *Experimental and Therapeutic Medicine, 14*(4), 3894–3900. https://doi.org/10.3892/etm.2017.5016

Panwalkar, P., Moiyadi, A., Goel, A., Shetty, P., Goel, N., Sridhar, E., & Shirsat, N. (2015). MiR-206, a cerebellum enriched miRNA, is downregulated in all medulloblastoma subgroups, and its overexpression is necessary for growth inhibition of medulloblastoma cells. *Journal of Molecular Neuroscience : MN, 56*(3), 673–680. https://doi.org/10.1007/s12031-015-0548-z

Park, J. E., Heo, I., Tian, Y., Simanshu, D. K., Chang, H., Jee, D., Patel, D. J., & Kim, V. N. (2011). Dicer recognizes the 5' end of RNA for efficient and accurate processing. *Nature, 475*(7355), 201–205. https://doi.org/10.1038/nature10198

Parker, A. L., Kavallaris, M., & McCarroll, J. A. (2014). Microtubules and their role in cellular stress in cancer. *Frontiers in Oncology*, 4, 153. https://doi.org/10.3389/fonc.2014.00153

Parker, N. R., Correia, N., Crossley, B., Buckland, M. E., Howell, V. M., & Wheeler, H. R. (2013). Correlation of microRNA 132 up-regulation with an unfavorable clinical outcome in patients with primary glioblastoma multiforme treated with radiotherapy plus concomitant and adjuvant temozolomide chemotherapy. *Translational Oncology, 6*(6), 742–748. https://doi.org/10.1593/tlo.13553

Parsons, D. W., Jones, S., Zhang, X., Lin, J. C., Leary, R. J., Angenendt, P., Mankoo, P., Carter, H., Siu, I. M., Gallia, G. L., Olivi, A., McLendon, R., Rasheed, B. A., Keir, S., Nikolskaya, T., Nikolsky, Y., Busam, D. A., Tekleab, H., Diaz, L. A., Jr, Hartigan, J., … Kinzler, K. W. (2008). An integrated genomic analysis of human glioblastoma multiforme. *Science, 321*(5897), 1807–1812. https://doi.org/10.1126/science.1164382

Patel, A., Patel, S., Patel, P., & Tanavde, V. (2022). Saliva based liquid biopsies in head and neck cancer: How far are we from the clinic? *Frontiers in Oncology, 12*, 828434. https://doi.org/10.3389/fonc.2022.828434

Paulsen, C. E., & Carroll, K. S. (2013). Cysteine-mediated redox signaling: Chemistry, biology, and tools for discovery. *Chemical Reviews, 113*(7), 4633–4679. https://doi.org/10.1021/cr300163e

Pavanello, L., Hall, M., & Winkler, G. S. (2023). Regulation of eukaryotic mRNA deadenylation and degradation by the Ccr4-Not complex. *Frontiers in Cell and Developmental Biology, 11*, 1153624. https://doi.org/10.3389/fcell.2023.1153624

Pazarlar, B. A., Aripaka, S. S., Petukhov, V., Pinborg, L., Khodosevich, K., & Mikkelsen, J. D. (2022). Expression profile of synaptic vesicle glycoprotein 2A, B, and C paralogues in temporal neocortex tissue from patients with temporal lobe epilepsy (TLE). *Molecular Brain*, 15(1), 45. https://doi.org/10.1186/s13041-022-00931-w

Pei, Z., Lee, K. C., Khan, A., Erisnor, G., & Wang, H. Y. (2020). Pathway analysis of glutamate-mediated, calcium-related signaling in glioma progression. *Biochemical Pharmacology*, 176, 113814. https://doi.org/10.1016/j.bcp.2020.113814

Penfold, C., Joannides, A. J., Bell, J., & Walter, F. M. (2017). Diagnosing adult primary brain tumours: Can we do better? *The British Journal of General Practice, 67*(659), 278–279. https://doi.org/10.3399/bjgp17X691277

Perry, J. R., Bélanger, K., Mason, W. P., Fulton, D., Kavan, P., Easaw, J., Shields, C., Kirby, S., Macdonald, D. R., Eisenstat, D. D., Thiessen, B., Forsyth, P., & Pouliot, J. F. (2010). Phase II trial of continuous dose-intense temozolomide in recurrent malignant glioma: RESCUE study. *Journal of Clinical Oncology, 28*(12), 2051–2057. https://doi.org/10.1200/JCO.2009.26.5520

Perry, J. R., Laperriere, N., O'Callaghan, C. J., Brandes, A. A., Menten, J., Phillips, C., Fay, M., Nishikawa, R., Cairncross, J. G., Roa, W., Osoba, D., Rossiter, J. P., Sahgal, A., Hirte, H., Laigle-Donadey, F., Franceschi, E., Chinot, O., Golfinopoulos, V., Fariselli, L., Wick, A., … Trial Investigators. (2017). Short-course radiation plus temozolomide in elderly patients with glioblastoma. *The New England Journal of Medicine, 376*(11), 1027–1037. https://doi.org/10.1056/NEJMoa1611977

Peterson, K., Turos-Cabal, M., Salvador, A. D., Palomo-Caturla, I., Howell, A. J., Vieira, M. E., Greiner, S. M., Barnoud, T., & Rodriguez-Blanco, J. (2024). Mechanistic insights into medulloblastoma relapse. *Pharmacology & Therapeutics, 260*, 108673. https://doi.org/10.1016/j.pharmthera.2024.108673

Petrescu, G. E. D., Sabo, A. A., Torsin, L. I., Calin, G. A., & Dragomir, M. P. (2019). MicroRNA based theranostics for brain cancer: Basic principles. *Journal of Experimental & Clinical Cancer Research : CR, 38*(1), 231. https://doi.org/10.1186/s13046-019-1180-5

Pillai-Kastoori, L., Heaton, S., Shiflett, S. D., Roberts, A. C., Solache, A., & Schutz-Geschwender, A. R. (2020). Antibody validation for Western blot: By the user, for the user. *The Journal of Biological Chemistry, 295*(4), 926–939. https://doi.org/10.1074/jbc.RA119.010472

Pink, R. C., Beaman, E. M., Samuel, P., Brooks, S. A., & Carter, D. R. F. (2022). Utilising extracellular vesicles for early cancer diagnostics: benefits, challenges and recommendations for the future. *British Journal of Cancer*, 126(3), 323–330. https://doi.org/10.1038/s41416-021-01668-4

Pirlog, R., Susman, S., Iuga, C. A., & Florian, S. I. (2019). Proteomic Advances in Glial Tumors through Mass Spectrometry Approaches. *Medicina (Kaunas, Lithuania)*, 55(8), 412. https://doi.org/10.3390/medicina55080412

Plaha, P., Camp, S., Cook, J., McCulloch, P., Voets, N., Ma, R., Taphoorn, M. J. B., Dirven, L., Grech-Sollars, M., Watts, C., Bulbeck, H., Jenkinson, M. D., Williams, M., Lim, A., Dixon, L., Price, S. J., Ashkan, K., Apostolopoulos, V., Barber, V. S., Taylor, A., … Nandi, D. (2022). FUTURE-GB: Functional and ultrasound-guided resection of glioblastoma - A two-stage randomised control trial. *BMJ Open, 12*(11), e064823. https://doi.org/10.1136/bmjopen-2022-064823

Platten, M., Bunse, L., Wick, A., Bunse, T., Le Cornet, L., Harting, I., Sahm, F., Sanghvi, K., Tan, C. L., Poschke, I., Green, E., Justesen, S., Behrens, G. A., Breckwoldt, M. O., Freitag, A., Rother, L. M., Schmitt, A., Schnell, O., Hense, J., Misch, M., … Wick, W. (2021). A vaccine targeting mutant IDH1 in newly diagnosed glioma. *Nature, 592*(7854), 463–468. https://doi.org/10.1038/s41586-021-03363-z

Polisetty, R. V., Gautam, P., Sharma, R., Harsha, H. C., Nair, S. C., Gupta, M. K., Uppin, M. S., Challa, S., Puligopu, A. K., Ankathi, P., Purohit, A. K., Chandak, G. R., Pandey, A., & Sirdeshmukh, R. (2012). LC-MS/MS analysis of differentially expressed glioblastoma membrane proteome reveals altered calcium signaling and other protein groups of regulatory functions. *Molecular & Cellular Proteomics: MCP, 11*(6), M111.013565. https://doi.org/10.1074/mcp.M111.013565

Pontén, J., & Macintyre, E. H. (1968). Long term culture of normal and neoplastic human glia. *Acta Pathologica et Microbiologica Scandinavica, 74*(4), 465–486. https://doi.org/10.1111/j.1699-0463.1968.tb03502.x

Pore, N., Liu, S., Haas-Kogan, D. A., O'Rourke, D. M., & Maity, A. (2003). PTEN mutation and epidermal growth factor receptor activation regulate vascular endothelial growth factor (VEGF) mRNA expression in human glioblastoma cells by transactivating the proximal VEGF promoter. *Cancer Research, 63*(1), 236–241. PMID: 12517803.

Porter, A. B., Wen, P. Y., & Polley, M. C. (2023). Molecular Profiling in Neuro-Oncology: Where We Are, Where We're Heading, and How We Ensure Everyone Can Come Along. *American Society of Clinical Oncology Educational Book. American Society of Clinical Oncology. Annual Meeting, 43*, e389322. https://doi.org/10.1200/EDBK_389322

Postel, M. D., Culver, J. O., Ricker, C., & Craig, D. W. (2022). Transcriptome analysis provides critical answers to the "variants of uncertain significance" conundrum. *Human Mutation, 43*(11), 1590–1608. https://doi.org/10.1002/humu.24394

Prapa, M., Chiavelli, C., Golinelli, G., Grisendi, G., Bestagno, M., Di Tomaso, N., & Dominici, M. (2021). GD2 CAR T cells against human glioblastoma. *npj Precision Oncology, 5*, 93. https://doi.org/10.1038/s41698-021-00233-9

Prather, K. Y., O'Neal, C. M., Westrup, A. M., Tullos, H. J., Hughes, K. L., Conner, A. K., Glenn, C. A., & Battiste, J. D. (2022). A systematic review of amino acid PET in assessing treatment response to temozolomide in glioma. *Neuro-Oncology Advances, 4*(1), vdac008. https://doi.org/10.1093/noajnl/vdac008

Pratt, A. J., & MacRae, I. J. (2009). The RNA-induced silencing complex: A versatile gene-silencing machine. *The Journal of Biological Chemistry, 284*(27), 17897–17901. https://doi.org/10.1074/jbc.R900012200

Pulumati, A., Pulumati, A., Dwarakanath, B. S., Verma, A., & Papineni, R. V. L. (2023). Technological advancements in cancer diagnostics: Improvements and limitations. *Cancer Reports (Hoboken, N.J.), 6*(2), e1764. https://doi.org/10.1002/cnr2.1764

Qin, S., Jiang, J., Lu, Y., Nice, E. C., Huang, C., Zhang, J., & He, W. (2020). Emerging role of tumor cell plasticity in modifying therapeutic response. *Signal Transduction and Targeted Therapy, 5*(1), 228. https://doi.org/10.1038/s41392-020-00313-5

Qu, C., Yan, C., Cao, W., Li, F., Qu, Y., Guan, K., Si, C., Yu, Z., & Qu, Z. (2020). miR-128-3p contributes to mitochondrial dysfunction and induces apoptosis in glioma cells via targeting pyruvate dehydrogenase kinase 1. *IUBMB Life, 72*(3), 465–475. https://doi.org/10.1002/iub.2212

Qu, K., Lin, T., Pang, Q., Liu, T., Wang, Z., Tai, M., Meng, F., Zhang, J., Wan, Y., Mao, P., Dong, X., Liu, C., Niu, W., & Dong, S. (2016). Extracellular miRNA-21 as a novel biomarker in glioma: Evidence from meta-analysis, clinical validation and experimental investigations. *Oncotarget, 7*(23), 33994–34010. https://doi.org/10.18632/oncotarget.9188

Qu, S., Guan, J., & Liu, Y. (2015). Identification of microRNAs as novel biomarkers for glioma detection: A meta-analysis based on 11 articles. *Journal of the Neurological Sciences, 348*(1-2), 181–187. https://doi.org/10.1016/j.jns.2014.11.036

Queensland University of Technology (QUT). (2021). New saliva oral and throat cancer diagnosis test receives FDA approval. Accessed: 10th August 20224, from QUT News.

Rachet, B., Mitry, E., Quinn, M. J., Cooper, N., & Coleman, M. P. (2008). Survival from brain tumours in England and Wales up to 2001. *British Journal of Cancer, 99*(Suppl 1), S98–S101. https://doi.org/10.1038/sj.bjc.6604603

Radaelli, E., Ceruti, R., Patton, V., Russo, M., Degrassi, A., Croci, V., Caprera, F., Stortini, G., Scanziani, E., Pesenti, E., & Alzani, R. (2009). Immunohistopathological and neuroimaging characterization of murine orthotopic xenograft models of glioblastoma multiforme recapitulating the most salient features of human disease. *Histology and Histopathology, 24*(7), 879–891. https://doi.org/10.14670/HH-24.879

Raez, L. E., Brice, K., Dumais, K., Lopez-Cohen, A., Wietecha, D., Izquierdo, P. A., Santos, E. S., & Powery, H. W. (2023). Liquid biopsy versus tissue biopsy to determine front line therapy in metastatic non-small cell lung cancer (NSCLC). *Clinical Lung Cancer, 24*(2), 120–129. https://doi.org/10.1016/j.cllc.2022.11.007

Rambabu, G., Kiran, Y. B. R., Tarakeswar, Y., Khalivulla, S. I., Barbosa, L. C. A., & Vijayakumar, V. (2022). Montmorillonite K10 clay catalyzed synthesis of novel β-aminocarbonyl compounds and their biological evaluation. *Chemistry & Biodiversity, 19*(10), e202200669. https://doi.org/10.1002/cbdv.202200669

Ramón Y Cajal, S., Sesé, M., Capdevila, C., Aasen, T., De Mattos-Arruda, L., Diaz-Cano, S. J., Hernández-Losa, J., & Castellví, J. (2020). Clinical implications of intratumor heterogeneity: Challenges and opportunities. *Journal of Molecular Medicine (Berlin, Germany), 98*(2), 161–177. https://doi.org/10.1007/s00109-020-01874-2

Rascio, F., Spadaccino, F., Rocchetti, M. T., Castellano, G., Stallone, G., Netti, G. S., & Ranieri, E. (2021). The pathogenic role of PI3K/AKT pathway in cancer onset and drug resistance: An updated review. *Cancers, 13*(16), 3949. https://doi.org/10.3390/cancers13163949

Raue, R., Frank, A. C., Syed, S. N., & Brüne, B. (2021). Therapeutic targeting of microRNAs in the tumor microenvironment. *International Journal of Molecular Sciences, 22*(4), 2210. https://doi.org/10.3390/ijms22042210

Ray, P. D., Huang, B. W., & Tsuji, Y. (2012). Reactive oxygen species (ROS) homeostasis and redox regulation in cellular signaling. *Cellular Signalling, 24*(5), 981–990. https://doi.org/10.1016/j.cellsig.2012.01.008

Razavi, S. M., Lee, K. E., Jin, B. E., Aujla, P. S., Gholamin, S., & Li, G. (2016). Immune evasion strategies of glioblastoma. *Frontiers in Surgery, 3*, 11. https://doi.org/10.3389/fsurg.2016.00011

Reardon, D. A., Brandes, A. A., Omuro, A., Mulholland, P., Lim, M., Wick, A., Baehring, J., Ahluwalia, M. S., Roth, P., Bähr, O., Phuphanich, S., Sepulveda, J. M., De Souza, P., Sahebjam, S., Carleton, M., Tatsuoka, K., Taitt, C., Zwirtes, R., Sampson, J., & Weller, M. (2020). Effect of Nivolumab vs Bevacizumab in patients with recurrent glioblastoma: The CheckMate 143 Phase 3 randomized clinical trial. *JAMA Oncology, 6*(7), 1003–1010. https://doi.org/10.1001/jamaoncol.2020.1024

Reda El Sayed, S., Cristante, J., Guyon, L., Denis, J., Chabre, O., & Cherradi, N. (2021). MicroRNA therapeutics in cancer: Current advances and challenges. *Cancers, 13*(11), 2680. https://doi.org/10.3390/cancers13112680

Ren, D., Lin, B., Zhang, X., Peng, Y., Ye, Z., Ma, Y., Liang, Y., Cao, L., Li, X., Li, R., Sun, L., Liu, Q., Wu, J., Zhou, K., & Zeng, J. (2017). Maintenance of cancer stemness by miR-196b-

5p contributes to chemoresistance of colorectal cancer cells via activating STAT3 signaling pathway. *Oncotarget*, 8(30), 49807–49823. https://doi.org/10.18632/oncotarget.17971

Renovanz, M., Hickmann, A. K., Nadji-Ohl, M., Keric, N., Weimann, E., Wirtz, C. R., Singer, S., Ringel, F., & Coburger, J. (2020). Health-related quality of life and distress in elderly vs. younger patients with high-grade glioma-results of a multicenter study. *Supportive Care in Cancer: Official Journal of the Multinational Association of Supportive Care in Cancer*, 28(11), 5165–5175. https://doi.org/10.1007/s00520-020-05354-8

Richard, S. A. (2024). The pivotal role of irradiation-induced apoptosis in the pathogenesis and therapy of medulloblastoma. *Cancer Reports (Hoboken, N.J.), 7*(4), e2048. https://doi.org/10.1002/cnr2.2048

Riolo, G., Cantara, S., Marzocchi, C., & Ricci, C. (2020). miRNA targets: From prediction tools to experimental validation. *Methods and Protocols*, *4*(1), 1. https://doi.org/10.3390/mps4010001

Rivera, A. L., Pelloski, C. E., Gilbert, M. R., Colman, H., De La Cruz, C., Sulman, E. P., Bekele, B. N., & Aldape, K. D. (2010). MGMT promoter methylation is predictive of response to radiotherapy and prognostic in the absence of adjuvant alkylating chemotherapy for glioblastoma. *Neuro-Oncology, 12*(2), 116–121. https://doi.org/10.1093/neuonc/nop020

Roadcap, D. W., Clemen, C. S., & Bear, J. E. (2000-2013). The role of mammalian coronins in development and disease. In *Madame Curie Bioscience Database*. Austin (TX): Landes Bioscience.

Robinson, G. A., Biggs, V., & Walker, D. G. (2015). Cognitive screening in brain tumors: Short but sensitive enough? *Frontiers in Oncology, 5*, 60. https://doi.org/10.3389/fonc.2015.00060

Robinson, S. D., de Boisanger, J., Pearl, F. M. G., Critchley, G., Rosenfelder, N., & Giamas, G. (2024). A brain metastasis liquid biopsy: where are we now? *Neuro-Oncology Advances, 6*(1), vdae066. https://doi.org/10.1093/noajnl/vdae066

Robinson, S. D., Samuels, M., Jones, W. et al. Confirming size-exclusion chromatography as a clinically relevant extracellular vesicles separation method from 1mL plasma through a comprehensive comparison of methods. *BMC Methods, 1*, 7 (2024). https://doi.org/10.1186/s44330-024-00007-2

Rodriguez, S. M. B., Kamel, A., Ciubotaru, G. V., Onose, G., Sevastre, A. S., Sfredel, V., Danoiu, S., Dricu, A., & Tataranu, L. G. (2023). An overview of EGFR mechanisms and their implications in targeted therapies for glioblastoma. *International Journal of Molecular Sciences, 24*(13), 11110. https://doi.org/10.3390/ijms241311110

Rong, L., Li, N., & Zhang, Z. (2022). Emerging therapies for glioblastoma: Current state and future directions. *Journal of Experimental & Clinical Cancer Research, 41*(1), 142. https://doi.org/10.1186/s13046-022-02349-7

Rosentreter, A., Hofmann, A., Xavier, C. P., Stumpf, M., Noegel, A. A., & Clemen, C. S. (2007). Coronin 3 involvement in F-actin-dependent processes at the cell cortex. *Experimental Cell Research, 313*(5), 878–895. https://doi.org/10.1016/j.yexcr.2006.12.015

Rossi, R., Arjmand, S., Bærentzen, S. L., Gjedde, A., & Landau, A. M. (2022). Synaptic vesicle glycoprotein 2A: Features and functions. *Frontiers in Neuroscience, 16*, 864514. https://doi.org/10.3389/fnins.2022.864514

Roth, P., Wischhusen, J., Happold, C., Chandran, P. A., Hofer, S., Eisele, G., Weller, M., & Keller, A. (2011). A specific miRNA signature in the peripheral blood of glioblastoma patients. *Journal of Neurochemistry, 118*(3), 449–457. https://doi.org/10.1111/j.1471-4159.2011.07307.x

Rybakin, V., & Clemen, C. S. (2005). Coronin proteins as multifunctional regulators of the cytoskeleton and membrane trafficking. *BioEssays: News and Reviews in Molecular, Cellular and Developmental Biology, 27*(6), 625–632. https://doi.org/10.1002/bies.20235

Sadelain, M., Rivière, I., & Riddell, S. (2017). Therapeutic T cell engineering. *Nature, 545*(7655), 423–431. https://doi.org/10.1038/nature22395

Saenz-Antoñanzas, A., Auzmendi-Iriarte, J., Carrasco-Garcia, E., Moreno-Cugnon, L., Ruiz, I., Villanua, J., Egaña, L., Otaegui, D., Samprón, N., & Matheu, A. (2019). Liquid Biopsy in Glioblastoma: Opportunities, Applications and Challenges. *Cancers*, 11(7), 950. https://doi.org/10.3390/cancers11070950

Sakshi, S., Jayasuriya, R., Ganesan, K., Xu, B., & Ramkumar, K. M. (2021). Role of circRNA-miRNA-mRNA interaction network in diabetes and its associated complications. *Molecular Therapy. Nucleic Acids, 26*, 1291–1302. https://doi.org/10.1016/j.omtn.2021.11.007

Salfer, B., Li, F., Wong, D. T. W., & Zhang, L. (2022). Urinary cell-free DNA in liquid biopsy and cancer management. *Clinical Chemistry, 68*(12), 1493–1501. https://doi.org/10.1093/clinchem/hvac122

Sanai, N., & Berger, M. S. (2018). Surgical oncology for gliomas: The state of the art. *Nature Reviews Clinical Oncology, 15*(2), 112–125. https://doi.org/10.1038/nrclinonc.2017.171

Sarkar, S., Zemp, F. J., Senger, D., Robbins, S. M., & Yong, V. W. (2015). ADAM-9 is a novel mediator of tenascin-C-stimulated invasiveness of brain tumor-initiating cells. *Neuro-oncology, 17*(8), 1095–1105. https://doi.org/10.1093/neuonc/nou362

Sati, I. S. E. E., & Parhar, I. (2021). MicroRNAs regulate cell cycle and cell death pathways in glioblastoma. *International Journal of Molecular Sciences, 22*(24), 13550. https://doi.org/10.3390/ijms222413550

Scarola, M., Schoeftner, S., Schneider, C., & Benetti, R. (2010). miR-335 directly targets Rb1 (pRb/p105) in a proximal connection to p53-dependent stress response. *Cancer Research, 70*(17), 6925–6933. https://doi.org/10.1158/0008-5472.CAN-10-0141

Schieber, M., & Chandel, N. S. (2014). ROS function in redox signaling and oxidative stress. *Current Biology, 24*(10), R453–R462. https://doi.org/10.1016/j.cub.2014.03.034

Schipmann, S., Müther, M., Stögbauer, L., Zimmer, S., Brokinkel, B., Holling, M., Grauer, O., Suero Molina, E., Warneke, N., & Stummer, W. (2020). Combination of ALA-induced fluorescence-guided resection and intraoperative open photodynamic therapy for recurrent

glioblastoma: Case series on a promising dual strategy for local tumor control. *Journal of Neurosurgery, 134*(2), 426–436. https://doi.org/10.3171/2019.11.JNS192443

Schneider, C. A., Rasband, W. S., & Eliceiri, K. W. (2012). NIH Image to ImageJ: 25 years of image analysis. *Nature Methods, 9*(7), 671–675. https://doi.org/10.1038/nmeth.2089

Schob, S., Meyer, J., Gawlitza, M., Frydrychowicz, C., Müller, W., Preuss, M., Bure, L., Quäschling, U., Hoffmann, K. T., & Surov, A. (2016). Diffusion-weighted MRI reflects proliferative activity in primary CNS lymphoma. *PloS One, 11*(8), e0161386. https://doi.org/10.1371/journal.pone.0161386

Segal, M., & Slack, F. J. (2020). Challenges identifying efficacious miRNA therapeutics for cancer. *Expert Opinion on Drug Discovery, 15*(9), 987–992. https://doi.org/10.1080/17460441.2020.1765770

Seker-Polat, F., Pinarbasi Degirmenci, N., Solaroglu, I., & Bagci-Onder, T. (2022). Tumor cell infiltration into the brain in glioblastoma: From mechanisms to clinical perspectives. *Cancers, 14*(2), 443. https://doi.org/10.3390/cancers14020443

Sempere, L. F., Azmi, A. S., & Moore, A. (2021). MicroRNA-based diagnostic and therapeutic applications in cancer medicine. *Wiley Interdisciplinary Reviews: RNA*, *12*(6), e1662. https://doi.org/10.1002/wrna.1662

Sengupta, S., Marrinan, J., Frishman, C., & Sampath, P. (2012). Impact of temozolomide on immune response during malignant glioma chemotherapy. *Clinical & Developmental Immunology, 2012*, 831090. https://doi.org/10.1155/2012/831090

Senrung, A., Tripathi, T., Aggarwal, N., Janjua, D., Chhokar, A., Yadav, J., Chaudhary, A., Thakur, K., Singh, T., & Bharti, A. C. (2023). Anti-angiogenic potential of trans-chalcone in an in vivo chick chorioallantoic membrane model: An ATP antagonist to VEGFR with predicted blood-brain barrier permeability. *Cardiovascular & Hematological Agents in Medicinal Chemistry*. Advance online publication. https://doi.org/10.2174/0118715257250417231019102501

Seo, J. S., Ju, Y. S., Lee, W. C., Shin, J. Y., Lee, J. K., Bleazard, T., Lee, J., Jung, Y. J., Kim, J. O., Shin, J. Y., Yu, S. B., Kim, J., Lee, E. R., Kang, C. H., Park, I. K., Rhee, H., Lee, S. H., Kim, J. I., Kang, J. H., & Kim, Y. T. (2012). The transcriptional landscape and mutational profile of lung adenocarcinoma. *Genome Research, 22*(11), 2109–2119. https://doi.org/10.1101/gr.145144.112

Sexton, R. E., Al-Hallak, M. N., Al-Share, B., Li, Y., Aboukameel, A., Landesman, Y., Kashyap, T., Kim, S., Mohammad, R. M., Philip, P. A., & Azmi, A. S. (2021). Mir-7974: An oncogenic miRNA that perpetuates gastric cancer. *Cancer Research, 81*(13_Supplement), 2383. https://doi.org/10.1158/1538-7445.AM2021-2383

Seyhan, A. A. (2024). Trials and tribulations of microRNA therapeutics. *International Journal of Molecular Sciences, 25*(3), 1469. https://doi.org/10.3390/ijms25031469

Shaikh, M. A. J., Altamimi, A. S. A., Afzal, M., Gupta, G., Singla, N., Gilhotra, R., Almalki, W. H., Kazmi, I., Alzarea, S. I., Prasher, P., Singh, S. K., & Dua, K. (2024). Unraveling the

impact of miR-21 on apoptosis regulation in glioblastoma. *Pathology, Research and Practice*, *254*, 155121. https://doi.org/10.1016/j.prp.2024.155121

Shan, Z. N., Tian, R., Zhang, M., Gui, Z. H., Wu, J., Ding, M., Zhou, X. F., & He, J. (2016). miR128-1 inhibits the growth of glioblastoma multiforme and glioma stem-like cells via targeting BMI1 and E2F3. *Oncotarget, 7*(48), 78813–78826. https://doi.org/10.18632/oncotarget.12385

Shang, R., Lee, S., Senavirathne, G., & Lai, E. C. (2023). MicroRNAs in action: Biogenesis, function, and regulation. *Nature Reviews Genetics, 24*(12), 816–833. https://doi.org/10.1038/s41576-023-00611-y

Sharma, P., Aaroe, A., Liang, J., & Puduvalli, V. K. (2023). Tumor microenvironment in glioblastoma: Current and emerging concepts. *Neuro-Oncology Advances, 5*(1), vdad009. https://doi.org/10.1093/noajnl/vdad009

Shea, A., Harish, V., Afzal, Z., Chijioke, J., Kedir, H., Dusmatova, S., Roy, A., Ramalinga, M., Harris, B., Blancato, J., Verma, M., & Kumar, D. (2016). MicroRNAs in glioblastoma multiforme pathogenesis and therapeutics. *Cancer Medicine*, *5*(8), 1917–1946. https://doi.org/10.1002/cam4.775

Shen, X., Kong, S., Ma, S., Shen, L., Zheng, M., Qin, S., Qi, J., Wang, Q., Cui, X., & Ju, S. (2022). Hsa_circ_0000437 promotes pathogenesis of gastric cancer and lymph node metastasis. *Oncogene, 41*(42), 4724–4735. https://doi.org/10.1038/s41388-022-02449-w

Sheng, H., Li, H., Zeng, H., Zhang, B., Lu, Y., Liu, X., Xu, Z., Zhang, J., & Zhang, L. (2024). Heterogeneity and tumoral origin of medulloblastoma in the single-cell era. *Oncogene, 43*(12), 839–850. https://doi.org/10.1038/s41388-024-02967-9

Sheng, Q., Vickers, K., Zhao, S., Wang, J., Samuels, D. C., Koues, O., Shyr, Y., & Guo, Y. (2017). Multi-perspective quality control of Illumina RNA sequencing data analysis. *Briefings in Functional Genomics, 16*(4), 194–204. https://doi.org/10.1093/bfgp/elw035

Sheng, W., Zhang, C., Mohiuddin, T. M., Al-Rawe, M., Zeppernick, F., Falcone, F. H., Meinhold-Heerlein, I., & Hussain, A. F. (2023). Multiplex immunofluorescence: A powerful tool in cancer immunotherapy. *International Journal of Molecular Sciences, 24*(4), 3086. https://doi.org/10.3390/ijms24043086

Shi, R., Wang, P. Y., Li, X. Y., Chen, J. X., Li, Y., Zhang, X. Z., Zhang, C. G., Jiang, T., Li, W. B., Ding, W., & Cheng, S. J. (2015). Exosomal levels of miRNA-21 from cerebrospinal fluids associated with poor prognosis and tumor recurrence of glioma patients. *Oncotarget, 6*(29), 26971–26981. https://doi.org/10.18632/oncotarget.4699

Shi, Z. M., Wang, J., Yan, Z., You, Y. P., Li, C. Y., Qian, X., Yin, Y., Zhao, P., Wang, Y. Y., Wang, X. F., Li, M. N., Liu, L. Z., Liu, N., & Jiang, B. H. (2012). MiR-128 inhibits tumor growth and angiogenesis by targeting p70S6K1. *PloS One, 7*(3), e32709. https://doi.org/10.1371/journal.pone.0032709

Shiravand, Y., Khodadadi, F., Kashani, S. M. A., Hosseini-Fard, S. R., Hosseini, S., Sadeghirad, H., Ladwa, R., O'Byrne, K., & Kulasinghe, A. (2022). Immune checkpoint inhibitors in cancer

therapy. *Current Oncology (Toronto, Ont.), 29*(5), 3044–3060. https://doi.org/10.3390/curroncol29050247

Shu, M., Zheng, X., Wu, S., Lu, H., Leng, T., Zhu, W., Zhou, Y., Ou, Y., Lin, X., Lin, Y., Xu, D., Zhou, Y., & Yan, G. (2011). Targeting oncogenic miR-335 inhibits growth and invasion of malignant astrocytoma cells. *Molecular Cancer, 10*, 59. https://doi.org/10.1186/1476-4598-10-59

Shu, S. Y., Qing, D., Wang, B., Zeng, Q. Y., Chen, Y. C., Jin, Y., Zeng, C. C., & Bao, R. (2013). Comparison of microRNA expression in hippocampus and the marginal division (MrD) of the neostriatum in rats. *Journal of Biomedical Science, 20*(1), 9. https://doi.org/10.1186/1423-0127-20-9

Shvarts-Serebro, I., Sheinin, A., Gottfried, I., Adler, L., Schottlender, N., Ashery, U., & Barak, B. (2021). miR-128 as a regulator of synaptic properties in 5xFAD mice hippocampal neurons. *Journal of Molecular Neuroscience, 71*(12), 2593–2607. https://doi.org/10.1007/s12031-021-01862-2

Sies, H., & Jones, D. P. (2020). Reactive oxygen species (ROS) as pleiotropic physiological signalling agents. *Nature Reviews Molecular Cell Biology, 21*(7), 363–383. https://doi.org/10.1038/s41580-020-0230-3

Simon, T., Jackson, E., & Giamas, G. (2020). Breaking through the glioblastoma micro-environment via extracellular vesicles. *Oncogene, 39*(23), 4477–4490. https://doi.org/10.1038/s41388-020-1308-2

Singh, R. R., Mondal, I., Janjua, T., Popat, A., & Kulshreshtha, R. (2023). Engineered smart materials for RNA-based molecular therapy to treat Glioblastoma. *Bioactive Materials, 33*, 396–423. https://doi.org/10.1016/j.bioactmat.2023.11.007

Sinha, K., Sangani, S. S., Kehr, A. D., Rule, G. S., & Jen-Jacobson, L. (2016). Metal Ion Binding at the Catalytic Site Induces Widely Distributed Changes in a Sequence Specific Protein-DNA Complex. *Biochemistry*, 55(44), 6115–6132. https://doi.org/10.1021/acs.biochem.6b00919

Skowron, P., Ramaswamy, V., & Taylor, M. D. (2015). Genetic and molecular alterations across medulloblastoma subgroups. *Journal of Molecular Medicine (Berlin, Germany)*, 93(10), 1075–1084. https://doi.org/10.1007/s00109-015-1333-8

Slika, H., Shahani, A., Wahi, R., Miller, J., Groves, M., & Tyler, B. (2024). Overcoming Treatment Resistance in Medulloblastoma: Underlying Mechanisms and Potential Strategies. *Cancers, 16*(12), 2249. https://doi.org/10.3390/cancers16122249

Solga, R., Behrens, J., Ziemann, A., Riou, A., Berwanger, C., Becker, L., Garrett, L., de Angelis, M. H., Fischer, L., Coras, R., Barkovits, K., Marcus, K., Mahabir, E., Eichinger, L., Schröder, R., Noegel, A. A., Clemen, C. S., & German Mouse Clinic Consortium (2019). CRN2 binds to TIMP4 and MMP14 and promotes perivascular invasion of glioblastoma cells. *European Journal of Cell Biology, 98*(5-8), 151046. https://doi.org/10.1016/j.ejcb.2019.151046

Son, Y., Cheong, Y. K., Kim, N. H., Chung, H. T., Kang, D. G., & Pae, H. O. (2011). Mitogen-activated protein kinases and reactive oxygen species: How can ROS activate MAPK pathways?. *Journal of Signal Transduction, 2011*, 792639. https://doi.org/10.1155/2011/792639

Song, H., Zhang, Y., Liu, N., Wan, C., Zhang, D., Zhao, S., ... & Yuan, L. (2016). miR-92b regulates glioma cells proliferation, migration, invasion, and apoptosis via PTEN/Akt signaling pathway. *Journal of Physiology and Biochemistry*, 72, 201-211.
Song, J., Ma, Q., Hu, M., Qian, D., Wang, B., & He, N. (2018). The inhibition of miR-144-3p on cell proliferation and metastasis by targeting TOP2A in HCMV-positive glioblastoma cells. *Molecules, 23*(12), 3259. https://doi.org/10.3390/molecules23123259

Song, Q., An, Q., Niu, B., Lu, X., Zhang, N., & Cao, X. (2019). Role of miR-221/222 in tumor development and the underlying mechanism. *Journal of Oncology, 2019*, 7252013. https://doi.org/10.1155/2019/7252013

[a]Song, Y., He, M., Zhang, J., & Xu, J. (2020). High expression of microRNA 221 is a poor predictor for glioma. *Medicine, 99*(49), e23163. https://doi.org/10.1097/MD.0000000000023163

[b]Song, Y., Zhang, J., He, M., & Xu, J. (2020). Prognostic role of microRNA 222 in patients with glioma: A meta-analysis. *BioMed Research International, 2020*, 4689689. https://doi.org/10.1155/2020/4689689

Souhami, L., Seiferheld, W., Brachman, D., Podgorsak, E. B., Werner-Wasik, M., Lustig, R., Schultz, C. J., Sause, W., Okunieff, P., Buckner, J., Zamorano, L., Mehta, M. P., & Curran, W. J., Jr. (2004). Randomized comparison of stereotactic radiosurgery followed by conventional radiotherapy with carmustine to conventional radiotherapy with carmustine for patients with glioblastoma multiforme: Report of Radiation Therapy Oncology Group 93-05 protocol. *International Journal of Radiation Oncology, Biology, Physics, 60*(3), 853–860. https://doi.org/10.1016/j.ijrobp.2004.04.011

Stenvang, J., Petri, A., Lindow, M., Obad, S., & Kauppinen, S. (2012). Inhibition of microRNA function by antimiR oligonucleotides. *Silence, 3*(1), 1. https://doi.org/10.1186/1758-907X-3-1

Steponaitis, G., & Tamasauskas, A. (2021). Mesenchymal and proneural subtypes of glioblastoma disclose branching based on GSC associated signature. *International Journal of Molecular Sciences, 22*(9), 4964. https://doi.org/10.3390/ijms22094964

Steponaitis, G., Kucinskas, V., Golubickaite, I., Skauminas, K., & Saudargiene, A. (2022). Glioblastoma molecular classification tool based on mRNA analysis: From wet-lab to subtype. *International Journal of Molecular Sciences, 23*(24), 15875. https://doi.org/10.3390/ijms232415875
Stergiopoulou, D., Markou, A., Strati, A., Zavridou, M., Tzanikou, E., Mastoraki, S., Kallergi, G., Georgoulias, V., & Lianidou, E. (2023). Comprehensive liquid biopsy analysis as a tool for the early detection of minimal residual disease in breast cancer. *Scientific Reports, 13*(1), 1258. https://doi.org/10.1038/s41598-022-25400-1

Sticht, C., De La Torre, C., Parveen, A., & Gretz, N. (2018). miRWalk: An online resource for prediction of microRNA binding sites. *PloS ONE*, *13*(10), e0206239. https://doi.org/10.1371/journal.pone.0206239

Storey, J. D., & Tibshirani, R. (2003). Statistical significance for genomewide studies. *Proceedings of the National Academy of Sciences of the United States of America*, 100(16), 9440–9445. https://doi.org/10.1073/pnas.1530509100

Stummer, W., Pichlmeier, U., Meinel, T., Wiestler, O. D., Zanella, F., Reulen, H. J., & ALA-Glioma Study Group. (2006). Fluorescence-guided surgery with 5-aminolevulinic acid for resection of malignant glioma: A randomised controlled multicentre phase III trial. *The Lancet Oncology, 7*(5), 392–401. https://doi.org/10.1016/S1470-2045(06)70665-9

Stupp, R., Hegi, M. E., Mason, W. P., van den Bent, M. J., Taphoorn, M. J., Janzer, R. C., Ludwin, S. K., Allgeier, A., Fisher, B., Belanger, K., Hau, P., Brandes, A. A., Gijtenbeek, J., Marosi, C., Vecht, C. J., Mokhtari, K., Wesseling, P., Villa, S., Eisenhauer, E., Gorlia, T., … National Cancer Institute of Canada Clinical Trials Group. (2009). Effects of radiotherapy with concomitant and adjuvant temozolomide versus radiotherapy alone on survival in glioblastoma in a randomised phase III study: 5-year analysis of the EORTC-NCIC trial. *The Lancet Oncology, 10*(5), 459–466. https://doi.org/10.1016/S1470-2045(09)70025-7

Stupp, R., Mason, W. P., van den Bent, M. J., Weller, M., Fisher, B., Taphoorn, M. J., Belanger, K., Brandes, A. A., Marosi, C., Bogdahn, U., Curschmann, J., Janzer, R. C., Ludwin, S. K., Gorlia, T., Allgeier, A., Lacombe, D., Cairncross, J. G., Eisenhauer, E., Mirimanoff, R. O., … National Cancer Institute of Canada Clinical Trials Group. (2005). Radiotherapy plus concomitant and adjuvant temozolomide for glioblastoma. *The New England Journal of Medicine, 352*(10), 987–996. https://doi.org/10.1056/NEJMoa043330

Su, L. J., Zhang, J. H., Gomez, H., Murugan, R., Hong, X., Xu, D., Jiang, F., & Peng, Z. Y. (2019). Reactive oxygen species-induced lipid peroxidation in apoptosis, autophagy, and ferroptosis. *Oxidative Medicine and Cellular Longevity, 2019*, 5080843. https://doi.org/10.1155/2019/5080843

Suarez-Arnedo, A., Torres Figueroa, F., Clavijo, C., Arbeláez, P., Cruz, J. C., & Muñoz-Camargo, C. (2020). An Image J plugin for the high throughput image analysis of in vitro scratch wound healing assays. *PLOS ONE, 15*(7), e0232565. https://doi.org/10.1371/journal.pone.0232565

Sufianov, A., Begliarzade, S., Ilyasova, T., Liang, Y., & Beylerli, O. (2022). MicroRNAs as prognostic markers and therapeutic targets in gliomas. *Non-coding RNA Research, 7*(3), 171–177. https://doi.org/10.1016/j.ncrna.2022.07.001

Suk, Y., Gwynne, W. D., Burns, I., Venugopal, C., & Singh, S. K. (2022). Childhood Medulloblastoma: An Overview. *Methods in Molecular Biology (Clifton, N.J.)*, *2423*, 1–12. https://doi.org/10.1007/978-1-0716-1952-0_1

Sun, J., Liao, K., Wu, X., Huang, J., Zhang, S., & Lu, X. (2015). Serum microRNA-128 as a biomarker for diagnosis of glioma. *International Journal of Clinical and Experimental Medicine, 8*(1), 456–463.

Sun, L., Su, Y., Jiao, A., & Zhou, J. (2023). T cells in health and disease. *Signal Transduction and Targeted Therapy, 8*, 235. https://doi.org/10.1038/s41392-023-01471-y

Sun, R., Yang, L., Wang, Y., Zhang, Y., Ke, J., & Zhao, D. (2021). DNAJB11 predicts a poor prognosis and is associated with immune infiltration in thyroid carcinoma: A bioinformatics analysis. *The Journal of International Medical Research, 49*(11), 3000605211053722. https://doi.org/10.1177/03000605211053722

Sunkin, S. M., Ng, L., Lau, C., Dolbeare, T., Gilbert, T. L., Thompson, C. L., Hawrylycz, M., & Dang, C. (2013). Allen Brain Atlas: An integrated spatio-temporal portal for exploring the central nervous system. *Nucleic Acids Research*, *41*(Database issue), D996–D1008. https://doi.org/10.1093/nar/gks1042

Sunny, D. E., Amoo, M., Al Breiki, M., Teng, E. D. W., Henry, J., & Javadpour, M. (2022). Prevalence of incidental intracranial findings on magnetic resonance imaging: A systematic review and meta-analysis. *Acta Neurochirurgica, 164*(10), 2751–2765. https://doi.org/10.1007/s00701-022-05225-7

Suwala, A. K., Stichel, D., Schrimpf, D., Maas, S. L. N., Sill, M., Dohmen, H., Banan, R., Reinhardt, A., Sievers, P., Hinz, F., Blattner-Johnson, M., Hartmann, C., Schweizer, L., Boldt, H. B., Kristensen, B. W., Schittenhelm, J., Wood, M. D., Chotard, G., Bjergvig, R., Das, A., … Sahm, F. (2021). Glioblastomas with primitive neuronal component harbor a distinct methylation and copy-number profile with inactivation of TP53, PTEN, and RB1. *Acta Neuropathologica, 142*(1), 179–189. https://doi.org/10.1007/s00401-021-02302-6

Suzuki, H. I., Katsura, A., Matsuyama, H., & Miyazono, K. (2015). MicroRNA regulons in the tumor microenvironment. *Oncogene, 34*(24), 3085–3094. https://doi.org/10.1038/onc.2014.254

Suzuki, H., Kumar, S. A., Shuai, S., Diaz-Navarro, A., Gutierrez-Fernandez, A., De Antonellis, P., Cavalli, F. M. G., Juraschka, K., Farooq, H., Shibahara, I., Vladoiu, M. C., Zhang, J., Abeysundara, N., Przelicki, D., Skowron, P., Gauer, N., Luu, B., Daniels, C., Wu, X., Forget, A., … Taylor, M. D. (2019). Recurrent noncoding U1 snRNA mutations drive cryptic splicing in SHH medulloblastoma. *Nature, 574*(7780), 707–711. https://doi.org/10.1038/s41586-019-1650-0

Svoronos, A. A., Engelman, D. M., & Slack, F. J. (2016). OncomiR or tumor suppressor? The duplicity of microRNAs in cancer. *Cancer Research, 76*(13), 3666–3670. https://doi.org/10.1158/0008-5472.CAN-16-0359

Szklarczyk, D., Gable, A. L., Lyon, D., Junge, A., Wyder, S., Huerta-Cepas, J., Simonovic, M., Doncheva, N. T., Morris, J. H., Bork, P., Jensen, L. J., & Mering, C. V. (2019). STRING v11: Protein-protein association networks with increased coverage, supporting functional discovery in genome-wide experimental datasets. *Nucleic Acids Research*, *47*(D1), D607–D613. https://doi.org/10.1093/nar/gky1131

Szklarczyk, D., Gable, A. L., Nastou, K. C., Lyon, D., Kirsch, R., Pyysalo, S., Doncheva, N. T., Legeay, M., Fang, T., Bork, P., Jensen, L. J., & von Mering, C. (2021). The STRING database in 2021: Customizable protein-protein networks, and functional characterization of user-uploaded gene/measurement sets. *Nucleic Acids Research*, *49*(D1), D605–D612. https://doi.org/10.1093/nar/gkaa1074

Taal, W., Bromberg, J. E., & van den Bent, M. J. (2015). Chemotherapy in glioma. *CNS Oncology, 4*(3), 179–192. https://doi.org/10.2217/cns.15.2

Tagliatela, A. C., Hempstead, S. C., Hibshman, P. S., Hockenberry, M. A., Brighton, H. E., Pecot, C. V., & Bear, J. E. (2020). Coronin 1C inhibits melanoma metastasis through regulation of MT1-MMP-containing extracellular vesicle secretion. *Scientific Reports, 10*(1), 11958. https://doi.org/10.1038/s41598-020-67465-w

[a]Tan, A. C., Ashley, D. M., López, G. Y., Malinzak, M., Friedman, H. S., & Khasraw, M. (2020). Management of glioblastoma: State of the art and future directions. *CA: A Cancer Journal for Clinicians, 70*(4), 299–312. https://doi.org/10.3322/caac.21613

Tan, D. C., Roth, I. M., Wickremesekera, A. C., Davis, P. F., Kaye, A. H., Mantamadiotis, T., Stylli, S. S., & Tan, S. T. (2019). Therapeutic targeting of cancer stem cells in human glioblastoma by manipulating the renin-angiotensin system. *Cells, 8*(11), 1364. https://doi.org/10.3390/cells8111364

[b]Tan, W. C. C., Nerurkar, S. N., Cai, H. Y., Ng, H. H. M., Wu, D., Wee, Y. T. F., Lim, J. C. T., Yeong, J., & Lim, T. K. H. (2020). Overview of multiplex immunohistochemistry/immunofluorescence techniques in the era of cancer immunotherapy. *Cancer Communications (London, England), 40*(4), 135–153. https://doi.org/10.1002/cac2.12023

Tandel, G. S., Biswas, M., Kakde, O. G., Tiwari, A., Suri, H. S., Turk, M., Laird, J. R., Asare, C. K., Ankrah, A. A., Khanna, N., Madhusudhan, B. K., Saba, L., & Suri, J. S. (2019). A review on a deep learning perspective in brain cancer classification. *Cancers, 11*(1), 111. https://doi.org/10.3390/cancers11010111

Tang, R., Ma, F., Li, W., Ouyang, S., Liu, Z., & Wu, J. (2017). miR-206-3p Inhibits 3T3-L1 Cell Adipogenesis via the c-Met/PI3K/Akt Pathway. *International Journal of Molecular Sciences*, 18(7), 1510. https://doi.org/10.3390/ijms18071510

[a]Tang, S., Qin, C., Hu, H., Liu, T., He, Y., Guo, H., Yan, H., Zhang, J., Tang, S., & Zhou, H. (2022). Immune checkpoint inhibitors in non-small cell lung cancer: Progress, challenges, and prospects. *Cells, 11*(3), 320. https://doi.org/10.3390/cells11030320

Tang, T., Yang, Z., Wang, D., et al. (2020). The role of lysosomes in cancer development and progression. *Cell Bioscience*, 10, 131. https://doi.org/10.1186/s13578-020-00489-x

[b]Tang, W., Pei, M., Li, J., Xu, N., Xiao, W., Yu, Z., Zhang, J., Hong, L., Guo, Z., Lin, J., Dai, W., Xiao, Y., Wu, X., Liu, G., Zhi, F., Li, G., Xiong, J., Chen, Y., Zhang, H., Xiang, L., … Wang, J. (2022). The miR-3648/FRAT1-FRAT2/c-Myc negative feedback loop modulates the metastasis and invasion of gastric cancer cells. *Oncogene, 41*(43), 4823–4838. https://doi.org/10.1038/s41388-022-02451-2

Tarev, I., & Cekov, A. (2024). Cerebellar glioblastoma: A literature review and case analysis. *Cureus, 16*(2), e55135. https://doi.org/10.7759/cureus.55135

Tarhan, L., Bistline, J., Chang, J., Galloway, B., Hanna, E., & Weitz, E. (2023). Single Cell Portal: An interactive home for single-cell genomics data. *bioRxiv : The Preprint Server for Biology*, 2023.07.13.548886. https://doi.org/10.1101/2023.07.13.548886

Tarnowski, B. I., Spinale, F. G., & Nicholson, J. H. (1991). DAPI as a useful stain for nuclear quantitation. *Biotechnic & Histochemistry, 66*(6), 297–302.

Tassone, P., Di Martino, M. T., Arbitrio, M., Fiorillo, L., Staropoli, N., Ciliberto, D., Cordua, A., Scionti, F., Bertucci, B., Salvino, A., Lopreiato, M., Thunarf, F., Cuomo, O., Zito, M. C., De Fina, M. R., Brescia, A., Gualtieri, S., Riillo, C., Manti, F., Caracciolo, D., … Tagliaferri, P. (2023). Safety and activity of the first-in-class locked nucleic acid (LNA) miR-221 selective inhibitor in refractory advanced cancer patients: A first-in-human, phase 1, open-label, dose-escalation study. *Journal of Hematology & Oncology, 16*(1), 68. https://doi.org/10.1186/s13045-023-01468-8

Teplyuk, N. M., Mollenhauer, B., Gabriely, G., Giese, A., Kim, E., Smolsky, M., Kim, R. Y., Saria, M. G., Pastorino, S., Kesari, S., & Krichevsky, A. M. (2012). MicroRNAs in cerebrospinal fluid identify glioblastoma and metastatic brain cancers and reflect disease activity. *Neuro-Oncology, 14*(6), 689–700. https://doi.org/10.1093/neuonc/nos074

Teplyuk, N. M., Uhlmann, E. J., Wong, A. H., Karmali, P., Basu, M., Gabriely, G., Jain, A., Wang, Y., Chiocca, E. A., Stephens, R., Marcusson, E., Yi, M., & Krichevsky, A. M. (2015). MicroRNA-10b inhibition reduces E2F1-mediated transcription and miR-15/16 activity in glioblastoma. *Oncotarget, 6*(6), 3770–3783. https://doi.org/10.18632/oncotarget.3009

Testa, U., Castelli, G., & Pelosi, E. (2018). Genetic abnormalities, clonal evolution, and cancer stem cells of brain tumors. *Medical Sciences, 6*(4), 85. https://doi.org/10.3390/medsci6040085

Tetta, C., Ghigo, E., Silengo, L., Deregibus, M. C., & Camussi, G. (2013). Extracellular vesicles as an emerging mechanism of cell-to-cell communication. *Endocrine*, 44(1), 11–19. https://doi.org/10.1007/s12020-012-9839-0

Thal, D., Xavier, C. P., Rosentreter, A., Linder, S., Friedrichs, B., Waha, A., Pietsch, T., Stumpf, M., Noegel, A., & Clemen, C. (2008). Expression of coronin-3 (coronin-1C) in diffuse gliomas is related to malignancy. *The Journal of Pathology, 214*(4), 415–424. https://doi.org/10.1002/path.2308

Thul, P. J., & Lindskog, C. (2018). The human protein atlas: A spatial map of the human proteome. *Protein Science: A Publication of the Protein Society*, *27*(1), 233–244. https://doi.org/10.1002/pro.3307

Tilak, M., Holborn, J., New, L. A., Lalonde, J., & Jones, N. (2021). Receptor tyrosine kinase signaling and targeting in glioblastoma multiforme. *International Journal of Molecular Sciences, 22*(4), 1831. https://doi.org/10.3390/ijms22041831

Tomasello, L., Distefano, R., Nigita, G., & Croce, C. M. (2021). The microRNA family gets wider: The isomiRs classification and role. *Frontiers in Cell and Developmental Biology, 9*, 668648. https://doi.org/10.3389/fcell.2021.668648

Tomczak, K., Czerwińska, P., & Wiznerowicz, M. (2015). The Cancer Genome Atlas (TCGA): An immeasurable source of knowledge. *Contemporary Oncology (Poznan, Poland)*, *19*(1A), A68–A77. https://doi.org/10.5114/wo.2014.47136

Torp, S. H., Solheim, O., & Skjulsvik, A. J. (2022). The WHO 2021 classification of central nervous system tumours: A practical update on what neurosurgeons need to know—a minireview. *Acta Neurochirurgica, 164*(9), 2453–2464. https://doi.org/10.1007/s00701-022-05301-y

Trevisi, G., Barbone, P., Treglia, G., Mattoli, M. V., & Mangiola, A. (2020). Reliability of intraoperative ultrasound in detecting tumor residual after brain diffuse glioma surgery: A systematic review and meta-analysis. *Neurosurgical Review, 43*(5), 1221–1233. https://doi.org/10.1007/s10143-019-01160-x

U.S. National Library of Medicine. (2024). Blood-brain barrier disruption (BBBD) for liquid biopsy in subjects with glioblastoma brain tumor. *ClinicalTrials.gov*. Accessed: 12th August 2024, from https://clinicaltrials.gov/ct2/show/NCT05383872

U.S. National Library of Medicine. (2024). Laboratory study of early tumor markers in the peripheral blood of glioblastoma multiforme patients. *ClinicalTrials.gov*. Accessed: 12th August 2024, from https://clinicaltrials.gov/ct2/show/NCT01135875

U.S. National Library of Medicine. (2024). Pembrolizumab and a vaccine (ATL-DC) for the treatment of surgically accessible recurrent glioblastoma. *ClinicalTrials.gov*. Accessed: 12th August 2024, from https://clinicaltrials.gov/ct2/show/NCT04201873

U.S. National Library of Medicine. (2024). Profiling program of cancer patients with sequential tumor and liquid biopsies (PLANET). *ClinicalTrials.gov*. Accessed: 12th August 2024, from https://clinicaltrials.gov/ct2/show/NCT05099068

U.S. National Library of Medicine. (2024). Tessa Jowell BRAIN MATRIX - platform study (BRAIN MATRIX). *ClinicalTrials.gov*. Accessed: 12th August 2024, from https://clinicaltrials.gov/ct2/show/NCT04274283

U.S. National Library of Medicine. (2024). The circTeloDIAG: A new approach of liquid biopsy for the diagnosis and follow-up of patients with glioma tumor. *ClinicalTrials.gov*. Accessed: 12th August 2024, from https://clinicaltrials.gov/ct2/show/NCT04931732

Vaitkiene, P., Pranckeviciene, A., Stakaitis, R., Steponaitis, G., Tamasauskas, A., & Bunevicius, A. (2019). Association of miR-34a expression with quality of life of glioblastoma patients: A prospective study. *Cancers, 11*(3), 300. https://doi.org/10.3390/cancers11030300

Valle-Garcia, D., Pérez de la Cruz, V., Flores, I., Salazar, A., Pineda, B., & Meza-Sosa, K. F. (2024). Use of microRNAs as diagnostic, prognostic, and therapeutic tools for glioblastoma. *International Journal of Molecular Sciences, 25*(5), 2464. https://doi.org/10.3390/ijms25052464

van Kessel, E., Baumfalk, A. E., van Zandvoort, M. J. E., Robe, P. A., & Snijders, T. J. (2017). Tumor-related neurocognitive dysfunction in patients with diffuse glioma: A systematic review of neurocognitive functioning prior to anti-tumor treatment. *Journal of Neuro-Oncology, 134*(1), 9–18. https://doi.org/10.1007/s11060-017-2503-z

van Niel, G., D'Angelo, G., & Raposo, G. (2018). Shedding light on the cell biology of extracellular vesicles. *Nature Reviews. Molecular Cell Biology*, 19(4), 213–228. https://doi.org/10.1038/nrm.2017.125

van Santwijk, L., Kouwenberg, V., Meijer, F., Smits, M., & Henssen, D. (2022). A systematic review and meta-analysis on the differentiation of glioma grade and mutational status by use of perfusion-based magnetic resonance imaging. *Insights into Imaging, 13*(1), 102. https://doi.org/10.1186/s13244-022-01230-7

van Zandwijk, N., Pavlakis, N., Kao, S. C., Linton, A., Boyer, M. J., Clarke, S., Huynh, Y., Chrzanowska, A., Fulham, M. J., Bailey, D. L., Cooper, W. A., Kritharides, L., Ridley, L., Pattison, S. T., MacDiarmid, J., Brahmbhatt, H., & Reid, G. (2017). Safety and activity of microRNA-loaded minicells in patients with recurrent malignant pleural mesothelioma: A first-in-man, phase 1, open-label, dose-escalation study. *The Lancet Oncology, 18*(10), 1386–1396. https://doi.org/10.1016/S1470-2045(17)30621-6

Veliz, I., Loo, Y., Castillo, O., Karachaliou, N., Nigro, O., & Rosell, R. (2015). Advances and challenges in the molecular biology and treatment of glioblastoma—is there any hope for the future?. *Annals of Translational Medicine, 3*(1), 7. https://doi.org/10.3978/j.issn.2305-5839.2014.10.06

Venkataraman, S., Alimova, I., Fan, R., Harris, P., Foreman, N., & Vibhakar, R. (2010). MicroRNA 128a increases intracellular ROS level by targeting Bmi-1 and inhibits medulloblastoma cancer cell growth by promoting senescence. *PLOS ONE, 5*(6), e10748. https://doi.org/10.1371/journal.pone.0010748

Venkatesh, H. S., Morishita, W., Geraghty, A. C., Silverbush, D., Gillespie, S. M., Arzt, M., Tam, L. T., Espenel, C., Ponnuswami, A., Ni, L., Woo, P. J., Taylor, K. R., Agarwal, A., Regev, A., Brang, D., Vogel, H., Hervey-Jumper, S., Bergles, D. E., Suvà, M. L., Malenka, R. C., … Monje, M. (2019). Electrical and synaptic integration of glioma into neural circuits. *Nature, 573*(7775), 539–545. https://doi.org/10.1038/s41586-019-1563-y

Villalpando-Rodriguez, G. E., & Gibson, S. B. (2021). Reactive oxygen species (ROS) regulates different types of cell death by acting as a rheostat. *Oxidative Medicine and Cellular Longevity, 2021*, 9912436. https://doi.org/10.1155/2021/9912436

Vojdani, S., Ghaderian, S. M. H., Zali, A., Rakhshan, A., Oraee Yazdani, S., Poursheikhani, A., Bidari Zerehpoush, F., & Sharifi, G. (2021). Altered expression of EGFR and miR-34a derived from serum and tumoral tissue was associated with glioblastoma multiform. *Experimental and Molecular Pathology, 121*, 104655. https://doi.org/10.1016/j.yexmp.2021.104655

Von Deimling, A., Korshunov, A., & Hartmann, C. (2011). The next generation of glioma biomarkers: MGMT methylation, BRAF fusions, and IDH1 mutations. *Brain Pathology, 21*(1), 74–87. https://doi.org/10.1111/j.1750-3639.2010.00454.x

Wach, J., Vychopen, M., Kühnapfel, A., Seidel, C., & Güresir, E. (2023). A systematic review and meta-analysis of supramarginal resection versus gross total resection in glioblastoma: Can we enhance progression-free survival time and preserve postoperative safety? *Cancers, 15*(6), 1772. https://doi.org/10.3390/cancers15061772

Walter, F. M., Penfold, C., Joannides, A., Saji, S., Johnson, M., Watts, C., Brodbelt, A., Jenkinson, M. D., Price, S. J., Hamilton, W., & Scott, S. E. (2019). Missed opportunities for diagnosing brain tumours in primary care: A qualitative study of patient experiences. *The British Journal of General Practice, 69*(681), e224–e235. https://doi.org/10.3399/bjgp19X701861

[a]Wang, B., Han, Y., Zhang, Y., Zhao, Q., Wang, H., Wei, J., Meng, L., Xin, Y., & Jiang, X. (2023). Overcoming acquired resistance to cancer immune checkpoint therapy: Potential strategies based on molecular mechanisms. *Cell & Bioscience, 13*(1), 120. https://doi.org/10.1186/s13578-023-01073-9

Wang, C., Liu, Y., Chen, R., Wang, X., Wang, Y., Wei, J., Zhang, K., & Zhang, C. (2022). Electrochemical biosensing of circulating microRNA-21 in cerebrospinal fluid of medulloblastoma patients through target-induced redox signal amplification. *Mikrochimica Acta, 189*(3), 105. https://doi.org/10.1007/s00604-022-05210-y

[a]Wang, H., Liu, D., & Yang, J. (2019). Prognostic risk model construction and molecular marker identification in glioblastoma multiforme based on mRNA/microRNA/long non-coding RNA analysis using random survival forest method. *Neoplasma*, 66(3), 459–469. https://doi.org/10.4149/neo_2018_181008N746

[a]Wang, H., Xu, Y., Jin, M., Li, H., & Li, S. (2021). miR-383 reduces keratinocyte proliferation and induces apoptosis in psoriasis via disruption of LCN2-dependent JAK/STAT pathway activation. *International Immunopharmacology*, 96, 107587. https://doi.org/10.1016/j.intimp.2021.107587

[b]Wang, J., Liu, J., Sun, G., Meng, H., Wang, J., Guan, Y., Yin, Y., Zhao, Z., Dong, X., Yin, S., Li, H., Cheng, Y., Wu, H., Wu, A., Yu, X., & Chen, L. (2019). Glioblastoma extracellular vesicles induce the tumour-promoting transformation of neural stem cells. *Cancer Letters, 466*, 1–12. https://doi.org/10.1016/j.canlet.2019.09.004

[c]Wang, J., Lu, L., Luo, Z., Li, W., Lu, Y., Tang, Q., & Pu, J. (2019). miR-383 inhibits cell growth and promotes cell apoptosis in hepatocellular carcinoma by targeting IL-17 via STAT3 signaling pathway. *Biomedicine & Pharmacotherapy*, 120, 109551. https://doi.org/10.1016/j.biopha.2019.109551

Wang, J., Tsouko, E., Jonsson, P., Bergh, J., Hartman, J., Aydogdu, E., & Williams, C. (2014). miR-206 inhibits cell migration through direct targeting of the actin-binding protein coronin 1C in triple-negative breast cancer. *Molecular Oncology, 8*(8), 1690–1702. https://doi.org/10.1016/j.molonc.2014.07.006

[a]Wang, L., Ge, J., Lan, Y., Shi, Y., Luo, Y., Tan, Y., Liang, M., Deng, S., Zhang, X., Wang, W., Tan, Y., Xu, Y., & Luo, T. (2020). Tumor mutational burden is associated with poor outcomes in diffuse glioma. *BMC Cancer, 20*(1), 213. https://doi.org/10.1186/s12885-020-6658-1

[b]Wang, L., Lang, B., Zhou, Y., Ma, J., & Hu, K. (2021). Up-regulation of miR-663a inhibits the cancer stem cell-like properties of glioma via repressing the KDM2A-mediated TGF-β/SMAD signaling pathway. *Cell Cycle (Georgetown, Tex.), 20*(19), 1935–1952. https://doi.org/10.1080/15384101.2021.1966962

[d]Wang, N., Zheng, J., Chen, Z., Liu, Y., Dura, B., Kwak, M., Xavier-Ferrucio, J., Lu, Y. C., Zhang, M., Roden, C., Cheng, J., Krause, D. S., Ding, Y., Fan, R., & Lu, J. (2019). Single-cell microRNA-mRNA co-sequencing reveals non-genetic heterogeneity and mechanisms of microRNA regulation. *Nature Communications*, *10*(1), 95. https://doi.org/10.1038/s41467-018-07981-6

Wang, Q., Li, P., Li, A., Jiang, W., Wang, H., Wang, J., & Xie, K. (2012). Plasma specific miRNAs as predictive biomarkers for diagnosis and prognosis of glioma. *Journal of Experimental & Clinical Cancer Research : CR, 31*(1), 97. https://doi.org/10.1186/1756-9966-31-97

[b]Wang, S., Xu, J., Guo, Y., Cai, Y., Zhu, W., Meng, L., Jiang, C., & Lu, S. (2023). Successful transfection of microRNA mimics or inhibitors in a regular cell line and in primary cells derived from patients with rheumatoid arthritis. *Bio-protocol, 13*(18), e4823. https://doi.org/10.21769/BioProtoc.4823

Wang, W., Dai, L. X., Zhang, S., Yang, Y., Yan, N., Fan, P., Dai, L., Tian, H. W., Cheng, L., Zhang, X. M., Li, C., Zhang, J. F., Xu, F., Shi, G., Chen, X. L., Du, T., Li, Y. M., Wei, Y. Q., & Deng, H. X. (2013). Regulation of epidermal growth factor receptor signaling by plasmid-based microRNA-7 inhibits human malignant gliomas growth and metastasis in vivo. *Neoplasma, 60*(3), 274–283. https://doi.org/10.4149/neo_2013_036

Wang, X., Ding, G., Lai, W., Liu, S., & Shuai, J. (2018). MicroRNA-383 upregulation protects against propofol-induced hippocampal neuron apoptosis and cognitive impairment. *Experimental and Therapeutic Medicine, 15*(4), 3181–3188. https://doi.org/10.3892/etm.2018.5838

Wang, X., Wang, L., Lin, H., Zhu, Y., Huang, D., Lai, M., Xi, X., Huang, J., Zhang, W., & Zhong, T. (2024). Research progress of CTC, ctDNA, and EVs in cancer liquid biopsy. *Frontiers in Oncology, 14*, 1303335. https://doi.org/10.3389/fonc.2024.1303335

[b]Wang, X., Xu, D., Pei, X., Zhang, Y., Zhang, Y., Gu, Y., & Li, Y. (2020). CircSKA3 modulates FOXM1 to facilitate cell proliferation, migration, and invasion while confining apoptosis in medulloblastoma via miR-383-5p. *Cancer Management and Research, 12*, 13415–13426. https://doi.org/10.2147/CMAR.S272753

[c]Wang, Y., Qi, H., Liu, Y., Duan, C., Liu, X., Xia, T., Chen, D., Piao, H. L., & Liu, H. X. (2021). The double-edged roles of ROS in cancer prevention and therapy. *Theranostics, 11*(10), 4839–4857. https://doi.org/10.7150/thno.56747

[d]Wang, Z., Jia, L., Sun, Y., Li, C., Zhang, L., Wang, X., & Chen, H. (2021). CORO1C is associated with poor prognosis and promotes metastasis through PI3K/AKT pathway in colorectal cancer. *Frontiers in Molecular Biosciences, 8*, 682594. https://doi.org/10.3389/fmolb.2021.682594

Wanis, H. A., Møller, H., Ashkan, K., & Davies, E. A. (2021). The incidence of major subtypes of primary brain tumors in adults in England 1995-2017. *Neuro-Oncology, 23*, 1371–1382.
Wasilewski, A., Serventi, J., Kamalyan, L., Wychowski, T., & Mohile, N. (2017). Acute care in glioblastoma: The burden and the consequences. *Neuro-Oncology Practice, 4*(4), 248–254. https://doi.org/10.1093/nop/npw032

Waszak, S. M., Robinson, G. W., Gudenas, B. L., Smith, K. S., Forget, A., Kojic, M., Garcia-Lopez, J., Hadley, J., Hamilton, K. V., Indersie, E., Buchhalter, I., Kerssemakers, J., Jäger, N., Sharma, T., Rausch, T., Kool, M., Sturm, D., Jones, D. T. W., Vasilyeva, A., Tatevossian, R. G., … Pfister, S. M. (2020). Germline Elongator mutations in Sonic Hedgehog medulloblastoma. *Nature, 580*(7803), 396–401. https://doi.org/10.1038/s41586-020-2164-5

Watts, C., & Sanai, N. (2016). Surgical approaches for the gliomas. *Handbook of Clinical Neurology, 134*, 51–69. https://doi.org/10.1016/B978-0-12-802997-8.00004-9

Weenink, B., French, P. J., Sillevis Smitt, P. A. E., Debets, R., & Geurts, M. (2020). Immunotherapy in glioblastoma: Current shortcomings and future perspectives. *Cancers, 12*(3), 751. https://doi.org/10.3390/cancers12030751

Wei, D. C., & Morrison, E. H. (2023). Histology, astrocytes. In *StatPearls*. StatPearls Publishing. https://www.ncbi.nlm.nih.gov/books/NBK545142/

Weiland, S., Hickmann, T., Lederer, M., Marquardt, J., & Schwindenhammer, S. (2021). The 2030 agenda for sustainable development: Transformative change through the sustainable development goals? *Politics and Governance, 9*(1), 90-95.

Welcker, D., Stein, C., Feitosa, N. M., Armistead, J., Zhang, J. L., Lütke, S., Kleinridders, A., Brüning, J. C., Eming, S. A., Sengle, G., Niehoff, A., Bloch, W., & Hammerschmidt, M. (2021). Hemicentin-1 is an essential extracellular matrix component of the dermal-epidermal and myotendinous junctions. *Scientific Reports*, 11(1), 17926. https://doi.org/10.1038/s41598-021-96824-4

Weller, M., & Le Rhun, E. (2020). How did lomustine become standard of care in recurrent glioblastoma? *Cancer Treatment Reviews, 87*, 102029. https://doi.org/10.1016/j.ctrv.2020.102029

Weller, M., van den Bent, M., Preusser, M., Le Rhun, E., Tonn, J. C., Minniti, G., Bendszus, M., Balana, C., Chinot, O., Dirven, L., French, P., Hegi, M. E., Jakola, A. S., Platten, M., Roth, P., Rudà, R., Short, S., Smits, M., Taphoorn, M. J. B., von Deimling, A., … Wick, W. (2021). EANO guidelines on the diagnosis and treatment of diffuse gliomas of adulthood. *Nature Reviews Clinical Oncology, 18*(3), 170–186. https://doi.org/10.1038/s41571-020-00447-z

Wen, D., Danquah, M., Chaudhary, A. K., & Mahato, R. I. (2015). Small molecules targeting microRNA for cancer therapy: Promises and obstacles. *Journal of Controlled Release, 219*, 237–247. https://doi.org/10.1016/j.jconrel.2015.08.011

Wen, P. Y., Weller, M., Lee, E. Q., Alexander, B. M., Barnholtz-Sloan, J. S., Barthel, F. P., Batchelor, T. T., Bindra, R. S., Chang, S. M., Chiocca, E. A., Cloughesy, T. F., DeGroot, J. F., Galanis, E., Gilbert, M. R., Hegi, M. E., Horbinski, C., Huang, R. Y., Lassman, A. B., Le Rhun, E., Lim, M., … van den Bent, M. J. (2020). Glioblastoma in adults: A Society for Neuro-

Oncology (SNO) and European Society of Neuro-Oncology (EANO) consensus review on current management and future directions. *Neuro-Oncology, 22*(8), 1073–1113. https://doi.org/10.1093/neuonc/noaa106

Westermark, B., Pontén, J., & Hugosson, R. (1973). Determinants for the establishment of permanent tissue culture lines from human gliomas. *Acta Pathologica et Microbiologica Scandinavica. Section A, Pathology, 81*(6), 791–805. https://doi.org/10.1111/j.1699-0463.1973.tb03573.x

Westholm, J. O., & Lai, E. C. (2011). Mirtrons: MicroRNA biogenesis via splicing. *Biochimie, 93*(11), 1897–1904. https://doi.org/10.1016/j.biochi.2011.06.017
White, J., White, M. P. J., Wickremesekera, A., Peng, L., & Gray, C. (2024). The tumour microenvironment, treatment resistance, and recurrence in glioblastoma. *Journal of Translational Medicine, 22*(1), 540. https://doi.org/10.1186/s12967-024-05301-9

Wick, W., & Platten, M. (2018). Understanding and treating glioblastoma. *Neurologic Clinics, 36*(3), 485–499. https://doi.org/10.1016/j.ncl.2018.04.006

Wightman, B., Ha, I., & Ruvkun, G. (1993). Posttranscriptional regulation of the heterochronic gene lin-14 by lin-4 mediates temporal pattern formation in C. elegans. *Cell, 75*(5), 855–862. https://doi.org/10.1016/0092-8674(93)90530-4

Williams, A. H., Valdez, G., Moresi, V., Qi, X., McAnally, J., Elliott, J. L., Bassel-Duby, R., Sanes, J. R., & Olson, E. N. (2009). MicroRNA-206 delays ALS progression and promotes regeneration of neuromuscular synapses in mice. *Science, 326*(5959), 1549–1554. https://doi.org/10.1126/science.1181046

Wishart, D. S., Tian, S., Allen, D., Oler, E., Peters, H., Lui, V. W., Gautam, V., Djoumbou-Feunang, Y., Greiner, R., & Metz, T. O. (2022). BioTransformer 3.0—a web server for accurately predicting metabolic transformation products. *Nucleic Acids Research, 50*(W1), W115–W123. https://doi.org/10.1093/nar/gkac313

Wojtukiewicz, M. Z., Rek, M. M., Karpowicz, K., Górska, M., Polityńska, B., Wojtukiewicz, A. M., Moniuszko, M., Radziwon, P., Tucker, S. C., & Honn, K. V. (2021). Inhibitors of immune checkpoints—PD-1, PD-L1, CTLA-4—New opportunities for cancer patients and a new challenge for internists and general practitioners. *Cancer Metastasis Reviews, 40*(3), 949–982. https://doi.org/10.1007/s10555-021-09976-0

Wortzel, I., Dror, S., Kenific, C. M., & Lyden, D. (2019). Exosome-Mediated Metastasis: Communication from a Distance. *Developmental Cell*, 49(3), 347–360. https://doi.org/10.1016/j.devcel.2019.04.011

Wu, A., & Lim, M. (2023). Advancing combination therapy for recurrent glioblastoma. *Nature Medicine, 29*, 1318–1319. https://doi.org/10.1038/s41591-023-02350-3

[a]Wu, J., Zhang, X., Wang, Y., Sun, Q., Chen, M., Liu, S., & Zou, X. (2018). Licochalcone A suppresses hexokinase 2-mediated tumor glycolysis in gastric cancer via downregulation of the Akt signaling pathway. *Oncology Reports, 39*(3), 1181–1190. https://doi.org/10.3892/or.2017.6155

[b]Wu, K., He, J., Pu, W., & Peng, Y. (2018). The role of Exportin-5 in microRNA biogenesis and cancer. *Genomics, Proteomics & Bioinformatics, 16*(2), 120–126. https://doi.org/10.1016/j.gpb.2017.09.004

Wu, L., Zhao, Z., Shin, Y. J., Yin, Y., Raju, A., Vaiyapuri, T. S., Idzham, K., Son, M., Lee, Y., Sa, J. K., Chua, J. Y. H., Unal, B., Zhai, Y., Fan, W., Huang, L., Hu, H., Gunaratne, J., Nam, D. H., Jiang, T., & Tergaonkar, V. (2024). Tumour microenvironment programming by an RNA-RNA-binding protein complex creates a druggable vulnerability in IDH-wild-type glioblastoma. *Nature Cell Biology, 26*(6), 1003–1018. https://doi.org/10.1038/s41556-024-01428-5

Wu, Q., Qin, H., Zhao, Q., & He, X. X. (2015). Emerging role of transcription factor-microRNA-target gene feed-forward loops in cancer. *Biomedical Reports, 3*(5), 611–616. https://doi.org/10.3892/br.2015.477

Wu, W., Klockow, J. L., Zhang, M., Lafortune, F., Chang, E., Jin, L., Wu, Y., & Daldrup-Link, H. E. (2021). Glioblastoma multiforme (GBM): An overview of current therapies and mechanisms of resistance. *Pharmacological Research, 171*, 105780. https://doi.org/10.1016/j.phrs.2021.105780

[a]Wu, Y., Chang, J., Ge, J., Xu, K., Zhou, Q., Zhang, X., Zhu, N., & Hu, M. (2022). Isobavachalcone's alleviation of pyroptosis contributes to enhanced apoptosis in glioblastoma: Possible involvement of NLRP3. *Molecular Neurobiology, 59*(11), 6934–6955. https://doi.org/10.1007/s12035-022-03010-2

[b]Wu, Y., Yi, M., Niu, M., Mei, Q., & Wu, K. (2022). Myeloid-derived suppressor cells: An emerging target for anticancer immunotherapy. *Molecular Cancer, 21*(1), 184. https://doi.org/10.1186/s12943-022-01657-y

Xavier, C. P., Eichinger, L., Fernandez, M. P., et al. (2013) Evolutionary and functional diversity of coronin proteins. In: *Madame Curie Bioscience Database*. Austin (TX): Landes Bioscience; 2000-2013.

Xavier, C. P., Rastetter, R. H., Blömacher, M., Stumpf, M., Himmel, M., Morgan, R. O., Fernandez, M. P., Wang, C., Osman, A., Miyata, Y., Gjerset, R. A., Eichinger, L., Hofmann, A., Linder, S., Noegel, A. A., & Clemen, C. S. (2012). Phosphorylation of CRN2 by CK2 regulates F-actin and Arp2/3 interaction and inhibits cell migration. *Scientific Reports, 2*, 241. https://doi.org/10.1038/srep00241

Xing, W., Feng, H., Jiang, B., Gao, B., Liu, J., Xie, Z., Zhang, Y., Hu, X., Sun, J., Greenblatt, M. B., Zhou, B. O., & Zou, W. (2024). Itm2a expression marks periosteal skeletal stem cells that contribute to bone fracture healing. *The Journal of Clinical Investigation*, 134(17), e176528. https://doi.org/10.1172/JCI176528

Xu, D., Ma, P., Gao, G., Gui, Y., Niu, X., & Jin, B. (2015). MicroRNA-383 expression regulates proliferation, migration, invasion, and apoptosis in human glioma cells. *Tumour Biology: The Journal of the International Society for Oncodevelopmental Biology and Medicine, 36*(10), 7743–7753. https://doi.org/10.1007/s13277-015-3378-2

Xu, L., Cao, H., Xie, Y., Zhang, Y., Du, M., Xu, X., ... & Liu, X. (2019). Exosome-shuttled miR-92b-3p from ischemic preconditioned astrocytes protects neurons against oxygen and glucose deprivation. *Brain Research*, 1717, 66-73.

[a]Xu, P., Wu, Q., Yu, J., Rao, Y., Kou, Z., Fang, G., Shi, X., Liu, W., & Han, H. (2020). A systematic way to infer the regulation relations of miRNAs on target genes and critical miRNAs in cancers. *Frontiers in Genetics, 11*, 278. https://doi.org/10.3389/fgene.2020.00278

[b]Xu, Q., & Xu, Z. (2020). miR-196b-5p Promotes Proliferation, Migration and Invasion of Lung Adenocarcinoma Cells via Targeting RSPO2. *Cancer Management and Research*, 12, 13393–13402. https://doi.org/10.2147/CMAR.S274171

Xue, L., Zhang, W. J., Fan, Q. X., & Wang, L. X. (2018). Licochalcone A inhibits PI3K/Akt/mTOR signaling pathway activation and promotes autophagy in breast cancer cells. *Oncology Letters, 15*(2), 1869–1873. https://doi.org/10.3892/ol.2017.7451

Yalçın, B., & Monje, M. (2021). Microenvironmental interactions of oligodendroglial cells. *Developmental Cell, 56*(13), 1821–1832. https://doi.org/10.1016/j.devcel.2021.06.006

Yan, H., Parsons, D. W., Jin, G., McLendon, R., Rasheed, B. A., Yuan, W., Kos, I., Batinic-Haberle, I., Jones, S., Riggins, G. J., Friedman, H., Friedman, A., Reardon, D., Herndon, J., Kinzler, K. W., Velculescu, V. E., Vogelstein, B., & Bigner, D. D. (2009). IDH1 and IDH2 mutations in gliomas. *The New England Journal of Medicine, 360*(8), 765–773. https://doi.org/10.1056/NEJMoa0808710

Yan, T., Zhang, Z., & Li, D. (2020). NGF receptors and PI3K/AKT pathway involved in glucose fluctuation-induced damage to neurons and α-lipoic acid treatment. *BMC Neuroscience, 21*(1), 38. https://doi.org/10.1186/s12868-020-00588-y

Yan, Y. Y., Guo, Q. R., Wang, F. H., Adhikari, R., Zhu, Z. Y., Zhang, H. Y., Zhou, W. M., Yu, H., Li, J. Q., & Zhang, J. Y. (2021). Cell-free DNA: hope and potential application in cancer. *Frontiers in Cell and Developmental Biology, 9*, 639233. https://doi.org/10.3389/fcell.2021.639233

[a]Yang, B., Wang, S., Zeng, J., Zhang, Y., Ruan, X., Han, W., Yin, B., Yuan, J., Qiang, B., Ying, W., Qian, X., & Peng, X. (2015). Proteomic screening and identification of microRNA-128 targets in glioma cells. *Proteomics, 15*(15), 2602–2617. https://doi.org/10.1002/pmic.201400128

[a]Yang, C. H., Yue, J., Pfeffer, S. R., Fan, M., Paulus, E., Hosni-Ahmed, A., Sims, M., Qayyum, S., Davidoff, A. M., Handorf, C. R., & Pfeffer, L. M. (2014). MicroRNA-21 promotes glioblastoma tumorigenesis by down-regulating insulin-like growth factor-binding protein-3 (IGFBP3). *The Journal of Biological Chemistry, 289*(36), 25079–25087. https://doi.org/10.1074/jbc.M114.593863

[b]Yang, G., Han, D., Chen, X., Zhang, D., Wang, L., Shi, C., ... & Zhao, S. (2014). MiR-196a exerts its oncogenic effect in glioblastoma multiforme by inhibition of IκBα both in vitro and in vivo. *Neuro-Oncology*, 16(5), 652-661.

Yang, H., Lou, C., Sun, L., Li, J., Cai, Y., Wang, Z., Li, W., Liu, G., & Tang, Y. (2019). admetSAR 2.0: Web-service for prediction and optimization of chemical ADMET properties. *Bioinformatics (Oxford, England), 35*(6), 1067–1069. https://doi.org/10.1093/bioinformatics/bty707

Yang, J., Roy, A., & Zhang, Y. (2013). BioLiP: A semi-manually curated database for biologically relevant ligand-protein interactions. *Nucleic Acids Research, 41*(Database issue), D1096–D1103. https://doi.org/10.1093/nar/gks966

Yang, N., Zhu, S., Lv, X., Qiao, Y., Liu, Y. J., & Chen, J. (2018). MicroRNAs: Pleiotropic regulators in the tumor microenvironment. *Frontiers in Immunology, 9*, 2491. https://doi.org/10.3389/fimmu.2018.02491

Yang, X., Krowiorz, K., Buelow, D., Bhayadia, R., Kohlschmidt, J., Nicolet, D., Maetzig, T., Pabst, C., Hui, J., Shad, A., Gao, S., Stephenson, M., Wu, S. W., van den Bosch, M., Escano, L., Lock, F., Panahi, A., Macphee, L., Maksakova, I., Amoah, A., … Kuchenbauer, F. (2023). P422: Targeting the WT1mut-miR-193a transcriptional axis with INT-1B3, a novel lipid nanoparticle-formulated miR-193a-3p mimic in acute myeloid leukemia. *HemaSphere, 7*(Suppl), e43178c6. https://doi.org/10.1097/01.HS9.0000968596.43178.c6

[b]Yang, X., Zhang, C., Guo, T., Feng, Y., Liu, Q., Chen, Y., & Zhang, Q. (2015). Reduced expression of microRNA 206 regulates cell proliferation via cyclinD2 in gliomas. *Molecular Medicine Reports, 11*(5), 3295–3300. https://doi.org/10.3892/mmr.2015.3171

[c]Yang, Z., & Wang, K. K. (2015). Glial fibrillary acidic protein: From intermediate filament assembly and gliosis to neurobiomarker. *Trends in Neurosciences, 38*(6), 364–374. https://doi.org/10.1016/j.tins.2015.04.003

Yi, Q., Xie, W., Sun, W., Sun, W., & Liao, Y. (2022). A Concise Review of MicroRNA-383: Exploring the Insights of Its Function in Tumorigenesis. *Journal of Cancer, 13*(1), 313–324. https://doi.org/10.7150/jca.64846

Yin, C. Y., Kong, W., Jiang, J., Xu, H., & Zhao, W. (2019). miR-7-5p inhibits cell migration and invasion in glioblastoma through targeting SATB1. *Oncology Letters, 17*(2), 1819–1825. https://doi.org/10.3892/ol.2018.9777

Yin, K., Yin, W., Wang, Y., Zhou, L., Liu, Y., Yang, G., Wang, J., & Lu, J. (2016). MiR-206 suppresses epithelial mesenchymal transition by targeting TGF-β signaling in estrogen receptor positive breast cancer cells. *Oncotarget*, 7(17), 24537–24548. https://doi.org/10.18632/oncotarget.8233

Yu, C. F., Chen, F. H., Lu, M. H., Hong, J. H., & Chiang, C. S. (2017). Dual roles of tumour cells-derived matrix metalloproteinase 2 on brain tumour growth and invasion. *British Journal of Cancer, 117*(12), 1828–1836. https://doi.org/10.1038/bjc.2017.362

Yu, D., Li, Y., Wang, M., Gu, J., Xu, W., Cai, H., Fang, X., & Zhang, X. (2022). Exosomes as a new frontier of cancer liquid biopsy. *Molecular Cancer, 21*(1), 56. https://doi.org/10.1186/s12943-022-01509-9

[a]Yu, X., Duan, W., Wu, F., Yang, D., Wang, X., Wu, J., Zhou, D., & Shen, Y. (2023). LncRNA-HOTAIRM1 promotes aerobic glycolysis and proliferation in osteosarcoma via the miR-664b-3p/Rheb/mTOR pathway. *Cancer Science, 114*(9), 3537-3552. https://doi.org/10.1111/cas.15881

[b]Yu, Y. (2023). The Function of NK Cells in Tumor Metastasis and NK Cell-Based Immunotherapy. *Cancers*, 15(8), 2323. https://doi.org/10.3390/cancers15082323

Yuan, Y., & Weidhaas, J. B. (2019). Functional microRNA binding site variants. *Molecular Oncology, 13*(1), 4–8. https://doi.org/10.1002/1878-0261.12421

Zhang, C. B., Wang, Z. L., Liu, H. J., Wang, Z., & Jia, W. (2023). Characterization of tumor-associated reactive astrocytes in gliomas by single-cell and bulk tumor sequencing. *Frontiers in Neurology, 14*, 1193844. https://doi.org/10.3389/fneur.2023.1193844

Zhang, C., Zhang, J., Hao, J., Shi, Z., Wang, Y., Han, L., Yu, S., You, Y., Jiang, T., Wang, J., Liu, M., Pu, P., & Kang, C. (2012). High level of miR-221/222 confers increased cell invasion and poor prognosis in glioma. *Journal of Translational Medicine, 10*, 119. https://doi.org/10.1186/1479-5876-10-119

Zhang, H., Huang, T., Yuan, S., Long, Y., Tan, S., Niu, G., Zhang, P., & Yang, M. (2022). Circ_0020123 plays an oncogenic role in non-small cell lung cancer depending on the regulation of miR-512-3p/CORO1C. *Thoracic Cancer, 13*(9), 1406–1418. https://doi.org/10.1111/1759-7714.14408

[a]Zhang, J. J. Y., Lee, K. S., Voisin, M. R., Hervey-Jumper, S. L., Berger, M. S., & Zadeh, G. (2020). Awake craniotomy for resection of supratentorial glioblastoma: A systematic review and meta-analysis. *Neuro-Oncology Advances, 2*(1), vdaa111. https://doi.org/10.1093/noajnl/vdaa111

[a]Zhang, Y., & Hunter, T. (2014). Roles of Chk1 in cell biology and cancer therapy. *International Journal of Cancer, 134*(5), 1013–1023. https://doi.org/10.1002/ijc.28226

Zhang, Y., Alexander, P. B., & Wang, X. F. (2017). TGF-β family signaling in the control of cell proliferation and survival. *Cold Spring Harbor Perspectives in Biology, 9*(4), a022145. https://doi.org/10.1101/cshperspect.a022145

Zhang, Y., Dube, C., Gibert, M., Jr., Cruickshanks, N., Wang, B., Coughlan, M., Yang, Y., Setiady, I., Deveau, C., Saoud, K., Grello, C., Oxford, M., Yuan, F., & Abounader, R. (2018). The p53 pathway in glioblastoma. *Cancers, 10*(9), 297. https://doi.org/10.3390/cancers10090297

[b]Zhang, Y., Yang, X., Zhu, X. L., Hao, J. Q., Bai, H., Xiao, Y. C., Wang, Z. Z., Hao, C. Y., & Duan, H. B. (2020). Bioinformatics analysis of potential core genes for glioblastoma. *Bioscience Reports*, 40(7), BSR20201625. https://doi.org/10.1042/BSR20201625

[b]Zhang, Z. Y., Zhu, Y. H., Zhou, C. H., Liu, Q., Lu, H. L., Ge, Y. J., & Wang, M. W. (2014). Development of β-amino-carbonyl compounds as androgen receptor antagonists. *Acta Pharmacologica Sinica, 35*(5), 664–673. https://doi.org/10.1038/aps.2013.201

Zhao, J., Tao, Y., Zhou, Y., Qin, N., Chen, C., Tian, D., & Xu, L. (2015). MicroRNA-7: A promising new target in cancer therapy. *Cancer Cell International, 15*, 103. https://doi.org/10.1186/s12935-015-0259-0

Zhao, J., Zhou, Y., Guo, M., Yue, D., Chen, C., Liang, G., & Xu, L. (2020). MicroRNA-7: Expression and function in brain physiological and pathological processes. *Cell & Bioscience, 10*, 77. https://doi.org/10.1186/s13578-020-00436-w

Zhao, L. N., Wang, P., Liu, Y. H., Cai, H., Ma, J., Liu, L. B., Xi, Z., Li, Z. Q., Liu, X. B., & Xue, Y. X. (2017). MiR-383 inhibits proliferation, migration and angiogenesis of glioma-exposed endothelial cells in vitro via VEGF-mediated FAK and Src signaling pathways. *Cellular Signalling, 30*, 142–153. https://doi.org/10.1016/j.cellsig.2016.09.007

[a]Zhao, L. Y., Xin, G. J., Tang, Y. Y., Li, X. F., Li, Y. Z., Tang, N., & Ma, Y. H. (2022). miR-664b-3p inhibits colon cell carcinoma via negatively regulating Budding uninhibited by benzimidazole 3. *Bioengineered, 13*(3), 4857–4868. https://doi.org/10.1080/21655979.2022.2036400

[b]Zhao, R., Fu, J., Zhu, L., Chen, Y., & Liu, B. (2022). Designing strategies of small-molecule compounds for modulating non-coding RNAs in cancer therapy. *Journal of Hematology & Oncology, 15*(1), 14. https://doi.org/10.1186/s13045-022-01230-6

Zhao, X., Xiao, Z., Li, B., Li, H., Yang, B., Li, T., & Mei, Z. (2021). miRNA-21 may serve as a promising noninvasive marker of glioma with a high diagnostic performance: A pooled analysis of 997 patients. *Therapeutic Advances in Medical Oncology, 13*, 1758835920987650. https://doi.org/10.1177/1758835920987650

[a]Zhao, Y., Li, X., Ye, C., Huang, C., Lv, X., & Li, J. (2023). The biogenesis, mechanism and function of the tRNA-derived small RNA (tsRNA): A review compared with microRNA. *American Journal of Cancer Research, 13*(5), 1656–1666.

[b]Zhao, Y., Ye, X., Xiong, Z., Ihsan, A., Ares, I., Martínez, M., Lopez-Torres, B., Martínez-Larrañaga, M. R., Anadón, A., Wang, X., & Martínez, M. A. (2023). Cancer metabolism: The role of ROS in DNA damage and induction of apoptosis in cancer cells. *Metabolites, 13*(7), 796. https://doi.org/10.3390/metabo13070796

[a]Zhou, F., Cao, W., Xu, R., Zhang, J., Yu, T., Xu, X., Zhi, T., Yin, J., Cao, S., Liu, N., Wang, Y., & Zhao, C. (2019). MicroRNA-206 attenuates glioma cell proliferation, migration, and invasion by blocking the WNT/β-catenin pathway via direct targeting of Frizzled 7 mRNA. *American Journal of Translational Research, 11*(7), 4584–4601.

Zhou, S. S., Jin, J. P., Wang, J. Q., Zhang, Z. G., Freedman, J. H., Zheng, Y., & Cai, L. (2018). miRNAs in cardiovascular diseases: Potential biomarkers, therapeutic targets, and challenges. *Acta Pharmacologica Sinica, 39*(7), 1073–1084. https://doi.org/10.1038/aps.2018.30

Zhou, Y., Tao, L., Qiu, J., Xu, J., Yang, X., Zhang, Y., Tian, X., Guan, X., Cen, X., & Zhao, Y. (2024). Tumor biomarkers for diagnosis, prognosis and targeted therapy. *Signal Transduction and Targeted Therapy, 9*(1), 132. https://doi.org/10.1038/s41392-024-01823-2

[b]Zhou, Y., Yang, L., Zhang, X., Chen, R., Chen, X., Tang, W., & Zhang, M. (2019). Identification of potential biomarkers in glioblastoma through bioinformatic analysis and evaluating their prognostic value. *BioMed Research International, 2019*, 6581576. https://doi.org/10.1155/2019/6581576

Zhu, H., Tang, L., Zhang, C., Wei, B., Yang, P., He, D., Zheng, L., & Zhang, Y. (2019). Synthesis of chalcone derivatives: Inducing apoptosis of HepG2 cells via regulating reactive oxygen species and mitochondrial pathway. *Frontiers in Pharmacology, 10*, 1341. https://doi.org/10.3389/fphar.2019.01341

Zienius, K., Chak-Lam, I., Park, J., Ozawa, M., Hamilton, W., Weller, D., Summers, D., Porteous, L., Mohiuddin, S., Keeney, E., Hollingworth, W., Ben-Shlomo, Y., Grant, R., & Brennan, P. M. (2019). Direct access CT for suspicion of brain tumour: An analysis of referral pathways in a population-based patient group. *BMC Family Practice, 20*(1), 118. https://doi.org/10.1186/s12875-019-1003-y

Zong, H., Parada, L. F., & Baker, S. J. (2015). Cell of origin for malignant gliomas and its implication in therapeutic development. *Cold Spring Harbor Perspectives in Biology, 7*(5), a020610. https://doi.org/10.1101/cshperspect.a020610

Appendices

Appendix 1. Continuous professional development

1.1. Attended workshops and seminars

- Patient and Public Involvement (PPI) Workshops – 23rd March 2023, 12th April 2023, 10th May 2023
- Travel Safety Awareness and Travel Risk Approver training – 12th June 2023
- Researcher Development Summer School Programme – 14th-16th September 2022
- How to Write a Scientific Paper (and get it accepted!) – 5th May 2022
- Maximise Your Memory – 17th April 2022
- Writer's Block and How to Overcome – 24th March 2022
- Reference Management – 23rd March 2022
- Creative Thinking and Problem Solving – 17th February 2022
- Registration and Doctoral Review Assessment – 16th February 2022
- The Viva and Process of Research Degree Examination – 3rd February 2022
- Literature Review – 20th January 2022
- RDP00041 NHS Ethics – 19th January 2022

1.2. Attended conferences and webinars

- 21st International Symposium on Pediatric Neuro-Oncology (ISPNO 2024), Philadelphia, US – 29th June – 2nd July 2024
- UH LMS Annual Research Conference, Hatfield, UK – 11th June 2024
- Berlin Early Cancer Forum, Berlin, Germany – 21st-22nd November 2023
- UH LMS Annual Research Conference, Hatfield, UK – 13th June 2023
- PGR Student Conference – Sustainability and Research, Hatfield, UK – 9th June 2023
- Illumina Webinar: Empower your Research with RNA sequencing (online) – 23rd May 2023
- RNA Microsymposium, Vienna, Austria – 3rd-5th May 2023
- 1st LMTKs International Virtual Meeting (online) – 28th April 2023
- 7th Annual Next-Gen Immuno-Oncology Conference, London, UK – 9th-10th March 2023
- The Festival of Genomics & Biodata, London, UK – 25th-26th January 2023
- Tri-Omics Summit Europe, London, UK – 18th-20th October 2022
- 4th Annual Biomarker and Companion Diagnostics Conference, London, UK – 6th-7th October 2022
- 54th Congress of the International Society of Paediatric Oncology, Barcelona, Spain – 28th September – 1st October 2022
- Cancer Research UK Brain Tumour Conference, London, UK– 5th-7th September 2022
- The RNA Isoform Landscape of Cancer (online) – 20th July 2022
- Cancer Genomics ONLINE - Webinar 1: Interrogating and targeting the complexities of the cancer genome (online) -5th July 202241
- UH LMS Research Conference, Hatfield, UK – 21st June 2022
- Liquid Biopsy ONLINE - Webinar 1: Liquid Biopsy: Where are we now? (online) – 16th June 2022
- UCL Cancer Domain Symposium, London, UK – 11th May 2022
- 6th Annual Next gen Immuno-Oncology Conference, London, UK – 10th-11th March 2022

Appendix 2. Publications and extended abstracts

2.1. Peer-reviewed journal publications

1. **Mustafov, D.**, Ahmad, M. S., Serrano, A., Braoudaki, M., & Siddiqui, S. S. **(2024)**. MicroRNA:Siglec crosstalk in cancer progression. *Current opinion in chemical biology*, *81*, 102502. https://doi.org/10.1016/j.cbpa.2024.102502

2. **Mustafov, D.**, Siddiqui, S. S., Kukol, A., Lambrou, G. I., Shagufta, Ahmad, I., & Braoudaki, M. **(2024).** MicroRNA-Dependent Mechanisms Underlying the Function of a β-Amino Carbonyl Compound in Glioblastoma Cells. *ACS omega*, *9*(29), 31789–31802. https://doi.org/10.1021/acsomega.4c02991

3. **Mustafov, D.,** Siddiqui, S. S., Klena, L., Karteris, E., & Braoudaki, M. **(2024)**. SV2B/miR-34a/miR-128 axis as prognostic biomarker in glioblastoma multiforme. *Scientific reports*, *14*(1), 6647. https://doi.org/10.1038/s41598-024-55917-6

4. Orton, S., Karkia, R., **Mustafov, D.,** Gharanei, S., Braoudaki, M., Filipe, A., Panfilov, S., Saravi, S., Khan, N., Kyrou, I., Karteris, E., Chatterjee, J., & Randeva, H. S. **(2024).** In Silico and In Vitro Mapping of Receptor-Type Protein Tyrosine Phosphatase Receptor Type D in Health and Disease: Implications for Asprosin Signalling in Endometrial Cancer and Neuroblastoma. *Cancers*, *16*(3), 582. https://doi.org/10.3390/cancers16030582

5. Ogbodo, A. K., **Mustafov, D.,** Arora, M., Lambrou, G. I., Braoudaki, M., & Siddiqui, S. S. **(2024).** Analysis of *SIGLEC12* expression, immunomodulation and prognostic value in renal cancer using multiomic databases. *Heliyon*, *10*(2), e24286. https://doi.org/10.1016/j.heliyon.2024.e24286

6. **Mustafov, D.,** Karteris, E., & Braoudaki, M. **(2023).** Deciphering the Role of microRNA Mediated Regulation of Coronin 1C in Glioblastoma Development and Metastasis. *Non-coding RNA*, *9*(1), 4. https://doi.org/10.3390/ncrna9010004

7. Braoudaki, M., Ahmad, M. S., **Mustafov, D.**, Seriah, S., Siddiqui, M. N., & Siddiqui, S. S. **(2022).** Chemokines and chemokine receptors in colorectal cancer; multifarious roles and clinical impact. *Seminars in cancer biology*, *86*(Pt 2), 436–449. https://doi.org/10.1016/j.semcancer.2022.06.002

2.2. Journal papers in press

1. **Mustafov, D.,** Siddiqui, S.S., Shagufta, Ahmad, I., Gkantalis, J., Rodriguez, P., Braoudaki, M. **(2024)**. New chalcone compound exhibits microRNA-mediated anticancer properties in glioblastoma. *In press*.

2. **Mustafov, D.,** Lambrou, G.I., Siddiqui, S.S., & Braoudaki, M. **(2024).** New kinder miRNA-based therapies shared between medulloblastoma and glioblastoma. *In press.*

2.3. Journal papers in preparation

1. Filipe, A., **Mustafov, D**., Panfilov, S., Bangar, S., Mousavikivaj, S., Savari, S., Sisu, C., Braoudaki, M., & Karteris, E. **(2024).** Investigation of *CIP2A,* its expression, its inhibition, and its impact on Ovarian cancer. *In preparation.*

2.4. Extended abstracts (peer-reviewed)

1. **Mustafov, D.,** Lambrou, G., Siddiqui, S.S., & Braoudaki, M. **(2024).** BIOM-11. Tumour suppressive roles of miR-206 and miR-383 via *CORO1C* and *SV2B* in aggressive paediatric and adult brain malignancies. *Neuro-Oncology*. 26. 10.1093/neuonc/noae064.030.

2.5. Book chapters

1. **Mustafov, D.**, Seriah, S., Malik, R., & Braoudaki, M. **(2022)**. MicroRNA Biomarkers in Primary Brain Malignancies. DOI:10.5772/intechopen.108386.

Appendix 3. Poster and oral presentations

3.1. Poster presentations

June 2024	**Mustafov, D.,** Lambrou, G., Siddiqui, S.S., & Braoudaki, M. Tumour suppressive roles of miR-206 and miR-383 via *CORO1C* and *SV2B* in aggressive paediatric and adult brain malignancies – ISPNO Conference, Philadelphia, US
June 2024	Serrano, A., **Mustafov, D.,** & Braoudaki, M. Elucidating the role of miR-217-3p/*REPS2* axis in childhood medulloblastoma – UH LMS Conference, Hatfield, UK
June 2024	Rodriguez, P., **Mustafov, D.,** & Braoudaki, M. Exploring microRNA expression signatures in glioblastoma cells upon treatment with a new chalcone – UH LMS Conference, Hatfield, UK
June 2023	**Mustafov, D.,** Siddiqui, S.S., & Braoudaki, M. MiR-21- and miR-128a-dependent regulation of *CORO1C* in glioblastoma cells upon treatment with a new carbonyl compound - UH PGR Conference, Hatfield, UK
April 2023	**Mustafov, D.,** Siddiqui, S.S., & Braoudaki, M. Downregulation of miR-21 and *CORO1C* in glioblastoma cells upon treatment with a new carbonyl compound - 17th Microsymposium on RNA Biology, Vienna, Austria
June 2022	**Mustafov, D.,** Karteris, E., & Braoudaki, M. The biological function of miR-128a and miR-21 in glioblastoma multiforme - UH LMS Conference, Hatfield, UK

3.2. Oral presentations

June 2024	**Mustafov, D.** Deciphering the microRNA pattern in the realm of high-grade brain malignancies – UH LMS Conference, Hatfield, UK
April 2024	**Mustafov, D.** New carbonyl compound leads to glioblastoma cell death through inhibition of miR-21 and *CORO1C* – University of San Francisco, Barcellos-Hoff Lab, San Francisco, US
November 2023	**Mustafov, D.** New carbonyl compound leads to glioblastoma cell death through inhibition of miR-21 and *CORO1C*" - Early Cancer Forum Berlin, Germany

Appendix 4. Awards and grants

June 2024	**Best Oral Presentation – Annual LMS conference UH**
March 2024	**Applied Microbiology International Society award - outstanding PhD Bioscience student**
November 2021-October 2024	**UH funded PhD studentship**
April 2024 April 2023 April 2022	**Funding Support for Conference Attendance from the UH Doctoral College**
June 2023	**Best Postgraduate Poster at UH PGR-conference**

Appendix 5. Ethics approval notification

University of Hertfordshire UH

HEALTH, SCIENCE, ENGINEERING AND TECHNOLOGY ECDA

ETHICS APPROVAL NOTIFICATION

TO	**Denis Mustafov**
CC	**Dr Maria Braoudaki**
FROM	**Dr Rosemary Godbold, Health. Science, Engineering and Technology ECDA**
DATE	**17/04/2024**

Protocol number:	aLMS/PGR/UH/05146(2)
Title of study:	Circulating miRNAs in central nervous system malignancies; functional role and clinical relevance.

Your application to modify and extend the existing protocol as detailed below has been accepted and approved by the ECDA for your School and includes work undertaken for this study by the named additional workers below:

No additional workers named

Modification:

As detailed in the EC2

General conditions of approval:

Ethics approval has been granted subject to the standard conditions below:

Original protocol: Any conditions relating to the original protocol approval remain and must be complied with.

Permissions: Any necessary permissions for the use of premises/location and accessing participants for your study must be obtained in writing prior to any data collection commencing. Failure to obtain adequate permissions may be considered a breach of this protocol.

External communications: Ensure you quote the UH protocol number and the name of the approving Committee on all paperwork, including recruitment advertisements/online requests, for this study.

Invasive procedures: If your research involves invasive procedures you are required to complete and submit an EC7 Protocol Monitoring Form, and copies of your completed consent paperwork to this ECDA once your study is complete.

Submission: Students must include this Approval Notification with their submission.

Validity:

This approval is valid:

From: 30/05/2024

To: 30/10/2024

Please note:

Failure to comply with the conditions of approval will be considered a breach of protocol and may result in disciplinary action which could include academic penalties.
Additional documentation requested as a condition of this approval protocol may be submitted via your supervisor to the Ethics Clerks as it becomes available. All documentation relating to this study, including the information/documents noted in the conditions above, must be available for your supervisor at the time of submitting your work so that they are able to confirm that you have complied with this protocol.

Should you amend any aspect of your research or wish to apply for an extension to your study you will need your supervisor's approval (if you are a student) and must complete and submit a further EC2 request.
Approval applies specifically to the research study/methodology and timings as detailed in your Form EC1A or as detailed in the EC2 request. In cases where the amendments to the original study are deemed to be substantial, a new Form EC1A may need to be completed prior to the study being undertaken.

Failure to report adverse circumstance/s may be considered misconduct.
Should adverse circumstances arise during this study such as physical reaction/harm, mental/emotional harm, intrusion of privacy or breach of confidentiality this must be reported to the approving Committee immediately.

Appendix 6. Relevant publications to work done in Chapter 2, Journal: *Non-coding RNA*

non-coding RNA

MDPI

Article

Deciphering the Role of microRNA Mediated Regulation of Coronin 1C in Glioblastoma Development and Metastasis

Denis Mustafov [1,2], Emmanouil Karteris [2] and Maria Braoudaki [1,*]

[1] School of Life and Medical Sciences, University of Hertfordshire, Hatfield AL10 9AB, UK
[2] College of Health, Medicine and Life Sciences, Brunel University London, Uxbridge UB8 3PH, UK
* Correspondence: m.braoudaki@herts.ac.uk

Abstract: Glioblastoma multiforme (GBM) is a highly heterogenic and malignant brain tumour with a median survival of 15 months. The initial identification of primary glioblastomas is often challenging. Coronin 1C (CORO1C) is a key player in actin rearrangement and cofilin dynamics, as well as enhancing the processes of neurite overgrowth and migration of brain tumour cells. Different bioinformatic databases were accessed to measure CORO1C expression at the mRNA and protein level in normal and malignant brains. CORO1C expression was observed in brain regions which have retained high synaptic plasticity and myelination properties. CORO1C was also expressed mainly within the hippocampus formation, including the Cornu Ammonis (CA) fields: CA1–CA4. Higher expression was also noticed in paediatric GBM in comparison to their adult counterparts. Pediatric cell populations were observed to have an increased log2 expression of CORO1C. Furthermore, 62 miRNAs were found to target the CORO1C gene. Of these, hsa-miR-34a-5p, hsa-miR-512-3p, hsa-miR-136-5p, hsa-miR-206, hsa-miR-128-3p, and hsa-miR-21-5p have shown to act as tumour suppressors or oncomiRs in different neoplasms, including GBM. The elevated expression of CORO1C in high grade metastatic brain malignancies, including GBM, suggests that this protein could have a clinical utility as a biomarker linked to an unfavorable outcome.

Keywords: CORO1C; mRNA; microRNA expression; brain; cancer; glioblastoma; pediatric; adult

check for updates

Citation: Mustafov, D.; Karteris, E.; Braoudaki, M. Deciphering the Role of microRNA Mediated Regulation of Coronin 1C in Glioblastoma Development and Metastasis. *Non-Coding RNA* **2023**, *9*, 4. https://doi.org/10.3390/ncrna9010004

Academic Editors: Hsiuying Wang and Y-h. Taguchi

Received: 2 December 2022
Revised: 28 December 2022
Accepted: 2 January 2023
Published: 4 January 2023

Copyright: © 2023 by the authors. Licensee MDPI, Basel, Switzerland. This article is an open access article distributed under the terms and conditions of the Creative Commons Attribution (CC BY) license (https://creativecommons.org/licenses/by/4.0/).

1. Introduction

1.1. Epidemiology and Molecular Characteristics

Presented with a 5-year survival rate of 5.6%, glioblastoma multiforme (GBM) remains one of the most aggressive and deadliest glial malignancies amongst adults [1]. The median onset of GBM is 64 years; however, the malignancy can occur at any age indiscriminatory [2]. GBM accounts for nearly 3350 newly diagnosed cases in the UK annually with an overall survival rate between 6–17 months. Proclaimed as an incurable brain tumour due to its infiltrative nature, complete surgical resection of the tumour burden is almost impossible, and thus inevitable progression of residual infiltrates enhance relapse and reoccurrence of the malignancy [3]. Postoperative radiotherapy and adjuvant chemotherapy with temozolomide are subsequently prescribed post tumour resection.

Paediatric glioblastomas (pGBM) possess distinctive molecular characteristics, which distinguish them from their adult counterparts. pGBM is a rare event accounting for 3–7% of all primary central nervous system (CNS) tumours in children [4]. The estimated median overall survival rate for paediatric GBM is 10.5 months, with children over 10 years of age being impacted more, due to a higher frequency of mutations detected when compared to younger children. A previous study on pGBM revealed that younger children had better overall survival outcomes [5]. Despite the fact that there is limited knowledge about the tumour microenvironment of paediatric GBM, the previous data demonstrated that this cohort of patients presented with significant alternations in mismatch repair (*MMR*)

genes, such as *MSH2* and *MSH6* [6]. Contradictive evidence regarding the isocitrate dehydrogenase 1 (*IDH1*) status in primary paediatric glioblastomas suggested that almost all cases within young children were *IDH*-wild type, whereas an adolescent's cohort with secondary paediatric GBM presented with an *IDH*-mutant molecular profile [7,8]. Despite the rarity of the malignancy, an exceptional study evaluating a cohort of 1173 pGBM could be subcategorised into several pathological entities based on the age of occurrence, diagnostics, molecular alternations, and location. These include paediatric high-grade glioma (PHGG), diffuse intrinsic pontine glioma (DIPG), and pediatric low-grade glioma (PLGG), with the latest being the most common type of CNS tumour found in children [9]. Gross resections of HGG have shown improved survival rates within patients, whereas such are unfeasible for DIPG due to the location of the tumour [10]. A further difference associated with the various survival rates within the pGBM population is the presence of *H3F3A* at the K27 mutation occurring in adolescents. This mutation defines a new subtype, diffuse midline glioma, which possesses distinct clinical and epigenetic profiles [11].

The undefined therapeutic approach for pGBM patients in comparison to their adult GBM counterparts has led to indistinguishable therapy routines, despite the inherent differences in their molecular profiles. However, radiation is often deferred for children's therapy, especially in infants, due to concerns for potential damage to the developing brain [12]. The location of pGBM also differs, with most tumours developing within the thalamus and brainstem leaving surgeons with limited routes for safe surgical resection [13].

1.2. MicroRNAs and Their Role in Glioblastoma Tumorigenesis and Diagnosis

MicroRNAs (miRNAs) are described as highly conserved, short, non-coding fragments of RNA (ncRNA) which constitute of around 22 nucleotides in length. Discovered nearly three decades ago, miRNAs are now recognised as post-transcriptional regulators for just over 60% of all protein-coding genes [14]. The biogenesis of miRNAs begins with post- or co-transcriptional processing of RNAse polymerase II/III [15]. Most intragenic miRNAs are transcribed from the introns of protein-coding genes, whereas very few are synthesised from the exons of such genes. Those miRNAs found to be intergenic have their own promoter regions and are transcribed autonomously to their host genes [16].

Validating miRNA biomarkers might provide a major advancement in the identification and treatment for brain cancer patients, with the hope they could predict how each patient's tumour is going to behave and respond to a particular targeted treatment. However, their clinical adaptation is still far from accepted, due to uncertainties in the experimental findings caused by the limited number of patient samples used in research [17]. Some miRNAs can act as tumour suppressors and others as oncogenes (oncomiRs). Detection of miRNA signatures in primary brain tumours has revealed unique avenues for assessing the diagnosis, prognosis, and monitoring of patients [18]. A systematic review has revealed that more than 300 miRNAs are affected in GBM tumorigenesis, with 253 being overexpressed and 95 under-expressed [19]. The short size of miRNAs allows them to bind imperfectly or complimentary to more than one mRNA and subsequently to regulate more than one target. It has been estimated that approximately 10,000 mRNAs can be regulated via this mechanism, allowing a single miRNA to be a direct or indirect target for multiple genes [20]. The deregulation of miRNAs in cancer is aided by different abnormalities in the biogenesis of miRNAs, such as amplification, deletion, epigenetic modification and silencing of miRNAs, translocation, and defective biosynthetic enzymes, that lead to either overexpression or downregulation.

Despite efforts made to combat deadly glioblastoma multiforme tumours, these types of brain cancers are still associated with poor prognosis and low overall survival rates. MiRNAs have demonstrated promising outcomes in their use as diagnostic, prognostic, and treatment agents. Elucidating aberrant miRNA expression in brain malignancies might provide novel biomarkers related to diagnosis, prognosis, and tailored therapy. For instance, miR-21 has been found to be overexpressed in many types of cancer, such as GBM, colorectal, and breast cancer. Nevertheless, miR-21 plays a pivotal role in the tumorigenesis of GBM

and is the only miRNA which has clearly defined diagnostic and prognostic properties to date. The levels of miR-21 drastically decrease post tumour resection, allowing the biomolecule to be used as a monitoring agent for patients and to detect early relapse [21]. Other miRNAs with potential diagnostic properties include miR-128 and miR-342-3p [22]. Previous research has confirmed the high analytical specificity and sensitivity of both, miR-21 and miR-128, in their use as diagnostic markers for GBM. For instance, Roth et al. (2011) demonstrated the significant downregulation of miR-128 in the peripheral blood samples of 20 GBM patients with an accuracy of 81%, and sensitivity and specificity of 79% and 81%, respectively [23].

1.3. Nanosensor-Based Diagnostic Approaches for GBM

Several approaches are currently incorporated in the diagnosis of GBM. Of these, magnetic resonance imaging (MRI) and computed tomography (CT) are of main use. A known drawback for these methods is that small tumour portions and infiltrations are hard to be detected [24]. Nanosensor-based diagnostic approaches offer a tailored way for the detection of GBM. For instance, molecular MRI utilises multifunctional iron oxide nanoparticles (IONP) which act as imaging agents for GBM and can be directly detected by MRI imaging [24]. These nanoparticles can also act as carriers of tumour-specific biomolecules. Polyethylene glycol (PEG) coated nanoparticles showed increased specificity of MRI contrast enhancement within GBM patients via the epidermal growth factor receptor variant III (EGFRvIII) antibody–IONP complex in vitro [25]. Even though nanosensor-based diagnostic approaches have shown promising results, the appearance of neurotoxicity from the application of nanoparticles remains a major concern. Thus, a careful consideration of unwanted side effects and the removal of nanoparticles from the brain should be comprehensively evaluated before their clinical utilisation.

1.4. Coronin 1C and Its Role in Glioblastoma Multiforme

Coronin 1C (CORO1C) has been shown to play a key role during the processes of migration and proliferation via its action upon actin rearrangement and cofilin dynamics. Potential miRNA tumour suppressors might aid helpfully in targeting *CORO1C*, rescuing its oncogenic phenotype. Previous research has identified that CORO1C is expressed significantly within migrating cells and its silencing demonstrated reduced proliferation and migration velocity within the glioblastoma cell lines A172 and U373 [26]. However, there is limited information on how CORO1C regulates these processes within glioblastoma patients. *CORO1C* was also found to be a direct target of miR-128a, showing upregulation when miR-128a was silenced [27]. However, the regulation of *CORO1C* via miRNAs is not fully examined and possible avenues for identifying novel miRNA targets exists.

The aforementioned existing differences between pediatric and adult glioblastomas' molecular profiles require new approaches for the diagnosis and treatment of the malignancy in different patient cohorts. Identifying a common, differentially expressed molecular biomarker for both pGBM and adult GBM could possibly aid in the early detection of GBM and provide a common therapeutic target.

In this in silico study, we sought to investigate the differential expression of the CORO1C protein across the brain profiles of paediatric and adult GBM patients. We demonstrated that the CORO1C mRNA expression was elevated within specific brain regions and within paediatric GBM patients, associated with highly aggressive brain neoplasms, suggesting that it potentially possesses oncogenic properties.

2. Results

2.1. CORO1C Normal Tissue Distribution

Figure 1 represents the mRNA expression profile of *CORO1C* within normal tissues. Specifically, in Figure 1a, the highest expression measured in normalized transcripts per million (nTPM) was detected in smooth muscle tissue (276.6 nTPM), followed by the endometrium (229.5 nTPM), urinary bladder (180.8 nTPM), adipose tissue (168.1 nTPM),

and lung (133.8 nTPM). When brain tissue and its associated regions were assessed separately, an average distribution of *CORO1C* of 39.2 nTPM across all regions was noted (Figure 1b). High expression of *CORO1C* mRNA was observed within the white matter (53.4 nTPM), followed by the medulla oblongata and hippocampal formation (43.9 and 41.3 nTMP, respectively). Single-cell analysis of the brain illustrated that *CORO1C* was highly expressed within neuronal cells. The glial cluster comprising of astrocytes, oligodendrocytes, oligodendrocyte precursor cells, and microglial cells revealed that CORO1C was highly expressed within all types of glial cells except for astrocytes (Figure 1c).

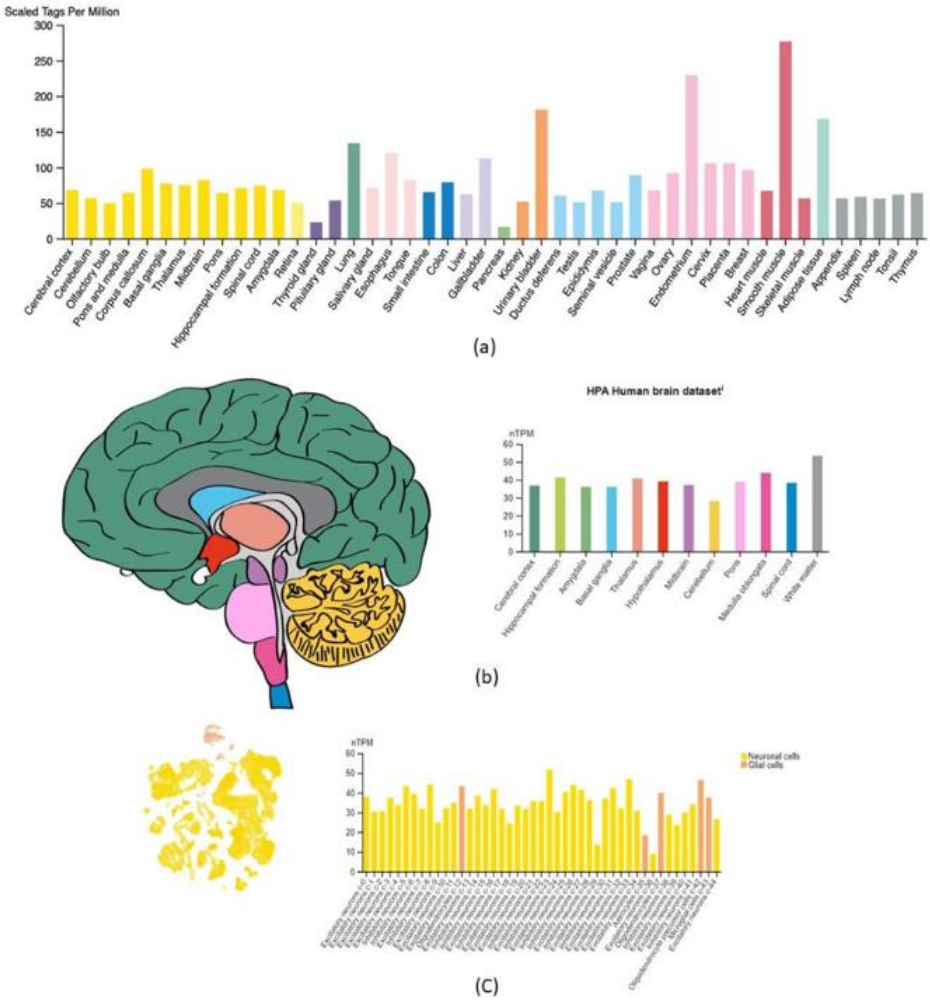


Figure 1. Detection of *CORO1C* mRNA across normal tissue types and brain [28,29]. (**a**) The Human Protein Atlas database was incorporated to examine the detection of *CORO1C* mRNA expression within different tissue types. Higher expression was observed within smooth muscle tissue, endometrium, urinary bladder, adipose, and lung tissues. (**b**) The average distribution of *CORO1C* mRNA throughout the brain demonstrated that the protein was highly expressed in the white matter, medulla oblongata, and hippocampal formation regions of the brain. (**c**) Single-cell cluster analysis obtained from normal brain tissue demonstrated high expression of *CORO1C* amongst neuronal cells, oligodendrocytes, oligodendrocyte precursor cells, and microglial cells.

2.2. CORO1C Regional Localization

The expression of CORO1C within the different brain regions of six patients was also evaluated via heatmaps of log2 expression values obtained using microarrays. High ex-pression of CORO1C is noticed within the hippocampal formation region of the brain. Figure 2 represented the Magnetic Resonance Imaging (MRI) scans and heatmaps from six healthy individuals who have succumbed from causes other than brain tumors. Ex-pression was mainly present across the CA1 (log2 expression 7.2 ± 2.5 and 7.5 ± 2.5), CA2 (log2 expression 7.7 ± 2.5), CA3 (log2 expression 7.0 ± 2.5), and CA4 (log2 expression 6.7 ± 2.5) fields, which are parts of the hippocampus. As observed in the heatmaps, high expression levels of CORO1C were also observed within the myelencephalon region of the brain (log2 expression 6.5 ± 2.5).

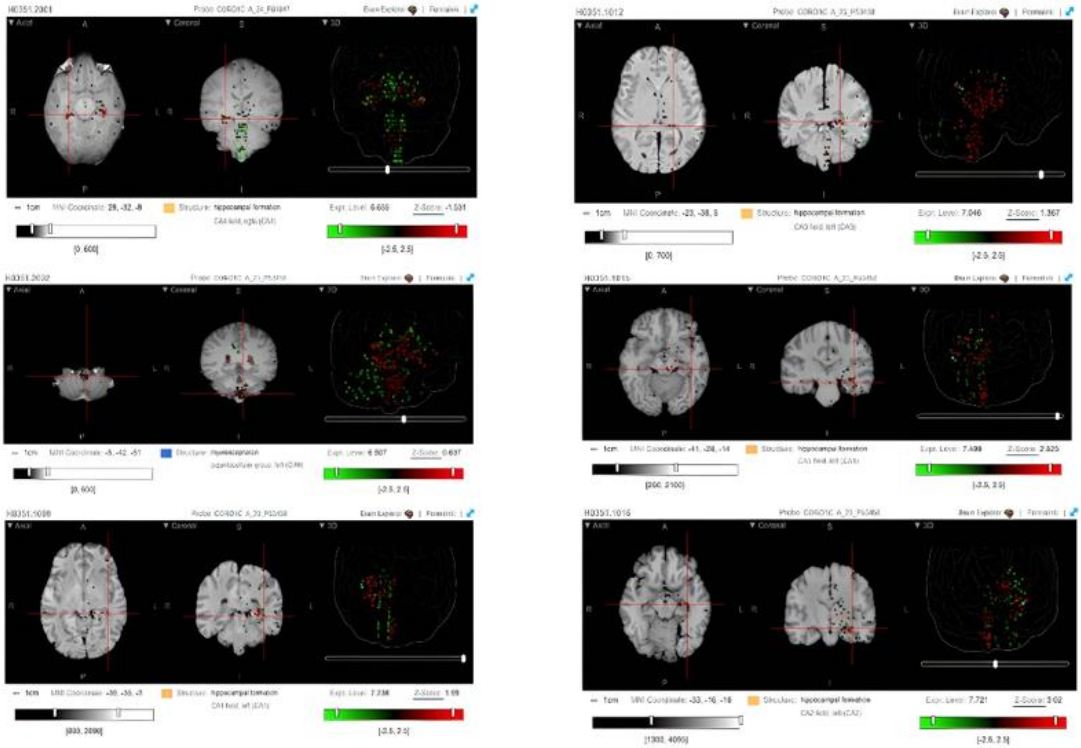


Figure 2. Heatmaps of log2 expression values of six patients obtained from microarrays experiments (Allen brain atlas). The Allen brain atlas database revealed that CORO1C is highly expressed within the hippocampal formation and myelencephalon regions of the brain [30].

2.3. CORO1C within Various Cancer Types

Figure 3 represented RNA-seq data available to the TCGA database to identify the degree of specificity of CORO1C in diverse cancer types. The RNA-seq data was expressed in a median number of fragments per kilobase of exon per million reads (FPKMs). Amongst the 17 different cancer types, the FPKM median expression was highest in head and neck cancers and gliomas, 33.4 FPKMs and 33.2 FPKMs, respectively. CORO1C expression determined by RNA-seq was also high in melanoma cancer, 32.3 FPKMs. Further analysis of CORO1C expression within normal and cancerous brain samples confirmed that CORO1C was significantly overexpressed within the brain tumour cohort, $p < 0.01$ (Figure 3b).

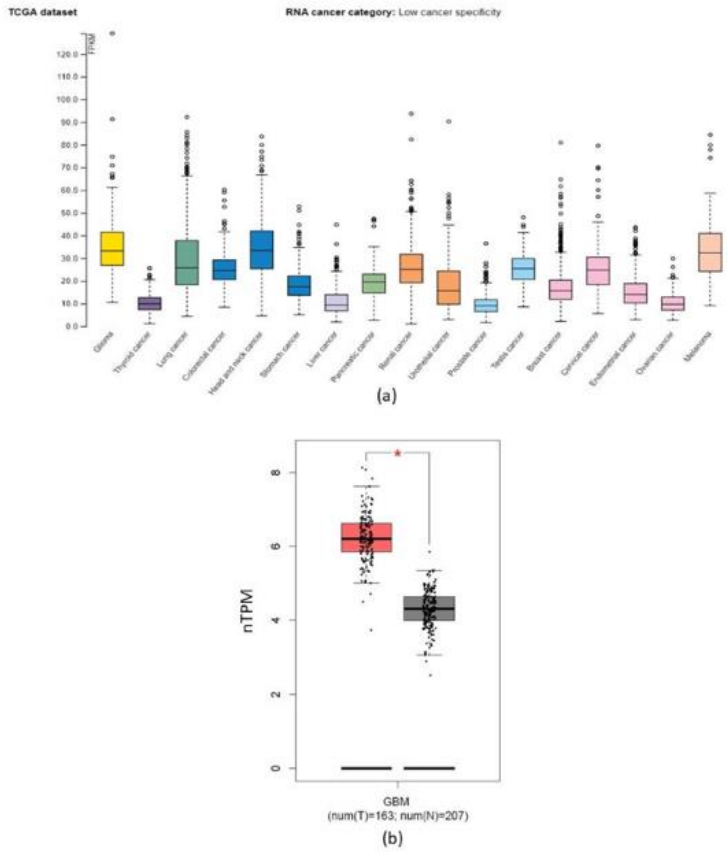


Figure 3. Expression of *CORO1C* in various cancerous tissues. (**a**) *CORO1C* expression across 17 cancer types revealed that the gene was highly expressed in head and neck cancer, gliomas, and melanomas. (**b**) *CORO1C* was significantly upregulated in GBM tumour samples (red) in comparison to normal brain tissue (grey) (One way ANOVA, * $p < 0.01$).

2.4. *CORO1C* Comparative Analysis of Expression between Paediatric and Adult GBM Cohorts

The expression of CORO1C based on patients' ages is illustrated in Figure 4a. Three GBM age groups ranging from 21–80 years of age had significantly increased CORO1C total protein expression levels when compared to normal patient samples. The highest significance was observed between normal samples versus the GBM age group 41–60 years, followed by the age groups 21–40 years and 61–80 years, respectively. Panel 4B provided a deeper insight on the expression levels of CORO1C within paediatric GBM samples. The age groups of 0–9 years, 10–19 years, and 20–19 years had higher median expression of CORO1C when compared to their counterparts at age $\geq$ 30 years (49.3 nTPM, 52.6 nTPM, 66.0 nTPM in comparison to 47.9 nTPM, respectively). However, no significant difference was observed. The expression of CORO1C in different types of paediatric brain malignancies is shown in Figure 4c. The highest median expression of the protein was detected in neurofibroma, chondroma, schwannoma, PHGG, and DIPG (70 nTPM, 69.4 nTPM, 68.0 nTPM, 62.8 nTPM, and 60.7 nTPM, respectively). This reached significance in neurofibromas only, when compared to PHGG. The overall expression levels of CORO1C within PLGG, DIPG, CRANIO, PTEN, ES, DNT, and CPP paediatric brain cancer subtypes were significantly lower in comparison to the expression of the protein found in HPGG.

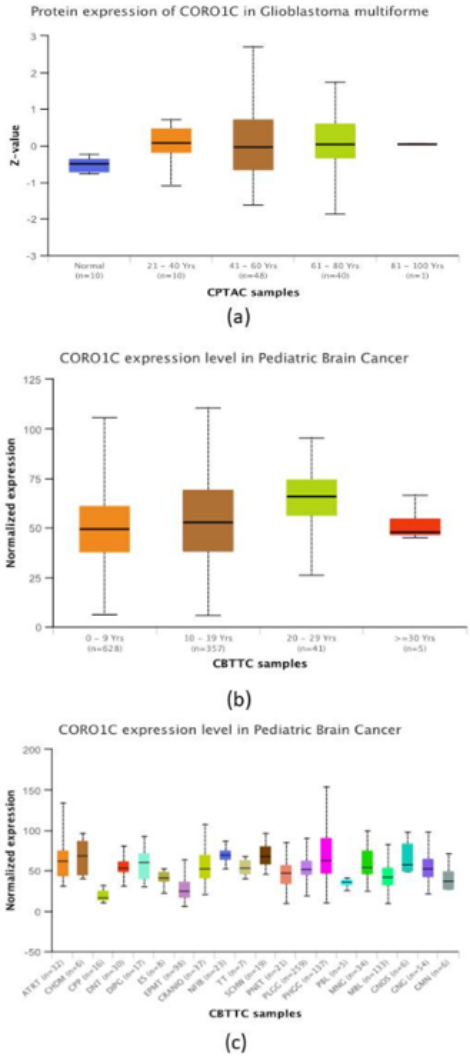


Figure 4. UALCAN comparative analysis of the expression of CORO1C within adult and paediatric glioblastoma patients. (**a**) Significantly high total protein levels of CORO1C were observed in all age groups compared to a normalised sample, except age group 81–100 years (normal versus age 21–40 years, $p < 6.015973 \times 10^{-3}$; normal versus age 41–60 years, $p < 4.724525 \times 10^{-4}$; normal versus age 61–80 years, $p < 1.753039 \times 10^{-3}$). (**b**) CORO1C expression was higher in age groups 0–9 years, 10–19 years, and 20–29 years in comparison to their counterparts at age ≥ 30 years of age. However, there was no statistical significance of expression between the different age groups. (**c**) Neurofibroma, chondroma, schwannoma, PHGG, and DIPG showed highest expression levels of CORO1C. Neurofibromas had significantly higher expression of CORO1C in comparison to PHGG ($p < 3.217085 \times 10^{-2}$). PLGG, DIPG, CRANIO, PTEN, ES, DNT, and CPP subtypes have significantly lower expressions of CORO1C in comparison to PHGG (PLGG versus PHGG, $p < 2.50863678369934 \times 10^{-7}$; DIPG versus PHGG $p < 3.535811 \times 10^{-3}$; CRANIO versus PHGG $p < 5.516405 \times 10^{-3}$; PTEN versus PHGG $p < 2.994696 \times 10^{-3}$; ES versus PHGG $p < 5.98540311685281 \times 10^{-8}$; DNT versus PHGG $p < 1.163218 \times 10^{-2}$; CPP versus PHGG $p < 1.75021275936207 \times 10^{-18}$).

2.5. CORO1C Single-Cell Expression Analysis in Various GBM Cell Clusters

The different types of cell clusters obtained from 28 individuals spanning both adult and paediatric GBM cohorts included macrophages, T-cells, malignant cells, and oligodendrocytes. In Figure 5a, the tSNE heatmap showed CORO1C expression within the left half of the malignant cell cluster, almost exclusively across the macrophage cluster and centre of the oligodendrocyte cell cluster. Limited expression was observed in the T-cell cluster. The expression of the protein was between log2 of 4 and log2 of 8 in these areas. A comparison between 8 paediatric cell populations and their 20 adult counterpart cell populations was performed as shown in Figure 5b. Expression of CORO1C within the paediatric cluster was higher, ranging between log2 of 6 and log2 of 8, when compared to cells from the adult cluster. The results revealed that paediatric cells occupied the left side of the malignant cell cluster, almost entirely the macrophage cluster and the centre of the oligodendrocyte cell cluster, an observation stated above regarding the increased log2 expression of CORO1C within these regions of the clusters. The expression of CORO1C was evaluated via the two-dimensional representation of each cellular state, including astrocyte like (AC-like), oligodendrocyte precursor cells (OPC-like), mesenchymal like (MES-like), and neural-progenitor-like cells (NPC-like). The heatmap of the log2 expression in Figure 5c revealed that CORO1C was expressed globally across all cellular states with an expression level of more than 4 logTPM. The expression of the protein within the NPC-like state was slightly higher in comparison to the rest of the cellular states: more than 6 logTPM, respectively.

2.6. miRNA Targets and Physical Interactions of CORO1C

Four databases were incorporated in finding common target miRNAs for the CORO1C gene, including miRSystem, TargetScan, miRWalk, and ENCORI. The results presented in the form of a Venn diagram shown in Figure 6 demonstrated that there were 62 (2.6%) common miRNA targets when all four miRNA analysis tools were used. Some of these common miRNAs included downregulation of hsa-miR-34a-5p, hsa-miR-128-3p, miR-9p, and miR-181a/b/d-5p and upregulation of hsa-miR-221-3p, hsa-miR-125p, and hsa-miR-21-5p and sha-miR-141-3p in glioblastomas. All six miRNAs have been previously shown to play key functions in glioblastomas. Also, miR-133a-3p and miR-206 were found overexpressed in the majority of the cancer types screened. The full list of all 62 miRNAs can be found in Supplementary Table S1.

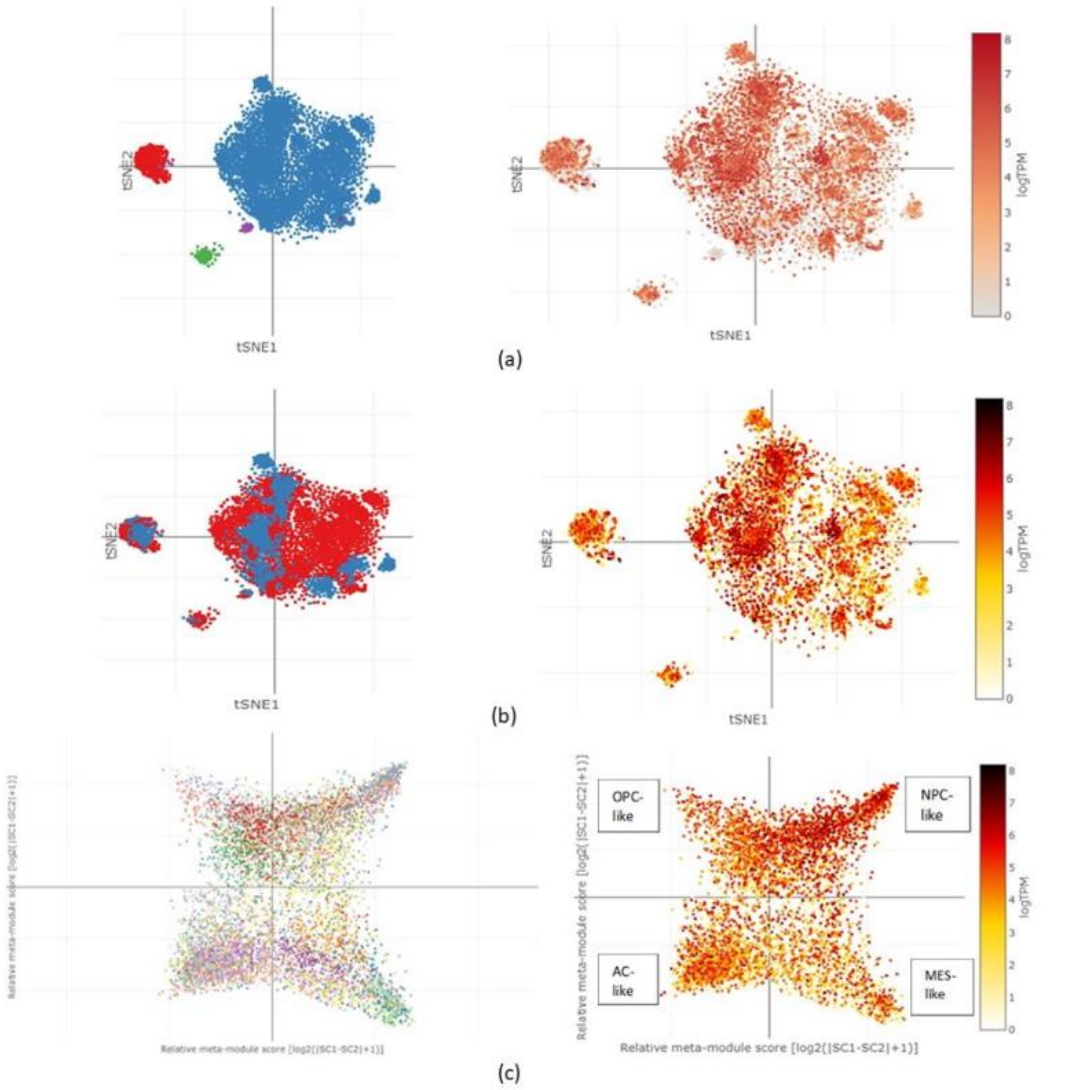


Figure 5. Single-cell analysis of glioblastoma cell clusters from paediatric and adult patients. (**a**) tSNE heatmap showed CORO1C expression within the left half of the malignant cell cluster (blue), almost exclusively across the macrophage cluster (red) and centre of the oligodendrocyte cell cluster (green). Little or no expression was observed within the T-cell cluster (purple). (**b**) Expression of CORO1C within the paediatric cluster (blue) was higher, ranging between log2 of 6 and log2 of 8, when compared to cells from the adult cluster (red). (**c**) Expression of CORO1C within astrocyte like (AC-like), oligodendrocyte precursor cells (OPC-like), mesenchymal like (MES-like), and neural-progenitor-like cells (NPC-like) demonstrated global expression across all cellular states with NPC-like state showing slightly higher expression of the protein (>log2 of 6).

miR-21-5p	↑
miR-221-3p	↑
miR-133-3p	↑
miR-128-3p	↓
miR-9-5p	↓
miR-206	↓

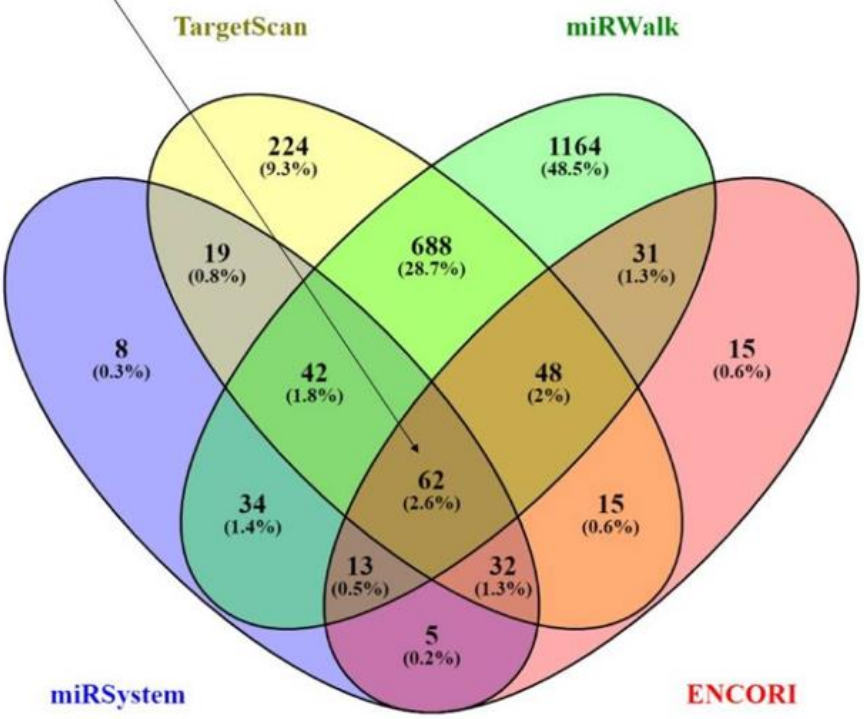


Figure 6. miRNA gene targets for *CORO1C* and physical interactions of *CORO1C* and other genes. Venn diagram incorporating miRSystem, TargetScan, miRWalk, and ENCORI databases. In total, 62 miRNAs were found to overlap between the 4 miRNA analysis tools (2.6%). Of these, miR-133-3p, hsa-miR-206, and miR-128-3p have been shown to be associated with *CORO1C* gene expression in different types of neoplasms.

3. Discussion

The oncogenic properties of CORO1C have been described in several types of cancer, including colorectal and liver cancers, non-small cell lung carcinoma, and melanomas [31–34]. The regulation of actin dynamics is essential for some disease states, including migration, cell polarity, signal transduction, and intracellular trafficking. Coronins are a family of highly conserved proteins that play an important role in cell motility and vesicle trafficking. *CORO1C* is a serum-induced gene and external stimuli, such as serum and growth factors, could up-regulate the transcriptional activation of the gene. However, little is known about the exact molecular mechanism that leads to increased transcriptional events. The gene product has emerged as a key player in actin rearrangement and cofilin dynamics via its

effects upon the assembly of actin-related proteins 2/3 (Arp2/3). Previous evidence has revealed that CORO1C exerts its effects via F-actin turnover during the processes of neurite overgrowth and migration of brain tumour cells [35]. The expression of *CORO1C* in astroglia cells and tumour cells is related to migrative and proliferative phenotypes. High levels of the protein are also associated with an increased grade of the malignancy, whereas neurons in the cortex of the brain show no significant expression of *CORO1C* [36]. The aim of this study was to in silico analyse the expression profiles of CORO1C in glioblastomas and to identify its diagnostic or prognostic potential.

Our results demonstrate that the average distribution of CORO1C throughout the brain was highest within the white matter, medulla oblongata, and hippocampal formation regions of the brain. CORO1C was also expressed amongst neuronal cells, oligodendrocytes, oligodendrocyte precursor cells, and microglial cells. Our results regarding the regional distribution of CORO1C, assessed by the Allen brain atlas also suggested overexpression of CORO1C within normal brain tissue, was present mainly in the hip-pocampal formation region of the brain, including the CA1-CA4 fields. Hippocampal pyramidal neurons and Purkinjean cells were shown to retain high levels of CORO1C during murine brain development. This feature enhanced a high level of synaptic plasticity which is inevitably linked to the processes of learning and memory [27]. CORO1C expression is also linked to the process of myelination, hence its high mRNA expression observed within the white matter, followed by the medulla oblongata and hippocampal formation. The localised expression of CORO1C suggested that the protein played an important role in differentiation, migration, the formation of neurites, and myeline sheets in oligodendrocytes [37]. Hasse et al. (2005) carried out in vitro experiments with neuro-2a and PC-12 cells transfected with GFP-tagged CORO1C versions. The team concluded that full-length CORO1C localised and supported outgrowing neurites, whereas truncated forms of the protein acted as suppressors for neurite formation. Thus, CORO1C appears to play a major role in the morphogenesis of neuronal cells [38]. The primary location of pGBM formation, the supratentorial brain, is found in close proximity to the CA fields. This is in line with our findings suggesting an elevated expression of CORO1C within areas near to the supratentorial region. On the other hand, adult GBM neoplasms are commonly found in cerebral hemispheres, especially in the frontal and temporal lobes of the brain. Our results did not show differential expression of CORO1C within these regions, suggesting that CORO1C levels might be elevated in pGBM cases due to their regional distribution. These findings might serve as a guidance for the clinical diagnosis of pGBM cases.

In the current study, overexpression of CORO1C in both adult and pediatric glioblastomas was observed. This is in line with Thal et al. (2008), who demonstrated high ex-pression of CORO1C in diffuse gliomas. They specifically showed that in normal brain tissue, the expression of CORO1C in cortex neurons was significantly reduced, whereas high grade benign brain neoplasms expressed increased levels of the protein. Thus, the expression of CORO1C is possibly dependent on tumour type and grade [36]. An experimental setting comprised from both in vitro and in vivo studies, demonstrated that CORO1C could promote glioma growth via the Wnt/β-catenin signalling pathway [39]. The overexpression of CORO1C in aggressive solid tumours such as glioblastomas and head and neck cancers are often associated with its metastatic powers [33]. In associations between 17 cancer types, the "crown-like" protein has exhibited the highest expression in head and neck cancers and gliomas. Nevertheless, it is not yet exclusively clear how CORO1C could enhance the metastatic and proliferative properties of GBM. Similar expression profiles have been observed in other types of malignancies. For instance, high expression of CORO1C has been observed in melanomas when compared to normal skin tissue. Specifically, evidence demonstrated that increased levels of the mRNA were found in BRAF mutant melanomas with high phosphor-Erk levels [31]. The frequent up- or down-regulation of CORO1C observed in microarray experiments of different cancer types, such as in glioblastomas and colorectal cancer (CRC) suggested that the protein is highly transcriptionally dynamic. As a member of a conserved protein family, the actin-binding

CORO1C has been shown to interact with trophoblast cell surface protein 2 (Trop2) in colorectal cancer [32]. Trop2 is an oncogenic protein that plays a vital role in stimulating the aggressive behavior of CRC. In the same research, it was also suggested that the overexpression of CORO1C in CRC patients was associated with lymph metastasis, distant metastasis, venous invasion, and perineuronal invasion. These findings suggested that elevated CORO1C might act as a prognostic factor for early metastasis events in different types of neoplasms and its clinical utilization as such could be beneficial for the early detection of metastatic formations.

The results obtained from UALCAN revealed that CORO1C was significantly overexpressed within patient groups in comparison to their normal counterparts, apart from the 81–100 years age group samples. However, a limitation of the study is that this age group is comprised from a limited number of patients. A comparison of the expression level of CORO1C within paediatric and adult GBM patients was also performed and differences were observed between younger ages and the > 30 years of age group; however, these did not reach significance. Previously, large molecular profiling studies have pointed out distinct molecular landscape differences between paediatric and adult glioblastomas [40,41]. Key driver epigenetic mutations within isocitrate dehydrogenase (*IDH1*) are classed as causative in adult GBM, and alterations in the *TP53*, *TERT*, and *ATRX* genes act as common prognostic and therapeutic targets. Unlike their adult counterparts, paediatric patients with GBM are likely to present with cancer predisposition syndromes, such as mismatch repair deficiency syndrome (CMMRD) [42]. A variety of malignant neoplasms are characteristic for children with CMMRD, including brain, gastrointestinal tract, and haematologic malignancies with a median onset of 7.5 years of age [43]. The difference between paediatric and adult GBM levels of CORO1C expression might be caused due to the high degree of neuronal plasticity found in children's developing brains. Another factor might be the high tumour mutational burden, which is characteristic for children with CMMRD. In most cases, such paediatric patients benefit from immune therapies, which commiserates the urgent need of early diagnostic and prognostic biomarkers.

A CBTTC dataset of the expression of CORO1C in different paediatric brain tumours depending on their histologic subtype was also incorporated in this research. Based on our results, the significantly highest median expression of the protein was obtained in the neurofibroma when compared to PHGG. Neurofibromas are benign nerve sheath brain tumours that grow on nerve cells and form soft bums under the skin [38]. Nevertheless, this type of benign malignancy has the potential to metastasize across the head and neck, and skin regions [44]. As aforementioned, CORO1C levels remain high in regions of myelination and differentiation. This finding is in agreement with the analysis using The Cancer Atlas dataset, which also revealed that the expression of CORO1C was highest in head and neck cancers, followed by gliomas and melanomas. The presence of CORO1C amongst these neoplasms might aid a possible poor prognostic biomarker associated with the metastatic capacity of the tumour and its spread. Other paediatric histological neoplasms, such as LGG, craniopharyngiomas, dysembryoplastic neuroepithelial tumours (DNT), and choroid plexus papilloma (CPP) are examples of lower grade brain tumours that grow slowly and are benign in most cases. The mRNA expression of CORO1C in these malignancies was significantly lower when compared to the highly malignant HGG neoplasms. This further supported the evidence that CORO1C could be exponentially expressed in tumours with malignant and invasive properties and hence could serve as a biomarker associated with an unfavorable prognosis. Furthermore, the presence of increased CORO1C levels within highly malignant pGBM cases correlates with the fact that the protein is expressed in brain regions with high synaptic plasticity. The factors concerning brain development and plasticity during childhood might serve as a possible explanation why CORO1C levels were found to be elevated in pediatric patients when compared to their adult counterparts. These findings could potentially improve the distinguishment of highly malignant tumors at an earlier stage and improve a patient's prognosis.

The single-cell RNA-sequencing dataset generated by Neftel et al. (2019) allowed the detection of CORO1C within different cell clusters obtained from individuals spanning both adult and paediatric patient cohorts [45]. CORO1C expression was evaluated amongst the intra-tumoral, heterogenic malignant cells obtained from all patients. Limited expression was noticed in the T-cell cluster. Glioblastoma tumours act as suppressors of the innate and adaptive immune systems [46]. The absence of CORO1C across the T-cell cluster might be explained by the fact that GBM neoplasms suppress T-cells, allowing neoplastic cells an immune-checkpoint escape and further proliferation. As CORO1C is required for the normal migration and proliferation of cells aiding its actin-binding properties and its involvement in the formation of neuronal lamellipodia, the presence of the protein within migrating malignant GBM cells is expected to be increased. Except for their supportive role within the brain, glial cell subtypes, such as microglial cells, are involved in the constant screening of the parenchyma of the brain [47,48]. Their dynamic action requires frequent cytoskeletal rearrangements, aided in part by CORO1C. Thus, the increased expression of CORO1C in brain microglial cells is expected, and observed in our findings. When the filter of the clusters was adjusted to show adult and paediatric cell populations, it became apparent that the paediatric cell population occupies the left side of the malignant cell cluster, almost entirely the macrophage cluster, and the centre of the oligodendrocyte cell cluster, an observation stated above regarding the increased log2 expression of CORO1C within these regions of the clusters. The high expression of CORO1C during brain development demonstrated specific expression patterns that correlated with our findings and supported the higher expression of the protein in paediatric patients when compared to their adult counterparts.

When the expression of CORO1C was evaluated via the two-dimensional representation of each cellular state, including AC-like, OPC-like, MES-like, and NPC-like, the heatmap of log2 expression demonstrated that CORO1C was expressed globally across all cellular states with an expression level of more than 4 logTPM. However, the expression of the protein within the NPC-like state was slightly higher in comparison to the rest of the cellular states. The increased expression of CORO1C in NPC-like cells was supported by the fact that these cells give rise to many, if not all, glial and neuronal cells found across the CNS; thus, they can differentiate. There is evidence that glioblastoma cells influence the migration of NPC-like cells towards the tumour site and enhances the expression of transformed phenotypes [34]. Though, not much is known about the process of communication between NPC-like cells and glioblastoma tumour cells [45].

The role of miRNAs hasn regulating the expression of CORO1C in different malignancies provides a novel way of targeting the deregulated expression of the gene and its protein product. A Venn diagram was generated using common target miRNAs from four miRNA bioinformatic tools. These included downregulation ofhasa-miR-128-3p, miR-9-5p, and miR-133a-3p and upregulation of hsa-miR-221-3p, hsa-miR-206, and hsa-miR-21-5p. All six miRNAs have been previously shown to play key functions in glioblastomas [49–55].

miR-128 was shown to possess an oncogenic property within breast cancer patients via enhancing proliferation and migration, and inhibiting apoptosis [56]. On the contrary, miR-128 has also been found downregulated in other types of malignancies, including glioblastomas and bladder cancer [57]. Restoring the normal levels of the brain-specific miR-128 within GBM has indicated tumor suppressive effects mediated through an interaction with the E3F3a and BMI1 genes and reducing the levels of proliferation and invasiveness [49]. Previously, CORO1C was found to be a direct target of miR-128a, and the protein product of the gene was subsequently enhanced when miR-128a was downregulated in GBM [58]. To the best of our knowledge, this is the only study that has previously identified an association between miR-128 and CORO1C by screening only a limited number of GBM patients. Overexpression of miR-128 was found to decrease the proliferative properties of NPC-like cells and drive their differentiation into neurons [58]. These findings, confirmed both in vitro and in vivo, suggested that miR-128 is an important player in the developing neocortex. This is in line with our findings, which showed high

expression of CORO1C within NPC-like cells obtained from GBM cell clusters. Thus, restoring the miRNA expression profile of miR-128a could potentially cease the activity of the gene product and the invasive potential of GBM cells via its interaction with CORO1C. The processes of cell cycle progression, cell transduction, and migration afforded possible pathways via which the gene might exert its tumorigenic potential. Hence, CORO1C might provide an effective therapeutic approach for GBM patients.

miR-9 has been found to possess dual tumour suppressive and promoting properties in different cancer tissues. For instance, miR-9 might act as an oncomiR in non-small cell lung cancers via its effects upon inhibiting E-cadherin [59]. Low expression of miR-9-5p has been associated with poor prognosis within GBM patient cohorts and thus could serve as a prognostic biomarker [50]. The overexpression of miR-9 in the glioblastoma cell lines U87MG and U251 revealed induction of apoptosis, reduced migration, and invasion within the cells [60]. Furthermore, elevated levels of miR-9-5p were shown to inhibit glioma proliferation by downregulating FOXP2 [61]. An interaction between miR-9-5p and CORO1C has been observed but not demonstrated in osteosarcoma pathogenesis [62]. To the best of our knowledge, currently, there is no evidence available directly linking miR-9-5p and CORO1C in glioblastoma cases. Yet, one can hypothesize that overexpression of miR-9-5p could influence CORO1C and cease its migratory properties.

Low levels of miR-133 were detected within GBM patient samples when compared to matched normal brain tissues [51]. Through in vitro experiments, Xu et al. (2015) demonstrated that the overexpression of miR-133 limited the growth of GBM cells and induced their apoptosis. This is in agreement with previous research indicating a similar role of miR-133a-3p and its interaction with CORO1C in hepatocellular carcinomas [63]. Specifically, it has been identified that overexpression of miR-133a-3p promoted apoptosis in hepatocellular carcinoma cells. Hence, this miRNA probably acted as a tumour suppressor and could potentially serve as a therapeutic target for this type of cancer. The direct interaction of miR-133-3p and CORO1C has not been previously evaluated to the best of our knowledge and this might potentially give rise to further research. On the other hand, there is evidence for the negative regulation of miR-206 in GBM patients upon its direct target Frizzled 7 (FZD7) [52]. Zhou et al. (2019) demonstrated that miR-206 has an inhibitory effect on the Wnt/β-catenin pathway by downregulating FZD7. The role of CORO1C in GBM was directly linked to the β-catenin growth dependent mechanism as part of the Wnt/β-catenin signaling pathway. Thus, restoring the levels of miR-206 to normal might have a potential therapeutic effect by ceasing migration and invasion processes. Demonstrated repressed proliferative and invasive properties of miR-206 within the non-small cell lung carcinoma (NSCLC) cell line A549 suggested that the overexpression of CORO1C was suppressed [64]. Even though this study provided a possible mechanism for a future therapeutic approach in targeting CORO1C in NSCLC, little is known about any induced metastatic properties of CORO1C in this type of cancer.

The aberrantly expressed miR-21-5p has been clearly defined as a diagnostic and prognostic biomarker for GBM. Several studies showed that miR-21 has an up-regulated profile in different types of cancer, including colorectal, prostate, and lung cancers, indicating its role as an oncomiR [65–68]. A rise in miR-21-5p was observed to increase the migration and invasion potential of glioma cells via increasing SOX2 expression [53]. Lou et al. (2017) showed that when the activity of miR-21-5p was suppressed and when SOX2 was inhibited, the beta-catenin levels decreased, leading to diminished invasiveness and migration. Subsequently, miR-21-5p has a direct effect upon the level of β-catenin. The association of CORO1C and miR-21 has not been well defined; however, acknowledging their involvement in the Wnt/β-catenin pathway initiates a possible avenue for research.

The overexpressed miRNA-221 acts as an oncomiR across diverse cancer types, including glioblastomas, gastric, bladder, and lung cancers [69,70]. Significantly high plasma levels ($p = 0.0001$) of miR-221/222 in glioma patients were associated with the degree of glioblastoma infiltration and a poorer overall survival within 95% of the studied cohort [54]. Possible molecular mechanisms via which the miR-221-3p acted during glioblastoma onco-

genesis involve promoting the S-phase of the cell cycle, inhibiting apoptosis, or regulating the invasiveness and proliferation of the cancer. However, the association of miR-221-3p and CORO1C and their occurrence in tandem with GBM has not yet been well defined to the best of our knowledge.

4. Materials and Methods

The Human Protein Atlas (HPA) (https://www.proteinatlas.org/ accessed on 30 September 2022) was incorporated to analyse the mRNA expression levels of *CORO1C*. HPA-RNA-seq data was used to demonstrate normal tissue expression of *CORO1C* across different tissue types measured in normalised transcripts per million (nTPM). The tool was also used to generate data of *CORO1C* mRNA expression across 17 different types of cancer. The data was obtained via The Cancer Genome Atlas (TCGA) database and was measured in a number of fragments per kilobase of exon per million (FPKM). A bar chart of a normal neuronal cell cluster was also available at the HPA. mRNA expression of *CORO1C* was measured in nTPM within individual brain cell clusters.

Visualisation of CORO1C expression across six brain donors (NM_014325.2) was performed via using the Allen brain atlas (https://portal.brain-map.org/ accessed on 30 September 2022). The results were presented as heatmaps of log2 expression. The data demonstrated in Figure 2 is publicly available from The Allen brain atlas. The UALCAN database (http://ualcan.path.uab.edu/ accessed on 30 September 2022) was incorporated to assess the different mRNA expressions of CORO1C amongst different GBM age groups and several paediatric brain phenotypes (CBTTC: https://pedcbioportal.kidsfirstdrc.org/study/summary?id=phgg_cbttc accessed on 30 September 2022. The single-cell portal was used to assess the log2 expression of CORO1C within 28 GBM cases (GSE131928), among of which there were 8 from a paediatric cohort and 20 from an adult cohort (https://singlecell.broadinstitute.org/single_cell accessed on 30 September 2022).

Venny2.1.0 was used to generate a Venn diagram of common target miRNAs for CORO1C (https://bioinfogp.cnb.csic.es/tools/venny/ accessed on 15 October 2022). Four different miRNA tools were used to generate miRNAs, which targeted CORO1C. These included miRSystem (http://mirsystem.cgm.ntu.edu.tw/index.php accessed on 15 October 2022), miRWalk (NM_001276471) (http://mirwalk.umm.uni-heidelberg.de/ accessed on 15 October 2022), TargetScan (ENST00000261401.3) (https://www.targetscan.org/vert_80/ accessed on 15 October 2022), and ENCORI (The Encyclopedia of RNA Interactomes, https://starbase.sysu.edu.cn/ accessed on 15 October 2022).

One-way ANOVA statistical analysis was used to compare disease states (Tumour or Normal) by GEPIA. Genes with higher log2FC values and lower q values than pre-set thresholds were statistically significance at p-value < 0.05. Significance of the TPM values utilised by UALCAN for the generation of boxplots was determined using a t-test PERL script with Comprehensive Perl Archive Network (CPAN) module "Statistics:TTest". Values of $p < 0.05$ were detonated statistically significant.

5. Conclusions

The current in silico investigation demonstrated that the overexpression of CORO1C appeared to be a distinctive feature for solid and highly malignant tumours of different origins, including glioblastomas. A higher expression of CORO1C was found in children with GBM when compared to their adult counterparts. The increased presence of the protein within NPC-like cells suggested high migratory power and potential differentiation of these cells in tumour cells. Expression of CORO1C within phenotypically different pediatric brain malignancies and adult GBM cases demonstrated that this protein could serve as a possible diagnostic biomarker associated with an inferior prognosis within GBM patients. The downregulation of miR-128-3p, miR-9-5p, and miR-133a-3p and upregulation of miR-221-3p, miR-206, and miR-21-5p could afford a potential GBM molecular signature relevant to the diagnosis and treatment to this aggressive type of malignancy.

Supplementary Materials: The following supporting information can be downloaded at: https://www.mdpi.com/article/10.3390/ncrna9010004/s1, Table S1: Common miRNAs (62) in "miRSystem", "TargetScan", "miRWalk", and "ENCORI".

Author Contributions: D.M. consulted the literature, and created the figures and the manuscript. E.K. and M.B. contributed to the critical revision and final edits of the article. All authors have read and agreed to the published version of the manuscript.

Funding: This research received no external funding.

Institutional Review Board Statement: Not applicable.

Informed Consent Statement: Not applicable.

Data Availability Statement: All data generated or analyzed during this study are included in this published article.

Conflicts of Interest: The authors declare no conflict of interest.

References

1. Zhang, X.; Zhang, W.; Mao, X.G.; Cao, W.D.; Zhen, H.N.; Hu, S.J. Malignant intracranial high grade glioma and current treatment strategy. *Curr. Cancer Drug Targets* **2019**, *19*, 101–108. [CrossRef] [PubMed]
2. Davis, M. Glioblastoma: Overview of disease and treatment. *Clin. J. Oncol. Nurs.* **2016**, *20*, S2–S8. [CrossRef] [PubMed]
3. Gillespie, C.; Bligh, E.; Poon, M.; Solomou, G.; Islim, A.; Mustafa, M.; Rominiyi, O.; Williams, S.; Kalra, N.; Mathew, R.; et al. Imaging timing after glioblastoma surgery (INTERVAL-GB): Protocol for a UK and Ireland, multicentre retrospective cohort study. *BMJ Open* **2022**, *12*, e063043. [CrossRef] [PubMed]
4. Ostrom, Q.; Cioffi, G.; Waite, K.; Kruchko, C.; Barnholtz-Sloan, J. CBTRUS statistical report: Primary brain and other central nervous system tumors diagnosed in the United States in 2014–2018. *Neuro-Oncology* **2021**, *23* (Suppl. 3), iii1–iii105. [CrossRef]
5. Liu, M.; Thakkar, J.; Garcia, C.; Dolecek, T.; Wagner, L.; Dressler, E.; Villano, J. National cancer database analysis of outcomes in pediatric glioblastoma. *Cancer Med.* **2018**, *7*, 1151–1159. [CrossRef]
6. Gestrich, C.; Jajosky, A.; Elliott, R.; Stearns, D.; Sadri, N.; Cohen, M.; Couce, M. Molecular profiling of pediatric and adult glioblastoma. *Am. J. Clin. Pathol.* **2020**, *155*, 606–614. [CrossRef]
7. Pollack, I.; Hamilton, R.; Sobol, R.; Nikiforova, M.; Lyons-Weiler, M.; La Framboise, B.P.; Brat, D.; Rosenblum, M.; Holmes, E.; Zhou, T.; et al. IDH1 mutations are common in malignant gliomas arising in adolescents: A report from the Children's Oncology Group. *Child's Nerv. Syst.* **2010**, *27*, 87–94. [CrossRef]
8. Pollack, I.; Finkelstein, S.; Woods, J.; Burnham, J.; Holmes, E.; Hamilton, R.; Yates, A.; Boyett, J.; Finlay, J.; Sposto, R. Expression of p53 and prognosis in children with malignant gliomas. *N. Engl. J. Med.* **2002**, *346*, 420–427. [CrossRef]
9. Miklja, Z.; Pasternak, A.; Stallard, S.; Nicolaides, T.; Kline-Nunnally, C.; Cole, B.; Beroukhim, R.; Bandopadhayay, P.; Chi, S.; Ramkissoon, S.; et al. Molecular profiling and targeted therapy in pediatric gliomas: Review and consensus recommendations. *Neuro-Oncology* **2019**, *21*, 968–980. [CrossRef]
10. Cohen, K.; Pollack, I.; Zhou, T.; Buxton, A.; Holmes, E.; Burger, P.; Brat, D.; Rosenblum, M.; Hamilton, R.; Lavey, R.; et al. Temozolomide in the treatment of high-grade gliomas in children: A report from the Children's Oncology Group. *Neuro-Oncology* **2011**, *13*, 317–323. [CrossRef]
11. Bailey, C.; Figueroa, M.; Mohiuddin, S.; Zaky, W.; Chandra, J. Cutting edge therapeutic insights derived from molecular biology of pediatric high-grade glioma and diffuse intrinsic pontine glioma (DIPG). *Bioengineering* **2018**, *5*, 88. [CrossRef] [PubMed]
12. Huynh-Le, M.; Walker, A.; Burger, P.; Jallo, G.; Cohen, K.; Wharam, M.; Terezakis, S. Management of pediatric intracranial low-grade gliomas: Long-term follow-up after radiation therapy. *Child's Nerv. Syst.* **2016**, *32*, 1425–1430. [CrossRef] [PubMed]
13. Chow, L.; Baker, S. Capturing the molecular and biological diversity of high-grade astrocytoma in genetically engineered mouse models. *Oncotarget* **2012**, *3*, 67–77. [CrossRef] [PubMed]
14. Kim, V.; Ha, M. Regulation of microRNA biogenesis. *FASEB J.* **2009**, *23*, 509–524. [CrossRef]
15. Kim, Y.; Kim, V. Processing of intronic microRNAs. *EMBO J.* **2007**, *26*, 775–783. [CrossRef] [PubMed]
16. Gatto, L.; Franceschi, E.; Di Nunno, V.; Tosoni, A.; Lodi, R.; Brandes, A. Liquid biopsy in glioblastoma manage-ment: From current research to future perspectives. *Oncologist* **2021**, *26*, 865–878. [CrossRef] [PubMed]
17. Areeb, Z.; Stylli, S.; Koldej, R.; Ritchie, D.; Siegal, T.; Morokoff, A.; Kaye, A.; Luwor, R. microRNA as potential biomarkers in glioblastoma. *J. Neuro-Oncol.* **2015**, *125*, 237–248. [CrossRef]
18. Møller, H.; Rasmussen, A.; Andersen, H.; Johnsen, K.; Henriksen, M.; Duroux, M. A systematic review of mi-croRNA in glioblastoma multiforme: Micro-modulators in the mesenchymal mode of migration and invasion. *Mol. Neurobiol.* **2012**, *47*, 131–144. [CrossRef]
19. Brennecke, J.; Stark, A.; Russell, R.; Cohen, S. Principles of microRNA–target recognition. *PLoS Biol.* **2005**, *3*, e85. [CrossRef]
20. Peng, Y.; Croce, C. The role of microRNAs in human cancer. *Signal Transduct. Target. Ther.* **2016**, *1*, 1–9. [CrossRef]

21. Qu, S.; Guan, J.; Liu, Y. Identification of microRNAs as novel biomarkers for glioma detection: A meta-analysis based on 11 articles. *J. Neurol. Sci.* **2015**, *348*, 181–187. [CrossRef]
22. Kalkan, R.; Atli, E. The impacts of miRNAs in glioblastoma progression. *Crit. Rev. Eukaryot. Gene Express.* **2016**, *26*, 137–142. [CrossRef]
23. Roth, P.; Wischhusen, J.; Happold, C.; Chandran, P.; Hofer, S.; Eisele, G.; Weller, M.; Keller, A. A specific miRNA signature in the peripheral blood of glioblastoma patients. *J. Neurochem.* **2011**, *118*, 449–457. [CrossRef]
24. Tomanek, B.; Iqbal, U.; Blasiak, B.; Abulrob, A.; Albaghdadi, H.; Matyas, J.R.; Ponjevic, D.; Sutherland, G.R. Evaluation of brain tumor vessels specific contrast agents for glioblastoma imaging. *Neuro-Oncology* **2012**, *14*, 53–63. [CrossRef]
25. Hadjipanayis, C.G.; Machaidze, R.; Kaluzova, M.; Wang, L.; Schuette, A.J.; Chen, H.; Wu, X.; Mao, H. EGFRvIII Anti-body–Conjugated Iron Oxide Nanoparticles for Magnetic Resonance Imaging–Guided Convection-Enhanced Delivery and Targeted Therapy of GlioblastomaEGFRvIII-Targeted Therapy of GBM by IONPs after CED. *Cancer Res.* **2010**, *70*, 6303–6312. [CrossRef]
26. Kleihues, P.; Cavenee, W.K. *Pathology and Genetics: Tumours of the Nervous System*; IARC-Press: Lyon, France, 2000.
27. Yang, B.; Wang, S.; Zeng, J.; Zhang, Y.; Ruan, X.; Han, W.; Yin, B.; Yuan, J.; Qiang, B.; Ying, W.; et al. Proteomic screening and identification of microRNA-128 targets in glioma cells. *Proteomics* **2015**, *15*, 2602–2617. [CrossRef]
28. Thul, P.J.; Åkesson, L.; Wiking, M.; Mahdessian, D.; Geladaki, A.; Ait Blal, H.; Alm, T.; Asplund, A.; Björk, L.; Breckels, L.M.; et al. A subcellular map of the human proteome. *Science* **2017**, *356*, eaal3321. [CrossRef]
29. Thul, P.J.; Lindskog, C. The human protein atlas: A spatial map of the human proteome. *Protein Sci. Publ. Protein Soc.* **2018**, *27*, 233–244. [CrossRef]
30. Hawrylycz, M.J.; Lein, E.S.; Guillozet-Bongaarts, A.L.; Shen, E.H.; Ng, L.; Miller, J.A.; van de Lagemaat, L.N.; Smith, K.A.; Ebbert, A.; Riley, Z.L.; et al. An anatomically comprehensive atlas of the adult human brain transcriptome. *Nature* **2012**, *489*, 391–399. [CrossRef]
31. Molinie, N.; Rubtsova, S.N.; Fokin, A.; Visweshwaran, S.P.; Rocques, N.; Polesskaya, A.; Schnitzler, A.; Vacher, S.; Den-isov, E.V.; Tashireva, L.A.; et al. Cortical branched actin determines cell cycle progression. *Cell Res.* **2019**, *29*, 432–445. [CrossRef]
32. Wang, Z.; Jia, L.; Sun, Y.; Li, C.; Zhang, L.; Wang, X.; Chen, H. CORO1C is associated with poor prognosis and promotes metastasis through PI3K/AKT pathway in colorectal cancer. *Front. Mol. Biosci.* **2021**, *8*, 682594. [CrossRef] [PubMed]
33. Shen, X.; Kong, S.; Ma, S.; Shen, L.; Zheng, M.; Qin, S.; Qi, J.; Wang, Q.; Cui, X.; Ju, S. Hsa_circ_0000437 promotes pathogenesis of gastric cancer and lymph node metastasis. *Oncogene* **2022**, *41*, 4724–4735. [CrossRef] [PubMed]
34. Pan, J.; Sheng, S.; Ye, L.; Xu, X.; Ma, Y.; Feng, X.; Qiu, L.; Fan, Z.; Wang, Y.; Xia, X.; et al. Extracellular vesicles derived from glioblastoma promote proliferation and migration of neural progenitor cells via PI3K-Akt pathway. *Cell Commun. Signal. CCS* **2022**, *20*, 7. [CrossRef]
35. Rosentreter, A.; Hofmann, A.; Xavier, C.P.; Stumpf, M.; Noegel, A.A.; Clemen, C.S. Coronin 3 involvement in F-actin-dependent processes at the cell cortex. *Exp. Cell Res.* **2007**, *313*, 878–895. [CrossRef] [PubMed]
36. Thal, D.; Xavier, C.P.; Rosentreter, A.; Linder, S.; Friedrichs, B.; Waha, A.; Pietsch, T.; Stumpf, M.; Noegel, A.; Clemen, C. Expression of coronin-3 (coronin-1C) in diffuse gliomas is related to malignancy. *J. Pathol.* **2008**, *214*, 415–424. [CrossRef]
37. Martorella, M.; Barford, K.; Winkler, B.; Deppmann, C.D. Emergent role of Coronin-1a in neuronal signaling. *Vitam. Horm.* **2017**, *104*, 113–131.
38. Hasse, A.; Rosentreter, A.; Spoerl, Z.; Stumpf, M.; Noegel, A.A.; Clemen, C.S. Coronin 3 and its role in murine brain morphogenesis. *Eur. J. Neurosci.* **2005**, *21*, 1155–1168. [CrossRef]
39. Wang, M.; Li, Q.; Yu, S.; Zhang, Z.; Qiu, P.; Zhang, Y.; Yang, W.; Xu, G.; Xu, T. Coronin 3 promotes the devel-opment of oncogenic properties in glioma through the Wnt/β-catenin signaling pathway. *OncoTargets Ther.* **2020**, *13*, 6661–6673. [CrossRef]
40. Campbell, P.J.; Getz, G.; Stuart, J.M.; Korbel, J.O.; Stein, L.D. ICGC/TCGA Pan-cancer analysis of whole genomes consortium Pan-cancer analysis of whole genomes. *Nature* **2020**, *578*, 82–93.
41. Michaeli, O.; Tabori, U. Pediatric high grade gliomas in the context of cancer predisposition syndromes. *J. Korean Neurosurg. Soc.* **2018**, *61*, 319–332. [CrossRef]
42. Tabori, U.; Hansford, J.R.; Achatz, M.I.; Kratz, C.P.; Plon, S.E.; Frebourg, T.; Brugières, L. Clinical management and tumor surveil-lance recommendations of inherited mismatch repair deficiency in childhood. *Clin. Cancer Res. Off. J. Am. Assoc. Cancer Res.* **2017**, *23*, e32–e37. [CrossRef]
43. Goldblum, J.R.; Weiss, S.W.; Folpe, A.L. *Enzinger and Weiss's Soft Tissue Tumors E-Book*; Elsevier Health Sciences: Amsterdam, The Netherlands, 2013.
44. Costa, A.D.A.; Gutmann, D.H. Brain tumors in neurofibromatosis type 1. *Neuro-Oncol. Adv.* **2020**, *2* (Suppl. 1), i85–i97. [CrossRef]
45. Neftel, C.; Laffy, J.; Filbin, M.G.; Hara, T.; Shore, M.E.; Rahme, G.J.; Richman, A.R.; Silverbush, D.; Shaw, M.L.; Hebert, C.M.; et al. An integrative model of cellular states, plasticity, and genetics for G glioblastoma. *Cell* **2019**, *178*, 835–849.e21. [CrossRef]
46. Borst, K.; Dumas, A.A.; Prinz, M. Microglia: Immune and non-immune functions. *Immunity* **2021**, *54*, 2194–2208. [CrossRef]
47. Broekman, M.L.; Maas, S.L.; Abels, E.R.; Mempel, T.R.; Krichevsky, A.M.; Breakefield, X.O. Multidimensional communication in the microenvirons of glioblastoma. *Nat. Rev. Neurol.* **2018**, *14*, 482–495. [CrossRef]
48. Wang, J.; Liu, J.; Sun, G.; Meng, H.; Wang, J.; Guan, Y.; Yin, Y.; Zhao, Z.; Dong, X.; Yin, S.; et al. Glioblastoma extracellular vesicles induce the tumour-promoting transformation of neural stem cells. *Cancer Lett.* **2019**, *466*, 1–12. [CrossRef]
49. Zhang, Y.; Chao, T.; Li, R.; Liu, W.; Chen, Y.; Yan, X.; Gong, Y.; Yin, B.; Liu, W.; Qiang, B.; et al. microRNA-128 inhibits glioma cells proliferation by targeting transcription factor E2F3a. *J. Mol. Med.* **2009**, *87*, 43–51. [CrossRef]
50. Hersi, H.M.; Raulf, N.; Gaken, J.; Folarin, N.; Tavassoli, M. MicroRNA-9 inhibits growth and invasion of head and neck cancer cells and is a predictive biomarker of response to plerixafor, an inhibitor of its target CXCR4. *Mol. Oncol.* **2018**, *12*, 2023–2041. [CrossRef]

51. Xu, F.; Li, F.; Zhang, W.; Jia, P. Growth of glioblastoma is inhibited by *miR*-133-mediated EGFR suppression. *Tumour Biol. J. Int. Soc. Oncodev. Biol. Med.* **2015**, *36*, 9553–9558. [CrossRef]
52. Zhou, F.; Cao, W.; Xu, R.; Zhang, J.; Yu, T.; Xu, X.; Zhi, T.; Yin, J.; Cao, S.; Liu, N.; et al. Mi-croRNA-206 attenuates glioma cell proliferation, migration, and invasion by blocking the WNT/β-catenin pathway via direct targeting of Frizzled 7 mRNA. *Am. J. Transl. Res.* **2019**, *11*, 4584–4601.
53. Luo, G.; Luo, W.; Sun, X.; Lin, J.; Wang, M.; Zhang, Y.; Luo, W.; Zhang, Y. MicroRNA-21 promotes migration and invasion of glioma cells via activation of Sox2 and β-catenin signaling. *Mol. Med. Rep.* **2017**, *15*, 187–193. [CrossRef] [PubMed]
54. Zhang, R.; Pang, B.; Xin, T.; Guo, H.; Xing, Y.; Xu, S.; Feng, B.; Liu, B.; Pang, Q. Plasma miR-221/222 family as novel descriptive and prognostic biomarkers for glioma. *Mol. Neurobiol.* **2016**, *53*, 1452–1460. [CrossRef] [PubMed]
55. Zhou, X.; Qi, L.; Tong, S.; Cui, Y.; Chen, J.; Huang, T.; Chen, Z.; Zu, X. *miR*-128 downregulation promotes growth and metastasis of bladder cancer cells and involves VEGF-C upregulation. *Oncol. Lett.* **2015**, *10*, 3183–3190. [CrossRef] [PubMed]
56. Li, Y.; Wang, Y.; Shen, X.; Han, X. *miR*-128 Functions as an OncomiR for the Downregulation of HIC1 in Breast Cancer. *Front. Pharmacol.* **2019**, *10*, 1202. [CrossRef] [PubMed]
57. Slack, F.; Chinnaiyan, A. The role of non-coding RNAs in oncology. *Cell* **2019**, *179*, 1033–1055. [CrossRef]
58. Zhang, W.; Kim, P.J.; Chen, Z.; Lokman, H.; Qiu, L.; Zhang, K.; Rozen, S.G.; Tan, E.K.; Je, H.S.; Zeng, L. *MiRNA*-128 regulates the proliferation and neurogenesis of neural precursors by targeting PCM1 in the developing cortex. *eLife* **2016**, *5*, e11324. [CrossRef]
59. Zhou, B.; Xu, H.; Xia, M.; Sun, C.; Li, N.; Guo, E.; Guo, L.; Shan, W.; Lu, H.; Wu, Y.; et al. Overexpressed miR-9 promotes tumor metastasis via targeting E-cadherin in serous ovarian cancer. *Front. Med.* **2017**, *11*, 214–222. [CrossRef]
60. Ben-Hamo, R.; Zilberberg, A.; Cohen, H.; Efroni, S. hsa-miR-9 controls the mobility behavior of glioblastoma cells via regulation of MAPK14 signaling elements. *Oncotarget* **2016**, *7*, 23170–23181. [CrossRef]
61. Zhang, H.; Li, Y.; Tan, Y.; Liu, Q.; Jiang, S.; Liu, D.; Chen, Q.; Zhang, S. MiR-9-5p Inhibits Glioblastoma Cells Proliferation Through Directly Targeting FOXP2 (Forkhead Box P2). *Front. Oncol.* **2019**, *9*, 1176. [CrossRef]
62. Luo, T.; Yi, X.; Si, W. Identification of miRNA and genes involving in osteosarcoma by comprehensive analysis of microRNA and copy number variation data. *Oncol. Lett.* **2017**, *14*, 5427–5433. [CrossRef]
63. Han, S.; Ding, X.; Wang, S.; Xu, L.; Li, W.; Sun, W. *miR*-133a-3p regulates hepatocellular carcinoma progression through targeting CORO1C. *Cancer Manag. Res.* **2020**, *12*, 8685. [CrossRef]
64. Liao, M.; Peng, L. *Mir*-206 may suppress non-small lung cancer metastasis by targeting Coro1c. *Cell. Mol. Biol. Lett.* **2020**, *25*, 1–13. [CrossRef]
65. Zhang, C.Z.; Zhang, J.X.; Zhang, A.L.; Shi, Z.D.; Han, L.; Jia, Z.F.; Yang, W.D.; Wang, G.X.; Jiang, T.; You, Y.P.; et al. MiR-221 and miR-222 target PUMA to induce cell survival in glioblastoma. *Mol. Cancer* **2010**, *9*, 229. [CrossRef]
66. Tan, X.; Tang, H.; Bi, J.; Li, N.; Jia, Y. MicroRNA-222-3p associated with Helicobacter pylori targets HIPK2 to promote cell proliferation, invasion, and inhibits apoptosis in gastric cancer. *J. Cell. Biochem.* **2018**, *119*, 5153–5162. [CrossRef]
67. Zhou, H.; Zhu, X. MicroRNA-21 and microRNA-30c as diagnostic biomarkers for prostate cancer: A meta-analysis. *Cancer Manag. Res.* **2019**, *11*, 2039–2050. [CrossRef]
68. Bica-Pop, C.; Cojocneanu-Petric, R.; Magdo, L.; Raduly, L.; Gulei, D.; Berindan-Neagoe, I. Overview upon miR-21 in lung cancer: Focus on NSCLC. *Cell. Mol. Life Sci. CMLS* **2018**, *75*, 3539–3551. [CrossRef]
69. Zeng, L.P.; Hu, Z.M.; Li, K.; Xia, K. *miR*-222 attenuates cisplatin-induced cell death by targeting the PPP2R2A/Akt/mTOR Axis in bladder cancer cells. *J. Cell. Mol. Med.* **2016**, *20*, 559–567. [CrossRef]
70. Zhang, Y.; Ma, T.; Yang, S.; Xia, M.; Xu, J.; An, H.; Yang, Y.; Li, S. High-mobility group A1 proteins enhance the expression of the oncogenic miR-222 in lung cancer cells. *Mol. Cell. Biochem.* **2011**, *357*, 363–371. [CrossRef]

Disclaimer/Publisher's Note: The statements, opinions and data contained in all publications are solely those of the individual author(s) and contributor(s) and not of MDPI and/or the editor(s). MDPI and/or the editor(s) disclaim responsibility for any injury to people or property resulting from any ideas, methods, instructions or products referred to in the content.

Appendix 7. Relevant publications to work done in Chapters 2, 3 & 4, Journal: *Scientific reports*

www.nature.com/scientificreports

scientific reports

Check for updates

OPEN

SV2B/miR-34a/miR-128 axis as prognostic biomarker in glioblastoma multiforme

D. Mustafov[1,2], S. S. Siddiqui[1], L. Klena[1], E. Karteris[2] & M. Braoudaki[1]✉

Glioblastoma (GBM) is a heterogenous primary brain tumour that is characterised with unfavourable patient prognosis. The identification of biomarkers for managing brain malignancies is of utmost importance. MicroRNAs (miRNAs) are small, non-coding RNAs implicated in cancer development. This study aimed to assess the prognostic significance of miRNAs and their gene targets in GBM. An in silico approach was employed to investigate the differentially expressed miRNAs in GBM. The most dysregulated miRNAs were identified and analysed via Sfold in association with their gene target. The candidate gene was studied via multi-omics approaches, followed by in vitro and in vivo experiments. The in silico analyses revealed that miR-128a and miR-34a were significantly downregulated within GBM. Both miRNAs displayed high binding affinity to the synaptic vesicle glycoprotein 2B (*SV2B*) 3′ untranslated region (3′UTR). SV2B exhibited upregulation within brain regions with high synaptic activity. Significantly higher SV2B levels were observed in high grade brain malignancies in comparison to their normal counterparts. SV2B expression was observed across the cytoplasm of GBM cells. Our findings underscored the downregulated expression patterns of miR-128a and miR-34a, alongside the upregulation of SV2B in GBM suggesting the importance of the *SV2B*/miR-34a/miR-128 axis as a potential prognostic approach in GBM management.

Glioblastoma multiforme (GBM) is an aggressive and heterogeneous primary brain malignancy characterised by its invasive nature and resistance to therapy. The tumour can originate in any part of the central nervous system (CNS), but it is frequently found in the frontal or temporal lobes[1]. GBM accounts for nearly 3350 newly diagnosed cases in the UK annually with an overall survival rate between 6–17 months[2]. Currently, aggressive multimodal therapeutic approaches involving maximal surgical resection followed by radiotherapy and chemotherapy with temozolomide have failed to improve overall survival rates and patients' prognosis remains poor[3]. Immunotherapies incorporating treatment with nivolumab and pembrolizumab have shown no safety concerns and neurotoxicity, but no survival improvements have been noticed in recurrent GBM[4,5]. Therefore, there is an urgent demand for innovative therapies for GBM, due to its aggressive nature and the limited effectiveness of current treatment options.

Responsible for approximately 50% of all gliomas and 15% of all intracranial neoplasms, GBM is associated with a complex heterogenic molecular profile[6]. The clinical application of molecular profiles for GBM diagnosis is often limited due to the dynamic microenvironment of GBMs and their ability to transition between different molecular subtypes. Current diagnostic practices for GBM are based on magnetic resonance imaging (MRI). However, relying solely on MRI for a conclusive clinical diagnosis can lead to errors in some instances[7]. Therefore, the need for tissue biopsy in the diagnostic decision-making process is nearly inevitable. Nonetheless, this approach has its limitations, including the invasive nature of the procedure, the lack of serial monitoring of the malignancy, tissue heterogeneity and the potential risk of neurological damage. To address these challenges, we have turned our attention to microRNAs (miRNAs).

MiRNAs are a class of small non-coding, single-stranded RNA molecules widely found in eukaryotic organisms consisting of approximately 22 nucleotides. The process of miRNA biogenesis undergoes intricate regulation at both the transcriptional and post-transcriptional levels to produce fully functional, mature miRNAs, which play a vital role in maintaining cellular homeostasis[8]. However, alternations of miRNAs functional properties do occur occasionally and could potentially lead to a transcriptome imbalance associated with different malignancies[9]. Deregulation of miRNAs in GBM can result from various faulty events during their biogenesis, such as amplifications, deletions, epigenetic modifications, translocations, and silencing. The overexpression of

[1]School of Life and Medical Sciences, University of Hertfordshire, College Lane Campus, Hatfield AL10 9AB, UK. [2]College of Health, Medicine and Life Sciences, Brunel University London, Uxbridge UB8 3PH, UK. ✉email: m.braoudaki@herts.ac.uk

certain miRNAs can lead to the suppression of tumour suppressor genes, while the downregulation of others can be associated with increased expression of oncogenes. Both scenarios could affect cell proliferation, differentiation, and apoptosis, ultimately contributing to the growth and progression of tumours[10]. The detection of miRNA signatures in primary brain tumours has provided valuable insights into the diagnosis, prognosis, and monitoring of patients[11], but more research is necessitated to unravel their exact role in the progression of those types of tumours.

Herein, we aimed to screen for the differentially expressed miRNAs and their target genes within GBM patients to identify valid prognostic biomarkers or therapeutic targets. Specifically, in silico analysis revealed that miR-34a and miR-128a were significantly downregulated in GBM cells and patients verifying their tumour suppressor properties. Additional bioinformatics analysis demonstrated that a common target gene for both miRNAs was the synaptic vesicle glycoprotein 2B (*SV2B*) gene which was found upregulated in GBM patients and hence manifesting oncogenic properties. The effect of current miRNA regulation on SV2B protein function was validated using brain tumour patient samples, including GBM. Based on current findings, we are proposing that the *SV2B*/miR-34a/miR-128 axis could serve as a putative prognostic biomarker for glioblastoma multiforme.

Results

miRNA analyses

Throughout our bioinformatics analysis, illustrated in Table 1, we analysed miRNAs and their gene targets using a formatted miRNA summary report, obtained from the NCBI and miRSystem databases. The summary of the hits between miRNAs and their target genes allowed us to select the four miRNAs with evident relevance within GBM pathogenesis, including miR-21-5p, miR-34a, miR-128a-3p, and miR-221-3p. Of these, miR-34a showed the highest number of hits against GBM oncogenes. Subsequent KEGG pathway analysis aided in depicting the differential expression profiles of these miRNAs (Fig. 1a). miR-34a and miR-128a were shown to be downregulated in GBM, whilst miR-21a and miR-221-3p were seen to be upregulated. Further analysis of the commonly co-expressed genes with *SV2B* and their miRNA regulatory pathways depicted miR-34a as the most important miRNA involved in overall gene regulation for this hub, whereas miR-128a was seen as the most important brain specific miRNA regarding the regulation of the gene hub and *SV2B* (Fig. 1b,c). Furthermore, common miRNAs targeting the *SV2B* gene including miR-128a and miR-34a were assessed by employing four databases: miRSystem, TargetScan, miRWalk, and ENCORI. The findings indicated that there were 26 common miRNA gene targets (1%) that were identified by all four databases. Within this set of shared miRNAs, miR-34a-5p was seen as downregulated and depicted as the main target for the gene (Fig. 1d). We selected the downregulated miR-34a and miR-128a for subsequent Sfold base-pair matching analysis. As illustrated in Fig. 1e, miR-34a featured a well conserved binding site for the 3′UTR of *SV2B* at site position 3909–3932, with a ΔGhybrid value of − 27.500. The binding type was 7mer-A1. Figure 1f–h revealed the Sfold predicted binding sites between *SV2B* and miR-128a. The outcome of the 3′UTR-miRNA binding depicted three site positions, including 8986–8999, 9532–9552, and 5671–5685. The hybrid binding interaction at these sites was − 17.900, − 19.300, and − 17.600, respectively. The seed interactions were described as 7mre-A1 for the first two sites, and as 6mer for the latest.

SV2B expression

Figure 2a illustrates the normal expression of the *SV2B* gene within various human tissues. The results demonstrated that the expression of this gene is highly elevated in the following brain regions: frontal cortex (BA9) (8.9 times), cortex (8.2 times), cerebellar hemisphere (7.2 times), anterior cingulate cortex (BA24) (7.1 times), and cerebellum (5.8 times). Furthermore, the proteomics analysis shown in Fig. 2b revealed that the median protein $\log^{10}$ normalized iBAQ intensity expression of SV2B was highest within the prefrontal cortex, the retina, and the brain as a whole (6.01, 5.98, and 5.48 iBAQ, respectively). The incorporated KEGG pathway analysis as shown in Fig. 2c depicted that members of the SV2 protein family were classed as proteoglycans that were involved in extracellular matrix–receptor interactions (ECM) with laminins. Specifically, *SV2B* was seen to interact closely with *SYT1* as part of the ECM-receptor interaction signalling.

String and survival analyses

Figure 3a illustrates a string interaction analysis of the *SV2B* gene and any co-expressed genes. As observed, synaptotagmin 1 (*SYT1*) was directly co-expressed alongside *SV2B* (score 0.128). Meanwhile, experimental, and

	Gene name and total no. of hits							
Name of miRNAs	*CDK6*	*NOTCH1*	*NOTCH2*	*JAG1*	*TIMP3*	*E2F3*	*BMI1*	Total
hsa-miR-21-5p	5	0	0	7	7	3	0	22
hsa-miR-34a-5p	7	7	8	8	0	8	0	38
hsa-miR-128a-3p	1	0	0	4	0	8	7	21
hsa-miR-221-3p	3	0	0	1	7	0	6	17

Table 1. Identification of miRNAs and associated target genes. The four depicted miRNAs; hsa-miR-21-5p, hsa-miR-34a-5p, hsa-miR-128-3p, hsa-miR-221-3p, aligned against the oncogenes Cyclin-dependent kinase 6 (*CDK6*), Neurogenic locus notch homolog protein 1 and 2 (*NOTCH1* and *NOTCH2*), Jagged Canonical Notch Ligand 1 (*JAG1*), TIMP Metallopeptidase Inhibitor 3 (*TIPM3*), E2F Transcription Factor (*E2F3*), and B lymphoma Mo-MLV insertion region 1 homolog (*BMI1*) found in GBM.

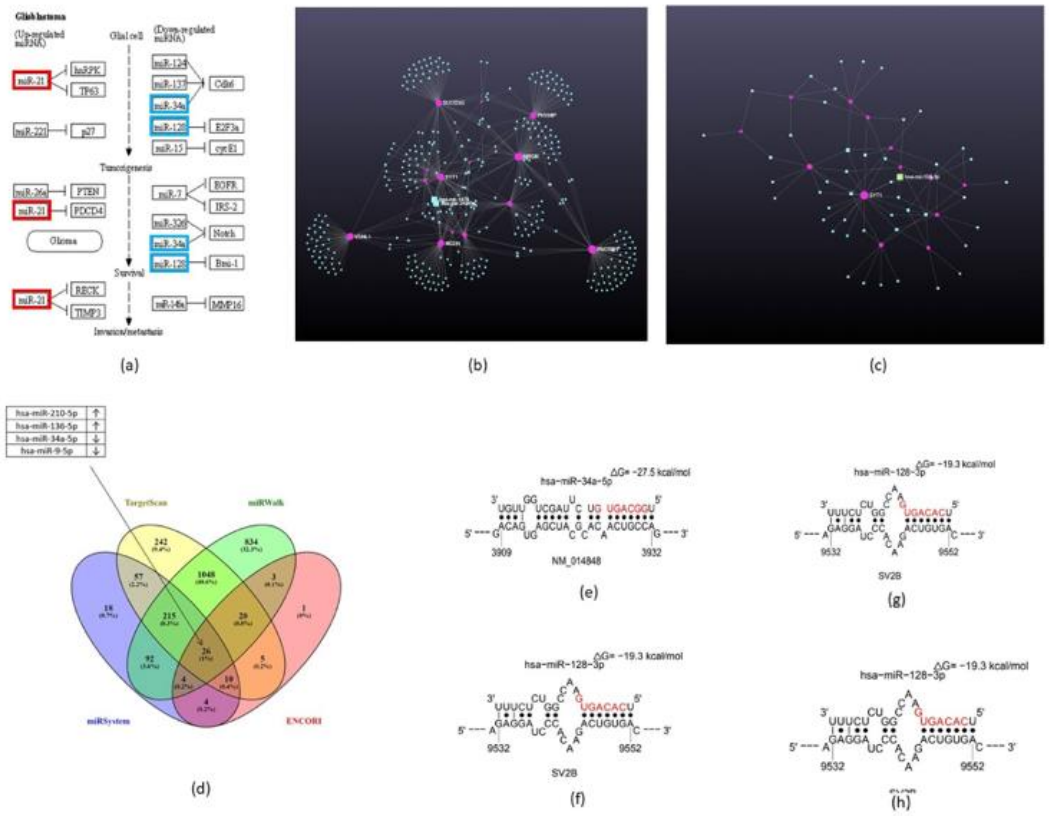


Figure 1. miRNA-*SV2B* interactions. (**a**) KEGG pathway analysis depicted the most differentially expressed miRNAs profiles in 529 GBM cases (grade 4). miR-21 and miR-221 (red boxes) were seen to be upregulated, whereas miR-34a and miR-128 (blue boxes) were downregulated. (**b**) miR-34a was depicted as one of the most important miRNAs involved in the overall gene regulation for *SV2B* co-expressed genes (*HRNBP3, SULT4A1, SLC12A5, PACSIN1, GRIN1, VSNL1, PHYHIP, SYN2, CAMK2A, GLS2, NCDN, NRGN, SYT1, AK5, NAPB*). (**c**) miR-128a was observed to be one of the most important brain specific miRNAs regarding gene hub associated with *SV2B*. (**d**) miR-34a-5p was identified as downregulated and depicted as a main target for *SV2B* out of 26 common miRNA gene targets. (**e**) 3′UTR of *SV2B* and miR-34a binding at site position 3909–3932, ΔGhybrid = – 27.500 kcal/mol. (**f**) 3′UTR of *SV2B* and miR-128-3p binding at site position 8986–8999, ΔGhybrid = – 17.900 kcal/mol. (**g**) 3′UTR of *SV2B* and miR-128-3p binding at site position 9532–9552, ΔGhybrid = – 19.300 kcal/mol. (**h**) 3′UTR of *SV2B* and miR-128-3p binding at site position 5671–5685, ΔGhybrid = – 17.600 kcal/mol.

biochemical data have demonstrated the relation between these two genes (score 0.292). Furthermore, a GeneMANIA interactive network was constructed, which also confirmed the strong co-expression between *SV2B* and *SYT1*, alongside *C6orf15, SCTR, SV2C,* and *SLC17A7*. The latest also showed that SV2B interacted with a great majority of laminins, supporting our aforementioned KEGG pathway observations (Fig. 3b,c). Our analysis also depicted the 15 genes that most positively correlated and co-expressed alongside *SV2B*, including: *HRNBP3, SULT4A1, SLC12A5, PACSIN1, GRIN1, VSNL1, PHYHIP, SYN2, CAMK2A, GLS2, NCDN, NRGN, SYT1, AK5,* and *NAPB* (Fig. 3d). Furthermore, survival analysis of primary GBM samples demonstrated that patient groups expressing higher levels of *SV2B* in comparison to those with lower expression levels had significantly shorter overall survival and disease specific survival ($p < 0.01119$ and $p < 0.02197$, respectively) (Fig. 3e,f). The variations between *SV2B* expression profiles within the progression free survival GBM analysis did not depict statistically significant differences (Fig. 3g).

Immunohistochemistry SV2B

The immunohistochemical analysis of SV2B performed within patient cohorts and normal brain samples revealed higher expression of the protein in all age patient groups in comparison to normal and normal adjacent brain tissue samples. However, only the age groups of 0–20 years and 61–80 years reached a significant difference

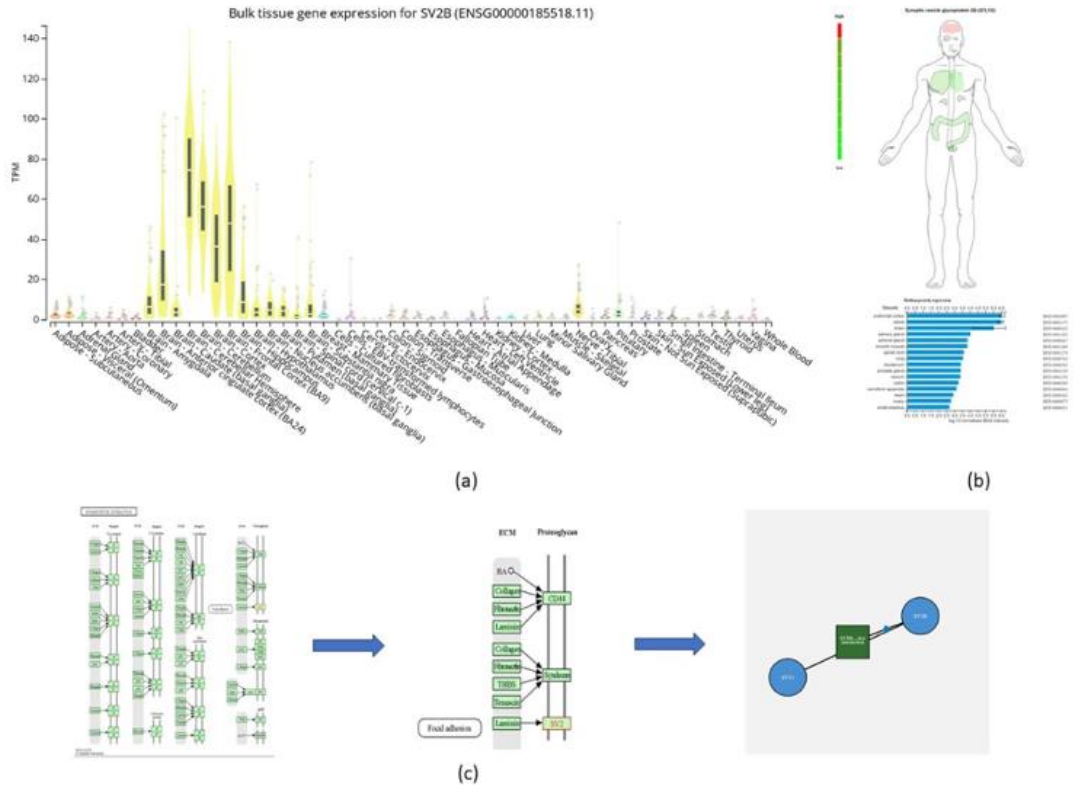


Figure 2. Expression of SV2B across the human body and its relation to biological pathways. (**a**) *SV2B* expression was observed to be highly elevated in various brain regions, including the frontal cortex (BA9) (8.9 times) (n = 56 females; n = 153 males), cortex (8.2 times) (n = 74 females; males = 181), cerebellar hemisphere (7.2 times) (n = 58 females; n = 157 males), anterior cingulate cortex (BA24) (7.1 times) (n = 48 females; n = 128 males), and cerebellum (5.8 times) (n = 67 females; n = 174 males). (**b**) SV2B proteomics analysis depicted that the protein's highest abundance was within the prefrontal cortex (6.01 iBAQ), the retina (5.98 iBAQ), and the brain as a whole (5.48 iBAQ). (**c**) The SV2 protein family was seen to be involved in extracellular matrix–receptor interactions (ECM) with laminins. *SV2B* was seen to interact closely with *SYT1* as part of the ECM-receptor interaction signalling.

regarding protein expression when compared to its normal counterparts (Fig. 4a). Figure 4b illustrates the different patterns of SV2B expression within different tumour types. The analysis depicted significant differences of SV2B levels between astrocytomas, IDH-wildtype diffuse astrocytic tumours, and oligodendrogliomas when compared to glioblastomas, the latter expressing higher protein abundance within patient samples. Medulloblastomas also possessed a significantly higher abundance of SV2B in comparison to astrocytomas. Malignant brain tumours evidently expressed higher levels of SV2B when compared to normal and normal adjacent tissue samples, reaching significance. Figure 4c depicted a significant increase of SV2B expression with increasing tumour grade. Significant differences of measured SV2B levels were seen between grades 1 and 2 in comparison to grade 4 brain tumour samples. Furthermore, the differences between grades 2 and 3 we also denoted with significance. Grades 3 and 4 were shown to express much higher levels of SV2B in comparison to lower tumour grades. As illustrated in the panel of microscopic images in Fig. 4d, the intensity of the brown colourised tissues sections increased within high grade tumours. The panels in Fig. 4e showed different patient samples with progressing tumour stages.

Immunofluorescence

The immunofluorescence analyses of stained GBM cells revealed that there was a specific localisation of SV2B within the cytoplasm of GBM cells. Figures 5a illustrated the negative control condition which did not visualise any specific binding. Beta-actin was used as a positive control and showed similarly uniform staining across both the U87MG and U251MG cell lines (Fig. 5b,c). Figure 5d,e represented that SV2B was enriched around the nucleus, suggesting a possibility of being localised in the endoplasmic reticulum or Golgi. Staining intensity was variable across the two cell lines. The U87MG cell line exhibited more intense SV2B staining (~ 1300–2200

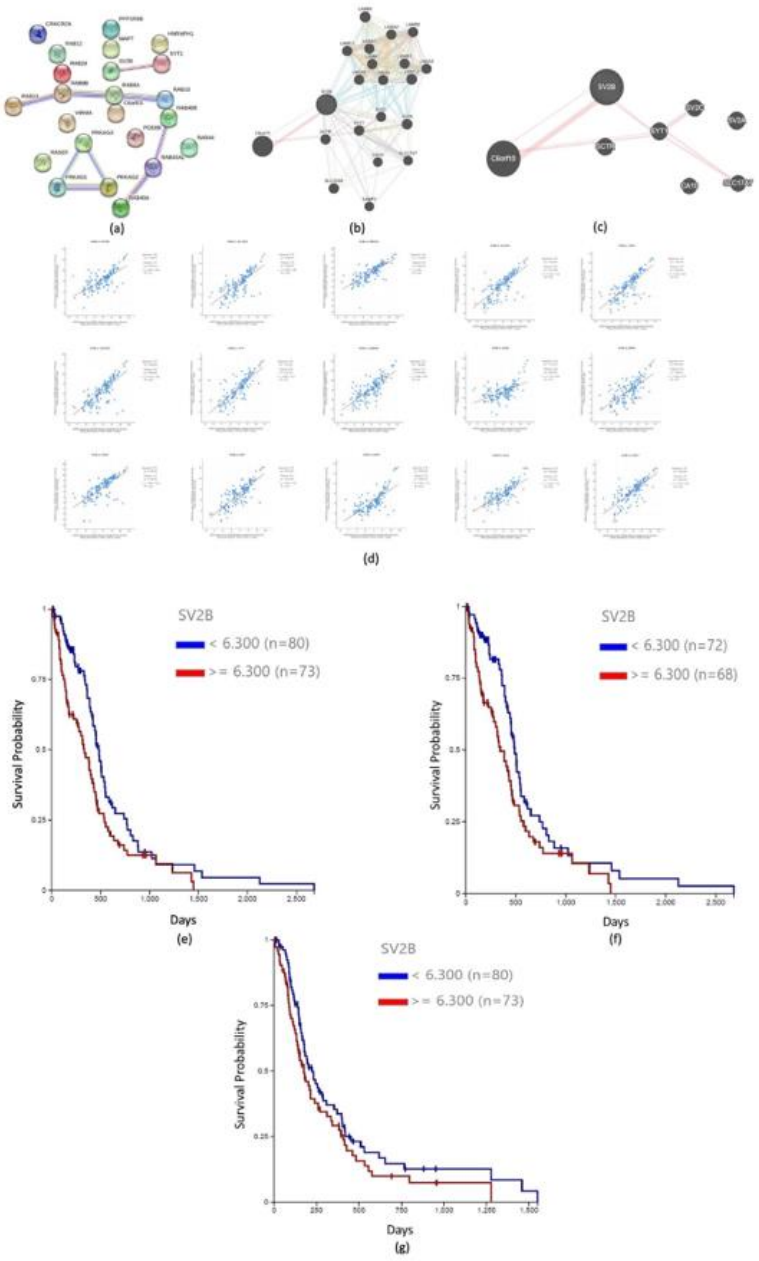


Figure 3. *SV2B* string interaction network. (**a**) String interaction analysis of *SV2B* depicted that synaptotagmin 1 (*SYT1*) was directly co-expressed alongside *SV2B* (score 0.128). (**b**,**c**) GeneMANIA interactive network also illustrated strong co-expression between *SV2B* and *SYT1*, *C6orf15*, *SCTR*, *SV2C*, and *SLC17A7*. (**d**) *HRNBP3*, *SULT4A1*, *SLC12A5*, *PACSIN1*, *GRIN1*, *VSNL1*, *PHYHIP*, *SYN2*, *CAMK2A*, *GLS2*, *NCDN*, *NRGN*, *SYT1*, *AK5*, and *NAPB* positively co-expressed with *SV2B*. (**e**) Survival analysis depicted that higher levels of *SV2B* were associated with significantly shorter overall survival ($p < 0.01119$). (**f**) Disease specific survival analysis indicated that high *SV2B* expression was associated with shorter disease specific survival ($p < 0.02197$). (**g**) Progression free survival GBM analysis did not depict statistically significant differences.

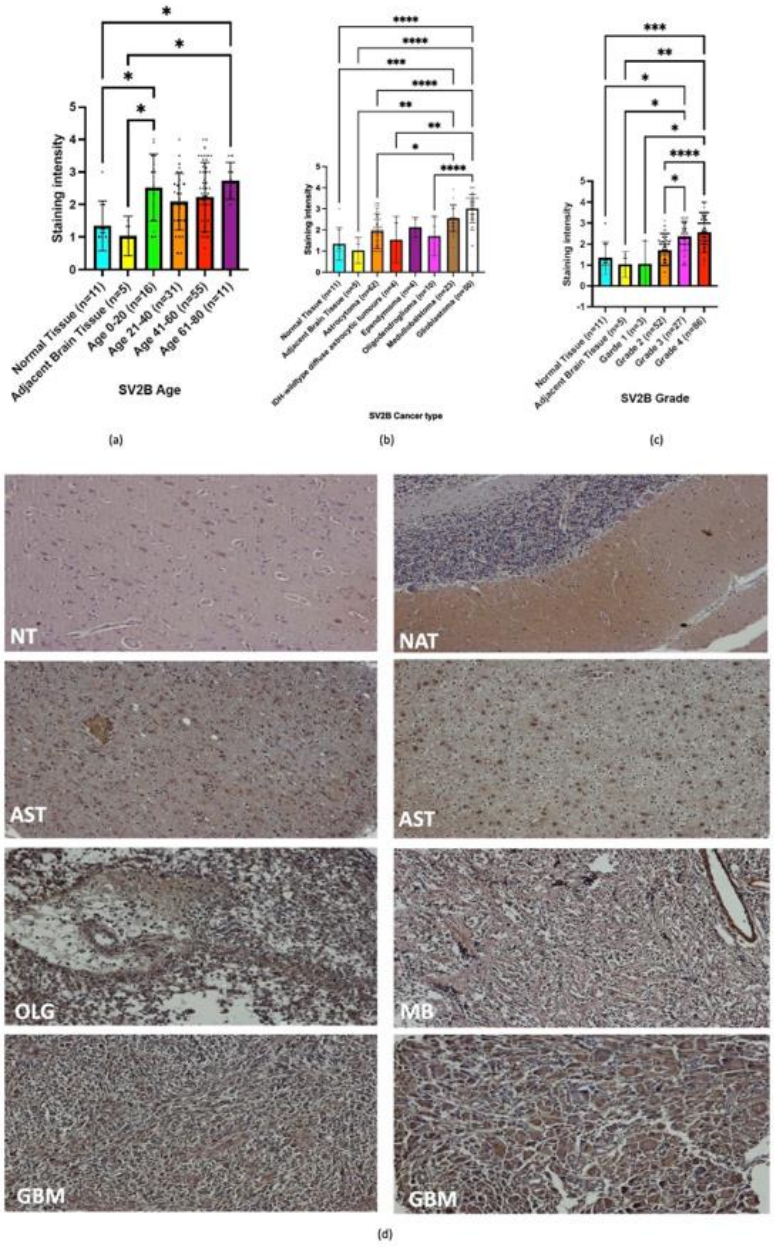


Figure 4. Immunohistochemistry analyses of SV2B. (**a**) The age groups of 0–20 years and 61–80 years reached significant difference in expression of SV2B when compared to their normal counterparts (Normal Tissue versus Age 0–20, $p < 0.0249$; Adjacent Brain Tissue versus Age 0–20, $p < 0.0344$; Normal Tissue versus Age 61–80, $p < 0.0200$; Adjacent Brain Tissue versus Age 61–80, $p < 0.0231$). (**b**) Significantly higher levels of the protein were observed within glioblastomas when compared to astrocytoma, IDH-wildtype diffuse astrocytic tumors, and oligodendrogliomas ($p \ll 0.0001$, $p < 0.0056$, and $p \ll 0.0001$, respectively). Medulloblastoma samples also reached statistical significance of high abundance of SV2B in comparison to astrocytoma ($p < 0.0245$). (**c**) Significant differences between tumor grades 3 and 4 in comparison to normal brain tissue were observed ($p < 0.0133$ and $p < 0.0002$, respectively). Significant differences between grades 1 and 2 in comparison to grade 4, and grades 2 and 3 we also depicted (Grade 1 versus Grade 4, $p < 0.0390$; Grade 2 versus Grade 4, $p < 0.0001$; Grade 2 versus Grade 3, $p < 0.0184$). (**d**) Microscopic images of SV2B stained tissues sections illustrating the staining intensity within normal brain tissue, tumor adjacent tissue, and different brain malignancies at × 100 magnification. (**e**) Microscopic images of SV2B stained tissues cores of normal brain tissue, tumor adjacent tissue, and different brain malignancies at × 40 magnification. *NT* normal tissue, *NAT* normal adjacent tissue, *AST* astrocytoma, *OLG* oligodendroglioma, *MB* medulloblastoma, *GBM* glioblastoma, *Ns* non-significant, *$p < 0.05$, **$p < 0.01$, ***$p < 0.001$, ****$p < 0.0001$.

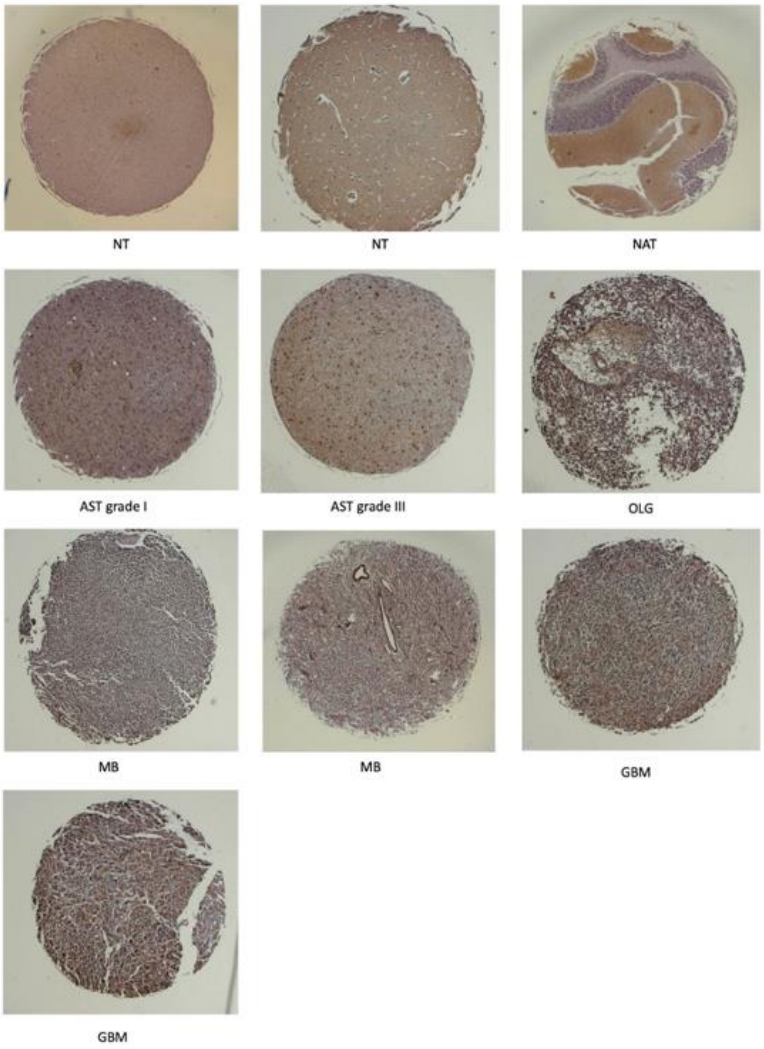


Figure 4. (continued)

range) compared to the U251MG cell line which exhibited lower intensity of staining for SV2B (~900–2000). Despite the higher intensity, there were less SV2B U87MG positive cells and therefore lower signal frequency than in U251MG cells, where the signal intensity was lower, but staining frequency was higher.

Discussion

The limited success in achieving favourable clinical outcomes for primary brain tumours has spurred increased efforts to comprehend the role of miRNAs. Our research attempted to elucidate the role of miR-128a and miR-34a, as emerged through our analyses, and their action upon their target gene *SV2B*.

The conducted in silico analysis demonstrated that miR-21 and miR-221 were overexpressed in GBM tumours, whereas miR-128a and miR-34a were downregulated. This was further supported by the KEGG pathway analysis, where miR-21 and miR-221 were observed to be upregulated, whilst miR-34a and miR-128a were found to be downregulated. Given the oncogenic nature of miR-21 and miR-221, they were excluded from further analysis in relation to *SV2B*.

The potential therapeutic use of miR-34a, which might function as a tumour suppressor by targeting gene promoters within the p53 pathway has arisen for patients with GBM[12]. Vaitkiene et al., 2019 also demonstrated

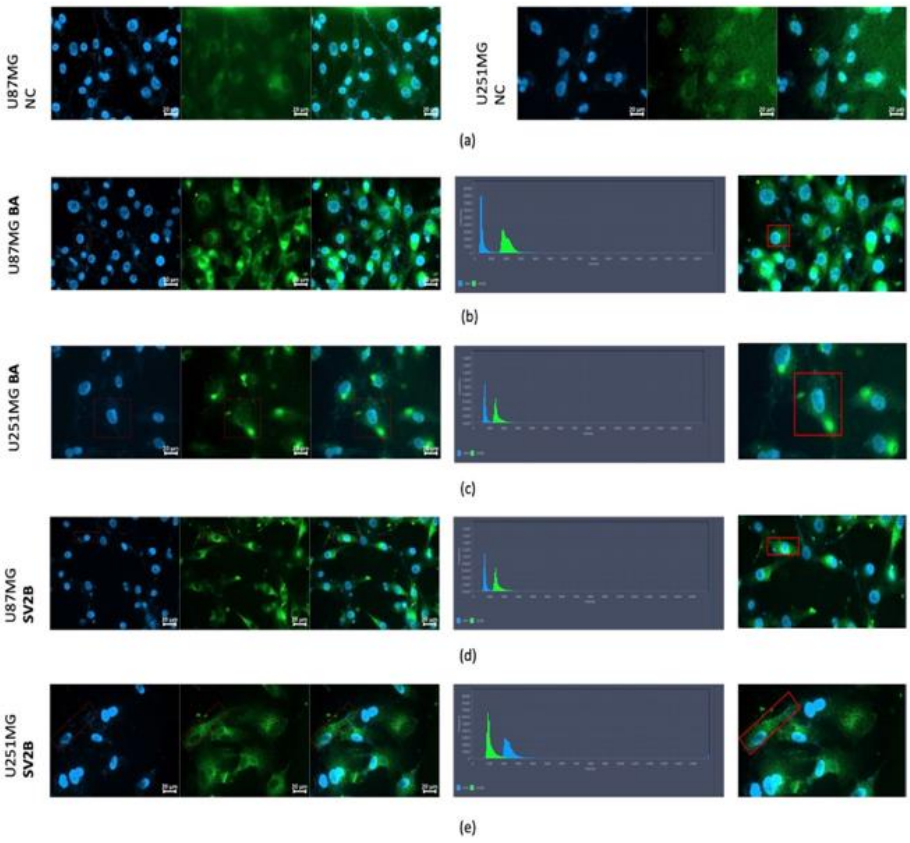


Figure 5. SV2B Immunofluorescence analysis. (**a**) There was no specific binding observed in the negative condition of the experiment. (**b**) Uniform staining across U87MG cells with beta-actin (positive control). (**c**) Uniform staining across U251MG cells with beta-actin (positive control). (**d**) The U87MG cell line exhibited intense SV2B staining (~ 1300–2200 range) enriched around the nucleus. (**e**) U251MG cells exhibited lower intensity of staining for SV2B (~ 900–2000). All microscopic images were taken under × 40 magnification.

lower miR-34a expression which was associated with larger tumour volume, decreased physical functioning, and lower Karnofsky Performance Status (KPS) scores in patients with GBM. However, these findings were described as preliminary, due to the small sample size incorporated in that study. miR-34a was also found significantly downregulated within patients' serums samples highlighting its relevance as a promising non-invasive biomarker for GBM[13]. However, larger sample size validations are further required to strengthen its clinical importance.

The miR-128a is an intronic miRNA primarily located in the brain and has been previously associated with normal brain development[14]. However, miRNA assays, RT-qPCR, and western blot analyses have indicated that miR-128a is expressed at lower levels in aggressive solid brain tumours, including GBM. On the contrary, Roth, et al., 2011 demonstrated that there were elevated levels of miR-128a within blood samples[15]. Our *in-silico* analysis revealed that miR-128a was downregulated within glioblastoma patient samples suggesting its tumour suppressive properties. These findings were in line with previous bioinformatics analyses which had identified low miR-128 levels in serum and tissue patient samples[16]. The low levels if miR-128a were associated with high pathological grade and low Karnofsky Performance Status score (KPS). This in turn has suggested that miR-128 could act as a serum detectable biomarker in GBM patients.

Our results demonstrated a potential interaction between miRNAs and the *SV2B* gene. *SV2B* is involved in synaptic vesicle trafficking and neurotransmitter release[17]. Our findings showed that miR-128a and miR-34a featured conserved binding sites towards *SV2B*. However, miR-34a stood out as a potential target for *SV2B*, as detected in all four miRNA-databases. To the best of our knowledge, the potential prognostic value of the miR-34a/mir-128a/*SV2B* axis has not been reported before. Previous work has demonstrated that miR-330-3p was implicated in *SV2B* regulation via directly targeting *SV2B* mRNA and inhibiting its expression in pancreatic β-cells[18]. In glioma tissues and cells, miR-330-3p was observed to exert low expression levels compared to

adjacent tissues and normal astrocytes[19]. Our *in-silico* analyses depicted that miR-330-3p and miR-34a targeted *SV2B* (Supplementary Table 1). Thus, an association between the two miRNAs and their target can potentially occur leading to the degradation of the gene. According to Morris et al., 2019 mir-134 was found to target *SV2B* in the brain[20]. In line with these findings, our bioinformatic analysis demonstrated that miR-134 had 167 binding sites in the 3′UTR-seedless region of *SV2B* (Supplementary Table 2) suggesting its high binding affinity to *SV2B*. In neuronal cells, miR-134 can downregulate *SV2B* expression, potentially affecting synaptic transmission and plasticity. The brain regional distribution between *SV2B* and miR-134 led to the suggestion that other brain specific miRNAs, such as miR-128a could act as targets for *SV2B* and thus influence its expression.

Expressed as a major form of the SV2 family, *SV2B* distribution across the brain was previously depicted and the gene was found to be exclusively expressed within glutamatergic neurons[21]. An immunohistochemical study has found the expression of the synaptic protein within the cerebellum, basal ganglia, and hippocampus[22]. This was in support to our findings which demonstrated that *SV2B* was predominantly expressed within synaptically active brain areas, such as the frontal cortex, cortex, cerebellar hemisphere, anterior cingulate cortex, and cerebellum. Given the primary function of *SV2B*, the protein product acts as a store of neurotransmitters and releases them upon neuronal excitation[23,24]. This has suggested that genes that align with the spatial location of GBM were associated with neuroactive ligand–receptor interactions and biological processes including the regulation of synapse organization, the modulation of chemical synaptic transmission, and interactions involving neuroactive ligands and receptors. Furthermore, genes associated with synapses, which possess postsynaptic structures and glutamate receptors, such as *SV2B*, have been observed to exhibit elevated expression levels in various subgroups of malignant gliomas[25]. When exposed to high levels of Ca^{2+} glioma cells increase the release of glutamate into the tumour microenvironment (TME). This in turn leads to excessive glutamatergic and calcium ion signalling and promotes the spread of glioma calls[26]. Our results demonstrated that high levels of *SV2B* led to shorter overall survival in patients with GBM, suggesting its diagnostic value for GBM patient cohorts. The energy conductivity observed in gliomas may indicate an intensified information transmission. Conversely, it is worth noting that this abnormal and prolonged activity can result in a reduction in the physiologically normal conductivity. Despite the heightened activity in gliomas, it is important to acknowledge that their activity may not be solely dependent on *SV2B*.

Our STRING analysis indicated that *SV2B* is significantly co-expressed with genes involved in the ECM-receptor interaction, making it an important hub gene associated with signalling transduction. Previous evidence suggested that *PAK-1* and *SV2B* might act as GBM prognostic biomarkers when studied together[27]. As apparent from our KEGG pathway and GeneMania results, *SV2B* had a very strong interaction and co-expression with Synaptotagmin-1 (*SYT1*) instead. *SYT1* is situated on the vesicular membrane of nerve and endocrine cells. It acts as a primary calcium (Ca^{2+}) sensor in the mechanisms of neurotransmission and hormone secretion, and it plays a crucial role in processes triggered by Ca^{2+} for secretion[28]. Given the involvement of *SYT1* and its calcium-binding protein product, this gene has appeared in GBM hub oncogene nodes alongside *SV2B*[29,30]. Moreover, a larger scale analysis of glioblastoma and normal brain tissue samples obtained from the TCGA and GEO databases revealed that *SYT1* was one of the core genes associated with GBM progression among the 552 differentially expressed genes in that analysis[31]. Nevertheless, Losada-Pérez et al.[30] identified that *SYT1* gathers on the membrane of *Drosophila* glial cells, which in turn appears to intensify its expression within GBM samples. These statements, along with our findings suggested that the *SV2B* and *SYT1* could act as potential prognostic biomarkers in combination for GBM patients as both oncogenes are associated with shorter overall survival.

Previous bioinformatics studies suggested that *SV2B* expression may be associated with glioma grade or unfavourable prognosis, suggesting its oncogenic properties[32,33]. Additionally, *SV2B* was found to be overexpressed within breast cancer tissue when compared to normal tissue[34]. This is in support with our IHC results, which depicted significantly high SV2B protein expression in high grade brain malignancies, such as medulloblastoma and GBM, respectively. To the best of our knowledge, no current immunohistochemical evidence of expression for SV2B within patient cohorts diagnosed with brain tumours exists. One of the possible reasons for the high accumulation of SV2B within high grade brain malignancies could be widely distributed *SV2B* messenger neurotransmitter within the brain. In turn, that leads to elevated intracellular Ca^{2+} levels which stimulate cell proliferation and migration, leading to glioma cells acquiring their tumorigenic characteristics[35]. Additionally, SV2B has been demonstrated to be associated with energy metabolism, as the substantial energy requirements within the tumour may heavily depend on SV2B for regulating transporter protein activity, glucose transport, and other functions[36]. Our IHC findings revealed that the expression of SV2B increased with tumour grade, which suggested that highly metabolically active malignancies might require more of the protein to be able to proliferate and metastasise. GBMs and medulloblastoma represent advanced stage in the development of brain malignancies, where numerous genes are differentially expressed to varying extents. Additionally, half of the newly diagnosed high grade brain tumours are found in patients over 65 years[37]. Our results showed that patients in the age group of 61–80 years presented significantly high expression of SV2B in comparison to their normal counterparts suggesting its prognostic relevance in high grade brain malignancies. The significant overexpression of SV2B in the age groups of 0–20 years also suggested that the protein is highly expressed within paediatric brain malignancies too. Moreover, the elevated levels of SV2B found in highly malignant paediatric brain malignancy cases could be associated with their expression in brain regions characterized by pronounced synaptic plasticity. Furthermore, the observed difference between NAT and high-grade tumours is worth noting. The significant under expression of SV2B within NAT could be a result of the particular characteristics within this type of tissue that makes it a separate entity and distinguishes it from both healthy and tumour tissue. Thus, it could be suggested that *SV2B* could potentially act as an oncogene hence its high abundance in highly malignant brain tumours. Furthermore, the expression levels SV2B suggested that it can act as a prognostic marker, enhancing its clinical relevance in combating yet incurable highly malignant brain tumours, such as glioblastoma and

medulloblastoma. Therefore, SV2B holds promising hopes in the search for new biomarkers. However, there is still little known regarding their potential oncogenic mechanisms within brain cancers.

In summary, this study focused on the role of miRNAs in brain tumours, particularly in GBMs. Our research aimed to unveil the expression patterns of miR-34a and miR-128a exploring their potential as prognostic biomarkers and therapeutic targets. In silico analyses revealed downregulation of miR-128a and miR-34a in GBM suggesting their tumour suppressor roles. Also, the study investigated the interaction of miR-34a and/or miR-128a and *SV2B*, a putative target gene. SV2B was found upregulated in high grade glioma tissues and exerted potential as a clinical prognostic marker.

Nevertheless, it is worth noting the potential limitations associated with this study, including the genetic and molecular variations between paediatric and adult brain malignancies, as well as the differences in their treatment approaches. Additionally, sample size limitations in patient and control groups must not be disregarded. The inclusion of functional assays could strengthen the reliability of our conclusions and could guide future experimental investigations. Nonetheless, our research could still pave the way for clinical interventions aimed at miR-128a and miR-34a and their target gene, *SV2B*.

Methods

In silico miRNA analyses

Bioinformatic analysis was conducted to select the miRNAs with potential clinical relevance for the diagnosis, prognosis, and treatment of glioblastoma. The NCBI database was incorporated in the identification of GBM dysregulated genes by employing the following filter form category "Popular": Entrez Gene records that are current; gene records annotated on RefSeq chromosome or contig accessions; gene records associated with gene-specific reports in dbSNP (VAR); and Genes with records in the ClinVar database. The miRSystem database (http://mirsystem.cgm.ntu.edu.tw/index.php) was used to generate a report of miRNAs targeting the GBM dysregulated genes from the NCBI report. The default parameter in miRSystem was set at three algorithm hits in order to increase the reliability of the generated results. The Kyoto Encyclopaedia of Genes and Genomes (KEGG; https://www.genome.jp/kegg/pathway.html)[38] was consequently utilised to study differentially expressed miRNAs and genes associated with glioblastoma and their relevance in tumorigenesis. The sample size included 529 GBM cases (grade 4). The miRBase database (https://mirbase.org) was used for miRNA sequences and annotations, whereas the Software for Statistical folding of nucleic acids and studies of regulatory RNAs (Sfold) (https://sfold.wadsworth.org/cgi-bin/starmirWeb.pl)[39] provided the probable binding sites of the chosen to miRNAs to their gene target. Subsequently, a Venn diagram of common target miRNAs for *SV2B*, was created via Venny2.1.0 (https://bioinfogp.cnb.csic.es/tools/venny/). Four different miRNA tools were employed to generate miRNAs that target *SV2B*. These included: miRSystem, miRWalk (*SV2B*—XM_017022761) (http://mirwalk.umm.uni-heidelberg.de/), TargetScan (*SV2B*-ENST00000394232.1), and ENCORI (The Encyclopaedia of RNA Interactomes) (https://starbase.sysu.edu.cn/). The four databases were employed to provide stronger evidence for functional miR–mRNA target interactions (MTIs) and to reduce the likelihood of false positive results. Following that, the miRNA-centric network visual analytics platform miRNet2.0 (https://www.mirnet.ca/)[40] was important in building a network of the miRNA-target interactions between the commonly co-expressed genes with *SV2B*.

In silico target gene analysis

To study the tissue gene expression of *SV2B* (ENSG00000185518.11), the Gtex Bulk database (https://www.gtexportal.org/home/gene/SV2B, GTEx Analysis Release V8, dbGaP Accession phs000424.v8.p2) was used. Expression values were shown in transcripts per million. Box plots were illustrated as median and 25th and 75th percentiles. Any points above or below the 1.5 times interquartile range were displayed as outliers. The protein expression of SV2B was depicted via the ProteomicsDB database (proteomics data—MS1, Q7L1I2) with no gender comparison conducted (https://www.proteomicsdb.org/proteomicsdb/#human/proteinDetails/Q7L1I2/expression). To elucidate the indolent of SV2B in a given biological pathway, KEGG Pathway (has:9899) and ProteomicsDB Pathway (Q7L1I2) analyses were conducted (https://www.genome.jp/entry/hsa:9899; https://www.proteomicsdb.org/proteomicsdb/#human/proteinDetails/Q7L1I2/interactions). To assess the effects of differential expression of SV2B upon GBM survival states, the Xena Functional Genomics Explorer (https://xenabrowser.net/)[41] was used where the TCGA Glioblastoma study (631 GBM patient samples, grade 4) was selected for analysis. Recurrent GBM tumour samples were omitted from the final analysis reducing the sample size to 619 primary GBM tumour samples (grade 4; aged 10–89 years old; n = 230 females; n = 389 males). String interaction analysis for *SV2B* and its co-expressed genes was conducted by GeneMANIA (https://genemania.org/search/homo-sapiens/sv2b/)[42] and STRING (https://string-db.org/cgi/network?pollingId=bsDyNqzn53bk&sessionId=bLTkmworrpXG&urldisam=b7Gi9w2abdot).

Cell culture

The glioblastoma cell lines U251MG and U87MG were obtained from the American Type Culture Collection (ATCC, Manassas, VA, USA). U251MG and U87MG cells were cultured in complete minimum essential media (MEM) (GibcoTM, Bleiswijk, NL) supplemented with 10% FBS (Gibco, Bleiswijk, NL) and 1% Pen/Strep (Gibco, Bleiswijk, NL). Maintained in a humidifying incubator at 37 °C with 5% CO_2, the cells were regularly tested for mycoplasma contamination.

Immunohistochemistry

Paraffin-embedded, commercially available, brain tumour tissue microarray slides (US Biomax Inc., London, UK; GL631, GL803c, GL2082a) were obtained in compliance with Health Insurance Portability and Accountability Act (HIPAA) approved protocols to ensure ethical standards. The slides contained 351 biopsy cores from

207 patients. The slides featured different brain malignancy types at different stages including astrocytoma, oligoastrocytomas (referred to as IDH-wildtype diffuse astrocytic tumours across the manuscript according to the world health organisation (WHO) classification of brain tumours, 2021), ependymomas, oligodendrogliomas, medulloblastomas, and glioblastomas, alongside normal and normal adjacent control tissue (Supplementary Table 3). The term "oligoastrocytoma" occurring in the IHC tissue microarray was used according to the old WHO classification brain tumours. This has been replaced with the term "IDH-wild type astrocytic tumours" according to the 2021 WHO classification of brain tumours which was used across this manuscript[43]. The protocol followed was previously described by Filipe et al.[44]. Post deparaffinized, rehydrated, antigen retrieval, treatment with H_2O_2, and blocking, the slides were incubated overnight at 4 °C with the SV2B primary antibody (1:200 dilution) (ProteinTech, Manchester, UK). Following an overnight incubation at 4 °C, the slides were incubated with a secondary anti-rabbit antibody from the Zytochem Plus HRP-DAB Kit (HRP008DAB-RB, Zytomed Systems, UK) for 1 h. Then, streptavidin-HRP conjugate was added, followed by a 45min incubation. Staining and counterstaining with DAB and haematoxylin was performed, respectively. Dehydration was performed using ethanol and HistoClear, and coverslips were applied with DPX mounting medium. Immunoreactivity was assessed by three independent viewers using a light microscope (Zeiss Microscopy, Oberkochen, Germany). The extent of brown staining was scored based on the percentage of positively stained cells. Scoring categories included: 0 (< 5% cells), 1 (5–25% cells), 2 (26–50% cells), 3 (51–75% cells), and 4 (> 75% cells). The average score from the three independent assessments was calculated.

Immunofluorescence

U87MG and U251MG glioblastoma cells were seeded on round coverslips in a 12-well plate at a cell density of 2.5×10^5 cells/well. The cells were grown in their respective media type for 24 h. Following that, the cells were fixed with 4% paraformaldehyde (PFA) (Sigma-AldrichTM, Dorset, UK) for 45 min. Two 5-min wash steps with phosphate buffered saline (PBS) (ThermofisherTM, CA, USA) were then performed. Blocking of the slides with 5% bovine serum albumin (BSA) (Sigma-AldrichTM, Dorset, UK) for 1 h was then carried out. The blocking solution was aspirated, and cells were incubated in primary antibody (in 5% BSA) overnight at 4 °C with gentle agitation. The dilutions for the SV2B (ProteinTech, Manchester, UK) and the Beta Actin (Bio-Rad Laboratories, California, US) primary antibodies were 1:100. Next day, the antibody solution was aspirated, and cells were washed three times with PBS for 5 min. For secondary antibody alone controls, cells were incubated in blocks without primary antibody. All cells were subsequently incubated in secondary antibody Alexa Fluor 488 Phalloidin (Applied Biosystems ThermoFisher, Pleasanton, CA) (prepared as for primary) at a dilution of 1:500 for 1 h at room temperature with gentle agitation. Cells were then washed three times with PBS for 5 min. The coverslips were then removed from the 12-well plate and excess liquid was gently dabbed off with tissue paper. A few drops of 4′,6-diamidino-2-phenylindole (DAPI) were applied to each slide, and the coverslip was gently dropped downwards at a 45° angle. The coverslips were the sealed using nail varnish. The slides were protected from light and stored at 4 °C overnight allowing the nail varnish to dry. Fluorescent images were obtained using a Zeiss Axioimager M2 microscope fitted with an Axiocam 503 imaging device using Zeiss ZEN software (Zeiss Microscopy × 40 magnification). Cell fluorescence was visualised using an EC Plan-Neofluar 63× (1.25) oil objective. The following channels were used for various fluorophores—DAPI (Ex. – 353, Em. – 465), and Alexa Fluor 488 (Ex. – 493, Em. – 517). The ZenBlue (Zeiss) software was used for image acquisition and subsequent analysis.

Statistical analysis

GraphPad Prism 9.4.1 software (GraphPad Software, San Diego, USA) was used for statistical analysis and graphical representations. Two-way ANOVA followed by Tukey's multiple comparisons test was used for three or more groups. A p-value of < 0.05 was considered statistically significant.

Data availability

The datasets generated and/or analysed during the current study are available upon reasonable request. Researchers interested in accessing the data can contact the corresponding authors.

Received: 23 November 2023; Accepted: 28 February 2024
Published online: 19 March 2024

References

1. Larjavaara, S. *et al.* Incidence of gliomas by anatomic location. *Neuro-oncology* **9**(3), 319–325 (2007).
2. Gillespie, C. *et al.* Imaging timing after glioblastoma surgery (INTERVAL-GB): Protocol for a UK and Ireland, multicentre retrospective cohort study. *BMJ Open* **12**(9), e063043. https://doi.org/10.1136/bmjopen-2022-063043 (2022).
3. Rong, L., Li, N. & Zhang, Z. Emerging therapies for glioblastoma: Current state and future directions. *J. Exp. Clin. Cancer Res. CR* **41**(1), 142. https://doi.org/10.1186/s13046-022-02349-7 (2022).
4. Van Gool, S. *et al.* Randomized controlled immunotherapy clinical trials for GBM challenged. *Cancers* **13**(1), 32. https://doi.org/10.3390/cancers13010032 (2020).
5. Omuro, A. Immune-checkpoint inhibitors for glioblastoma: What have we learned?. *Arquivos de neuro-psiquiatria* **80**(5 Suppl 1), 266–269 (2022).
6. Ozair, A. *et al.* DNA methylation and histone modification in low-grade gliomas: Current under-standing and potential clinical targets. *Cancers* **15**(4), 1342. https://doi.org/10.3390/cancers15041342 (2023).
7. Gilard, V. *et al.* Diagnosis and management of glioblastoma: A comprehensive perspective. *J. Pers. Med.* **11**(4), 258. https://doi.org/10.3390/jpm11040258 (2021).
8. O'Brien, J., Hayder, H., Zayed, Y. & Peng, C. Overview of microRNA biogenesis, mechanisms of actions, and circulation. *Front. Endocrinol.* **9**, 402. https://doi.org/10.3389/fendo.2018.00402 (2018).

9. Chen, S. *et al.* Mechanisms controlling microRNA expression in tumour. *Cells* **11**(18), 2852. https://doi.org/10.3390/cells11182852 (2022).
10. Chen, N., Peng, C. & Li, D. Epigenetic underpinnings of inflammation: A key to unlock the tumour microenvironment in glioblastoma. *Front. Immunol.* **13**, 869307. https://doi.org/10.3389/fimmu.2022.869307 (2022).
11. Areeb, Z. *et al.* MicroRNA as potential biomarkers in glioblastoma. *J. Neuro-oncol.* **125**(2), 237–248 (2015).
12. Vaitkiene, P. *et al.* Association of miR-34a expression with quality of life of glioblastoma patients: A prospective study. *Cancers* **11**(3), 300. https://doi.org/10.3390/cancers11030300 (2019).
13. Vojdani, S. *et al.* Altered expression of EGFR and miR-34a derived from serum and tumoral tissue was associated with glioblastoma multiform. *Exp. Mol. Pathol.* **121**, 104655. https://doi.org/10.1016/j.yexmp.2021.104655 (2021).
14. Franzoni, E. *et al.* miR-128 regulates neuronal migration, outgrowth and intrinsic excitability via the intellectual disability gene Phf6. *eLife* **4**, e04263. https://doi.org/10.7554/eLife.04263 (2015).
15. Roth, P. *et al.* A specific miRNA signature in the peripheral blood of glioblastoma patients. *J. Neurochem.* **118**(3), 449–457 (2011).
16. Sun, J. *et al.* Serum microRNA-128 as a biomarker for diagnosis of glioma. *Int. J. Clin. Exp. Med.* **8**(1), 456–463 (2015).
17. Requena, A. The role of the synaptic protein sv2b in embryonic development of the cerebral cortex. Doctoral dissertation, Universidad Miguel Hernández. https://hdl.handle.net/11000/25586 (2020).
18. Shirjang, S. *et al.* miR-330 regulates colorectal cancer oncogenesis by targeting BACH1. *Adv. Pharm. Bull.* **10**(3), 444–451 (2020).
19. Wang, M. *et al.* Coronin 3 promotes the development of oncogenic properties in glioma through the Wnt/β-catenin signalling pathway. *OncoTargets Ther.* **13**, 6661–6673 (2020).
20. Morris, G., Reschke, C. & Henshall, D. Targeting microRNA-134 for seizure control and disease modification in epilepsy. *EBioMedicine* **45**, 646–654 (2019).
21. Grønborg, M. *et al.* Quantitative comparison of glutamatergic and GABAergic synaptic vesicles unveils selectivity for few proteins including MAL2, a novel synaptic vesicle protein. *J. Neurosci.* **30**(1), 2–12 (2010).
22. Morgans, C. W. *et al.* Loss of the synaptic vesicle protein SV2B results in reduced neurotransmission and altered synaptic vesicle protein expression in the retina. *PLoS One* **4**(4), e5230. https://doi.org/10.1371/journal.pone.0005230 (2009).
23. Pazarlar, B. A. *et al.* Expression profile of synaptic vesicle glycoprotein 2a, b, and C paralogues in temporal neocortex tissue from patients with Temporal Lobe Epilepsy (TLE). *Mol. Brain* **15**(1), 45. https://doi.org/10.1186/s13041-022-00931-w (2022).
24. Bao, H. *et al.* New insights into glioma frequency maps: From genetic and transcriptomic correlate to survival prediction. *Int. J. Cancer* **152**(5), 998–1012 (2023).
25. Venkatesh, H. S. *et al.* Electrical and synaptic integration of glioma into neural circuits. *Nature* **573**(7775), 539–545 (2019).
26. Masui, K., Onizuka, H., Cavenee, W. K., Mischel, P. S. & Shibata, N. Metabolic reprogramming in the pathogenesis of glioma: Update. *Neuropathology* **39**(1), 3–13 (2019).
27. Long, H. *et al.* Prediction and analysis of key genes in glioblastoma based on bioinformatics. *BioMed Res. Int.* **2017**, 7653101. https://doi.org/10.1155/2017/7653101 (2017).
28. Banerjee, A., Lee, J., Nemcova, P., Liu, C. & Kaeser, P. S. Synaptotagmin-1 is the Ca^{2+} sensor for fast striatal dopamine release. *Life* **9**, e58359. https://doi.org/10.7554/eLife.58359 (2020).
29. Polisetty, R. V. *et al.* LC-MS/MS analysis of differentially expressed glioblastoma membrane proteome reveals altered calcium signaling and other protein groups of regulatory functions. *Mol. Cell. Proteom.* **11**(6), M111.013565. https://doi.org/10.1074/mcp.M111.013565 (2012).
30. Losada-Pérez, M., Hernández García-Moreno, M., García-Ricote, I. & Casas-Tinto, S. Synaptic components are required for glioblastoma progression in Drosophila. *PLoS Genet.* **18**(7), e1010329. https://doi.org/10.1371/journal.pgen.1010329 (2022).
31. Zhou, Y. *et al.* Identification of potential biomarkers in glioblastoma through bioinformatic analysis and evaluating their prognostic value. *BioMed Res. Int.* **2019**, 6581576. https://doi.org/10.1155/2019/6581576 (2019).
32. Wang, H., Liu, D. & Yang, J. Prognostic risk model construction and molecular marker identification in glioblastoma multiforme based on mRNA/microRNA/long non-coding RNA analysis using random survival forest method. *Neoplasma* **66**(3), 459–469 (2019).
33. Zhang, Y. *et al.* Bioinformatics analysis of potential core genes for glioblastoma. *Biosci. Rep.* **40**(7), BSR20201625. https://doi.org/10.1042/BSR20201625 (2020).
34. Bandala, C. *et al.* Synaptic vesicle protein 2 (SV2) isoforms. *Asian Pac. J. Cancer Prev. APJCP* **13**(10), 5063–5067 (2012).
35. Pei, Z., Lee, K. C., Khan, A., Erisnor, G. & Wang, H. Y. Pathway analysis of glutamate-mediated, calcium-related signaling in glioma progression. *Biochem. Pharmacol.* **176**, 113814. https://doi.org/10.1016/j.bcp.2020.113814 (2020).
36. Liu, Z. *et al.* Structural basis for botulinum neurotoxin E recognition of synaptic vesicle protein 2. *Nat. Commun.* **14**(1), 2338. https://doi.org/10.1038/s41467-023-37860-8 (2023).
37. Renovanz, M. *et al.* Health-related quality of life and distress in elderly vs. younger patients with high-grade glioma-results of a multicenter study. *Support Care Cancer.* **28**(11), 5165–5175. https://doi.org/10.1007/s00520-020-05354-8 (2020).
38. Kanehisa, M., Furumichi, M., Sato, Y., Kawashima, M. & Ishiguro-Watanabe, M. KEGG for taxonomy-based analysis of pathways and genomes. *Nucleic Acids Res.* **51**(D1), D587–D592. https://doi.org/10.1093/nar/gkac963 (2023).
39. Ding, Y., Chan, C. Y. & Lawrence, C. E. Sfold web server for statistical folding and rational design of nucleic acids. *Nucleic Acids Res.* **32**(Web Server Issue), W135–W141. https://doi.org/10.1093/nar/gkh449 (2004).
40. Chang, L. & Xia, J. MicroRNA regulatory network analysis using miRNet 2.0. *Methods Mol. Biol.* **2594**, 185–204 (2023).
41. Goldman, M. J. *et al.* Visualizing and interpreting cancer genomics data via the Xena platform. *Nat. Biotechnol.* **38**(6), 675–678 (2020).
42. Franz, M. *et al.* GeneMANIA update 2018. *Nucleic Acids Res.* **46**(W1), W60–W64. https://doi.org/10.1093/nar/gky311 (2018).
43. Louis, D. N. *et al.* The 2021 WHO classification of tumors of the central nervous system: A summary. *Neuro-oncology* **23**(8), 1231–1251. https://doi.org/10.1093/neuonc/noab106 (2021).
44. Filipe, A. *et al.* Differential expression of RAD51AP1 in ovarian cancer: Effects of siRNA in vitro. *J. Person. Med.* **12**(2), 201. https://doi.org/10.3390/jpm12020201 (2022).

Author contributions

D.M. performed all experiments, evaluated and interpreted data analyses, and drafted the manuscript. S.S. supervised the lab and in silico work and reviewed the manuscript. L.K. assisted in the experimental work. E.K. supervised the experimental work and reviewed the manuscript. M.B. designed, coordinated, supervised the study and reviewed the manuscript. All authors have read and agreed to the published version of the manuscript.

Competing interests

The authors declare no competing interests.

Additional information

Supplementary Information The online version contains supplementary material available at https://doi.org/10.1038/s41598-024-55917-6.

Correspondence and requests for materials should be addressed to M.B.

Reprints and permissions information is available at www.nature.com/reprints.

Publisher's note Springer Nature remains neutral with regard to jurisdictional claims in published maps and institutional affiliations.

Open Access This article is licensed under a Creative Commons Attribution 4.0 International License, which permits use, sharing, adaptation, distribution and reproduction in any medium or format, as long as you give appropriate credit to the original author(s) and the source, provide a link to the Creative Commons licence, and indicate if changes were made. The images or other third party material in this article are included in the article's Creative Commons licence, unless indicated otherwise in a credit line to the material. If material is not included in the article's Creative Commons licence and your intended use is not permitted by statutory regulation or exceeds the permitted use, you will need to obtain permission directly from the copyright holder. To view a copy of this licence, visit http://creativecommons.org/licenses/by/4.0/.

© The Author(s) 2024

Appendix 8. Relevant publications to work done in Chapter 5, Journal: *ACS omega*

ACS OMEGA

Open Access

This article is licensed under CC-BY 4.0

http://pubs.acs.org/journal/acsodf

Article

MicroRNA-Dependent Mechanisms Underlying the Function of a β-Amino Carbonyl Compound in Glioblastoma Cells

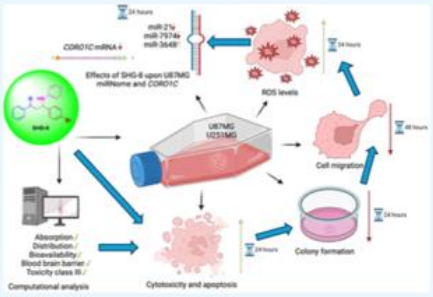
Denis Mustafov, Shoib S. Siddiqui, Andreas Kukol, George I. Lambrou, Shagufta, Irshad Ahmad, and Maria Braoudaki*

Cite This: *ACS Omega* 2024, 9, 31789−31802

Read Online

ACCESS | Metrics & More | Article Recommendations | Supporting Information

ABSTRACT: Glioblastoma (GB) is an aggressive brain malignancy characterized by its invasive nature. Current treatment has limited effectiveness, resulting in poor patients' prognoses. β-Amino carbonyl (β-AC) compounds have gained attention due to their potential anticancerous properties. *In vitro* assays were performed to evaluate the effects of an in-house synthesized β-AC compound, named SHG-8, upon GB cells. Small RNA sequencing (sRNA-seq) and biocomputational analyses investigated the effects of SHG-8 upon the miRNome and its bioavailability within the human body. SHG-8 exhibited significant cytotoxicity and inhibition of cell migration and proliferation in U87MG and U251MG GB cells. GB cells treated with the compound released significant amounts of reactive oxygen species (ROS). Annexin V and acridine orange/ethidium bromide staining also demonstrated that the compound led to apoptosis. sRNA-seq revealed a shift in microRNA (miRNA) expression profiles upon SHG-8 treatment and significant upregulation of miR-3648 and downregulation of miR-7973. Real-time polymerase chain reaction (RT-qPCR) demonstrated a significant downregulation of *CORO1C*, an oncogene and a player in the Wnt/β-catenin pathway. *In silico* analysis indicated SHG-8's potential to cross the blood−brain barrier. We concluded that SHG-8's inhibitory effects on GB cells may involve the deregulation of various miRNAs and the inhibition of *CORO1C*.



1. INTRODUCTION

Glioblastoma (GB) is the most aggressive, fastest growing, and heterogeneous primary brain malignancy occurring in adults. GB accounts for nearly 3350 newly diagnosed cases in the UK annually with an overall survival rate between 6−17 months.[1] Current, aggressive therapeutic approaches involving maximal surgical excision followed by radiotherapy and chemotherapy with temozolomide (TMZ) have failed to improve the overall survival rates, and patients' prognoses remain poor.[2] Furthermore, cisplatin is a highly effective chemotherapy drug. However, its application in treating GB is constrained by significant systemic toxicity and a limited ability to penetrate the brain tumor tissue, even with direct administration into the brain using standard delivery methods.[3] Thus, the essential need for researching alternative therapeutic strategies for managing the malignancy have brought attention to micro-RNAs (miRNAs) due to their multimodal targeting capabilities.

MiRNAs are short, noncoding RNAs that regulate various biological mechanisms at the post-transcriptional level.[4] In GB, the miRNA landscape reflects the disease stage and holds potential for prognostic evaluation and therapy selection. Previous research has demonstrated that miRNAs undergo dynamic alterations throughout the progression of the malignancy and have a direct involvement in GB tumorigenesis via regulating neo-angiogenesis, proliferation, invasion, and apoptosis.[5]

The functional relevance of GB-specific miRNAs highlights their dual roles as oncogenes and tumor-suppressors. Subsequently, miRNA expression profiling in GB aims to identify particular miRNA expression signatures associated with the tumorigenesis process and response to treatment. Several miRNAs have been found deregulated in GB and were associated with anticancer therapies. For instance, inhibition of miR-21 has been shown to increase the chemosensitivity of glioma cells to carmustine (BCNU), thereby enhancing the effectiveness of treatment.[6] Another example to sensitize GB cells toward TMZ chemotherapy is the overexpression of miR-128.[7] Thus, changes in the expression of miRNAs could underline their crucial role as therapeutic targets in GB and their potential in improving patient outcomes.

Meanwhile, the effectiveness of small-molecule inhibitors on miRNA expression remains a challenge and provides

Received: March 28, 2024
Revised: June 10, 2024
Accepted: June 18, 2024
Published: July 15, 2024



ACS Publications

© 2024 The Authors. Published by American Chemical Society

https://doi.org/10.1021/acsomega.4c02991
ACS Omega 2024, 9, 31789−31802

alternative therapeutic avenues. The biologically and medicinally important β-amino carbonyl (β-AC) compounds possess a β-amino carbonyl motif, which provides considerable stability and rigidity to the compound, resulting in enhanced pharmacokinetic dynamics and improved bioavailability.[8] Current research has demonstrated that β-AC compounds can act as anticancer agents by interfering with mitochondrial structures, thereby exhibiting antineoplastic properties. Specifically, some of these molecules decrease the mitochondrial membrane potential and generate reactive oxygen species (ROS), leading to programmed cell death.[9] The outcome of this cellular carbonyl stress might alter miRNA expression patterns and thus lead to their up- or downregulation. Further, oxidative stress might influence the miRNAs' stability and consequently their interactions with their mRNA targets.[10] To the best of our knowledge, the effects of β-AC compounds on miRNA regulation within cancer and particularly GB have not been studied before.

Several studies have reported the effectiveness of compounds possessing a carbonyl motif in GB management. For instance, the α,β-unsaturated carbonyl moiety of guaianolide sesquiterpene lactone cynaropicrin (1) expressed strong antiproliferative activity within U251MG glioblastoma cancer stem cells, suggesting potential therapeutic applications in targeting GB.[11] In addition, a different sesquiterpene compound, compound 12 (oxyphyllanene B, OLB), which also possess an α,β-unsaturated carbonyl moiety was observed to induce apoptosis in time- and dose-dependent manners within TMZ-resistant GB cells.[12]

In the current study, we sought to investigate the efficacy of an in-house synthesized β-AC compound, b3-(4-bromophenyl)-1-phenyl-3-(phenylamino)propan-1-one (SHG-8), and its effects upon miRNA regulation within GB cell models. The results demonstrated reduced cell migration and proliferation alongside induced cell death via ROS. The miRNA expression levels were drastically influenced by the drug with miR-21 being significantly downregulated after exposure to SHG-8.

2. MATERIALS AND METHODS

2.1. Synthesis of SHG-8. Considering the United Nations Sustainable Development Goals (SDGs), we have adopted a solid acid catalytic approach instead of Brønsted acid to synthesize SHG-8 (Supplementary Figure 1). The desired compound SHG-8 was synthesized by utilizing the sustainable sulfonic-acid-functionalized silica nanospheres (SAFSNS) nanocatalyst, which was prepared and characterized by Ahmad et al.[13] Details on the synthesis of SHG-8 can be found in the Supplementary Methodology (SM1).

2.2. Cell Culture. The U87MG and U251MG glioblastoma cell lines isolated from malignant gliomas were derived from the American Type Culture Collection (ATCC, Manassas, VA, USA). The cells were cultured in complete minimum essential medium (MEM; GibcoTM, Bleiswijk, NL) supplemented with 10% fetal bovine serum (FBS) (Gibco, Bleiswijk, Netherlands) and 1% penicillin/streptomycin (Gibco, Bleiswijk, Netherlands). Throughout the study, the cells were kept in a humidifying incubator at 37 °C with 5% CO_2 and were confirmed to be free of mycoplasma contamination.

2.3. *In Vitro* Functional Assays. Cell viability, colony forming, and wound-healing assays were performed as previously described by Vazhappilly et al.[14] U87MG and U251MG GB cells were seeded at different cell densities and subsequently treated with increasing SHG-8 concentrations (diluted in DMSO, Dubai, UAE). Dimethyl sulfoxide (DMSO; Thermofisher, CA, USA) was used as a negative control, whereas cisplatin (200 μM; Sigma-Aldrich, Dorset, UK) was used as a positive control. Further details on how the functional assays were performed can be found in the Supplementary Methodology (SM2−SM4).

2.4. Determination of ROS. A ROS assay kit (Abcam, Cambridge, UK) was used to assess the release of ROS within glioblastoma cell lines. U87MG and U251MG cells (1.5×10^4/well) were seeded in 96-well plates and incubated with 20 μL of Red ROS dye diluted in DMSO according to manufacturers' guidance. The plates were incubated for 1 h at 5% CO_2 and 37 °C. Subsequently, cells were treated with increasing SHG-8 concentrations (20 μM, 40 μM, 60 μM, 80 μM, and 100 μM), alongside PBS (negative control) and 1 mM H_2O_2 (positive control, Sigma-AldrichTM, Dorset, UK) for 30 min. Fluorescence increase of ROS was detected at an excitation wavelength of 520 nm and an emission wavelength of 605 nm using a CLARIOstar microplate reader at 0, 15, 30, 45, 60, 75, 90, 105, and 120 min.

2.5. Acridine Orange/Ethidium Bromide Staining. U87MG and U251MG cells were seeded at a density of 5×10^5 cells/well in six-well chambers with DMSO (negative control), 200 μM cisplatin (positive control), and SHG-8 (50 μM and 100 μM) for 24 h. Post-treatment, the media were removed, and the cells were washed twice with PBS. Following washes, cells were trypsinized and pelleted. The cells were centrifuged at 200*g* for 5 min. The pellets were then resuspended in 1 mL of ice-cold PBS and centrifuged again at 200*g* for 5 min. The pellets were then resuspended in 20 μL of ice-cold PBS and stained with 2 μL of acridine orange (100 μg/mL) and ethidium bromide (100 μg/mL; ThermoFisher, CA, USA) dye for 3 min at room temperature. The stained cell suspension was added on a glass slide. The coverslips were applied onto the slides, and immunofluorescence images were captured using a 40× objective on an EVOS fluorescent microscope (Life Technologies, CA, USA) that was set at 30 lx/s exposure.

2.6. Annexin-V/Propidium Iodide Apoptosis Assay. To assess the extent of apoptosis induction following SHG-8 treatment, U87MG and U251MG cells were seeded at a density of 3×10^6 cells/well in six-well chambers and allowed to adhere overnight. Subsequently, the wells containing cells were subjected to treatments with DMSO (negative control), 200 μM cisplatin (positive control), and SHG-8 (50 μM and 100 μM) for 24 h. Post-treatment, cells were washed twice with ice cold PBS, and 1×10^6 cells were harvested in 100 μL of suspension. RNase (1 μL, 10 mg/mL) was applied to each cell suspension, followed by labeling with Annexin-V FITC (5 μL) and propidium iodide (100 μg/mL). As per manufacturer instructions, each cell suspension was incubated with the dead cells Annexin-V/propidium iodide apoptosis kit for flow cytometry (Invitrogen, Inchinnan, UK) at room temperature for 15 min. After the incubation period, 400 μL of annexin binding buffer was applied to each sample and subsequently analyzed using the Guavasoft 3.1.1 software and the guava easyCyte HT system (Merck Millipore, Watford, UK).

2.7. RNA Isolation and TaqMan Expression Assays. RT-qPCR was performed as described by Braoudaki et al.[15] In brief, total RNA and miRNAs were extracted following the Trizol reagent (Ambion Life Technology, Aukland, New Zealand) protocol and mirVana isolation kit (ThermoFisher, Vilnius, Lithuania), respectively. The sample's quantity and

https://doi.org/10.1021/acsomega.4c02991
ACS Omega 2024, 9, 31789−31802

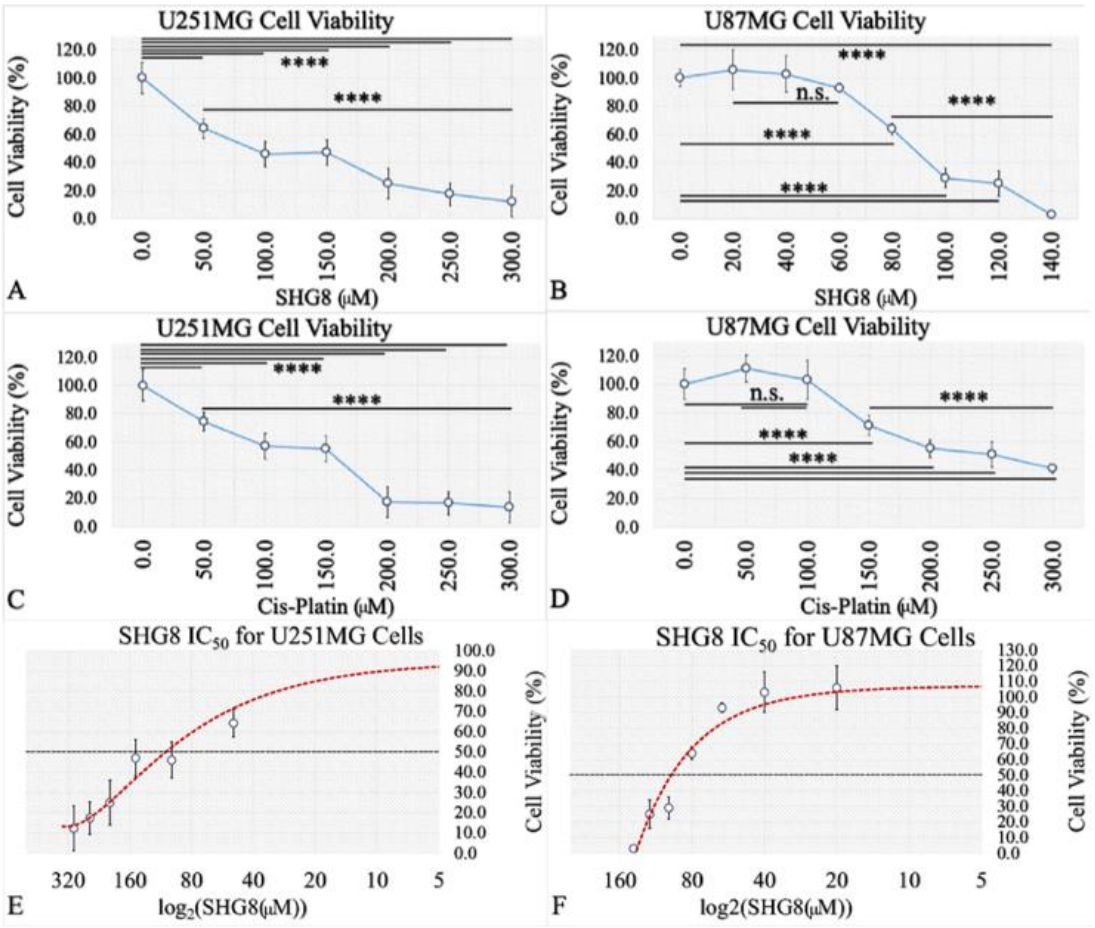


Figure 1. U251MG and U87MG glioma cell viability and proliferation dependency on SHG-8 concentration. MTT assay upon treatment with different concentrations of SHG-8 (50 μM, 100 μM, 150 μM, 200 μM, 250 μM, and 300 μM) for the U251MG cells revealing an IC_{50} of 100 μM (A, E). MTT assay upon treatment with SHG-8 (20 μM, 40 μM, 60 μM, 80 μM, 100 μM, 120 μM, and 140 μM) for the U87MG cells revealing an IC_{50} of 85 μM (B, F). MTT assay upon treatment with increasing concentrations of cisplatin (50 μM, 100 μM, 150 μM, 200 μM, 250 μM, and 300 μM) for both U251MG (C) as well as U87MG cells (D) manifested a significant cytotoxicity effect (legend: ns, nonsignificant, $*p < 0.05$, $**p < 0.01$, $***p < 0.001$, $****p < 0.0001$).

quality were assessed using Nanodrop (Nanodrop ND1000 Spectrophotometer, Marshall Scientific, Hampton, USA). Further details on RNA isolation and expression analysis can be found in the Supplementary Methodology (SM5).

2.8. Preparation of Samples for Small RNA Sequencing. U87MG RNA samples were extracted with Trizol. A nanodrop bioanalyzer was used to detect the purity of RNA samples, concentration, and integrity and to ensure the use of qualified samples for sequencing. RNA integrity was assessed using the RNA Screen Tape Kit of the Agilent Bioanalyzer 2100 system (Agilent Technologies, CA, USA). Samples with RNA integrity numbers (RINs) greater than seven were sent off for sRNA-seq to Biomarker Technologies (Biomarker Technologies, Germany). Further information on library preparation, clustering, sequencing, and data analyses can be found in the Supporting Information (SM6−13).

2.9. Metabolite and Toxicity Prediction of SHG-8. Metabolites of SHG-8 were predicted with Biotransformer 3.1.0 using the canonical Simplified Molecular-Input Line-Entry System (SMILES).[16] The set of "Human and Human Gut" metabolic transformations was selected with one reaction iteration and a "combined CYP450 mode". The absorption, distribution, metabolism, excretion, and toxicity (ADMET) properties of SHG-8 and metabolites were predicted with admetSAR 2.0 using the canonical SMILES with the option "ADMET properties for drug discovery" selected. AdmetSAR 2.0 predictions are based on machine learning methods based on molecular similarity utilizing data for 96 000 compounds.[17]

2.10. Molecular Docking Analysis. The crystal structure of human CORO1C was retrieved from the Protein Data Bank (https://www.rcsb.org). Docking analysis was then performed via utilizing CB-DOCK2 (https://cadd.labshare.cn/cb-dock2/index.php) to predict the stable binding configuration and molecular interactions between the receptor (CORO1C) and ligand (SHG-8). An SDF file of the query ligand was uploaded on CB-DOCK2, and blind docking was performed. The outcomes of the molecular docking between SHG-8 and the

https://doi.org/10.1021/acsomega.4c02991
ACS Omega 2024, 9, 31789−31802

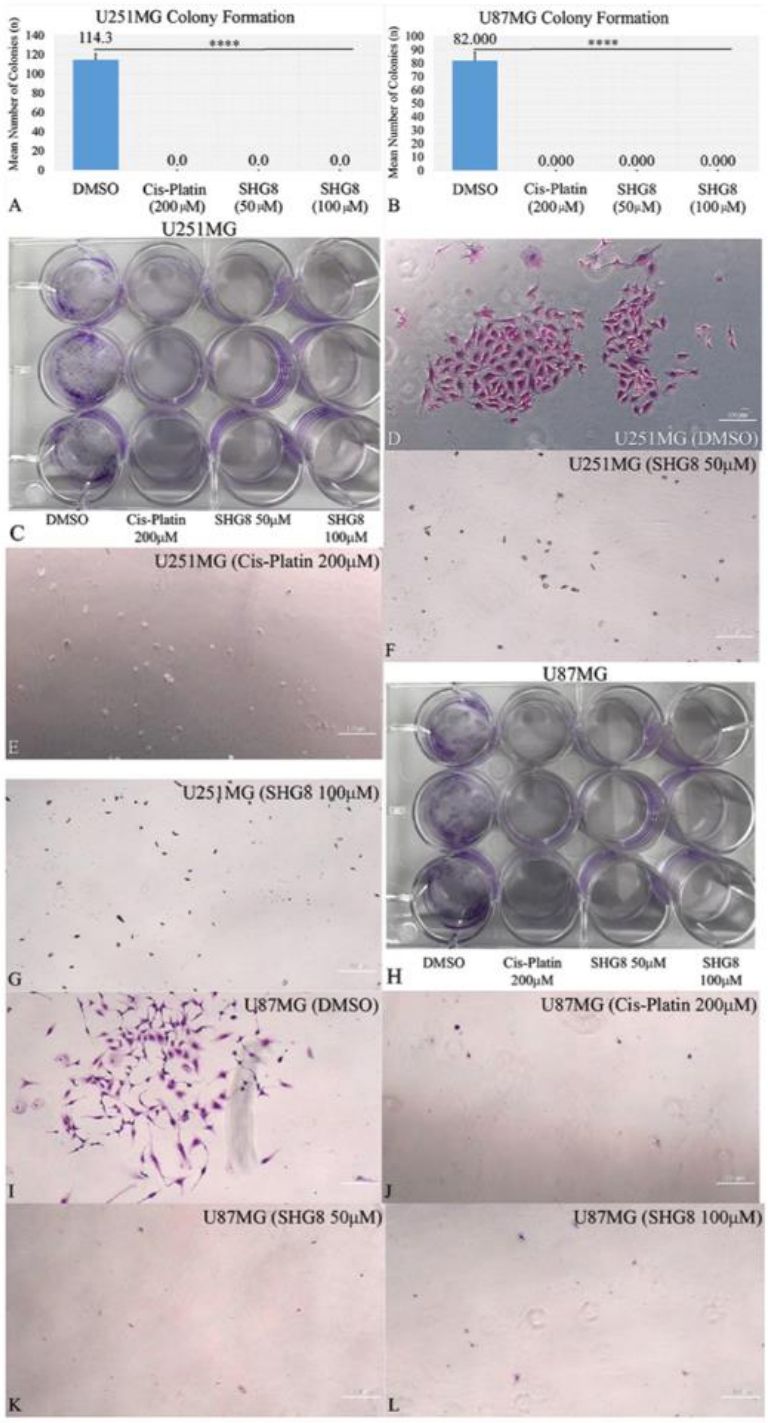


Figure 2. U251MG and U87MG glioma cell migration dependency on SHG-8 concentration. Significant decrease of U251MG colonies' proliferative clonal capacity upon 50 μM and 100 μM SHG-8 treatment (A). Significant decrease of U87MG colonies' proliferative clonal capacity upon 50 μM and 100 μM SHG-8 treatment (B). This was also manifested microscopically where the colony formation inhibition was observed for both the U251MG (C–G) and U87MG cells (H–L). Plates and microscopic images of colonies were taken under 40× magnification; legend: ns, nonsignificant, *$p < 0.05$, **$p < 0.01$, ***$p < 0.001$, ****$p < 0.0001$).

https://doi.org/10.1021/acsomega.4c02991
ACS Omega 2024, 9, 31789–31802

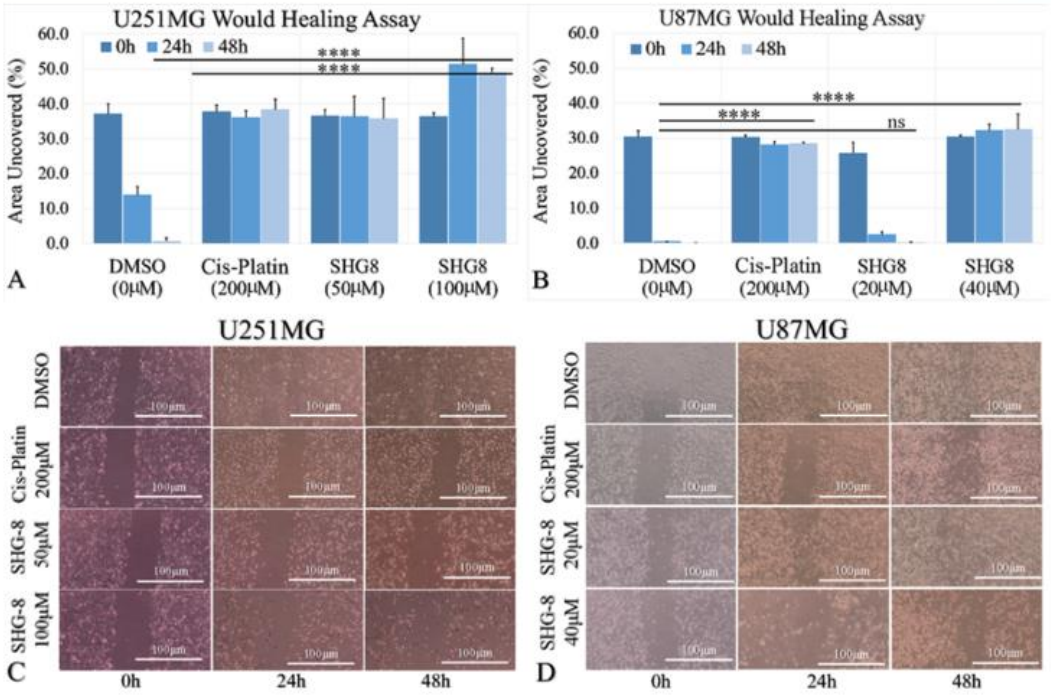


Figure 3. U251MG and U87MG glioma cells wound-healing assay dependency on SHG-8 concentration. (A) Quantification of the wound-healing assay of U251MG cells following treatment with DMSO, cisplatin, and SHG-8 (50 μM and 100 μM) across different time points. (B) Wound-healing area quantification of U87MG cells following treatment with DMSO, cisplatin, and SHG-8 (20 μM and 40 μM) across different time points. (C) Scratch images acquired at 0 h, 24 h and 48 h from U251MG cells treated as described above. (D) Wound (scratch) images acquired at 0 h, 24 h, and 48 h from U251MG cells treated as described above (legend: ns, nonsignificant; *p < 0.05, **p < 0.01, ***p < 0.001, ****p < 0.0001).

target protein were depicted using BioLip (version of 2021.09.15).[18]

2.11. Statistical Analysis. Statistical analysis was performed using GraphPad Prism 9.4.1 software (GraphPad Software, San Diego, USA), which was also used to create all graphical representations. One-way ANOVA was used to determine statistical differences between two groups, while two-way ANOVA tests followed by Tukey's multiple comparisons were used for the analysis of three or more groups; p values of <0.05 were regarded as statistically significant.

3. RESULTS AND DISCUSSION

3.1. SHG-8 Cytotoxicity Inhibited U251MG and U87MG Cells' Proliferative Ability. To investigate whether SHG-8 exhibited cytotoxic effects within GB cells, an MTT cell viability assay was performed in the U251MG and U87MG cell lines treated with DMSO (as a vehicle, which corresponds to 0 μM SHG-8) and increasing SHG-8 concentrations. In particular, for the U251MG cell line, the concentrations tested were 50 μM, 100 μM, 150 μM, 200 μM, 250 μM, and 300 μM. Respectively, for the U87MG cell line, the concentrations tested were 20 μM, 40 μM, 80 μM, 100 μM, 120 μM, and 140 μM. In addition, both cell lines were treated with cisplatin and, in particular, at 50 μM, 100 μM, 150 μM, 200 μM, 250 μM, and 300 μM for both cell lines.

Cells treated with SHG-8, as obtained from the MTT assay, revealed a significant reduction of cell viability in the treatment conditions from 50 μM to 300 μM for U251MG cells (Figure 1A), as well as in the treatment conditions of 80 μM and 100 μM for the U87MG cell (Figure 1B). At the same time, U251MG cells appeared to be also sensitive to cisplatin (Figure 1C), with less sensitivity manifested by the U87MG cells (Figure 1D). For the U251MG cells, the IC_{50} of SHG-8 was estimated to be at the 100 μM level (p < 0.0001; Figure 1E), while the IC_{50} for U87MG cells was 85 μM (p < 0.0001; Figure 1F). Overall, both SHG-8 and cisplatin manifested significant cytotoxicity in both cell lines, yet the SHG-8 agent manifested better results in the U87MG cell line (Figure 1B).

3.2. SHG-8 Cytotoxicity Inhibits U251MG and U87MG Cells Colony Formation Abilities. Following the observed cytotoxicity drug effects, the clonogenic capacity of U251MG and U871MG cells was examined after being treated with SHG-8 concentrations of 50 μM and 100 μM (Figure 2A–L). Cisplatin also significantly reduced the clonogenic abilities of GB cells (p < 0.0001).

3.3. SHG-8 Cytotoxicity Inhibits U251MG and U287 Cells Wound-Healing Capacity. The wound-healing assay results demonstrated that the percentage of the area uncovered remained unchanged at 50 μM and 100 μM SHG-8 exposure (U251MG cells) and 40 μM SHG-8 exposure (U87MG cells) when compared to DMSO (Figure 3A and B). The results obtained post-treatment of U251MG cells revealed that

https://doi.org/10.1021/acsomega.4c02991
ACS Omega 2024, 9, 31789−31802

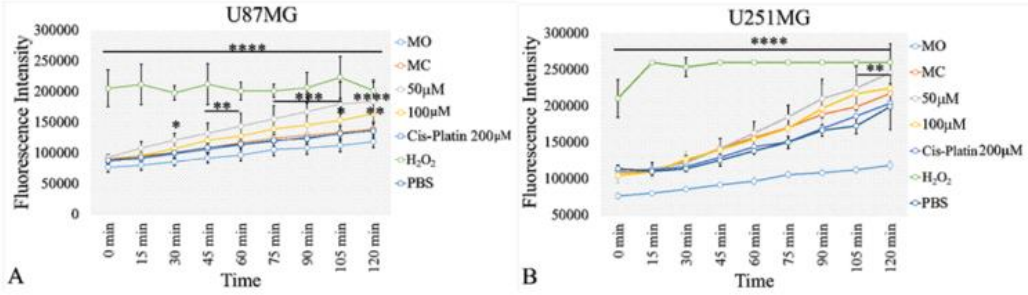


Figure 4. SHG-8 led to the release of ROS. (A) A significant but non-concentration-dependent elevation of ROS was observed post 30 min treatment period with 50 μM SHG-8 in comparison to the control condition. SHG-8 of 100 μM concentration induced ROS cytotoxicity at 90 min. At 120 min, both SHG-8 concentrations of 50 μM and 100 μM demonstrated significantly higher levels of ROS within U87MG. (B) A significant but non-concentration-dependent elevation of ROS observed post 105 min treatment period with 50 μM SHG-8 in comparison to the control condition for U251MG cells (legend: ns, nonsignificant; $*p < 0.05$, $**p < 0.01$, $***p < 0.001$, $****p < 0.0001$).

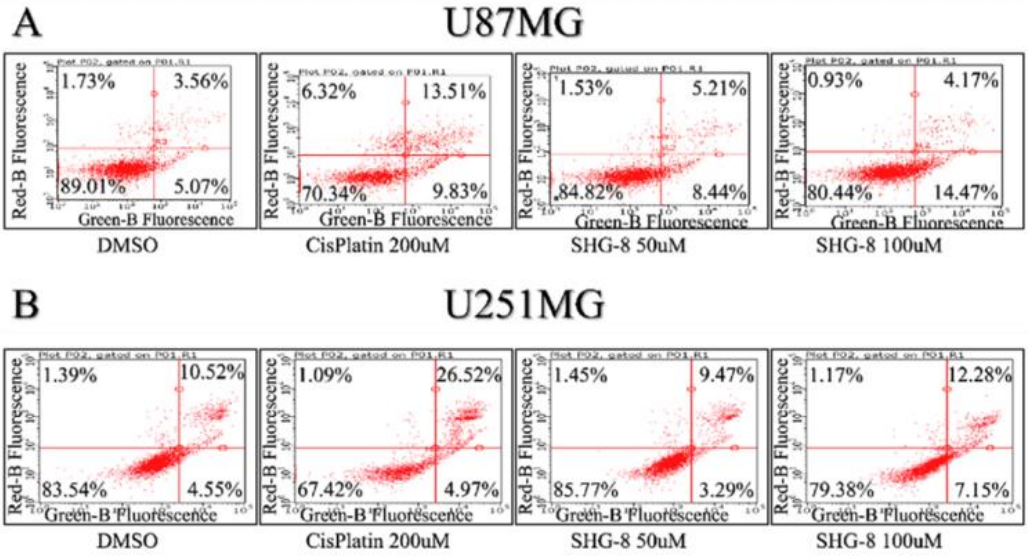


Figure 5. Annexin-V/propidium iodide (PI) staining of U87MG and U251MG cells treated with SHG-8. (A) Concentrations of 100 μM SHG-8 depicted a higher percentage of U87MG cells entering early apoptosis post-treatment (FITC positive and PI negative, lower right quadrant) in comparison to cisplatin, where more cells were seen in their late apoptosis stage (FITC positive and PI positive (upper right quadrant)). (B) Concentrations of 100 μM SHG-8 depicted a higher percentage of U251MG cells entering late apoptosis post-treatment (FITC positive and PI positive, upper right quadrant) in line with the positive control condition of cisplatin.

concentrations of 50 μM and 100 μM both significantly seized cell migration and led to no change in the percentage of area uncovered post-48 h incubation when compared to DMSO control cells ($p < 0.0001$). In fact, there was apparent cell death at 100 μM SHG-8 concentration (Figure 3C). At 24 h, the relative percentage of area uncovered was less within control cells in comparison to U87MG cells treated with 20 μM and 40 μM SHG-8, respectively ($p < 0.0001$). At 48 h, the relative area uncovered of control cells decreased further; however, so did the scratch at 20 μM, whereas the gap at 40 μM remained unchanged ($p < 0.0001$), indicating a concentration-dependent inhibitory effect upon U87MG cell migration (Figure 3D).

Beta-amino carbonyl derivatives have demonstrated promising potential in medicinal chemistry, drug development, and cancer therapy owing to their diverse biological activities and capacity to trigger apoptosis in cancerous cells.[19,20] This research incorporated an eco-friendly approach in an efficient, simple, and green catalytic process to produce SHG-8, aiming to demonstrate its *in vitro* cytotoxic effects on GB cell models.

The evaluation of the metabolic effects of SHG-8 upon GB cells revealed a significant decrease in cell viability and proliferation, suggesting that the β-AC compound possessed cytotoxic properties, which limit the growth and spread of cancer cells. Alongside the cytotoxic properties of the drug, the clonogenic potential of U87MG and U251MG cells was also significantly reduced, indicating impaired immortalization and

https://doi.org/10.1021/acsomega.4c02991
ACS Omega 2024, 9, 31789−31802

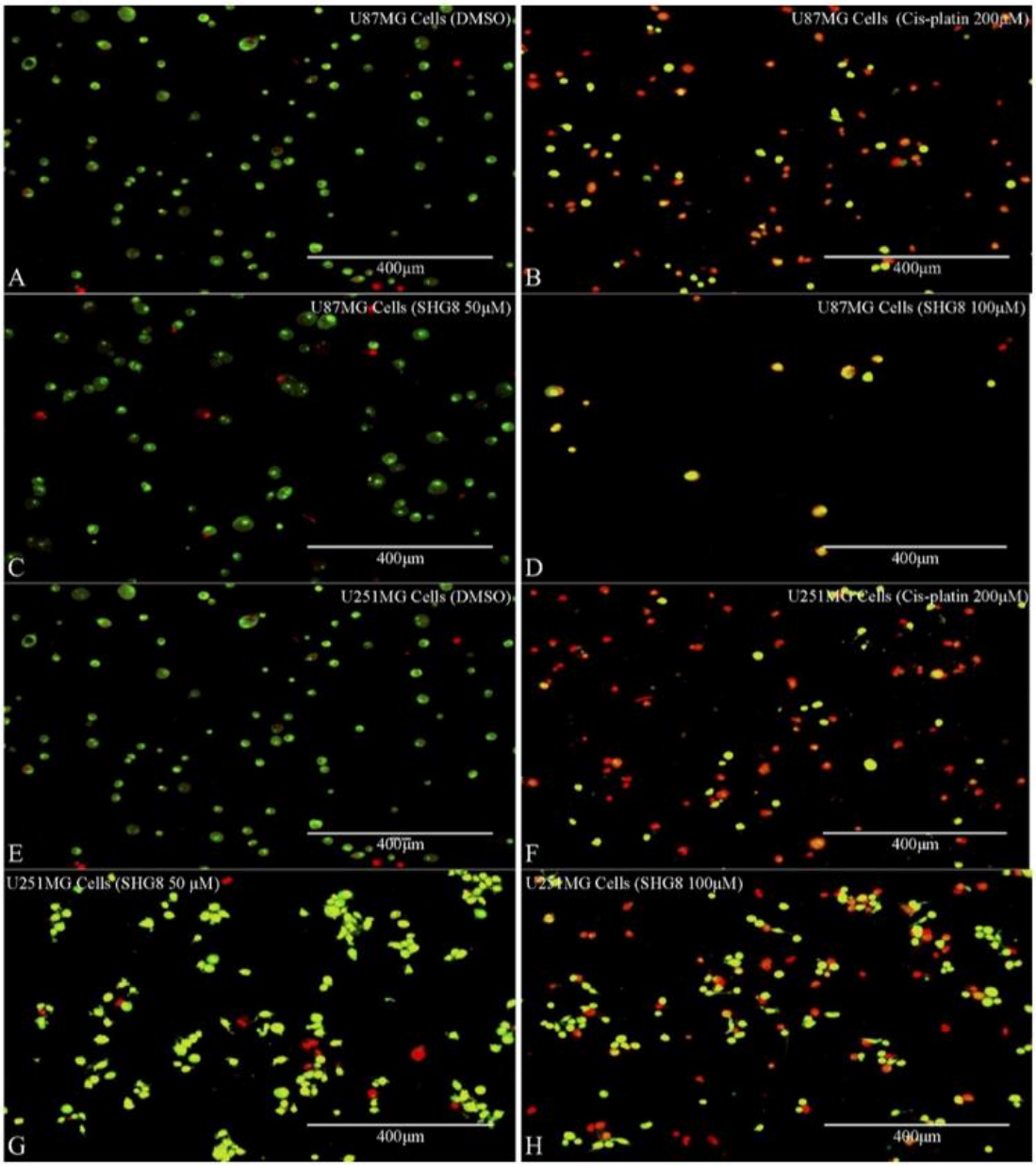


Figure 6. Acridine orange/ethidium bromide (AO/EB) staining. AO/EB fluorescent staining showing fluorescent microscopic images of U87MG and U251MG GB cells treated with DMSO (negative control), 200 μM cisplatin, and 50 μM and 100 μM of SHG-8 (A–H). Green cells were viable. Yellow cells indicated apoptosis, and orange/red cells indicated necrosis.

proliferation of cancer cells. The dose-dependent decrease in cell viability indicated that higher concentrations of the SHG-8 compound were required to increase cell death. Similar cytotoxic effects were previously observed with several β-AC compounds on human prostate cancer cells and colorectal cancer cells.[20,21] Currently, the most effective drug against gliomas is the chemotherapeutic agent TMZ. Combining chemotherapy with TMZ and radiotherapy is considered a gold standard therapeutic approach incorporated in the treatment regimens of GB patients with surgical tumor excision.[22] Nasir et al. demonstrated that TMZ doses as high as 1000 μM were most effective in inhibiting cell viability in U87MG cells.[23] The use of significantly high drug doses could lead to adverse effects on normal cells resulting in systemic toxicity, alongside intrinsic resistance to cytotoxic therapies. Subsequently, this contributes to treatment failure and tumor recurrence. Even though the actions of SHG-8 were observed to be dose-dependent, we demonstrated that concentrations

https://doi.org/10.1021/acsomega.4c02991
ACS Omega 2024, 9, 31789−31802

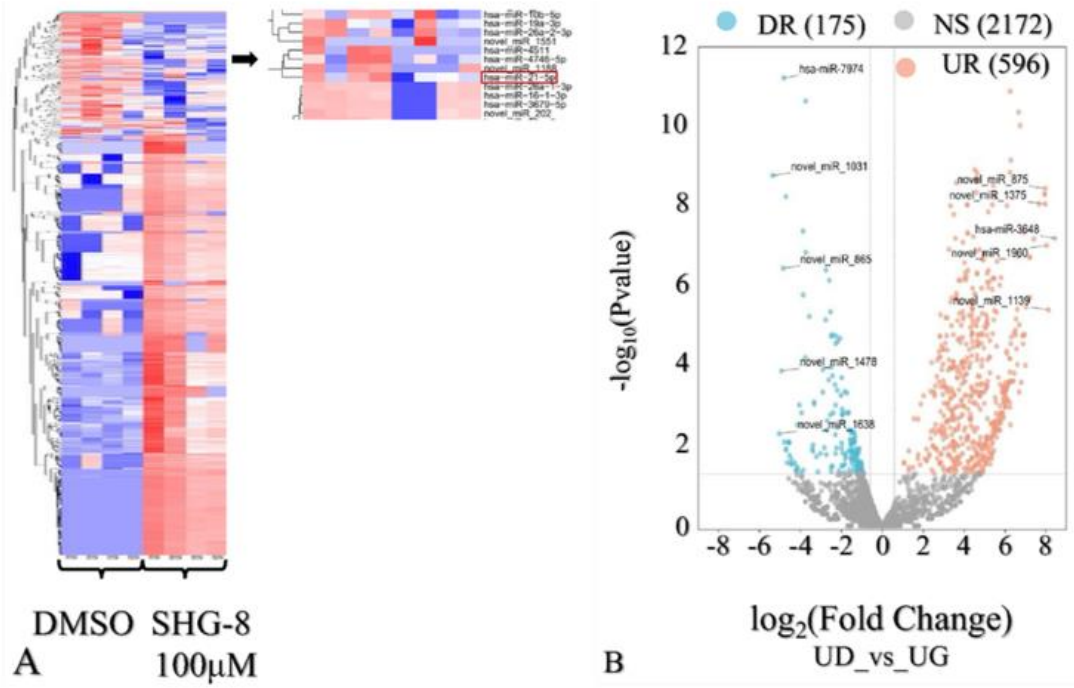


Figure 7. Comprehensive sRNA-seq analysis of SHG-8 treated samples. (A) Heatmap of deregulated miRNAs (groups: light blue, DMSO; light red, SHG-8 treated samples). (B) Volcano plot of miRNA expression revealed 771 deregulated miRNAs; 175 downregulated and 596 upregulated in the presence of SHG-8 (legend: NS, not significant; DR, downregulated; UR, upregulated).

below 100 μM were sufficient to induce restricted cell viability and cell proliferation due to induced cell cytotoxicity. These findings suggested SHG-8 can act effectively against brain tumor cells at low concentrations.

3.4. SHG-8 Induced Release of ROS and Led to Cell Death via Apoptosis. *3.4.1. ROS Release.* A significant elevation of ROS was observed during post 30 min treatment period of U87MG cells with 50 μM SHG-8 as compared to the control condition (Figure 4A). SHG-8 of 100 μM concentration induced ROS cytotoxicity later in time at 90 min. At 120 min, both SHG-8 concentrations demonstrated significantly higher levels of ROS within U87MG, resulting in oxidative damage of the U87MG GB cells. ROS release mechanisms of SHG-8-induced cytotoxicity in GB cells were observed to be time-dependent. A significant elevation for ROS was seen post 105 min within U251 treated cells with SHG-8 concentration at 50 μM (Figure 4B). Concentrations of 100 μM did not reveal significant ROS elevation for the later cell line.

3.4.2. ROS-Related Apoptosis. The Annexin V/PI assay revealed that U87MG cells treated with SHG-8 concentrations of 50 μM and 100 μM led to more cells entering an early apoptosis stage (8.44% and 14.47%, respectively; Figure 5A). The cisplatin positive control condition had a larger percentage of cells within the late apoptosis stage (13.51%). The degree of necrosis across all conditions was minimal. Cell cycle arrest analysis of U87MG cells demonstrated increased presence in the G2/M phase with SHG-8 at 50 μM. The results obtained from SHG-8-treated U251MG cells showed that more cells were entering late apoptosis with increasing SHG-8 concertation, similar to the results obtained from the positive control condition of cisplatin (Figure 5B). Cell cycle arrest was seen in the G2/M phase at 50 μM and 100 μM SHG-8-treated cells. It is notable that minor differences of the effect of SHG-8 on apoptosis between the two cell lines have been obtained, which could be attributed to variations in metabolic pathways such as glycolysis and purine metabolism. However, it is still evident that apoptosis was consistently detected in both cell lines, which validates the robustness of our results.

Compromising genomic integrity is a well-established cytotoxic mechanism of numerous genotoxic therapies.[24] High levels of ROS have been previously detected in multiple neurodegenerative disorders, such as Alzheimer's and Parkinson's diseases.[25] Thus, the therapeutic potential of ROS as a possible GB hallmark was evaluated in our study. To investigate if SHG-8 acted as a ROS-generating compound and its potential cytotoxic mechanism on DNA damage induction, ROS levels were measured upon treatment with the drug. Concentrations of 50 μM and 100 μM showed a significant impact on ROS release levels in a time-dependent manner. However, it is notable that 100 μM concentration induced ROS slower than did the 50 μM one, which could be attributed to the induced cell death caused by the higher concentration, resulting in less production of ROS. The antioxidant properties of ROS have also been observed in other inflammatory conditions, such as bowel disease.[26] This is in line with this study's findings, as GB is primarily associated with an inflammatory microenvironment signature that accelerates epigenetic changes, aiding tumor cells in avoiding immunological surveillance.[27] The oxidative stress exhibited upon U87MG and U251MG cells via ROS in our treatment conditions was further supported via subsequent Annexing

https://doi.org/10.1021/acsomega.4c02991
ACS Omega 2024, 9, 31789−31802

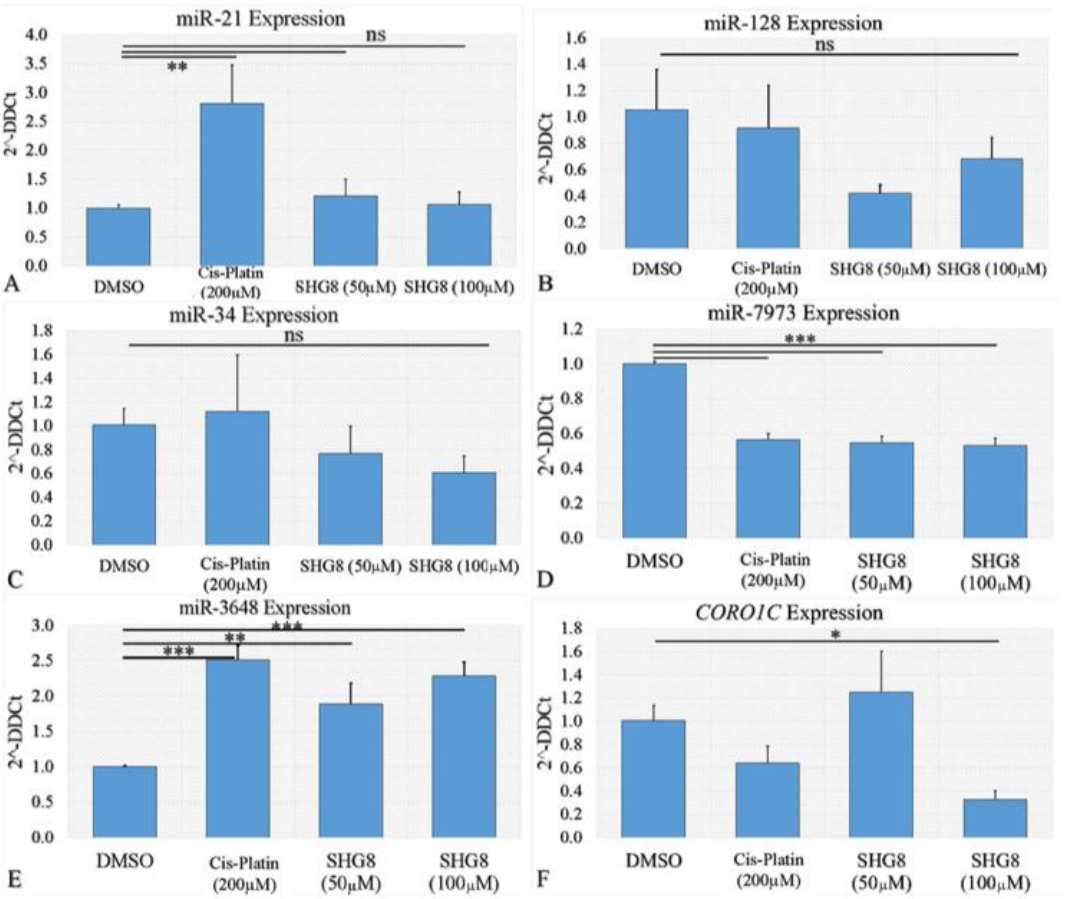


Figure 8. Relative RT-qPCR expression post exposure to SHG-8. Relative expression of miR-21 (A), miR-128a (B), miR-34a (C), miR-7973 (D), miR-3648 (E), and *CORO1C* (F) when treated with SHG-8 (q value < 0.05 and |log2 fold change| > 1; legend: ns, not significant, *p < 0.05, **p < 0.01, ***p < 0.001, ****p < 0.0001).

V/PI apoptosis assay. The SHG-8 treatment conditions (50 μM and 100 μM) resulted in the migration of U87MG cells toward the early apoptosis stage, while U251MG cells were seen to enter late apoptosis. These findings provide a potential explanation regarding the predominant cytotoxic mechanism of SHG-8 upon the inhibition of cell migration and proliferation, alongside the observed induction of apoptosis and tumor cell death.

3.5. Acridine Orange/EtBr (Ethidium Bromide) Staining. To detect if SHG-8 induced morphological alterations leading to apoptosis, AO/EtBr staining was performed for SHG-8-treated U87MG and U251MG cells (Figure 6A–H). The observed results depicted a high uptake of ethidium bromide at 100 μM SHG-8 concentrations, indicating a loss of membrane integrity and cell death. Concentrations of 50 μM depicted more U251MG cells entering early apoptosis in comparison to treated U87MG cells. Apoptotic and necrotic stages were also observed at 200 μM cisplatin, where more uptake of ethidium bromide was seen within U251MG treated cells. There was no indication of cell death in the negative control condition (DMSO), where the cells looked intact and in regular shape (Supplementary Table 2).

3.6. SHG-8 Downregulated miR-21 and *CORO1C*. sRNA-seq comprehensive miRNA expression and gene pathway analysis revealed that 771 miRNAs were either significantly upregulated or downregulated (Figure 7A). Of these, 175 miRNAs were downregulated, and 596 were upregulated in the SHG-8 treated conditions compared to the control samples (q value < 0.05 and |log2 fold change| > 1). The most downregulated miRNA was found to be miR-7974, which was associated with targeting 416 genes, while miR-3648 was the most upregulated miRNA, which targeted 212 genes (Figure 7B).

sRNA-seq miRNA analysis demonstrated that the commonly deregulated GB-specific miRNAs, miR-21-5p and miR-128a-3p were significantly downregulated. RT-qPCR results for these miRNAs did not reach a significant 2-fold change in expression (Figure 8A and B; p < 0.04 and p < 0.01, respectively). MiR-34a-5p (Figure 8C) showed no significant expression change in the sRNA-seq data and via RT-qPCR. RT-qPCR performed on miR-7974 (Figure 8D) and miR-3648 (Figure 8E) showed significant downregulation and upregulation, respectively. Furthermore, several genes involved in the Wnt/β-catenin pathway, such as *CORO2A*, *APC2*, and *WNT7A*, were direct

https://doi.org/10.1021/acsomega.4c02991
ACS Omega 2024, 9, 31789−31802

targets of the most upregulated or downregulated miRNAs (hsa-miR-3648 and hsa-miR-7974, respectively). Thus, the differential expression of the *CORO1C*, a potential oncogene and a player in this pathway, was assessed via RT-qPCR and found to be significantly downregulated in the 100 μM SHG-8 condition with a 2-fold change in expression ($p < 0.05$; Figure 8F).

MiRNAs have emerged as promising therapeutic targets in GB treatment. Their small size and stability are advantageous over targeting protein-coding genes, making them attractive candidates for therapeutic interventions.[27] Nevertheless miRNA-based therapies are not yet applicable due to their diverse binding abilities.

Thus, a response to a given drug may differ due to the multiple targets a single miRNA can regulate. To elucidate the action of SHG-8 upon the miRNA regulation within U87MG cells, sRNA-seq was conducted and revealed a plethora of deregulated miRNAs. The observed shift of miRNA expression profiles suggested that SHG-8 exerted prominent effects upon their regulation, which was further supported by the performed KEGG pathway analysis, which revealed that a sufficient number of miRNAs controlling genes were affected by the presence of SHG-8. The most downregulated miRNA was miR-7974, while the most upregulated miRNA was miR-3648, which were also confirmed by RT-qPCR. In support of these findings, Wang et al. also observed downregulation of miR-7974 within GB tissue samples.[28] Administration of an miR-7974 mimic within gastric cancer influenced tumor cell proliferation, confirming its potential oncogenic properties.[29] Thus, it can be hypothesized that miR-7974 could also act as an oncomiR within GB cells. The biological actions of miR-7974 within GB cells are yet to be elucidated, even though suggestions for its implication in the glycerophospholipid metabolism within tumor spheroids do exist.[30]

Regarding miR-3648, it has been associated with the inactivation of the Wnt/β-catenin signaling pathway in gastric cancer.[31] Tang et al. observed that miR-3648 acted as a tumor-suppressive miRNA via a negative miR-3648/FRAT1-FRAT2/c-Myc feedback loop. Even though the exact mechanism of action of miR-3648 within GB is not fully understood, its strong association with the Wnt/β-catenin signaling pathway suggested possible implications as a therapeutic target.[31]

Overall, given that the expression changes of miR-3648 and miR-7974 are prominent and confirmed by both sRNA-seq and RT-qPCR, they are more likely to be considered as the main contributors of SHG-8-mediated cytotoxicity. However, this remains to be elucidated.

The effects of SHG-8 upon three miRNAs that are highly deregulated and involved in the tumorigenesis of GB, including miR-21, miR-128a, and miR-34a, were also investigated. miR-21 was found upregulated in gliomas, contributing to enhanced tumor cell survival and invasiveness, alongside its potential to induce resistance to various treatments, including chemotherapy and radiotherapy.[32] Inhibition of miR-21-5p activity and suppression of *SOX2* resulted in reduced levels of β-catenin, leading to decreased invasiveness and migration. Consequently, the downregulation of miR-21-5p directly influenced the expression of β-catenin. In line with these findings, our sRNA-seq analysis showed that miR-21 was significantly downregulated by SHG-8, suggesting that reduced migratory and clonogenic abilities of glioma cells might be caused by the inhibition of miR-21. However, subsequent RT-qPCR analysis demonstrated unchanged miR-21 levels between the control and treatment conditions. This could be because real-time PCR is a more sensitive approach used in expression analysis, whereas sRNA-seq captures information on transcript isoforms and alternative splicing events.[33] Additionally, cisplatin did not exhibit inhibitory effects upon miR-21. However, cisplatin has the potential to inhibit cell growth and proliferation via other mechanisms that are compensating for this. Furthermore, RT-qPCR analysis did not reveal significant changes in the expression of miR-34a and miR-128a. sRNA-seq analysis also demonstrated that the expression of miR-34a remained unchanged, while miR-128a was observed to be downregulated by the drug. miR-128a has shown downregulation in various malignancies, such as GB and bladder cancer.[34]

Reinstating the proper levels of miR-128a specific to the brain has demonstrated tumor-suppressive effects. This occurs through its interaction with the *E3F3a* and *BMI1* genes, resulting in decreased proliferation and invasiveness.[35] Nevertheless, the SHG-8 influenced the downregulation of miR-128a, suggesting that the drug could not restore adequate levels of the miRNA, which could further suppress tumor proliferation and migration. On the contrary, miR-34a expression levels were not affected by the presence of SHG-8. miR-34a belongs to a family of tumor suppressor miRNAs, and its expression is significantly reduced in GB.[36] miR-34 is known to be transactivated and controlled by the tumor suppressor protein P53. Moreover, miR-34a expression is negatively correlated with the expression of c-Met in GB cells, inhibiting GB tumor growth *in vivo* and induction of cell death.[26] Thus, the unaffected expression of miR-34a is a limiting factor for SHG-8 due to its inability to enhance its expression and lead to desired tumor suppressive mechanisms. It is hard to elucidate the exact mechanisms underlying SHG-8 upon the discussed miRNA candidates; however potential downregulation or inhibition of miR-21 might serve beneficial for the suppression of tumor growth and metastasis.

KEGG pathway analysis of deregulated genes (DEG) revealed that they were primarily associated with axon guidance and microRNAs in cancer (q value < 0.05; Supplementary Figure 3A). Consecutive biological pathway analysis of DEG showed that the biological processes affected by SHG-8 were primarily associated with neuron development, homophilic cell adhesion via plasma membrane adhesion molecules, negative regulation of intracellular signal transduction, negative regulation of the Wnt/β-catenin pathway, and negative regulation of the neuron apoptotic process (q value < 0.01; Supplementary Figure 3B).

miR-21 and miR-3648 were both associated with the inactivation of the Wnt/β-catenin signaling pathway. The Wnt/β-catenin pathway plays a crucial role in controlling cancer progression. It is transduced through frizzled receptors and LRP5/LRP6 coreceptors, leading to a β-catenin signaling cascade. Some of the negative regulators influencing this pathway involve *APC*, *AXIN1*, *AXIN2*, and *PPARG*.[37] Our sRNA-seq analysis revealed that multiple oncogenes, including *IDH2*, *FGFR3*, *IGFBP3*, *MADD*, *NF2*, *CORO2A*, *PDCD1/2*, and *GFAP* were negatively influenced by SHG-8 supporting its tumor suppressive properties (Supplementary Figure 3B). For instance, the *GFAP* gene encodes the production of glial fibrillary acidic protein, which belongs to the intermediate filament protein family. Intermediate filaments play a crucial role in regulating the shape, movement, and function of glial cells.[38] Thus, the negative SHG-8 regulation exerted upon

https://doi.org/10.1021/acsomega.4c02991
ACS Omega 2024, 9, 31789−31802

Table 1. Prediction of Absorption, Distribution, and Toxicity Properties of SHG-8 and Metabolites Together with Aspirin and Ibuprofen Predictions[a]

	compound										
feature[1]	SHG-8	SHG-8-1	SHG-8-2	SHG-8-3	SHG-8-4	SHG-8-5	SHG-8-6	SHG-8-7	SHG-8-8	aspirin	ibuprofen
Caco-2 permeability	+	+	−	+	−	+	−	+	+	−	+
human intestinal absorption	+	+	+	+	+	+	+	+	+	+	+
human oral bioavailability	+	+	+	+	+	+	−	+	+	+	+
blood−brain barrier	+	+	+	+	+	+	+	+	+	−	+
P-glycoprotein inhibitior	−	−	−	−	−	−	−	−	−	−	−
P-glycoprotein substrate	−	−	−	−	−	−	−	−	−	−	−
plasma protein binding[2]	0.791	0.725	0.972	0.918	0.972	0.821	0.649	0.897	0.760	0.583	0.751
Ames mutagenesis	−	−	−	−	−	−	−	−	−	−	−
acute oral toxicity[3]	III	III	III	III	III	III	III	III	III	II	III
carcinogenicity (binary)	−	−	−	−	−	−	−	−	−	−	−
hepatotoxicity	+	−	+	+	+	+	+	+	+	+	+
hERG inhibition	+	+	−	−	−	+	+	−	−	−	−
mitochondrial toxicity	−	+	+	+	+	+	−	+	−	+	+
micronucleus test	−	−	+	+	+	+	+	+	−	+	−
nephrotoxicity	−	−	−	+	−	−	−	−	−	+	−
reproductive toxicity	−	−	+	−	+	+	+	+	−	+	+
respiratory toxicity	−	+	+	−	+	−	−	−	−	+	+

[a](a) A "+" symbol denotes a positive and a "−" symbol denotes a negative prediction or absence of a feature. (b) The numbers are fractions between 0 and 1. (c) The toxicity classes range from IV to I with class IV being the lowest possible toxicity class.

GFAP could lead to a disturbed glial balance and enhanced permeability within the blood−-brain barrier (BBB), allowing the passage of SHG-8 molecules and their direct targeting of GB. Furthermore, knocking out *MADD* (MAPK-activating death domain) within anaplastic thyroid cancer resulted in a notable decrease in cellular migration, invasion potential, and clonogenic capacity *in vitro*.[39] Thus, SHG-8 regulated silencing of *MADD* might lead to antimigratory and anti-invasive effects within GB, which could be accompanied by the inhibition of epithelial-mesenchymal transition (EMT) and Wnt-signaling pathways. The scientific evidence regarding both *GFAP* and *MADD* correlated with the RNA-seq findings related to the biological processes influenced by SHG-8, which included the effect on neuron development, negative regulation of intracellular signal transduction, negative regulation of the Wnt-signaling pathway, and negative regulation of the neuron apoptotic process. To strengthen the hypothesis that SHG-8 negatively regulated the Wnt-pathway, an *in vitro* RT-qPCR of *CORO1C* revealed that the gene was significantly downregulated in the presence of the drug. *CORO1C* acts as an F-actin turnover effector influencing neurite overgrowth and migration of brain tumor cells.[40] An elevated expression of *CORO1C* in metastatic malignancies, such as GB and colorectal cancer, was previously documented, indicating the potential clinical relevance of this gene as a biomarker associated with an unfavorable prognosis.[41] The negative effects of SHG-8 upon this oncogene supported the findings that SHG-8 exerted negative regulation upon *de novo* neurone overgrowth and the Wnt pathway, thus limiting the proliferative and migratory abilities of U87MG GB cells. Furthermore, the high affinity binding between the CORO1C protein receptor and the SHG-8 ligand demonstrated in our molecular docking analysis suggested that GB cell inhibition might be partially through targeting CORO1C (Supplementary Figure 4, Supplementary Table 1).

3.7. SHG-8 Possessed Sustainable Bioavailability. The nine predicted metabolites (SHG-8-1 to SHG-8-9, Supplementary Figure 2) are based on one reduction of the parent compound SHG-8 by carbonyl reductase as well as a number of hydroxylations and dealkylations predicted to be carried out by cytochrome P450 1A2 (CYP1A2). A selected number of absorption, distribution, and toxicity properties of SHG-8 and metabolites predicted with admetSAR 2.0 are shown in Table 1. For comparison, the over-the-counter painkillers aspirin and ibuprofen were included in the prediction. From Table 1, SHG-8 has predicted absorption and distribution features comparable with aspirin and ibuprofen, which suggests that SHG-8 is sufficiently absorbed and distributed in the body. In particular, SHG-8 was predicted to pass the blood−brain barrier. SHG-8 and all metabolites did fall into the acute oral toxicity class III (medium), while class IV is the lowest toxicity class. With regards to various toxicity predictions, SHG-8 and metabolites were comparable to ibuprofen, except for inhibition of hERG, a gene that encodes for the alpha-subunit of a cardiac potassium channel, inhibition of which could potentially lead to heart problems. SHG-8 was not associated with carcinogenicity and nephrotoxicity. Furthermore, a number of metabolites were predicted positive for the micronucleus test, indicating a potential for genotoxicity. SHG-8 and metabolites were not predicted to be mutagenic or carcinogenic in the Ames test.

Cytotoxicity presents challenges in GB treatment. For instance, the selectivity of the BBB restricts the entry of many therapeutic agents into the brain, limiting their efficacy against GB cells, while potentially causing toxicity to healthy brain tissue.[42] As predicted via the *in silico* analysis, SHG-8 can pass freely through the BBB, overcoming cytotoxicity-related challenges in GB treatment. The complex tumor microenvironment of GB and its rigid protection by the BBB can hinder the delivery and effectiveness of cytotoxic treatments.[43] We demonstrated that SHG-8 has the capacity to negatively regulate genes involved in the maintenance of the BBB, leading to its weakening and thus exerting direct cytotoxic effects upon GB cells. The low oral toxicity possessed by SHG-8 metabolites could prove beneficial for patient comfort and better quality of life during therapy. Furthermore, a number of

https://doi.org/10.1021/acsomega.4c02991
ACS Omega 2024, 9, 31789−31802

metabolites of SHG-8 were predicted as potential genotoxicity effectors, supporting the findings observed throughout the *in vitro* investigations. Genotoxicity is a valuable consideration in GB treatment as certain therapies, such as radiation and chemotherapeutic agents, including TMZ, can induce DNA damage and genomic instability.[44] Nevertheless, it is essential to mention that this could lead to potential adverse effects on normal cells and contribute to the development of secondary malignancies.[45]

The present study of testing a new, potential anticancer agent within glioblastoma cell models could benefit from incorporating *in vivo* experimentations which will strengthen the validity of the results. In addition, animal models represent the tumor microenvironment better and thus would help to elucidate the specific drug efficacy and impact within model organism. Furthermore, the predicted genotoxicity of SHG-8 and its metabolites via the ADMET prediction highlights the need of further toxicity and efficacy evaluations before its clinical application. Our findings suggested that SHG-8 could act as a potential anticancer therapeutic and influences the miRNome of GB cells; however, sample size must be considered as a potential limitation.

In summary, the environmentally sustainable and economical synthesis of SHG-8 and its biological inhibitory effects upon GB cell viability, migration, and proliferation suggested that the compound might be a beneficial therapeutic agent against GB. SHG-8 demonstrated genotoxic properties via the release of ROS and promoting cells toward apoptotic stages. Inhibition of Wnt/β-catenin pathway-associated oncogenes, supported via the significant downregulation of miR-21 and *CORO1C*, might serve as a guiding point to understanding the mechanisms of action of the drug.

■ ASSOCIATED CONTENT

Data Availability Statement

The data presented in this research paper have been uploaded at Mendeley. Release date: 02/12/2023 (https://data.mendeley.com/datasets/v5mcf8hpsz/1).

Supporting Information

The Supporting Information is available free of charge at https://pubs.acs.org/doi/10.1021/acsomega.4c02991.

> Additional details on the methodology; supplementary figures on SHG-8 synthesis, metabolites of SHG-8, KEGG pathway and biological pathway bioinformatics analyses of sRNA-sequencing, and molecular docking of SHG-8; supplementary tables of molecular docking analysis and quantification of apoptosis (PDF)

■ AUTHOR INFORMATION

Corresponding Author

Maria Braoudaki − *School of Life and Medical Sciences, University of Hertfordshire, Hatfield AL10 9AB, United Kingdom; University Research Institute of Maternal and Child Health and Precision Medicine, National and Kapodistrian University of Athens, 11527 Athens, Greece;* Email: m.braoudaki@herts.ac.uk

Authors

Denis Mustafov − *School of Life and Medical Sciences, University of Hertfordshire, Hatfield AL10 9AB, United Kingdom; College of Health, Medicine and Life Sciences, Brunel University London, Uxbridge UB8 3PH, United Kingdom;* orcid.org/0009-0008-2244-600X

Shoib S. Siddiqui − *School of Life and Medical Sciences, University of Hertfordshire, Hatfield AL10 9AB, United Kingdom*

Andreas Kukol − *School of Life and Medical Sciences, University of Hertfordshire, Hatfield AL10 9AB, United Kingdom*

George I. Lambrou − *Choremeio Research Laboratory, First Department of Pediatrics, School of Medicine, National and Kapodistrian University of Athens, Athens, Greece, 11527 Athens, Greece; University Research Institute of Maternal and Child Health and Precision Medicine, National and Kapodistrian University of Athens, 11527 Athens, Greece*

Shagufta − *Department of Biotechnology, School of Arts and Sciences, American University of Ras Al Khaimah, Ras Al Khaimah, United Arab Emirates;* orcid.org/0000-0003-1028-7888

Irshad Ahmad − *Department of Biotechnology, School of Arts and Sciences, American University of Ras Al Khaimah, Ras Al Khaimah, United Arab Emirates*

Complete contact information is available at: https://pubs.acs.org/10.1021/acsomega.4c02991

Author Contributions

D.M. performed all experiments and drafted the manuscript. S.S.S. contributed to the experimental design and assisted in experiment performance. A.K. performed the SHG-8 bioinformatic analyses. G.I.L. revised the manuscript and provided critical insight. S. and I.A. synthesized the SHG-8 compound. M.B. designed, coordinated, and supervised the study; gave final approval for publication. All authors contributed to writing, reading, and approval of the final version of the manuscript.

Funding

The authors I.A. and S. appreciate the financial support provided by the School of Graduate Studies and Research, American University of Ras Al Khaimah, Ras Al Khaimah, UAE, through seed grant funded project no. AAS/002/19.

Notes

The authors declare no competing financial interest.

■ ACKNOWLEDGMENTS

We are grateful to the School of Life and Medical Sciences, University of Hertfordshire, United Kingdom for the support in this work.

■ ABBREVIATIONS

GB = glioblastoma
miRNA = microRNA
RT-qPCR = real-time polymerase chain reaction
ROS = reactive oxygen species
β-AC = β-amino carbonyl
sRNA-seq = small RNA-sequencing
TMZ = temozolomide
TME = tumor microenvironment
SAFSNS = sulfonic acid-functionalized silica nanospheres
SHG-8 = β3-(4-bromophenyl)-1-phenyl-3-(phenylamino)-propan-1-one
MTT = 3-(4,5-dimethylthiazol-2-yl)-2,5-diphenyltetrazolium bromide
DMSO = dimethyl sulfoxide

GO = gene ontology
KEGG = Kyoto Encyclopaedia of Genes and Genomes

REFERENCES

(1) Gillespie, C. S.; Bligh, E. R.; Poon, M. T. C.; Solomou, G.; Islim, A. I.; Mustafa, M. A.; Rominiyi, O.; Williams, S. T.; Kalra, N.; Mathew, R. K.; et al. Imaging timing after glioblastoma surgery (INTERVAL-GB): protocol for a UK and Ireland, multicentre retrospective cohort study. *BMJ. open* **2022**, *12* (9), No. e063043.

(2) Rong, L.; Li, N.; Zhang, Z. Emerging therapies for glioblastoma: current state and future directions. *Journal of experimental & clinical cancer research: CR* **2022**, *41* (1), 142.

(3) Zhang, C.; Nance, E. A.; Mastorakos, P.; Chisholm, J.; Berry, S.; Eberhart, C.; Tyler, B.; Brem, H.; Suk, J. S.; Hanes, J. Convection enhanced delivery of cisplatin-loaded brain penetrating nanoparticles cures malignant glioma in rats. *Journal of controlled release: official journal of the Controlled Release Society* **2017**, *263*, 112−119.

(4) Braoudaki, M.; Lambrou, G. I. MicroRNAs in pediatric central nervous system embryonal neoplasms: the known unknown. *Journal of Hematol. Oncol.* **2015**, *8*, 6.

(5) Dawoud, A.; Ihab Zakaria, Z.; Hisham Rashwan, H.; Braoudaki, M.; Youness, R. A. Circular RNAs: New layer of complexity evading breast cancer heterogeneity. *Non-coding RNA research* **2023**, *8* (1), 60−74.

(6) Wang, G. B.; Liu, J. H.; Hu, J.; Xue, K. MiR-21 enhanced glioma cells resistance to carmustine via decreasing Spry2 expression. *Eur. Rev. Med. Pharmacol. Sci.* **2017**, *21* (22), 5065−5071.

(7) Budi, H. S.; Younus, L. A.; Lafta, M. H.; Parveen, S.; Mohammad, H. J.; Al-Qaim, Z. H.; Jawad, M. A.; Parra, R. M. R.; Mustafa, Y. F.; Alhachami, F. R.; et al. The role of miR-128 in cancer development, prevention, drug resistance, and immunotherapy. *Frontiers in oncology* **2023**, *12*, No. 1067974.

(8) Singh, R.; Bhasin, G.; Srivastava, R. *β*-Aminocarbonyl Compounds: Chemistry and Biological Activities. *Mini-Reviews in Organic Chemistry* **2016**, *13* (2), 143−153.

(9) Hossain, M.; Das, U.; Dimmock, J. R. Recent advances in alpha,beta-unsaturated carbonyl compounds as mitochondrial toxins. *European journal of medicinal chemistry* **2019**, *183*, No. 111687.

(10) Ebrahimi, S. O.; Reiisi, S.; Shareef, S. miRNAs, oxidative stress, and cancer. A comprehensive and updated review. *Journal of Cellular Physiology* **2020**, *235* (11), 8812−8825.

(11) Araki, K.; Hara, M.; Hamada, S.; Matsumoto, T.; Nakamura, S. Antiproliferative Activities of Cynaropicrin and Related Compounds against Cancer Stem Cells. *Chemical & pharmaceutical bulletin* **2024**, 72 (2), 200−208.

(12) Cui, P.; Chen, F.; Ma, G.; Liu, W.; Chen, L.; Wang, S.; Li, W.; Li, Z.; Huang, G. Oxyphyllanene B overcomes Temozolomide resistance in glioblastoma: Structure-activity relationship and mitochondria-associated ER membrane dysfunction. *Phytomedicine: international journal of phytotherapy and phytopharmacology* **2022**, *94*, No. 153816.

(13) Ahmad, I.; Shagufta; Dhar, R.; Hisaindee, S.; Hasan, K. An Environmentally Benign Solid Acid Nanocatalyst for the Green Synthesis of Carboxylic Acid Ester. *Chemistryselect* **2021**, *6* (36), 9645−9652.

(14) Vazhappilly, C. G.; Hodeify, R.; Siddiqui, S. S.; Laham, A. J.; Menon, V.; El-Awady, R.; Matar, R.; Merheb, M.; Marton, J.; Al Zouabi, H. A. K.; et al. Natural compound catechol induces DNA damage, apoptosis, and G1 cell cycle arrest in breast cancer cells. *Phytotherapy research: PTR* **2021**, *35* (4), 2185−2199.

(15) Braoudaki, M.; Lambrou, G. I.; Papadodima, S. A.; Stefanaki, K.; Prodromou, N.; Kanavakis, E. MicroRNA expression profiles in pediatric dysembryoplastic neuroepithelial tumors. *Medical oncology (Northwood, London, England)* **2016**, *33* (1), 5.

(16) Wishart, D. S.; Tian, S.; Allen, D.; Oler, E.; Peters, H.; Lui, V. W.; Gautam, V.; Djoumbou-Feunang, Y.; Greiner, R.; Metz, T. O. BioTransformer 3.0-a web server for accurately predicting metabolic transformation products. *Nucleic acids research* **2022**, *50* (W1), W115−W123.

(17) Yang, H.; Lou, C.; Sun, L.; Li, J.; Cai, Y.; Wang, Z.; Li, W.; Liu, G.; Tang, Y. admetSAR 2.0: web-service for prediction and optimization of chemical ADMET properties. *Bioinformatics (Oxford, England)* **2019**, *35* (6), 1067−1069.

(18) Yang, J.; Roy, A.; Zhang, Y. BioLiP: a semi-manually curated database for biologically relevant ligand-protein interactions. *Nucleic Acids Research* **2012**, *41* (D1), D1096−D1103.

(19) Kaur, B.; Kumar, H. Ultrasound-Promoted One-Pot Three-Component Synthesis of *β*−Amino Carbonyl Compounds Using Manganese Perchlorate. *Organic Preparations and Procedures International* **2020**, *52* (5), 474−477.

(20) Ahmad, M. S.; Braoudaki, M.; Patel, H.; Ahmad, I.; Shagufta; Siddiqui, S. S. Novel Siglec-15-Sia axis inhibitor leads to colorectal cancer cell death by targeting miR-6715b-3p and oncogenes. *Frontiers in immunology* **2023**, *14*, No. 1254911.

(21) Zhang, Z. Y.; Zhu, Y. H.; Zhou, C. H.; Liu, Q.; Lu, H. L.; Ge, Y. J.; Wang, M. W. Development of beta-amino-carbonyl compounds as androgen receptor antagonists. *Acta pharmacologica Sinica* **2014**, *35* (5), 664−673.

(22) Yang, K.; Wu, Z.; Zhang, H.; Zhang, N.; Wu, W.; Wang, Z.; Dai, Z.; Zhang, X.; Zhang, L.; Peng, Y.; et al. Glioma targeted therapy: insight into future of molecular approaches. *Molecular cancer* **2022**, *21* (1), 39.

(23) Nasir, S.; Nazir, S.; Hanif, R.; Javed, A. Glioblastoma Multiforme: Probing Solutions to Systemic Toxicity towards High-Dose Chemotherapy and Inflammatory Influence in Resistance against Temozolomide. *Pharmaceutics* **2023**, *15* (2), 687.

(24) Sies, H.; Jones, D. P. Reactive oxygen species (ROS) as pleiotropic physiological signalling agents. *Nature reviews. Molecular cell biology* **2020**, *21* (7), 363−383.

(25) Wang, L.; Fan, F.; Cao, W.; Xu, H. Ultrasensitive ROS-Responsive Coassemblies of Tellurium-Containing Molecules and Phospholipids. *ACS Appl. Mater. Interfaces* **2015**, *7* (29), 16054−16060.

(26) Li, S.; Xie, A.; Li, H.; Zou, X.; Zhang, Q. A self-assembled, ROS-responsive Janus-prodrug for targeted therapy of inflammatory bowel disease. *Journal of controlled release: official journal of the Controlled Release Society* **2019**, *316*, 66−78.

(27) Chen, M.; Medarova, Z.; Moore, A. Role of microRNAs in glioblastoma. *Oncotarget* **2021**, *12* (17), 1707−1723.

(28) Wang, S.; Zhou, H.; Zhang, R.; Zhang, Y. Integrated Analysis of Mutations, miRNA and mRNA Expression in Glioblastoma. *International journal of general medicine* **2021**, *14*, 8281−8292.

(29) Sexton, R. E.; Al-Hallak, M. N.; Al-Share, B.; Li, Y.; Aboukameel, A.; Landesman, Y.; Kashyap, T.; Kim, S.; Mohammad, R. M.; Philip, P. A.; Azmi, A. S. Abstract 2383: Mir-7974: An oncogenic miRNA that perpetuates gastric cancer. *Cancer Res.* **2021**, *81* (13_Supplement), 2383−2383.

(30) Mucino-Olmos, E. A.; Vazquez-Jimenez, A.; Lopez-Esparza, D. E.; Maldonado, V.; Valverde, M.; Resendis-Antonio, O. MicroRNAs Regulate Metabolic Phenotypes During Multicellular Tumor Spheroids Progression. *Frontiers in oncology* **2020**, *10*, No. 582396.

(31) Tang, W.; Pei, M.; Li, J.; Xu, N.; Xiao, W.; Yu, Z.; Zhang, J.; Hong, L.; Guo, Z.; Lin, J.; et al. The miR-3648/FRAT1-FRAT2/c-Myc negative feedback loop modulates the metastasis and invasion of gastric cancer cells. *Oncogene* **2022**, *41* (43), 4823−4838.

(32) Aloizou, A. M.; Pateraki, G.; Siokas, V.; Mentis, A. A.; Liampas, I.; Lazopoulos, G.; Kovatsi, L.; Mitsias, P. D.; Bogdanos, D. P.; Paterakis, K.; et al. The role of MiRNA-21 in gliomas: Hope for a novel therapeutic intervention? *Toxicology reports* **2020**, *7*, 1514−1530.

(33) Coenye, T. Do results obtained with RNA-sequencing require independent verification? *Biofilm* **2021**, *3*, No. 100043.

(34) Slack, F. J.; Chinnaiyan, A. M. The Role of Non-coding RNAs in Oncology. *Cell* **2019**, *179* (5), 1033−1055.

(35) Zhang, Y.; Chao, T.; Li, R.; Liu, W.; Chen, Y.; Yan, X.; Gong, Y.; Yin, B.; Liu, W.; Qiang, B.; et al. MicroRNA-128 inhibits glioma cells proliferation by targeting transcription factor E2F3a. *Journal of molecular medicine (Berlin, Germany)* **2009**, *87* (1), 43−51.

https://doi.org/10.1021/acsomega.4c02991
ACS Omega 2024, 9, 31789−31802

(36) Vaitkiene, P.; Pranckeviciene, A.; Stakaitis, R.; Steponaitis, G.; Tamasauskas, A.; Bunevicius, A. Association of miR-34a Expression with Quality of Life of Glioblastoma Patients: A Prospective Study. *Cancers* **2019**, *11* (3), 300.
(37) Manfreda, L.; Rampazzo, E.; Persano, L. Wnt Signaling in Brain Tumors: A Challenging Therapeutic Target. *Biology* **2023**, *12* (5), 729.
(38) Guan, R.; Zhang, X.; Guo, M. Glioblastoma stem cells and Wnt signaling pathway: molecular mechanisms and therapeutic targets. *Chinese neurosurgical journal* **2020**, *6*, 25.
(39) van Bodegraven, E. J.; van Asperen, J. V.; Robe, P. A. J.; Hol, E. M. Importance of GFAP isoform-specific analyses in astrocytoma. *Glia* **2019**, *67* (8), 1417−1433.
(40) Mustafov, D.; Karteris, E.; Braoudaki, M. Deciphering the Role of microRNA Mediated Regulation of Coronin 1C in Glioblastoma Development and Metastasis. *Non-coding RNA* **2023**, *9* (1), 4.
(41) Wang, Z.; Jia, L.; Sun, Y.; Li, C.; Zhang, L.; Wang, X.; Chen, H. CORO1C is Associated With Poor Prognosis and Promotes Metastasis Through PI3K/AKT Pathway in Colorectal Cancer. *Frontiers in molecular biosciences* **2021**, *8*, No. 682594.
(42) Arvanitis, C. D.; Ferraro, G. B.; Jain, R. K. The blood-brain barrier and blood-tumour barrier in brain tumours and metastases. *Nature reviews. Cancer* **2020**, *20* (1), 26−41.
(43) Karmur, B. S.; Philteos, J.; Abbasian, A.; Zacharia, B. E.; Lipsman, N.; Levin, V.; Grossman, S.; Mansouri, A. Blood-Brain Barrier Disruption in Neuro-Oncology: Strategies, Failures, and Challenges to Overcome. *Frontiers in oncology* **2020**, *10*, No. 563840.
(44) Lang, F.; Liu, Y.; Chou, F. J.; Yang, C. Genotoxic therapy and resistance mechanism in gliomas. *Pharmacology & therapeutics* **2021**, *228*, No. 107922.
(45) Domenech, J.; Rodriguez-Garraus, A.; Lopez de Cerain, A.; Azqueta, A.; Catalan, J. Genotoxicity of Graphene-Based Materials. *Nanomaterials (Basel, Switzerland)* **2022**, *12* (11), 1795.

https://doi.org/10.1021/acsomega.4c02991
ACS Omega 2024, 9, 31789−31802